Towards Selective Small Cation Chelation

A thesis presented
in partial fulfilment of the requirements
for the degree of
Doctor of Philosophy in Chemistry
at Massey University, Palmerston North

Karl Jürgen Shaffer

2010

Acknowledgements

First and foremost I would like to thank my supervisor Paul Plieger who was always friendly and supportive throughout my study. He encouraged me to put my own twist on the thesis and this has fostered the development of my independent research and problem-solving abilities.

I would like to thank Anthony Burrell and Mark McCleskey for hosting me when I visited the Los Alamos National Laboratory to conduct the beryllium coordination chemistry aspects of this thesis. Whilst there, Himashinie Diyabalanage provided much insight regarding the particular aspects of conducting this challenging field of chemistry.

Ross Davidson deserves a special mention for providing a wealth of knowledge on the inorganic chemistry and computational aspects of this thesis. Marco Wenzel must be thanked for taking time away from his own research to run most of my crystals on the diffractometer.

I would also like to acknowledge the New Zealand Government for providing financial support in the form of a Top Achiever Doctoral Scholarship.

Finally, I wish to thank my parents for supporting my efforts to pursue a PhD.

Abstract

This thesis sought to identify ligands which could be used in sensing or sequestering applications for the toxic element beryllium. The overall aim was to search for ligands with tight binding cavities and those capable of fully encapsulating the small Be(II) cation. Please refer to the foldout at the end of this book for ligand descriptions.

Proton sponge ligands **L1** – **L13** were synthesised and evaluated for their use as simple bidentate small cation chelators. An efficient modified route to **L1** was developed. The derivatisation and properties of these unexplored ligands were investigated. X-ray crystallography gave insight into the structures of these unique molecules. Ligands of type **L1** had an ideal size-fit for the small cation B(III), used as a structural analogue for Be(II), as indicated by the crystal structure of the boron complex. Due to their high basicity they were unsuitable for coordination to Be(II) in aqueous systems due to competition for protonation. The larger Cu(II) cation was a poor fit for these ligands and a rare crystal structure showed large distortions of the metal ion from the ligand plane. The Cu(II) complexes were unstable and hydrolysed readily.

A fundamentally new type of tetra-coordinate ligand, **L14**, was synthesised and while untested in this thesis offers promise as an ideal Be(II) chelator.

The ligands **L15** – **L21** were evaluated for use as fully encapsulating Be(II) chelators and those containing three oxygen donors were found to be most suitable. The rigidity imparted by the locking of certain conformations of the ligands **L18** and **L19** upon Be(II) coordination gave rise to fluorescence. The ligands containing carboxylic acid groups (**L17** and **L18**) enabled good water solubility and **L18** in particular showed the most promise as a ligand for beryllium sensing or sequestering applications.

Contents

List of Abbreviations

Acac	Acetylacetonate
BODIPY	Boron dipyrromethene
-^{n}Bu	Normal butyl group
-^{t}Bu	Tertiary butyl group
CBD	Chronic beryllium disease
CCSD	Cambridge crystal structure database
Cg	Centroid
COSY	Correlation spectroscopy
DFT	Density functional theory
DMAD	Dimethylacetylene dicarboxylate
DMAE	Dimethyaminoethanol
DMAN	1,8-Bis(dimethylamino)naphthalene
DMF	Dimethylformamide
DMSO	Dimethylsulfoxide
Dppe	1,2-Bis(diphenylphosphino)ethane
EDTA	Ethylenediaminetetraacetic acid
EPA	Environmental Protection Agency
ESR	Electron spin resonance
-Et	Ethyl group
GIAO	Gauge including atomic orbital
HEPA	High efficiency particulate air
Hfac	Hexafluoroacetylacetonate
HMQC	Heteronuclear multiple quantum coherence
HOMO	Highest occupied molecular orbital
LUMO	Lowest unoccupied molecular orbital
-Me	Methyl group
MS	Mass spectroscopy
NBS	N-Bromosuccinimide
NMR	Nuclear magnetic resonance

-OAc	Acetoxy group
-Ph	Phenyl group
RT	Room temperature
SERS	Surface enhanced Raman spectroscopy
TLC	Thin layer chromatography
TMS	Tetramethylsilane
TOF	Time of flight
UV-Vis	Ultraviolet-Visible spectroscopy

List of Figures, Tables and Reaction Schemes

Chapter 1: Literature Review

1.1 Introduction to Beryllium

Beryllium has unique and unusual material properties which make it an important industrial metal. It is a key component in the aerospace and electronics industries, particularly when alloyed with metals such as copper.[1] Beryllium is also used in nuclear applications due to its small neutron capture cross-section. Unfortunately, beryllium is one of the most toxic non-radioactive metals on the periodic table.[2] It can cause the often-fatal lung disease CBD (Chronic Beryllium Disease)[3-5] and it is listed as a Class A EPA carcinogen in the USA.[6] Operations such coal-fired plants, industrial manufacturing, nuclear weapons production and disposal operations release beryllium to the environment. There is the potential to expose workers and the public to beryllium.

1.1.1 Properties, Production and Uses

Beryllium is a valuable metal as it is extremely lightweight, six times stiffer than steel, has a high melting point of 1285 ^{o}C and a high heat-adsorption capacity. It is nonmagnetic and corrosion resistant, and has the lowest thermal neutron adsorption cross-section of any metal.[7] This property is utilised in X-ray windows for various instruments in the fields of science and medicine. Beryllium was isolated in 1828 but not used extensively until the 1920's when it was alloyed with copper as a 2 % addition to give an alloy six times stronger than copper alone.[7-9] The only available oxidation state for beryllium is +2. Beryllium has a relatively high ionisation potential, with a charge-to-size-ratio of 5.7 (+2/0.35 Å), and the highest Pauling electronegativity (6.3 kJ/g atom) of the alkali and alkaline earth elements.

Beryllium is mined from naturally occurring silicates including beryl ($Al_2Be_3Si_6O_{18}$, 5 % by weight beryllium) and bertrandite ($Be_4(OH)_2Si_2O_7$, 15 % by weight beryllium).[10]

Bertrandite is primarily mined in the state of Utah in the USA, while beryl is imported to the USA from Argentina and Brazil.[9] The world's resources of beryllium are estimated at approximately 80,000 tons.[11] The USA is the world's leading producer, processor and consumer of beryllium products. In the year 2000 the USA used 390 tons of beryllium with an estimated value of USD $140 million.[9]

Beryllium can be used as a pure metal, mixed with other metals to form high-strength alloys, processed to salts that dissolve in water, or processed to form oxides and ceramic materials. Its unique structural and mechanical properties find applications in the aerospace and electronics industries.[12-15] Beryllium is used in aircraft bearing and bushings because it can sustain heavy loads without adding weight or losing material strength. Its material strength makes it useful as a component of fuel containers for solid propulsion jet and rocket fuel systems, gyros and re-entry vehicles. A beryllium-aluminium alloy (Beralcast®) is being used in the manufacture of US military fighter planes, helicopters and missile systems. In the electronics industry, beryllium is used to make springs, switches, relays, connectors and electronic systems for computers, telecommunications (fiber optics and cellular network communication systems), appliances (optical laser scanners in copy machines, photo separators, and airport luggage handlers), and automotive applications (air bag sensors, ignition switches, power steering systems).[16, 17] Beryllium oxide ceramics have a thermal conductivity second only to diamond among electrically insulating materials, dissipating nearly 300 W/mK at room temperature.[16] The ceramics provide circuit performance at high frequencies and are stable under oxidising and reducing, high humidity environments making them excellent semiconductor devices and integrated circuits that require thermal dissipation. The medicinal community relies on beryllium for production of pacemakers, lasers, high-resolution X-ray images and dental alloys for manufacturing crowns, bridges and dental plates.[9] The sports industry has utilised beryllium for golf clubs and bicycle frames. The nuclear defense industry uses beryllium for its neutron adsorption and reflection properties.

1.1.2 Health Hazards and Safety Precautions

Although beryllium is an important industrial metal, it presents health hazards that are of critical importance to consider before proceeding with processing or handling pure beryllium metal, oxide or materials contaminated with beryllium. The significant health risk is developing the potentially fatal lung disease, berylliosis or Chronic Beryllium Disease (CBD).[3-5] CBD is a granulomatous lung disease that develops from a cell-mediated immune response to inhaled beryllium in 1 – 15 % of exposed individuals.[17-19] It is characterised by a hypersensitivity that can be delayed in onset several months to 40 years. There is no clear relationship between the extent of exposure and the severity of the resultant disease.[3, 17-21] Beryllium disease is treatable but incurable.[19]

The primary route of potential human exposure to beryllium and beryllium compounds is inhalation. In the current biomolecular understanding of how beryllium initiates CBD, beryllium inhaled into the lungs is solubilised and transported into the cell. Once in the cell, it is believed that beryllium interacts with a specific protein that binds beryllium at a receptor site. The binding of the beryllium results in auto-immune presentation of the protein, initiates the body's immune response, and triggers the onset of beryllium sensitisation and CBD.[5] The human immune system responds to beryllium by producing blood cells that engulf beryllium particles in the lung forming granulomas and eventually fibroids that make it increasingly difficult for victims to breathe.[5, 19] Occupational workers are the highest risk group for contracting CBD, although individuals with minimal exposure such as plant secretaries, security staff and spouses of the beryllium workers have also contracted the disease.

The evidence suggests that the development of CBD in certain individuals may be due to two risk factors, beryllium exposure and genetic susceptibility. Research associated with genetic susceptibility has shown that a high degree of association exists between individuals with CBD and a variation in a specific gene, the HLA-DPB1 locus, which is believed to code for the beryllium binding protein.[5, 22] Research on homozygous substitution of a glutamic acid in the Glu69 portion of the HLA-DPB1 gene translated into

a higher risk for the development of beryllium sensitisation and CBD.[23] In a study of CBD victims, 30 % possessed homozygous glutamic acid in Glu69 while 1.3 % of beryllium exposed workers that were not affected by CBD possessed this variation of chain alleles.[23]

Aside from causing CBD, beryllium has high cytotoxicity.[15, 24, 25] Beryllium binds strongly to sites in complex biomolecules that are unavailable to most other metals. It can displace divalent cations (such as magnesium) in these environments. Beryllium can impact enzyme function, DNA synthesis, protein phosphorylation and cell division.[25, 26] In animal studies, beryllium is a known carcinogen causing lung tumours and carcinomas. These effects occur for beryllium metal, alloys, ore, and as salts when the animals are exposed by inhalation and intratracheally.

1.2 Beryllium Coordination Chemistry

Study in the area of beryllium coordination chemistry has been aimed toward developing chelation agents for the treatment of CBD,[27] the development of fluorescent sensors for studying biological systems,[28] and environmental remediation.[29] There are two main groups worldwide who are actively pursuing research in the area of beryllium coordination chemistry.[27, 30] As of 2010, it is getting increasingly difficult to establish collaborations with research groups still active in this area.

Oxygen and nitrogen donor ligands are pertinent when comparing the complexes studied in this thesis. Complexes with donor atoms other than oxygen or nitrogen have been omitted. The following sections are not comprehensive; rather, they provide an overview of the types of chelates beryllium forms with oxygen and nitrogen donor ligands. This is a summary of the numerous reviews[15, 24, 31, 32] and the references cited therein, with a focus on those complexes with direct structural evidence for coordination to beryllium with the aim of identifying the key components needed in a beryllium selective ligand.

1.2.1 Beryllium Complexes with Oxygen Donors

The most widely studied complexes to beryllium involve ligands with strong σ oxygen donors such as carboxylic acid and phenolic moieties. The following examples were found in the CCSD (v5.30, Nov 2008, 1 update). In aqueous environments an equimolar ratio of L (L being a two-oxygen chelating ligand) with Be(II) at low pH will typically give the *mono*-ligand chelate $[BeL(H_2O)_2]^{n+}$ while a 2:1 ratio of L to Be(II) at pH greater than 7 will typically give the *bis*-ligand chelate $[BeL_2]^{n+}$ (n is the charge of the complex and is dependent on whether L can be singly or doubly deprotonated for complexation).[32] At intermediate pH of approximately 5 – 7, complicated beryllium hydroxo cluster species usually form.[32] One example of such a cluster complex is basic beryllium acetate $Be_4O(O_2CMe)_6$, with four Be(II) ions tetrahedrally arranged around one O^{2-} with six bridging acetates along the edges of the tetrahedron (Figure 1.1).[33] The role of beryllium –

oxygen cluster formation at physiological pH has been studied to understand the development of chronic beryllium disease and identify possible chelation treatments,[34, 35] including the investigation of beryl-like structures which were stable and soluble in phosphate media.[36] While an important class of beryllium complexes, the following discussion will be limited to *mono*-ligand and *bis*-ligand chelates.

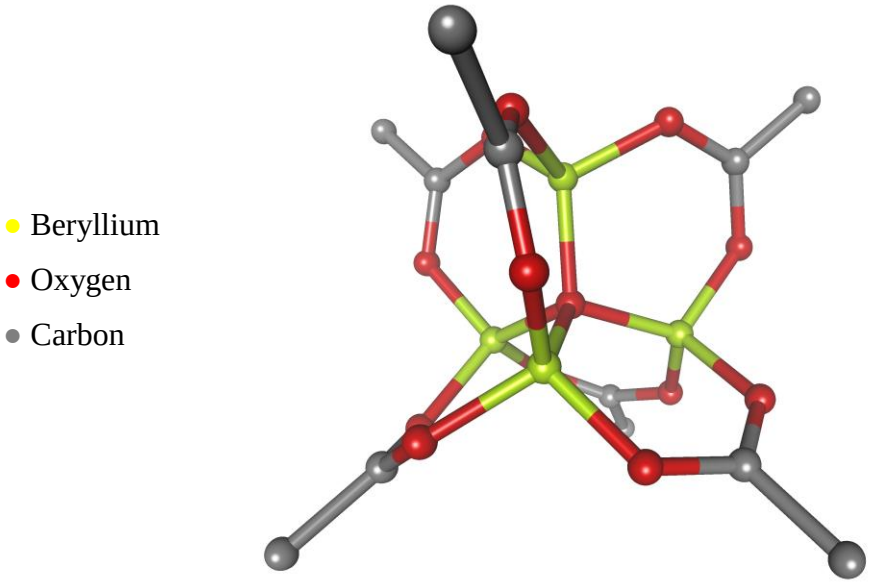

Figure 1.1: Structure of beryllium acetate[33]

Dicarboxylic acid ligands offer very strong σ oxygen donors to beryllium. Beryllium retains a tetrahedral geometry with one or two chelating dicarboxylic acid ligands depending on the pH range; e.g. $[BeL(H_2O)_2]$, $[BeL_2]^{2-}$. Dicarboxylic acid complexes with six-membered chelate rings (e.g. beryllium complexes of **102**, **104**, Figure 1.2) offer the best "fit" for beryllium. These have the least ring and torsional strain and are most compatible with the tetrahedral geometry of the beryllium ion. The dicarboxylic acids in Figure 1.2 have reported crystal structures complexed to Be(II) of the form $[BeL_2]^{2-}$ and are balanced by suitable cations (such as K^+).[37-40] The crystal structure of $K_2[Be(\mathbf{104})_2]$ had bond lengths (for one ligand Be – O; 1.598(3) and 1.613(3) Å) and a bite angle of (for one ligand O–Be–O; 107.5(1)^o), both units of **104** were symmetrical.[41]

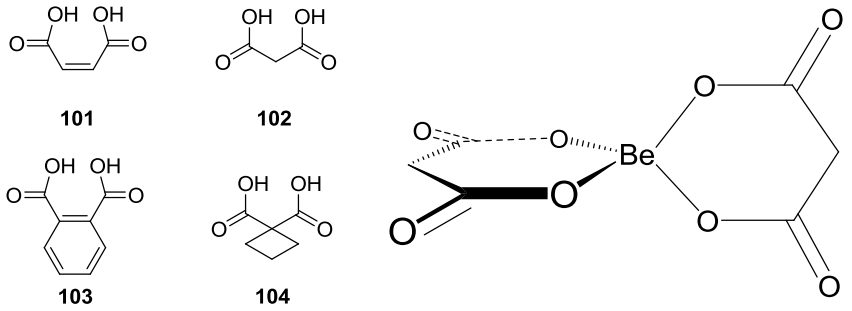

*Figure 1.2: Selection of dicarboxylic acids and a representative complex of K_2[Be(**102**)$_2$]*

An interesting dicarboxylic acid which was modified for solid support was **105** (Figure 1.3).[42] A single ligand and two water molecules were bound tetrahedrally to beryllium as shown in the crystal structure with an equimolar ratio of **105** to Be(II). The crystal structure of [Be(**105**)(H_2O)$_2$][H**105**] had bond lengths (Be – O; 1.599(2) Å) and a bite angle of (O–Be–O; 115.4(1)^o). The lengths of the Be – O bonds water molecules were slightly elongated at 1.616(2) and 1.643(2) Å. When two equivalents of **105** were used the *bis*-ligand chelate formed. Beryllium was also shown in a rare instance to bind to **105** after it was grafted onto a polymer. Polymer binding of metals is well established in water treatment and many other processes that require the purification and sequestering of metal ions.[43, 44]

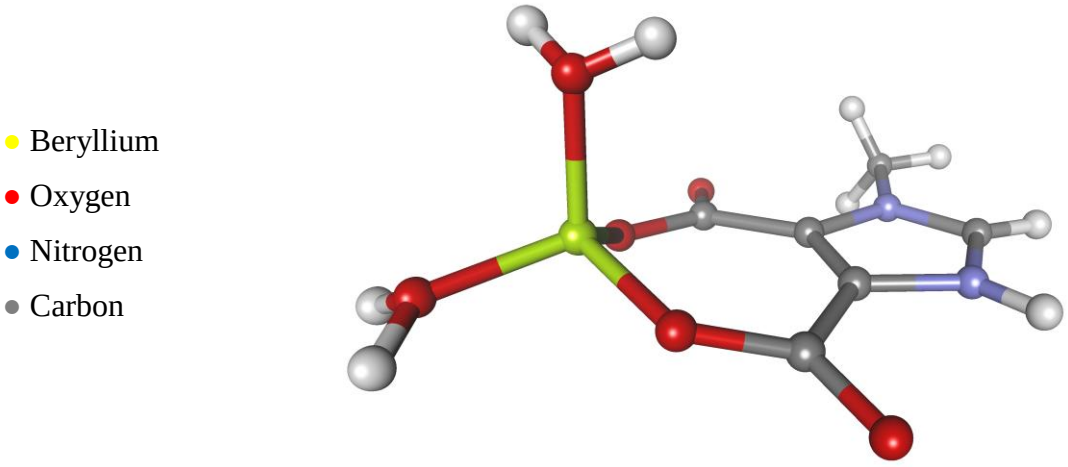

*Figure 1.3: Crystal structure of beryllium bound to dicarboxyimidazole, **105***

Hydroxy-keto-heterocycles have a pseudo-aromatic tautomer arising from π donation from the heteroatom into the aromatic ring (Figure 1.4). These ligands were developed for

chelation therapy of iron overload;[45] however, the unusually strong chelation of pyridinones observed with Fe(III) does not apply to the Be(II) ion.

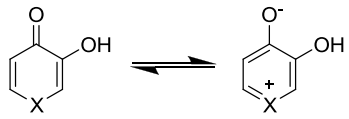

Figure 1.4: Resonance structure of hydroxy-keto-heterocycles

Cecconi and co-workers[46] crystallised the 1:2 adducts of **106** and **107** with beryllium as part of an investigation into a series of related compounds (Figure 1.5). Compared to the dicarboxylic acid ligands above, these ligands are weaker and competition with the beryllium hydroxo species present in aqueous systems was evident. The Be – O bond lengths for [Be(**106**)$_2$] were elongated to 1.646(4) Å for the ketone donor and 1.617(4) Å for the alcohol donor. The bite angle; O–Be–O, of the five-membered chelate ring was 98.8(1)^o.

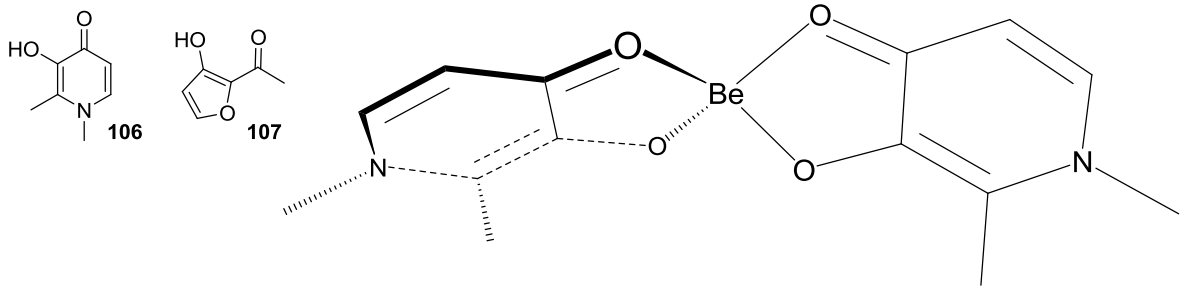

*Figure 1.5: Selection of hydroxy-keto-heterocycles and a representative complex [Be(**106**)$_2$]*

Hydroxy-carboxylic-heterocycles such as salicylic acid, **108**, and its derivatives have been investigated for chelation therapy for the treatment of beryllium poisoning (Figure 1.6).[15] Deprotonation of the phenolate moiety is achieved through delocalisation of charge onto the aromatic ring and coordination of beryllium to **108** offers an ideal six-membered chelate ring. Both the *mono*-ligand[47] (dihydrate) and *bis*-ligand[48] chelates to beryllium have been determined by X-ray crystallography. The Be – O bond lengths for [Be(**108**)(H_2O)$_2$] were 1.572(2) Å for the phenol donor and 1.612(2) Å for the carboxyl donor. The bite angle; O–Be–O, of the unstrained six-membered chelate ring was an ideal 109.7(1)^o. The Be – O bond lengths for K_2[Be(**108**)$_2$] were 1.59(1) Å for the phenol donor and 1.63(1) Å

for the carboxyl donor. The bite angle; O–Be–O, of the unstrained six-membered chelate ring was an ideal 108.7(6)°. The sulfonated analogue, **109**, is typically used for solution studies due to the increased water solubility.[15, 49]

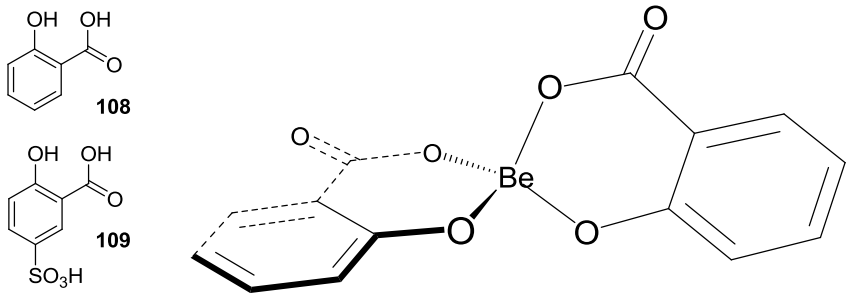

*Figure 1.6: Salicylic acid, **108**, and its sulfonated analogue, **109**, and the complex of K_2[Be(**108**)]*

Polyols such as catechol, **110**,[50] and its derivatives have also been proposed for use in chelation therapy of beryllium (Figure 1.7).[15] The Be – O bond lengths for Na_2[Be(**110**)$_2$] were 1.641(5) and 1.638(6) Å for the phenol donors. The bite angle; O–Be–O, of the five-membered chelate ring was now 99.8(3)°. Tiron, **111**,[51] conferred increased water solubility and reduced oxidation to semiquinones and benzoquinones. The strongest chelate in this series was a related ligand, chromotropic acid, **112**,[52] demonstrating a preference for Be(II) to form six-membered chelates rather than the five-membered chelates of the phenolic two oxygen donor sets of **110** and **111**. A related aliphatic diol; **113**, was shown to form a *bis*-ligand complex with beryllium by Klufers and co-workers.[53]

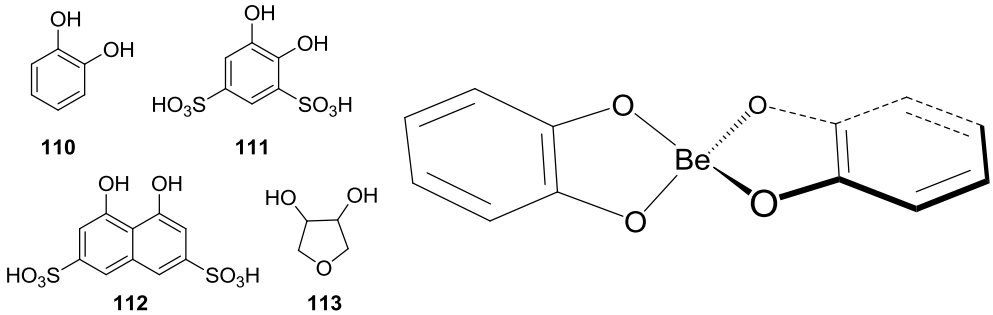

*Figure 1.7: Catechol, **110**, and related polyols, and the complex Na_2[Be(**110**)$_2$]*

1.2.2 Beryllium Complexes with Mixed Oxygen and Nitrogen Donors

When coupled with a strong oxygen donor, beryllium coordinates effectively to nitrogen donor ligands; the following were obtained from the CCSD (v5.30, Nov 2008, 1 update).

One interesting complex was that formed between nitrilotripropionic acid, **114**, and beryllium (Figure 1.8).[54] The authors complexed a series of polyamino carboxylic acids to beryllium and found that coordination could be achieved close to physiological pH which is one of the criteria in selecting suitable chelators for beryllium poisoning. Beryllium binds to **114** through the central amine and the three carboxyl groups wrap around creating the tetrahedral cavity for beryllium. The bond lengths for Na[Be(**114**)] were (Be – O; 1.596(1) Å) for the carboxyl donors and (Be – N; 1.780(3) Å) for the amine donor. The bond angles were (O–Be–O; 110.0(1)^{o}) and for the unstrained six-membered chelate rings (O–Be–N; 108.9(1)^{o}).

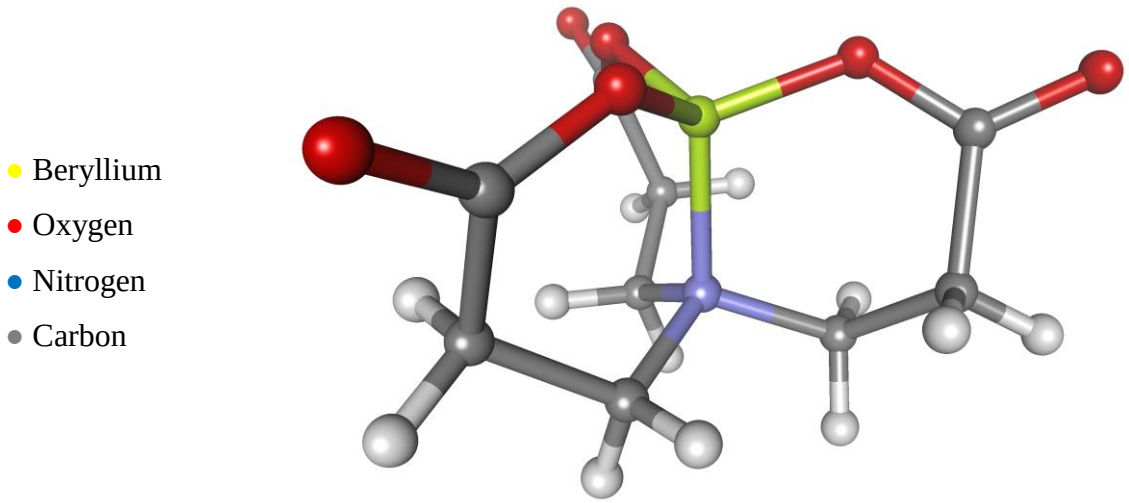

Figure 1.8: Crystal structure of beryllium bound to nitrilotripropionic acid, ***114***

Salicylaldimines were shown to form *bis*-ligand chelates to beryllium which had slightly distorted tetrahedral geometries; the following two ligands have reported crystal structures (Figure 1.9).[55] The *bis*-ligand chelates were formed by refluxing two equivalents of salicylaldehyde and the appropriate amine with beryllium sulfate in a basic water / ethanol mixture. A precipitate developed which was collected, recrystallised and structurally

characterised. The bond lengths for [Be(**116**)$_2$] were (Be – O; 1.53(2), 1.54(2), 1.59(2), 1.63(2) Å) for the phenol donors and (Be – N; 1.73(2), 1.73(2), 1.75(2), 1.77(2) Å) for the imine donors (two independent molecules were present in the asymmetric unit). The bite angles were (N–Be–O; 104.5(12), 105.2(12), 105.8(12), 106.6(12)^o) for the unstrained six-membered chelate rings.

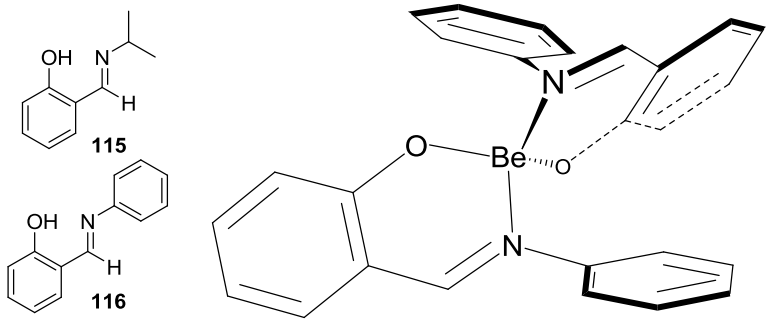

Figure 1.9: Salicylaldimines which formed bis-ligand chelates with beryllium

Hydroxyphenyl pyridine, **117**, is a molecule with a similar donor set configuration to salicylaldimines (Figure 1.10). Tetrahedral *bis*-ligand chelates were formed by reacting two equivalents with of hydroxyphenyl pyridine to beryllium sulfate in basic methanol to give a precipitate which was recrystallised and analysed by X-ray crystallography.[56] The bond lengths for [Be(**117**)$_2$] were (Be – O; 1.564(2) Å) for the phenol donors and (Be – N; 1.747(2) Å) for the pyridine donors with bite angle (N–Be–O; 105.2(1)^o). The luminescent properties of the beryllium complex were investigated and the complex could be used as a blue emitting material or as a host material to fabricate organic electroluminescent devices.[56]

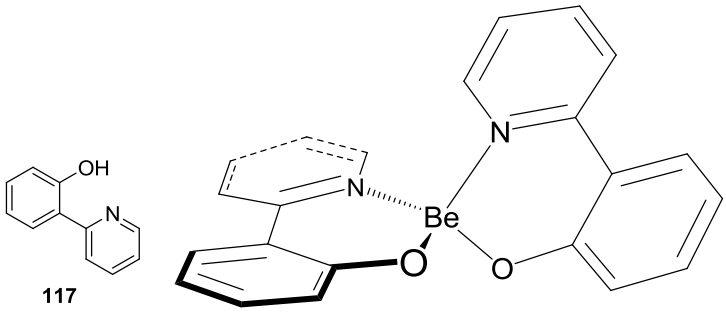

*Figure 1.10: 2-(Pyridin-2-yl)phenol, **117**, and the bis-ligand beryllium chelate*

Tong and co-workers[57] examined the photoluminescence of the hydroxyphenyl indole ligand **118** coordinated as a *bis*-ligand chelate to beryllium formed analogously to **117** above also for the purpose of constructing light-emitting devices (Figure 1.11). The luminescence could be tuned slightly by varying X = NH, O or S. They obtained crystal structures for all three ligands which coordinate to beryllium in the standard *bis*-ligand tetrahedral arrangement. The three different crystal structures all showed slight variation in bond lengths and angles; Be – O lengths ranged from 1.560(3) – 1.598(3) Å, Be – N lengths ranged from 1.698(3) – 1.754(3) Å. The O – Be – N bite angles ranged from 103.6(1) – 105.6(1)^{o}.

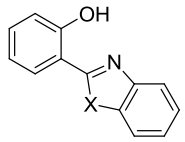

*Figure 1.11: Hydroxyphenyl indole ligand, **118**, X: NH, O, or S these do not participate in coordination*

The beryllium *bis*-ligand chelate of **119** has also received much attention for use as an electroluminescent device (Figure 1.12).[58-60]

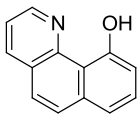

*Figure 1.12: Benzo[h]quinolin-10-ol, **119***

The colourmetric properties of Be(II) complexation with a sulfonated analogue of **119** is currently used in commercial test kits for the detection of beryllium contamination on surfaces (Figure 1.13).[61]

Figure 1.13: A colourmetric beryllium test kit utilising a sulfonated analogue of ***119***

Oxine, **120**, and its substituted derivatives also form *bis*-ligand chelates with beryllium in tetrahedral geometry (Figure 1.14).[62] The tetrahedral geometry of the *bis*-ligand chelates with beryllium was distorted due to the five-membered chelate rings formed.

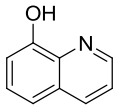

Figure 1.14: 8-Hydroxyquinoline, ***120***

1.2.3 Beryllium Complexes with Nitrogen Donors

Ligands containing nitrogen donors coordinated to beryllium with crystal structures are uncommon. In fact, a search of the CCSD (v5.30, Nov 2008, 1 update) for beryllium complexes consisting of only nitrogen donors yields only rare instances.[63-65] These

examples cannot be considered similarly to the ligands discussed above as they require the generation of an anionic ligand in anhydrous conditions and use of reactive beryllium salt to achieve complexation. The examples discussed previously all complex to hydrated beryllium sulfate in either water or alcoholic solvents.

2-(Pyridin-2-yl)-1*H*-indole, **121**, is one such example of a nitrogen-only donor where a tetrahedral five-membered *bis*-ligand chelate was formed with beryllium (Figure 1.15).[66] The complex was formed under anhydrous conditions by treating **121** with *n*-butyllithium in THF at low temperature then reacting the anionic ligand with beryllium chloride. It is unlikely such a complex would form under aqueous conditions. The bond lengths for [Be(**121**)$_2$] were (Be – N; 1.753(6) Å) for the pyridine donors and (Be – N; 1.668(5) Å) for the indole donors with a bite angle for the five-membered chelate ring of (N–Be–N; 93.3(2)^o). The complex; [Be(**121**)$_2$], was synthesised for the purpose of constructing electroluminescent devices.

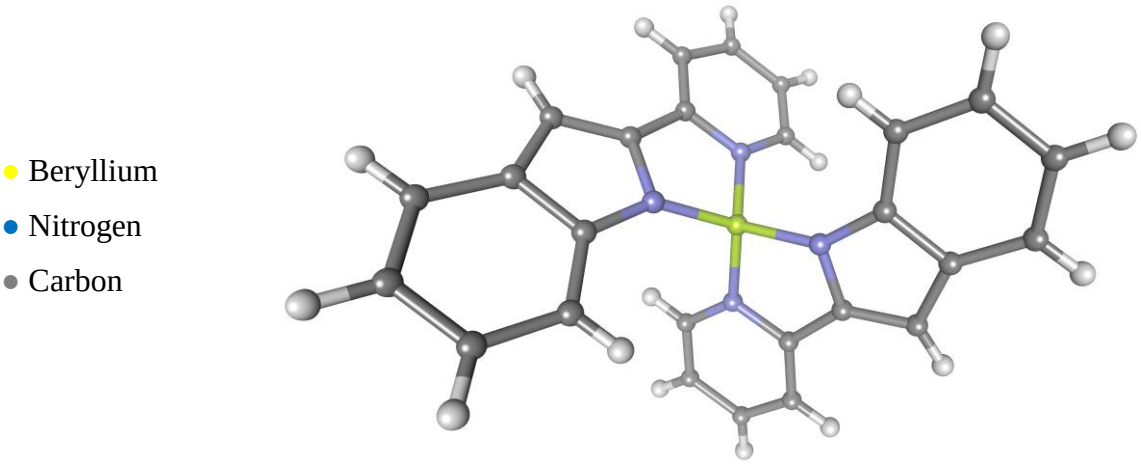

Figure 1.15: Crystal structure of beryllium bound to 2-(pyridin-2-yl)-1H-indole, ***121***

1.2.4 Summary of Existing Beryllium Complexes

Almost all beryllium complexes are four-coordinate and have tetrahedral geometry, often with some minor distortion owing to the particular orientation of the donor atoms on the particular ligand. In fact, there are only a few rare instances where beryllium forms two

and three-coordinate complexes.[63, 67] The tetrahedral geometry can accommodate a wide variety of ligands forming five, six and seven membered chelate rings once coordinated to beryllium. The six-membered chelate ring is considered to be the most favourable as steric and torsional strain within the ligand is minimised.[15]

Beryllium binds most readily to ligands which contain ionisable protons. The best examples of such ligands are those which contain carboxylic acid or phenolic moieties. A ligand containing nitrogen donors usually requires the additional presence of ionisable oxygens in the donor set to provide initial association followed by complexation via chelation. Ligands containing only nitrogen donors are considered weak, and typically only coordinate under special circumstances and certainly not in aqueous environments. The hard Be(II) cation requires coordination with hard oxygen donors in aqueous environments in order to displace the water solvent shell surrounding the beryllium cation.

1.3 The Search for a Beryllium Selective Ligand

1.3.1 Introduction

In the preceding section, beryllium was shown to form many complexes with a variety of different ligands. However, all of the molecules discussed in Section 1.2 coordinate not only to beryllium, but, to a host of other metal cations. If there were a ligand that could bind preferentially to beryllium over other metal cations then it may be used to separate beryllium from a source containing a mixture of metal ions. Beryllium is an expensive metal whereby recovery of this element from waste sources instead of disposal may prove valuable. Additionally, due to the toxicity of beryllium, separating this element from waste sources could simplify expensive disposal measures.

If a ligand was found such that the cavity was small enough to predominantly bind Be(II) and exclude other larger metal cations, it could be used to separate beryllium from waste sources. The work of Plieger, John and coworkers[42] designed a ligand which could bind the Be(II) cation (Figure 1.16). The crystal structure revealed a cationic beryllium complex and an anionic form of the ligand to balance the charge.

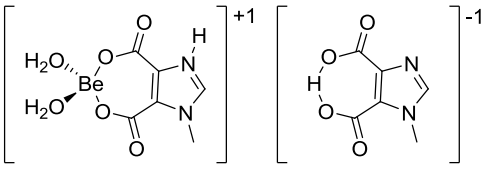

Figure 1.16: 1-Methyl-1H-imidazole-4,5-dicarboxylic acid with Be(II) bound (left) and the associated anionic ligand (right)

Comparing the cationic and anionic components of the structure highlights the tendency for Be(II) to coordinate in place of deshielded protons arising from strong hydrogen bonding interactions. This is an emerging theme in recent papers striving to achieve beryllium selective ligands.[28] A test kit for the detection of beryllium on surfaces was developed based on the fluorescence of Be(II) bound to the sulfonated analogue (for water solubility)

of **119** (Figure 1.17).[61] The Be(II) cation displaces a tightly bound hydrogen bonded proton located between the phenolic oxygen and the heterocyclic nitrogen.

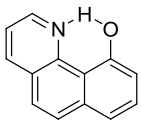

*Figure 1.17: Benzo[h]quinolin-10-ol, **119** showing the internal hydrogen bonding interaction*

As the Be(II) cation appears to behave like a proton, a potentially ideal class of molecules which are as yet untested for coordination to Be(II) are "proton sponges". Proton sponges are generally derived from 1,8-diaminonaphthalene and have very high basicities. The unique separation of the two nitrogen atoms causes a destabilising overlap of lone electron pairs. To overcome this destabilisation they form especially strong hydrogen bonds effectively "trapping" a highly deshielded proton in the process (Figure 1.18).

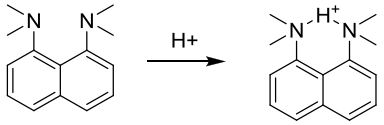

Figure 1.18: Mode of proton binding in 1,8-bis(dimethylamino)naphthalene

While there is no precedence for Be(II) coordinating to neutral nitrogen donors in aqueous environments the highly deshielded proton might be displaced by Be(II) in this instance. Further, these neutral nitrogen donor ligands show poor coordination to larger metal cations largely due to the cavity size meaning potential coordination of Be(II) would not be complicated by competition from other metals in sensing and sequestering applications. This can be exemplified by Table 1.1:

Ligand	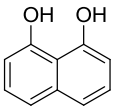 **122**	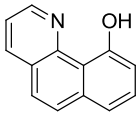 **119**	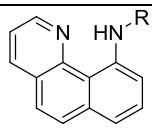 **123**	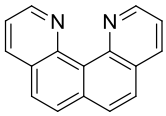 **124**
Number of References[a]	314	208	5	1
Metals bound	**Be**,[52] most other metal cations	**Be**,[58] Mg, Al, Fe, Co, Ni, Cu, Zn, Ga, Zr, Pd, In, Ir, Au, Eu, Tb	**Be**,[68] Al,[68] Zn,[68] Pd,[69-71]	Mn,[72] Pd,[72] Re,[72] Pt[72]

Table 1.1: Relative selectivity of proton sponge ligands for metal cations, [a] Number of references (including patents) upon searching Scifinder Scholar for metal complexes of each ligand, R= $SO_2C_6H_4NO_2$

The four ligands shown all have a similar bite angle and rigid naphthalene backbone and form six-membered chelate rings upon metal coordination. The decreasing number of metal complexes reported is directly tied to the binding strength of each ligand. The first two ligands, **119** and **122**, contain ionisable oxygen donors which have a high affinity for most metal cations. The ligand containing one ionisable nitrogen and one neutral nitrogen, **123**, has been scarcely studied with several palladium complexes reported[69-71] and an unverified account of beryllium, aluminium and zinc complexes in a patent.[68] Lastly, the proton sponge ligand with two neutral nitrogen donor atoms, **124**, only binds to particular metal cations in special cases. Most importantly, this type of ligand has not been tested for its ability to complex beryllium, while the others already have reported beryllium complexes.

Naphthalene-1,8-diol, **122**, is a commercially available ligand which has been extensively used in the formation of transition metal complexes (Figure 1.19). It was shown to coordinate with beryllium tetrahedrally via a *bis*-ligand chelate.[52]

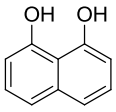

*Figure 1.19: Naphthalene-1,8-diol, **122***

Although **119** has a similar rigidity and bite angle to proton sponges, the binding strength of the phenol moiety enables the ligand to also bind to most other metal and non-metal cations (Figure 1.20). The test kit utilising a sulfonated analogue of **119** for the detection of beryllium on surfaces required an excess of EDTA to remove the interfering metal cations.[61] Given that proton sponges are neutral nitrogen donors, their weak binding to larger metal cations may support the preferential binding of small cations such as beryllium.

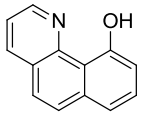

Figure 1.20: Benzo[h]quinolin-10-ol, ***119***

The mid-point between **119** and the neutral nitrogen donor **124** is the ligand **123** (Figure 1.21)[73] This has the same bite angle and rigidity as **119**, only, the phenol has been replaced by a sp^3 hybridised nitrogen. The ability for this ligand to bind beryllium has been proposed in a patent dealing with electroluminescent materials but has yet to be proven.[68] This ligand has also been shown to bind zinc,[68] aluminium[68] and palladium. [69-71]

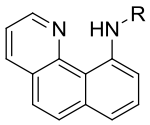

Figure 1.21: Benzo[h]quinolin-10-amine, ***123****, R= -$SO_2C_6H_4NO_2$, -C_6H_5, -Ac*

This leaves the class of compounds known as proton sponges which will be discussed in the following sections.

1.3.2 Aryl Amine Proton Sponges

The first example of a aryl amine proton sponge was shown by Alder where methylation of 1,8-diaminonaphthalene yielded **125** (Figure 1.22).[74]

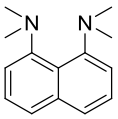

*Figure 1.22: Alkylated proton sponge; 1,8-bis(dimethylamino)naphthalene, **125***

The pK_{BH+} was measured as 12.1 (in H_2O and 35% DMSO/H_2O) and it was extracted into aqueous solutions at pH 8 and below. The pK_{BH+} is the affinity for the protonated conjugate acid of the neutral proton sponge to release a proton according to the following equation:

$pK_{BH+} = -\log K_{BH+}$ and $K_{BH+} = [B][H_3O^+]/[BH^+]$ for $BH^+ + H_2O \rightarrow B + H_3O^+$

In TFA the ^1H NMR of **125** revealed the bound proton bridging the two nitrogen atoms. The four methyl groups were split into a doublet due to the coupling of this bound proton. The molecule was clearly strained and the stresses are relieved upon protonation. Subsequently, a host of derivatives involving varying alkylation on the nitrogens[75, 76] and substitution at the 2,6-positions on the naphthalene backbone adjacent to the amines were reported.[77-82]

By analogy to the above work, Staab and co-workers synthesised methyl-substituted fluorene, **126**, and derivatives based on **127** (Y = O, S, NH, Figure 1.23).[83, 84] The slightly shorter N-N distance angled the lone electron pairs further toward each other. This gave a higher pK_{BH+} of 13.5 when compared to **125**.

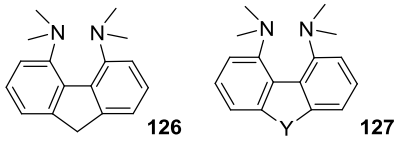

*Figure 1.23: Fluorenediamine, **126**, and related derivatives based on **127** (Y = O, S, NH)*

1.3.3 Heterocyclic Imine Proton Sponges

The first and only fully heterocyclic proton sponge, **124**, was reported by Zirnstein and Staab in 1987 (Figure 1.24).[85] The pK_{BH+} was estimated to be 12.8 by analogy to **125**. The cavity created between the two fused pyridine rings is not sterically hindered compared to the aryl amine-based proton sponges making it an attractive target for potential coordination of small metal cations.

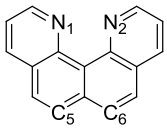

*Figure 1.24: Quino[7,8-h]quinoline, **124***

The crystal structure was later reported and revealed **124** had a flattened aromatic ring structure with a $N_1 – N_2$ distance of 2.727(2) Å and a $C_5 – C_6$ distance of 2.450(2) Å.[86] The repulsion of electron density on the two nitrogens accounts for the slight elongation of the $N_1 – N_2$ distance and the compressed $C_5 – C_6$ distance.

1.3.4 Aryl Imine Proton Sponges

Raab and co-workers presented a series of new proton sponges having guanidino, **128, 129**,[87, 88] and phosphazene, **130**,[89] type motifs (Figure 1.25). The pK_{BH+} of **128** – **130** was 25.1, 25.8 and 29.9 respectively, and were classified as "super basic" proton sponges.

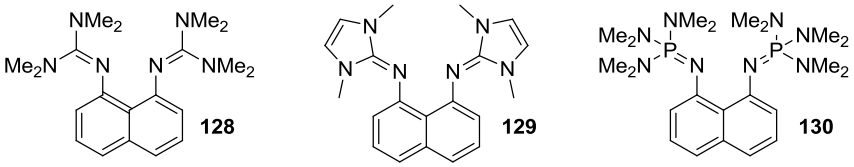

Figure 1.25: Aryl imine type proton sponges

1.3.5 Proton Sponge Metal Coordination Complexes

The use of proton sponges as metal chelators has received relatively little study. This is in stark contrast to other neutral nitrogen donor ligands such as 1,10-phenanthroline or 2,2'-bipyridine which have thousands of reported complexes. It was only in recent years that a select few papers have been published on the coordination chemistry of proton sponges.

In 2001 Wustefeld and co-workers[72] reported that they had made complexes of 4,9-dichloroquino[7,8-*h*]quinoline, **131**, with Pt(II), Pd(II), Re(I), and Mn(I) (Figure 1.26). They obtained crystal structures for the Pt(II) and Re(I) derivatives (Figures 1.27 and 1.28).

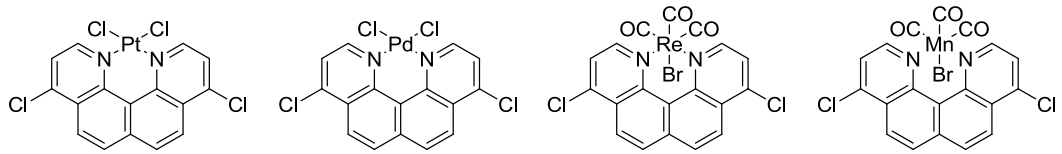

*Figure 1.26: Metal complexes with 4,9-dichloroquino[7,8-h]quinoline, **131***

The small nitrogen – nitrogen distance along with the high basicity of **131** limited the use to an aprotic solvent in the synthesis of these complexes. The platinum complex was formed by treating Zeise's dimer $[Pt_2(H_2C{=}CH_2)_2Cl_4]$ in CH_2Cl_2 with **131**. The crystal structure (Figure 1.27) of the complex revealed that the Pt ion sat out of the plane of the aromatic ring system and the aromatic system was strongly bowed. The extent of bowing was measured by averaging the displacement of the atoms in the aromatic system to give a "mean plane". The bend of the bow was 0.742 Å, compared to 0.151 Å in the unbound ligand. The platinum ion sat 1.432 Å above the mean plane (inset, Figure 1.27). The $N_1 – N_2$ distance was elongated to 2.812(2) Å relative to the crystal structure of the unbound ligand[86] while the $C_5 – C_6$ distance (Figure 1.24) on the rear of the ligand was compressed to 2.410(2) Å. While this complex would appear to be unstable, the exceptionally strong Pt –N bonds meant heating of the complex at 380 ^oC in concentrated H_2SO_4 for several days did not cause decomposition.

- Platinum
- Chlorine
- Nitrogen
- Carbon

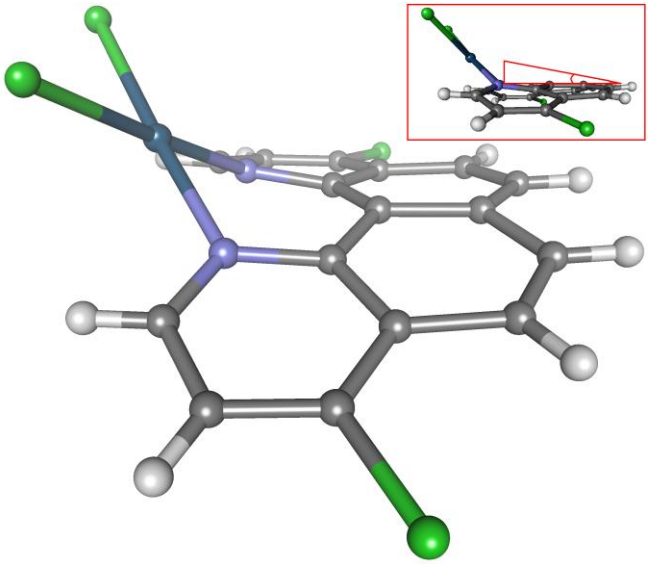

*Figure 1.27: Perspective view of the crystal structure of [Pt(**131**)Cl_2]*

For the rhenium complex the metal ion sat 1.419 Å above the mean plane (Figure 1.28). The $N_1 – N_2$ distance was elongated to 2.804(2) Å while the $C_5 – C_6$ distance on the rear of the ligand was compressed to 2.390(2) Å.

- Rhenium
- Chlorine
- Bromine
- Oxygen
- Nitrogen
- Carbon

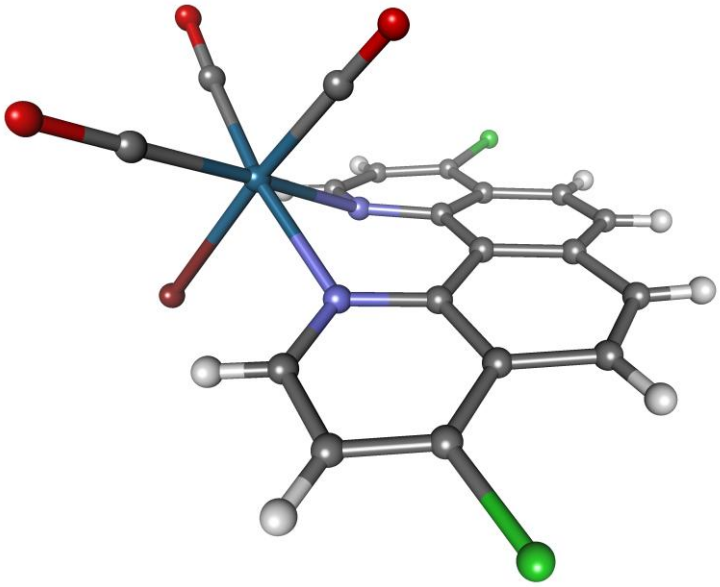

*Figure 1.28: Perspective view of the crystal structure of [Re(**131**)(CO)$_3$Br]*

In 2004 Yamasaki and co-workers[90] reported complexes of ligand **125** with palladium. They achieved this by first reacting [Pd(hfac)$_2$][2] (hfac is hexafluoroacetylacetonate) and **125** in hexane to form a charge transfer complex [Pd(hfac)$_2$](**125**) in 80 % yield as dark violet crystals. After standing for one week these crystals disappeared and red crystals of [Pd(hfac)(**125**)](hfac) in 63 % yield which could be reacted with β-diketones in ether to give yellow crystals of [Pd(β-diketone-*O,O'*)(**125**)](hfac), in 50 – 80 % yields (Figure 1.29). It was proposed that the intermediate charge transfer complex was necessary for the complexation to occur.

- Palladium
- Oxygen
- Nitrogen
- Carbon

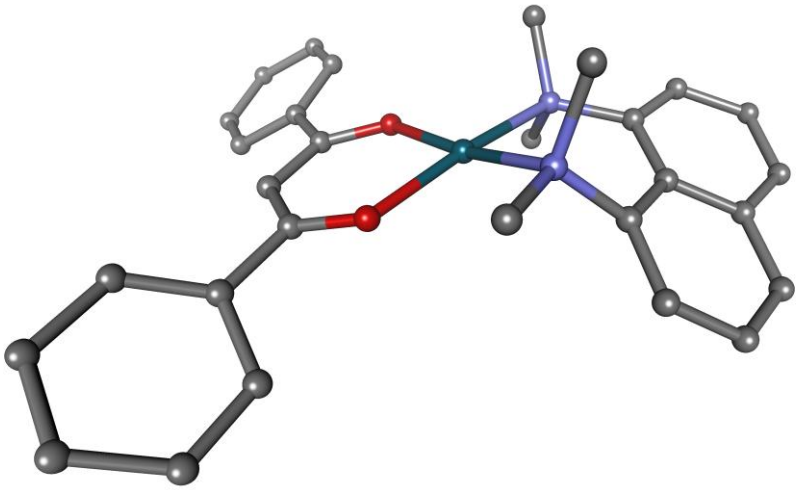

*Figure 1.29: Crystal structure of [Pd(β-diketone-O,O')(**125**)](hfac)*

When the mean plane was calculated in the context of this thesis from the ten carbons of the naphthalene ring, the palladium ion sat 0.825 Å above this plane. While this distortion was smaller than that of **131**, the mode of binding differs. The two amine groups orient in opposite directions from the mean plane, +0.629 Å and -0.564 Å, leaving the palladium ion more centralised. The large steric interference around the nitrogen donor atoms greatly decreases the coordination ability of **125**. Despite being a strong base, **125** is a very weak nucleophile. There was no indication of the complex's stability.

There are no known complexes for the proton sponges **126** and **127** (Figure 1.23).

In 2008, Wild and co-workers,[91] provided the first example of **128** bound to both Pd and Pt. The Pt cation sat 1.337 Å above the mean plane of the aromatic system and the ligand was slightly bowed (Figure 1.30). The Pd complex was nearly identical to the Pt complex and sat 1.331 Å above the mean plane.

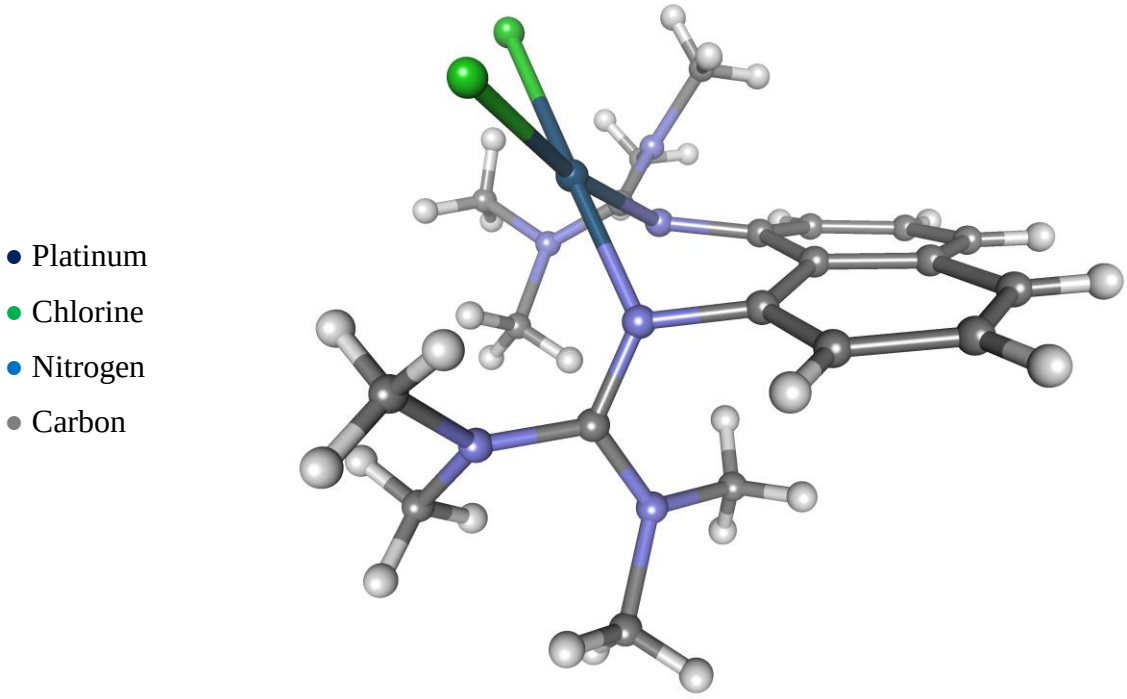

*Figure 1.30: Perspective view of the crystal structure of [Pt(**128**)Cl_2]*

With only three papers ever published on the coordination chemistry of proton sponges, the scope of metal complexes formed by these ligands remains largely unexplored. In all three proton sponge complexes, the metal ions sat a large distance out of the plane of the molecule and the proton sponge ligands showed unusual distortions. The spacing between the nitrogen atoms clearly restricts most metals from forming chelates. In the above cases, the metals used were known to bind strongly with nitrogen donor ligands (e.g. Pt, Pd). There was also careful choice of the starting metal compound, usually in the form of a dimer, where breakdown of the dimer during the reaction would lead to a naked site on the metal ion greatly enhancing complexation to the sterically hindered proton sponges.

It is possible that due to the smaller ionic radius of Be(II), coordination of beryllium to proton sponges may not proceed with such difficulty as with other larger metal cations. Under the aprotic conditions employed for the above metal complexations, along with suitable choice of a reactive beryllium metal salt, there is unlikely to be any difficulty in coordinating Be(II). The difficulty is expected to arise from investigation of the aqueous coordination chemistry of Be(II) and proton sponges as there will be competition between coordination and protonation of the ligands.

1.4 Encapsulation of Beryllium

1.4.1 Existing Ligands which Encapsulate Beryllium

A tetrahedral geometry is essentially the only possible geometry for a beryllium coordination complex. While the proton sponges discussed in the previous section would offer a tight binding cavity suited for small cations they would need to form *bis*-ligand chelates in order to fully encapsulate beryllium. A single compound which offered four donor atoms in a tetrahedral environment would be better suited to selectively coordinating beryllium. One example of such a complex fully encapsulating beryllium was **114** (Figure 1.31).[54] Complexes of **114** form with most other metals, a Scifinder search revealed 41 other metal complexes with **114**. The flexibility of **114** enabled the same four-coordinate mode of binding for beryllium with Cu, Zn and Co.[92, 93] The selectivity of **114** toward beryllium has yet to be tested.

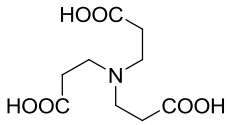

*Figure 1.31: Nitrilotripropionic acid, **114***

A recent example of full encapsulation of beryllium was with **132** (Figure 1.32). The beryllium cation coordinated via tetra-dentate tetrahedral coordination with both phenol and imine donors.[94] A Scifinder search gave 241 metal complexes of **132** (and substituted structural analogues) to other metals; some were M_2L_2 phenolate bridged complexes,[95] while others adopted a MLX binding mode were X is was an appropriate mono- or bi-dentate ligand which completed the coordination sphere around the particular metal ion.[96] Metal competition studies were not performed with this ligand.

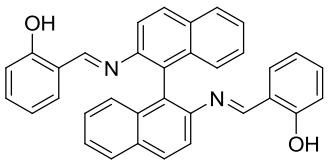

Figure 1.32: 2,2'-(1E,1'E)-(1,1'-Binaphthyl-2,2'-diylbis(azan-1-yl-1-ylidene))bis(methan-1-yl-1-ylidene)diphenol, ***132***

An example of partial encapsulation of beryllium was shown with **133** (Figure 1.33).[28] The two basic phenolates bind strongly to the Be(II) centre while the pyridine ring acted to transfer protons off the phenols. A water molecule completed the coordination sphere. A Scifinder search of **133** (and structural analogues) gave 102 other reported metal complexes, when **133** bound to Cu and Zn, multiple metals were involved with bridging phenolates to give 1D polyers.[97]

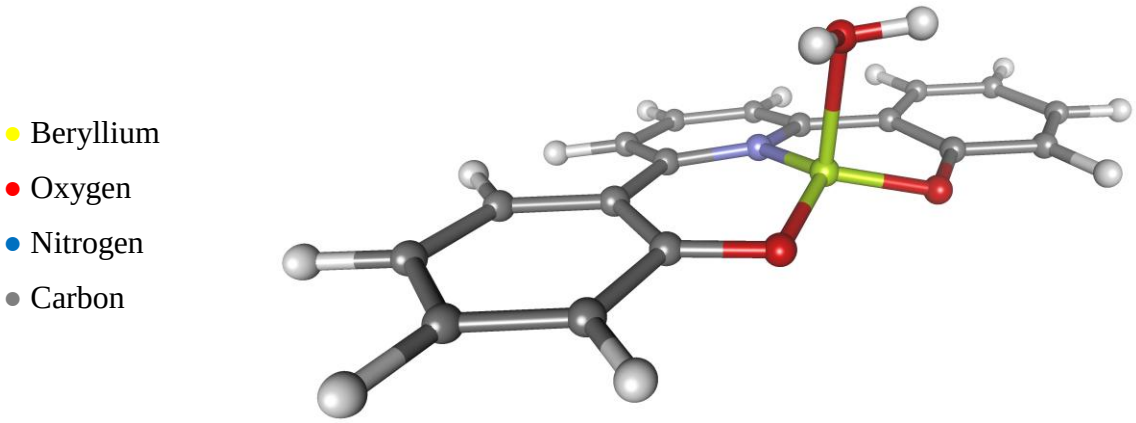

Figure 1.33: Beryllium complex of 2,6-bis(2-hydroxyphenyl)pyridine, ***133***

1.4.2 Design of New Ligands which Fully Encapsulate Beryllium

Coordination to beryllium may be further enhanced by combining the features of **114** and **133** and constructing tetra-coordinate ligands capable of fully encapsulating beryllium. If the aromaticity of **133** was broken, an additional donor arm could be incorporated to give **134** (Figure 1.34).

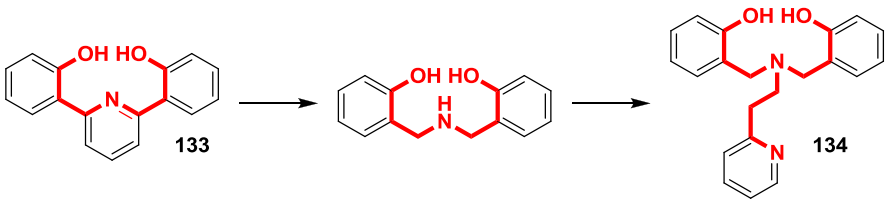

*Figure 1.34: Creation of a tetra-coordinate ligand, **134***

The tight proton sponge cavity may also be extended into the third dimension to give a compound capable of full encapsulation. Anything other than this geometry would be too large to offer selective binding to small cations (e.g. the geometry of phenanthroline). It is more desirable to use nitrogen donors rather than oxygen donating moieties in an attempt to lower selectivity for other metal cations. To extend the cavity of **124** into three dimensions it is not possible retain the aromaticity, so, the central carbon must become sp^3 hybridised. In a tetrahedral arrangement, this would lead to **135**, offering three of the four points of the required tetra-coordinate ligand (Figure 1.35).

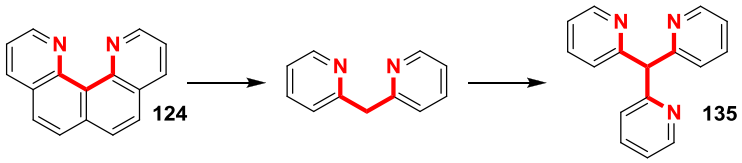

Figure 1.35: Conversion of a proton sponge into the third dimension

135 is already extensively reported in the literature and has been shown to complex with most metals. As the aim of this section is to create a compound capable of fully encapsulating beryllium, a fourth donor atom is required. A compound which offered a tetrahedral binding cavity would need a donor atom at the following position shown in Figure 1.36:

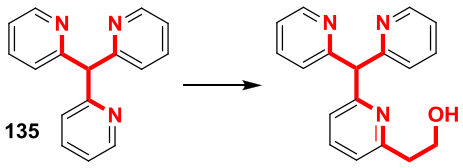

Figure 1.36: Location of an oxygen atom required to make tetrahedral binding cavity

There is no literature precedence of a compound with this exact arrangement of donor atoms, so an extensive synthetic effort would be required to design such ligands. Two examples of possible compounds are shown in Figure 1.37:

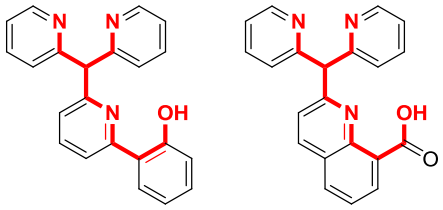

Figure 1.37: Possible compounds containing tetrahedral binding cavities for beryllium

The design and synthesis of new classes of tetra-coordinate ligands will be explored in this thesis for use as potential Be(II) chelators.

1.5 Boron as a Small Cation Analogue for Beryllium

Due to the safety considerations involved in handling beryllium there are only a handful of laboratories around the world set up to conduct this research. As none of the beryllium research will be conducted at Massey University, a small cation analogue was required to investigate the complexation of the ligands synthesised to small cations without heavy restrictions.

	CN	Radius Å	Geometry
B(III)	4	0.25	Tetrahedral
Be(II)	4	0.27	Tetrahedral

Table 1.2: Similarities between B(III) and Be(II)

Boron(III) was chosen as the most suitable analogue as the size-to-charge ratio is similar. While boron is a non-metal and doesn't display the same aqueous solution chemistry as Be(II), formation of boron complexes under aprotic conditions would allow for full characterisation. Determination of solid state structures by X-ray crystallography will allow comparison of the size-fit of the ligand's cavities for small cations over large metal cations.

The Lewis acidity of boron compounds (for example boron trifluoride) should provide favourable coordination to the proton sponges analysed, given that the lone electron pairs on the nitrogen atoms readily accept a proton to stabilise the overlapping electron pairs. Subsequent loss of one fluoride would lead to $[BF_2(\text{proton sponge})]^+$.[98]

While the use of boron is feasible for simple bidentate neutral nitrogen ligands such as the proton sponges, there is no precedent for the encapsulation of boron with a tetradentate ligand containing mixed oxygen / nitrogen donors. The thermodynamic stability of boron trihalides would prevent such an interaction. This is where the similarity between boron and beryllium ends as boron; being a non-metal, cannot be strictly used at a small metal cation analogue in all circumstances.

1.6 Proposed Aims

The objectives of this thesis can be divided into several major themes:

- Selection of a suitable candidate from the class of compounds known as proton sponges to test for coordination to Be(II) using the hypothesis that Be(II) can displace strongly deshielded protons.

- Exploration of the properties of the proton sponges through functionalisation to alter the physical and electronic properties of the molecules with the intention of enhancing the coordination strength and detection ability primary via enhanced fluorescence.

- Use the idea of a tight cavity for selective beryllium coordination and extend it to synthesising new molecules capable of forming tetra-coordinate fully encapsulated beryllium complexes.

- Complexation when possible of boron to these ligands to investigate predominantly structural aspects which are otherwise not possible using aqueous beryllium solution chemistry.

- Analyse the beryllium coordination chemistry of these ligands in aqueous environments and characterise using safe solution-based techniques such as ^{9}Be NMR and UV-Vis and fluorescence spectroscopy supported with computational chemistry to identify the beryllium species.

- Complexation of representative larger metal cations to gauge the ligand's ability to exclude large metal cations.

Chapter 2: Synthesis of Proton Sponges

2.1 Assessment of Proton Sponges

2.1.1 Introduction

There are a number of different types of proton sponges which are synthetically challenging to various degrees. It was therefore necessary to identify which type would make an ideal candidate to begin the investigation of proton sponge coordination to beryllium. It is only after successful initial studies that other proton sponge types should be synthesised and tested. Computational chemistry and literature precedent was utilised to select which type of proton sponge should be initially pursued.

2.1.2 Results / Discussion

To select the best candidate for beryllium coordination, the proton sponges were classified into three representative types; guanidine (e.g. **201**, introduced in Chapter 1 as **129**), quinoline derivative (e.g. **L2**, introduced in Chapter 1 as **124**) and aryl amine (e.g. **L3**, introduced in Chapter 1 as **125**). Using **201**, **L2** and **L3** as models for each type, they were optimised (B3LYP, 6-31(d)) as their beryllium *bis*-ligand chelate to exclude the influence of counter-ligands.

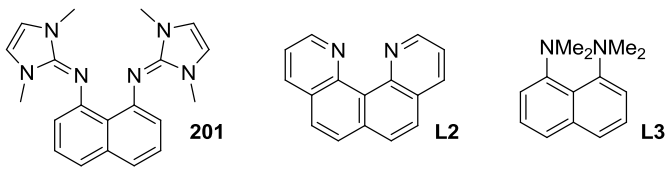

Figure 2.1: Proton sponges analysed by computational methods

As these calculations were initial guesses of theoretical compounds, diffuse functions were not included and only a single d function for heavy atoms was used. Diffuse functions allow orbitals to occupy a larger region of space and become important for systems where electrons are relatively far from the nucleus. Including diffuse functions and extra functions for heavy atoms and hydrogen atoms generally increases the precision of the computational results; however, with no experimental data to compare to it was unnecessary to perform the calculations at a higher level.

A summary of the important features of each optimised structure is given in Table 2.1. The Be – N distance can be related to known crystallographically observed structures to assess the likelihood of such a bond. The Be – mean plane distance is the perpendicular distance beryllium lies outside of the plane of the ligand cavity. The N-C-C-N torsion angle measures the twist present in the cavity of the ligand upon coordination.

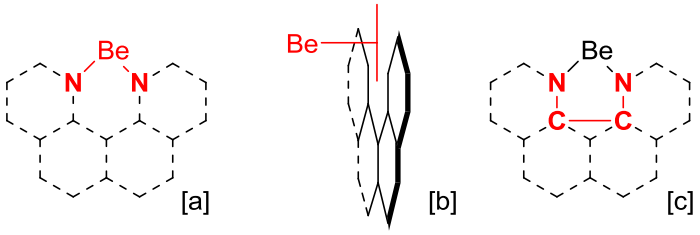

Figure 2.2: Highlighted structural parameters for the optimised models; [a] Be – N bond lengths, [b] Be – mean plane distance, [c] torsion angle

***Bis*-Chelate Complex**	**Be – N (Å)**	**Be – Mean Plane (Å)**	**φ(N-C-C-N) (°)**
$[Be(\mathbf{201})_2]^{2+}$	1.811	0	24.99
$[Be(\mathbf{L2})_2]^{2+}$	1.706	0	0
$[Be(\mathbf{L3})_2]^{2+}$	1.881, 1.843	0.836	26.39

Table 2.1: Important parameters from the optimised proton sponge beryllium complexes

A summary of the bond lengths for neutral N-donor complexes is shown in Table 2.2 (CCSD, v5.30, Nov 2008, 1 update). These were separated into neutral sp^2 and sp^3 N-donors, all anionic Be – N bonds (e.g. those where a covalent N – H bond is displaced for coordination) were excluded. An estimated mean and standard deviation was calculated based on these data sets.

Neutral N-Donor	Mean ± 3σ (Å)
sp^2	1.745 ± 0.132[a]
sp^3	1.781 ± 0.137[b]

Table 2.2: Estimated mean and standard deviation for bond lengths of neutral N-donors to beryllium, [a] N = 88, [b] = 34, no outliers were present at Q(95%)

The proton sponge **L3**[74] is non-nucleophilic and sterically crowded (Figure 2.3). This molecule shows very poor affinity toward binding metals, with only one rare example reported previously.[90]

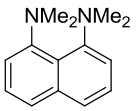

*Figure 2.3: 1,8-bis(Dimethylamino)naphthalene, **L3***

The optimised structure of $[Be(\mathbf{L3})_2]^{2+}$ indicated that in order for the beryllium ion to adopt the necessary tetrahedral geometry the ligand had to distort significantly from planarity with the beryllium ion located 0.836 Å from the mean plane of each ligand and the nitrogen atoms of each ligand twisted 26.39^o away from each other (Figure 2.4). The eight methyl groups surrounding the beryllium ion would cause severe steric hindrance to the initial formation of this complex. The Be – N bond lengths fell within 3σ of those documented crystallographically for a neutral sp^3 N-donors.

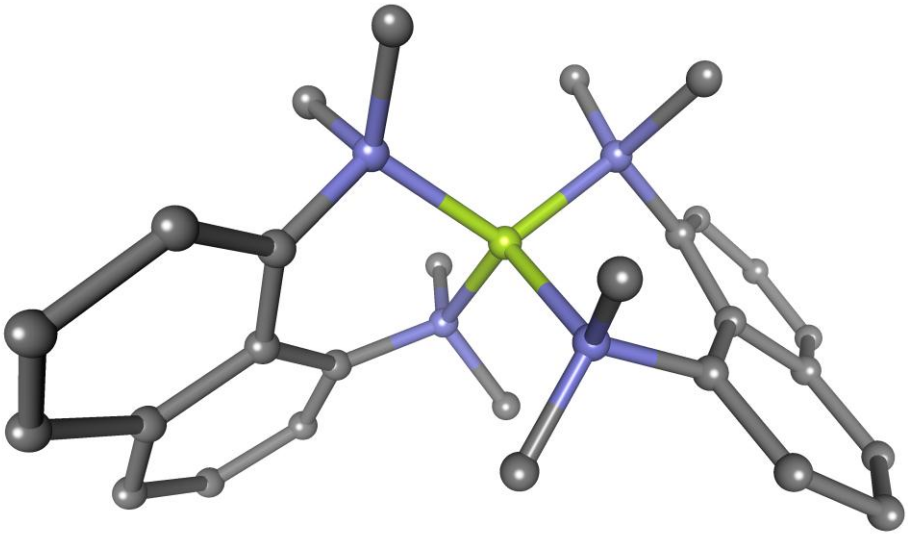

*Figure 2.4: Computer model of the beryllium bis-ligand chelate of **L3**, hydrogens are removed for clarity*

Metal complexation to a guanidine-type proton sponge related to **201** discussed in Chapter 1 was achieved under anhydrous conditions with careful choice of reactive metal reagents.[91]

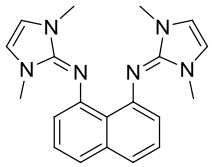

*Figure 2.5: N1,N8-bis(1,3-Dimethyl-1H-imidazol-2(3H)-ylidene)naphthalene-1,8-diamine, **201***

The optimised structure of $[Be(\mathbf{201})_2]^{2+}$ showed the beryllium ion sits directly within the mean planes of the ligands; however, the nitrogen atoms of each ligand twisted 24.99^{o} away from each other (Figure 2.6). This emphasises the inherent strain with such a tight bite angle. The imidazole moieties should cause less steric hindrance at the binding site compared to the methyl groups in **L3**. The alignment of the auxiliary imidazole moieties by π-stacking appeared to stabilise the interaction of two-equivalents of **201** with beryllium. The Be – N bond lengths were well within 3σ of those documented crystallographically for a neutral sp^2 N-donor.

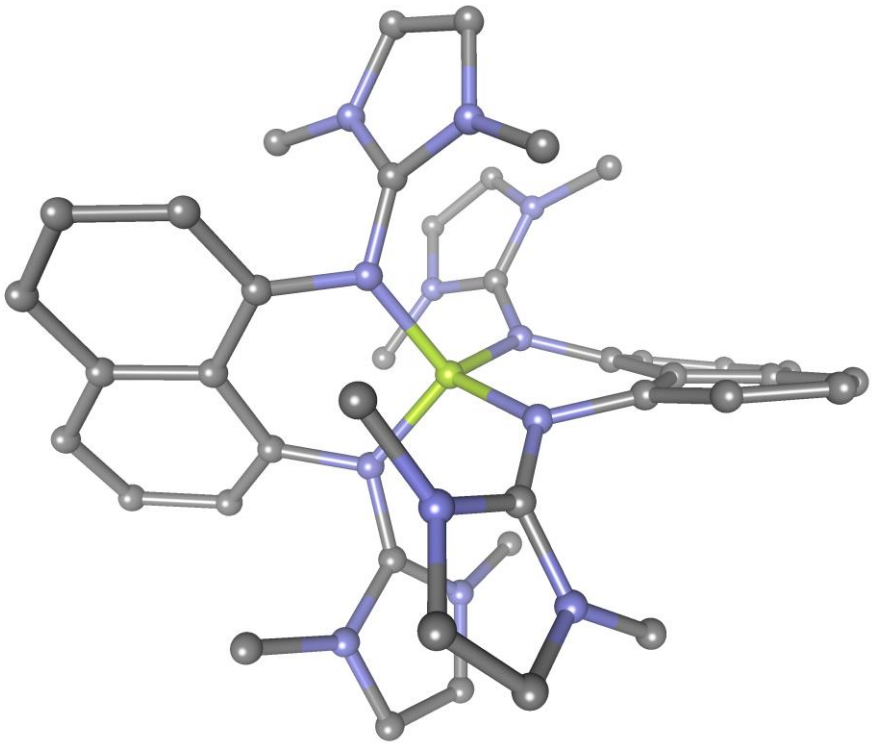

*Figure 2.6: Computer model of the beryllium bis-ligand chelate of **201**, hydrogens are removed for clarity*

The proton sponge **201**,[88] and its analogues,[87, 89] would potentially be the most suitable ligands for testing whether beryllium can displace a strongly deshielded proton bound to the ligand in aqueous environments due to their extremely high basicity. The only problem is the steric hindrance associated with the substituted imidazole moieties. In aqueous environments the water solvent shell must first be displaced for Be(II) to coordinate; ligands having sterically blocked coordination sites may cause further hindrance.

The compromise between extremely high basicity and a sterically hindered coordination site may come in the form of **L2** (Figure 2.7).

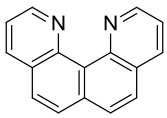

*Figure 2.7: Quino[7,8-h]quinoline, **L2***

The sp^2 hybridisation of the nitrogen atoms offers minimal steric hindrance compared to the alkylated nitrogen donors of **L2**. It does not have the high basicity of **201** meaning a bound proton is not as significantly deshielded. While metal coordination was shown in anhydrous media with careful choice of reactive metal reagents,[72] the scope of metal coordination to **L2** has not been investigated.

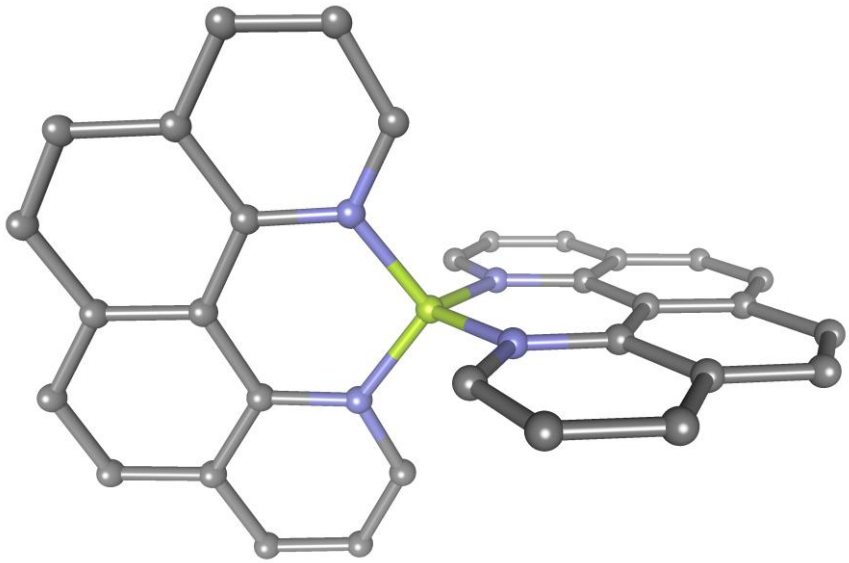

*Figure 2.8: Computer model of the beryllium bis-chelate of **L2**, hydrogens are removed for clarity*

The optimised structure of $[Be(\mathbf{L2})_2]^{2+}$ showed the beryllium ion sits directly within the mean plane of the ligands and there was no twisting present in the ligands (Figure 2.8). The ligand was free from any obvious steric hindrance due to substitution seen in **201** and **L3**, which may account for the remarkably short Be – N bond lengths. Despite having a structurally ideal cavity for beryllium coordination, it is not possible to predict whether this ligand will chelate to beryllium using theoretical methods alone. In aqueous environments there is expected to be competition between protonation of **L2** and coordination to beryllium.

2.1.3 Summary

All the proton sponges have the potential to coordinate beryllium; the choice is essentially limited to the conditions imposed for safely conducting beryllium coordination chemistry research. The only available beryllium source for these investigations was an aqueous solution of beryllium sulfate as this avoided the need to handle beryllium powders. If there were no such restrictions, a suitable beryllium reagent (e.g. beryllium chloride) and use of anhydrous conditions would likely coordinate beryllium to the neutral form of the proton sponges as evidenced by the previous papers dealing with metal coordination chemistry to proton sponges.

Under the conditions imposed the proton sponges would be expected to exist as the cationic protonated species upon exposure to water. It is anticipated that Be(II) will coordinate only by displacement of the deshielded proton bound between the two nitrogen donors. For Be(II) to displace this proton it may be preferential to have a ligand which is not sterically encumbered by substitution so it is for this reason the initial investigation will utilise the ligand **L2** (Figure 2.9).

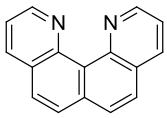

*Figure 2.9: Quino[7,8-h]quinoline, **L2***

L3 was commercially available and was used as a comparison to **L2**. The remaining proton sponges were synthetically challenging and they did not receive further examination in this initial study.

2.2 Zirnstein and Staab Synthesis

2.2.1 Introduction

The Staab synthesis is currently the only confirmed and reproducible method of achieving **L2**.[85] The first reported synthesis of **L2** was in 1950,[99] but, was later shown to be the structural isomer; **202**.[100] In 1967, the synthesis of **L2** was again reported after 1,8-*bis*(acetimido)naphthalene was subjected to a double Skraup reaction.[101] However, this was proved incorrect and the product was subsequently correctly identified as **203**.[85, 102]

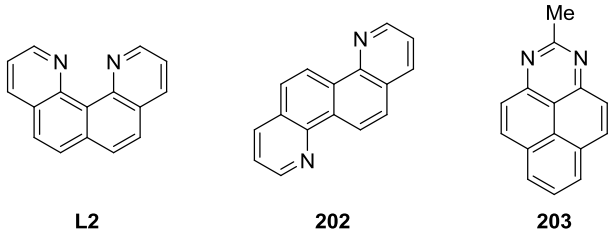

*Figure 2.10: Quino[7,8-h]quinoline, **L2**, and misreported products formed, **202** and **203***

The first confirmed synthesis of **L2** was by Zirnstein and Staab,[85] where they later provided a crystal structure.[86] Their method is shown in Scheme 2.1 and was the starting point in the synthesis of **L2**.

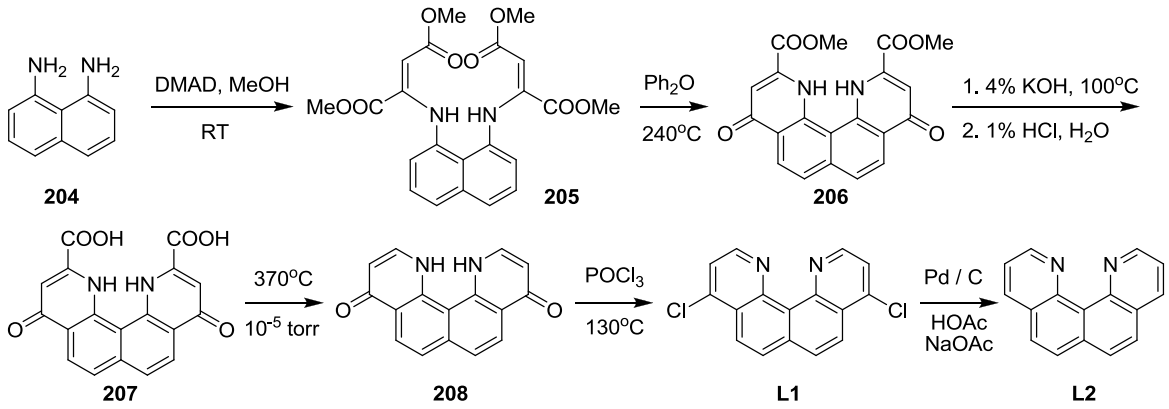

*Scheme 2.1: Synthesis of quino[7,8-h]quinoline, **L2***

2.2.2 Results / Discussion

The original literature preparation of **205** (Scheme 2.2) used several recrystallisations for purification;[103] however, when ethanol was used as the solvent in place of methanol, **205** precipitated from the reaction mixture was simply washed with ethanol and used directly in the next step.

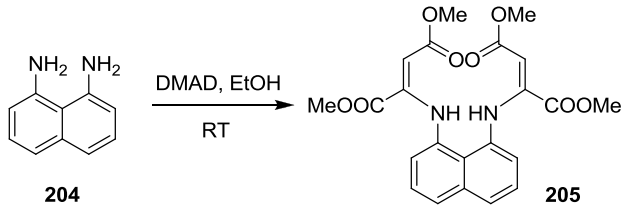

*Scheme 2.2: Synthesis of tetramethyl 2,2'-(naphthalene-1,8-diylbis(azanediyl))difumarate, **205***

Thermal cyclisation of **205** in phenyl ether gave **206** (Scheme 2.3). Thorough rinsing, sonication and filtration of the insoluble precipitate with three volumes of acetone was required to effectively remove impurities and solvent locked into the clay-like solid **206**. Due to the insolubility of **206**, full characterisation was not possible; however, elemental analysis gave good agreement with calculated CHN values and was closer than those previously reported.[103]

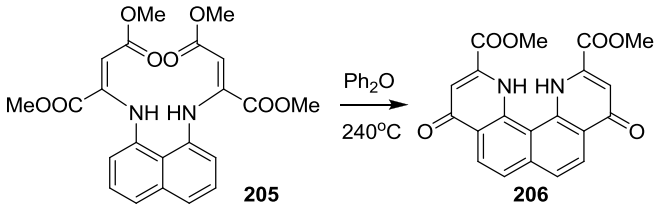

*Scheme 2.3: Synthesis of dimethyl 4,9-dioxo-1,4,9,12-tetrahydroquinolino[7,8-h]quinoline-2,11-dicarboxylate, **206***

The next two steps in the Staab's synthesis involved hydrolysis of the di-ester **206** followed by high temperature – low pressure thermal decarboxylation to achieve **208** (Scheme 2.4).

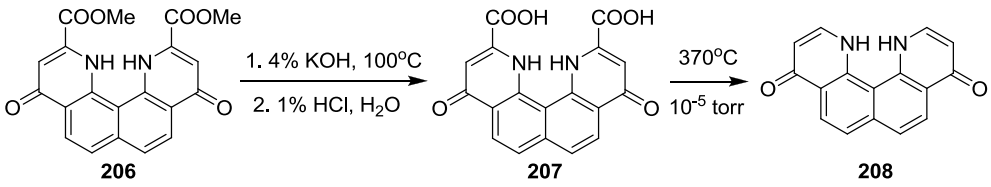

Scheme 2.4: Synthesis of quinolino[7,8-h]quinoline-4,9(1H,12H)-dione, ***208***

A related compound to **206** where ester cleavage was required is indole, **210**. The Fischer Indole synthesis is widely used; however, a decarboxylation step is needed to generate **210**. With the use of a microwave reactor, Strauss and Trainor,[104] converted ethyl indole-2-carboxylate to indole in twenty minutes using the weak base sodium acetate in low concentration and water as the solvent (Scheme 2.5).

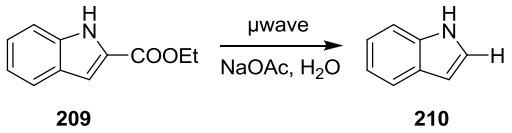

Scheme 2.5: Microwave assisted ester cleavage of ethyl indole-2-carboxylate, ***210***

This simple reaction was used to shorten the two steps utilised in the Staab synthesis (Scheme 2.6).

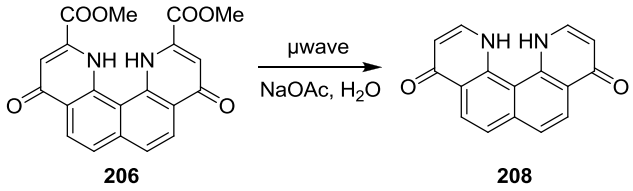

Scheme 2.6: Microwave assisted ester cleavage of dimethyl 4,9-dioxo-1,4,9,12-tetrahydroquinolino[7,8-h]quinoline-2,11-dicarboxylate, ***206***

The reaction did proceed as indicated; the microwave reactor could achieve this reaction in one hour at 250 ^{o}C. While **206** and **208** are insoluble in almost all solvents, including water, the combination of the heat and pressure of this reaction permits this reaction which was heterogeneous at RT to occur. However, despite being rated to 300 ^{o}C and 100 bar the microwave vessels would fail over time and were expensive to replace. The reaction was instead shifted to a Teflon-lined stainless steel bomb placed inside an oven at 250 ^{o}C

overnight. This achieved the same result and also allowed the reaction to be performed on an increased scale (0.1 g scale to 0.8 g scale). When the conversion of **206** to **208** was incomplete due to insufficient reaction time, a side-product formed after the halide substitution reaction with phosphorus oxychloride, **L13** (Scheme 2.7). This was also synthesised by directly reacting **206** with phosphorus oxychloride and will be discussed in Chapter 3.

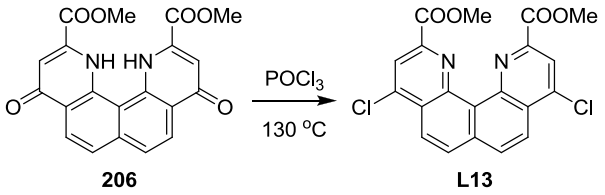

206 **L13**

*Scheme 2.7: Synthesis of dimethyl 4,9-dichloroquinolino[7,8-h]quinoline-2,11-dicarboxylate, **L13***

Due to the insolubility of **208**, full characterisation was not possible. The elemental analysis did not match calculated CHN values within acceptable limits; however, the impurity of **208** did not impact the subsequent dehydration reaction, which, after workup, did give an agreeable CHN analysis and full characterisation of **L1**. The unsubstituted **208** treated with phosphorus oxychloride to obtain **L1** (Scheme 2.8). The overall yield for the revised two steps from **206** – **L1** was 58 – 68 % which was similar to the reported yield of 57 % over three steps for the Staab synthesis.

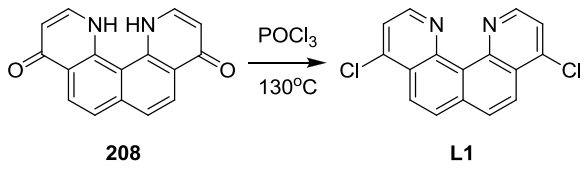

208 **L1**

*Scheme 2.8: Synthesis of 4,9-dichloroquino[7,8-h]quinoline, **L1***

While **208** has not been fully characterised, measurement of the infrared spectrum reveals what might be a more realistic structure for this molecule. As drawn in Scheme 2.8, the two protons lie close to one another requiring a twist in the molecule to overcome this unfavourable interaction. The infrared spectrum of **208** showed a characteristic broad OH stretch indicating that the tautomer of **208** may form instead (Figure 2.11). The tautomer

would relieve the strain by allowing intramolecular hydrogen bonding between the two nitrogen atoms resulting in a flattened molecule. Both **208** and the potassium bromide used to make the disc for measurement were dried in an oven at 110 ^{o}C overnight to exclude the possibility of atmospheric water giving rise to the signal. Crystallographic evidence of compounds resulting from nucleophilic substitutions on **L1** which will be discussed in Chapter 3 also showed this similar tautomerism.

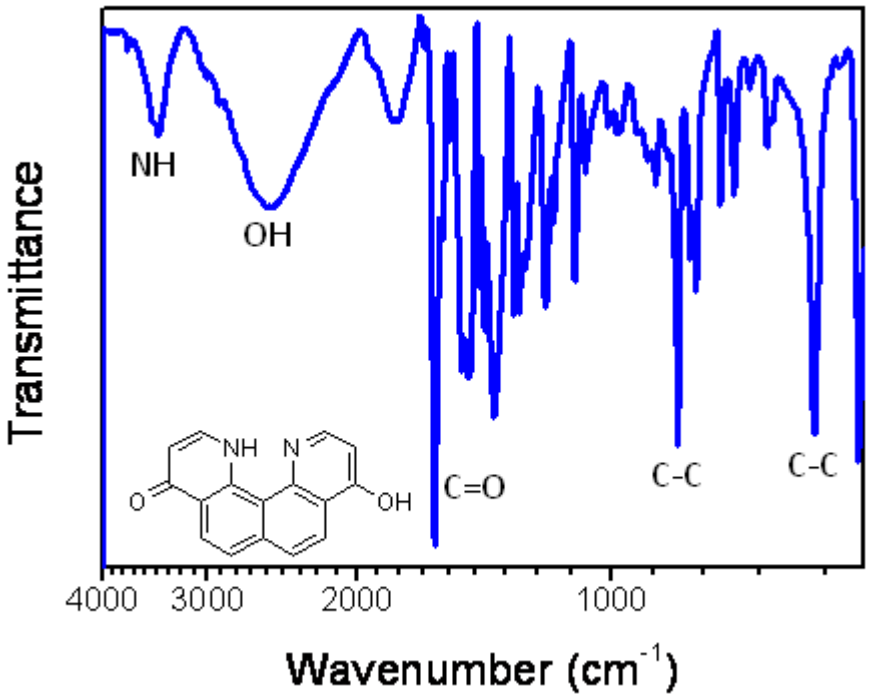

*Figure 2.11 IR spectra for the tautomer of **208** showing a broad OH vibration at 2500 cm^{-1}*

The stretching vibrations for standard phenols are typically around 3500 cm^{-1},[105] however, in this instance the vibration for the OH stretch was 2500 cm^{-1}. The lower energy vibration is due to delocalisation into the heterocyclic ring system. The IR spectra of 3-pyridinol showed an OH stretch at a similar energy of 2500 cm^{-1}.[105] Energy calculations (B3LYP/6311++g(2d,p) on both potential structures showed the tautomer of **208** drawn in Figure 2.11 was 48 kJ mol^{-1} lower in energy than the sterically encumbered twisted form.

Finally, the unsubstituted **L2** was formed by catalytic hydrogenation with Pd / C, glacial acetic acid, and sodium acetate (Scheme 2.9).

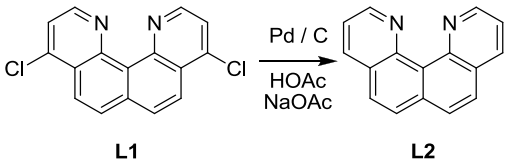

Scheme 2.9: Synthesis of quino[7,8-h]quinoline, ***L2***

To further confirm the successful application of the synthesis, a crystal structure was obtained for **L1** by slow cooling of a saturated solution in chloroform at 0 ^{o}C. The asymmetric unit consisted of one molecule of **L1** and two chloroform molecules. This crystal structure was important as it revealed that in non-protic media there was inherent distortion in the ring which had not been evidenced in previous examples of solid state structures of **L2**. The hydrogens on the two chloroform molecules are oriented toward the nitrogens on **L1** with closest distances of H40A – N2 of 2.2900(18) Å and H30A – N1 of 2.3300(18) Å. The torsion angle between the nitrogens on **L1** was 20.02(9)^{o} which is enough to relieve the strain of the overlapping lone electron pairs on the nitrogens. Figure 2.13 shows this twisting of the fused aromatic rings on **L1** with N1 – N2 2.7683(16) Å.

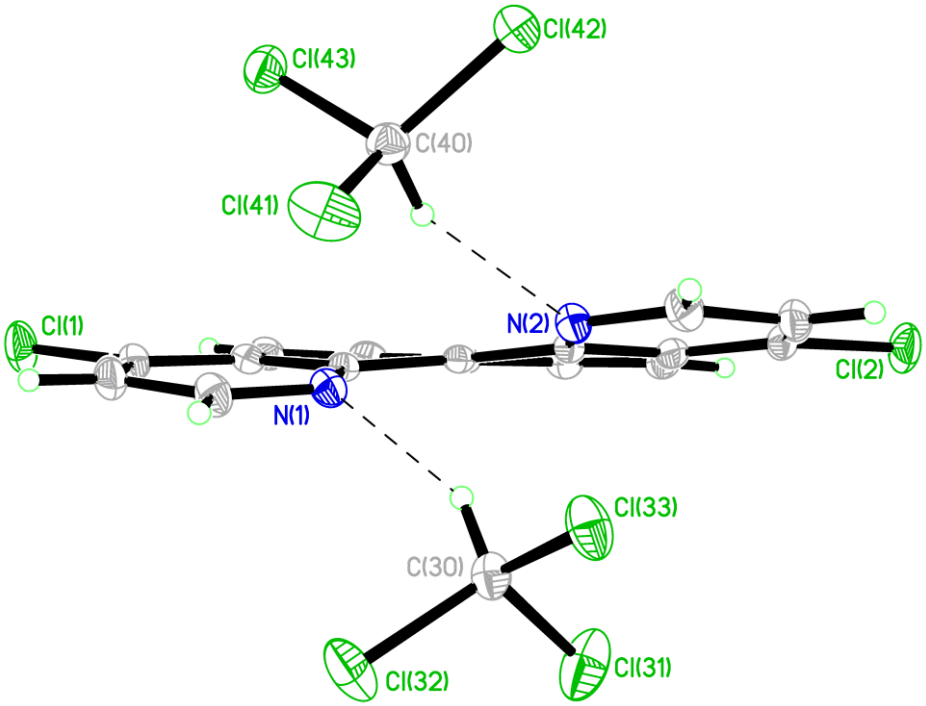

Figure 2.12: Crystal structure showing twisting of the heterocyclic ring system in ***L1****,*

ellipsoids drawn at the 50% probability level

Due to the solvent molecules occupying a large proportion of the crystal and the buckling of the aromatic rings, there are very few π – π interactions typical for solid-state structures of aromatic molecules.[106]

The nature of the π – π stacking interactions can be described by the following parameters (Figure 2.13).[107] The Cg – Cg distance is the distance between the centroids of two six-membered aromatic rings. The two angles of significance are: α, the angle between the two planes, and β, the angle between the ring normal and the two centroids. The aromatic rings are considered to be interacting when the Cg – Cg distance is approximately 3.8 Å or lower and the β angle is 20° or less.

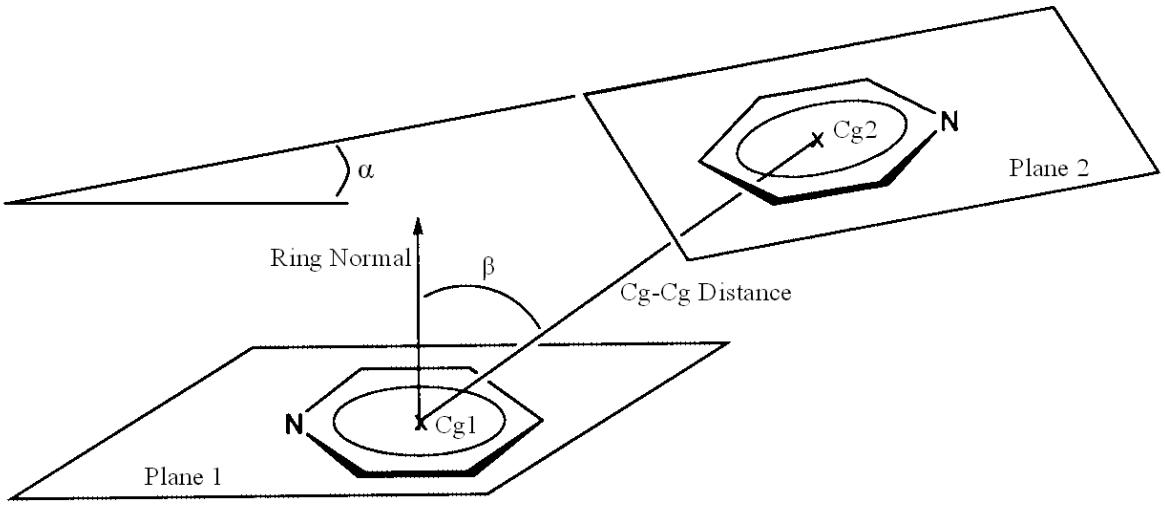

Figure 2.13: Parameters describing π – π stacking interactions, modified diagram from ref 106

The edges of two molecules of **L1** overlap very weakly with a large offset π – π stacking interaction (Figure 2.14); Cg1a – Cg3b 3.6698(10) Å, and β 19.29°, and Cg3a – Cg1b 3.6552(10) Å, and β 18.55°.

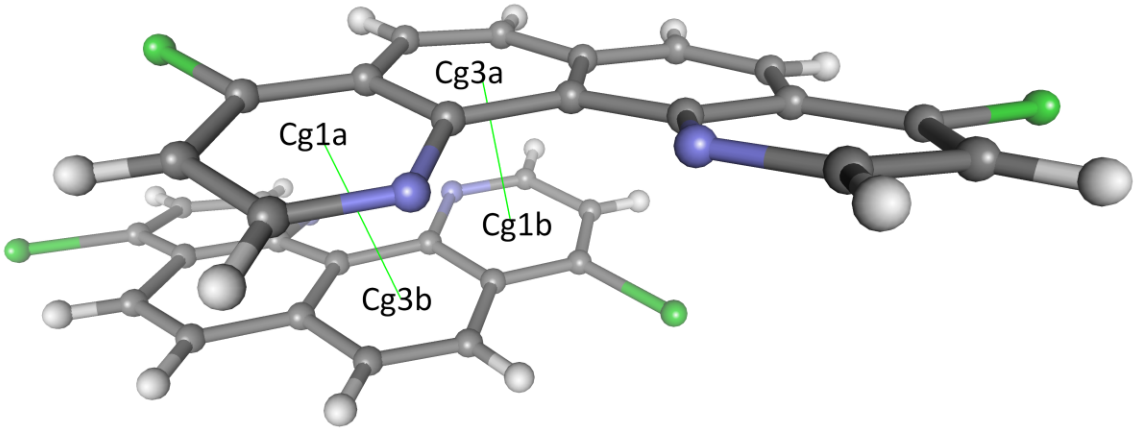

Figure 2.14: Example of stacking π – π stacking interactions between two molecules of ***L1***

The crystal structure of the unsubstituted **L2** (Figure 2.15) originally reported by Zirnstein and Staab[86] is in stark contrast to what was observed for **L1**. In this case the crystals of **L2** were formed by slow evaporation of acetone and water. The result was a more closely packed structure with one water molecule bridging two molecules of **L2**. The presence of the water molecule alleviates the unfavourable N to N interaction resulting in a flattened ring structure (Figure 2.15) with N1 – N2 2.7271(18) Å.

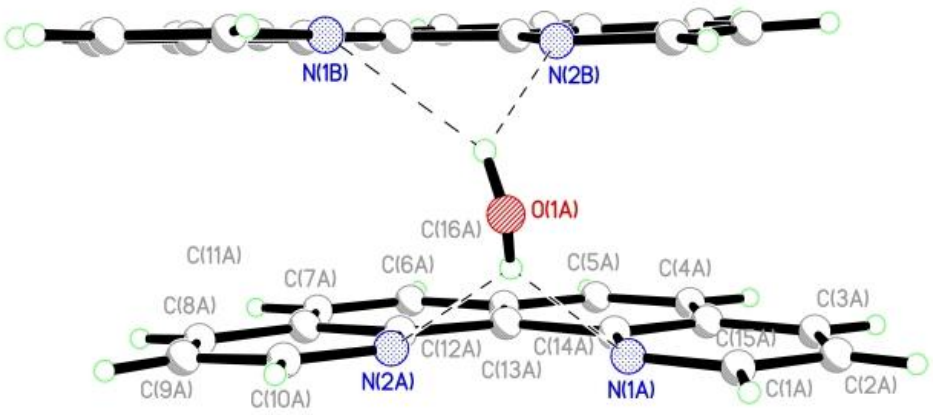

Figure 2.15: Crystal structure of Zirnstein and Staab showing flattened heterocyclic ring system of ***L2***[86]

The water molecules engage in similar hydrogen contact interactions seen in **L1** with N2A – H11E of 2.324(14) Å and N1A – H11E of 2.390(14) Å. While not initially recognised as hydrogen bonding by Staab, recent classifications of hydrogen bonding in the solid state[108] specify these interactions as a three centred[109] moderate electrostatic hydrogen bonds, with

the closest O – H – N (N2A – H11E – O1A) angle being 138.6(13) ^{o} and the closest O – N (N2A – O1A) distance being 3.004(2) Å.

The relief in torsional strain upon proton binding is well documented for proton sponges, however, it was not previously observed in the solid state for quino[7,8-*h*]quinolines. To confirm this, the protonated tetrafluoroborate salt of **L1** was crystallised by vapour diffusion of diethyl ether into acetonitrile. This was a side product to the boron complex which formed upon treatment with boron trifluoride diethyl etherate. The asymmetric unit consisted of one molecule of [H(**L1**)][BF_4] and one tetrafluoroborate anion, modelled for disorder due to rotation along the B1 – F1 bond. The proton on the nitrogen was located by difference map. For this protonated species, the torsion angle between the nitrogens on **L1** was now 0.10(15)^{o}. The proton has relieved the strain of the overlapping lone electron pairs on the nitrogens. The hydrogen bonding was three centred with N1 – N2 2.591(2) Å and N1 – F4 2.738(10) Å.

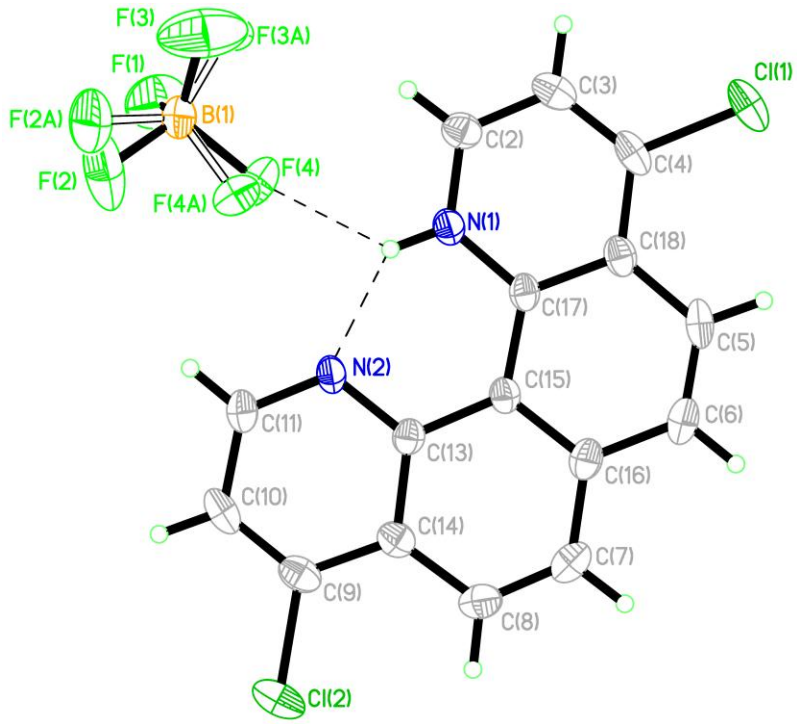

*Figure 2.16: Face view of the crystal structure of [H(**L1**)][BF4] showing hydrogen bonding, ellipsoids drawn at the 50% probability level*

Without solvent present, as in the crystal structure of neutral **L1**, extensive offset π stacking was present between molecules of [H(**L1**)][BF_4] (Figure 2.17); Cg1a – Cg2b 3.4650(13) Å, and β 16.15°, and Cg2a – Cg1b 3.4417(13) Å, and β 14.77°. The tetrafluoroborate anions lie between the stacks.

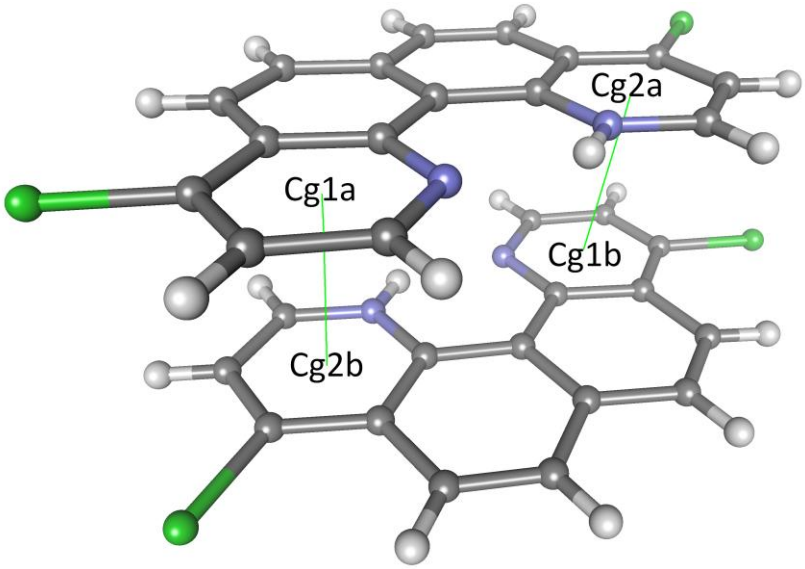

*Figure 2.17: Example of stacking π – π stacking interactions between two molecules of [H(**L1**)][BF4]*

The hydrogen bonding interactions for the three crystal structures above are summarised in Table 2.3.

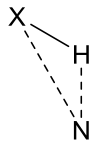

*Figure 2.18: Classification of important bond lengths and angles associated with hydrogen bonding, X = C ($CHCl_3$, **L1**), N, F (ring N, BF_4^-, [H(**L1**)][BF4]), O (H_2O, **L2**)*

	N – H (Å)	N – X (Å)	N – H – X (°)
L1	N1-H30A 2.3300(18)	N1-C30 3.2383(18)	N1-H30A-C30 154.00(18)
	N1-H40A 2.4500(17)	N1-C40 3.2110(17)	N1-H40A-C40 134.00(18)
	N2-H30A 2.5700(18)	N2-C30 3.3227(18)	N2-H30A-C30 134.00(18)
	N2-H40A 2.2900(18)	N1-C40 3.2091(18)	N2-H40A-C40 155.00(18)
[H(**L1**)][BF_4]	N2-H1N 1.9000(2)	N1-N2 2.591(2)	N1-H1N-N2 136.00(2)
	F4-H1N 2.0900(10)	N2-F4 2.738(10)	F4-H1N-N2 131.00(10)
L2	N1-H11 2.390(14)	N1-O1 3.1286(16)	N1-H11-O1 147.4(13)
	N2-H11 3.324(14)	N2-O1 3.0038(19)	N2-H11-O2 138.6(13)

Table 2.3: Important bond lengths and angles associated with hydrogen bonding in quino[7,8-h]quinolines

A summary of the relief in torsional strain upon proton binding is shown for the main types of proton sponges in Table 2.4.

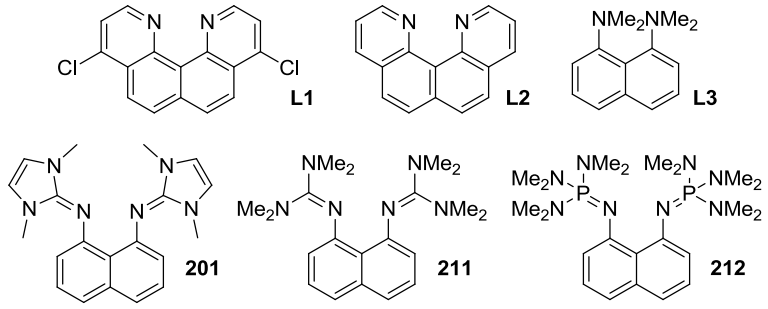

Figure 2.19: Selection of proton sponges with recorded crystal structures

Proton Sponge	φ(N-C-C-N) (°)	
	Free Base	H^+ Bound
L1	20.02(9)[a]	0.10(15)[a]
L2	3.73[86b]	N / A
L3	19.99[110]	3.99±11.67[c]
201	2.33[88b]	1.89[88]
211	32.36[87]	5.46[87]
212	16.65[89]	8.15[89]

Table 2.4: Proton sponge torsion angles in the solid state, [a] present work, [b] does not fit trend for reasons discussed below, [c] mean (N = 83)

The exceptions to the trend are when the stabilising effect of non-covalent interactions are present. Hydrogen bonding in **L2** overcame the repulsion of the lone electron pairs on the

nitrogens. $\pi - \pi$ stacking of the imidazoles of **201** essentially rotated the nitrogens 90^{o} rather than the nitrogens twisting out of plane as in **211**. The large 3σ for H^{+}**L3** was due to the wide variety of environments it was crystallised in.

2.3 Ila et al. Synthesis

2.3.1 Introduction

The Staab synthesis of **L2** was reported in 1987 and subsequently modified in 2004.[111] The alternate method was reported by Ila and co-workers which used a double Skraup condensation with 3-*bis*(methylthio)acrolein on 1,8-diaminonaphthalene **204** which gave **213** in 40 % yield. Although this was not attempted, it was mentioned that reduction with Raney Nickel would lead to the unsubstituted **L2** (Scheme 2.10).

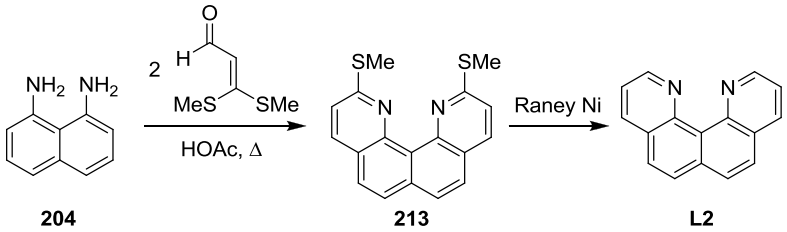

Scheme 2.10: Synthesis of 2,11-bis(methylthio)quino[7,8-h]quinoline, ***213***

2.3.2 Results / Discussion

All attempts to follow the procedure of Ila et al. did not lead to the expected **213**. Subsequent modification of both temperature and reaction time did not yield any discrete products after chromatography. A common problem encountered in this thesis when attempting to construct heterocycles starting from **204** was addition across the nitrogens (Appendix B). The NMR and MS of the crude reaction mixture did not show any evidence of **213** forming. The reaction failure was identified as specific to **204** as repeating the reaction with methoxy-substituted anilines reported gave the expected quinolines.

Eventually, by purifying the 3-*bis*(methylthio)acrolein by chromatography prior to the reaction, distilling the acetic acid and using a drying tube (i.e. using an air atmosphere) it

was possible to obtain a 2 % yield of the half product, **214**. This was subsequently confirmed by single crystal X-ray determination.

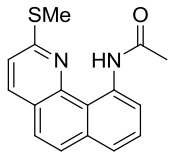

*Figure 2.20: N-(2-(Methylthio)benzo[h]quinolin-10-yl)acetamide, **214***

Clearly there is discrepancy between these reactions and the particular case which would lead to **213**. When the authors were contacted about this, they assured us that no special conditions were needed to form **213**. As no spectroscopic and analytical data was supplied in the paper to support the formation of **213** it is debatable whether this molecule was ever synthesised. The method required chromatography and it is unlikely the compound they isolated could have been **213** as it is not possible to purify quino[7,8-*h*]quinolines using the silica gel column chromatography conditions described (9:1 hexanes / EtOAc). All of the quino[7,8-*h*]quinoline (including those with 2,11 substitution) compounds synthesised in this thesis stayed firmly at the baseline of a hexane and ethyl acetate gradient. Purification by chromatography of these compounds was only possible in the extremely polar gradient 47:47:6 CH_2Cl_2 / MeOH / NEt_3.

There is a patent concerning electroluminescent materials,[68] of which **215** (Figure 2.21), a related ligand to **214** is proposed to coordinate beryllium as a *bis*-ligand chelate. While beryllium coordination to benzo[*h*]quinolin-10-amines had not been published in any journal, it is expected that with a suitable choice of beryllium reagent and reaction conditions, coordination would occur.

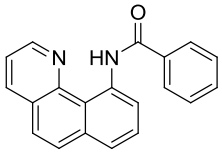

*Figure 2.21: N-(Benzo[h]quinolin-10-yl)benzamide, **215***

The asymmetric unit of the crystal structure of **214** consisted of one molecule of **214** and no solvent molecules. The acetamide group oriented such that a moderate electrostatic hydrogen bond[108] (located from a difference map) existed between the central nitrogen atoms; N2 – H 1.9400(14) Å, N1 – N2 2.6385(14) Å, N1 – H – N2 138.00(14)°. The ^{1}H NMR shift of this hydrogen was 14.3 ppm indicating this hydrogen bond was also present in solution.

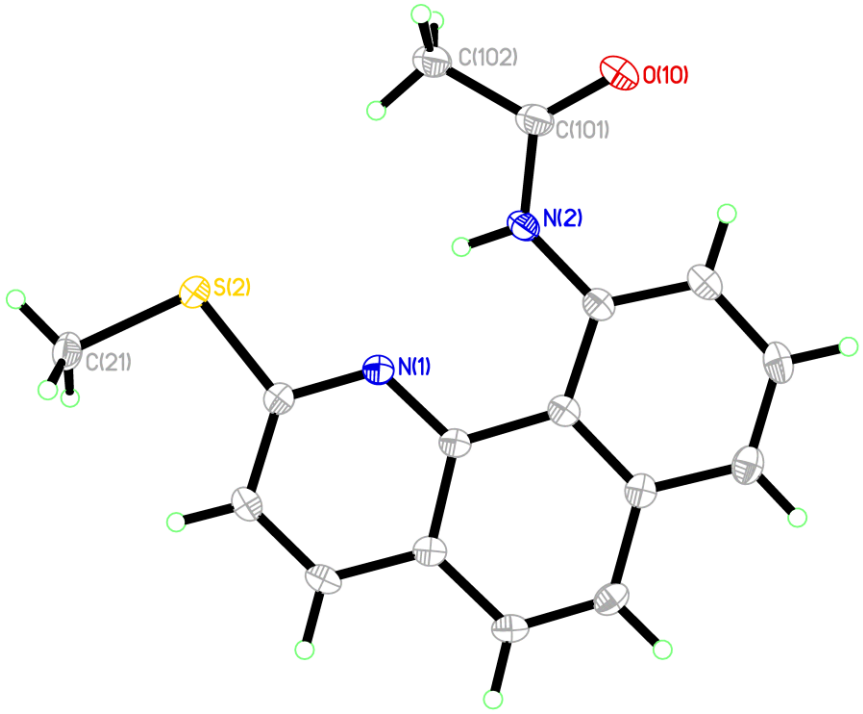

*Figure 2.22: Crystal structure of **214**, grown by D. Parr, ellipsoids drawn at the 50% probability level*

In the absence of any solvent, the adjacent molecules in the crystal structure were closely packed (Figure 2.23). Weak offset π stacking was present between the molecules of **214**, however, there was only one pair of aromatic rings with a close π – π stacking interaction, Cg1 – Cg2 3.5896(8) Å, α 1.15(6)° and β 20.59(6)°. The other main packing interaction was the CH – Cg interaction shown in Figure 2.21; H21B – Cg3 2.68 Å, C21 – H21B – Cg3 148°, and C21 – Cg3 3.5257(16) Å.

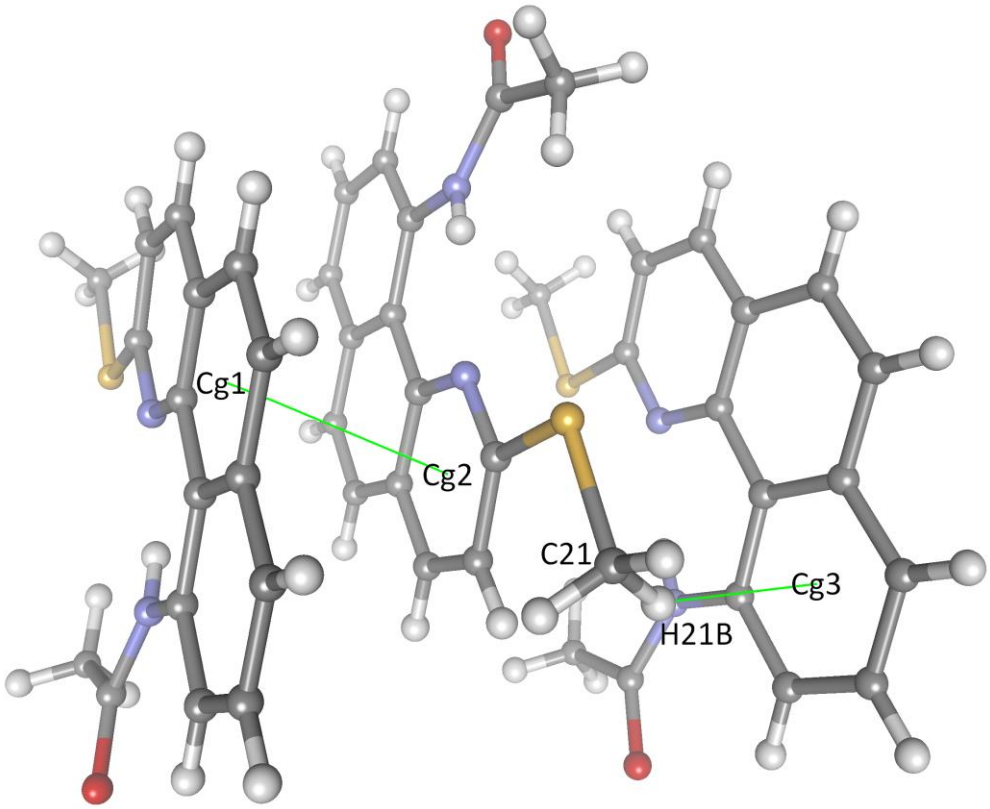

*Figure 2.23: Crystal packing of **214***

The beryllium *bis*-ligand chelate of **214** was computationally modelled (B3LYP - 6-31g(d)). This is shown (with hydrogens removed for clarity) in Figure 2.24. The beryllium ion lay nearly within the mean planes of the ligands (< 0.1 Å) which were almost perpendicular to one another (88.06^{o}). The torsion angle between the two nitrogen atoms was 16.49^{o}.

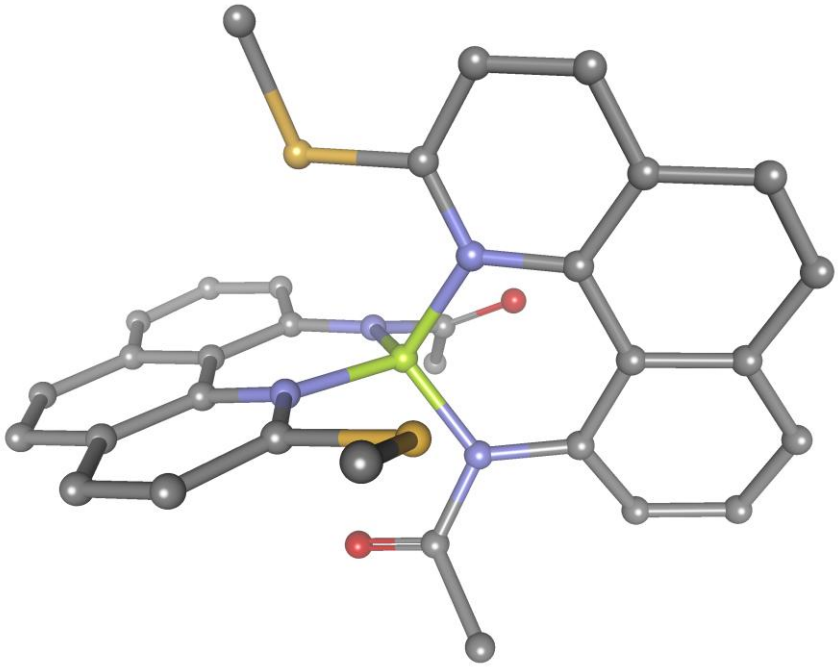

*Figure 2.24: Computer model of the beryllium bis-ligand chelate of **214**, hydrogens removed for clarity, beryllium is shown in light green*

While offering the potential for beryllium coordination, due to the capricious nature of the reaction, sufficient quantities of **214** could not be produced for testing.

2.4 Summary

The ligands chosen as a result of computational analysis were synthesised by modification of the Staab synthesis. The alternative ester cleavage method offered a more readily accessible route to **L1** and **L2** without requiring specialised equipment. Aside from the original paper produced by Staab there had only been one investigation on the coordination chemistry of **L1**,[72] perhaps due to the difficult synthetic procedure. A crystal structure of **L1** provided a unique insight into the conformation adopted in the absence of protic media. The coordination chemistry of the ligands in Figure 2.25 will be investigated in Chapter 4.

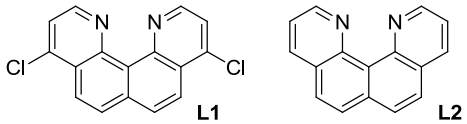

Figure 2.25: Successfully synthesised proton sponge ligands

The methodology put forward by Ila and co-workers proceeded efficiently using activated methoxy-substituted anilines, the original focus of the paper. Unfortunately, this did not extend to the synthesis of **213**.

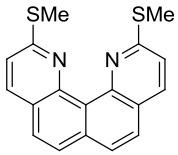

*Figure 2.26: 2,11-bis(Methylthio)quinolino[7,8-h]quinoline, **213***

Chapter 3: Synthesis of Proton Sponge Derivatives

3.1 Introduction

This chapter outlines attempts to functionalise the basic molecules encountered in Chapter 2 in order to enhance their coordination ability. The coordination ability of the ligand could be enhanced by increasing the number of donor arms to create tetra-dentate ligands (2,11 substitution at position R', Figure 3.1), or by adjusting the basicity and solubility through substitution of functional groups onto the ligand (4,9 substitution at position R, Figure 3.1).

Incorporating groups which allow water solubility of the ligand is crucial for sensing beryllium ions in aqueous environment. Substituting either electron-withdrawing or electron-donating groups may tune the basicity of the central cavity to better meet the requirements for small cation complexation over protonation. Including bulky alkyl groups may enhance the solubility in kerosene in order to allow industrial extraction of beryllium from an aqueous waste source.

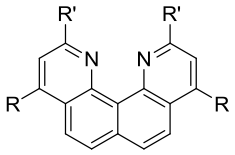

Figure 3.1: Potential sites for modification of on quino[7,8-h]quinoline

Incorporation of chromophores onto the ligand could enhance the fluorescence of the ligand upon beryllium coordination. Currently safe handling of beryllium requires that the beryllium concentration must not exceed 0.2 µg / m^3 in beryllium work areas.[61] A fluorescent sensor would be able to detect whether such trace amounts are present.

As shown in Figure 3.2, if more donor atoms were incorporated into quino[7,8-*h*]quinoline, full encapsulation of beryllium or other small cations of interest may be possible. A tighter

cavity might enable better selectivity for sequestering beryllium over other metals from a waste source. Including oxygen donors will enhance the binding strength of the ligand to beryllium over the relatively weaker nitrogen donors on the native quino[7,8-*h*]quinoline.

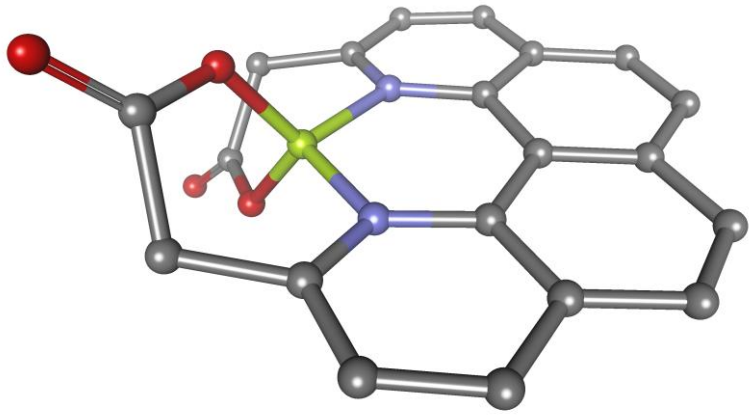

Figure 3.2: Computer model showing potential encapsulation of beryllium through 2,11 substitution of acetic acid moieties on quino[7,8-h]quinoline, beryllium is shown in yellow

3.2 Modification of 4,9 Substitution of Quino[7,8-*h*]quinoline

3.2.1 Results / Discussion

This section focuses on modification of the chlorides of 4,9-dichloroquino[7,8-*h*]quinoline, **L1**, to alter the physical and electronic properties of the resultant complexes.

Schmittel and Ammon demonstrated that a range of phenols and anilines could be substituted onto 4,7-dihalogenated 1,10-phenanthrolines as part of a paper dealing with the synthesis of precursors for macrocyclic oligophenanthrolines.[112] This concept was utilised with **L1** for the purpose of adding chromophores to give compounds with enhanced fluorescence (Scheme 3.1).

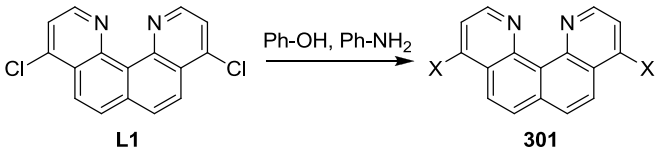

*Scheme 3.1: General scheme for the synthesis of substituted **301** where X is Ph-O or Ph-NH*

As a test reaction for chloride substitution on **L1** with phenols, 4-^{t}Bu-phenol was used; however, nearly quantitative conversion to **L4** after aqueous workup occurred (Scheme 3.2). **L4** has good solubility and purification by chromatography and full characterisation was possible, contrasting with the neutral form of quino[7,8-*h*]quinolines.

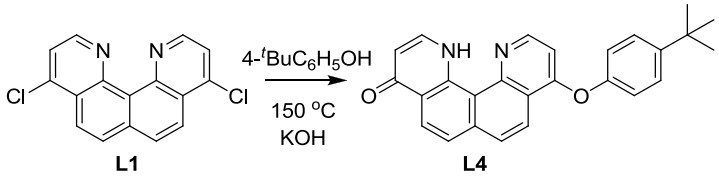

*Scheme 3.2: Synthesis of 9-(4-tert-butylphenoxy)quinolino[7,8-h]quinolin-4(1H)-one, **L4***

The tautomerism observed between quinolin-4-ol, **302** and quinolin-4(1*H*)-one, **303** (Figure 3.3),[113] may offer an explanation for the formation of **L4**. Unlike **303**, the high basicity of **L4**, appears to drive the tautomerism equilibrium towards the ketone with the hydrogen tightly bound between the nitrogen atoms. The reaction in Scheme 3.2 was performed in a melt of neat 4-^{t}Bu-phenol and KOH, under these conditions both chlorides were substituted by 4-^{t}Bu-phenol, as evidenced by the MS of the reaction mixture. Upon aqueous workup, conversion to **L4** occurs, which could be enhanced by using dilute HCl. This suggests that initial protonation between the nitrogens destabilises the molecule and allows the tautomerism to **L4** to occur via nucleophilic substitution of one phenol.

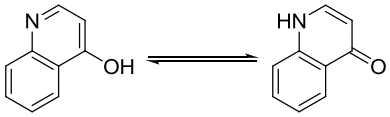

302 **303**

*Figure 3.3: Tautomerism of quinolin-4-ol, **302***

Attempts to crystallise **L4** in the presence of copper perchlorate by vapour diffusion of diethyl ether in acetonitrile resulted in the isolation of protonated **L4** as the perchlorate salt and no metal complex (from an attempted reaction in Chapter 4). CHN analysis of the bulk crystallised material suggested the formulation **L4**.$HClO_4$; however, upon analysis of a single crystal suitable for X-ray determination, the asymmetric unit consisted of two molecules of **L4** and only one perchlorate. While this single crystal was a minor product compared to the bulk material, it allowed identification of the structural features of **L4** to reinforce the NMR and MS results. The charge was balanced by a central proton (located via the difference Fourier map) which formed a bridge between the two molecules of **L4** (Figure 3.4). The bulk material of formula **L4**.$HClO_4$ most likely had all O9 positions protonated with the charge balanced by a perchlorate anion.

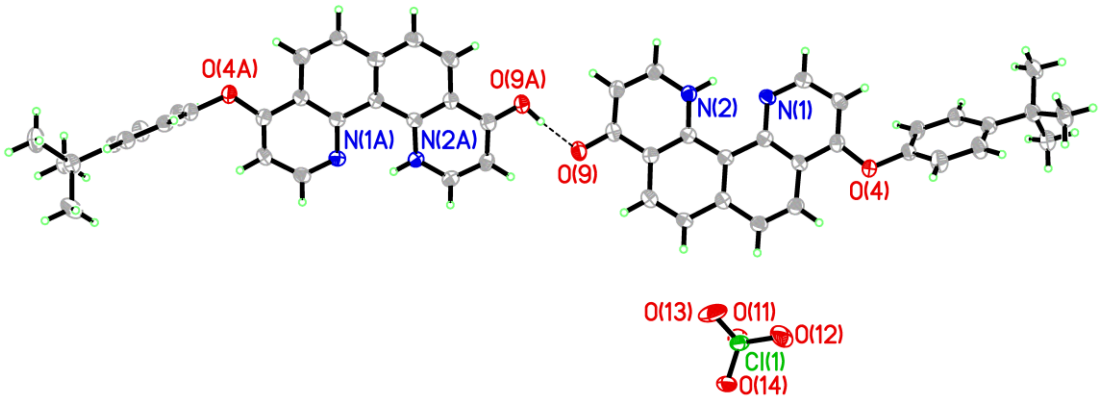

*Figure 3.4: Crystal structure of **L4** showing the bridging proton, H9AA, ellipsoids drawn at the 50% probability level*

Both carbonyls associated with this bridging hydrogen were elongated to a partial double bond length of 1.300(3) Å. The difference map placed the proton as a formal bond to O9A with a strong hydrogen bond[108] to O9; O9A – H9AA 1.610(2) Å, O9A – O9 2.444(2) Å, and an O9A – H9AA – O9 angle of 175.00(2)^{o}. The expansion of the crystal structure shown in Figure 3.5 details the differences in the double-bond character resulting from the quinolinone part; C(9) – O(9), C(10) – C(11) and C(13) – C(14), and the quinolinol part; N(1) – C(2), C(3) – C(4) and C(17) – C(18).

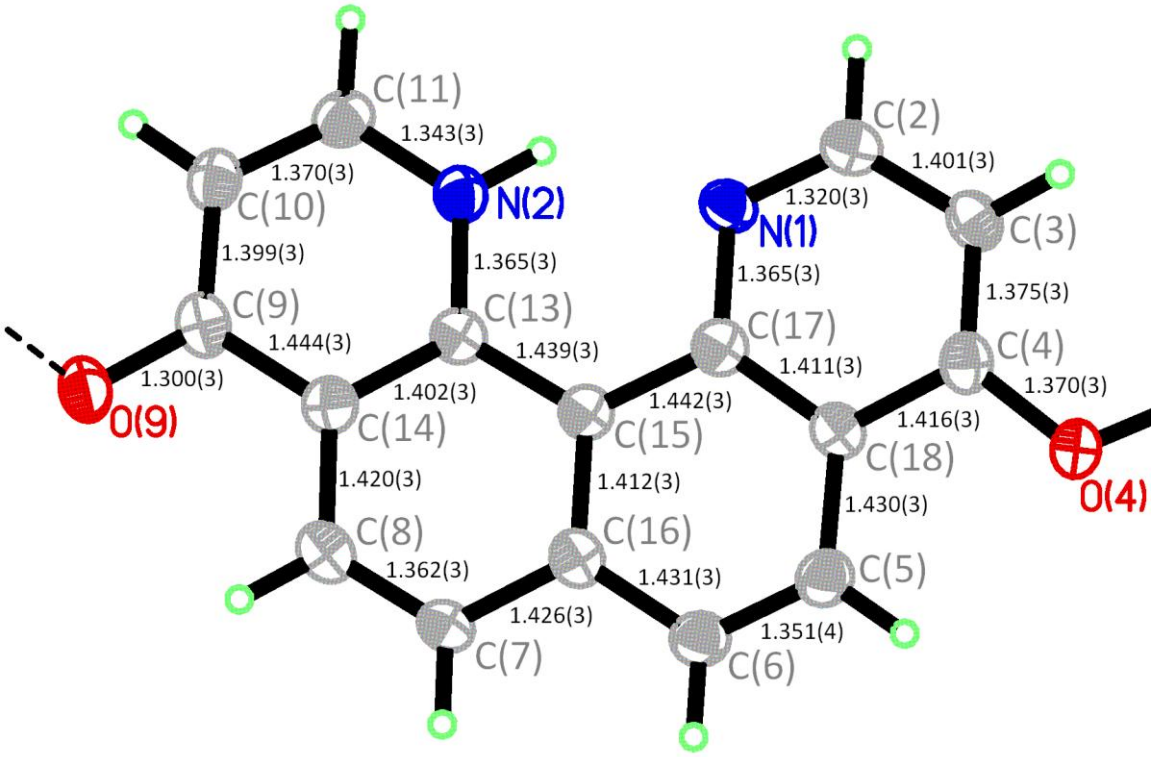

*Figure 3.5: Expanded crystal structure of **L4** showing the bonds with single and double bond character, ellipsoids drawn at the 50% probability level*

The crystal packed primarily via offset π stacking between adjacent heterocycles shown in Figure 3.6, there were also minor C-H π interactions between adjacent 4-^{t}Bu-phenol substituents.

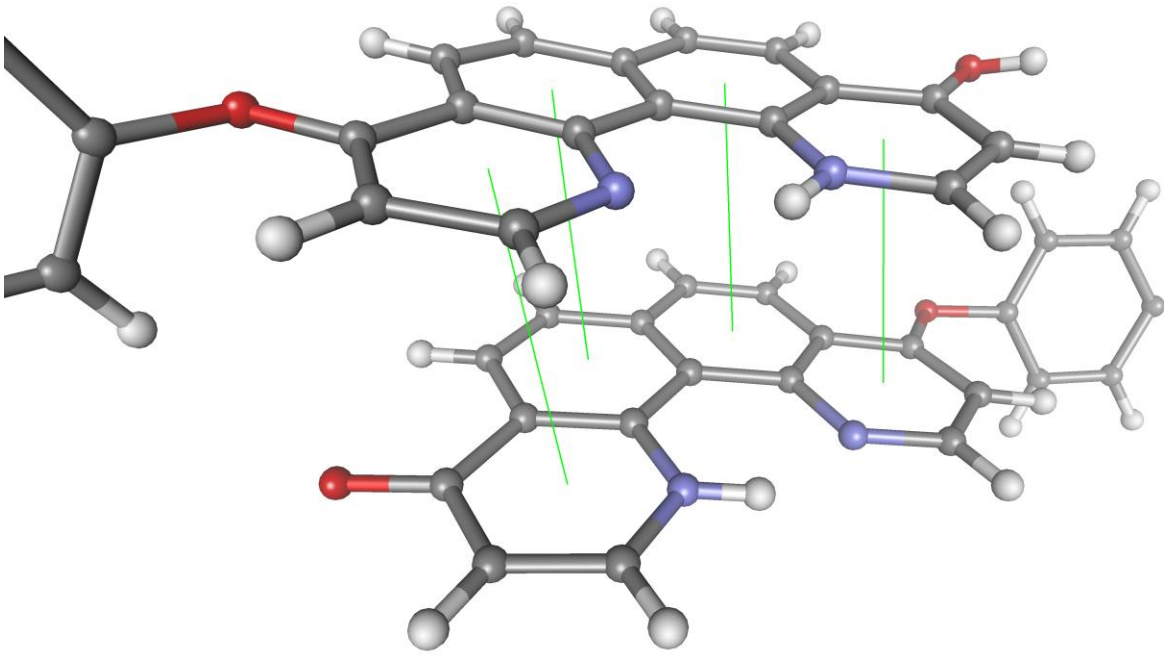

*Figure 3.6: Crystal packing in **L4***

In order to convert **L4** back into a dipyridine-type donating ligand, treatment with phosphorus oxychloride gave the unsymmetrical **L5** (Scheme 3.3). This may have interesting electronic properties due to net charge transfer across the ligand. Moreover, the substitution on **L5** improved the solubility in a range of polar solvents compared with **L1** which had solubility limited to halogenated solvents. It was subsequently found that **L5** could be formed directly by refluxing **L1** and 4-^{t}Bu-phenol (4 equiv.) in toluene; however, it was difficult to separate **L5** from the unreacted 4-^{t}Bu-phenol. The ability to purify **L4** by chromatography first was preferable to purification of **L5** after direct synthesis from **L1**.

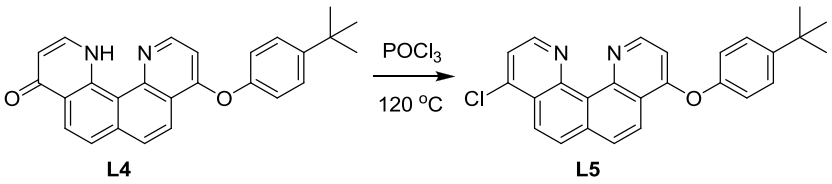

*Scheme 3.3: Synthesis of 4-(4-tert-butylphenoxy)-9-chloroquinolino[7,8-h]quinoline, **L5***

Substitution of the chlorides on **L1** with anilines was also possible; *p*-toludine was used to test the reaction methodology. Mono-substitution of *p*-toludine (4 equiv.) onto **L1** was achieved by refluxing in toluene (Scheme 3.4). This offered a clean and efficient method

of substitution as **L1** would solubilise upon reaction with *p*-toludine then precipitate as **L6** which allowed a convenient method of separating unreacted *p*-toludine by filtration.

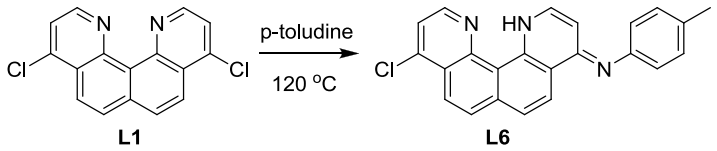

*Scheme 3.4: Synthesis of (E)-N-(9-chloroquinolino[7,8-h]quinolin-4(1H)-ylidene)-4-methylaniline, **L6***

The ^{1}H NMR of **L6** recorded in deuterated methanol did not show the nitrogen-bound proton as shown in Scheme 3.4 due to exchange. The proton shift could be detected as **L6** was sparingly soluble in hot deuterated dimethylsulfoxide and the ^{1}H NMR showed this proton at 14.62 ppm.

Di-substitution with *p*-toludine to form **L7** could be achieved as a melt in neat *p*-toludine. Purification proved to be much more complicated compared to **L6** (Scheme 3.5).

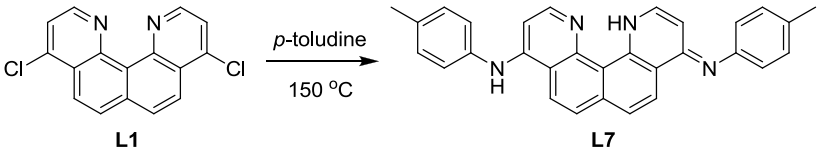

*Scheme 3.5: Synthesis of (E)-N-p-tolyl-9-(p-tolylimino)-9,12-dihydroquinolino[7,8-h]quinolin-4-amine, **L7***

Quino[7,8-*h*]quinoline-based compounds are generally unable to be purified by silica gel column chromatography until the solvent gradient becomes excessively polar (e.g. 8:8:1 CH_2Cl_2 / MeOH / NEt_3). These compounds will not move in a CH_2Cl_2 / MeOH gradient alone. Usually, at high MeOH concentrations, silica gel begins to dissolve, however, if purification was started at 90:10 CH_2Cl_2 / MeOH to remove unreacted *p*-toludine, this appeared to deactivate the silica such that it didn't dissolve when the higher methanol concentrations were used. Initial elution with 90:10 CH_2Cl_2 / MeOH removed most of the impurities, and then the gradient was increased to 50:50 CH_2Cl_2 / MeOH which shifted any insoluble degraded by-products and left **L7** at the baseline of the column. Finally, **L7** was slowly eluted using a 8:8:1 CH_2Cl_2 / MeOH / NEt_3 gradient. The product separated did not

give an agreeable CHN analysis, perhaps owing to the silica dissolution problem. A high resolution mass spectrum and NMR analysis confirmed the presence of **L7**.

A crystal structure was obtained by cooling **L7** at 4 ^{o}C in CH_2Cl_2 / MeOH overnight. The asymmetric unit (Figure 3.7) unexpectedly revealed that upon crystallisation **L7** had formed a tautomer stabilised by one methanol solvent molecule, with the hydrogen located on N2 rather than N91 (the hydrogen was located via the fourier difference map). The C9-N91 bond length, 1.311(2) Å, had partial double bond character relative to C4-N41, 1.367(2) Å. For this to occur, the basicity of this molecule must have increased due to the electron-donating substituted amine groups. The proton was also observed in the ^{1}H NMR spectra at 16.41 ppm; the large downfield shift is typical for a highly deshielded proton located between the ring nitrogens.

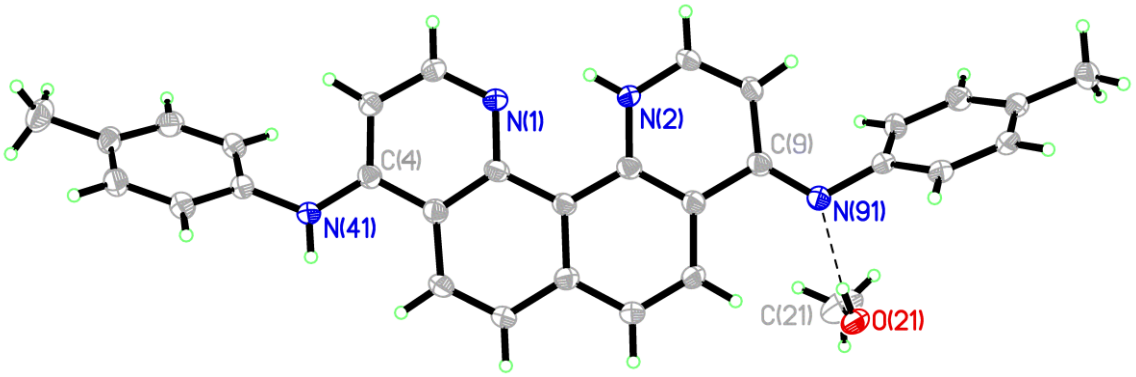

*Figure 3.7: Crystal structure of **L7**, ellipsoids drawn at the 50% probability level*

The methanol solvent interacts with a moderate electrostatic hydrogen bond[108] with O21 – H21 0.820(2) Å, N91 – H21 1.950(2) Å, O21 – N91 2.753(2) Å, and an O21 – H21 – N91 angle of 167.00(2)^{o}. There was no significant π-stacking within the crystal lattice. Edge to face π packing was evident between two adjacent toludine substituents; H93A – Cg1 2.690(2) Å, C93 – H93A – Cg1 153.00(2)^{o} and C93 – Cg1 3.551(2) Å, Figure 3.8.

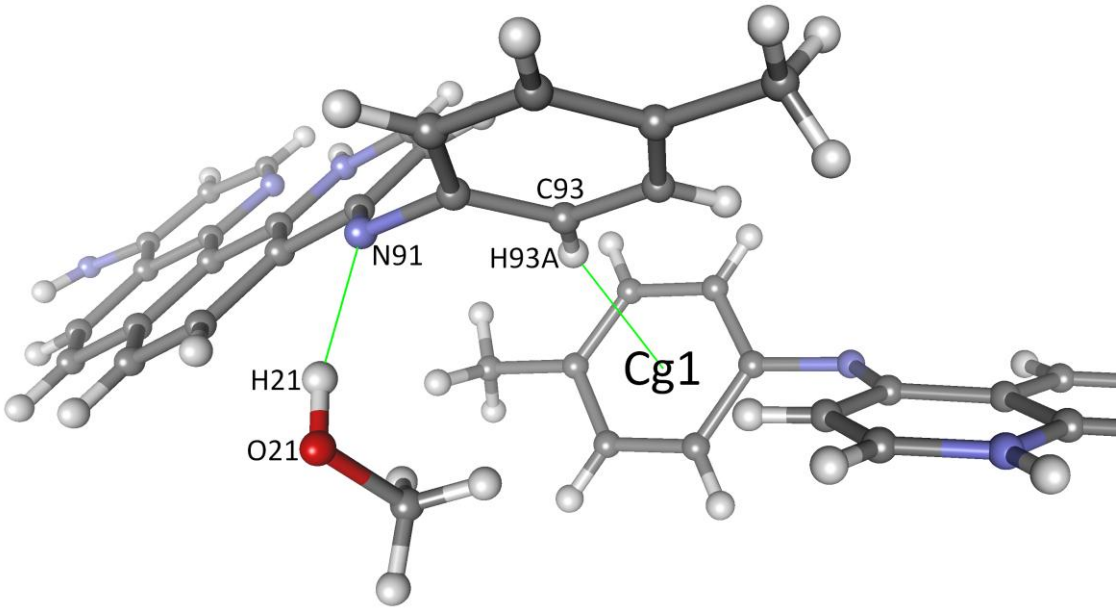

*Figure 3.8: Hydrogen bonding and edge to face π packing interactions in **L7***

A protonated form of **L7** could be crystallised as the tetrafluoroborate salt by reaction with boron trifluoride diethyl etherate. The crystals formed by vapour diffusion of diethyl ether into a methanolic solution containing **L7**. The asymmetric unit consisted of one molecule of **L7** and one tetrafluoroborate anion (Figure 3.9). The hydrogens on N4 and N9 and the proton on N1 were located via the fourier difference map. As expected, the C4 – N4, 1.354(4) Å, and C9 – N9, 1.374(4) Å, bonds lengths were now longer than those in the neutral form of **L7** (Figure 3.7). The protonation state was additionally confirmed by ^{1}H NMR which showed the central NH proton at 18.79 ppm and the two secondary amine protons at 10.11 ppm. The ^{1}H NMR shift of the central NH was now further downfield compared to the 16.41 ppm shift for neutral form.

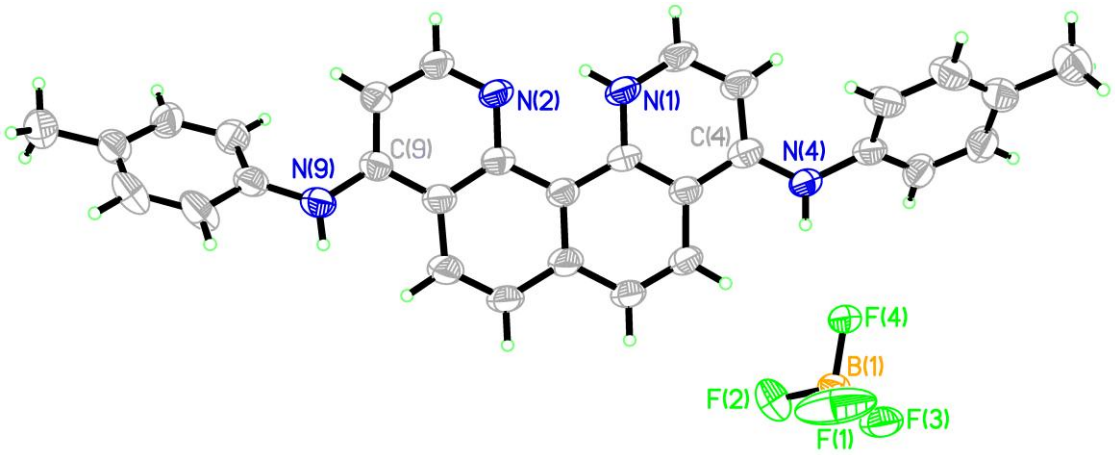

*Figure 3.9: Crystal structure of [H(**L7**)][BF_4], ellipsoids drawn at the 50% probability level*

The tetrafluoroborate anion interacts with a moderate hydrogen bond[108] ; F4 – H4A 2.080(3) Å, N4 – F4 2.869(3) Å, and an N4 – H4A – F4 angle of 152.00(3)^o. Compared to the tautomer, the packing was now primarily offset π-stacking interactions, the closest centroid interactions are shown in Figure 3.10.

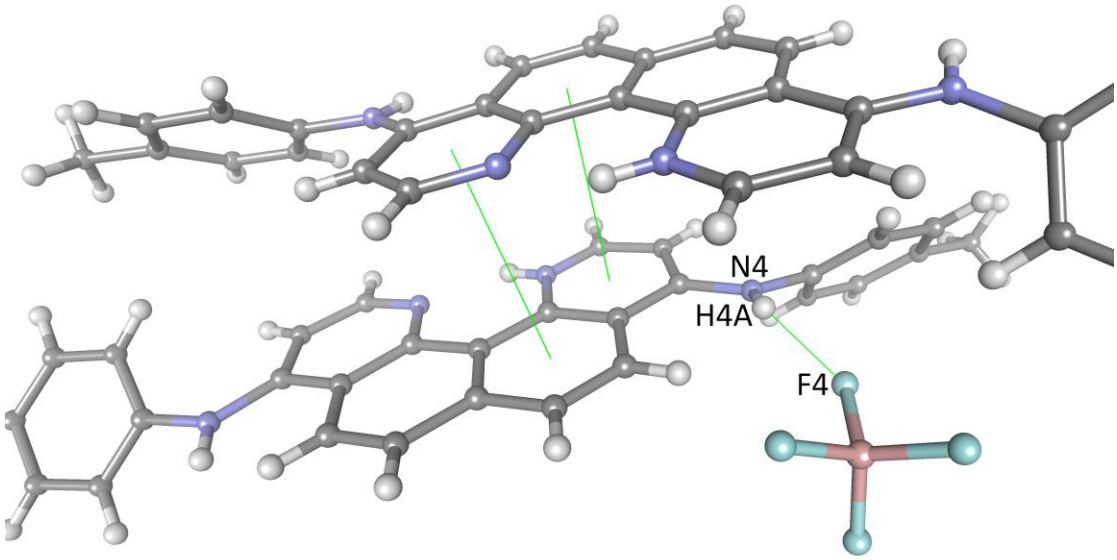

*Figure 3.10: Crystal packing of [H(**L7**)][BF_4]*

With a route to forming diamine derivatives of **L1** established, methyl 2-aminobenzoate, **304**, was selected from a range of substituted anilines available because it was strongly

fluorescent when viewed under an UV light. This is due to the hydrogen bonding interaction between the adjacent amine and methyl ester shown in Figure 3.11.

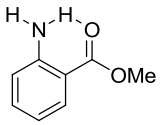

*Figure 3.11: Hydrogen bonding in methyl 2-aminobenzoate, **304***

Substitution of methyl 2-aminobenzoate gave the orange coloured compound **L8** (Scheme 3.6), a marked change to **L1** which did not absorb in the visible spectrum. The ^{1}H NMR of **L8** recorded in deuterated methanol did not show the nitrogen-bound proton as shown in Scheme 3.6 due to exchange. The proton shift could be detected as **L8** was sparingly soluble in hot deuterated dimethylsulfoxide and the ^{1}H NMR showed this proton at 15.69 ppm.

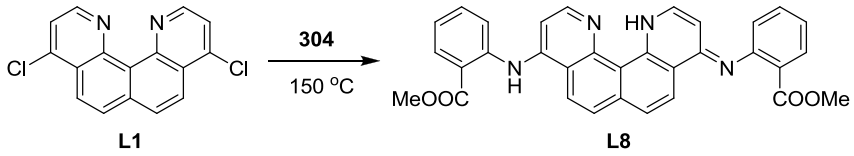

L1 **L8**

*Scheme 3.6: Synthesis of (E)-methyl 2-(9-(o-tolylamino)quinolino[7,8-h]quinolin-4(1H)-ylideneamino)benzoate, **L8***

The enhanced fluorescence of the protonated form of **L8** over **L7** is best illustrated by Figure 3.12. Protonation occurs on the imine which is evidenced by the crystal structure of **L7** described earlier (Figure 3.9). Although no crystals were grown, it is reasonable to assume protonation occurs at the same position for **L8**.

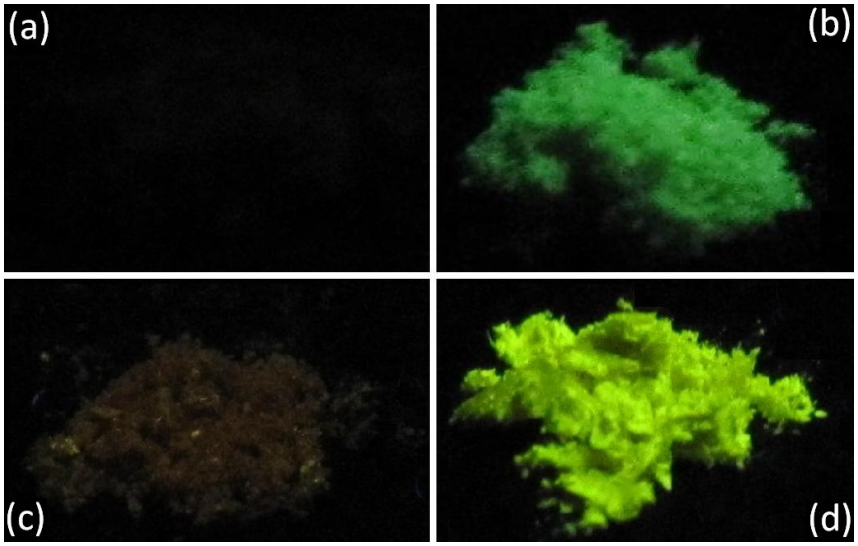

*Figure 3.12: Compounds; (a) **L7**, (b) [H(**L7**)][BF_4], (c) **L8**, (d) [H(**L8**)][BF_4], viewed in the dark under a long wave 385 nm UV lamp*

The strong fluorescence of [H(**L8**)][BF_4], (d), must arise from delocalisation across the entire system as the neutral form **L8**, (c), is not fluorescent. The crystal structures of [H(**L7**)][BF_4] and neutral **L7**.MeOH both show the substituted anilines rotated away from the plane of the heterocyclic ring. Although no crystal structure was obtained, the hydrogen bonding present between the 2^o amines and the methyl esters of [H(**L8**)][BF_4] may align the aniline substituents with the central heterocycle. This shows that with careful choice of substituent, quino[7,8-*h*]quinoline can be modified into a fluorescent compound.

The optimised geometries of both [H(**L7**)][BF_4] and [H(**L8**)][BF_4] were calculated at the B3LYP/6-311++g(2d,p) level. The angles between the aniline substituents and the heterocyclic ring for [H(**L7**)][BF_4] were 67.57^o and 71.37^o. The angles between the aniline substituents and the heterocyclic ring for [H(**L8**)][BF_4] were reduced to 43.90^o and 41.20^o as a result of the hydrogen bonding.

Analysis of the molecular orbitals involved in the $\pi - \pi^*$ transitions for [H(**L7**)][BF_4] and [H(**L8**)][BF_4] provide more evidence for these empirical observations (Figure 3.13). The weak fluorescence observed for [H(**L7**)][BF_4], Figure 3.12, image (b), is due to a partial intramolecular charge transfer from one aniline substituent into the heterocyclic ring.

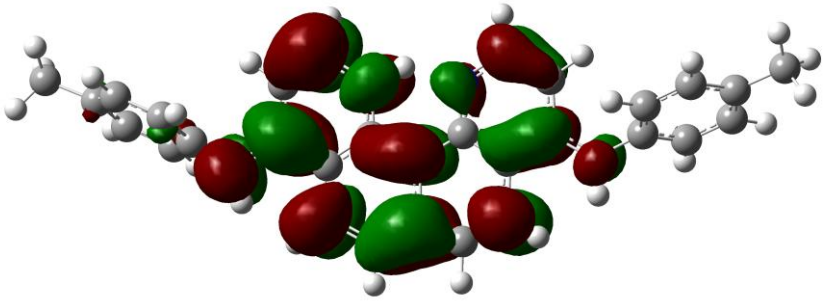

LUMO, -0.185 eV

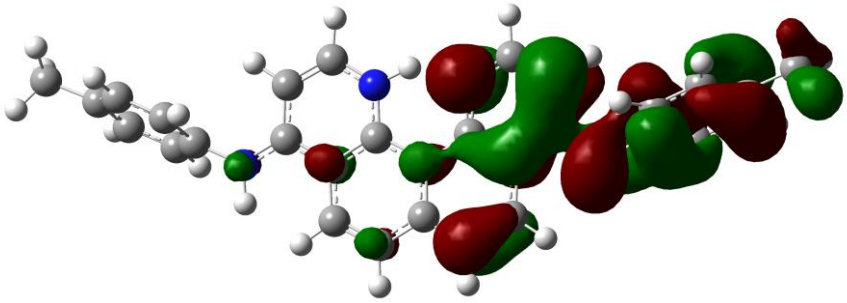

HOMO, -0.308 eV

Figure 3.13: Molecular orbitals associated with the π – π transition for [H(**L7**)][BF_4]*

Based on this analysis, the strong fluorescence observed for [H(**L8**)][BF_4], Figure 3.12, image (d), is due to an intramolecular charge transfer from one aniline substituent into the heterocyclic ring and the opposite aniline substituent (Figure 3.14).

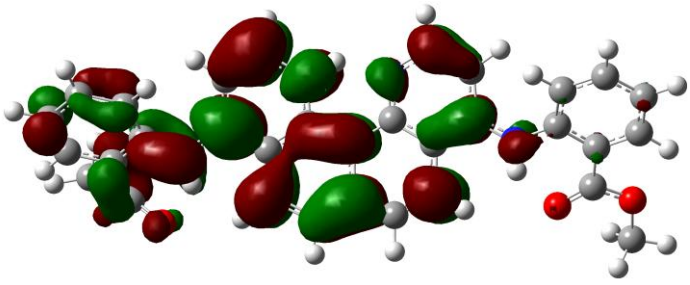

LUMO, -0.180 eV

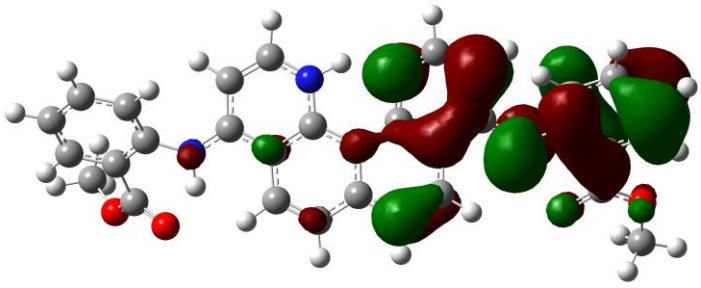

HOMO, -0.292 eV

Figure 3.14: Molecular orbitals associated with the π – π transition for [H(**L8**)][BF_4]*

Substitution of *p*-toludine onto **L5** did not proceed selectively on the chloride; both the 4 and 9-positions were substituted to give **L7** (Scheme 3.7). While not offering the anticipated result, this does show the leaving ability of the phenol and explains why the tautomer **L4** forms instead of a di-aryl ether substituted product.

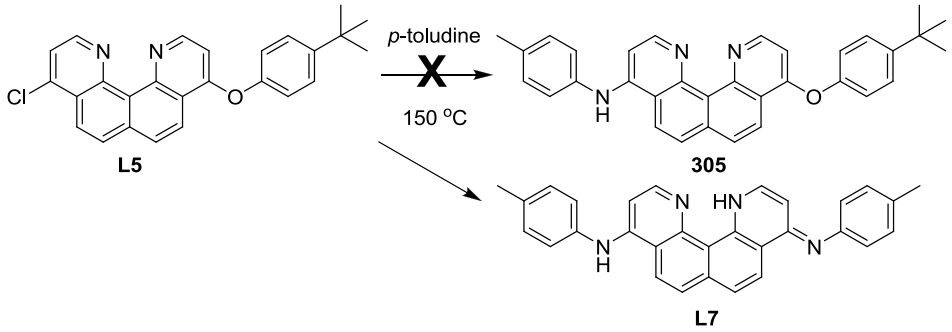

*Scheme 3.7: Attempted synthesis of the asymmetrically substituted **305***

In order to give enhanced fluorescence, it was desirable to have substitution that gave rise to increased conjugation. Nitration of **L1** for 2 min in fuming HNO_3 / H_2SO_4 gave selective electrophilic substitution of two NO_2 groups (Scheme 3.8).

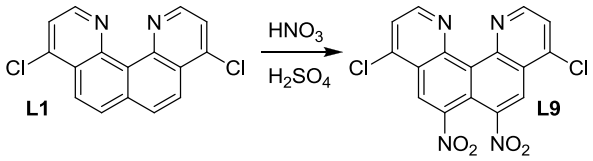

*Scheme 3.8: Synthesis of 4,9-dichloro-6,7-dinitroquinolino[7,8-h]quinoline, **L9***

The mass spectra revealed the chlorides had remained intact and the NO_2 groups had replaced two hydrogens. This was confirmed by a CHN analysis of the tetrafluoroborate salt. The compound had poor solubility; however, a ^1H NMR recorded in DMSO-d6 was only able to definitively characterise the hydrogens 1, 2 and 3 shown in Figure 3.15.

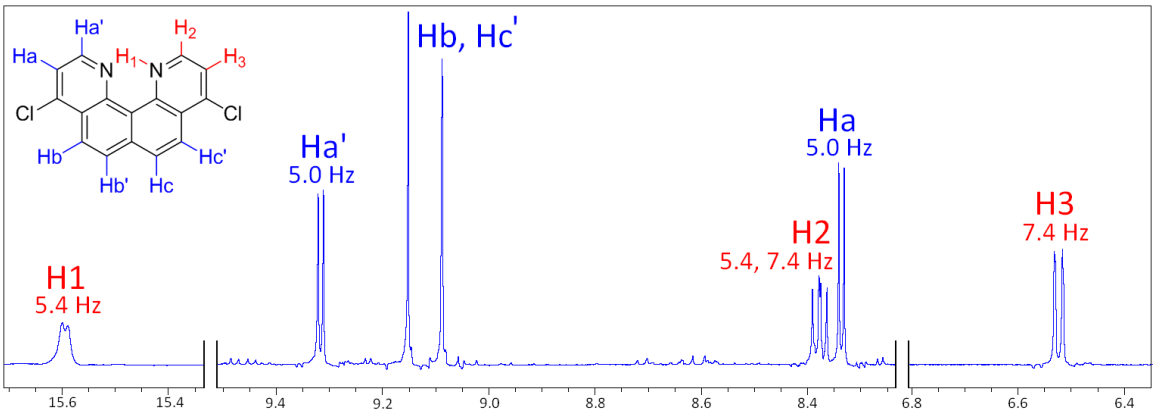

*Figure 3.15: ^{1}H NMR of the nitrated quinolino[7,8-h]quinoline, **L9***

The two nitro groups on **L9** are most likely substituted at the Hb' and Hc positions. In the absence of a crystal structure it is only possible to speculate this; however, nitrations under similar conditions of the proton sponge **L3** lead to substitution at these positions.[114] One of the nitrogen atoms of **L9** was protonated and exchange on the NMR timescale was slow, this causes the observed different chemical shifts and couplings in the ^{1}H NMR spectrum for the otherwise symmetrically identical hydrogens. When the solid was viewed under 385 nm UV light the protonated form of **L9** was not fluorescent, most likely as a result of rotation of the NO_2 groups out of the plane of the aromatic ring, the crystal structure of the nitrated **L3** showed the trigonal planar NO_2 groups rotated 30.4^{o} out of the aromatic plane.[114] The nitro groups can potentially offer points for further substitution or attachment to polymers or surfaces.

To utilise ligands such as **L1** in analytical applications, water solubility is a desirable property, therefore the ability to sulfonate **L1** was explored. It should be possible to substitute the chloride groups with sulfonic acid groups by a reaction with sodium sulfite. An equivalent chloride-substitution reaction had been performed with 4-chloropyridine.[115] A mass spectrum of the reaction mixture showed some di-substitution of the chloride on **L1** with sulfonic acid moieties, unfortunately, the only stable product formed over a range of reaction times and temperatures was **L10** (Scheme 3.8). The large downfield NH shift of 15.47 ppm in the ^{1}H NMR spectrum and the carbonyl peak at 176.5 ppm ^{13}C NMR spectrum confirmed the existence of **L10** rather than the phenol tautomer. Unfortunately, **L10** could not purified sufficiently to give an agreeable CHN analysis. This hydrolysed

product was consistent with the observed hydrolysis of **L4** encountered earlier. When good leaving groups are substituted, tautomerism is favoured giving oxo-species such as **L4** and **L10**. Attempted treatment of **L10** with phosphorus oxychloride did not give the anticipated **306**.

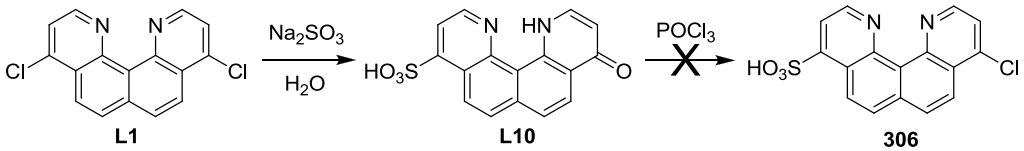

*Scheme 3.9: Synthesis of 9-oxo-9,12-dihydroquinolino[7,8-h]quinoline-4-sulfonic acid, **L10***

Alkoxides may be used to exchange the chlorides with ether linkages. A greater range of solvent solubility was required for **L1** as it was only soluble in halogenated solvents. An analogous reaction has been achieved with 4-chloroquinoline.[113]

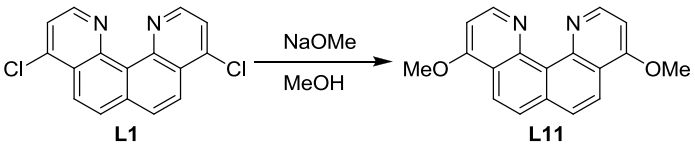

*Scheme 3.10: Synthesis of 4,9-dimethoxyquino[7,8-h]quinoline, **L11***

The displacement of the chlorides by methoxide substitution proceeded smoothly and gave the di-substituted product; **L11** (Scheme 3.9). This was fully characterised and was resistant to the tautomerism observed for **L4** and **L10**. This was exemplified when **L11** was heated to dissolution in DMSO and upon slow cooling gave crystals of **L11**. The asymmetric unit consisted of three molecules of the neutral form of **L11**. As the methoxide moieties are poor leaving groups, the observed tautomerism in **L4** and **L10** did not occur. The only solvent with good solubility for **L11** was methanol.

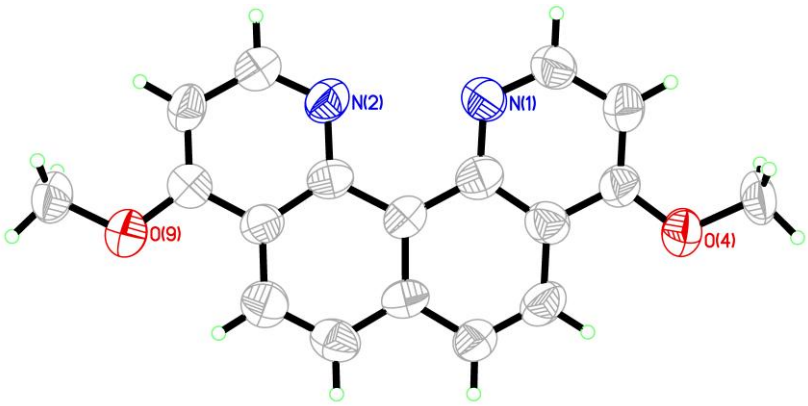

*Figure 3.16: Crystal structure of **L11**, ellipsoids drawn at the 50% probability level*

Aside from long range C-H π interactions, there were no notably strong packing interactions within the crystal (Figure 3.17). The three molecules of **L11** in the asymmetric unit had N1-C17-C13-N2 torsion angles of 13.73(49), 8.83(49) and 8.13(50)^{o}; less than the twisting in the crystal structure of the neutral form of **L1** discussed in Chapter 2; 20.02(9)^{o}. As both the chloride and methoxide substituents are electron withdrawing groups, the larger twisting observed for **L1** is likely primarily due to the interaction between the heterocyclic nitrogens and the hydrogens on the two chloroform solvent molecules with the crystal structure. There were no solvent molecules in the crystal structure of **L11** suggesting the torsion angles are representative of a neutral quino[7,8-*h*]quinoline molecule in the relaxed state.

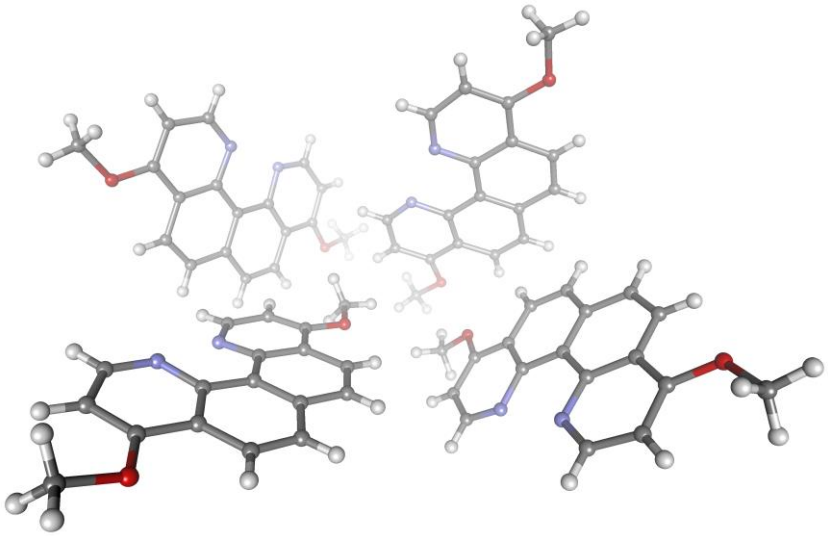

*Figure 3.17: Crystal packing of **L11***

A manganese-catalyzed cross-coupling reaction could potentially be used to replace the chlorides with a range of alkyl groups (Scheme 3.11). This should give better solubility in petroleum-based solvents, i.e. those which would be used in an industrial extraction of beryllium from an aqueous waste source. This reaction has been investigated successfully with 4-chloroquinoline.[116]

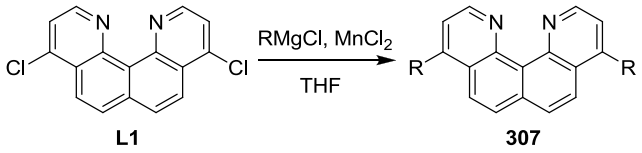

L1 **307**

*Scheme 3.11: General scheme for the synthesis of alkyl-substituted **307**, R = alkyl group*

The alkylation of **L1** by manganese cross-coupling substituted at the chloro 4,9-positions; however, the 2,11-positions were also alkylated. The electron withdrawing effect of the nitrogen heteroatoms likely made the adjacent 2,11-positions more electropositive. With four possible sites of substitution, a number of products were observed by MS. By varying the ratio of tertiary butylmagnesium chloride and the temperature it was possible to change the ratio of products but never to a single product, so this route was abandoned. The products all had similar polarity and solubility so purification was not possible.

In order to access a range of other substitutions, it was desirable to have bromides instead of the chlorides at the 4,9-postions of **L1**. For Suzuki couplings,[117, 118] the bromide is several orders of magnitude more reactive than the chloride. This was achieved by reacting **308** with phosphorus oxybromide in place of phosphorus oxychloride in the substitution step (Scheme 3.12). Bromination of **308** using phosphorus oxybromide proceeded analogously to the reaction with phosphorus oxychloride. An increase in the reaction time and temperature was required to achieve efficient conversion of **308** to **L12**, 120 to 200 ^{o}C and 8min to 30min. It was possible to achieve useful quantities of **L12** for further reactions with the yield being on par with the analogous reaction with phosphorus oxychloride. Suzuki coupling reactions and conversion of the bromides into carboxylic acids is the

current focus of our research group. As a dicarboxylic acid, a potentially novel building block in the synthesis of metal organic frameworks may be achieved.

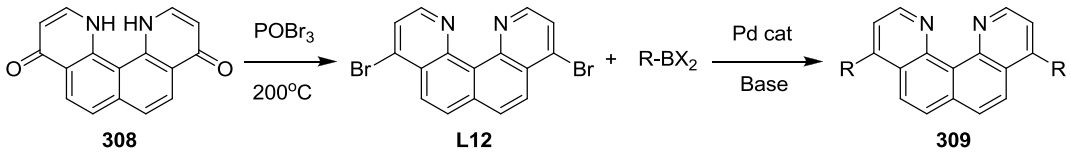

308 **L12** **309**

*Scheme 3.12: Proposed generalised Suzuki coupling reaction with **L12***

Given the crystal structure of **L7** showed a tautomer had formed, there is clearly a substituent influence on the basicity of each ligand. Due to the large differences in solubility of each ligand, measurement of the pK_{BH+} would not offer direct comparison between the series of quino[7,8-*h*]quinolines. Measurement of the ^{1}H NMR shift of the NH shift is also not directly related to pK_{BH+} of proton sponges as this depends on the molecular structure of the compound and the solvent used for measurements. For example;

Compound	Solvent	^{1}H NMR NH Shift (ppm)	pK_{BH+}
L2	DMSO-d6	19.4	12.8
L3	CD_3CN	18.6	18.2
L3	$DMSO/H_2O$	9.5	12.1
310	CD_3CN	14.3	25.1

Table 3.1: Lack of relationship between ^{1}H NMR NH shift and pK_{BH+}

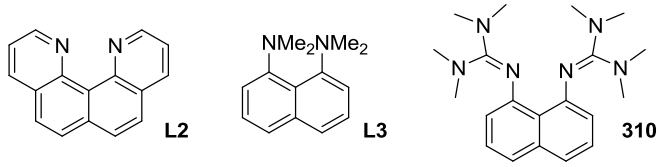

L2 **L3** **310**

Figure 3.18: Proton sponges with different chemical environments

As our series of compounds all had the same molecular cavity so long as the solvent environment was identical, the relative basicity could be investigated by looking at the NH shift. In this particular solvent system, 2:1 DMSO-d6 / MeOD, the NH shift was not as far downfield as in polar aprotic solvents; however, the relative magnitude of each shift reflects

the basicity. When the ^{1}H NMR sprectra were recorded immediately after dissolution, the exchange of the NH proton due to MeOD was not a problem.

4,9 Substituents	δ NH ppm[a]	Charge N[b]
L7; 2x NH-Ph	18.80	-0.241030, -0.232271
L6; 1x NH-Ph, 1x Cl	16.44	-0.251407, -0.193139
L5; 1x O-Ph, 1x Cl	15.76	-0.244144, -0.197436
L11; 2x O-Me	15.68	-0.227521
L2; 2x H	15.63	-0.212772
L1; 2x Cl	15.40	-0.214037

Table 3.2: Relative basicity of quino[7,8-h]quinolines, [a] 2:1 DMSO-d6 / MeOD, acetate salt, referenced to DMSO-d6 at δ 2.50, [b] B3LYP, 6-311++g(2d,p)

The calculated Mulliken charge on the central nitrogens becomes more negative as the NH shift of each compound increases. A greater negative charge suggests a stronger attraction for initial protonation. The NH shift is not solely related to the charge. The ^{1}H NMR shifts of aromatic hydrogens are strongly deshielded by the aromatic ring. This is due to the ring current, which is the circulation of delocalised π electrons producing a small local magnetic field. It is reasonable to assume that an increase of electron density into the heterocyclic ring system from electron donating substituents will enhance this ring current. Hence the NH shift is more than 3 ppm downfield when the ring has electron donating substituents.

3.3 Modification of 2,11 Substitution of Quino[7,8-*h*]quinoline

3.3.1 Results / Discussion

In the Staab synthesis pursued in Chapter 2, the esters on **311** were cleaved; however, a reaction directly with phosphorus oxychloride led to a new methyl ester substituted proton sponge **L13** (Scheme 3.13). The methyl esters provided a scaffold for potential further modification to create molecules which could fully encapsulate beryllium. To the best of our knowledge, this is currently the only confirmed quino[7,8-*h*]quinoline with 2,11 substitution and the best chance to create a tetra-coordinate ligand.

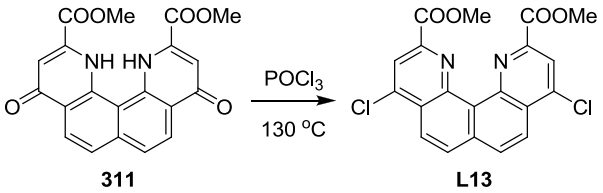

Scheme 3.13: Synthesis of dimethyl 4,9-dichloroquinolino[7,8-h]quinoline-2,11-dicarboxylate, ***L13***

A crystal structure of the protonated **L13** confirmed the esters were retained during this reaction. The tetrafluoroborate salt was obtained from a reaction with boron trifluoride diethyl etherate and crystals were formed by vapour diffusion of diethyl ether into acetonitrile (Figure 3.19). The asymmetric unit consisted of two molecules of **L13** and two tetrafluoroborate anions. The protons on N2 and N2B (from the second molecule in the asymmetric unit) were found via the fourier difference map.

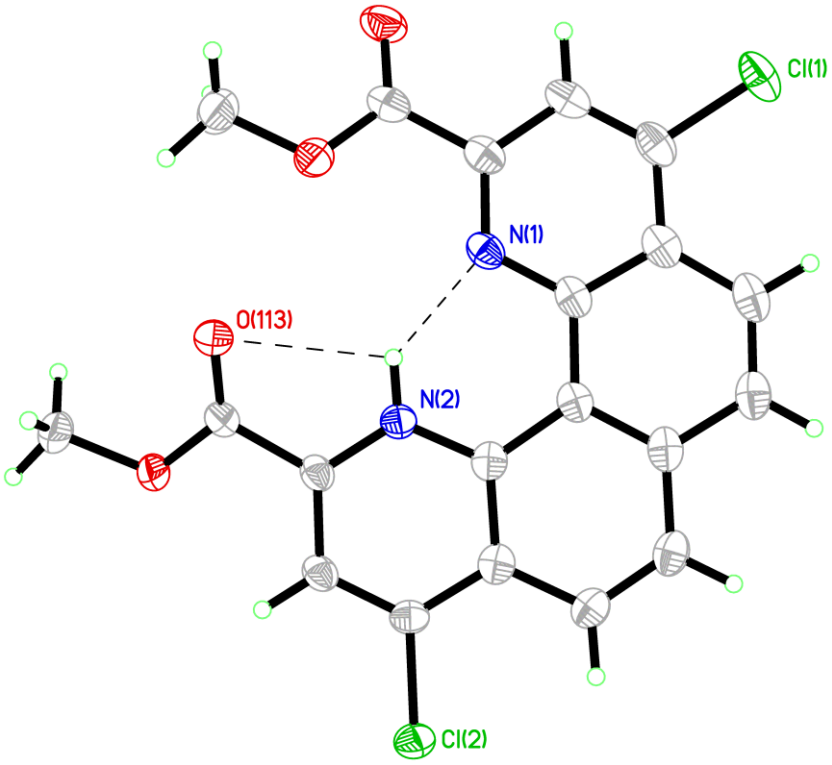

*Figure 3.19: Crystal structure of [H(**L13**)][BF_4] showing H2 close contacts, ellipsoids drawn at the 50% probability level*

An important distinction between this molecule and the crystal structures of other protonated proton sponges was that there was no auxiliary three-centred hydrogen bonding from anions or solvent to the central proton.[109] The three-centred hydrogen bond now consisted of an interaction between N1 and N2 and between N2 and O113.

N – H (Å)	**N – X (Å)**	**N – H – X (°)**
N2-H2 1.9500(3)	N2-N1 2.643(3)	N2-H2-N1 135.00(3)
O113-H2 2.4800(3)	O113-N1 2.790(3)	N2-H2-O113 101.00(3)
N1-H2B 1.9600(3)	N1-N2 2.646(3)	N1-H2B-N1 135.00(3)
O31B-H2B 2.3900(3)	O31B -N1 2.730(3)	N2-H2B-O31B 103.00(3)

*Table 3.3: Important bond lengths and angles associated with the hydrogen bonding of H2 and H2B in [H(**323**)][BF_4]*

The crystal packed primarily through anion-π interactions and similar π contacts with the chlorides and carbonyl oxygens. There was only very weak π-π stacking present due to the

large offset of adjacent heterocycles. The closest contacts are shown in Figure 3.19; F8 – Cg1 3.265(2) Å, B2 – F8 – Cg1 114.28(15)°, B2 – Cg1 4.052(4) Å and Cl2 – Cg2 3.4084(13) Å, C9 – Cl2 – Cg2 79.06(9)°, C9 – Cg2 3.514(3) Å.

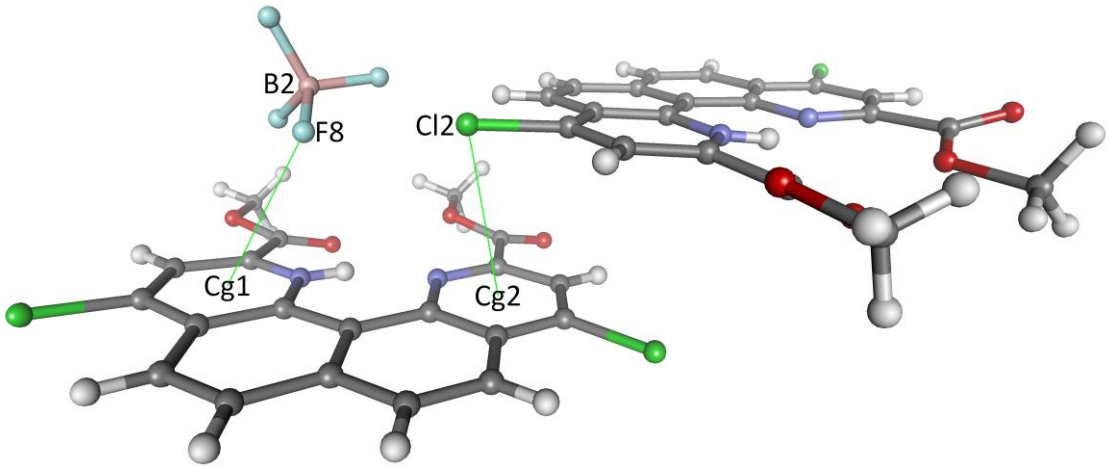

*Figure 3.20: Crystal packing of [H(**L13**)][BF_4]*

The methyl esters appear to shield the proton binding site. In a recent review chapter on proton sponges,[119] the authors proposed that four criterion needed to be met for a molecule to be classified as a proton sponge and that the unsubstituted quino[7,8-*h*]quinoline was in violation of the fourth requirement. That is, there needed to be the presence of a hydrophobic environment at the nitrogen atoms to account for the low rate of proton addition – elimination and to prevent coordination of all Lewis acids except the proton. In reality, there is no molecule which matches all the criteria perfectly. The original proton sponge, 1,8-*bis*(dimethylamino)naphthalene, **L3**, has been shown to complex to boron.[98] It would appear that **L13**, meets the criterion of a proton sponge more effectively in this case as the cavity can only support a proton due to the greater steric influence of the methyl esters.

The previously reported[120] crystal structure of the analogous tetrafluoroborate salt of **L3** also reveals there were no significant auxiliary hydrogen bonding interactions. A symmetry generated tetrafluoroborate lies above the proton cavity, Figure 3.21, but the short contacts exceed what would be considered weak hydrogen bonding. For a molecule based on quino[7,8-*h*]quinoline, **L13** replicates this shielding of the proton well.

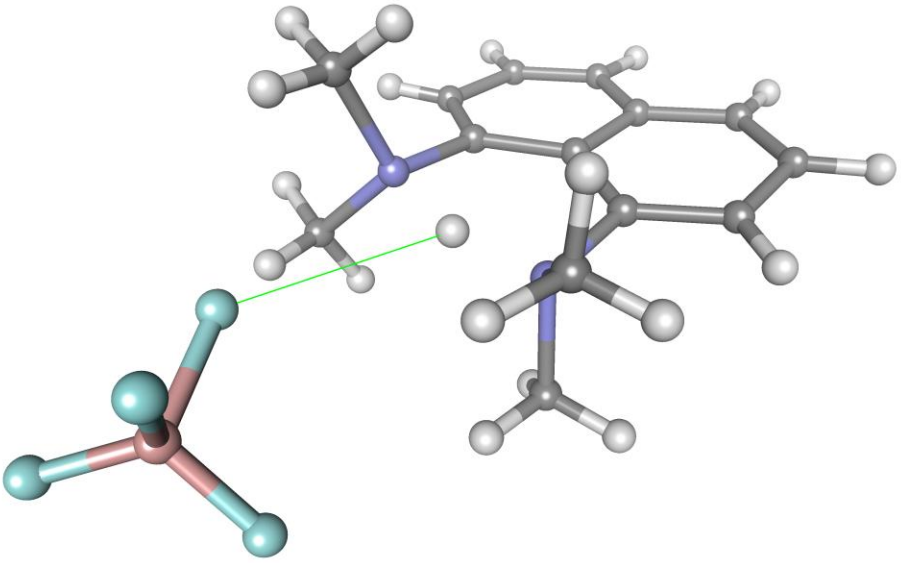

*Figure 3.21: Crystal structure of [H(**L3**)][BF_4] with a long range contact to a BF_4^- anion*

As we were interested in coordinating more than just a proton, it was necessary to modify the methyl esters to reduce steric hindrance and incorporate additional donors. While sterically encumbered beryllium complexes can adopt flattened geometries in special cases,[63, 121] they are unstable and hydrolyse readily.[121] Direct ester hydrolysis of **L13** to **312** would provide additional donors for coordination to beryllium, but, be limited due to the rigid geometry of the donor set (Scheme 3.14). The ester hydrolysis of **L13** was attempted; however the insolubility of the resulting compound made characterisation difficult. Attempts to re-crystallise the insoluble product by slow cooling in hot DMSO to obtain crystallographic evidence of the structure were unsuccessful.

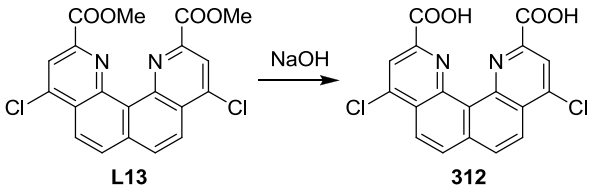

L13 **312**

*Scheme 3.14: Proposed ester hydrolysis of **L13***

While it would be interesting to test whether **312** formed a four coordinate species with beryllium, an extra CH_2 group placed at the 2,11 substituents should enhance the flexibility

of the donor set to allow six-membered chelate ring formation (Scheme 3.15). A possible route could proceed via the following transformations; reduction of **L13** should give **313**, activation of **313** with a suitable protecting group followed by nucleophilic substitution should lead to **315**, extending the substituents by one carbon each. Functionalisations of the nitrile would then give the desired geometry to create a tetrahedral binding pocket.

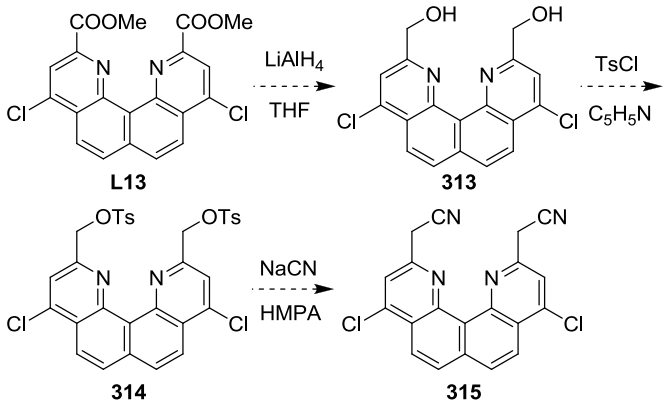

Scheme 3.15: Proposed synthesis of 2,2'-(4,9-dichloroquinolino[7,8-h]quinoline-2,11-diyl)diacetonitrile, ***315***

Finally, hydrolysis of **315** would give **316** as shown in Scheme 3.16. This is one example of the range of potential functionalisations of **315**.

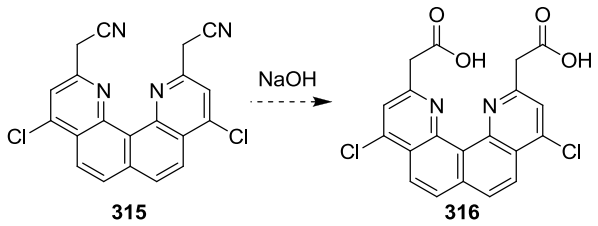

Scheme 3.16: Proposed synthesis of 2,2'-(4,9-dichloroquinolino[7,8-h]quinoline-2,11-diyl)diacetic acid, ***316***

The first step was to convert the esters of **L13** into functional groups capable of further modification; in this case an alcohol was necessary. Two methods which could achieve this are lithium aluminium hydride reduction[122] or sodium borohydride / methanol reduction.[123]

Under standard conditions, the reduction with lithium aluminium hydride showed none of the desired product by mass spectrometry. This may be due to coordination of lithium to

the ligand causing deactivation. Sodium borohydride / methanol reduction did show some of the correct product by mass spectrometry, however, the reaction did not proceed cleanly as a number of side reactions occurred. Unfortunately, once the solvent was removed from the reaction mixture a completely insoluble precipitate developed. **313** might have been stabilised by solvent in solution and strong intermolecular hydrogen bonding could give the insoluble precipitate. Another possibility is the formation of a coordination polymer as deprotonation of the alcohol moieties, due to the high basicity of the ligand could allow side reactions to occur, e.g. nucleophilic displacement of the chlorides.

To elucidate what was occurring, it was necessary to isolate the esters and eliminate potential side reactions. One potentially novel route to achieving this was to form **317** (Scheme 3.17). Substituting the chlorides and blocking basic nitrogen centre, may avoid the potential side reactions encountered earlier. Substitution with *t*-butylphenol and subsequent oxidation upon purification should lead to **317**.

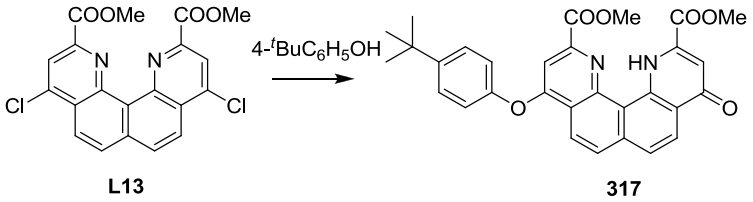

L13 **317**

*Scheme 3.17: Proposed limitation of side reactions through substitution of the chlorides on **317***

The substitution of both chlorides (as evidenced by MS) was achieved by refluxing in toluene for four hours. In contrast to **L1** where only mono-substitution occurred, the greater solubility due to the presence of the ester groups allowed both chlorides to be displaced. Unfortunately the tautomerism which occurred for **L4** could not be reproduced to give **317**, which would have enabled purification by column chromatography. Unlike the tautomer **L4** which could be purified by chromatography, the products associated with the attempted formation of **317** were inseparable. It seemed polymerisation was occurring as suggested by the streaking on the silica column and the lack of discrete products separated. The reaction also did not proceed using a stoichiometric quantity of *t*-butylphenol, the protonated form of **L13** was predominantly formed.

Given the time constraints on the project, it was not possible to post-synthetically modify **L13**; creating tetra-coordinate ligands in this manner had to be abandoned.

3.4 Summary

The modification of quino[7,8-*h*]quinolines was difficult due to the insolubility of the products obtained and inability to purify using conventional chromatography or recrystallisation techniques. In spite of this, reactions which lead to single products could be fully characterised. Substitution of **L1** with oxygen linked substituents lead to nucleophilic substitution of both substituents followed by hydrolysis and tautomerism of one when the substituent was a good leaving group (Scheme 3.18). The exception was found when methoxy groups were substituted, **L11**, which are relatively poor leaving groups and gave the di-substituted compound more stability.

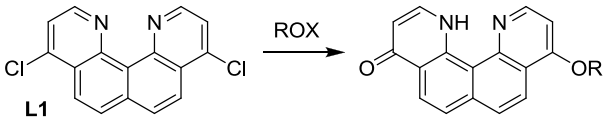

*Scheme 3.18: Generalised tautomerised product when oxygen-containing groups were substituted, this occurred for **L4** and **L10***

When possible, treatment with phosphorus oxychloride could reform the full heterocyclic ring system creating novel unsymmetrical compounds such as **L5**.

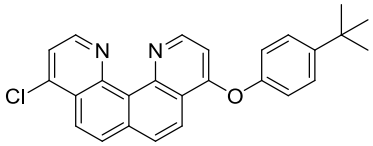

*Figure 3.22: 4-(4-tert-Butylphenoxy)-9-chloroquinolino[7,8-h]quinoline, **L5***

Mono- or di-substitution of anilines onto **L1** could be achieved by altering the reaction conditions and using the solubility of the product in the reaction mixture. Mono-substitution occurred by refluxing in toluene where the precipitated product could be purified by filtration to give **L6**. Di-substitution was achieved in the melt of the appropriate aniline at a slightly higher temperature to give **L7**. Both **L6** and **L7** showed tautomerism

similar to that observed in Scheme 3.18, however, rather than hydrolysis, one of the nitrogens adopted partial double bond character, Scheme 3.19.

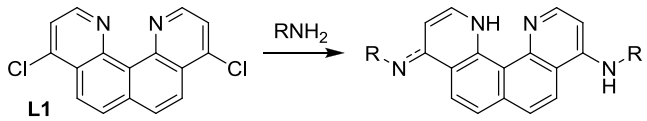

Scheme 3.19: Generalised tautomerised product when anilines were substituted

With a suitable choice of aniline, the substituents of gave rise to fluorescence due to enhanced π-delocalisation across the entire molecule. The protonated form of **L8** is worthy of further investigation to exploit the fluorescent properties of the molecule. Fluorescent dyes are often attached to light harvesting devices such as dye-sensitised solar cells.[124]

Nitration of **L1** lead to substitution of two nitro groups at positions previously inaccessible, **L9**, if required these could act as points for further substitution or attachment to polymers or surfaces.

The ^{1}H NMR shift of the proton bound (in the protonated form of the molecules) between the nitrogen heteroatoms was shifted further downfield when electron-donating substituents were present, **L7**. This trend was reflected in the calculated charge on nitrogen atoms which became more negative with increased electron-donation into the heterocyclic ring system.

Despite showing promise for creation of a four coordinate ligand, which might fully encapsulate beryllium, modification of the 2,11 positions on **L13** with useful functional groups proved technically difficult and had to be abandoned due to time constraints.

Chapter 4: Coordination Chemistry of Proton Sponges

4.1 Complexation of Proton Sponges to Boron

4.1.1 Introduction

Boron was used as a size analogue for beryllium to better study small cation complexation to proton sponges. Boron complexes have received attention for their potential use as fluorescent dyes. For example, boron-dipyrromethene complexes are known to have intense fluorescence quantum yields. An example is a paper which utilised the ligands shown in Figure 4.1 reported quantum yields in the range of 0.56 – 0.98.[125] These had sharp excitation and emission bands with small Stokes shifts.

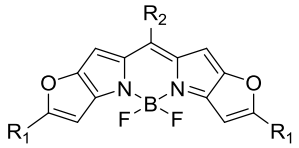

Figure 4.1: Example of a boron-dipyrromethene complex with a high quantum yield

Complexes of boron with bidentate neutral N-donor ligands are reasonably well documented. A paper published by Hartman and Shoemaker,[98] dealt with the ligands 2,2'-bipyridine, 1,10-phenanthroline, and **L3** (Figure 4.2).

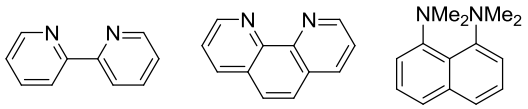

Figure 4.2: Neutral nitrogen donor ligands reported to complex boron; 2,2'-bipyridine, 1,10-phenanthroline, and 1,8-bis(dimethylamino)naphthalene respectively

All were shown to form difluoroboron and dichloroboron cations and all except DMAN could form dibromoboron cations. All complexes were analysed by ^{19}F and ^{11}B NMR and Mass Spectrometry. There is currently no crystallographic structural evidence for these compounds. The flexibility imparted by the backbone of the dipyrromethene unit allows all boron and transition metal complexes to be planar. Based on the two known transition metal structures, the rigidity of the fully aromatic quino[7,8-*h*]quinoline proton sponge scaffold meant transition metal complexes had large out of plane distortions (Figure 4.3).[72] Coordination of a smaller cation such as B(III) to these types of proton sponge types should offer a better size fit.

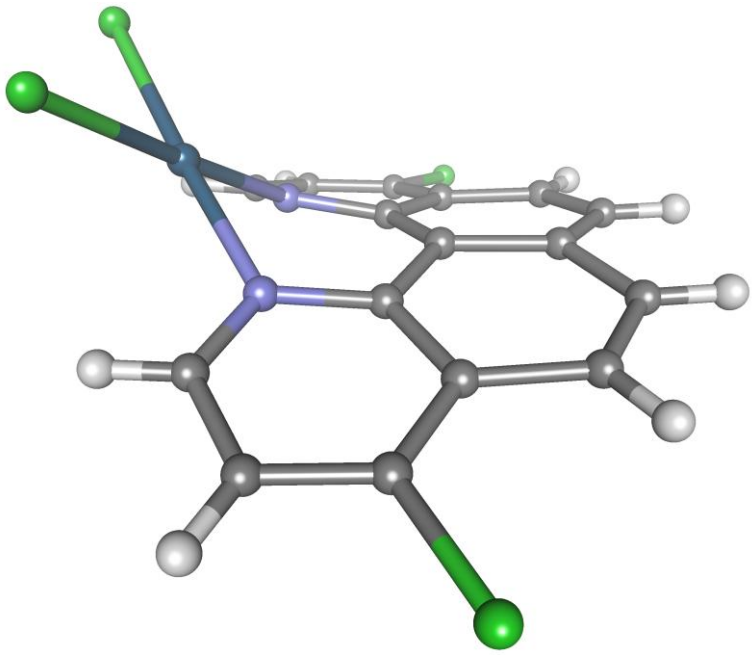

*Figure 4.3: Perspective view of the crystal structure of [Pt(**L1**)Cl_2]*

4.1.2 Results / Discussion

Boron trifluoride diethyl etherate was added to **L1** (Figure 4.4) in dry CH_2Cl_2 and a precipitate of [BF_2(**L1**)][BF_4] formed immediately. The precipitate was washed with diethyl ether and was crystallised by vapour diffusion of diethyl ether into an acetonitrile solution containing the complex.

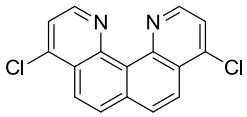

*Figure 4.4: 4,9-Dichloroquino[7,8-h]quinoline, **L1***

Pale yellow prismatic crystals suitable for X-ray determination were obtained. These crystals darkened in the presence of light so the crystallisation setup was kept in the dark. A side-product later identified to be [H(**L1**)][BF_4] also crystallised co-currently as yellow needles, the crystal structure was discussed in Chapter 2.

The crystal structure of [BF_2(**L1**)][BF_4] had space group $P2_1/n$ and the asymmetric unit consisted of one boron difluoride cation of **L1** balanced by one disordered tetrafluoroborate anion (Figure 4.5). The crystal structure revealed **L1** had a flattened aromatic ring system with the boron ion located only slightly above the mean plane of the aromatic ring (0.096(6) Å, the mean plane was calculated using the five central atoms N1, C17, C15, C13, N2). This was analogous to the crystal structure of [H(**L1**)][BF_4] discussed in Chapter 2 (Figure 2.16) where the aromatic rings were flattened compared to the torsional twist present in the crystal structure of neutral **L1** (Figure 2.12). Thus, the cavity of **L1** was an ideal size to support the small B(III) cation.

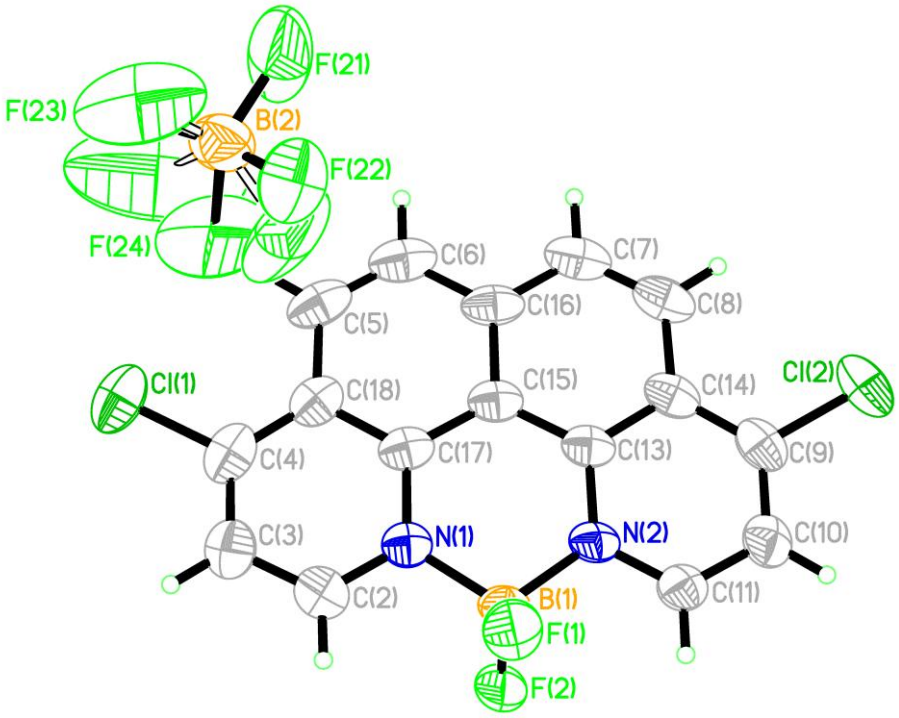

*Figure 4.5: Side view of the crystal structure of [BF_2(**L1**)][BF_4], ellipsoids drawn at the 50% probability level*

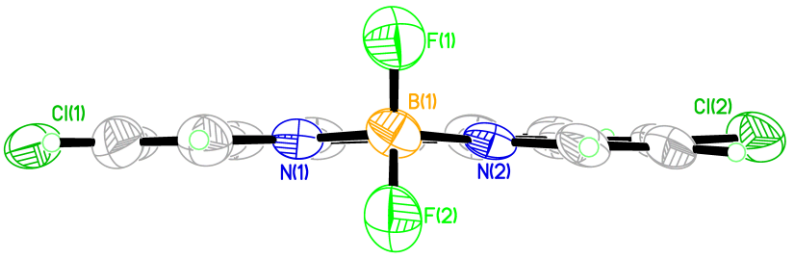

*Figure 4.6: Top view of the crystal structure of [BF_2(**L1**)][BF_4], (tetrafluoroborate anion not shown), ellipsoids drawn at the 50% probability level*

The chlorine atoms and the tetrafluoroborate anions prevent the close packing of the flattened ring systems such that only minor π-stacking interactions outside of what would be considered an interaction were present in the crystal (Figure 4.7).

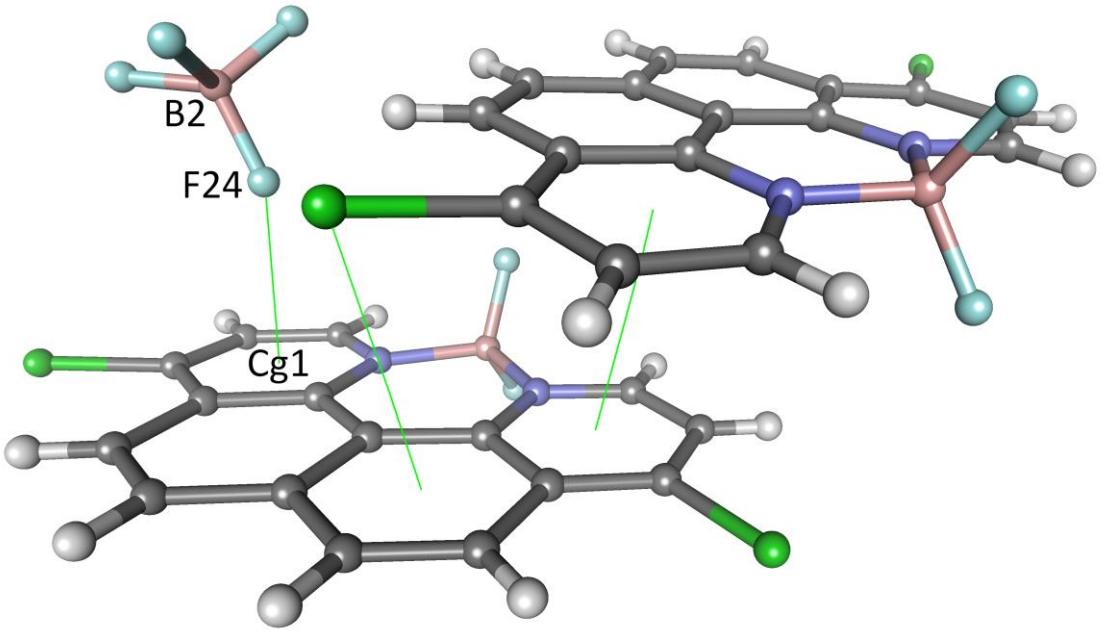

*Figure 4.7: Packing within the structure of [BF_2(**L1**)][BF_4]*

Recently, a series of theoretical studies[126-128] investigated the presence of favourable non-covalent interactions between electron deficient (π-acidic) aromatic rings and anions. These had binding energies comparable to hydrogen bonds (20 – 50 kJ/mol). The majority of reported anion-π interactions are longer than 3.0 Å and it is considered rare that the contacts are shorter than this. Such a contact with the tetrafluoroborate anions to the centroid of the ring containing both the chloride and ring nitrogen was observed (Figure 4.7); F24 – Cg1 2.808(8) Å, B2 – F24 – Cg1 145.5(8)°, B2 – Cg1 3.926(6) Å. This close interaction was presumably due to the electron-withdrawing effect of the ring nitrogen and the substituted chloride. There were no such interactions occurring on either of the two unsubstituted non-heterocyclic rings of the ligand. This distance is one of the shortest anion-π interactions that have been observed crystallographically.

An analogous reaction occurred with **L2** (Figure 4.8) and boron trifluoride diethyl etherate giving both [BF_2(**L2**)][BF_4] and the side product [H(**L2**)][BF_4] discussed in Chapter 2.

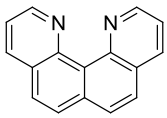

*Figure 4.8: Quino[7,8-h]quinoline, **L2***

The bulk of $[BF_2(\mathbf{L2})][BF_4]$ crystallised as needles, which did not diffract; however, a single prismatic crystal was identified that was suitable for X-ray determination. The crystal structure of $[BF_2(\mathbf{L2})][BF_4]$ grew in space group $P2_1/c$ and the asymmetric unit consisted of one boron difluoride cation of **L2** balanced by one tetrafluoroborate anion with one acetonitrile solvent molecule (Figure 4.9). The crystal structure had a similar flattened aromatic ring system to $[BF_2(\mathbf{L1})][BF_4]$ with the boron ion located 0.186(4) Å above the mean plane of the aromatic ring (Figure 4.10). This was further out of plane than the crystal structure for $[BF_2(\mathbf{L1})][BF_4]$ and the variation may be due to crystal packing.

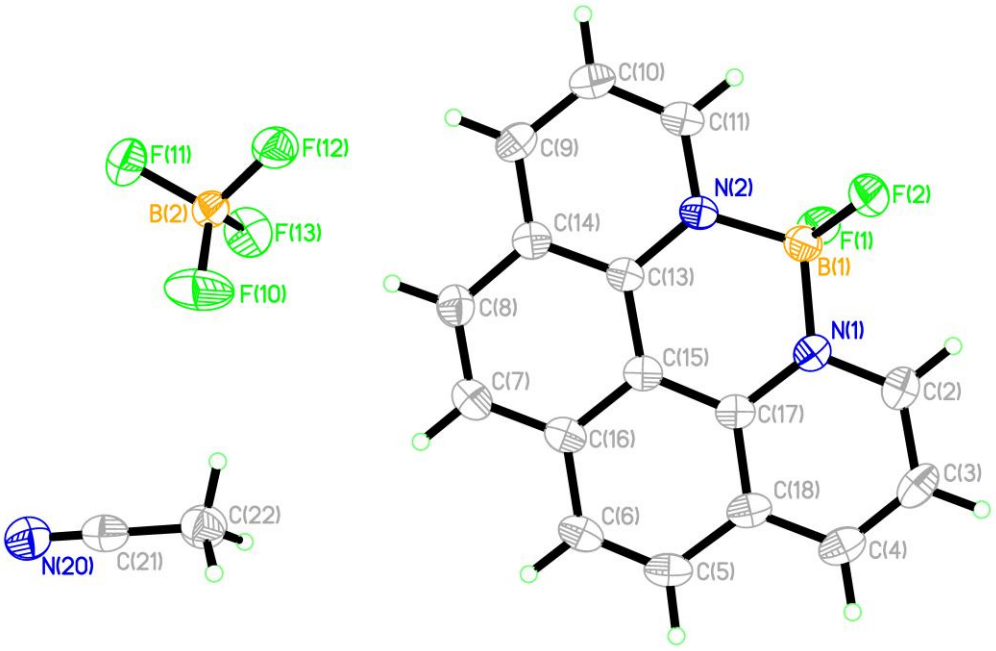

Figure 4.9: Side view of the crystal structure of $[BF_2(\mathbf{L2})][BF_4]$, ellipsoids drawn at the 50% probability level

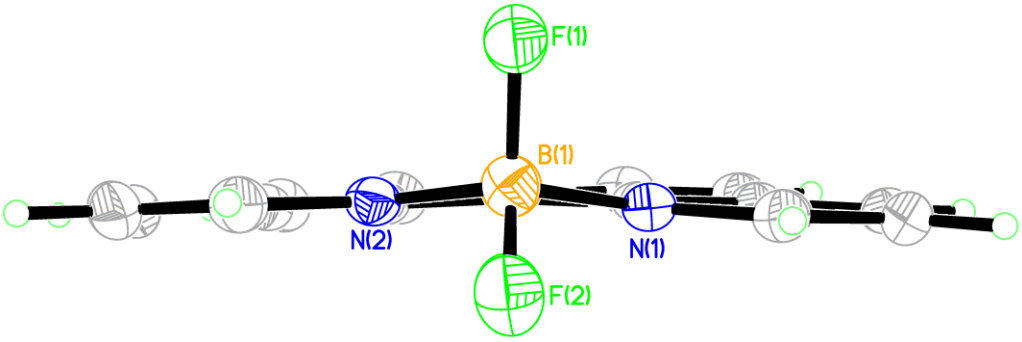

*Figure 4.10: Top view of the crystal structure of [BF_2(**L2**)][BF_4], ellipsoids drawn at the 50% probability level*

These crystals were suspected to contain ~10% of [BF_2(**L1**)][BF_4] present as indicated by a low percentage of electron density approximately 1.8 Å from C4 and C9. This contamination appeared to act as a template for crystal growth. The presence of **L1** in this crystal indicated the conversion of **L1** to **L2** was not fully completed; however, only a minute trace of **L1** was present. There were too few of these crystals to run an elemental analysis.

In the absence of the chlorine substitution in the 4 and 9 positions of the ligand, the anion-π interaction is more diffuse and distributed across two six-membered rings (Figure 4.11); F12 – Cg1 3.288(2) Å, B2 – F12 – Cg1 124.63(16)^o, B2 – Cg1 4.249(3) Å and F12 – Cg2 3.326(8) Å, B2 – F12 – Cg2 108.59(15)^o, B2 – Cg2 4.004(3) Å. There are closer offset π-stacking interactions present within the structure than the analogous **L1** complex and also a π-ring interaction with the nitrogen on the acetonitrile solvent molecule is now present, interacting across two six-membered rings; N20 – Cg4 3.416(3) Å, C21 – N20 – Cg4 103.0(2)^o, C21 – Cg4 3.845(3) Å and N20 – Cg3 3.413(3) Å, C21 – N20 – Cg3 85.9(2)^o, C21 – Cg3 3.524(3) Å.

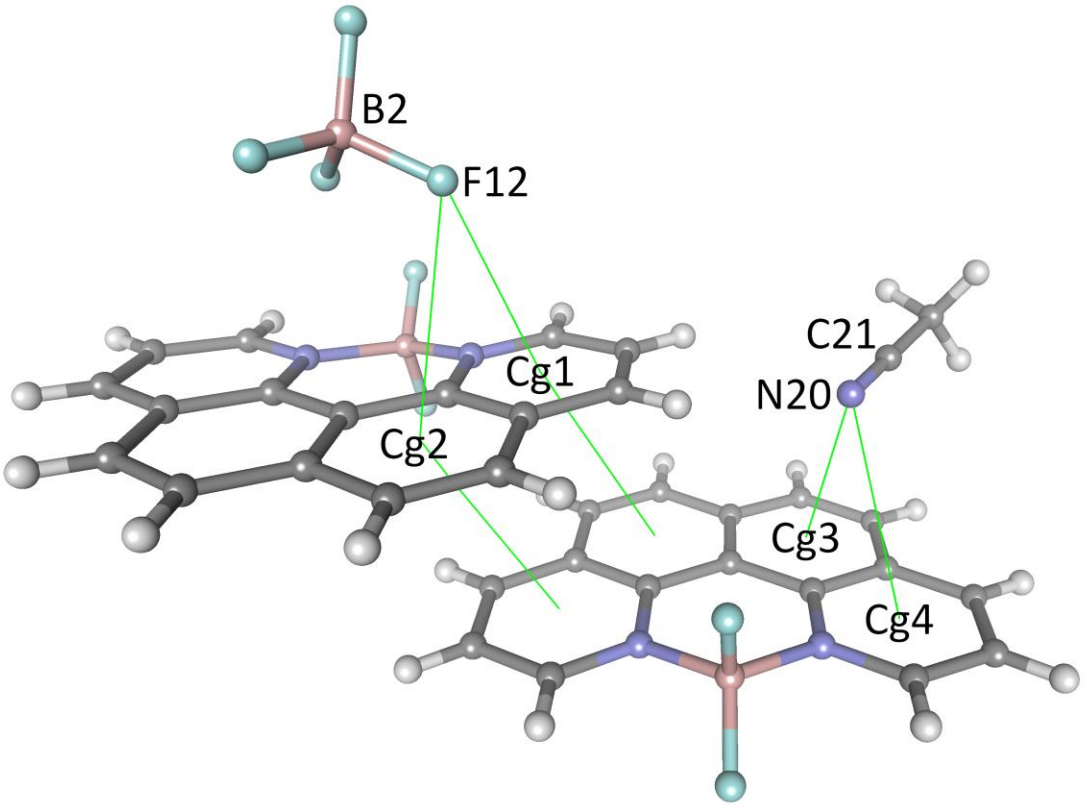

*Figure 4.11: Packing within the structure of [BF_2(**L2**)][BF_4]*

The platinum and rhenium ion complexes reported by Wustefeld and co-workers[72] had coordinated metal cations which were 0.999 Å and 1.133 Å respectively above the mean plane. In addition, there was significant bowing of the aromatic heterocycles to accommodate metal chelation which was in stark contrast to the flattened ring systems and minor deviation from the aromatic mean plane observed in the B(III) complexes.

The remaining ligands investigated in Figure 4.12 did not show conclusive coordination to B(III) for a number of reasons outlined below, these are shown.

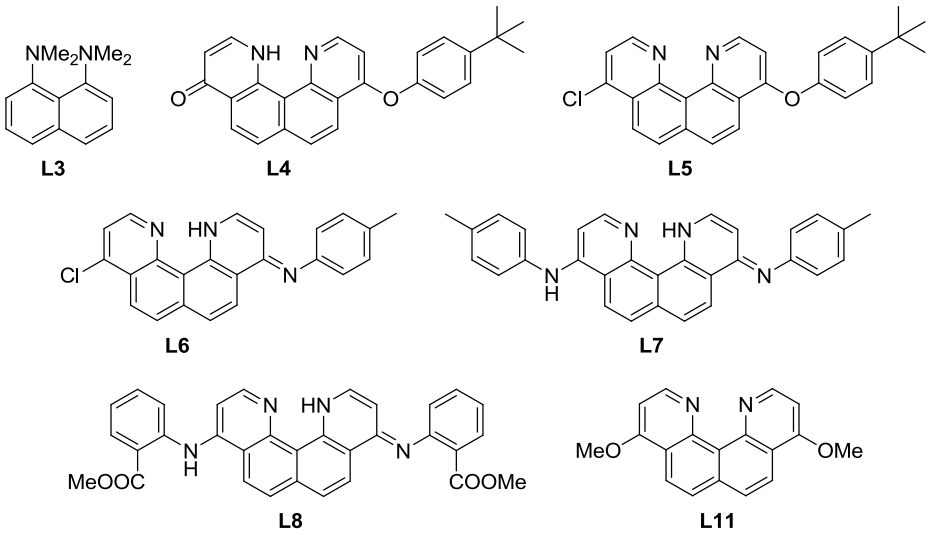

Figure 4.12: Ligands which did not show good coordination to B(III)

While the boron difluoride complex of **L3** has already been reported,[98] no crystal structure has been documented. For comparison purposes, crystallisation was attempted, however, due to the weak nature of the ligand and the oxygen free conditions required for the formation of the boron complex, no crystals were ever achieved. The ligand had a strong preference for hydrolysis and deposition of protonated **L3**.

L4 did not complex with boron trifluoride diethyl etherate. The hydrogen was not displaced by boron and **L4** was recovered unreacted. The reaction was repeated in the presence of a number of bases (NEt_3, *n*BuLi, NaH, NaOMe) none of which were capable of promoting the reaction.

L5 showed some coordination to boron; however, there was always a roughly equal ratio of the protonated species formed (according to the MS). Crystallisation could not be used to separate out the boron coordinated species for further analysis which was used successfully for **L1** and **L2**.

L6, **L7** and **L8** showed no coordination to boron. As noted in Chapter 3, they exist as a tautomer with one hydrogen located on a central heterocyclic nitrogen and one of the auxiliary nitrogens displaying partial imine behaviour. Attempting to use the bases as above for initial deprotonation did not allow coordination.

The limitation of **L11** to coordinate boron arose from the inability to dissolve in a suitable polar aprotic solvent necessary for the reaction with boron trifluoride diethyl etherate to occur. While **L11** has good solubility in methanol, the use of this solvent caused exclusive formation of the protonated species and could not be suppressed using the bases as above.

4.2 Spectroscopy of Boron Proton Sponge Complexes

4.2.1 Introduction

Boron-dipyrromethene (BODIPY) complexes are well-known as versatile fluorescent dyes with intense fluorescence quantum yields (Φ_F), sharp absorption and emission spectra, and high photo- and chemostability.[129] It was hoped that the rigid, planar fused aryl systems of the quino[7,8-*h*]quinoline-based proton sponges might give rise to a fluorescent complex when boron was coordinated.

The quantum yield (Φ_F) is the ratio of emitted photons to absorbed photons. When the correct equipment is not available to measure the absolute quantum yield, it is possible to measure the relative quantum yield.[130] This is achieved by relating the fluorescence efficiency of an unknown sample to a standard dye with known quantum yield. The equation is given below:

$$\Phi_{F(X)} = (A_S/A_X)(F_X/F_S)(n_X/n_S)^2\Phi_{F(S)}$$

A is the absorbance at the excitation wavelength, F is the area under the corrected emission curve (expressed as number of photons), and n is the refractive index of the solvents used. Subscripts s and x refer to the standard and the unknown respectively. A accounts for the number of absorbed photons, F accounts for the number of emitted photons and the refractive index is a correction factor.

4.2.2 UV-Vis Spectroscopy

The normalised UV-Vis spectra of $[BF_2(\mathbf{L1})][BF_4]$ and $[BF_2(\mathbf{L2})][BF_4]$ at 10^{-4} M are shown in Figure 4.13. The absorption spectrum for $[BF_2(\mathbf{L1})][BF_4]$ was slightly red-

shifted. This placed the tail of the absorbance at 389 nm into the visible region and the resulting solution was pale yellow compared to the colourless solution of $[BF_2(\mathbf{L2})][BF_4]$.

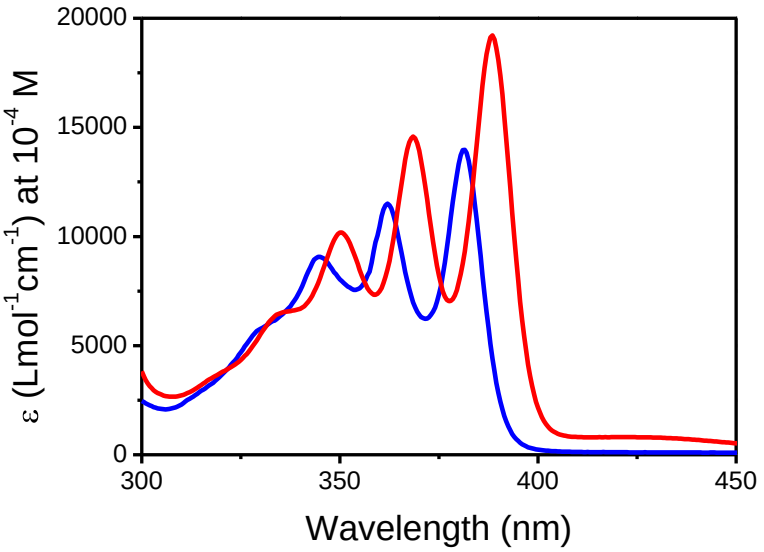

*Figure 4.13: UV-Vis spectra of $[BF_2(\mathbf{L2})][BF_4]$ (**blue**) and $[BF_2(\mathbf{L1})][BF_4]$ (**red**) showing the π – π* transitions at 10^{-4} M in MeCN*

The other main difference between the two complexes is the presence of a very weak charge transfer peak for $[BF_2(\mathbf{L1})][BF_4]$. The intensity of the π – π* transitions masks this at concentrations of 10^{-4} M shown in Figure 4.13. However, at 10^{-6} M (the concentration typically required for fluorescence quantum yield determination) a charge transfer peak at 422 nm for $[BF_2(\mathbf{L1})][BF_4]$ becomes more prominent (Figure 4.14). The prominence of the charge transfer band at low concentration suggests that quenching due to solute – solute interactions may occur at higher concentrations. The presence of halides is a known cause of fluorescence quenching, BODIPY dyes substituted with chlorides had very low quantum yields of less than 1%.[131] The chloride group is typically only used as a precursor to further functionalisation. The fluorescence resulting from excitation of this absorbance will be discussed in 4.2.3.

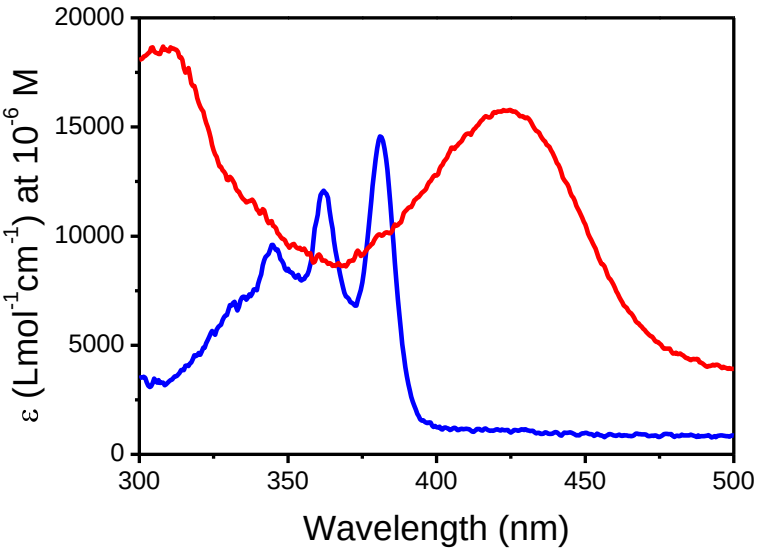

*Figure 4.14: UV-Vis spectra of [BF_2(**L2**)][BF_4] (**blue**) and [BF_2(**L1**)][BF_4] (**red**) showing the charge transfer peak for[BF_2(**L1**)][BF_4] at 10^{-6} M*

The UV-Vis spectrum of the protonated species; [H(**L1**)][BF_4], showed a red-shift relative to the neutral **L1**. When diluted to 10^{-6} M, a charge transfer peak at 427 nm for [H(**L1**)][BF_4], similar to that observed for [BF_2(**L1**)][BF_4], was present. The fluorescence resulting from excitation of this peak will be discussed in 4.2.3.

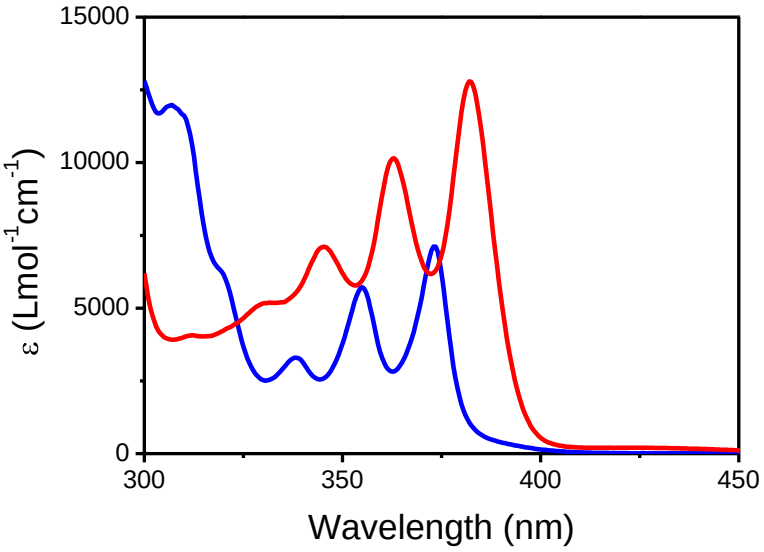

*Figure 4.15: UV-Vis spectra of **L1** (**blue**) and [H(**L1**)][BF_4] (**red**) showing the $\pi - \pi^*$ transitions*

A summary of the differences in the major peaks between the various forms of quino[7,8-*h*]quinoline at wavelengths longer than 300 nm is shown in Table 4.1. The last row contains the minor charge transfer peaks of [H(**L1**)][BF_4] and [BF_2(**L1**)][BF_4]. The peaks of [BF_2(**L1**)][BF_4] were slightly red-shifted relative to [H(**L1**)][BF_4] indicating different species were present and the boron complex had not merely hydrolysed to the protonated species.

L1	*[H(**L1**)][BF_4]*	*[BF_2(**L2**)][BF_4]*	*[BF_2(**L1**)][BF_4]*
-	331 nm	333 nm	336 nm
338 nm	346 nm	345 nm	350 nm
355 nm	363 nm	362 nm	369 nm
373 nm	382 nm	382 nm	389 nm
-	427 nm	-	422 nm

Table 4.1: Comparison of the π – π transitions and charge transfer peaks for quino[7,8-h]quinolines*

Theoretical structural optimisation of the boron difluoride complex of **L1** revealed that the location of the B(III) ion within the mean plane may be influenced by solvent interaction and or crystal packing. The crystal structure and computer model utilising a solvent model (acetonitrile) both showed the B(III) ion in a similar position close to the mean plane of the aromatic ring. The gas phase computer model placed the B(III) ion a relatively larger distance of 0.385 Å out of the plane of the ring. Hence, the acetonitrile solvent model was used for all further calculations.

[BF_2(**L1**)]$^+$	**Crystal Structure Å**	**Gas Phase Model[a] Å**	**Solvent Model MeCN[a] Å**
B1 – mean plane	0.096(6)	0.385	0.136
B1 – N1	1.566(6)	1.583	1.570
B1 – N2	1.564(7)	1.583	1.570
B1 – F1	1.360(6)	1.369	1.385
B1 – F2	1.367(6)	1.367	1.381

Table 4.2: Comparison of bond parameters for the B(III) ion between the crystal structure and calculated models, [a] B3LYP, 6-311++g(2d,p)

Next, calculations where the exchange correlation functionals were varied between B3LYP and OLYP were run. The basis set 6-311++g(2d,p) and an acetonitrile solvent model was used for both calculations. To assess which functional gave better precision, the IR spectrum of [BF_2(**L1**)][BF_4] and **L1** were measured and compared with the frequency output for each functional (Figure 4.16). The following scaling factors were used to correlate the measured and experimental frequencies; B3LYP – 0.9679[132] and OLYP – 0.9839.[133]

While the relative intensities were not predicted that well, the OLYP functional gave an overall better prediction of the relative spread of vibrational frequencies for [BF_2(**L1**)][BF_4]. The broad underlying peak around 1000-1200 cm^{-1} in the experimental spectra (**red**) is attributed to the tetrafluoroborate anion and were not present in the calculations of the [BF_2(**L1**)]$^+$ cation. The broad peak at 1000-1200 cm^{-1} is typical for tetrafluoroborate anions.[105]

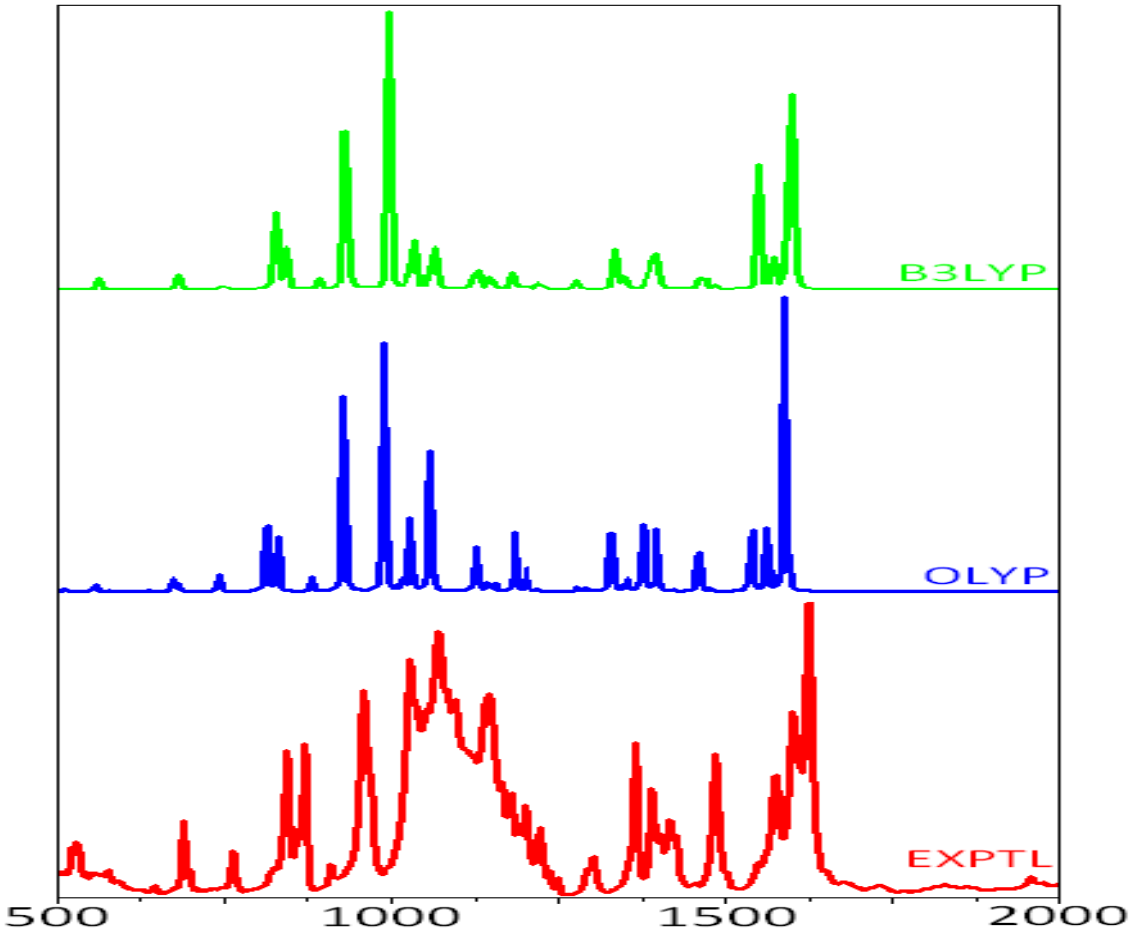

*Figure 4.16: Comparison between the IR spectra of [BF_2(**L1**)][BF_4]; measured as KBr disc (**red**), OLYP (**blue**) and B3LYP (**green**), the frequency is shown in cm^{-1}*

Both the OLYP and B3LYP functionals gave reasonable predictions of the vibrational frequencies for **L1**; OLYP predicted the relative spread and intensities slightly better (Figure 4.17).

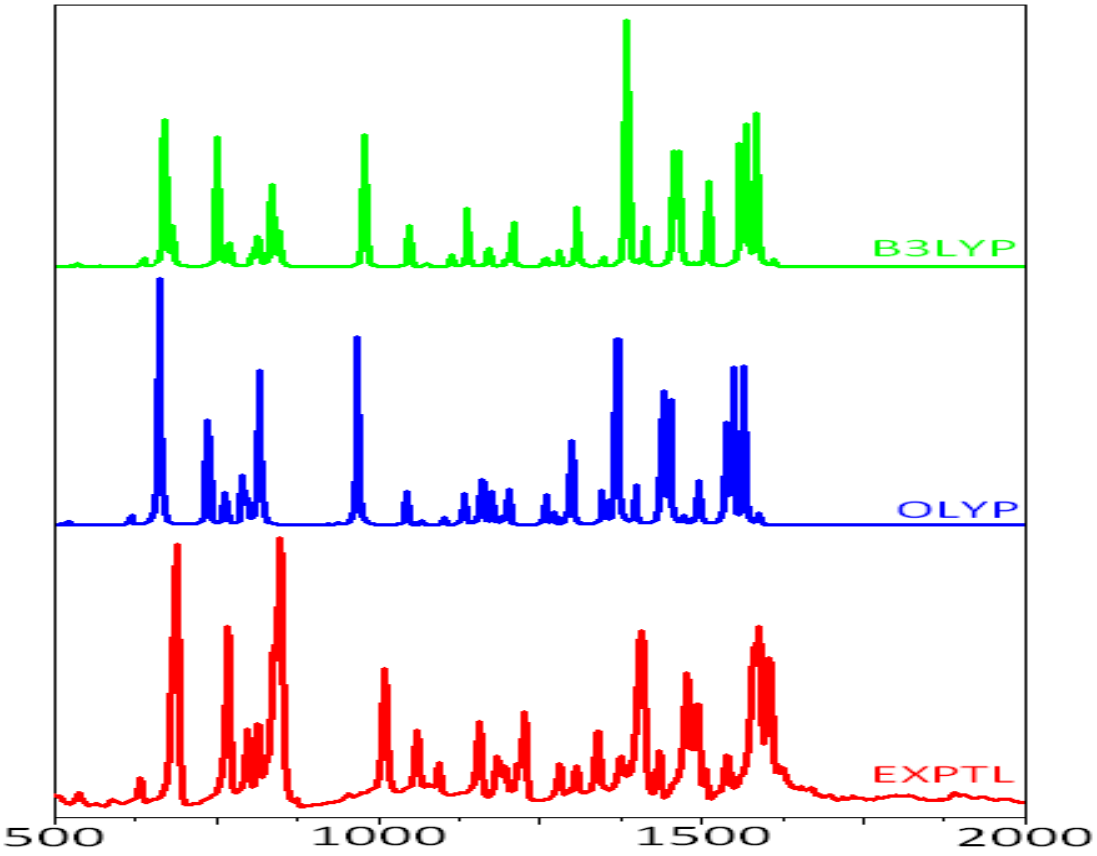

*Figure 4.17: Comparison between the IR spectra of **L1**; measured as KBr disc (**red**), OLYP (**blue**) and B3LYP (**green**), the frequency is shown in cm^{-1}*

The OLYP functional gave a substantially better model of the UV-Vis spectrum for $[BF_2(\mathbf{L1})][BF_4]$ than B3LYP (Figure 4.18).

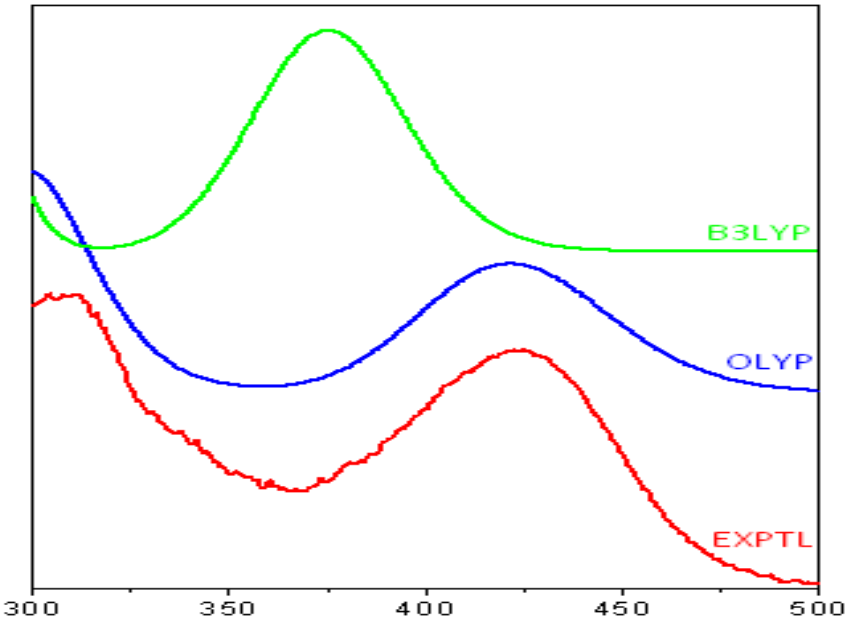

*Figure 4.18: Comparison between the UV-Vis spectra of $[BF_2(\mathbf{L1})][BF_4]$; measured in MeCN at 10^{-6} M (**red**), OLYP (**blue**) and B3LYP (**green**), the wavelength is shown in nm*

The UV-Vis spectrum for **L1** was not well predicted with either functional, however, OLYP gave a better account of the spectrum profile (Figure 4.19).

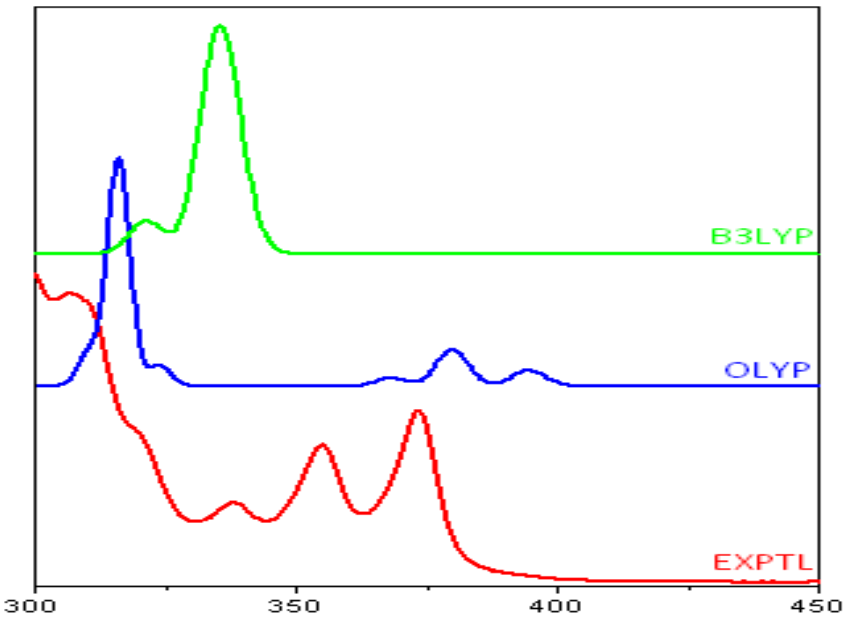

*Figure 4.19: Comparison between the UV-Vis spectra of **L1**; measured in MeCN (**red**), OLYP (**blue**) and B3LYP (**green**), the wavelength is shown in nm*

Overall, the OLYP functional was superior to B3LYP in this instance, and calculation of the molecular orbitals using this functional will be used when discussing the transitions which give rise to the observed fluorescence.

4.2.3 Fluorescence Spectroscopy

$[BF_2(\mathbf{L1})][BF_4]$ had a distinctive charge transfer peak at 422 nm. Excitation of the peak at 422 nm in a fluorometer showed an emission at 532 nm; none of the other absorbances were fluorescence active. $[BF_2(\mathbf{L2})][BF_4]$, did not fluoresce within several orders of magnitude of $[BF_2(\mathbf{L1})][BF_4]$, and the dye standards. The absorption and emission spectra of $[BF_2(\mathbf{L1})][BF_4]$ are shown in Figure 4.20.

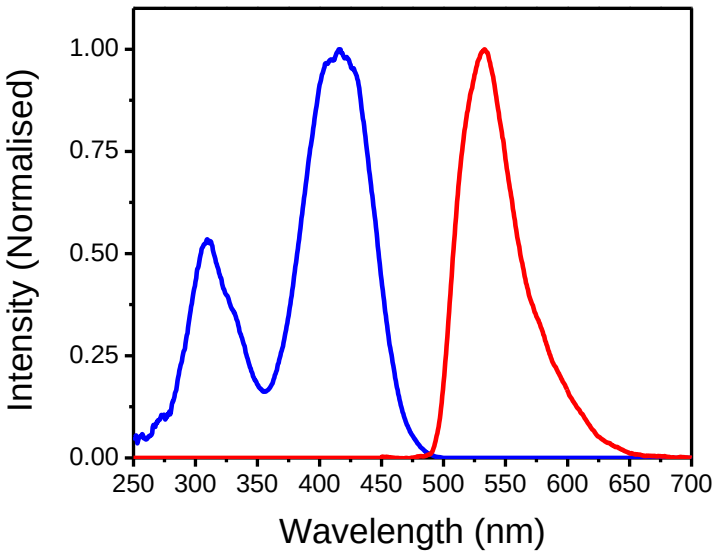

*Figure 4.20: Normalised absorption and emission spectra of $[BF_2(\mathbf{L1})][BF_4]$, absorption (**blue**) and emission (**red**)*

The major molecular orbitals which gave rise to the fluorescence are the HOMO and LUMO shown in Figure 4.21. The donor orbitals are the aromatic system as well as the *p* orbitals on the substituted chlorides. As the boron complex of **L2** (without chloride substitution) did not show this activity, electron donation from the chlorides appears to

make an important contribution to the fluorescence. The acceptor orbitals have contribution from the boron cation. The band gap difference between the HOMO and LUMO for the boron complexes of **L1** and **L2** was negligible suggesting the weak internal charge transfer occurring in $[BF_2(\mathbf{L1})][BF_4]$ offers an alternate route of deactivation of the excited state.

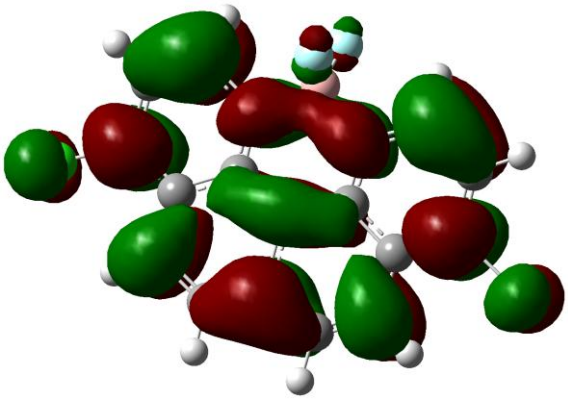

LUMO, -0.144 eV

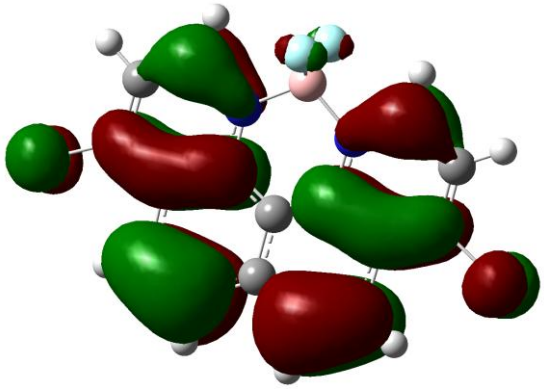

HOMO, -0.240 eV

Figure 4.21: Molecular orbitals associated with the fluorescence for $[BF_2(\mathbf{L1})][BF_4]$

The absorption and emission spectra of $[H(\mathbf{L1})][BF_4]$ had a similar, but, weaker profile to $[BF_2(\mathbf{L1})][BF_4]$. Excitation of the peak at 427 nm in a fluorometer showed an emission at 532 nm. Given the protonated species can illicit this emission, the fluorescence is clearly associated with an intra-ligand charge transfer attributed to flattening of the aromatic ring system, rather than being specifically due to coordination to boron.

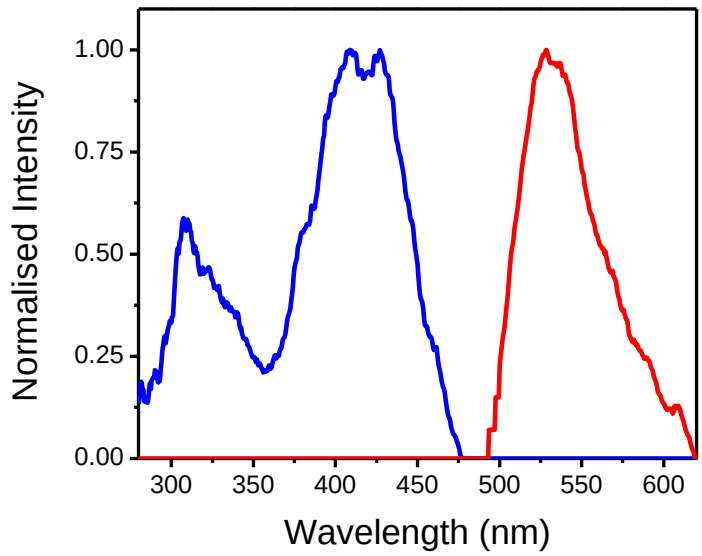

*Figure 4.22: Normalised absorption and emission spectra of [H(**L1**)][BF_4], absorption (**blue**) and emission (**red**)*

The major molecular orbitals which gave rise to the fluorescence were the HOMO and LUMO shown in Figure 4.23. In this instance the asymmetry of the molecule resulting from one of the nitrogens being protonated appears to account for the weak intramolecular charge transfer. As pictured in Figure 4.23, the donor orbitals are the aromatic system as well as the *p* orbitals on the substituted chlorides and the acceptor orbitals have contribution from the protonated nitrogen.

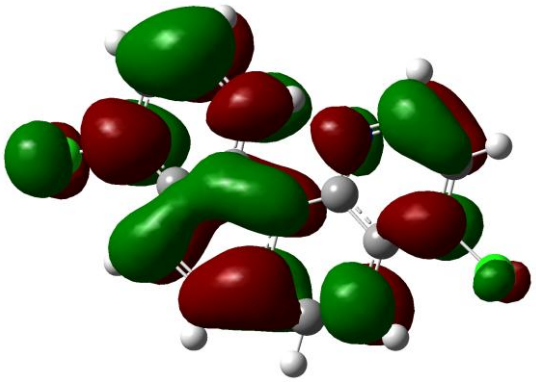

LUMO, -0.133 eV

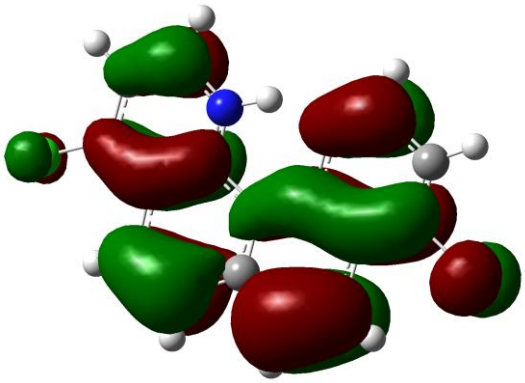

HOMO, -0.231 eV

*Figure 4.23: Molecular orbitals associated with the fluorescence for [H(**L1**)][BF_4]*

Coumarin 153 and acridine orange were selected as the two standards as they had similar absorption and emission profiles to [BF_2(**L1**)][BF_4], Appendix A.5.7 has the details for each dye. The following equation was used to compare the precision of the measured relative quantum yields of the two dyes and measure the relative quantum yield of [BF_2(**L1**)][BF_4] to both dye standards.

$$\Phi_{F(X)} = (A_S/A_X)(F_X/F_S)(n_X/n_S)^2\Phi_{F(S)}$$

The following table summarises these calculations.

Unknown (X)	Standard (S)	Literature Φ	Measured $\Phi_{F(X)}$
Coumarin 153	Acridine Orange	0.56[134]	0.47
Acridine Orange	Coumarin 153	0.20[135]	0.24
[H(**L1**)][BF_4], new[a]	Coumarin 153	-	0.03
[H(**L1**)][BF_4], new[a]	Acridine Orange	-	0.02
[BF_2(**L1**)][BF_4], new[a]	Coumarin 153	-	0.07
[BF_2(**L1**)][BF_4], new[a]	Acridine Orange	-	0.06
[BF_2(**L1**)][BF_4], old[b]	Coumarin 153	-	0.009
[BF_2(**L1**)][BF_4], old[b]	Acridine Orange	-	0.008

Table 4.3: Calculation of relative quantum yields, $\Phi_{F(X)}$, [a] fluorescence measured the same day the solution was prepared, [b] fluorescence measured after standing of the solution for one week

There is some discrepancy between the literature values of the standards and the measured relative quantum yield, however, the variation is acceptable for these types of experiments. Disappointingly, [BF_2(**L1**)][BF_4] had a very low relative quantum yield compared to similar boron difluoride heteroaryl nitrogen complexes. Moreover, the weak fluorescence was only observed in a freshly prepared solution suggesting contaminants (e.g. dissolved oxygen) quench the fluorescence.

While the fusion of aryl moieties extends the π-system of a ligand; it is not the determining factor for a complex to have a high fluorescence quantum yield. The low quantum yield of [BF_2(**L1**)][BF_4] could be due to the ligand being a neutral nitrogen donor and the resulting boron complex being cationic. Analogous boron complexes with dipyrromethene form a neutral species (as a result of losing a proton upon complexation) giving more intense electronic transitions. Additionally, it is preferable to have π-sufficient heteroaryl moieties capable of intramolecular charge transfer rather than just aryl moieties when selecting a ligand to have a high fluorescence quantum yield. The only substituents on **L1** are chlorides (which are known to cause poor fluorescence).[131] These particular boron complexes in their present form are unsuitable for application as fluorescent dyes. However, it was shown in Chapter 3 that modification of **L1** to increase the π –conjugation greatly enhanced the observed fluorescence, the protonated form of **L8** (Figure 3.12) highlights this.

4.2.4 Surface Enhanced Raman Spectroscopy

In addition to the above fluorescence measurements, the Raman spectrum of $[BF_2(\mathbf{L1})][BF_4]$ adsorbed on silver colloidal nanoparticles was measured (courtesy of T.M. McLean). This correlated well with DFT calculations of the Raman spectrum of the complex only at the B3LYP/6-311g(2d,p) level without using scaling factors (Figure 4.24 and Table 4.4).

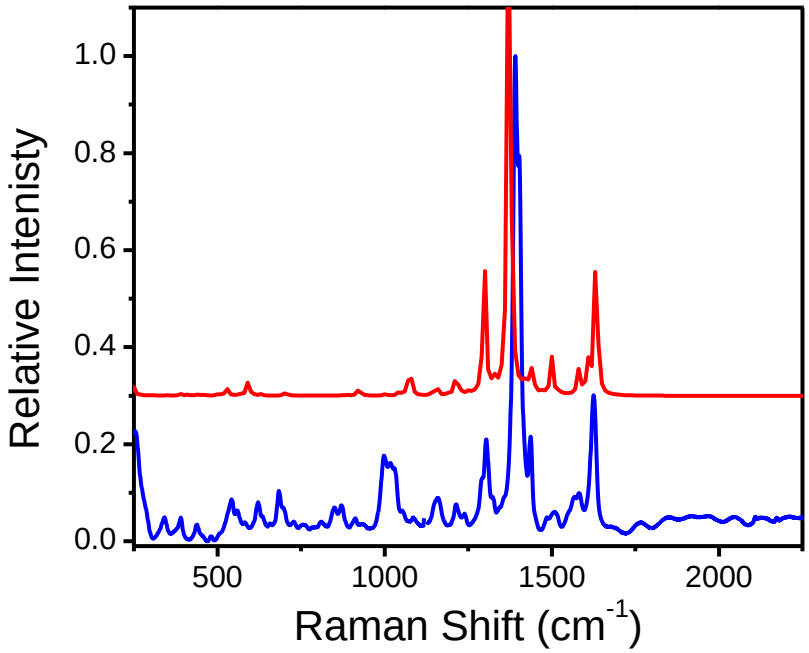

*Figure 4.24: Raman spectra of $[BF_2(\mathbf{L1})][BF_4]$; calculated (**red**) and SERS (**blue**)*

The enhanced signals correspond to in-plane stretching and bending vibrations in the aromatic ring-system. Further investigations would be required to determine the mechanism for this SERS enhancement.

$\mathbf{V_{SERS}}$ **(cm^{-1})**	$\mathbf{V_{CALC}}$ **(cm^{-1})**
1303	1298
1393	1372
1625	1630

Table 4.4: Related bands for the SERS and calculated Raman spectra of $[BF_2(\mathbf{L1})][BF_4]$

4.3 Complexation of Proton Sponges to Beryllium

4.3.1 Introduction

As discussed in Chapter 1, studies on the coordination of beryllium to neutral nitrogen donors are extremely scarce. Coordination is usually necessitated by having strong anionic counter ligands to balance the charge. A close analogue to quino[7,8-*h*]quinoline investigated in this chapter is 2,2'-bipyridine, which was last investigated for coordination to beryllium nearly 50 years ago (Figure 4.25).[136] The paper reported on beryllium 2,2'-bipyridine complexes with; dihalides, dicarbanions and diamides, using melting point and cryoscopy measurements for characterisation.

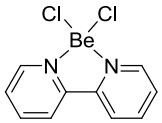

Figure 4.25: Coordination of beryllium to 2,2'-bipyridine

In order for beryllium to coordinate to 2,2'-bipyridine, reactive beryllium reagents were used such as dimethyl-beryllium and beryllium chloride. It was also necessary to use anhydrous solvents with Schlenk and dry-box techniques. Due to heavy safety restrictions on the handling of beryllium solids, a number of the techniques employed in the above paper are no longer conducted in laboratories today.

For an overview on the safety aspects of conducting beryllium coordination chemistry refer to Appendix A.2. The characterisation techniques employed in this section were essentially limited to NMR and UV-Vis spectroscopy (i.e. solution techniques) due to the safety considerations of performing this research. The beryllium source used for the coordination chemistry was limited to a 0.99 M beryllium sulfate solution in water. The beryllium coordination chemistry was conducted off-site at the Los Alamos National Laboratory, New Mexico during a three month trip. In order to be permitted to conduct research at this

facility, extensive training was required which was completed within six weeks of the three month period. Beryllium coordination chemistry should never be attempted without the proper safety precautions and training. At the time, the following quino[7,8-*h*]quinoline based ligands were available for testing:

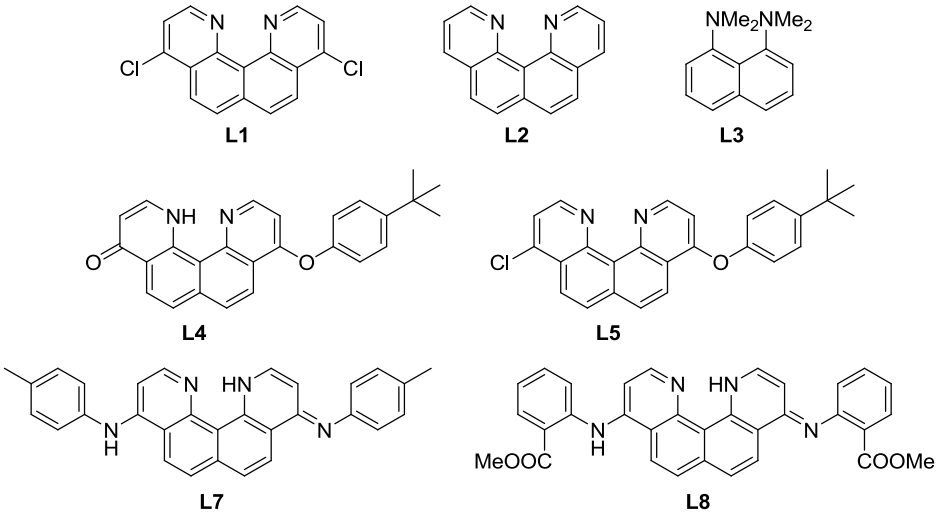

Figure 4.26: Proton sponge ligands tested for beryllium coordination

4.3.2 Aqueous Coordination Chemistry of Beryllium to Proton Sponges

Given the conditions required to enable coordination of beryllium to 2,2'-bipyridine, and the significant problem of protonation of quino[7,8-*h*]quinolines, proving coordination to beryllium under the limited testing conditions was extremely challenging. The following experiments were performed to elucidate whether protonation or beryllium coordination was occurring.

The dichloro-substituted, **L1** (Figure 4.27) in $CHCl_3$ was mixed with $BeSO_4$ (as a 0.99 M solution in H_2O, diluted with MeOH to allow a single phase reaction). An identical experiment was performed using dilute H_2SO_4 in place of the $BeSO_4$ to simulate the acidic pH generated by dissolving beryllium sulfate in water.

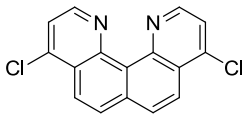

Figure 4.27: 4,9-Dichloroquino[7,8-h]quinoline, ***L1***

Colourless solids precipitated for both the beryllium and non-beryllium solutions, which were insoluble in all organic solvents and only water soluble. The mother liquor was drawn off each, taking care to leave the precipitates wetted. The precipitates were washed with aliquots of MeOH. The precipitates were dissolved in water and diluted to 10^{-5} M for spectral measurements (as no drying or weighing of the solids were permitted, the concentrations are approximations). The fluorescence spectra of both were measured, the excitation wavelength was 345 nm and the emission wavelength was 405 nm. Both experiments showed large increases in fluorescence intensity relative to the neutral ligand, but, gave identical spectra indicated in Figure 4.28.

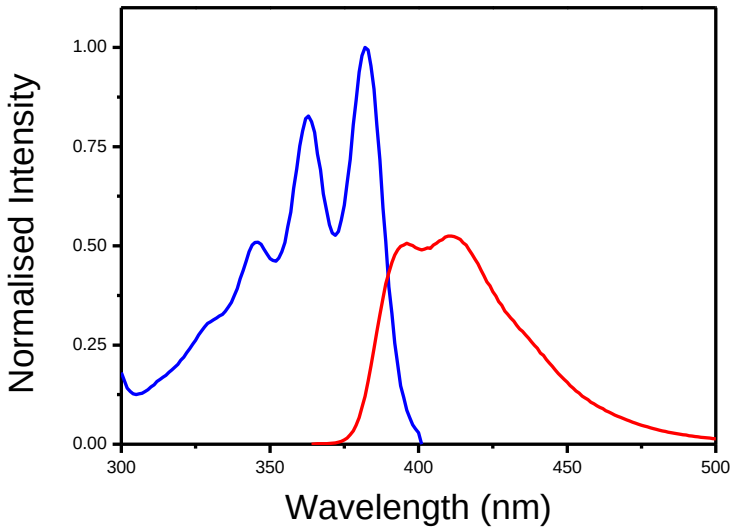

*Figure 4.28: Normalised absorption (****blue****) and emission spectra (****red****) at 10^{-5} M of* ***L1*** *after $BeSO_4$ or H_2SO_4 addition*

The UV-Vis spectrum of both showed a large change relative to the neutral ligand, however, both the precipitates gave identical spectra (Figure 4.29).

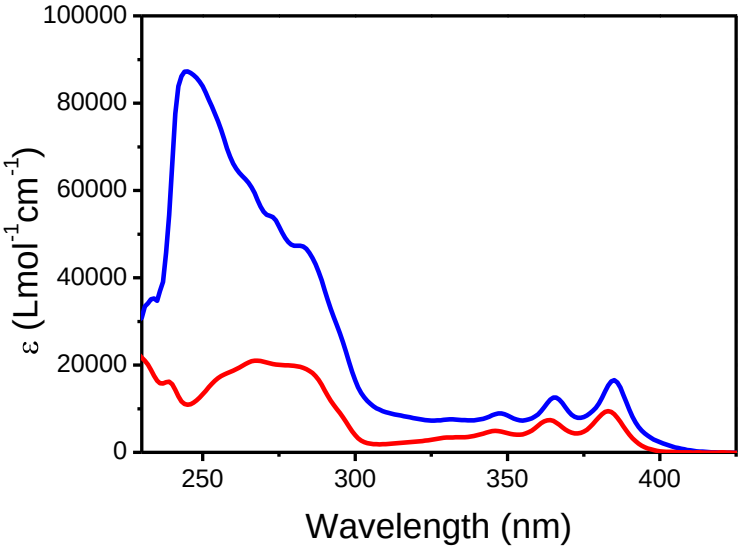

*Figure 4.29: Change in UV-Vis spectrum at 10^{-5} M of neutral **L1** (**blue**) and after $BeSO_4$ or H_2SO_4 addition (**red**)*

There was evidently a significant problem in proving beryllium coordination was occurring over protonation and the above results suggest the acidic beryllium sulfate was merely causing precipitation of protonated **L1**.

The aqueous soluble precipitate resulting from the reaction with beryllium sulfate did have a ^{9}Be NMR shift of 0.87 ppm which was distinct from the reference $Be(H_2O)_4^{2+}$ shift in water of 0 ppm. ^{1}H and ^{13}C NMR revealed that **L1** was present in the precipitate. The observed ^{9}Be NMR chemical shift must have been a result of co-precipitation of a beryllium species with the protonated form of **L1**. The beryllium species was most likely a cluster of the $[Be_n(OH)_n(H_2O)_{2n}]^{n+}$ type as the pH of the resulting aqueous solution (~ pH 4.5) was in the range where these form and the ^{9}Be NMR shift was typical for such a cluster. **L1** in this case simply acted as a base and partially neutralised the acidic beryllium sulfate solution from pH 2.0 to pH 4.5.

Due to the extreme basicity of proton sponges, the problem of ligand protonation was expected. It was hoped that the Be(II) cation could displace this proton; however, there was no strong evidence to confirm coordination to **L1**.

Unfortunately, there was no pH in an aqueous environment where beryllium showed coordination to **L1**. Be(II) is present as the soluble $[Be(H_2O)_4]^{2+}$ at pH ~ 5 and below, and **L1** exists as the strongly bound protonated species which was not displaced by beryllium. Between pH ~ 5 and 12 the insoluble $[Be(OH)_2]$ precipitates. **L1** can be deprotonated at pH ~ 12 where it then precipitates, at this pH the sparingly soluble $[Be(OH)_4]^{2-}$ starts to form, however, there was no evidence of coordination to **L1**. The general distribution of beryllium species is shown in Figure 4.30,[137] however, with the inclusion of a coordinating ligand this is usually perturbed toward complex formation. This was not the case with **L1** as the strongly bound protonated species was resistant to any interaction.

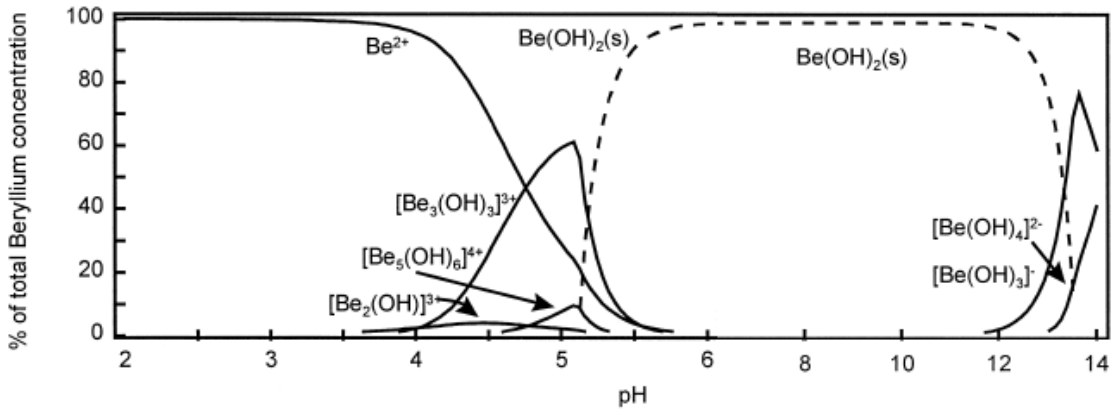

Figure 4.30: Calculated distribution of beryllium hydroxo species at C_{Be} = 0.002 M, from ref 137

4.3.3 Non-Aqueous Coordination Chemistry of Beryllium to Proton Sponges

In order to counter the effect of the acidity of the aqueous beryllium sulfate causing protonation of **L1**, a slight excess of triethylamine (10 equiv.) in an organic solvent was used. The ideal solvent to observe apparent coordination of **L1** to beryllium was DMF as this solubilised both the reactants and the resulting complex. DMSO appeared to cause breakdown of the resulting species and all other organic solvents did not solubilise the resulting beryllium species. The mixture of **L1**, $BeSO_4$(aq), NEt_3 in DMF was stirred at 50 ^oC for 16 h during this time the solution changed from colourless to yellow.

To determine the influence of DMF and NEt_3 on **L1** and beryllium sulfate, two extra experiments were set up; one containing no **L1** to observe whether the ^{9}Be NMR shift was due to coordination of DMF or NEt_3 and the other using dilute H_2SO_4 in place of beryllium sulfate to determine if the UV-Vis spectrum was actually a protonated form of **L1**.

Excitation of the beryllium coordinated **L1** at 425 nm showed an emission at 530 nm that was not present in the neutral or protonated form of the ligand. It should be noted that these were only weak as the background fluorescence observed for neutral **L1** is a similar order of magnitude. This would suggest that the complex is either weakly fluorescent, or, if a complex formed it was only to a small extent.

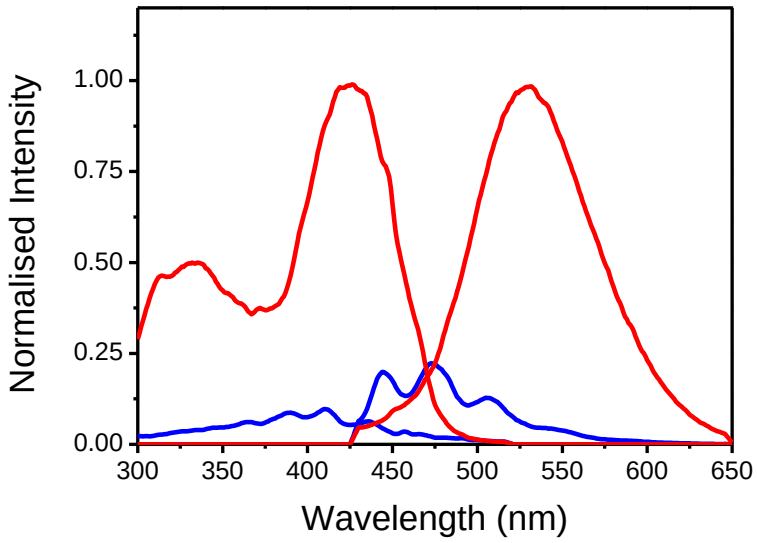

*Figure 4.31: Normalised absorption and emission spectra at 10^{-5} M of neutral **L1** (**blue**) and after $BeSO_4$ addition (**red**) in DMF and NEt_3*

The UV-Vis spectrum (Figure 4.32) showed the appearance of a new peak which now absorbed in the visible part of the spectrum, accounting for the pale yellow colour. However, the heating of only **L1** in DMF generated a very similar spectrum and also gave a yellow solution. The mass spectrum of this reaction showed no **L1** remaining, rather peaks attributed to nucleophilic substitution of one or both chlorides with dimethylamine (a breakdown product of DMF) were observed.

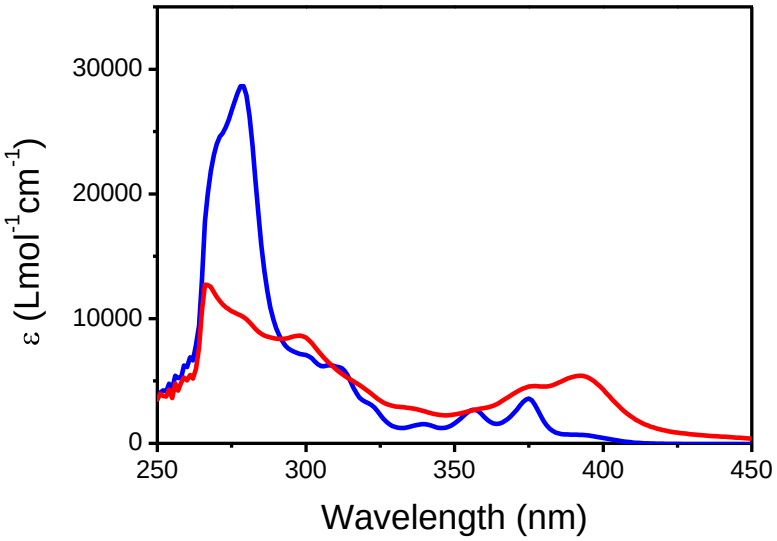

*Figure 4.32: Shift in UV-Vis spectrum at 10^{-5} M of neutral **L1** (**blue**) and after $BeSO_4$ addition or simply heating **L1** in DMF and NEt_3 (**red**)*

The ^{9}Be NMR spectra of both experiments containing Be(II) were measured. The solution containing **L1** showed a very broad shift centred around 2.25 ppm which was distinct to the solution containing no **L1** which was centred around 0.47 ppm. This suggested **L1** had some influence on the ^{9}Be NMR spectra; however, the ^{9}Be signal was much too broad to be attributed to a single species. For single species the width at half height can be related to the coordination number of Be(II) and the only complexes to show high values (i.e. broad peaks) are two or three coordinate species.[138] A four-coordinate species typically has a width at half height of around 50 Hz. The only plausible explanation is that more than one species is present, which is probably due to polymeric species. The solution containing no **L1** was also broad suggesting a variety of coordination modes to the solvent and triethylamine. In addition, the apparent dimethylamine displacement of the chlorides on **L1** would enable the now free chlorides to participate in beryllium coordination.

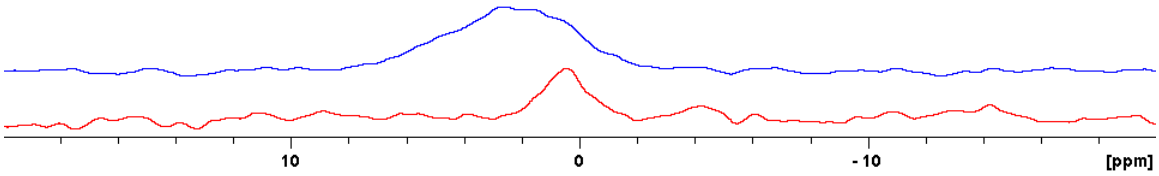

*Figure 4.33: ^{9}Be NMR shift of **L1** coordinated to beryllium (**blue**) and $BeSO_4$ in DMF / NEt_3 (**red**)*

Potential beryllium complexes of **L1** can be proposed via interpretation of the calculated ^{9}Be NMR shift after optimisation of theoretical models (Table 4.5). This was investigated by Plieger and co-workers[138] and has been used to confirm speciation in subsequent papers.[94] In the present work, the theoretical models were optimised using Becke's three-parameter hybrid exchange correlation functional containing the nonlocal gradient correlation of Lee, Yang, and Parr (B3LYP), in conjunction with the 6-311++g(2d,p) basis set. The shielding tensor is related to the NMR chemical shift by comparison to a standard of known chemical shift and its calculated shielding tensor. The GIAO (gauge-including atomic orbital) NMR method and the same gradient correlation and basis set as were used in the optimisation were used to calculate the shielding tensor for each model. Aqueous beryllium sulfate, $Be(H_2O)_4^{2+}$, is defined with a NMR shift of 0.00 ppm and a shielding tensor of 109.10 ppm at the 6-311++g(2d,p) level.

Complex	δ_{ref}	δ_{model}	$\delta_{(ref-model)}$	δ_{exptl}	$\lvert\Delta_{exptl-calc}\rvert$
$Be(H_2O)_4^{2+}$	109.10	109.10	0.00	0.00	0.00
$[Be(\mathbf{L1})_2]^{2+}$		101.02	8.08	2.25	5.83
$[Be(\mathbf{L1})(H_2O)_2]^{2+}$		104.11	4.99	2.25	2.74
$[Be(\mathbf{L1})(SO_4)]$		105.35	3.75	2.25	1.50
$[Be_3(OH)_3(\mathbf{L1})_3]^{3+}$		103.19	5.91	2.25	3.66

*Table 4.5: NMR analysis of beryllium complexes with **L1***

In this instance there were no calculated ^{9}Be NMR shifts for beryllium complexes of **L1** which correlated closely to experimentally observed value. The value of Δ should be close to 0 ppm if the theoretical model is a correct prediction of the experimentally observed species. It is possible to rule out $[Be(\mathbf{L1})_2]^{2+}$ as the Δ value of 5.83 ppm suggests two equivalents of **L1** do not coordinate to beryllium. The species in solution may contain one equivalent of **L1** to beryllium, but, the exact species cannot be determined. Complexes

where hydrogen bonding interactions are important are known to have poorly correlated calculated NMR shifts and can vary by 2 or more ppm.[138] The closest beryllium complex with neutral nitrogen donors and a measured ^{9}Be NMR was $[Be(NH_3)_4]^{2+}$ and the Δ between the calculated and experimental shift was 2.1 ppm, so it is possible that a species such as [Be(**L1**)(SO_4)] formed where Δ was 1.50. Characterisation was impeded by the complex reaction mixture. Attempted modelling of the four-coordinate complex [Be(**L1**-NMe_2)Cl_2] where the chlorides on **L1** were displaced by dimethylamine (from DMF) and the chlorides them coordinated to Be(II) gave a Δ of 5.93.

L2 did not give a similar result to **L1**. In the absence of triethylamine, **L2** gave exclusive precipitation of the protonated ligand. In the presence of NEt_3 in DMF the protonated ligand also precipitated. This suggests that the ^{9}Be NMR shifts observed when **L1** was present with NEt_3 in DMF may be the displaced chlorides interacting with beryllium to give a beryllium chloride species.

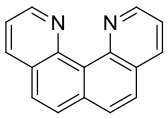

*Figure 4.34: Quino[7,8-h]quinoline, **L2***

No complexation to **L3** was observed with or without triethylamine, nor was a precipitate of the protonated species obtained. Protonation of the ligand most likely occurred; however, it was soluble and remained in solution.

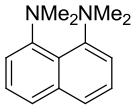

*Figure 4.35: 1,8-bis(Dimethylamino)naphthalene, **L3***

No complexation to **L4** was observed, the hydrogen could not be displaced and attempted use of strong inorganic bases was not compatible with the aqueous beryllium sulfate solution.

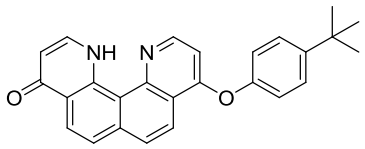

Figure 4.36: 9-(4-tert-Butylphenoxy)quinolino[7,8-h]quinolin-4(1H)-one, ***L4***

A similar observation to **L1** occurred for **L5** as evidenced by a new beryllium species in the ^{9}Be NMR (Figure 4.37). The mixture of **L5**, $BeSO_4$(aq), NEt_3 in DMF was stirred at 50 ^{o}C for 16 h during this time the solution changed from colourless to yellow.

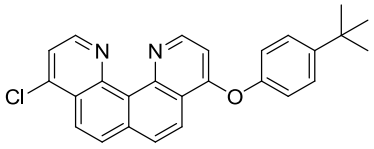

Figure 4.37: 4-(4-tert-butylphenoxy)-9-chloroquinolino[7,8-h]quinoline, ***L5***

The ^{9}Be NMR of this mixture showed a broad peak at 1.69 ppm. The broad peak would likely contain a large number of beryllium species involving solvent and triethylamine. Chloride (from **L5** displaced by the breakdown product of DMF) likely contribute to the observed ^{9}Be NMR shift by participating in these complex beryllium species.

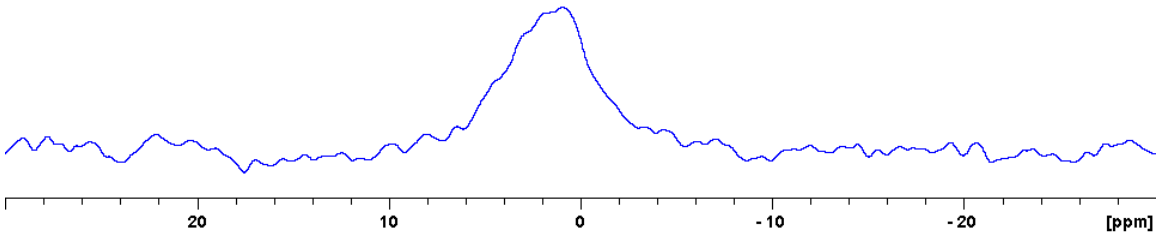

Figure 4.38: The broad ^{9}Be NMR shift for the reaction mixture of beryllium and ***L5*** *in DMF / NEt_3*

A 20 µL aliquot of the reaction mixture was diluted with DMF (10 mL) to give a concentration of 48.5 µmol L^{-1} which was measured against an identical sample containing neutral **L5** and a partial change was observed in the UV-Vis and fluorescence spectras.

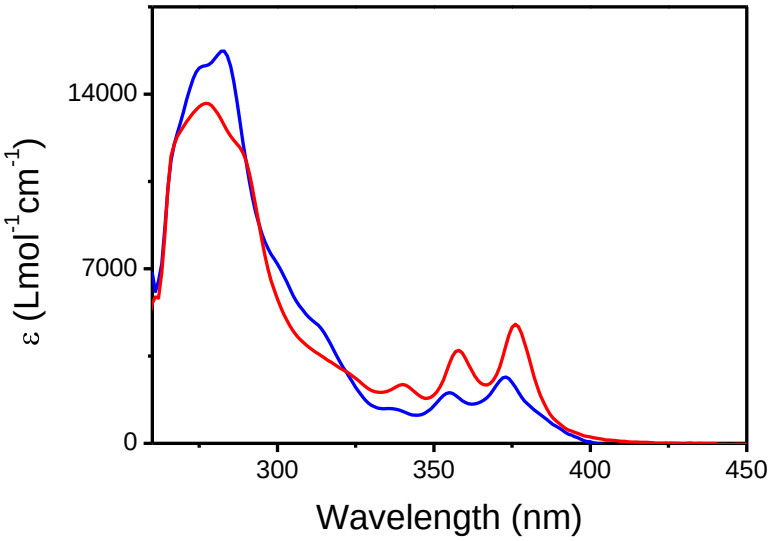

*Figure 4.39: Shift in UV-Vis spectrum at 10^{-5} M of neutral **L5** (**blue**) and after $BeSO_4$ addition (**red**) in DMF and NEt_3*

Excitation of the reaction mixture at 405 nm showed a very weak emission at 495 nm that was not present in the neutral ligand.

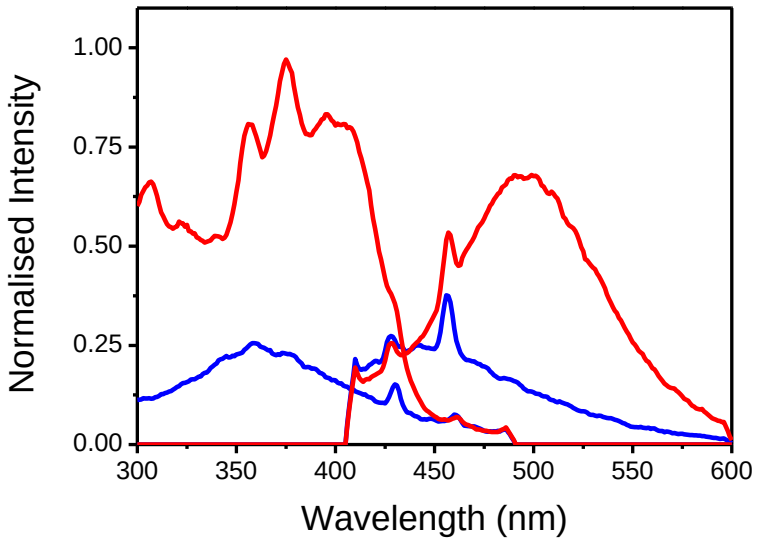

*Figure 4.40: Normalised absorption and emission spectras at 10^{-5} M of neutral **L5** (**blue**) and after $BeSO_4$ addition (**red**) in DMF and NEt_3*

Due to the tautomer forms of **L7** and **L8**, they showed no coordination to beryllium. The central proton was not displaced in order to coordinate beryllium.

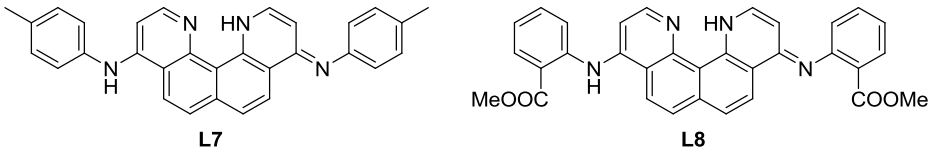

Figure 4.41: Proton sponges with tautomers incapable of coordinating to Be(II)

4.4 Complexation of Proton Sponges to Transition Metals

4.4.1 Introduction

In order to emphasise the size selectivity of proton sponges toward small cations, it was necessary to investigate whether they can be bound to larger cations such as transition metals. There are a few papers in existence where metal complexes were formed with various different types of proton sponges.[72, 90, 91] These complexes were formed using metals that form strong M – N bonds. Carefully selected dimeric metal salts (such as Zeise's dimer $[Pt_2(H_2C{=}CH_2)_2Cl_4]$), which have weakly coordinating bridging ligands also allowed easy displacement by the chelating ligand.

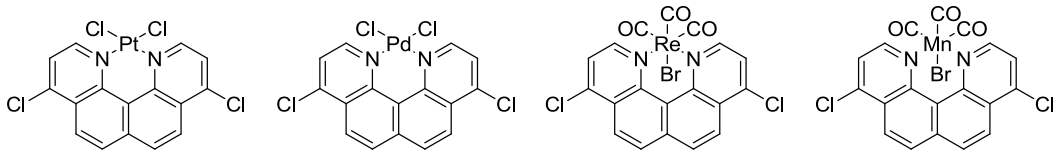

*Figure 4.42: Metal complexes with **L1***

The following section will explore whether quino[7,8-*h*]quinolines can complex to various metal salts to deduce the strength of coordination with transition metals.

4.4.2 Results / Discussion

To begin with; a series of copper(II) salts were tested for their coordination to **L1**; copper sulfate, acetate, chloride and perchlorate. Acetonitrile was used as the solvent creating a polar aprotic environment (aside from the water present in the metal salts) and could provide additional coordinating ligands if required. In all cases an initial colour change to green was observed indicating formation of a copper complex followed by rapid precipitation of a colourless solid, which was the protonated form of **L1**, caused by hydrolysis. The exception to this was the perchlorate salt which did not give the rapid

precipitate of protonated **L1** and could be analysed further. The perchlorate anion is one of the least coordinating anions and gave the greatest stability toward hydrolysis of the metal complex given by the following general equations (L = **L1**, M = Cu, X = anion):

$$L + MX_2 \rightarrow [LM][X_2]$$
$$[LM][X_2] + H_2O \rightarrow [LH][X] + [MOH][X]$$

Use of triethylamine as an auxiliary base did not hinder the formation of protonated **L1** for the sulfate, acetate and chloride salts. According to the Hofmeister Series,[139] the anion most likely influences the hydrolysis as a strongly hydrated anion brings water in close proximity to the metal complex, water is present in all the metal salt reagents. As perchlorate anions are weakly hydrated, they did not induce rapid hydrolysis.

With perchlorate established as a suitable anion for preventing hydrolysis, perchlorate salts of nickel, zinc and cobalt were also tested for coordination to **L1**. They all showed what appeared to be initial complexation followed by rapid precipitation within seconds of protonated **L1**. Thus, the only 1st row transition metal in the current investigation to show some stability was copper as a perchlorate salt. The stability of copper complexes relative to other 1st row transition metals is well documented according to the Irving-Williams series.[140]

The complexation of **L1** with copper perchlorate in acetonitrile gave $[Cu(\mathbf{L1})(CH_3CN)_3][(ClO_4)_2]$. Single crystals suitable for X-ray determination were obtained by vapour diffusion of diethyl ether into acetonitrile containing $[Cu(\mathbf{L1})(CH_3CN)_3][(ClO_4)_2]$. The crystals were not air stable and collapsed due to solvent loss. In addition the crystals were transient, after initial crystallisation the crystals would redissolve and protonated ligand was precipitated within 24 hours. When care was taken not to expose the crystals to air it was possible to record the X-ray structure. Elemental analysis of the isolated dried crystals gave the formula of the complex as $[Cu(\mathbf{L1})(H_2O)_3][(ClO_4)_2]$, essentially the water molecules had replaced the coordinated

acetonitrile molecules in the inner coordination sphere during the drying and analysis process.

The structure crystallised in space group $P2_1/c$ and the asymmetric unit consisted of a complex and accompanying anions. The crystal structure revealed **L1** had a bowed aromatic ring system with the copper ion located 0.867(4) Å above the mean plane of the aromatic ring. The aromatic ring was also bowed similar to the platinum and rhenium complexes reported previously.[72] The cavity was not an ideal fit for the Cu(II) ion.

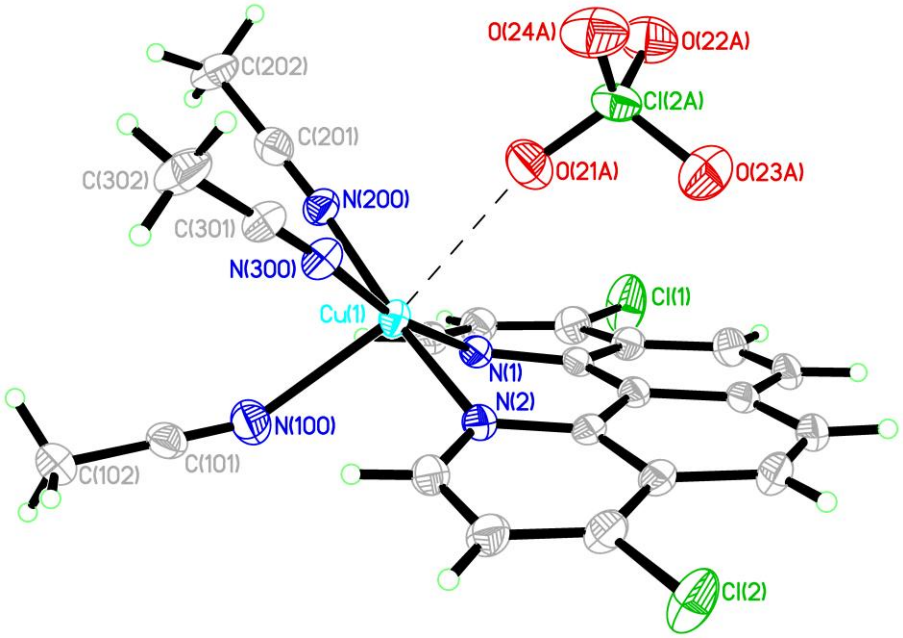

*Figure 4.43: Perspective view of the crystal structure of [Cu(**L1**)$(CH_3CN)_3$][$(ClO_4)_2$], ellipsoids drawn at the 50% probability level, the second ClO_4^- is omitted for clarity*

The complex adopts a square pyramidal geometry with one perchlorate providing a long range interaction of 2.626(4) Å filling the vacant sixth site. The second perchlorate lies to one side of the complex (not pictured). The bond angles passing through the metal centre all deviate from the ideal 90° (Table 4.5). A symmetry generated perchlorate from an adjacent molecule lies in a "pocket" created by the three coordinated acetonitrile molecules (Figure 4.44).

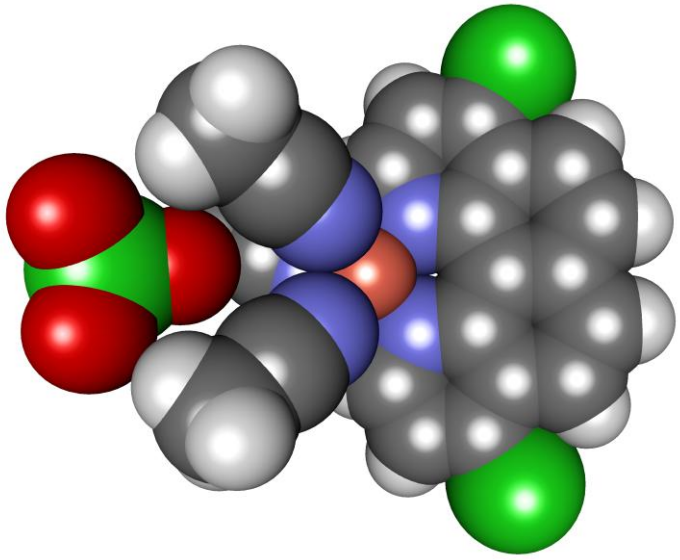

Figure 4.44: Space-filling diagram showing a perchlorate stabilising the acetonitrile ligands

The complex also showed typical Jahn-Teller distortion of the axial ligands, the lengths are summarised in Table 4.6:

Parameter	Length (Å)	Parameter	Angle (°)	Parameter	Angle (°)
Cu1–N1 (eq)	1.982(3)	N1–Cu1–N2	88.25(12)	N2–Cu1–O21A	95.18(13)
Cu1–N2 (eq)	1.966(3)	N1–Cu1–N100	101.69(13)	N100–Cu1–N200	88.40(13)
Cu1–N200 (eq)	2.008(4)	N1–Cu1–N200	92.83(12)	N100–Cu1–N300	88.42(13)
Cu1–N300 (eq)	2.022(3)	N1–Cu1–O21A	83.21(13)	N200–Cu1–N300	85.66(14)
Cu1–N100 (ax)	2.316(4)	N2–Cu1–N100	97.00(13)	N300–Cu1–O21A	86.54(13)
Cu1–O21A (ax)	2.623(4)	N2–Cu1–N300	92.26(14)		

*Table 4.6: Major structural parameters for the geometry of the Cu(II) ion in [Cu(**L1**)(CH_3CN)$_3$][(ClO_4)$_2$]*

No significant π-stacking interactions were in the crystal; however, anion-π interactions of between the oxygens on the perchlorates and centroids on the rings of the heterocycle were present. The perchlorate associated with the copper had an intramolecular interaction with the heterocycle (Figure 4.45); O23A – Cg2 3.254(4) Å, Cl2A – O23A – Cg2 126.7(2)°, Cl2A – Cg2 4.287(3) Å. An intermolecular interaction with another symmetry generated perchlorate contacts via two oxygens and two six-membered rings; O13 – Cg2 2.967(7) Å, Cl10 – O13 – Cg2 124.2(3)°, Cl10 – Cg2 3.927(2) Å and O14 – Cg1 3.415(4) Å, Cl10 – O14 – Cg1 104.66(16)°, Cl10 – Cg1 4.029(2) Å.

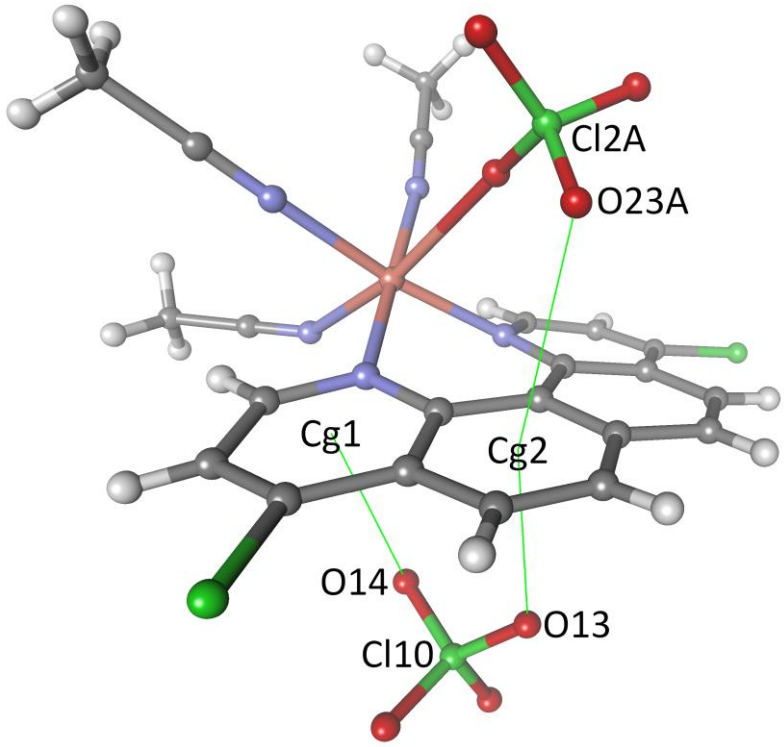

*Figure 4.45: Crystal packing of [Cu(**L1**)(CH_3CN)$_3$][(ClO_4)$_2$]*

The UV-Vis spectrum showed a broad d-d transition at 625 nm with ε = 50 L mol^{-1} cm^{-1}. The Cu(II) ion sat a large distance out of the plane of the ring system of **L1** in the crystal structure so there was not expected to be any metal – ligand charge transfer interactions.

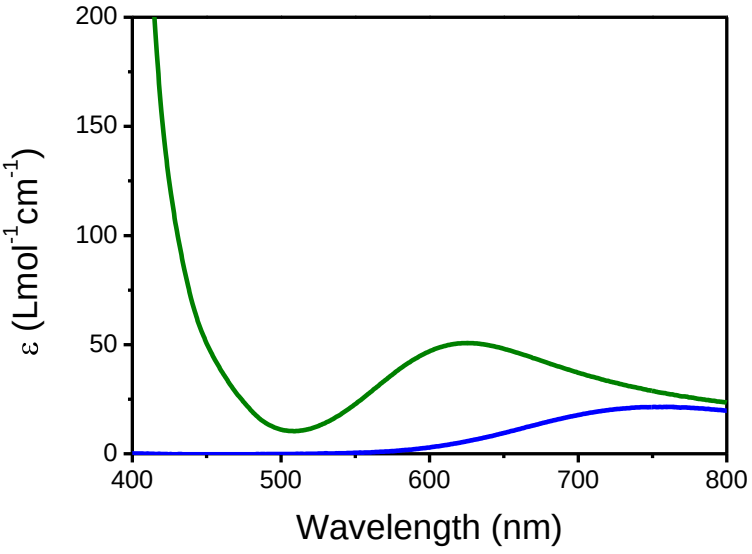

*Figure 4.46: UV-Vis of [Cu(**L1**)(CH_3CN)$_3$][(ClO_4)$_2$] (**green**) and copper perchlorate (**blue**) in acetonitrile*

The shape and position of the d-d transition can sometimes distinguish the geometry of the ligands around a Cu(II) ion. According to Figure 4.47, the axial acetonitrile is coordinating in solution as well as the solid state. If the Cu(II) complex of **L1** was square-planar, a sharper d-d transition closer to 500 nm would be expected. In this instance the broad transition centred around 625 nm is closer to that observed for square-based pyramidal complexes.

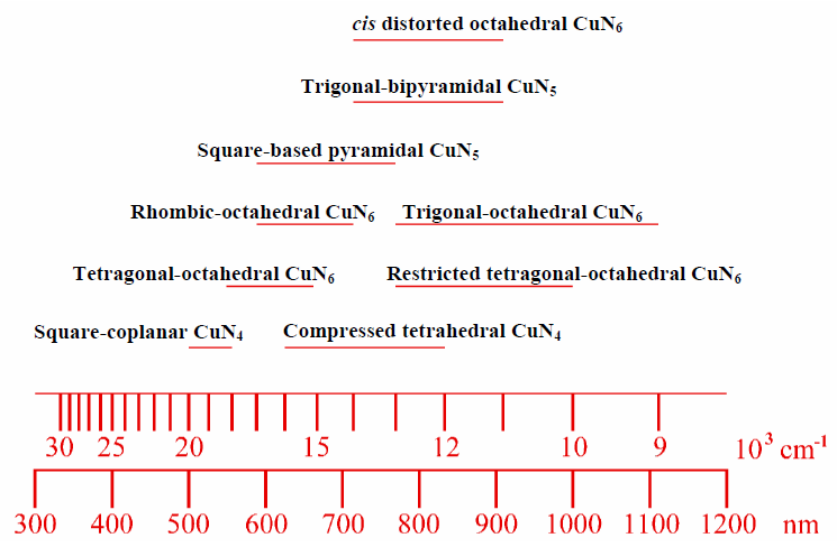

Figure 4.47: Summary of energy ranges for closely related CuN_x chromophores with different stereochemistries, figure from S. Kirk's thesis,[141] adapted from Lever[142]

The complexation of **L2** with copper perchlorate in acetonitrile gave the complex, $[Cu(\mathbf{L2})(CH_3CN)_3][(ClO_4)_2]$ which had similar stability and crystallised under the same conditions to the complex with **L1**. Elemental analysis of the isolated dried crystals gave $[Cu(\mathbf{L2})(H_2O)_3][(ClO_4)_2]$, the expected outcome from solvent removal. The structure crystallised in space group *P*-1 and the asymmetric unit consisted of a complex and accompanying anions. The crystal structure revealed **L2** had a bowed aromatic ring system with the copper ion located 0.849(6) Å above the mean plane of the aromatic ring.

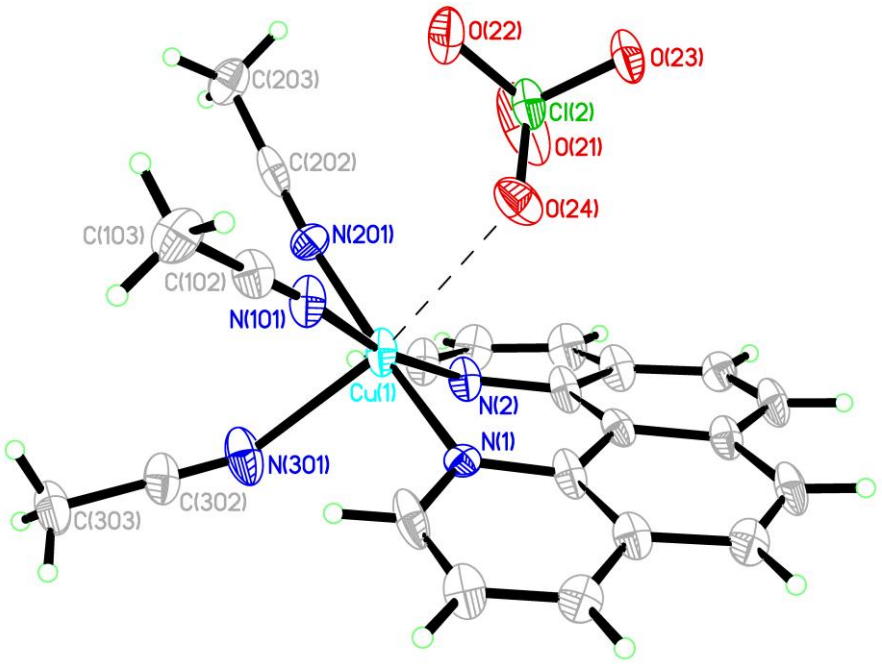

*Figure 4.48: Perspective view of the crystal structure of [Cu(**L2**)(CH_3CN)$_3$][(ClO_4)$_2$], ellipsoids drawn at the 50% probability level, the second ClO_4^- is omitted for clarity*

The complex adopted a square pyramidal geometry with one perchlorate providing a long range interaction of 2.651(4) Å occupying the sixth site. The bond lengths and angles shows only minor deviations to [Cu(**L1**)(CH_3CN)$_3$][(ClO_4)$_2$].

Parameter	Length (Å)	Parameter	Angle (°)	Parameter	Angle (°)
Cu1–N1 (eq)	1.963(4)	N1–Cu1–N2	88.83(19)	N2–Cu1–O21	84.47(17)
Cu1–N2 (eq)	1.984(5)	N1–Cu1–N101	91.47(19)	N101–Cu1–N201	86.2(2)
Cu1–N201 (eq)	1.971(5)	N1–Cu1–N301	95.36(19)	N101–Cu1–N301	89.80(19)
Cu1–N301 (eq)	2.032(5)	N1–Cu1–O21A	94.24(17)	N201–Cu1–N301	88.4(2)
Cu1–N101 (ax)	2.305(5)	N2–Cu1–N201	92.8(2)	N201–Cu1–O21	81.86(18)
Cu1–O21 (ax)	2.651(4)	N2–Cu1–N301	100.41(19)		

*Table 4.7: Major structural parameters for the geometry of the Cu(II) ion in [Cu(**L2**)(CH_3CN)$_3$][(ClO_4)$_2$]*

No significant π-stacking interactions in the crystal; however, anion-π interactions between the oxygens on perchlorate and centroids on the rings of the heterocycle were present. The perchlorate associated with the copper had an intramolecular interaction with the heterocycle (Figure 4.48); O21 – Cg1 3.498(7) Å, Cl2 – O21 – Cg1 114.7(3)°, Cl2 – Cg1

4.291(3) Å. An intermolecular interaction with another symmetry generated perchlorate contacts via two oxygens and two six-membered rings; O12 – Cg2 3.102(5) Å, Cl1 – O12 – Cg2 130.7(3)^{o}, Cl1 – Cg2 4.18(3) Å and O13 – Cg3 3.426(5) Å, Cl1 – O13 – Cg3 114.1(2)^{o}, Cl1 – Cg3 4.226(3) Å. The lengths of these interactions are shorter for [Cu(**L1**)$(CH_3CN)_3$][$(ClO_4)_2$] due to the electron withdrawing effect of the chlorides decreasing the electron density on the heterocyclic rings. A similar trend in the anion-π interactions was observed in the crystal structures of the boron complexes of **L1** and **L2**.

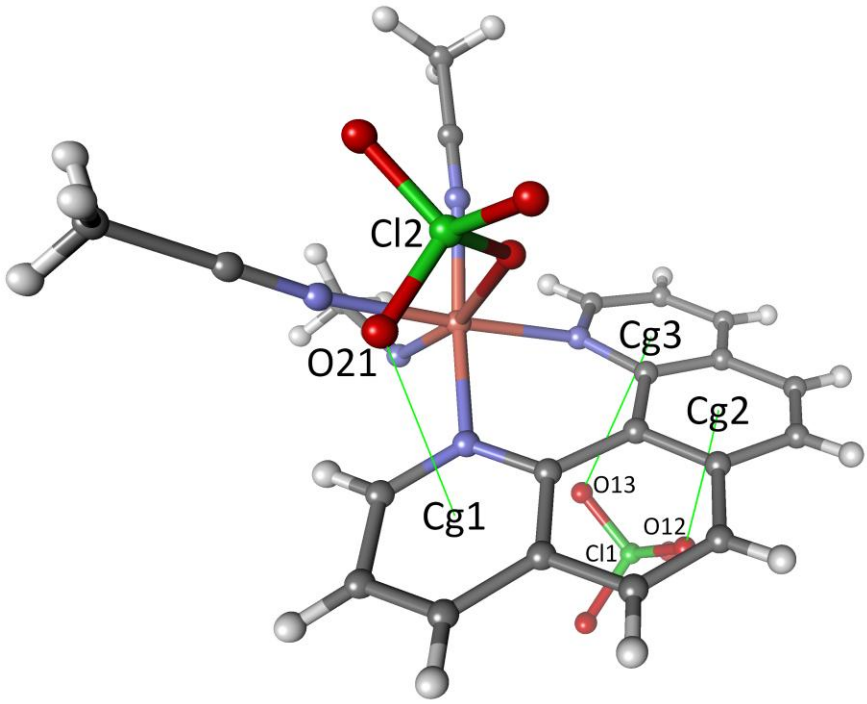

*Figure 4.49: Crystal packing of [Cu(**L2**)$(CH_3CN)_3$][$(ClO_4)_2$]*

The UV-Vis of [Cu(**L2**)$(CH_3CN)_3$][$(ClO_4)_2$] showed a similar weak d-d transition to the copper complex of **L1**, the maximum absorbance was at 613 nm with ε = 67 L mol^{-1} cm^{-1}.

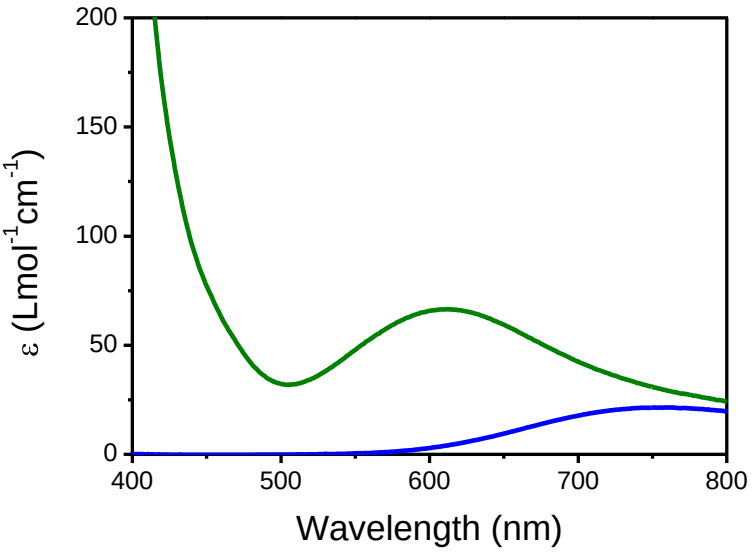

*Figure 4.50: UV-Vis of [Cu(**L2**)(CH_3CN)$_3$][(ClO_4)$_2$] (**green**) and copper perchlorate (**blue**) in acetonitrile*

X-Band ESR spectra (Table 4.8) of both complexes were recorded in acetonitrile at liquid nitrogen temperatures, courtesy of E. Ainscough. Both complexes showed essentially identical spectra suggesting the chlorides on **L1** have almost no influence on the Cu(II) complex relative to **L2** containing only hydrogens. The $g_{\|} > g_{\perp}$ values are typical for monomeric axial Cu(II) complexes and confirm the crystal structures.[143, 144] Well-resolved hyperfine lines in the $g_{\perp}$ region were not observed.

Cu(II) Complex	**ESR**		
	$g_{\|}$	**$g_{\perp}$**	**$A_{\|}$ (cm^{-1})**
L1	2.3133	2.0899	173 x 10^{-4}
L2	2.3133	2.0935	173 x 10^{-4}

*Table 4.8: ESR data for the copper complexes of **L1** and **L2***

The size-fit of quino[7,8-*h*]quinolines can be analysed by comparing the distances between the following adjacent atoms (Figure, 4.51, Table 4.9).

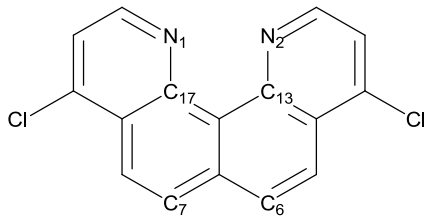

Figure 4.51: Atoms used to relate the size-fit of various cations for quino[7,8-h]quinolines

Compound	Atomic Distances (Å)			Torsion Angle (°)
	N1 – N2	C13 – C17	C6 – C7	N1 – C17 – C13 – N2
L1	2.768(2)	2.585(2)	2.444(2)	20.02(9)
[H(**L1**)][BF_4]	2.591(2)	2.539(2)	2.467(3)	0.17(13)
[BF_2(**L1**)][BF_4]	2.553(5)	2.508(6)	2.469(8)	1.30(24)
[BF_2(**L2**)][BF_4]	2.560(3)	2.500(4)	2.470(4)	2.43(18)
[Cu(**L1**)$(MeCN)_3$][ClO_4]$_2$	2.749(5)	2.560(5)	2.427(6)	0.71(28)
[Cu(**L2**)$(MeCN)_3$][ClO_4]$_2$	2.762(6)	2.572(8)	2.443(9)	4.99(43)
[Pt(**L1**)Cl_2]	2.812(2)	2.481(2)	2.410(2)	0.00
[Re(**L1**)$(CO)_3$Br]	2.804(2)	2.585(2)	2.390(2)	1.69

*Table 4.9: Atom distances to relate the size-fit of various cations for **L1***

A good size-fit cation shows shortened N1 – N2 and C13 – C17 distances and slightly lengthened C6 – C7 distances relative to the neutral ligand. The atomic displacements behave similarly to the opening and closing of a peg (Figure 4.52). For both the small B(III) and H^+ cations the atomic distances are shortened around the binding cavity and lengthened on the opposing side of the pivot (**red** arrows). For the larger metal cations the atomic distances have the reverse trend (**blue** arrows).

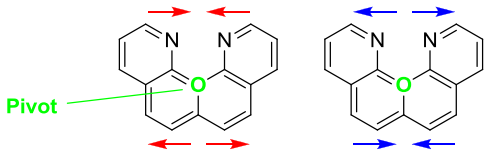

Figure 4.52: Atomic motion relative to cation size, small cations cause the displacement shown in red while larger cations give the displacement shown in blue

The neutral ligand, **L1**, has a slightly elongated N1 – N2 distance of 2.768(2) Å due to the repulsion of the lone electron pairs on the nitrogens, which in turn compresses the C6 – C7

distance to 2.444(2) Å on the backend of the molecule. This strain is relieved in the protonated form of **L1** with the N1 – N2 distance now reduced to 2.591(2) Å with a slight elongation of the C6 – C7 distance to 2.467(3) Å. The B(III) cation offered a further improvement to this reduction in strain as the boron **L1** and **L2** complexes have the shortest N1 – N2 distances of 2.553(5) Å and 2.560(3) Å respectively. This is due to the presence of two covalent B – N bonds while the protonated form has one N – H bond and a weaker hydrogen bond to the adjacent nitrogen. The Cu(II) complex gave a slightly shorter N1 – N2 distance compared to the previously reported Pt(II) complex, which may be explained by the smaller ionic radii of Cu(II).

4.5 Summary

To better investigate the coordination of small cations to quino[7,8-*h*]quinolines, boron difluoride complexes were formed and crystallographic evidence showed there was a good size-fit for small cations. It was hoped that the boron complexes would show potential as fluorescent dyes, however, these complexes exhibited very low quantum yields and the fluorescence was not preserved over time.

Boron trifluoride was ideally suited to coordinating quino[7,8-*h*]quinoline as the incomplete electron octet of boron was readily filled by the lone electron pairs of the heterocyclic nitrogens of quino[7,8-*h*]quinoline. Full coordination was facilitated by having a second boron trifluoride molecule remove a fluoride to give the tetrafluoroborate anion which balances the charge of the cationic boron difluoride complex of quino[7,8-*h*]quinoline (Figure 4.53).

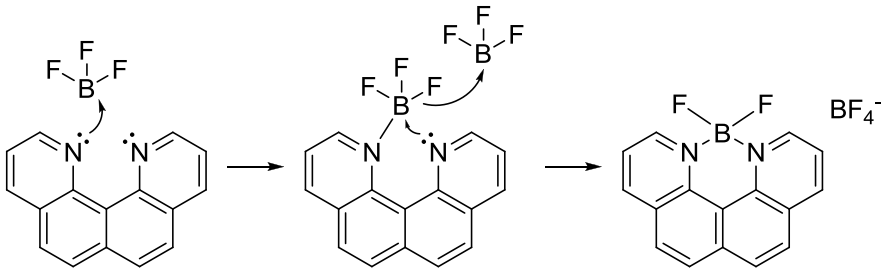

Figure 4.53: Coordination of boron trifluoride to quino[7,8-h]quinoline

The excellent coordination to B(III) and poor coordination to Be(II) comes down to the differing reaction environments and choice of Be(II) starting reagent. Favourable ligand coordination to Be(II) in an aqueous environment is best explained comparing the coordination of Be(II) to the analogous benzo[*h*]quinolin-10-ol (Figure 4.54).[61] Benzo[*h*]quinolin-10-ol has an electron-rich phenolic oxygen which has two sets of unpaired electrons. The pyridine adjacent to this phenol weakens the OH bond by forming a strong intramolecular hydrogen bond. The weakening of the OH bond enhances the nucleophilicity of the phenolic oxygen by facilitating the formation of the phenoxide ion. It is the nucleophilic phenoxide ion which coordinates to the Be(II) cation. After removal of

the pyridine-associated proton, complete coordination by one molecule of benzo[*h*]quinolin-10-ol to Be(II) is achieved by solvent loss and association of Be(II) with the remaining pyridine.

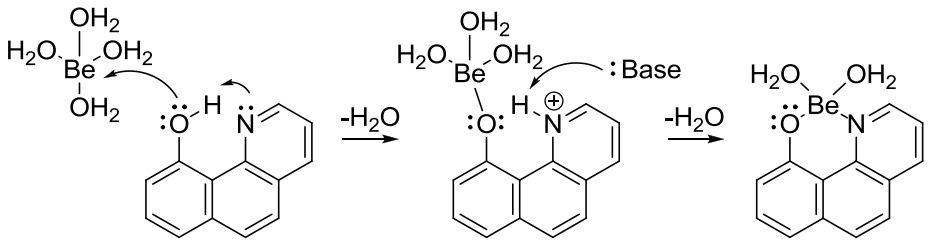

Figure 4.54: Coordination of beryllium hydrate to benzo[h]quinolin-10-ol

The crucial difference for quino[7,8-*h*]quinoline is there is apparently no driving force for initial Be(II) association. Each sp^2 nitrogen in quino[7,8-*h*]quinoline has one lone electron pair which both get tied up upon protonation. Once this occurs the cationic molecule has no available electron pair capable of disrupting the cationic beryllium hydrate species, Figure 4.55.

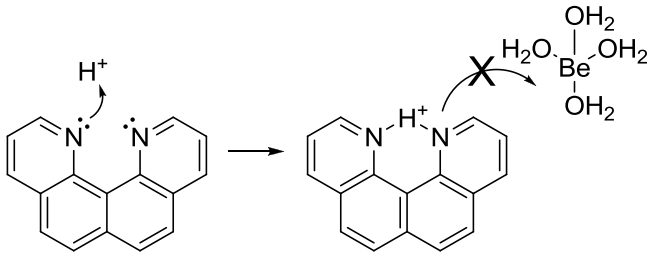

Figure 4.55: Inactivation of quino[7,8-h]quinoline by protonation

The investigation into whether Be(II) would coordinate to proton sponges has confirmed the critical features for creating a suitable ligand for complexation of beryllium. Had the means and materials been available, it is more than likely a beryllium complex of quino[7,8-*h*]quinoline could have been formed in aprotic media with a suitable beryllium reagent, similar to that used for the boron complex. In aqueous systems the beryllium aqua species, whether it is the tetrahydrate species in acidic pH, a cluster species at intermediate pH or the hydroxide species at basic pH; are considered moderately stable species. It is imperative to utilise strong anionic oxygen donors to break this hydration sphere and

achieve coordination. Despite providing a cavity structurally suited for the small Be(II) cation, the binding strength of the quino[7,8-*h*]quinolines after protonation was not sufficient to displace the water molecules surrounding Be(II) and achieve coordination. The tendency for the ligands to rapidly protonate effectively inactivates them toward beryllium complexation. Once this happened there was no longer a driving force to coordinate beryllium, and the anticipated displacement of strongly deshielded proton by beryllium did not occur.[28, 61] Displacement of a deshielded proton is necessitated by having a mixed oxygen – nitrogen donor ligand.

When coordination to transition metals was attempted, for all intents and purposes quino[7,8-*h*]quinolines met the criteria for excluding large metal cations. Extremely weak copper complexes (copper having the highest stabilities according to the Irving-Williams series) were formed with copper perchlorate in acetonitrile which existed briefly. Crystallisation of this complex showed a large distortion of the copper ion out of the plane of the heterocyclic ring. No other 1st row transition metal complexes were formed.

Quino[7,8-*h*]quinolines were generally unsuitable for making useful complexes and remain a structural novelty. While they do have an ideal size-fit for small cations, as shown in the crystal structure of the B(III) complex, the inherent weakness of the neutral nitrogen donors combined with the high susceptibility for protonation mean they would be a poor choice for any Be(II) sensing for sequestering applications in aqueous environments. The remainder of this thesis investigated compounds which should give stronger beryllium complexes and attempt to use encapsulation for selectivity.

Chapter 5: Synthesis of Tetra-Coordinate Ligands

5.1 Assessment of Tetra-Coordinate Ligands

In contrast to the proton sponges investigated in Chapter 4, the ligands described in this chapter have greater flexibility due to the less strained geometries. The binding cavities are still relatively tight and have the advantage of offering four donor atoms and the possibility for full encapsulation of Be(II). These ligands also incorporate oxygen donors to provide a better opportunity for initial association with Be(II) which was the likely shortfall of the proton sponges. While the remaining donor arms on these ligands have weak nitrogen donors, it is hoped that Be(II) will coordinate via chelation to all four donor atoms. This was the assumption made for the theoretical calculations, which were performed with the same level of theory used for assessing the proton sponges in Chapter 2; B3LYP and 6-31(d).

The first ligand, **501**, consists of three pyridine units with nitrogen donors linked via a central carbon atom (Figure 5.1). An oxygen donor in the form of a phenol moiety substituted onto one of the pyridines caps the tetrahedral binding cavity. Full encapsulation of Be(II) would involve all three nitrogen donors and an oxygen donor from the deprotonated phenol. There are currently no known ligands which provide this type of enclosed tetrahedral binding cavity.

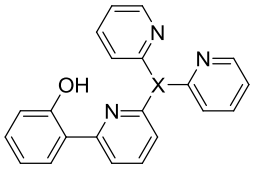

*Figure 5.1: 2-(6-(Dipyridin-2-ylmethyl)pyridin-2-yl)phenol, **501**, X = C, N*

The only ligand marginally related to **501** is shown in Figure 5.2 which appeared in a patent for use as a potassium ion channel modulator for therapeutic and diagnostic applications.[145]

This ligand would not provide an ideal tetrahedral geometry and the four neutral nitrogen donor atoms would be unsuitable for coordination to Be(II).

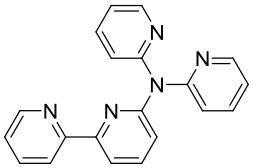

*Figure 5.2: A related four-coordinate ligand to **501***

A computer generated model of the beryllium complex of **501** is shown in Figure 5.3. The three nitrogen atoms make a trigonal pyramidal base providing three points of the tetrahedral cavity. The oxygen from the phenol caps the complex to give what appears to be an ideal tetrahedral geometry for beryllium with favourable bond lengths and angles around the Be(II) centre.

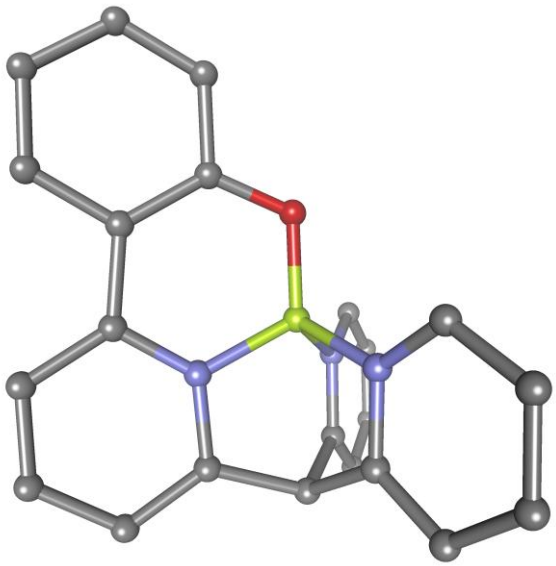

*Figure 5.3: Computer model of beryllium coordinated to **501**, hydrogens removed for clarity*

The second ligand, **502**, consists of quinoline-8-carboxylic acid and two pyridine units (Figure 5.4). Full encapsulation of Be(II) would involve all three nitrogen donors and an oxygen donor from the deprotonated carboxylic acid in a similar arrangement to **501**.

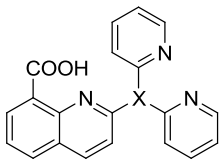

*Figure 5.4: 2-(Dipyridin-2-ylmethyl)quinoline-8-carboxylic acid, **502**, X = C, N*

A computer generated model of the beryllium complex of **502** is shown in Figure 5.5. The three nitrogen atoms make a trigonal pyramidal base and the oxygen from the deprotonated carboxylic acid caps the complex. This provides a tetrahedral geometry for Be(II) analogously to **501**.

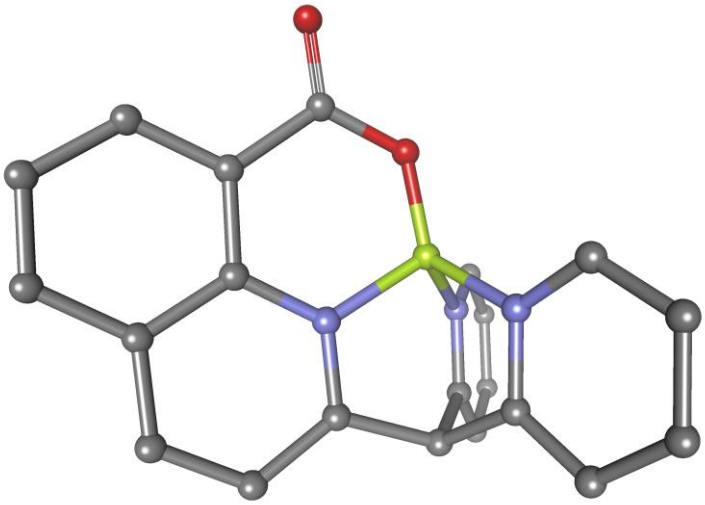

*Figure 5.5: Computer model of beryllium coordinated to **502**, hydrogens removed for clarity*

The final set of ligands considered in this thesis are based on tertiary amines, the central amine offers one point of coordination and the arms offer the remaining donors which consist of phenols, pyridines, carboxylic acids or quinoline moieties (Figure 5.6).

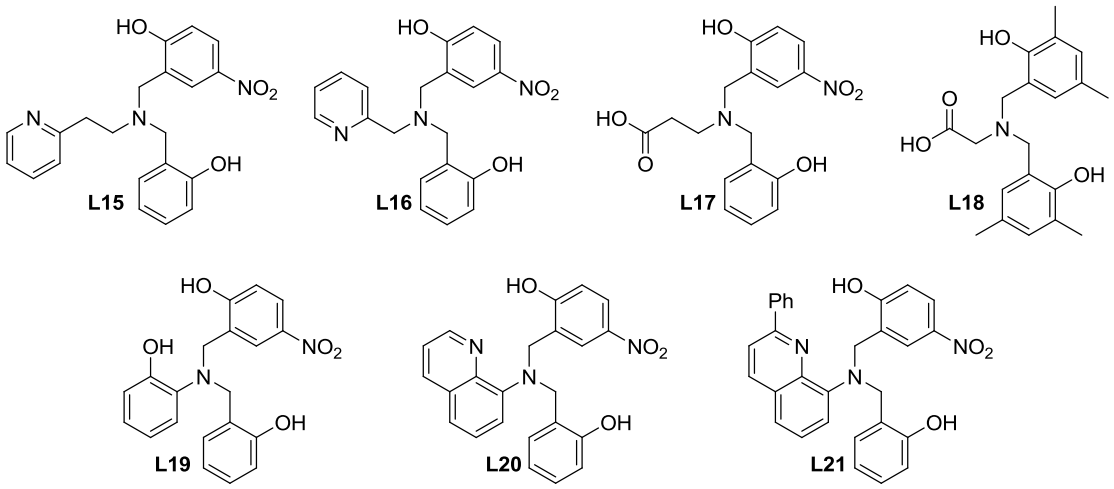

Figure 5.6: Range of tetra-coordinate amine-capped ligands

Unlike compounds **501** and **502** above, molecules **L15** through **L21** are open to coordination outside of the central cavity; however, when optimisation was attempted utilising the three donor arms with the fourth donor being a solvent molecule (H_2O) the minimised structure found displaced the water molecule and placed the Be(II) cation within the central cavity bound through the tertiary amine (Figure 5.7). The water molecule initially placed as the fourth point of coordination to Be(II) was displaced in favour of Be(II) coordination to the central amine.

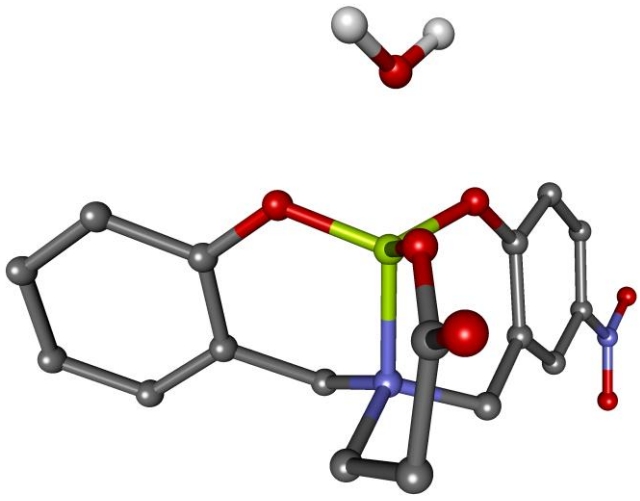

*Figure 5.7: Computer model of beryllium coordinated to **L17** and the water molecule initially placed as the fourth coordination point displaced after geometry optimisation, hydrogen atoms have been removed for clarity*

5.2 Synthesis of a Phenol-Capped Tetra-Coordinate Ligand

5.2.1 Introduction

If **501** is first considered with a carbon atom linking the three pyridine groups, the logical disconnection for would be to split it into the halide substituted 2-(pyridin-2-yl)phenol, **503**, and the methylene-bridged dipyridine, **504** (Figure 5.8).

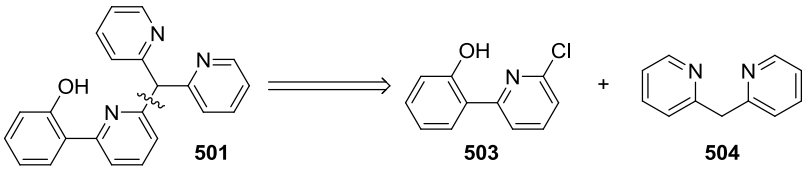

*Figure 5.8: Disconnection of 2-(6-(dipyridin-2-ylmethyl)pyridin-2-yl)phenol, **501***

The desired **503** has been reported previously.[146] The methylated phenol, **509**, should hopefully avoid undesired side reactions from the phenol group participating in the coupling with **504**. A Corriu-Kumada-Tamao coupling between the Grignard of the commercially available **505** and **507** gives **508** (Scheme 5.1).

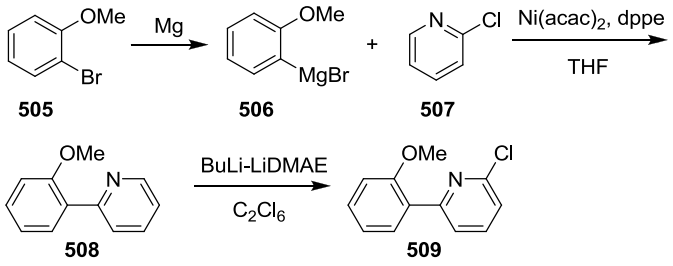

*Scheme 5.1: Synthesis of 2-chloro-6-(2-methoxyphenyl)pyridine, **509***

The substitution of a chloride selectively at the 2-position on **508**, was proposed to occur via chelation of the aggregate BuLi-DMAE (LiDMAE = $Me_2N(CH_2)_2OLi$, Figure 5.9).

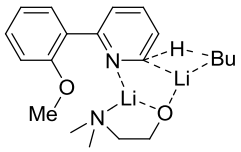

Figure 5.9: Proposed model for external chelations in substituted phenylpyridines leading to chloride substitution at the 2-position

While **504** is available commercially, it was more cost effective to synthesise it from the constituent pyridines. A number of papers have reported the synthesis of **504**, the most convenient was deemed to be that by Dyker and Muth.[147]

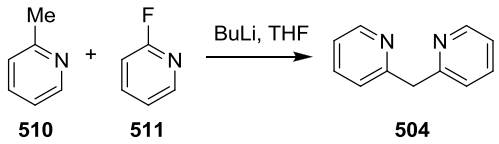

*Scheme 5.2: Synthesis of 2-(2-pyridylmethyl)pyridine, **504***

5.2.2 Results / Discussion

The synthesis of **504** and **509** proceeded as described in the literature. The coupling of **504** and **509**; however, did not proceed (Scheme 5.3).

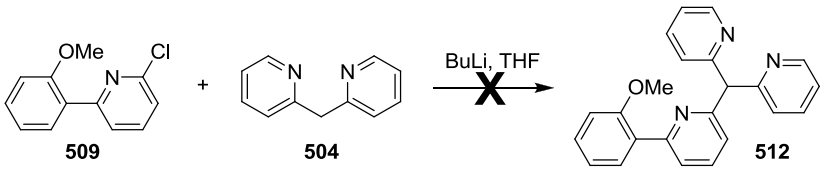

*Scheme 5.3: Attempted synthesis of 2-(dipyridin-2-ylmethyl)-6-(2-methoxyphenyl)pyridine, **512***

Firstly, the coupling was attempted by generating a carbanion of **504** with *n*-butyllithium. Although the exact coupling is unprecedented, a carbanion formed at the methylene bridge of **504** generated by treatment with *n*-butyllithium has been used in several carbon – carbon bond forming reactions previously.[147-150] The carbanion was formed by treatment of **504** with *n*-butyllithium at -78 ^{o}C in one hour, then the electrophile, **509**, was introduced and the reaction was either warmed slowly to RT over 4 hr or heated to reflux for 30 min.

There was no evidence of formation of **512** in either case by mass spectrometry of the reaction mixture or discrete products isolated by silica gel column chromatography.

In an attempt to make a better leaving group on **509**, a bromide was placed at the 2-position on the pyridine ring instead of the chloride to give **513**. The methodology of Parmentier and co-workers[146] was followed to give the previously unreported pyridylphenol; **513**. This was achieved by using carbon tetrabromide as the electrophile source in place of hexachloroethane in the final step of Scheme 5.1.

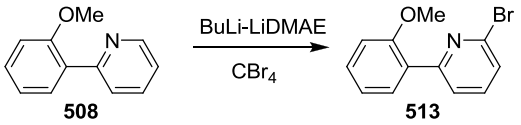

*Scheme 5.4: Synthesis of 2-bromo-6-(2-methoxyphenyl)pyridine, **513***

There was also no evidence for the formation of **512** when **513** was the electrophile in the attempted carbanion coupling reaction (Scheme 5.5).

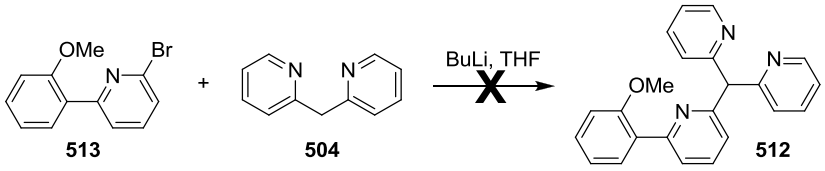

*Scheme 5.5: Attempted synthesis of 2-(dipyridin-2-ylmethyl)-6-(2-methoxyphenyl)pyridine, **512***

Nucleophilic substitution should occur at the 2-position of **509** or **513** as halides typically make good leaving groups and the 2-carbon should be slightly more electrophilic due to the influence of the slightly electron withdrawing nitrogen. The carbanion of **504** may not be a strong nucleophile, perhaps due to charge delocalisation onto the adjacent pyridine rings. Next, the roles in the coupling reaction were reversed by attempting to make carbanions of **509** and **513** by displacing the halides with *n*-butyllithium and using derivatives of **504** as the electrophile. **504** was substituted with a bromide at the methylene bridge using N-bromosuccinimide (NBS)[151] (Scheme 5.6) to add a leaving group and promote nucleophilic displacement by **509** or **513**.

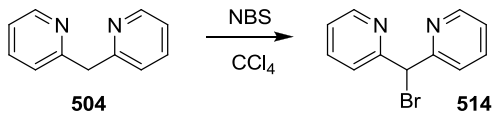

*Scheme 5.6: Synthesis of 2,2'-(bromomethylene)dipyridine, **514***

The coupling still did not proceed when the carbanion of **509** or **513** was reacted with **514** (Scheme 5.7). Although there was no precedence of **514** acting as an electrophile in carbon – carbon bonding forming reactions, it was hoped that *n*-butyllithium would displace the halides on **509** and **513** making a carbanion at the 2-position on the pyridine ring. Charge delocalisation may also make **509** and **513** poor nucleophiles.

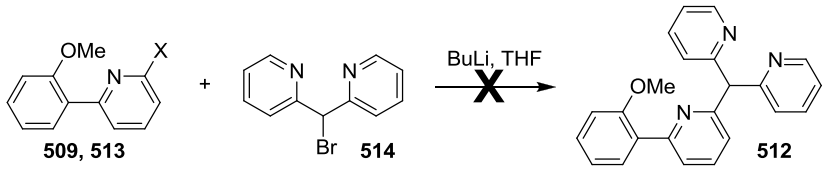

*Scheme 5.7: Attempted synthesis of 2-(dipyridin-2-ylmethyl)-6-(2-methoxyphenyl)pyridine, **512**, X=Br,Cl*

Similarly, when dipyridin-2-ylmethanone, **515**, was used as the electrophile in place of **514** there was still no coupling observed (Scheme 5.8). A coupling of **515** and an aromatic bromide has been reported[152] and with a N-substituted pyrrole with a bromide at the 2-position.[153] The problem must be isolated to the attempted use of **509** or **513** as the nucleophiles.

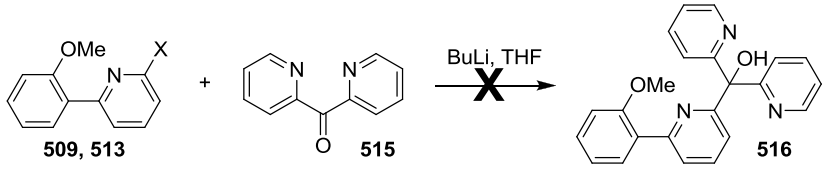

*Scheme 5.8: Attempted synthesis of (6-(2-methoxyphenyl)pyridin-2-yl)dipyridin-2-ylmethanol, **516**, X=Br,Cl*

It was apparently not possible to construct **512** or **516** using this methodology. Finally, the coupling via nucleophilic substitution of carbanions was abandoned altogether and the nucleophile was switched to dipyridin-2-ylamine, **517** (Figure 5.10).

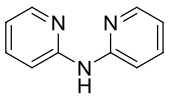

*Figure 5.10: Dipyridin-2-ylamine, **517***

While **517** would change the backbone of the resultant tetra-coordinate species to **518** (Scheme 5.9) there is no obvious drawback to having an amine in place of the central carbon of **512**. The central amine would not be expected to participate in coordination to Be(II) as unfavourable four-membered N(amine) – Be – N(pyridine) chelate rings would need to form. It is expected that Be(II) coordination would still proceed via the three pyridines and phenol.

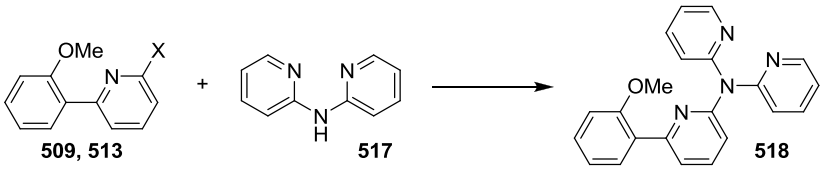

*Scheme 5.9: Proposed synthesis of 6-(2-methoxyphenyl)-N,N-di(pyridin-2-yl)pyridin-2-amine, **518**, X=Br,Cl*

Nucleophilic substitution of **517** onto aromatic bromides is a known coupling reaction as reported by Aubouy and co-workers.[154] This reaction involved a melt of **517** and an aromatic bromide with K_2CO_3 and $CuSO_4.5H_2O$ heated to 210 ^oC for 6 hr.

When the same reaction conditions were applied to **513** and **517** only trace quantities of **518** were formed as evidenced by TLC and mass spectrometry. The solventless high-temperature thermal reaction was not suitable in this instance and significant charring of reagents occurred over the course of the reaction.

The solventless reaction was also attempted with microwave heating for shorter time periods of 5 – 15 min at 160 ^oC; however, only trace quantities of **518** were formed as evidenced by TLC. Attempted microwave heating for longer time periods 15 – 60 min at lower temperature, 120 ^oC did not improve coupling. The problem was most likely caused by inadequate mixing of the reagents and the stability of **513** so the reaction was re-designed to use 6M KOH as both the solvent and base (in place of K_2CO_3). Now, the

reaction proceeded smoothly after 15 min at 160 ^{o}C heating by microwave irradiation. The only minor issue was in purification as both unreacted **517** and the product **518** had similar polarity making silica gel column chromatography difficult. This was solved by using two equivalents of **513** and this achieved nearly quantitative conversion of **517** to **518**. This represented a novel and efficient route to **518** (Scheme 5.10).

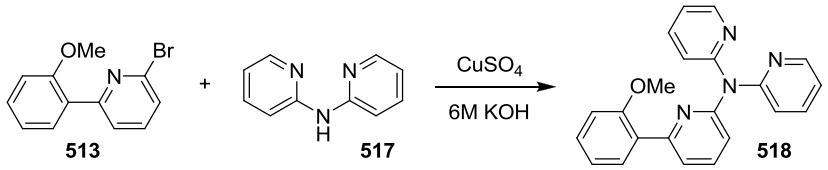

*Scheme 5.10: Synthesis of 6-(2-methoxyphenyl)-N,N-di(pyridin-2-yl)pyridin-2-amine, **518***

The synthesis of **518** was confirmed by ^{1}H, ^{13}C NMR and high resolution mass spectroscopy. While the aromatic signals were overlapped in the ^{1}H NMR, a 2D COSY NMR experiment in conjunction with comparison of some of the original shifts for **513** and **517** allowed identification of the three distinct regions of coupled aromatic protons (Figure 5.11).

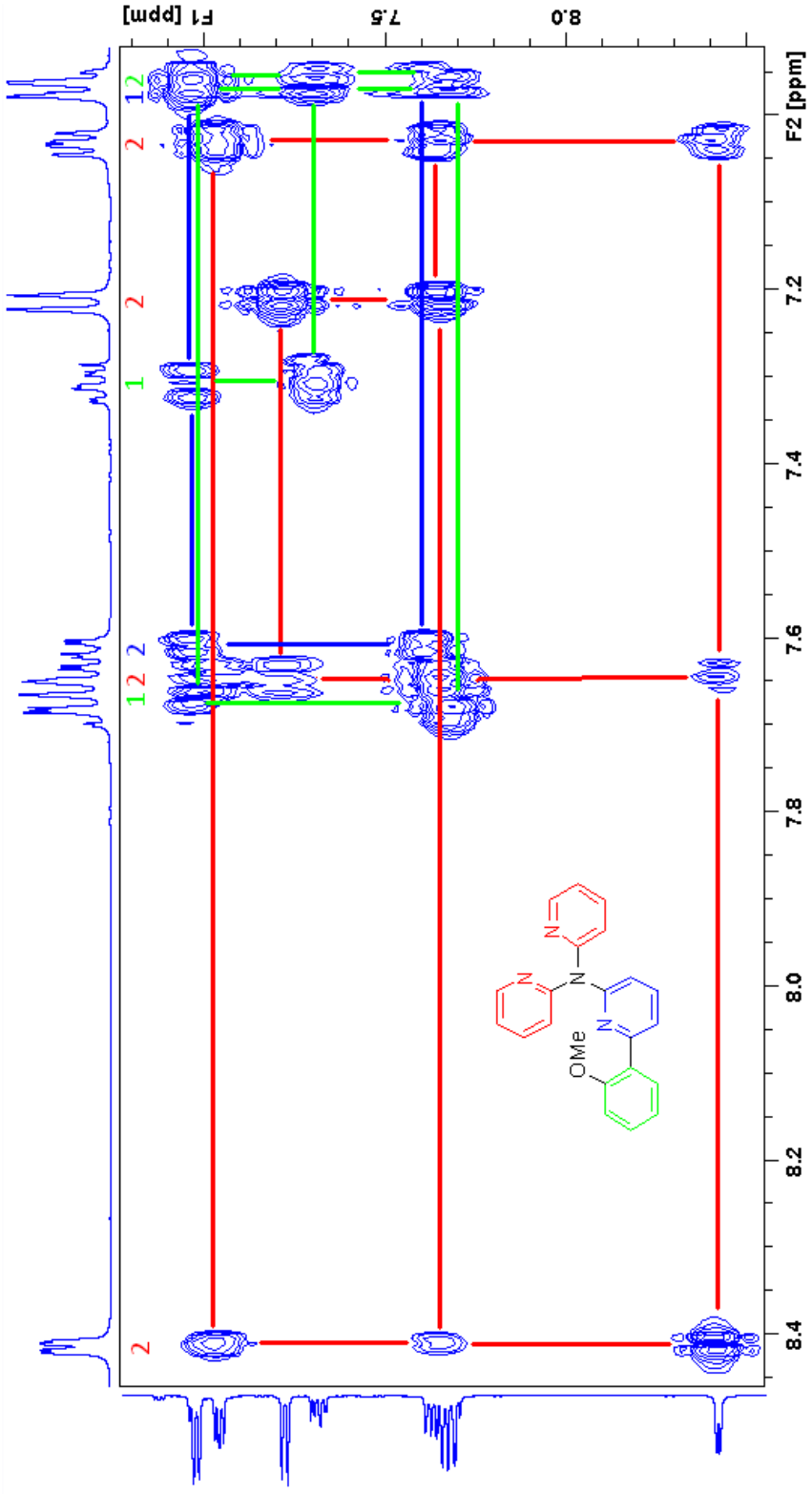

Figure 5.11: COSY of 6-(2-methoxyphenyl)-N,N-di(pyridin-2-yl)pyridin-2-amine, ***518***

Finally a 2D HMQC NMR experiment identified the 15 carbons coupled to protons (the carbons in **red** are symmetric so 11 actual carbon peaks are observed) and 6 quaternary carbons (the carbons in **red** are symmetric so 5 actual carbon peaks are observed) (Figure 5.12).

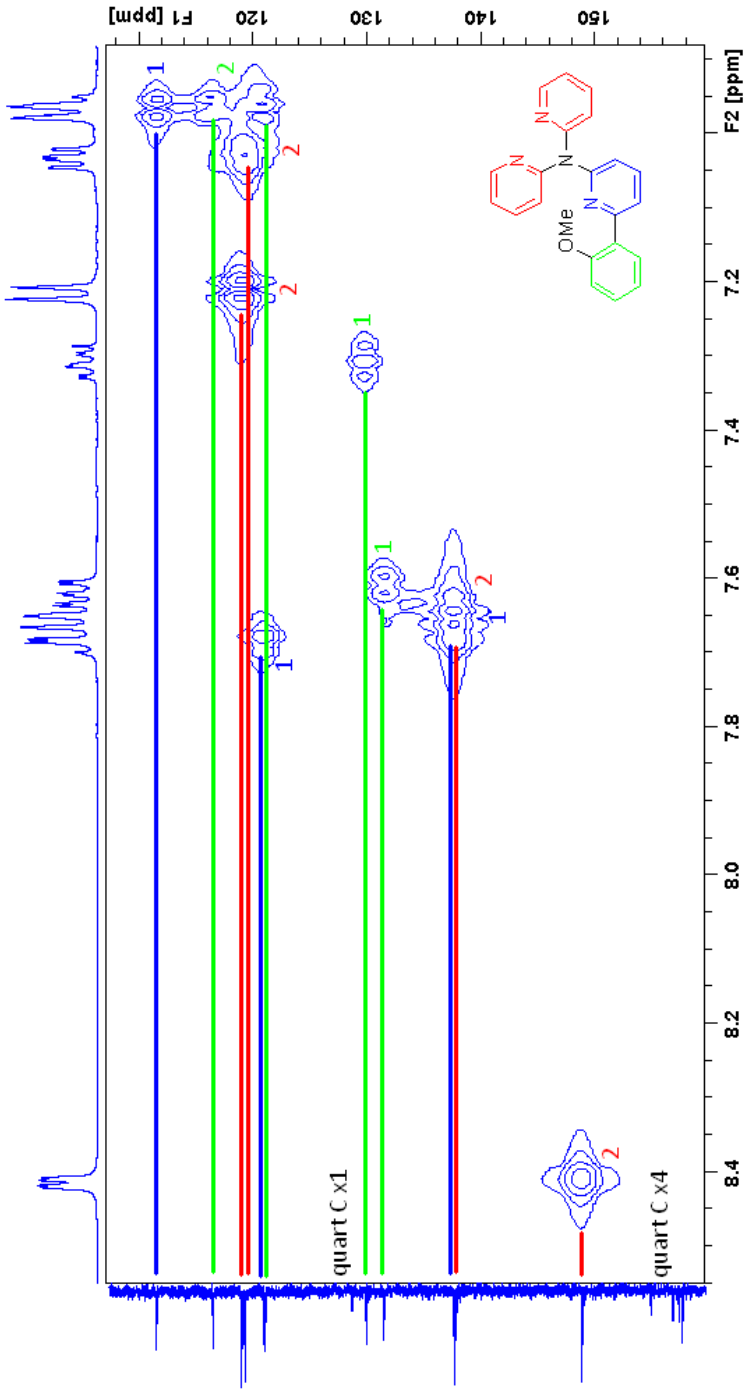

Figure 5.12: HMQC of 6-(2-methoxyphenyl)-N,N-di(pyridin-2-yl)pyridin-2-amine, ***518***

Demethylation of **518** was achieved using BBr_3 to give **L14** in 79 % yield (Scheme 5.11), a ligand potentially capable of fully encapsulating Be(II). The HBr generated upon aqueous workup protonated the nitrogen atoms on **L14**, the aqueous phase was neutralised with 2M NaOH where **L14** moved into the organic phase. The correct product was identified by NMR and high resolution mass spectroscopy after purification by silica gel column chromatography. The notable difference from the NMR of **518** and **L14** was the disappearance of the methoxide peak at 3.87 ppm and the appearance of phenol proton at 12.54 ppm in the ^1H NMR spectrum. A misleading peak in the low resolution mass spectrum with the same mass as **518** could be seen when the solvent was dichloromethane. This is actually **L14**.CH_2^+ as pyridine is known to slowly react with dichloromethane to form methylenebispyridinium salts and is readily observed in the ionising conditions of the mass spectrometer.[155]

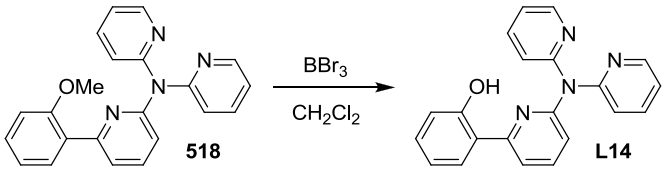

*Scheme 5.11: Synthesis of 2-(6-(dipyridin-2-ylamino)pyridin-2-yl)phenol, **L14***

The overall yield of **L14** over four steps was 29 %. The ^1H NMR of **L14** highlights the promise for an ideal Be(II) chelator (Figure 5.13). The phenolic proton is deshielded due to hydrogen bonding to the adjacent pyridine and appears at 12.55 ppm. This should enhance the ability of the phenolic oxygen to initially coordinate to Be(II) while the proton is shuttled off via the pyridine. After initial coordination to Be(II) via the phenol, full encapsulation of Be(II) through the remaining pyridines will hopefully readily occur via chelation.

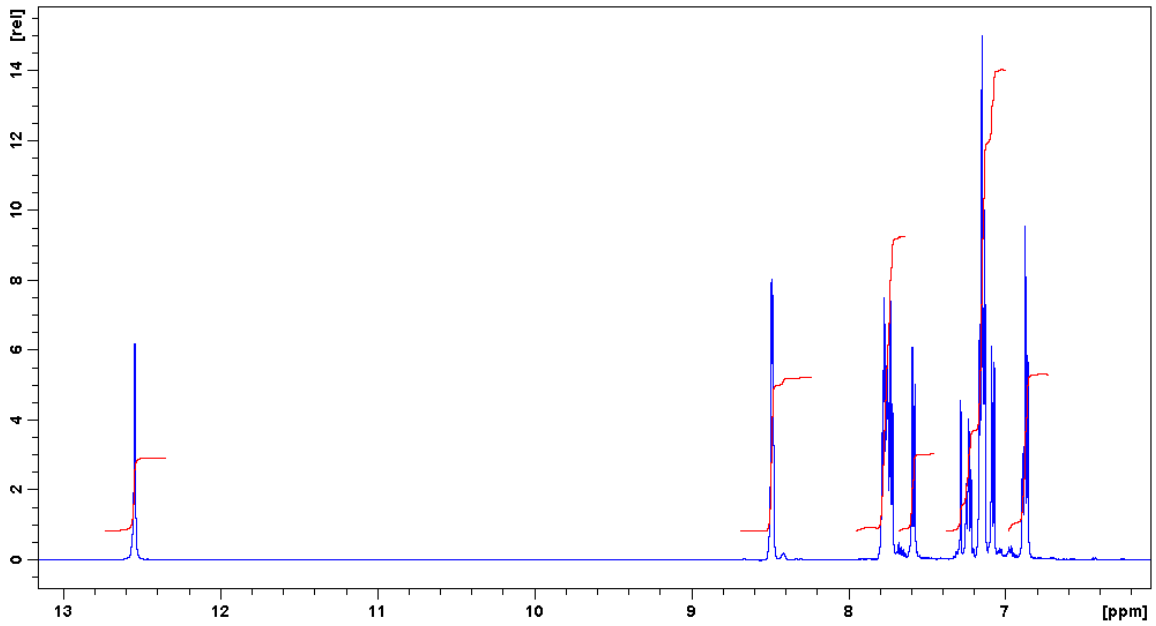

Figure 5.13: ^{1}H NMR of 2-(6-(dipyridin-2-ylamino)pyridin-2-yl)phenol, ***L14*** *showing the deshielded proton at 12.55 ppm.*

5.3 Synthesis of a Carboxylic Acid-Capped Tetra-Coordinate Ligand

5.3.1 Introduction

As with **501**, the logical disconnection for **502** would be to split it into a substituted quinoline **519** and the methylene-bridged dipyridine used earlier, **504** (Scheme 5.12). Both **519** and **504** are accessible using existing literature syntheses.

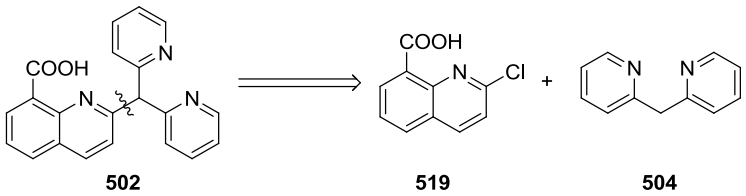

*Scheme 5.12: Disconnection of 2-(dipyridin-2-ylmethyl)quinoline-8-carboxylic acid, **502***

The exact quinoline, **519**, had not been previously fully characterised. However, Cottet and co-workers[156] synthesised a range of trifluoromethyl-substituted quinolinecarboxylic acids, one of which was **520** (Figure 5.14).

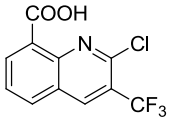

*Figure 5.14: 2-Chloro-3-(trifluoromethyl)quinoline-8-carboxylic acid, **520***

The synthesis of **520** can be altered by avoiding the 3-trifluoromethyl substitution step such that the final compound would be the desired **519** (Scheme 5.13).

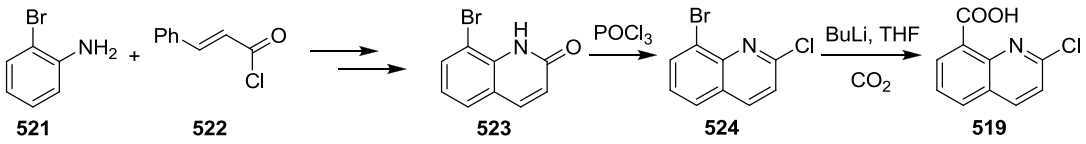

*Scheme 5.13: Proposed synthesis of 2-chloroquinoline-8-carboxylic acid, **519***

Attempting to couple the free carboxylic acid, **519**, with **504** may be problematic due to undesired side-reactions so the carboxylic acid will be protected. Alternatively, ethyl chloroformate might form a protected ester directly from **524** (Scheme 5.14). The esterification of an aromatic bromide has been reported previously.[157]

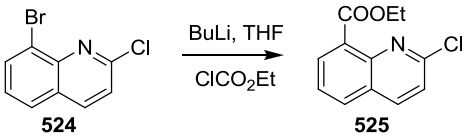

524 **525**

*Scheme 5.14: Proposed synthesis of ethyl 2-chloroquinoline-8-carboxylate, **525***

An alternative to this synthesis might be to start off with an ester at the 2-position of the aniline by using **526** instead of 2-bromoaniline, **521** (Scheme 5.15). There is no precedent for quinoline formation resulting in an ester at the 8-postion directly, however, the cheap starting material **526** makes this route worthwhile to attempt.

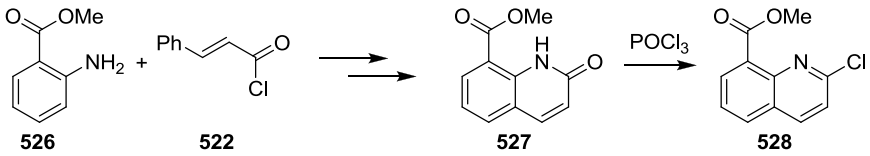

526 **522** **527** **528**

*Scheme 5.15: Proposed synthesis of methyl 2-chloroquinoline-8-carboxylate, **528***

It is hoped the carbanion of **504** generated by treatment with *n*-butyllithium will couple by nucleophilic substitution of the chloride at the 2-position on **525** (Scheme 5.16).

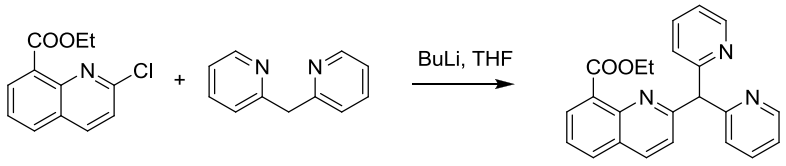

525 **504** **529**

*Scheme 5.16: Proposed synthesis of ethyl 2-(dipyridin-2-ylmethyl)quinoline-8-carboxylate, **529***

A related compound was formed shown in Scheme 5.17.[158] A carbanion of **530** was generated by treatment with *n*-butyllithium and reacted first with **507**, and then finally in a

second analogous carbanion reaction with **531** as the electrophile. The central amine was protected by treatment with acetic anhydride to give **532**.

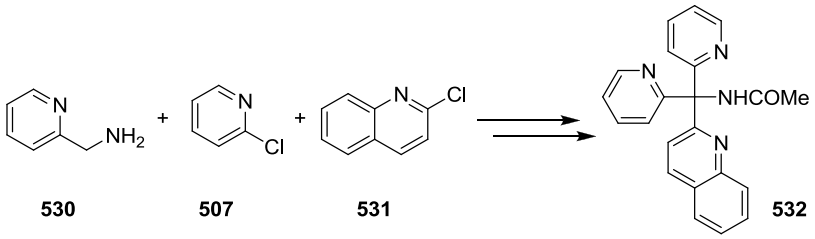

Scheme 5.17: Synthesis of N-(dipyridin-2-yl(quinolin-2-yl)methyl)acetamide, ***532***[158]

532 was part of a larger paper which dealt with tripodal pyridine complexes of copper and zinc. No crystal structures of metal complexes with **532** was obtained, however, it was deduced to have the structure $[Cu(SO_4)(\mathbf{532})(H_2O)].3H_2O$. A crystal structure of a similar complex with the tridentate pyridine showed a distorted square pyramidal geometry. A non-coordinated water molecule occupied the sixth coordination site in octahedral geometry. The target compound in this section should hopefully provide a steric hindrance to coordination of most metals ions larger than Be(II).

5.3.2 Results / Discussion

The synthesis of **504** proceeded in nearly quantitative yield as described previously (Scheme 5.18).[147] After aqueous workup and solvent evaporation, **504** was used without purification.

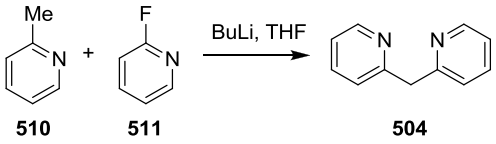

Scheme 5.18: Synthesis of 2-(2-pyridylmethyl)pyridine, ***504***

The synthesis of the quinoline precursor, **524**, proceeded without difficulty in accord with the literature preparation (Scheme 5.19).[156] **533** was used without recrystallisation as stated

in the original preparation. In the cyclisation step to form **523**, toluene was used as the solvent in place of chlorobenzene and silica gel column chromatography was required instead of recrystallisation. Purification of **524** by silica gel column chromatography was followed by recrystallisation by slow cooling of a solution of **524** in hot hexane.

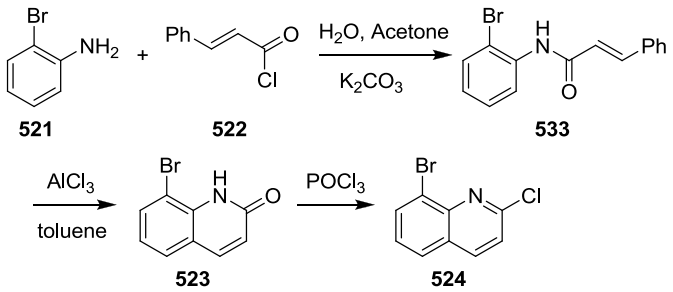

521 **522** **533** **523** **524**

*Scheme 5.19: Synthesis of 8-bromo-2-chloroquinoline, **524***

Conversion of the bromide at the 8-position of **524** to an ester directly was unsuccessful. When ethyl chloroformate was added to the carbanion of **524** over a range of reaction conditions, only trace amounts (< 1%) of **525** could be isolated by chromatography which contained a side-product with the same polarity as **525**. As no other discrete products were isolated self-polymerisation of **524** most likely occurred as there are two electrophilic sites on the molecule.

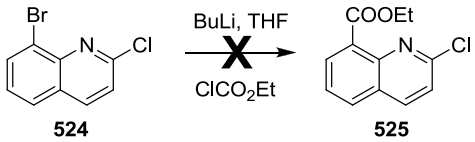

524 **525**

*Scheme 5.20: Unsuccessful esterification of **525***

Under optimal conditions the side-product (B, Figure 5.15) was present in a 6:5 ratio over **525** (A, Figure 5.15) according to ^{1}H NMR integrals. Full characterisation of **525** and the side-product B was not attempted due to the poor yielding reaction. Instead, an alternate route to placing an ester at the 8-position of **525** was successfully pursued in two steps by carboxylation then protection of the carboxylic acid as an ester.

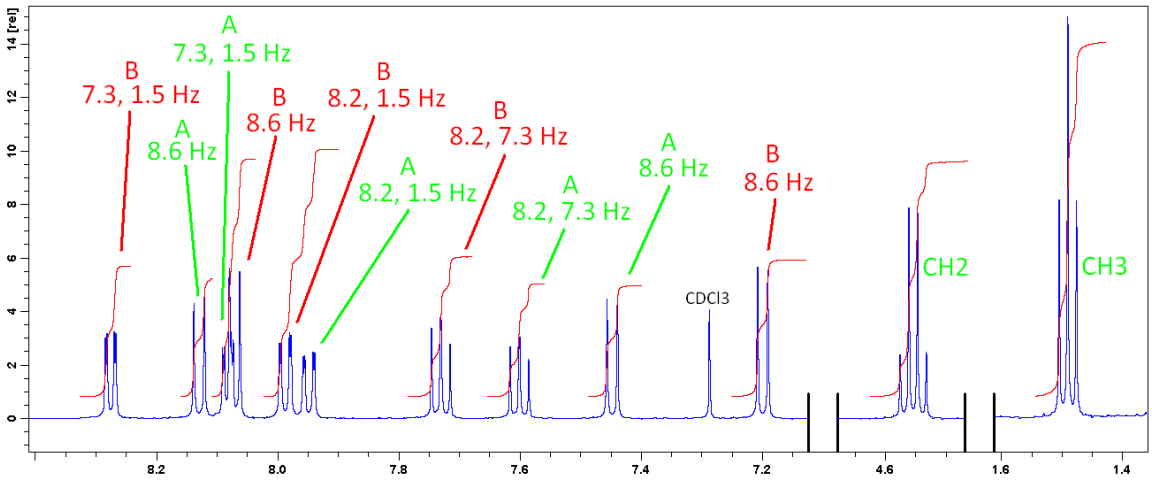

*Figure 5.15: ^{1}H NMR of the trace amount of **525** (A) and the side-product (B) isolated in Scheme 5.19*

The carboxylation reaction reported by Cottet and co-workers[156] (Scheme 5.21) shows that upon treatment with *n*-butyllithium a carbanion forms by displacing the bromide preferentially to the chloride and then reacts with carbon dioxide to give **520**.

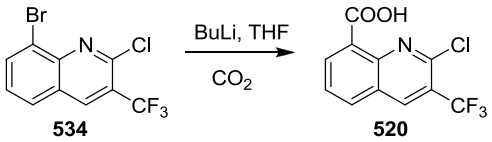

*Scheme 5.21: Synthesis of 2-chloro-3-(trifluoromethyl)quinoline-8-carboxylic acid, **520***

The above reaction used dry ice as the CO_2 source; however, bubbling of CO_2 gas from a cylinder through the reaction mixture could achieve **519** (Scheme 5.22). While **520** was obtained in 68% yield, the yield of **519** was only 42%. The trifluoromethyl group at the 3-postion of **520** appears to prevent an elimination side reaction which was apparently more problematic with **524**. Nevertheless, small quantities of **519** were formed in 18 % yield over 4 steps.

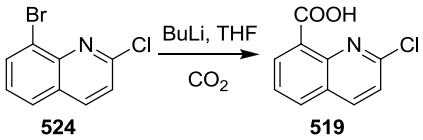

*Scheme 5.22: Synthesis of 2-chloroquinoline-8-carboxylic acid, **519***

The ^{1}H NMR of **519** highlights why this makes an excellent ligand precursor for potential Be(II) coordination (Figure 5.16). The proton on the carboxylic acid is deshielded as a result of hydrogen bonding to the heterocyclic nitrogen and appears at 14.82 ppm. This is reminiscent of the deshielded protons seen for proton sponges but has the added benefit of the oxygen donor to promote initial coordination to Be(II) while the deshielded proton may be removed via the heterocyclic nitrogen.

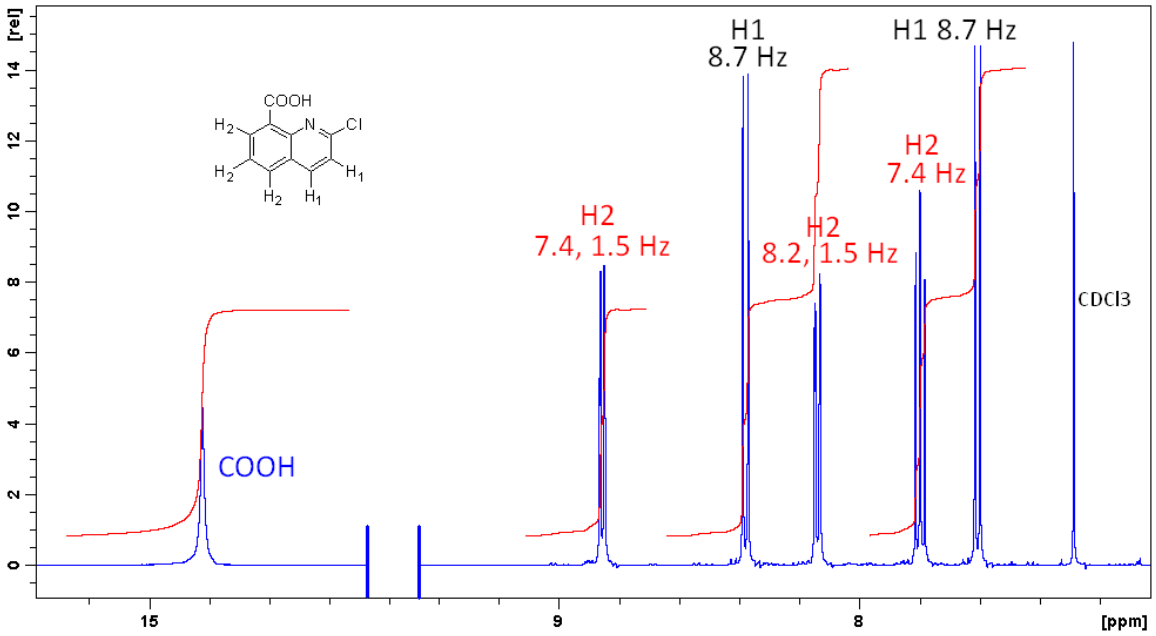

*Figure 5.16: ^{1}H NMR of 2-chloroquinoline-8-carboxylic acid, **519***

Finally, the carboxylic acid group of **519** was protected as a methyl ester by treating the caesium salt with methyl iodide (Scheme 5.23) according to a standard procedure for protecting carboxylic acids.[159]

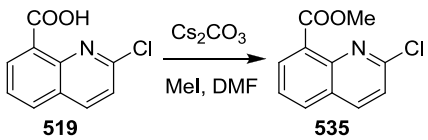

*Scheme 5.23: Synthesis of methyl 2-chloroquinoline-8-carboxylate, **535***

When the ester substituted aniline, **526**, was used to attempt to form **535** directly, the cyclisation step did not proceed. The amide **536** formed without issue in 95 % yield;

however, **536** did not undergo cyclisation upon treatment with $AlCl_3$. There were no discrete products obtained and no formation of **527**.

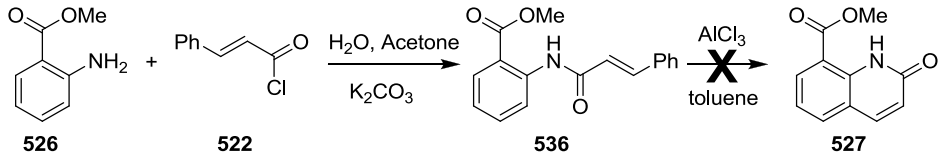

*Scheme 5.24: Attempted synthesis of methyl 2-oxo-1,2-dihydroquinoline-8-carboxylate, **527***

The coupling of the carbanion of **504** with **519** or **535** was attempted; however no desired reaction was observed (Scheme 5.25). The carbanion of **504** most likely removed the proton from the carboxylic acid on **519**, yet, when two equivalents of *n*-butyllithium were used to compensate for the presence of the carboxylic acid there was still no coupling. The ester protected variant, **535**, also did not show the desired substitution at the 2-chloro position. There was no indication by mass spectroscopy that **502** had formed.

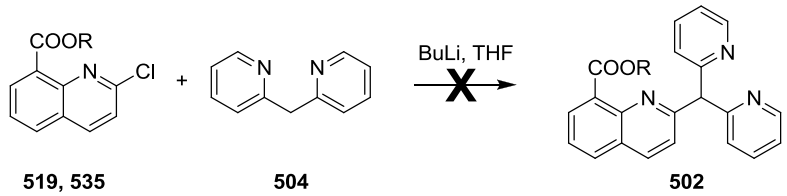

*Scheme 5.25: Attempted synthesis of 2-(dipyridin-2-ylmethyl)quinoline-8-carboxylic acid, **502**, R=H, Me*

Since direct coupling proved problematic with the carboxylic acid or ester in place, it may be possible to substitute the carboxylic acid in a later step. When the carbanion of **504** was coupled with **524**, the reaction proceeded as indicated in Scheme 5.26. The carbanion selectively substituted at the 2-chloride and not with the 8-bromide as confirmed by mass spectroscopy. While a bromide typically makes a better leaving group than a chloride, the 2-position is likely activated by being adjacent to the slightly electronegative nitrogen atom. The yield was 75 – 78 %.

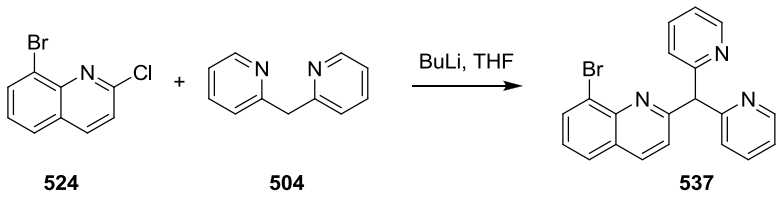

*Scheme 5.26: Synthesis of 8-bromo-2-(dipyridin-2-ylmethyl)quinoline, **537***

Unfortunately, all attempts to modify the bromide on **537** to a carboxyl group by treatment with *n*-butyllithium and carbon dioxide were unsuccessful (Scheme 5.27). After first acidifying the reaction mixture with 2M HCl then neutralising to pH 7 with 2M NaOH, there was no indication by mass spectroscopy or ^{1}H NMR that the organic layer extracted contained **502**. When treated with *n*-butyllithium, both the central sp^3 proton (there was an absence of this distinct peak in the ^{1}H NMR) and the bromide were displaced and the lack of discrete product formation suggested degradation or polymerisation was occurring. Using two equivalence of *n*-butyllithium to simultaneously displace both the bromide and the central sp^3 proton in an attempt to curb possible polymerisation did not solve this problem and a similarly messy ^{1}H NMR spectrum was obtained.

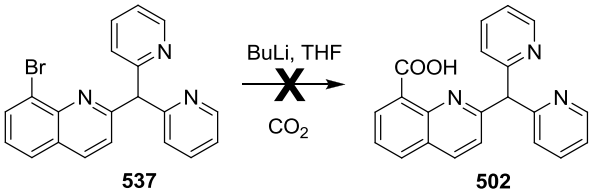

*Scheme 5.27: Attempted synthesis of 2-(dipyridin-2-ylmethyl)quinoline-8-carboxylic acid, **502***

An alternative route to **502** may be hydrolysis of a nitrile at the 8-position on the quinoline. A cyanation using copper cyanide with an aromatic bromide allows substitution of a nitrile.[160] When this reaction was attempted on **524**, the reaction proceeded selectively on the 8-bromide and not the 2-chloride to give **538** in 63 % yield (Scheme 5.28). This was confirmed by high resolution mass spectroscopy and a new nitrile peak in the ^{13}C NMR spectra.

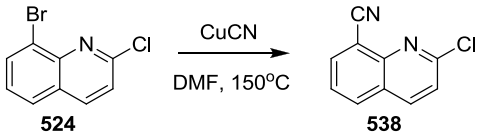

524 538

Scheme 5.28: Synthesis of 2-chloroquinoline-8-carbonitrile, ***538***

Subsequently the nitrile-substituted quinoline, **538**, was used as the electrophile in the coupling reaction with **504**, which proceeded by selective displacement of the chloride on **546** to give **539** in 69 % yield (Scheme 5.29).

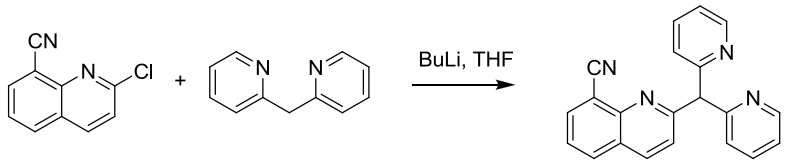

538 504 539

Scheme 5.29: Synthesis of 2-(dipyridin-2-ylmethyl)quinoline-8-carbonitrile, ***539***

Hydrolysis of the nitrile on **539** was attempted in both acidic (6M HCl) and basic (6M NaOH) conditions, refluxing for 4 h at 110 ^{o}C. After neutralisation and organic extraction, in both cases none of the desired product, **502**, was observed by ^{1}H NMR or mass spectroscopy. Again, the lack of discrete products obtained is apparently owed to the reactive nature of the central sp^3 proton as this distinct peak was absent in the ^{1}H NMR spectrum.

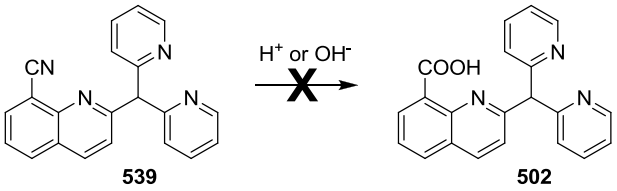

539 502

Scheme 5.30: Attempted synthesis of 2-(dipyridin-2-ylmethyl)quinoline-8-carboxylic acid, ***502***

Lastly, the same reaction methodology which enabled the successful synthesis of **L14** in Section 5.2 was attempted with **519** and **535** (Scheme 5.31). Sadly, in this instance the chlorides were not susceptible toward nucleophilic attack of **517** under the reaction

conditions and no evidence of coupling was observed, a bromide at the 2-postion may be required.

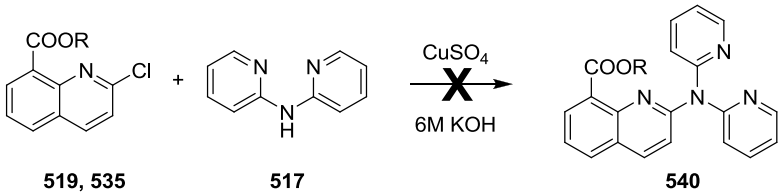

*Scheme 5.31: Attempted synthesis of 2-(dipyridin-2-ylamino)quinoline-8-carboxylic acid, **540**, R=H, Me*

As a representative ligand of this type had eventually been synthesised with a phenol as the oxygen donor, **L14** (Figure 5.17); further investigation into synthesis of the carboxylic acid variant was halted due to the time restrictions on this project. Should the phenol variant **L14** prove an excellent ligand for beryllium the synthesis of the carboxylic acid variant; **540**, could be restarted.

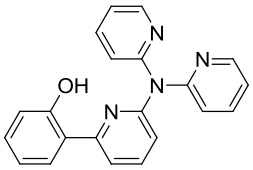

*Figure 5.17: Successfully synthesised 2-(6-(dipyridin-2-ylamino)pyridin-2-yl)phenol, **L14***

One possible route to achieving **540** laid out in Scheme 5.30 could be to form **541** by using phosphorus oxybromide in the dehydration step of the quinoline synthesis (Scheme 5.32).

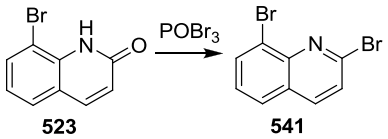

*Scheme 5.32: Proposed synthesis of 2,8-dibromoquinoline, **541***

While it seems counter-intuitive to have bromides at both the 2- and 8-positions, the 2-position should be activated due to the influence of the nitrogen atom. The successful coupling of **524** and **504** showed the 2-position was activated toward nucleophilic substitution and the 2-chloride was displaced in favour of the 8-bromide (Scheme 5.33).

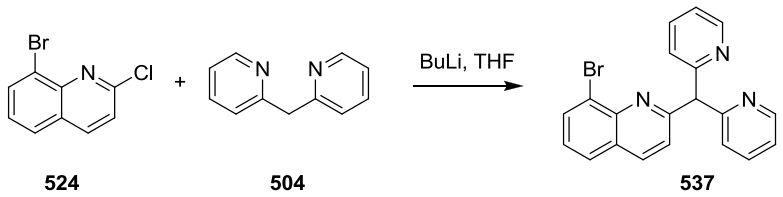

524 **504** **537**

*Scheme 5.33: Synthesis of 8-bromo-2-(dipyridin-2-ylmethyl)quinoline, **537***

If the coupling of **541** and **517** were successful (Scheme 5.34), the 8-bromide may be easier to convert to a carboxylic acid compared to that on **537** as there would not be a central sp^3 proton susceptible to treatment with *n*-butyllithium which caused degradation and polymerisation problems.

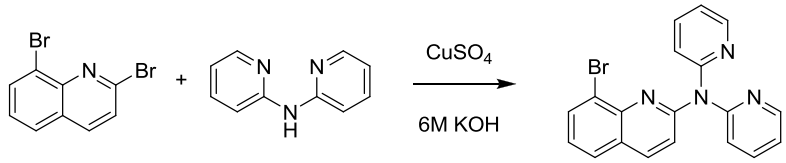

541 **517** **542**

*Scheme 5.34: Proposed synthesis of 8-bromo-N,N-di(pyridin-2-yl)quinolin-2-amine, **542***

5.4 Synthesis of Amine-Capped Tetra-Coordinate Ligands

5.4.1 Introduction

All of the ligands synthesised in this section followed a commonly utilised series of reactions. An example is shown in Scheme 5.35. The secondary amine **545** was obtained from a Schiff base condensation of a component amine and aldehyde followed by reduction.[161] Further substitution to provide the final donor arm, **546**, by nucleophilic displacement of a chloride gave the tetra-coordinate ligand, **547**.[162] When coordinated to transition metals, ligands of this type typically form diphenoxo-bridged $[M_2L_2]$ complexes.[162]

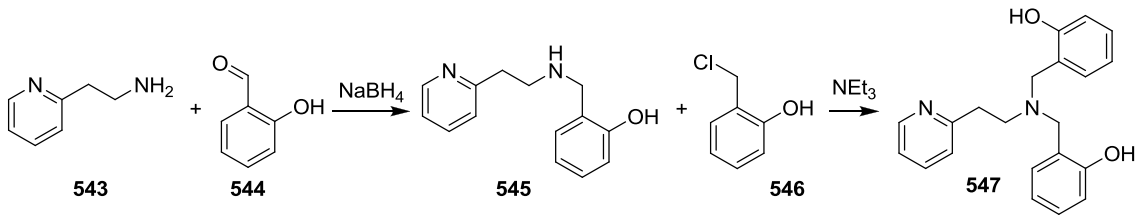

*Scheme 5.35: Synthesis of the tetra-coordinate ligand, **547***

By analogy to the above synthesis, a series of structurally related ligands may also be constructed (Figure 5.18). Exchanging **543** with an amine containing a suitable donor provides a different tetra-coordinate ligand. For ease of synthesis, in place of **546**, the commercially available 2-(chloromethyl)-4-nitrophenol (**548**) was used. The drawback of this was that upon coordination to Be(II) all the complexes become chiral due to the two phenol arms being non-identical. The unbound ligands are not chiral as the central amine inverts. With the exception of the nitro group substitution on one of the phenols, ligands **L15**,[162] **L16**[163] and **L19**[164] have been synthesised previously. The exact ligand **L18** has been reported previously.[165] The ligands **L17**, **L20** and **L21** have not been previously reported.

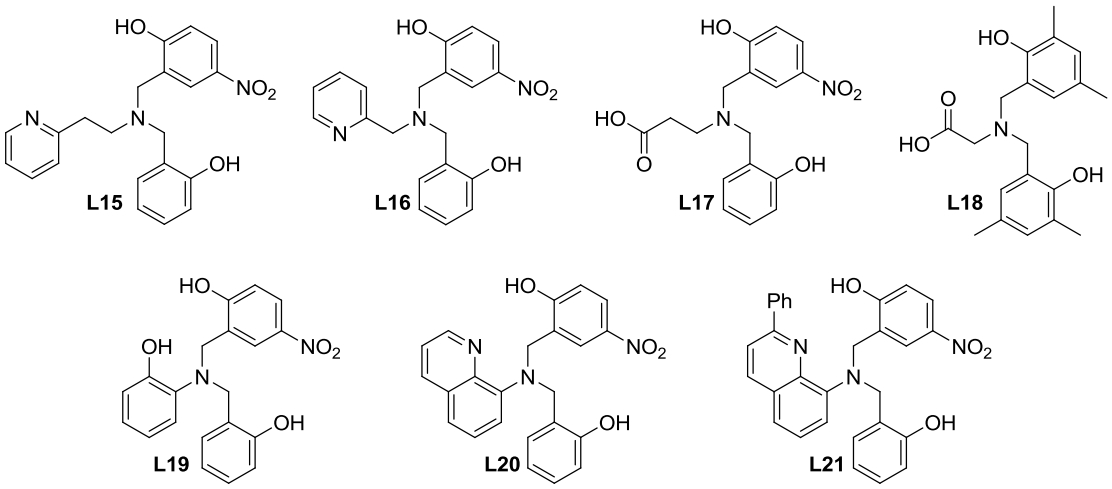

Figure 5.18: Variety of amine-capped tetra-coordinate ligands

5.4.2 Results / Discussion

The initial Schiff base condensations for **L15** to **L17** were complete after 30 min. The Schiff base condensation for **L19** was moderately slower taking 6 hr and those for **L20** and **L21** were extremely slow due to the delocalisation into the aromatic system and took 1 week each. After *in situ* reduction with sodium borohydride the yields for the secondary amines were 68 – 89 % (Scheme 5.36). The only new secondary amines were those for **L17** and **L21** so were further characterised (in addition to NMR) by elemental analysis or high resolution mass spectroscopy. The remaining secondary amines agreed with the previous characterisation data.

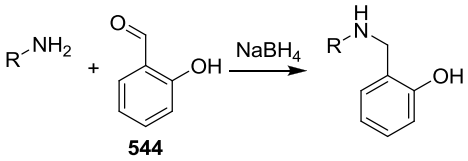

*Scheme 5.36: Generalised reductive aminations for ligands **L15**, **L16**, **L17**, **L19**, **L20** and **L21**; R is the appropriate ligand arm*

The tertiary amines, **L15**, **L16**, **L17**, **L19**, **L20** and **L21** were synthesised according to a standard preparation via substitution of **548** in 46 – 69 % yields (Scheme 5.37). The final

products after purification by silica gel column chromatography were sticky oils due to residual solvent. To obtain solid powders, the oils were dissolved in a small volume of dichloromethane and an excess of hexane was added. After solvent removal under reduced pressure, the oils eventually became solid foams and could be collected in powder form. Due to the presence of the nitro substituent, all six ligands were technically new compounds so were further characterised (in addition to NMR) by elemental analysis or high resolution mass spectroscopy.

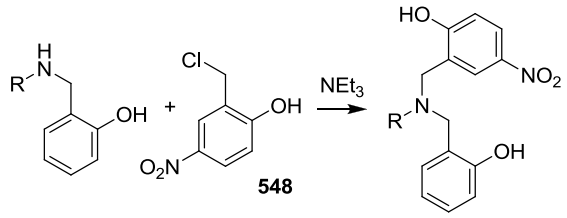

*Scheme 5.37: Generalised reaction scheme for tertiary amines **L15**, **L16**, **L17**, **L19**, **L20** and **L21**; R is the appropriate ligand arm*

As a representative example to show the new ligands have been correctly synthesised, the particular COSY NMR characterisation of **L20** will be described in detail (Figure 5.19). While some of the aromatic signals were overlapped in the ^{1}H NMR, a 2D COSY NMR experiment in conjunction with comparison of some of the original shifts for the component secondary amine and **548** allowed identification of the four distinct regions of coupled aromatic protons. Aside from the aromatic protons, the four CH_2 protons (4.49 ppm) which should ordinarily give sharp uncoupled singlets appeared unusually broadened. This could be rationalised by observing the two downfield phenol shifts at 10.43 and 12.61 ppm which imply intra-molecular hydrogen-bonding interactions with each of the nitrogens. The locking of the molecule's geometry via hydrogen bonding causes the CH_2 protons to become chemically inequivalent leading to the observed broadened ^{1}H NMR signal.

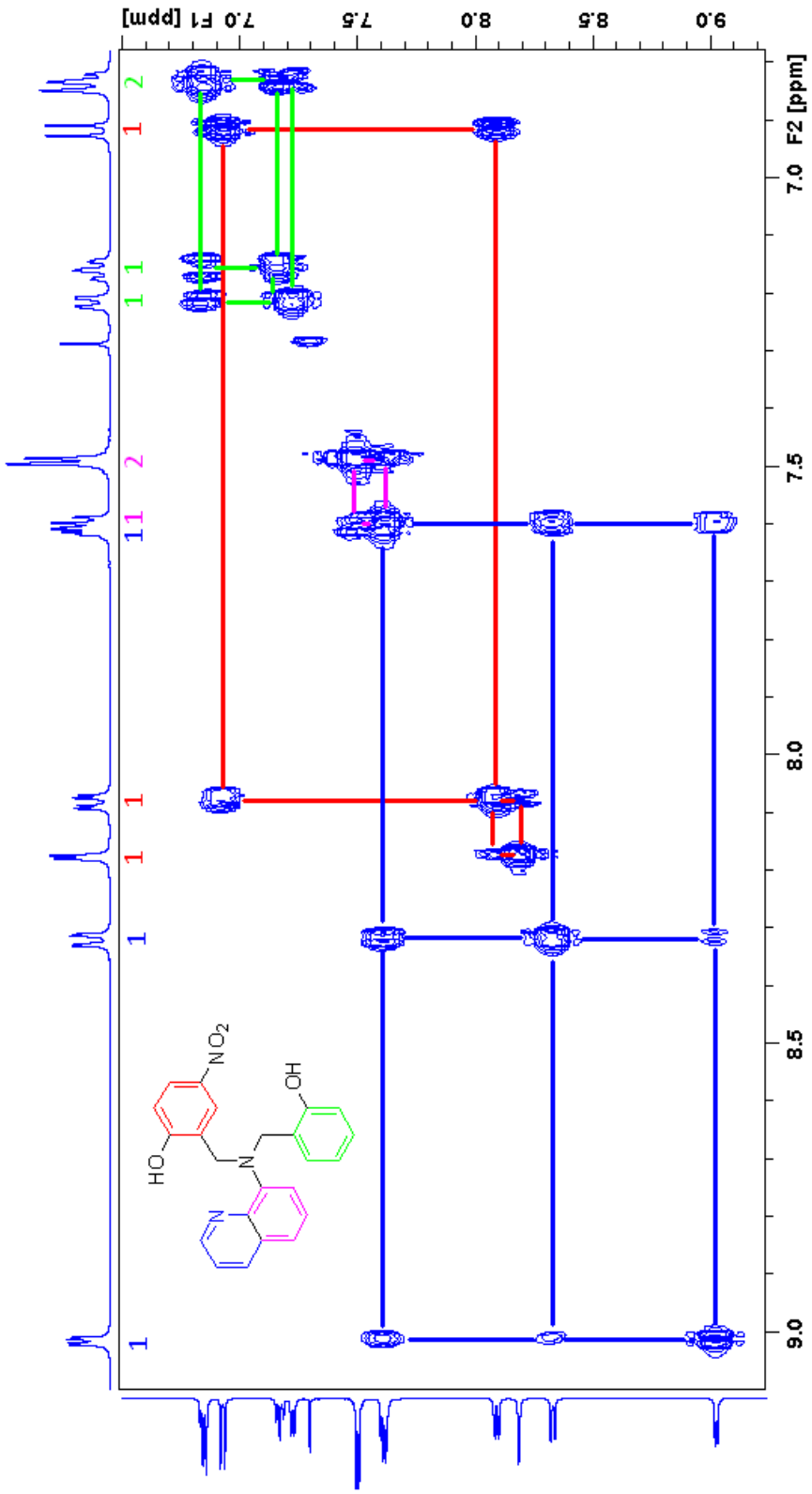

Figure 5.19: COSY of 2-(((2-hydroxybenzyl)(quinolin-8-yl)amino)methyl)-4-nitrophenol, ***L20***

Finally a 2D HMQC NMR experiment identified the 13 carbons coupled to protons and 8 uncoupled quaternary carbons (Figure 5.20).

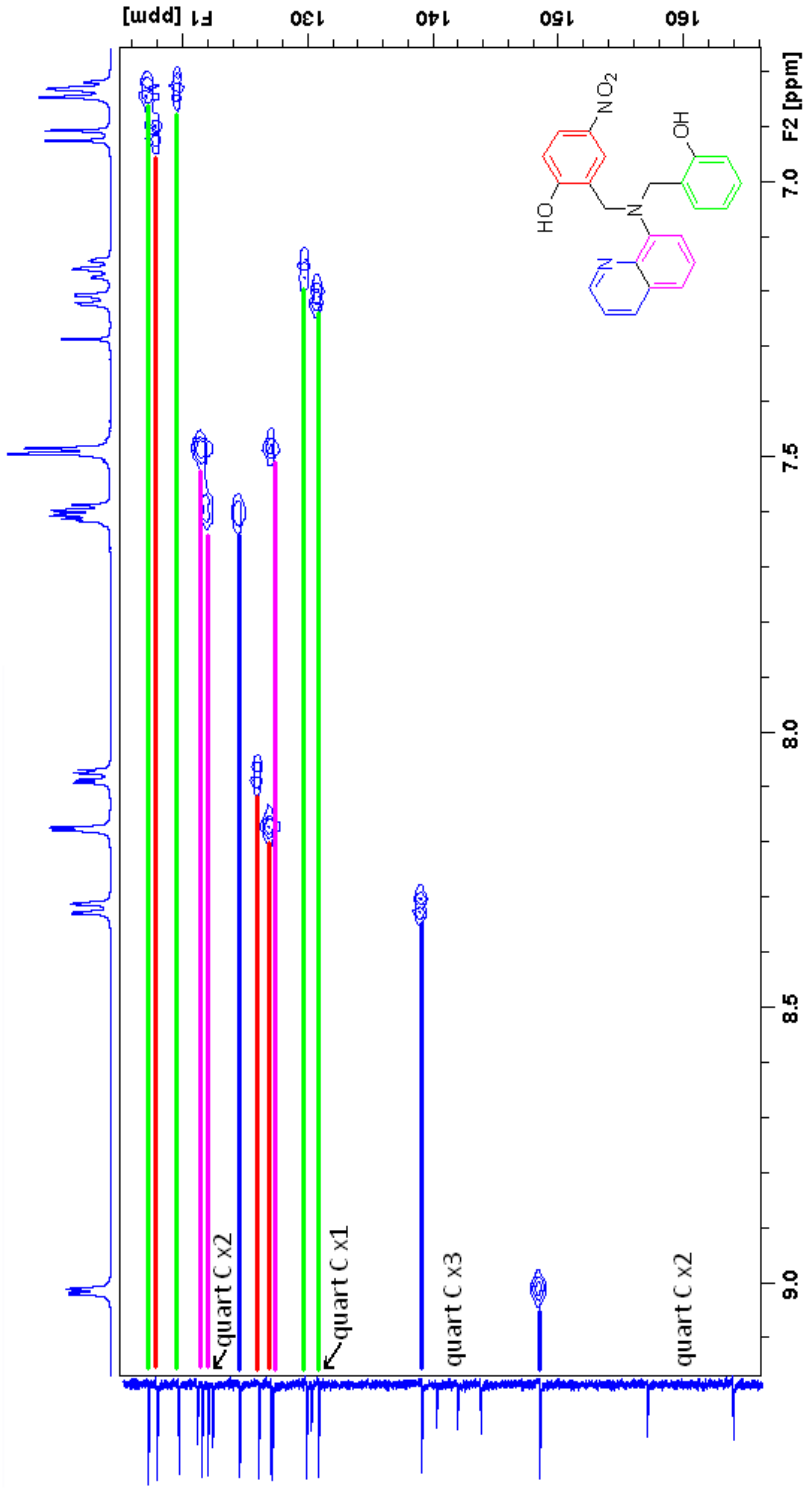

Figure 5.20: HMQC of 2-(((2-hydroxybenzyl)(quinolin-8-yl)amino)methyl)-4-nitrophenol, ***L20***

The tertiary amine **L17** was synthesised according to the above scheme as the protected methyl ester, **549** (Scheme 5.38). Deprotection of the methyl ester was achieved by refluxing in 6M HCl for 4 h at 110 ^{o}C. The potential for zwitterion formation of **L17** meant careful pH control was needed for an organic extraction workup. The acidic aqueous phase was first washed with dichloromethane and this organic layer was discarded. The aqueous phase was then neutralised to pH 7 with NaOH which allowed **L17** to be extracted into an organic phase of 9:1 dichloromethane / methanol. After solvent removal **L17** was precipitated from a minimum of dichloromethane in excess hexane and filtered to give **L17** in 47 % yield for the ester hydrolysis step. Both **549** and **L17** were further characterised (in addition to NMR) by elemental analysis or high resolution mass spectroscopy.

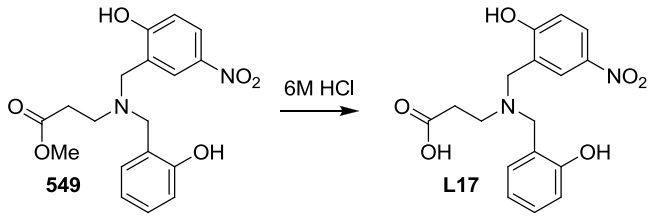

*Scheme 5.38: Acid hydrolysis of **549** to achieve **L17***

The ligand **L18** was prepared as previously reported via a Mannich reaction of 2,4-dimethylphenol, formaldehyde and glycine (Scheme 5.39), the characterisation data agreed with the literature.[165]

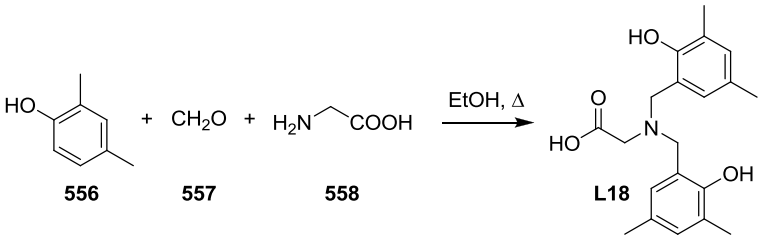

*Scheme 5.39: Mannich reaction to achieve **L18***

5.5 Summary

The highlight of this chapter was the synthesis of the phenol-capped ligand **L14** (Figure 5.21). This represents a fundamentally new type of ligand capable of offering an enclosed tetrahedral binding cavity. As this ligand was synthesised at a late stage in this project, coordination to Be(II) could not be tested and will have to be part of a future collaboration with a group still actively pursuing beryllium research.

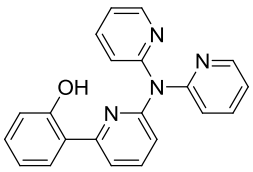

*Figure 5.21: Successfully synthesised 2-(6-(dipyridin-2-ylamino)pyridin-2-yl)phenol, **L14***

Despite an extensive investigation, the synthesis of the analogous carboxylic acid-capped ligand **502** was not completed within the time-constraints of this project (Figure 5.22). The ligand **L14** provides a representative example for these enclosed ligands. The ligand **502** was close to completion and should **L14** prove to be a good Be(II) chelator, **502** may be synthesised in the future.

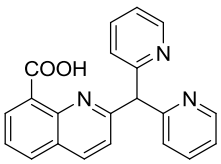

*Figure 5.22: Unsuccessfully synthesised 2-(dipyridin-2-ylmethyl)quinoline-8-carboxylic acid, **502***

The amine-capped ligands were synthesised according to robust well-established procedures without difficulty (Figure 5.23). As they were synthesised in good time, their coordination to Be(II) was investigated in this thesis. This is the focus of Chapter 6.

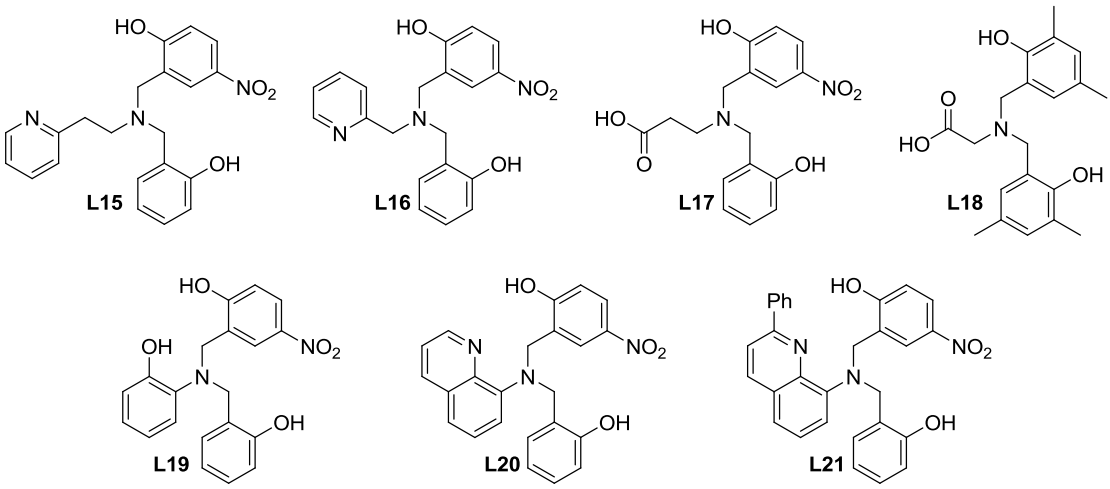

Figure 5.23: Variety of amine-capped tetra-coordinate ligands

Chapter 6: Coordination Chemistry of Encapsulating Compounds

6.1 Complexation of Encapsulating Compounds to Beryllium

6.1.1 Introduction

The proton sponges investigated in Chapter 4 showed promise for Be(II) complexation based on the ideal size-fit for B(III). Unfortunately, the coordination was difficult to observe for Be(II), largely due to the restrictions on the available beryllium salt used for the investigation. It is very likely that a Be(II) proton sponge complex could be formed in aprotic media with a suitable reactive beryllium salt such as beryllium chloride. Nonetheless, it was clear that to achieve good coordination to Be(II) in an aqueous environment, a suitable ligand must contain stronger oxygen donors and having only neutral nitrogen donors was not ideal. The ligands in this chapter have four donors which should enable full encapsulation of Be(II).

The tertiary amine ligands synthesised in Chapter 5 will be investigated for their coordination to beryllium in this chapter. While some of these ligands have reported complexes with other metals, for beryllium sensing applications it is possible to provide a non-competitive environment for beryllium through the use of buffers to control pH and EDTA to remove interfering metal ions.[61]

Structural analogues (i.e. those with the same structure but with minor differences in peripheral aromatic substitution) of **L16** have hundreds of reported metal complexes covering much of the periodic table. The complexes are usually of the form M_2L_2 with the phenolic oxygens bridging the cluster, representative example complexes include; Ti,[166] Co,[167] Zn[168] and Sc.[169] For example the bridged copper complex with a structural analogue

of **L16** (Figure 6.1).[163] Alternatively the ligand can form MLX complexes where a suitable counter ligand (X) balances the charge and occupies the remainder of the coordination sphere for the metal cation. Representative examples include complexes with; Ti,[166] W,[170] Mo,[170] Al,[171] Cr,[172] Mn,[173] Fe,[174] Ni,[175] Y,[176] Hf,[177] Zr,[177] Sc,[169] Re[178] and Zn.[179] A structural analogue of **L16** formed [Cu(**'L16'**H)(OAc)], the ligand was mono-protonated to balance the charge in this instance (Figure 6.1).[180]

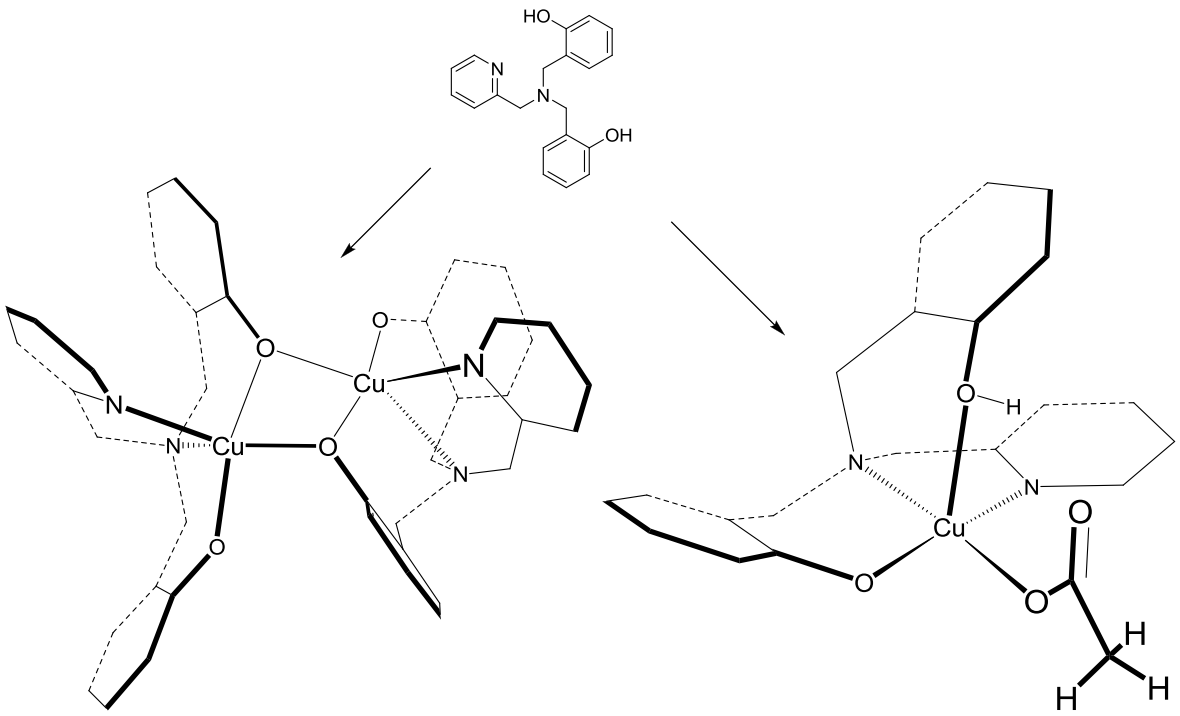

*Figure 6.1: Molecular structures of [Cu_2(**'L16'**)$_2$] and [Cu(**'L16'**H)(OAc)], peripheral aromatic substitution, double bonds and hydrogens removed for clarity*

The structural analogues of **L15** (Figure 6.2), with an extra CH_2 spacer on the pyridine arm, have received much less attention with only a relative handful of reported metal complexes. Similarly to the **L16** analogues, these were shown to form either phenolic bridged M_2L_2 clusters with Ni,[162] Zn,[162] Cu,[162] Co,[162] or MLX complexes with Cu,[162] Re,[181] Zr,[182] Zn[183] and Mo.[184]

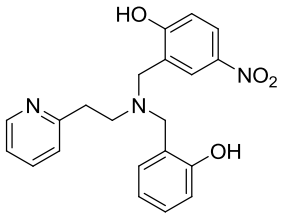

Figure 6.2: 2-(((2-Hydroxybenzyl)(2-(pyridin-2-yl)ethyl)amino)methyl)-4-nitrophenol, ***L15***

Structural analogues of **L18** only have a few reported metal complexes. M_2L_2 clusters for vanadium have been reported.[185] MLX complexes have been reported for iron; 2,2'-bipyridine (bipy) type ligands occupied the remainder of the coordination sphere (Figure 6.3).[186, 187]

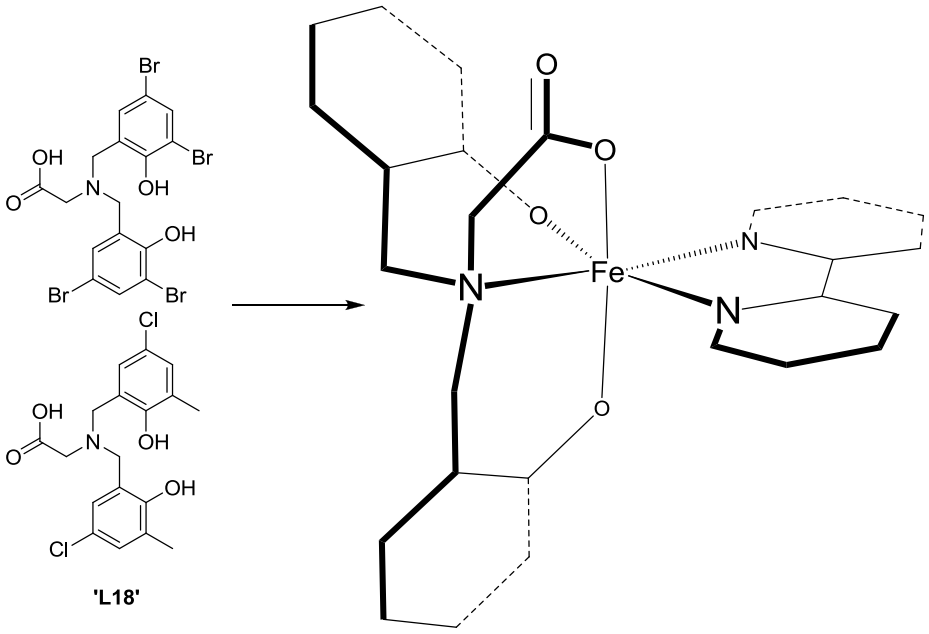

Figure 6.3: Molecular structure of [Fe(***'L18'****)(bipy)],*
peripheral aromatic substitution, double bonds and hydrogens removed for clarity

Investigations on structural analogues of **L19** (Figure 6.4) have shown M_2L_2 clusters with Zr,[164] and MLX complexes with Ti[164] and Fe.[188]

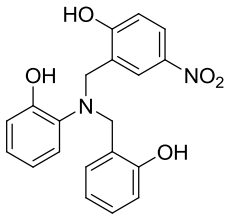

*Figure 6.4: 2-(((2-Hydroxybenzyl)(2-hydroxyphenyl)amino)methyl)-4-nitrophenol, **L19***

Ligands **L17**, **L20** and **L21** have not been previously synthesised (Figure 6.5).

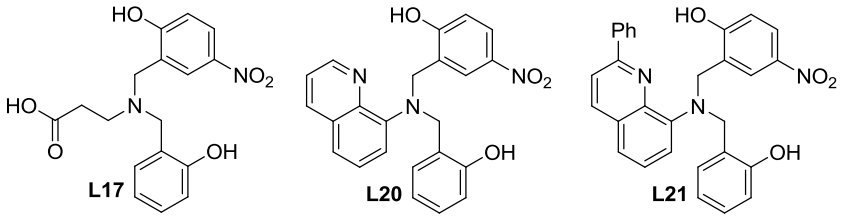

Figure 6.5: Previously unreported tertiary amine ligands

The above compounds were first screened for beryllium coordination using ^{1}H, ^{13}C and ^{9}Be NMR, and then the properties of the beryllium complexes further investigated using UV-Vis, fluorescence spectroscopy, and computational chemistry.

6.1.2 ^{9}Be NMR Analysis

With the exception of **L21**, all of the ligands **L15** through **L20** showed coordination to beryllium. The steric bulk of the phenyl substituent (**green**, Figure 6.6) possibly prevented coordination to beryllium. The bite angle between the neutral nitrogen donors (**red**, Figure 6.6) was not ideal for beryllium coordination where six-coordinate over five-coordinate chelate rings are preferred. The five-coordinate chelate ring would have kept potential metal coordination further from the sterically demanding phenyl group relative to a six coordinate chelate ring with adjacent phenyl substitution.

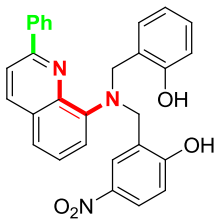

Figure 6.6: 2-(((2-hydroxybenzyl)(2-phenylquinolin-8-yl)amino)methyl)-4-nitrophenol, ***L21***

The following table summarises the ^{9}Be NMR shifts and line widths (width at ½ heights) carried out in a number of different solvents. In all cases the beryllium source was aqueous beryllium sulfate and 10 equivalents of triethylamine were required, the reactions were stirred for 16 h and warmed at 50 ^{o}C to enhance coordination. When possible the ^{1}H and ^{13}C NMR were recorded and are partially documented in Appendix A.7. As the ^{1}H and ^{13}C NMR were of reaction mixtures and often in non-deuterated solvents it was generally not possible to use either of these as definitive methods for confirming Be(II) coordination. If a suitable organic soluble beryllium starting material was available and a pure deuterated solvent such as chloroform was used, the shifts of the aromatic protons of the ligands and disappearance of phenolic protons would provide additional evidence for Be(II) coordination. In the current investigation there was shifting of the aromatic protons but the disappearance of the phenolic protons could be due to other factors such as the presence of triethylamine in the reaction mixture. The shifting of aromatic protons alone doesn't necessarily confirm the proposed four-coordinate species but merely indicated the ligand was interacting with Be(II). The use of the ^{9}Be NMR shifts was more conclusive as this involved interpretation of a single uncoupled peak in the spectrum and could be readily compared to the computational results.

Compound	^{9}Be NMR shift, ppm (Line Width, Hz)			
	DMF	DMSO-d6	MeOH	D_2O
[Be(**L15**)]	2.77 (62)	3.18 (123)	2.94 (150)	Insoluble
[Be(**L16**)]	4.51 (67)	No complex	4.18 (188)	Insoluble
[Be(**L17**)]$^{-}$	Not measured	2.11 (174)	2.33 (151)	2.60 (175)
[Be(**L18**)]$^{-}$	4.06 (66)	4.64 (130)	Insoluble	5.15 (104)
[Be(**L19**)]$^{-}$	4.40 (59)	5.10 (106)	5.28 (159)	Insoluble
[Be(**L20**)]	5.15 (89)	No complex	No complex	Insoluble
[Be(**L21**)]	No complex	No complex	No complex	Insoluble

Table 6.1: ^{9}Be NMR shifts and line widths of tetra-coordinate ligands in a number of different solvents

The line width is related to the symmetry of the complex.[138] Symmetrical four-coordinate species typically have line widths of less than 50 Hz. The line width broadens with unsymmetrical four-coordinate species, such as those reported by Niemeyer and Power.[63] As the compounds in this investigation provided four different donor arms, the resulting line widths could potentially broaden. In this instance, the most likely cause of the broadened line widths is the complexity of the reaction mixture. In addition to complex formation with the ligand, there is the possibility of minor beryllium species involving water, solvent, and triethylamine. When beryllium sulfate was subjected to the same conditions in the absence of the ligands a similar broadening of the line width was observed, however, the ^{9}Be NMR were distinctly shifted in the presence of the ligands so complexation was indeed occurring for the above reactions. In general, the use of DMF as the solvent prevented such extreme broadening of the line widths (Figure 6.7).

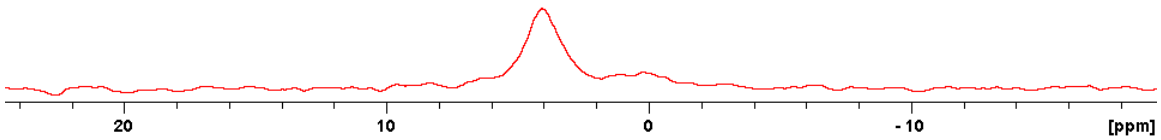

*Figure 6.7: ^{9}Be NMR shift of **L18** coordinated to beryllium in DMF (**red**)*

The complexes were modelled and optimised at the B3LYP level using the 6-311++g(2d,p) basis set as implemented in Gaussian 03 for windows. The nuclear magnetic shielding tensors were calculated using the same basis set. The results are summarised in Table 6.2.

For the ligands which had three ionisable oxygen donors, it was assumed that the anionic beryllium complex formed. It is possible protonation could occur on the ligand to give a neutral species. As shown in Table 6.1, the experimental shift showed some variation when measured in different solvents, for simplicity the closest ^{9}Be NMR shift was chosen for each to compare to the calculated values.

Complex	δ_{ref}	$\delta_{model[a]}$	$\delta_{(ref-model)}$	δ_{exptl}	$\lvert\Delta_{exptl-calc}\rvert$
$Be(H_2O)_4^{2+}$	109.10	109.10	0.00	0.00	0.00
[Be(**L15**)]		105.66	3.44	3.18 (DMSO-d6)	0.26
[Be(**L16**)]		103.12	5.98	4.51 (DMF)	1.47
[Be(**L17**)]$^-$		106.62	2.48	2.60 (D_2O)	0.12
[Be(**L18**)]$^-$		103.22	5.18	5.15 (D_2O)	0.03
[Be(**L19**)]$^-$		103.57	5.53	5.28 (MeOH)	0.25
[Be(**L20**)]		102.65	6.45	5.15 (DMF)	1.30

Table 6.2: Calculated ^{9}Be NMR shifts for tetra-coordinate ligands, [a] Gas phase model utilised as solvent models had negligible influence on the ^{9}Be shielding tensors

The calculated ^{9}Be NMR shifts for the beryllium complexes of **L15**, **L17**, **L18** and **L19** correlated well with the experimental shifts proving good evidence that the four-coordinate species formed in solution. A Δ of 0.5 ppm or less is considered an acceptable deviation for these types of calculations. The ligands all offered one tertiary amine donor, two phenol groups and each differed by one point of substitution. Be(II) coordinated to the central amine and the two phenols via six-membered chelate rings. The remaining arm on **L17**, **L18** and **L19** offered strong oxygen donors. **L18** and **L19** had five-membered chelate rings and **L17** had a six-membered chelate ring (**red**, Figure 6.8). **L15** had a weaker nitrogen donor, which formed an unstrained six-membered chelate ring.

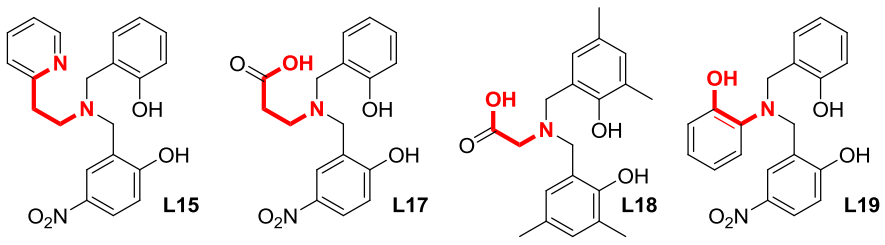

Figure 6.8: Tetra-coordinate ligands with well correlated ^{9}Be NMR shifts

The calculated ^{9}Be NMR shifts for the beryllium complexes of **L16** and **L20** did not correlate well with the experimental shifts. This suggested full encapsulation was not occurring. The fourth points of coordination in both cases were neutral nitrogen donors which needed to form strained five-membered chelate rings (**red**, Figure 6.9).

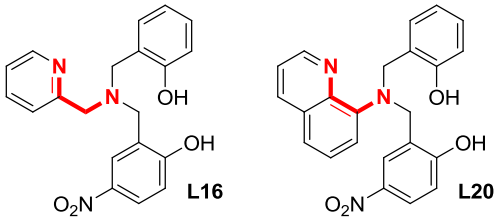

Figure 6.9: Tetra-coordinate ligands with poorly correlated ^{9}Be NMR shifts

The beryllium complex of **L16** was optimised with a water molecule in place of the pyridine arm (Figure 6.10) and the calculated ^{9}Be NMR shift was 3.58 ppm (Δ 0.77 ppm) which was closer to the experimental ^{9}Be NMR shift than the calculated shift for the tetra-coordinate species. This suggested full encapsulation of beryllium with **L16** was not occurring. The two-coordinate beryllium complex of **L16** bound through both phenols with two water molecules was unlikely to be the species present as the calculated ^{9}Be NMR shift of 1.92 ppm (Δ 2.59 ppm). Other possibilities could include cluster complexes such as those observed for other metal complexes discussed earlier or a polymeric species (e.g. if the water molecule in Figure 6.10 was a donor arm from another partially coordinated species a 1D polymer would form).

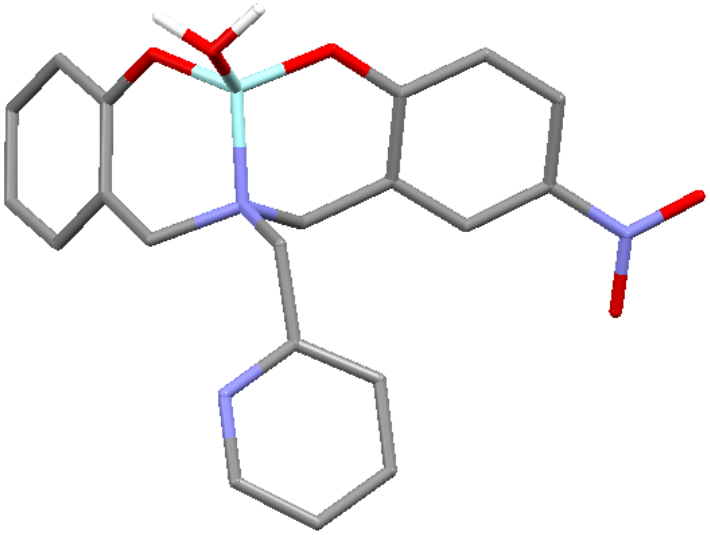

*Figure 6.10: Optimised model of [Be(**L16**)(H_2O)], Be(II) is light blue, O is red, N is blue and C is grey*

The steric bulk of the quinoline substituent on **L20** prevented the calculation of an analogous water-coordinated complex. A similar partially coordinated species was likely forming rather than the desired tetra-coordinate species.

6.1.3 UV-Vis Spectroscopy in Organic Solvents

UV-Vis spectra were measured by making appropriate dilutions to the reaction mixtures in 6.1.2. The UV-Vis spectra were measured for the reactions of beryllium with **L16** and **L20**; however, as the calculated ^{9}Be NMR did not match experimental they will not be discussed. The details for each experiment and any spectra not included here are given in Appendix A.7.

Coordination of **L15**, **L17** and **L19** to beryllium each gave blue-shifted $\pi - \pi^*$ transitions (for the transition associated with the nitro-substituted phenol group) relative to the unbound ligands (Figures 6.11, 6.12 and 6.13).

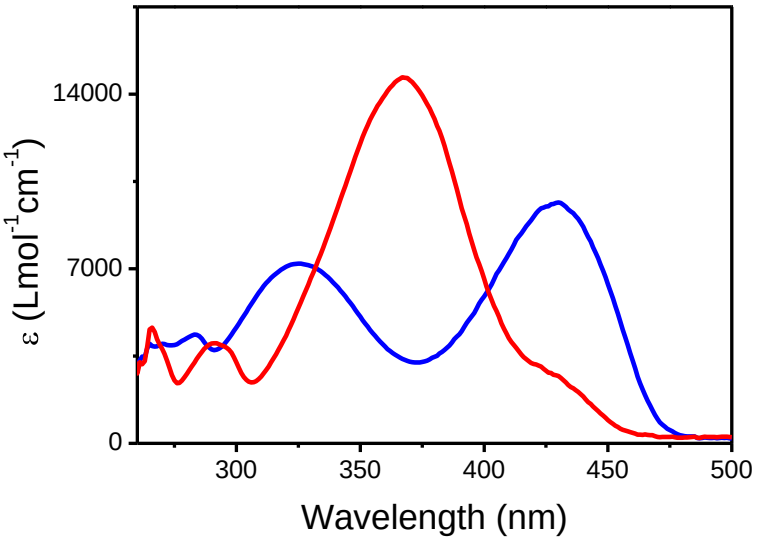

*Figure 6.11: Change in UV-Vis spectrum at 10^{-5} M of neutral **L15** (**blue**) and after $BeSO_4$ addition (**red**)*

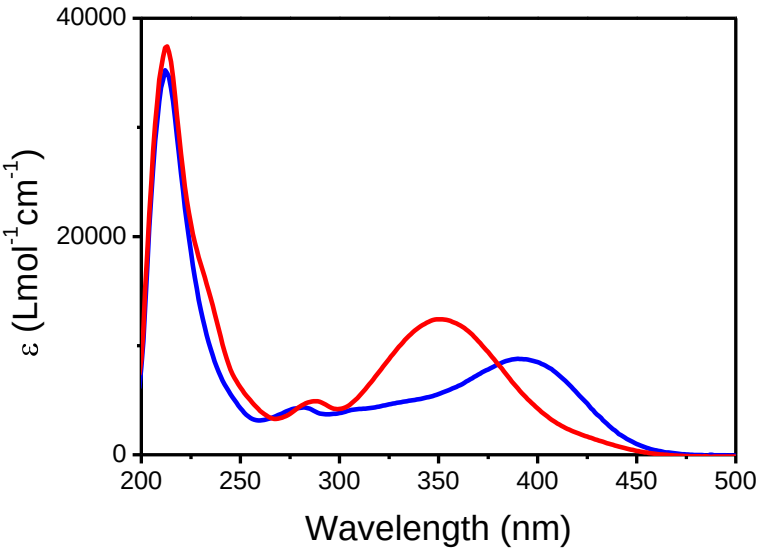

*Figure 6.12: Change in UV-Vis spectrum at 10^{-5} M of neutral **L17** (**blue**) and after $BeSO_4$ addition (**red**)*

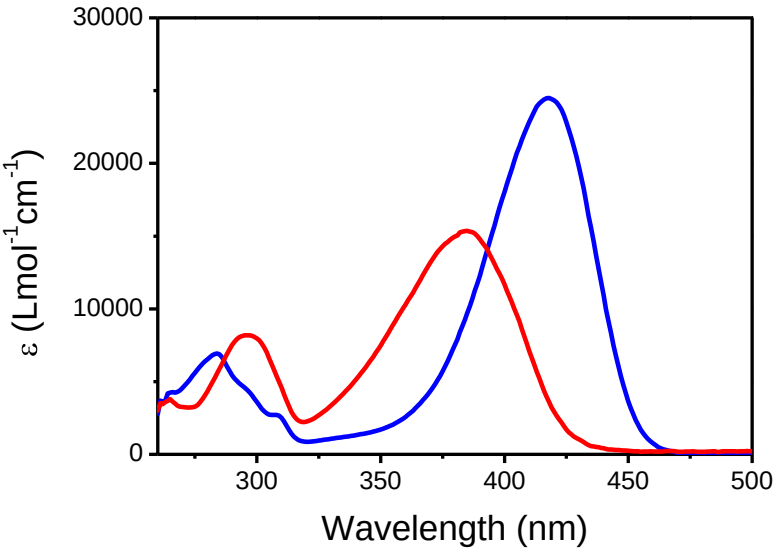

*Figure 6.13: Change in UV-Vis spectrum at 10^{-5} M of neutral **L19** (**blue**) and after $BeSO_4$ addition (**red**)*

Coordination of **L18** to beryllium gave red-shifted π – π* transitions (for the absorbance associated with the methyl-substituted phenol groups) relative to unbound **L18** (Figure 6.14).

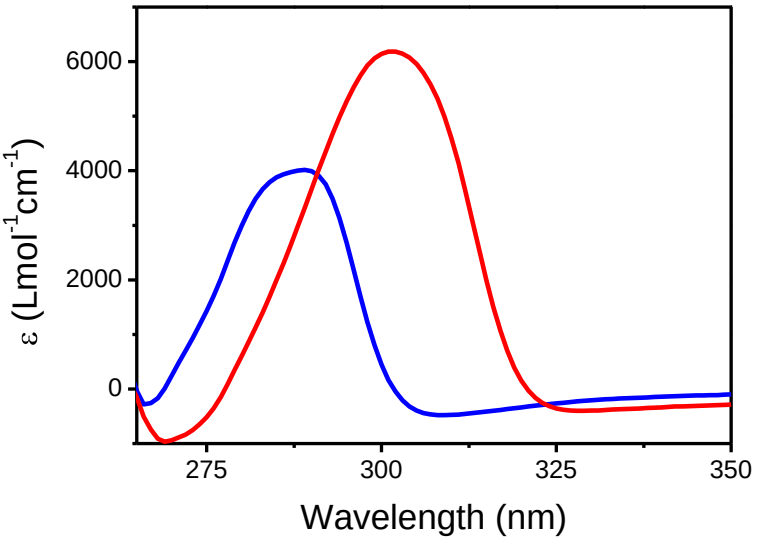

*Figure 6.14: Change in UV-Vis spectrum at 10^{-5} M of neutral **L18** (**blue**) and after $BeSO_4$ addition (**red**)*

Time domain calculations were employed to calculate the electronic spectra for each of the complexes at the B3LYP level using the 6-311++g(2d,p) basis set (Table 6.3). A solvent model was not employed due to the difficulty in modelling a solvent mix.

Compound	Transition nature	Wavelength (nm)		
		Calculated	Experimental	$\Delta_{exptl-calc}$
[Be(**L15**)]	π- π*	328	367	39
[Be(**L17**)]$^-$	π- π*	352	349	3
[Be(**L18**)]$^-$	π- π*	283	302	19
[Be(**L19**)]$^-$	π- π*	349	385	36

Table 6.3: Calculated and experimental maximum absorption wavelengths

Without a solvent model, the calculated and experimental absorbance varies by not more than 40 nm. As the measured spectra are of reaction mixtures as opposed to a purified complex in a single solvent it would not be practical to attempt to improve the accuracy. The use of solvent models or alternative functionals to improve the precision should only be utilised when the exact solute and solvent is characterised. Nonetheless, insight into the nature of the transitions can still be described in relative detail and will be the focus of the following sections.

6.1.4 Fluorescence Spectroscopy in Organic Solvents

Two of the above four complexes in Table 6.3; [Be(**L18**)]$^-$ and [Be(**L19**)]$^-$, were fluorescent. The fluorescence spectras were recorded and are shown in Figures 6.15 and 6.16. Excitation at 305 nm gave an emission at 335 nm for [Be(**L18**)]$^-$ and excitation at 355 nm gave an emission at 425 nm for [Be(**L19**)]$^-$.

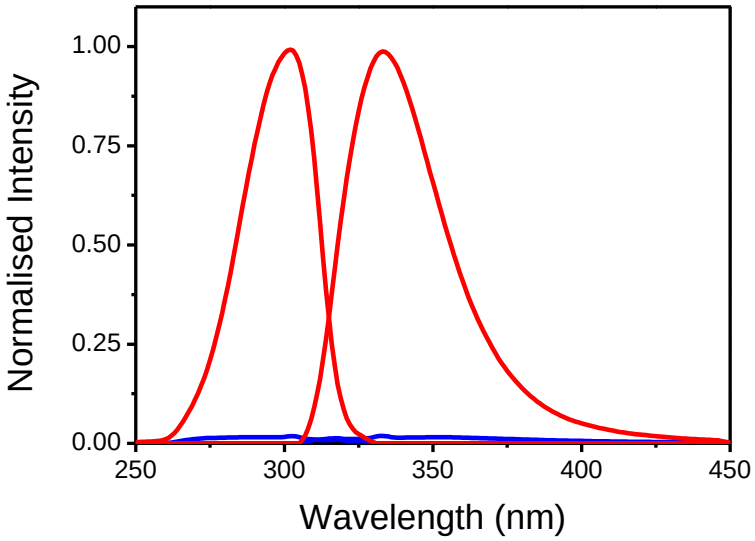

*Figure 6.15: Normalised absorption and emission spectras at 10^{-5} M of neutral **L18** (**blue**) and after $BeSO_4$ addition (**red**) in DMF and NEt_3*

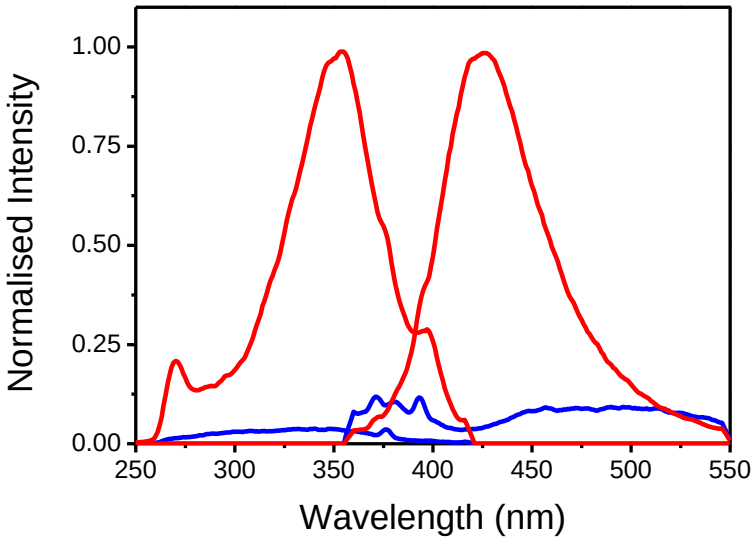

*Figure 6.16: Normalised absorption and emission spectras at 10^{-5} M of neutral **L19** (**blue**) and after $BeSO_4$ addition (**red**) in DMF and NEt_3*

The above fluorescence could be related to the rigidity and locking of certain conformations of the Be(II) complexes and these locked conformations will be discussed in the remainder of this section. By contrast, the flexibility of three six-membered chelate

rings formed upon coordination of beryllium to **L15** and **L17** allowed a single major conformer to be adopted (Figure 6.17).

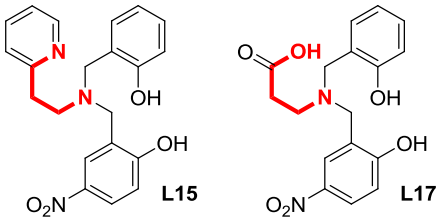

Figure 6.17: Flexible tetra-coordinate ligands with a single conformer upon beryllium coordination

Optimisation of the gas-phase models of [Be(**L15**)] and [Be(**L17**)]$^-$, lead to a single conformer (ignoring the possibility of optical isomers arising from the three different substituents surrounding the central nitrogen). The conformer can be described by the orientation of the hydrogens on the three CH_2 groups surrounding the central nitrogen donor. [Be(**L15**)] and [Be(**L17**)]$^-$ adopted what will herein be classed as an "anti" geometry about the central nitrogen. The equatorial hydrogens on the CH_2 groups (**green atoms**, Figure 6.18) all orient away from one another.

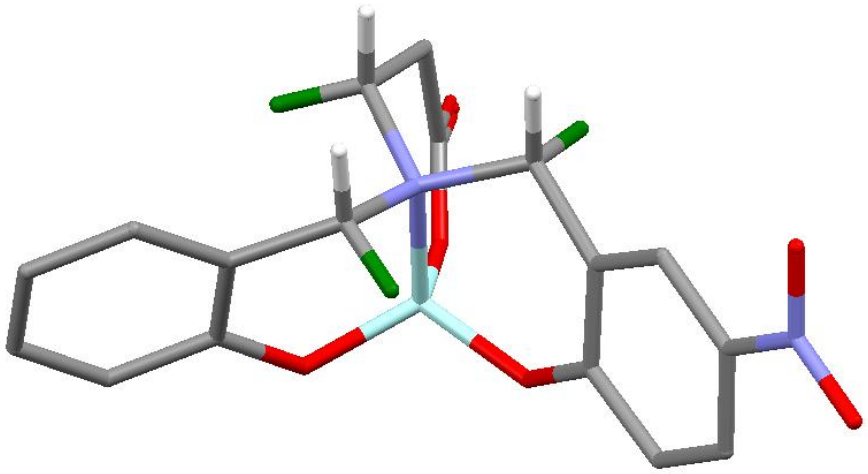

*Figure 6.18: Optimised model of [Be(**L17**)]$^-$ with anti geometry*

One of the few four-coordinate ligands ever reported to coordinate beryllium was **601** (Figure 6.19).[54]

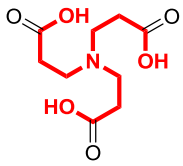

*Figure 6.19: 3,3',3''-nitrilotripropanoic acid, **601***

Upon coordination to Be(II), **601** formed three six-membered chelate rings (**red outlines**, Figure 6.19). The crystal structure revealed all the equatorial hydrogens on the CH_2 groups (**green atoms**, Figure 6.20) oriented away from one another in an anti conformation which was analogous to the optimised computer models for [Be(**L15**)] and [Be(**L17**)]$^-$.

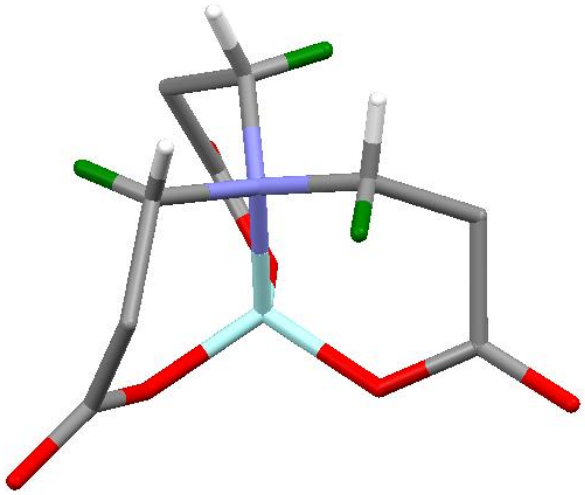

*Figure 6.20: Crystal structure of [Be(**601**)]$^-$ with anti geometry, Na^+ cation and solvent removed for clarity*

Modelling of [Be(**L18**)]$^-$ and [Be(**L19**)]$^-$ allowed the possibility for two distinct conformers to be adopted. The rigid five-membered chelate rings (**red outline**, Figure 6.21), in contrast to the six-membered chelate rings of **L15** and **L17**, were the cause for this.

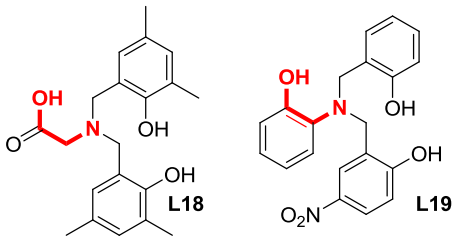

Figure 6.21: Strained four-coordinate ligands with two conformers upon beryllium coordination

Changing the orientation of one donor arm then optimising the gas-phase models lead to two distinct minimised structures for both [Be(**L18**)]$^-$ and [Be(**L19**)]$^-$. One conformer of [Be(**L18**)]$^-$ has a similar anti geometry to [Be(**L17**)]$^-$ above, with the equatorial hydrogens (**green atoms**, Figure 6.22) facing away from each other. The other adopts a "syn" geometry with the equatorial hydrogens (**green atoms**, Figure 6.22) facing toward each other. The syn conformer was calculated to be 10 kJ mol^{-1} higher in energy than the anti conformer. While this is a lower stability, the small energy difference (equivalent to the torsional energy barrier in simple bond rotations) suggests it is plausible that upon coordination to Be(II) a proportion of the resultant complexes are locked into the syn conformation.

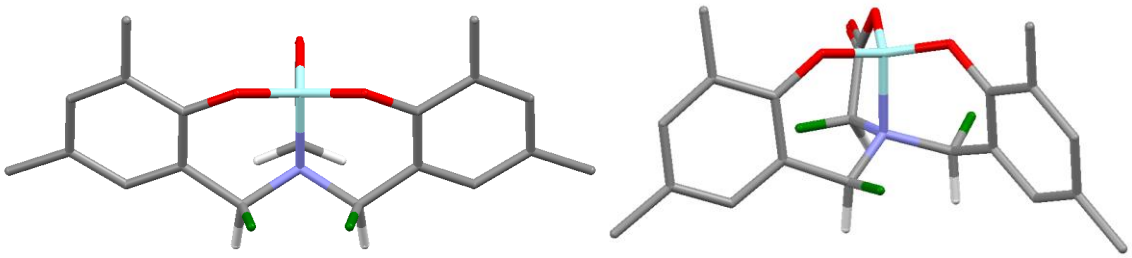

*Figure 6.22: Syn conformer (left) and anti conformer (right) of [Be(**L18**)]$^-$*

This syn orientation aligned the phenol groups, such that delocalisation of molecular orbitals across both rings was possible. The anti conformation prevented good alignment of the aromatic moieties (Figure 6.23).

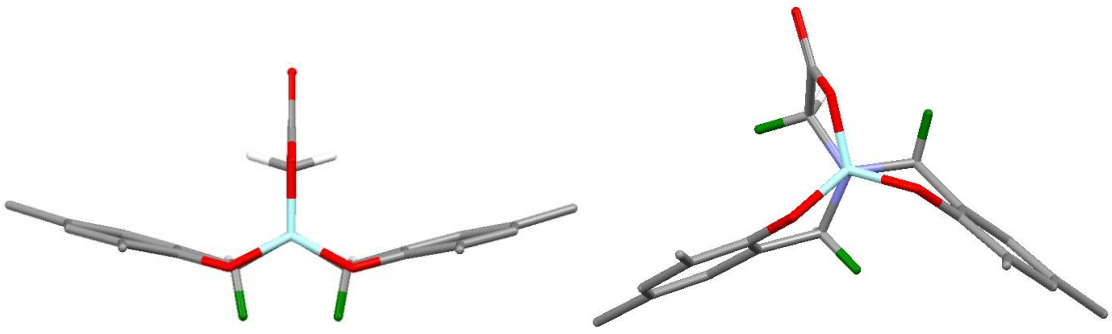

*Figure 6.23: Top view of the Syn conformer (left) and anti conformer (right) of [Be(**L18**)]$^-$*

The locking of the phenols into an aligned geometry in [Be(**L18**)]$^-$ and [Be(**L19**)]$^-$ may be attributed to the observed fluorescence. Analysis of the angle between the mean planes of the two aromatic phenol rings in the modelled beryllium complexes highlights the required alignment for fluorescence. Table 6.4 summarises these values.

Compound	Chelate Ring Sizes	Angle Between Mean Planes (°)		Fluorescent
		Anti	Syn	
[Be(**L15**)]	**6**,6,6	61.69	-	**No**
[Be(**L17**)]$^-$	**6**,6,6	61.89	-	**No**
[Be(**L18**)]$^-$	**5**,6,6	61.72	25.48	**Yes**
[Be(**L19**)]$^-$	**5**,6,6	-[a]	22.34	**Yes**

Table 6.4: Comparison of the angle of intersection between the aromatic phenol rings, [a] the second possible conformation was not exactly an anti geometry as defined here and will be discussed later

The rigidity of the locked complexes of [Be(**L18**)]$^-$ and [Be(**L19**)]$^-$ allowed alignment of the aromatic rings on opposing donor arms, which appeared to cause the observed fluorescence. Analysis of the major molecular orbital contributions for the $\pi - \pi^*$ transitions of all four complexes in Table 6.4 gave some evidence for this.

The major molecular orbitals attributed to the $\pi - \pi^*$ transitions present in the non-fluorescent [Be(**L15**)] and [Be(**L17**)]$^-$ were localised on the nitro-phenol group. The anti conformation prevented delocalisation onto the adjacent phenol group (Figures 6.24 and 6.25).

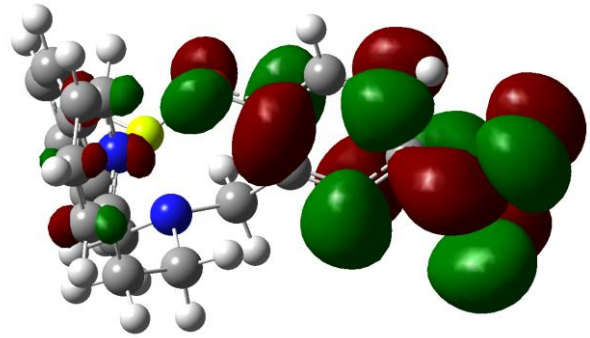

LUMO, -0.085 eV

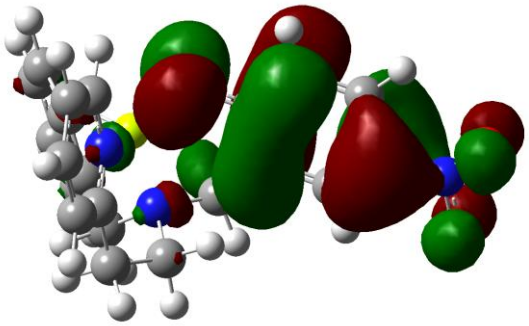

HOMO, -0.208 eV

Figure 6.24: Molecular orbitals associated with the π – π transition for [Be(**L15**)] (anti conformer)*

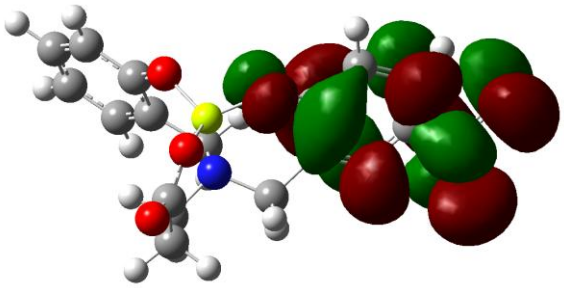

LUMO, +0.004 eV

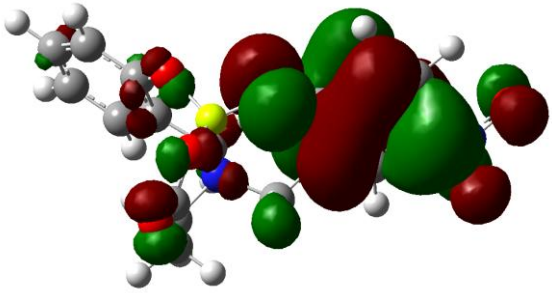

HOMO, -0.108 eV

Figure 6.25: Molecular orbitals associated with the π – π transition for [Be(**L17**)]⁻ (anti conformer)*

The major molecular orbitals attributed to the π – π* transitions of the syn conformer of the fluorescent [Be(**L18**)]⁻ showed delocalisation across both phenol rings (Figure 6.26).

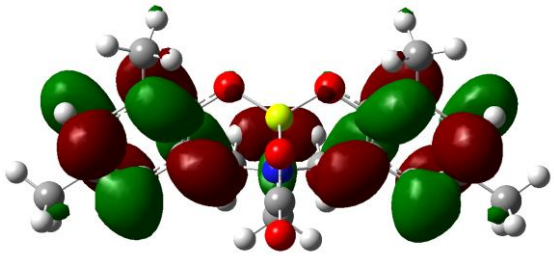

LUMO, +0.065 eV

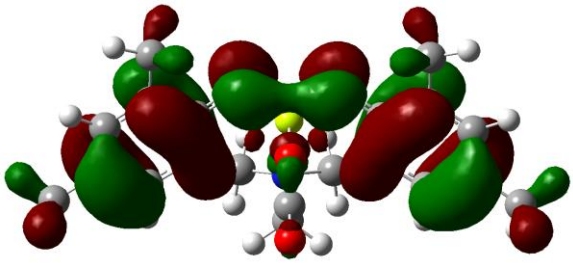

HOMO, -0.088 eV

Figure 6.26: Molecular orbitals associated with the π – π transition for [Be(**L18**)]⁻ (syn conformer)*

The anti conformer of [Be(**L18**)]⁻ did not have quite the same delocalisation observed with the syn conformer. Both phenol rings were still involved in the π – π* transition and a weaker fluorescence pathway might still exist for this conformation (Figure 6.27).

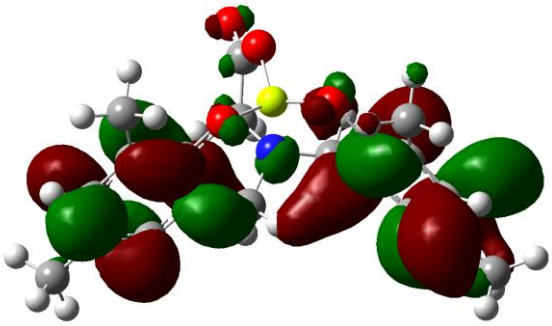

LUMO, +0.063 eV

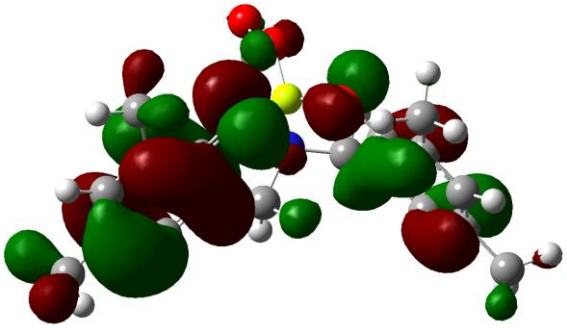

HOMO, -0.087 eV

Figure 6.27: Molecular orbitals associated with the π – π transition for [Be(**L18**)]⁻ (anti conformer)*

The complex of the fluorescent [Be(**L19**)]⁻ was a little more difficult to assign as the aminophenol moiety meant that there was more than one conformation which could give rise to delocalisation across two aromatic moieties. In this instance the calculated molecular orbitals for the syn conformer did not show the same delocalisation as [Be(**L18**)]⁻. The π – π* transition molecular orbitals were localised on the nitro-substituted phenol ring (Figure 6.28).

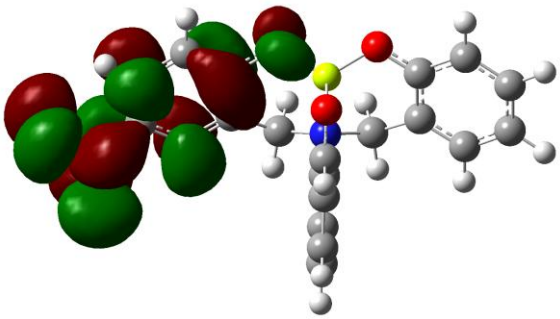

LUMO, +0.010 eV

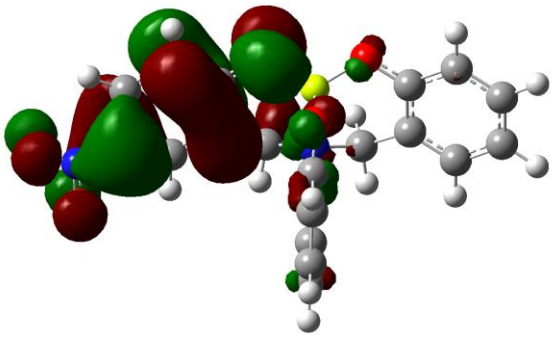

HOMO, -0.098 eV

Figure 6.28: Molecular orbitals associated with the π – π transition for [Be(**L19**)]⁻ (syn conformer)*

Optimisation of what would otherwise be described here as the anti conformer did not lead to an analogous geometry to the ligands **L15**, **L17** and **L18**. These had three sp^3 CH_2 groups surrounding the central nitrogen whereas the aminophenol group on **L19** was sp^2 hybridised. Due to the unfavourably close π – π stacking overlap between the aminophenol group and an adjacent phenol, computational modelling gave the minimised structure in Figure 6.29. This conformer was calculated to be 6 kJ mol^{-1} lower in energy than the syn conformer shown in Figure 6.28.

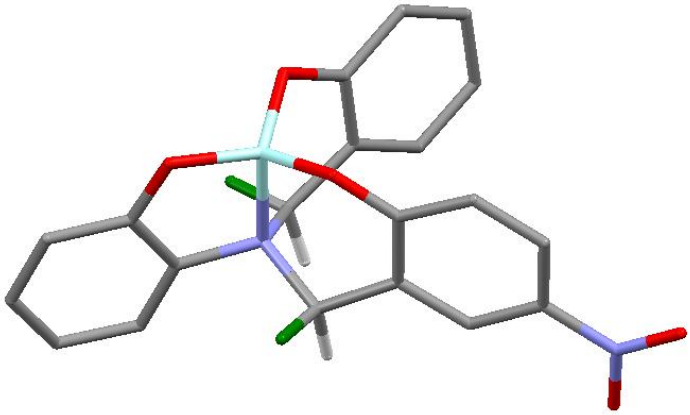

*Figure 6.29: Second possible minimised structure of [Be(**L19**)]⁻*

The major molecular orbitals attributed to the π – π* transitions of this conformer showed an apparently "bowl-like" delocalisation between the two phenols (not the aminophenol). The π* antibonding orbitals lie on the electron-withdrawing nitro-substituted phenol. This suggests an intra-molecular charge transfer from the unsubstituted phenol group to the nitro-substituted phenol occurs (Figure 6.30). Such charge transfers are typical in fluorescent molecules and perfectly flat aromatic systems are not a strict requirement for fluorescence.

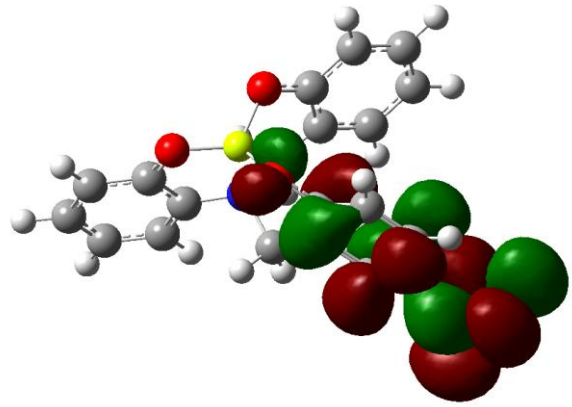

LUMO, +0.013 eV

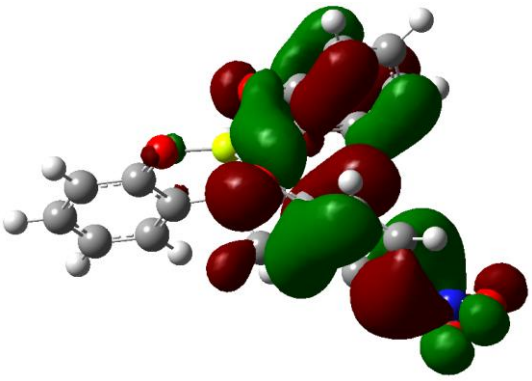

HOMO, -0.099 eV

Figure 6.30: Molecular orbitals associated with the π – π transition for [Be(**L19**)]⁻*

Overall, the locking of certain conformations due to the rigidity of five-membered chelate ring in [Be(**L18**)]⁻ and [Be(**L19**)]⁻ gave rise to fluorescence. [Be(**L15**)] and [Be(**L17**)]⁻ had more flexibility due to the six-membered chelates allowing adoption of anti conformations where no extended overlap of π orbitals was present.

6.1.5 UV-Vis and Fluorescence Spectroscopy in Water

The only ligands which had water solubility were those with carboxylic acid moieties, **L17** and **L18** (Figure 6.31).

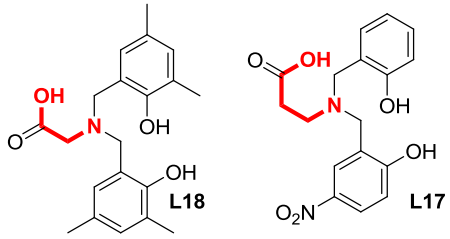

Figure 6.31: Water-soluble encapsulating ligands

Analogous experiments were performed to 6.1.3 above with water as the solvent in place of DMF and the following spectra were obtained (Figures 6.32 and 6.33).

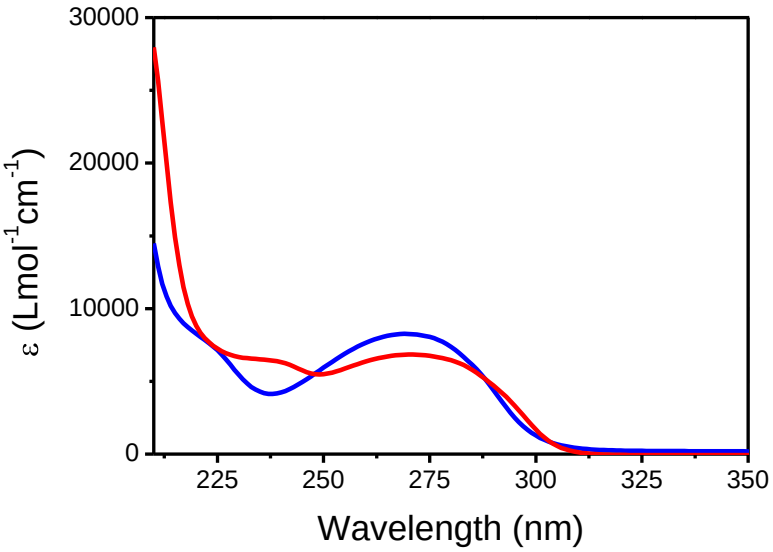

*Figure 6.32: Change in UV-Vis spectrum at 10^{-5} M of neutral **L18** (**blue**) and after $BeSO_4$ addition (**red**) in H_2O*

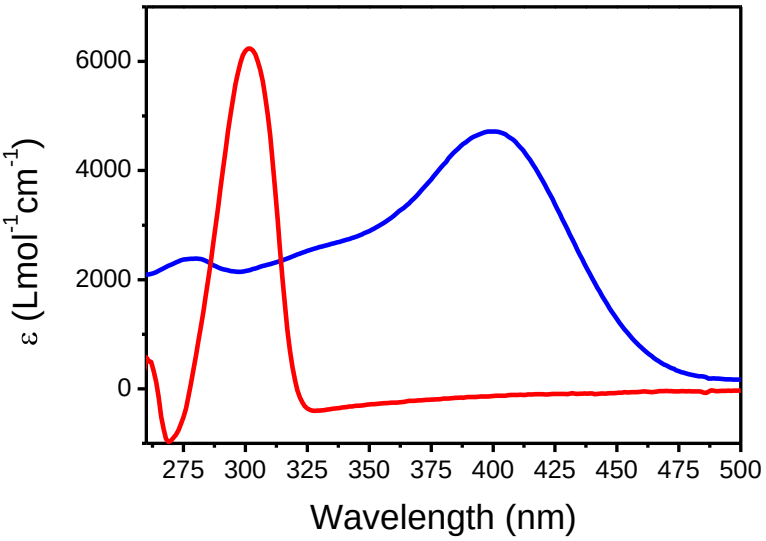

*Figure 6.33: Change in UV-Vis spectrum at 10^{-5} M of neutral **L17** (**blue**) and after $BeSO_4$ addition (**red**) in H_2O*

Similarly to 6.1.3, [Be(**L18**)]$^-$ was fluorescent and excitation at 290 nm gave an emission at 330 nm for (Figure 6.34).

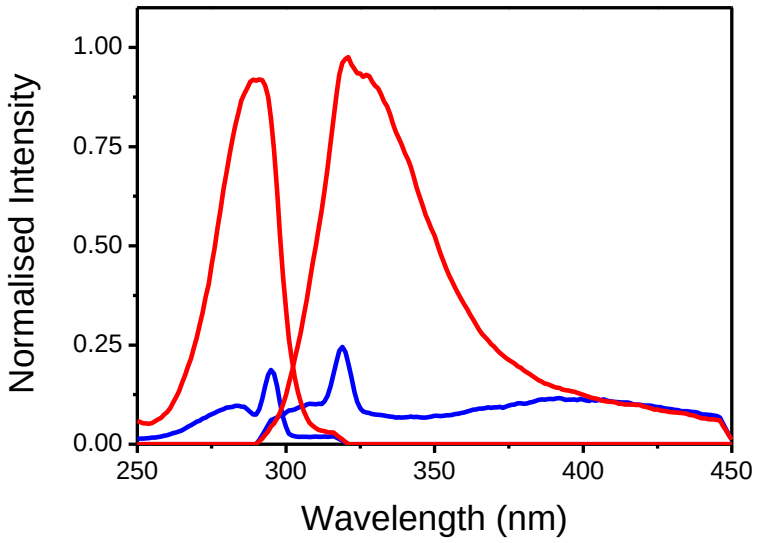

*Figure 6.34: Normalised absorption and emission spectras at 10^{-5} M of neutral **L18** (**blue**) and after $BeSO_4$ addition (**red**) in H_2O*

The ligand **L18** is the best candidate for a potential application for the detection of beryllium in an aqueous environment as measuring the fluorescence enables greatly enhanced sensitivity over straight measurement of the UV-Vis spectra. The UV-Vis spectra are unreliable as contaminants could easily give rise to increased absorbance at the wavelength where the beryllium species absorbs. The fluorescence is due to a specific excitation of the beryllium species that cannot be replicated by contaminants. Due to the time constraints of the short trip and the slow and careful pace which beryllium coordination chemistry must be conducted there was not time to perform any competition studies between other metal cations which would interfere the detection of beryllium.

6.2 Complexation of Encapsulating Compounds to Transition Metals

Variations on the tetra-coordinate ligands in this Chapter (e.g. variations in the peripheral substitution on the aromatic rings) have already been investigated for their coordination to transition metals. As an example, the current **L16** was coordinated to both copper and zinc and the crystal structures were determined and most importantly the spectroscopy was investigated to deduce whether coordination to other metal cations than Be(II) would lead to fluorescent compounds and hinder detection of Be(II).

The copper complex of **L16** was formed using copper acetate in MeOH and MeCN and crystallised via vapour diffusion of diethyl ether into the solution. The asymmetric unit consisted of one molecule **L16** and one copper ion (Figure 6.35). One molecule of methanol was present in the asymmetric unit and was located in a special position.

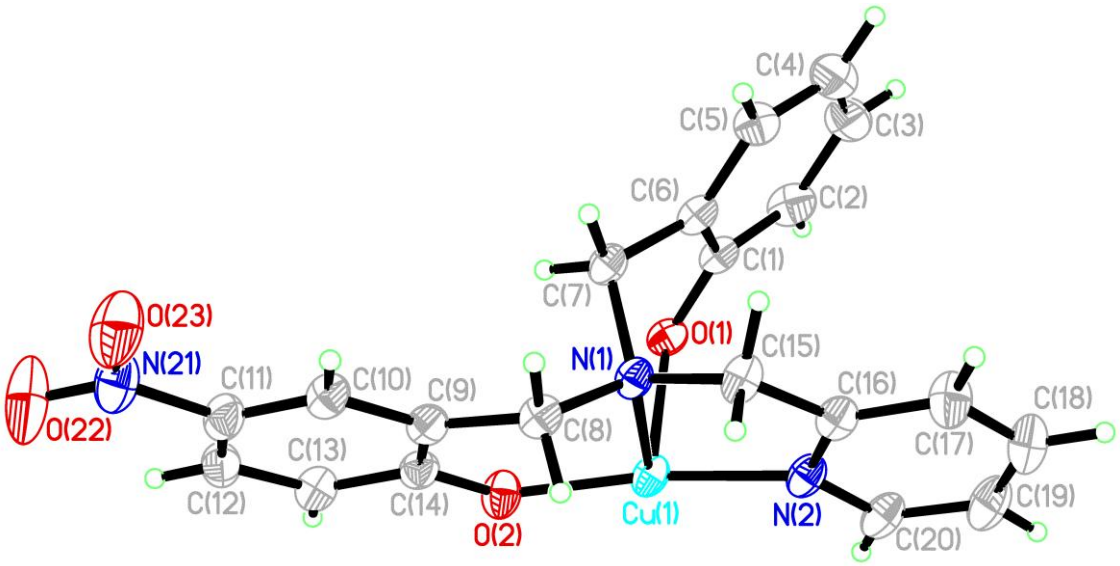

*Figure 6.35: Asymmetric unit for the crystal of [Cu(**L16**)], ellipsoids drawn at the 50% probability level*

The unit cell shows the full [Cu_2(**L16**)$_2$] bridged dimer (Figure 6.36). The copper ions have square pyramidal geometry with the fifth donor atom coming from a bridging phenolate on the adjacent ligand. The ligand packs with "syn" geometry discussed previously with one phenol arm and the pyridine arm aligning in plane.

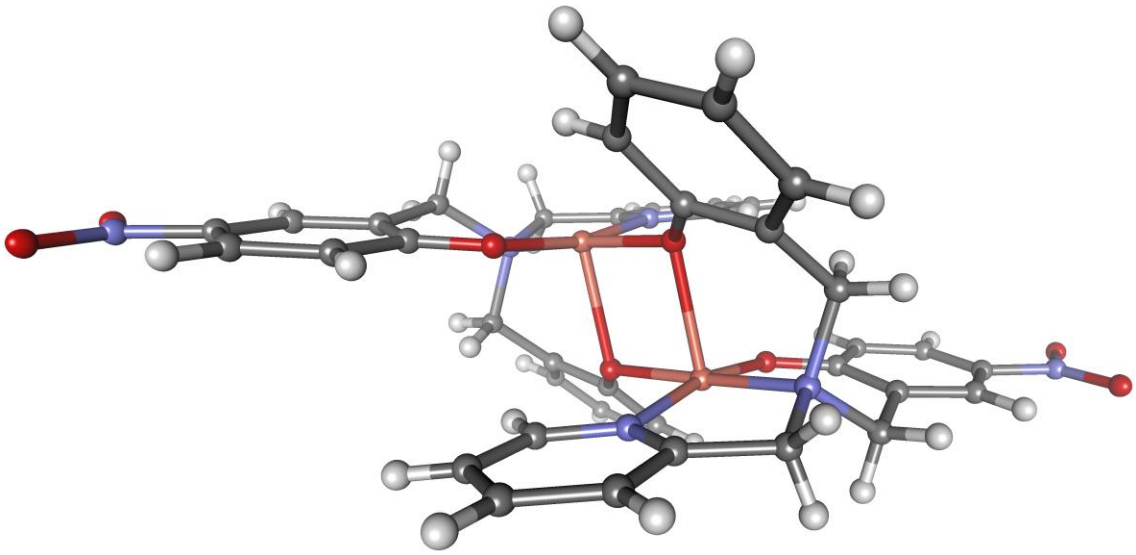

*Figure 6.36: The bridged dimer [Cu_2(**L16**)$_2$]*

The syn arrangement of the donor arms and square pyramidal metal geometry is typical for all the copper complexes of the structural analogues of **L16**, regardless of whether the complex is of the M_2L_2 or MLX type.[163, 179, 180, 189-191] The bond lengths and angles around the copper ion did not show any notable deviations from the complexes already reported (Table 6.5).

Parameter	Length (Å)	Parameter	Angle (°)	Parameter	Angle (°)
Cu1–O1	2.295(3)	O1–Cu1–O2	98.51(11)	N1–Cu1–N2	83.82(11)
Cu1–O2	1.905(2)	O1–Cu1–N1	93.21(11)	N2–Cu1–O1a	91.54(11)
Cu1–N1	2.044(3)	O1–Cu1–N2	93.17(10)		
Cu1–N2	1.992(2)	O1–Cu1–O1a	83.54(11)		
Cu1–O1a	1.958(3)	N2–Cu1–N1	92.20(11)		
		O2–Cu1–O1a	93.03(11)		

*Table 6.5: Major structural parameters for the geometry of the Cu(II) ion in [Cu_2(**L16**)$_2$]*

The UV-Vis of [Cu_2(**L16**)$_2$] showed the typical weak *d-d* transition at 685 nm and ε 129 L mol^{-1} cm^{-1} (Figure 6.37). The $\pi - \pi^*$ transition for the ligand was at 374 nm and ε 16700 L mol^{-1} cm^{-1} (Figure 6.38). When checked for fluorescence activity using similar

concentrations and entry/exit slit widths (10^{-5} M, 2.5nm) on the fluorometer to those used when analysing the Be(II) complexes there was no activity. This is despite the crystal structure of $[Cu_2(\mathbf{L16})_2]$ showing an alignment of adjacent aromatic rings on the ligand. The square pyramidal geometry of the copper complex does not place the rings at a significantly greater distance than that of tetrahedral geometry of the beryllium complex.

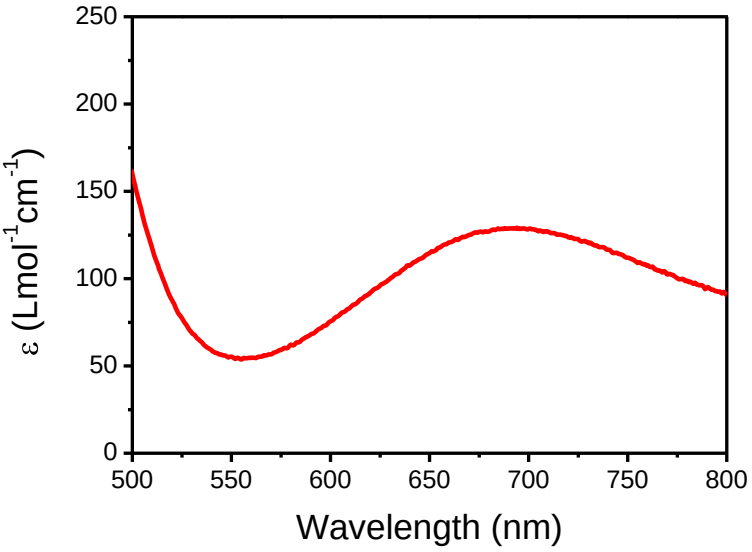

*Figure 6.37: UV-Vis of $[Cu_2(\mathbf{L16})_2]$ (**red**) at 10^{-4} M showing metal d – d transition in MeOH*

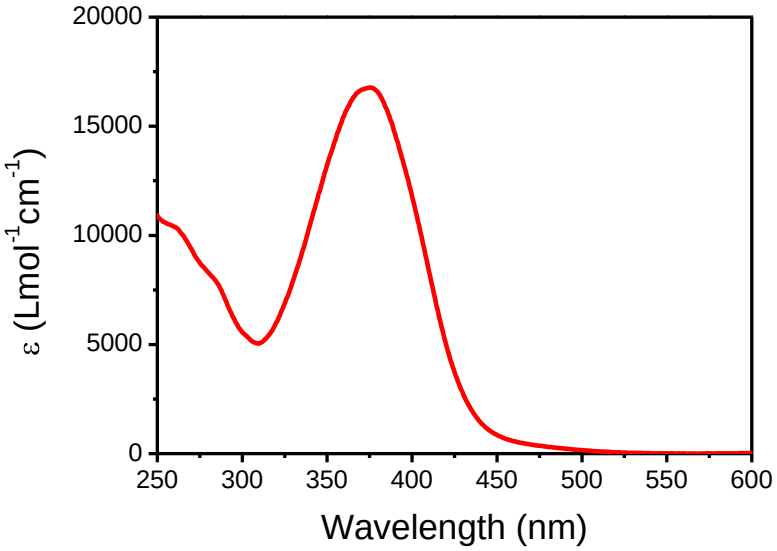

*Figure 6.38: UV-Vis of $[Cu_2(\mathbf{L16})_2]$ (**red**) at 10^{-5} M showing ligand $\pi - \pi^*$ transitions in MeOH*

The zinc complex of **L16** was formed using zinc acetate in MeOH and CH_2Cl_2 and crystallised via vapour diffusion of diethyl ether into the solution. The crystal structure of the zinc complex had more disorder than the copper complex. The asymmetric unit consisted of the $[Zn_2(\mathbf{L16})_2]$ bridged dimer (Figure 6.39). The solvent could not be modelled so 156 electrons were squeezed from the unit cell which is approximately two molecules of dichloromethane and four molecules of methanol.

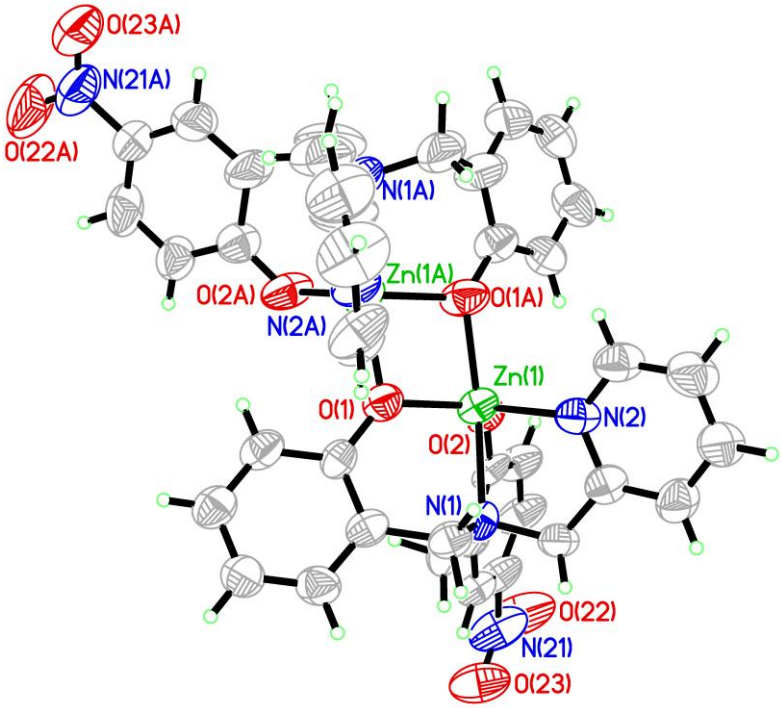

Figure 6.39: Crystal structure of $[Zn_2(\mathbf{L16})_2]$, ellipsoids drawn at the 50% probability level

The zinc ions adopt distorted trigonal bipyramidal geometries. The ligand packs with "anti" geometry discussed previously with no alignment of aromatic planes (Figure 6.40).

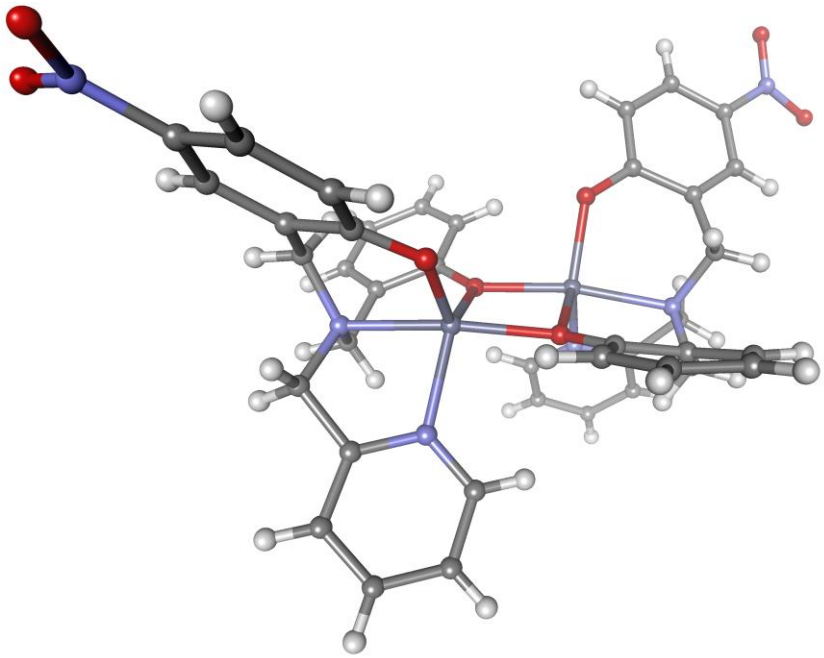

*Figure 6.40: Perspective view of [Zn_2(**L16**)$_2$]*

The anti arrangement of the donor arms and trigonal bipyramidal metal geometry is typical for the zinc complexes of the structural analogues of **L16**.[168] The bond lengths and angles around the zinc ion did not show any notable deviations from the complexes already reported (Table 6.6).

Parameter	Length (Å)	Parameter	Angle (°)	Parameter	Angle (°)
Zn1–O1	1.987(6)	O1–Zn1–O1A	78.0(2)	O1–Zn1A–O1A	78.2(2)
Zn1–O1A	2.054(5)	O1–Zn1–O2	122.8(2)	O1–Zn1A–O2A	98.5(2)
Zn1–O12	1.943(5)	O1–Zn1–N1	90.5(2)	O1–Zn1A–N1A	169.0(2)
Zn1–N1	2.158(6)	O1–Zn1–N2	124.5(2)	O1–Zn1A–N2A	96.6(2)
Zn1–N2	2.065(6)	O1A–Zn1–O2	104.9(2)	O1A–Zn1A–O2A	118.2(2)
Zn1A–O1	2.021(5)	O1A–Zn1–N1	164.0(2)	O1A–Zn1A–N1A	93.7(2)
Zn1A–O1A	2.013(6)	O1A–Zn1–N2	97.4(2)	O1A–Zn1A–N2A	114.3(3)
Zn1A–O2A	1.926(5)	O2–Zn1–N1	90.6(2)	O2A–Zn1A–N1A	91.8(2)
Zn1A–N1A	2.155(6)	O2–Zn1–N2	111.9(2)	O2A–Zn1A–N2A	127.3(3)
Zn1A–N2A	2.068(6)	N1–Zn1–N2	79.9(2)	N1A–Zn1A–N2A	79.9(2)

*Table 6.6: Major structural parameters for the geometry of the Zn(II) ion in [Zn_2(**L16**)$_2$]*

The UV-Vis of $[Zn_2(\mathbf{L16})_2]$ showed a similar $\pi - \pi^*$ transition for the ligand as the copper complex which was at 362 nm and ε 13400 L mol^{-1} cm^{-1} (Figure 6.41). When checked for fluorescence activity using similar concentrations and entry/exit slit widths on the fluorometer to those used when analysing the beryllium complexes there was no activity.

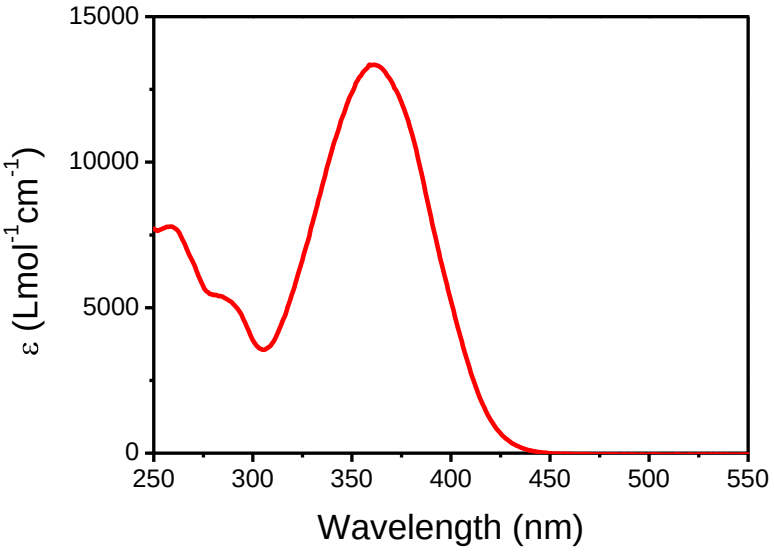

*Figure 6.41: UV-Vis of $[Zn_2(\mathbf{L16})_2]$ (**red**) at 10^{-5} M showing ligand $\pi - \pi^*$ transitions in MeOH*

It is expected the ligands **L15** – **L19** would show similar modes of coordination to metal cations as **L16**. Characterising all of the possible metal complexes of these ligands would represent a large detour from the aims of this thesis; however, it was most important to determine whether there was an influence on the fluorescence on the water soluble ligand **L18** (Figure 6.42).

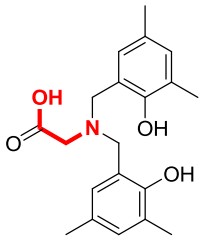

*Figure 6.42: Water-soluble and fluorescent encapsulating ligand, **L18***

L18 had the greatest potential for use as a water soluble fluorescent sensor for detection of Be(II). Coordination of **L18** to other metals only becomes a problem if they give rise to a fluorescent species. An excess of **L18** could be used in a sensor to ensure Be(II) coordination or a buffer and EDTA system could be used to coordinate Be(II) to **L18** preferentially to other metals. Current commercial beryllium sensors use buffers to precisely control the pH and EDTA to coordinate other metals to effectively detect beryllium with good sensitivity.[61] Both copper and zinc sulfate were coordinated to **L18** in water and the solutions were diluted and checked for any fluorescence at 290 nm (the excitation wavelength of the Be(II) complex, Figure 6.34) and there was no activity.

6.3 Summary

The use of tetra-coordinate ligands offered a vast improvement in the complexation of Be(II) compared to the proton sponges investigated in Chapter 4. The use of ^{9}Be NMR calculations allowed prediction of the correct species with good certainty and time domain calculations gave insight into the electronic transitions occurring for the fluorescent beryllium complexes.

The trade-off in use of these ligands is the potential loss in selectivity for beryllium over other metal cations. Future investigation will need to involve competition studies between beryllium and other metals for these ligands to evaluate the extent of this problem.

It should be noted that there is currently no known ligand which will bind only to beryllium and show no complexation with other metals. It is possible; however, to elicit selectivity through the use of buffers to control pH and EDTA to coordinate other interfering metal cations. Hence, a ligand such as **L18** has strong potential for development into a beryllium sensor.

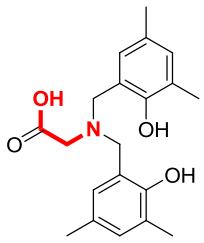

*Figure 6.43: Water-soluble and fluorescent encapsulating ligand, **L18***

Modification of the phenolic substituents on **L18** with suitable chromophores could further enhance the observed fluorescence increasing the sensitivity for detection of minute traces of beryllium.

Chapter 7: Conclusions

This investigation began by exploring the idea of size fit selectivity in an attempt to find a potentially beryllium selective ligand. The current "gold standard" for detection of beryllium in an aqueous environment is a sulfonated analogue of **701** (Figure 7.1), which is currently used commercially in a beryllium detection kit.[61]

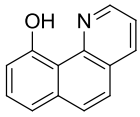

*Figure 7.1: Benzo[h]quinolin-10-ol, **701***

701 was not entirely selective for beryllium, and the test kit used a complex buffer system to maintain a precise pH to elicit coordination to beryllium and an excess amount of EDTA to bind all other metal ions. **701** would therefore be unsuitable for any large scale environmental remediation application.

It was thought that by retaining the rigid aromatic backbone of **701** and switching the strong phenolic oxygen donor to nitrogen, selectively for beryllium might be possible. We then began an extensive investigation into the ligand **L2** and its substituted derivatives (Figure 7.2).

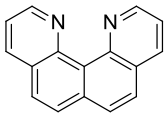

*Figure 7.2: Quinolino[7,8-h]quinoline, **L2***

L2 turned out to be a poor ligand for Be(II) coordination in aqueous environments. The unique spacing of the nitrogen donors resulted in a high affinity for protonation which was not matched by Be(II) in an aqueous environment. Once protonated, **L2** was essentially inactivated against any metal coordination with the high pK_{BH+} leaving no chance for

deprotonation and Be(II) coordination. It is still a firm belief that the use of a suitable beryllium salt (such as beryllium chloride) in an aprotic environment would achieve Be(II) coordination to **L2**. Coordination of **L2** to the similarly sized B(III) cation was achieved using aprotic conditions and the solid state structure revealed an excellent fit. Unfortunately, beryllium is not available in a wide variety of different salts, and preparation of a suitable reactive beryllium salt increases the danger due to the handling of beryllium solids. Hence, aqueous beryllium coordination chemistry was the only safe viable option, even then requiring the use of a special overseas facility.

In closing, to achieve coordination to beryllium in an aqueous system, it is essential to use hard electron-rich oxygen donors to coordinate with the hard beryllium dication. When considering simple rigid bidentate ligands, **701** is still the most suitable choice for Be(II) coordination.

The use of encapsulation to achieve selectivity for beryllium was then explored. A three-coordinate ligand which was recently investigated for the use of physiological detection of beryllium was **702** (Figure 7.3).[28]

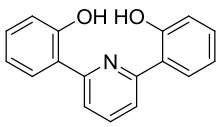

*Figure 7.3: 2,2'-(pyridine-2,6-diyl)diphenol, **702***

The Be(II) complex of **702** was presented to common interferants found in physiological media and was stable under these conditions. It is not known whether initial complexation to Be(II) would occur selectively with **702** in a complex media containing other metal cations.

The current investigation focused on ligands capable of full encapsulation, forming tetra-coordinate species with Be(II). The best ligands were those containing two or three oxygen donors which effectively coordinated to the beryllium aqua species, for example **L18** (Figure 7.4).

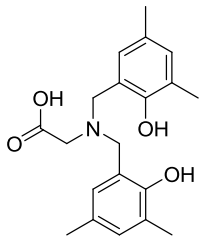

Figure 7.4: 2-(bis(2-Hydroxy-3,5-dimethylbenzyl)amino)acetic acid, ***L18***

Depending on the solubility of the ligand, they could be used for aqueous or organic solvent based applications. Due to the limited amount of time available to conduct the beryllium research at the overseas facility, competition studies for beryllium were not instigated.

The current state of affairs in the search for beryllium selective ligands still remains largely uncharted. The toxicity of beryllium means there are very few groups willing to work in the field of beryllium coordination chemistry. Figure 7.5 offers a rough schematic of how simple bidentate ligands coordinate to Be(II) relative to other metal cations. The requirement of hard oxygen donors to coordinate Be(II) means it is not possible to design a simple bidentate ligand which will coordinate Be(II) and not other metal ions. An enclosed tetra-coordinate ligand on the other hand may be better suited to excluding larger metal cations.

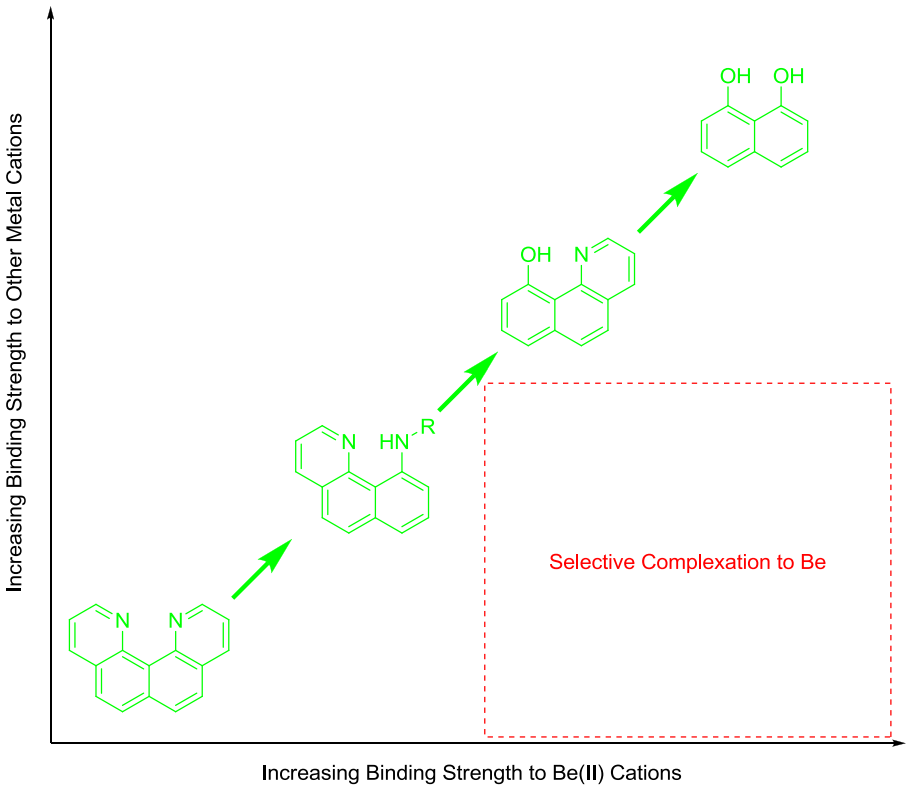

Figure 7.5: A representation of the lack of selectivity of simple bidentate ligands

Due to the time constraints of this project, the ligand **L14** could not be tested for Be(II) coordination (Figure 7.6). In light of the results of Chapter 6, it is anticipated this would show weak coordination to beryllium due to the lack of oxygen donors. Crucially however, the presence of the phenolic oxygen should promote initial coordination to Be(II) and full encapsulation via the weaker pyridine donors could potentially occur via chelation.

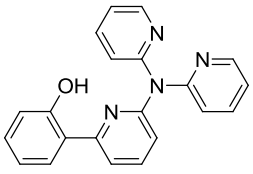

Figure 7.6: Successfully synthesised 2-(6-(dipyridin-2-ylamino)pyridin-2-yl)phenol, ***L14***

An enclosed ligand such as **L14** has not been previously synthesised and future studies may show the beginnings of selectivity toward smaller Be(II) cations over larger metal cations (Figure 7.7).

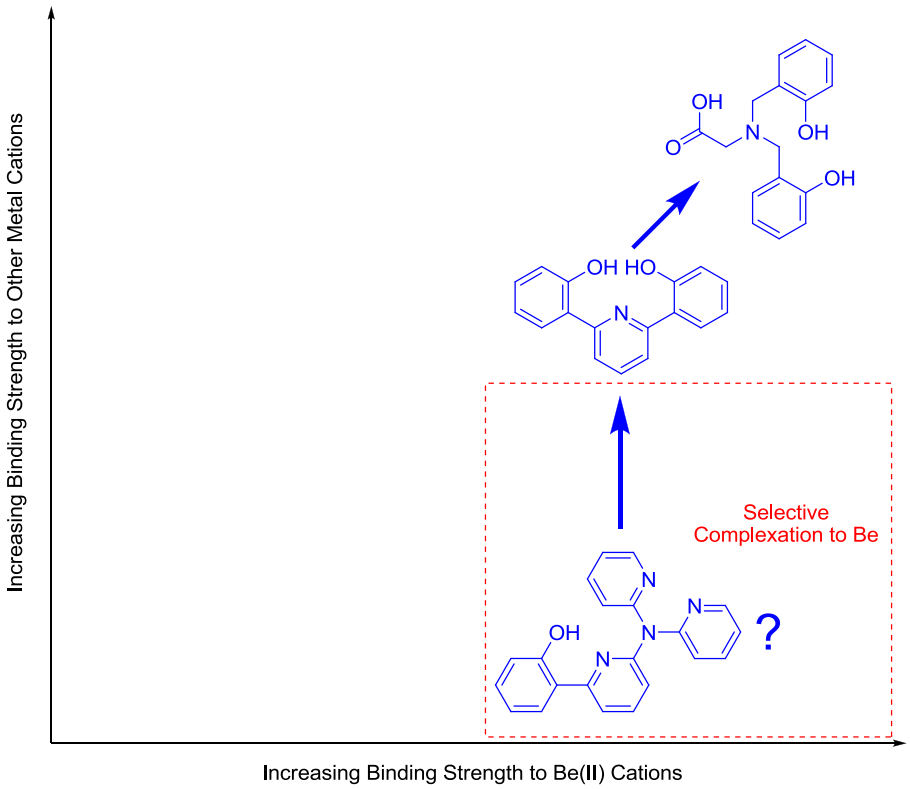

Figure 7.7: A representation of the potential selectivity of the encapsulating ligand ***L14***

The only way future research can effectively be achieved would be to start a beryllium research laboratory at Massey University. Travelling overseas to conduct the research is not a viable long term option, and the overseas laboratory used in this investigation is no longer available due to absence of beryllium trained staff and repurposing of the facilities. The major components of such a setup is a dedicated fumehood separate from all other activities and a separate reverse phase glove box for the handling of initial beryllium solids. Aside from these, the long term cost is the relatively small amount of beryllium contaminated waste generated which must be strictly contained. All liquid and solid waste (pipette tips, gloves, paper towels etc) must be separately contained and not allowed to mix with any other waste generated by the University. With the correct precautions put in place, excellent progress on this important research area could be made making New Zealand a world leader in this area.

Appendix A: Experimental

A.1 General Experimental

A.1.1 Reagents and Solvents

All starting materials were obtained from commercial sources and used without purification unless otherwise noted. All other reagents and solvents were obtained from commercial sources and used as supplied.

Solvents used in reactions were analytical grade and used directly. If stated as dry, they were subject to further purification as follows: Tetrahydrofuran, dichloromethane and toluene were passed through an alumina column on an in-house solvent purification system. Dimethylformamide was distilled from barium oxide and stored over 4 Å molecular sieves, under an atmosphere of nitrogen. Methanol was distilled from Mg turnings and I_2 and stored over 4 Å molecular sieves, under an atmosphere of nitrogen. Acetonitrile was distilled and stored over 4 Å molecular sieves, under an atmosphere of nitrogen.

A.1.2 Synthetic Methods

All reactions were carried out in oven-dried glassware, unless stated as being flame-dried, under an atmosphere of nitrogen or argon, with magnetic stirring. The reaction temperature refers to external sand bath temperature. All organic extracts were simultaneously filtered and dried over filter paper filled with magnesium sulfate. The solvents were removed under reduced pressure on a Büchi rotary evaporator. For characterisation purposes, or when strict drying of the compound was required for the next step, the last traces of solvent were removed using a high vacuum pump attached to a Schlenk line.

A.1.3 Chromatography

Reactions were followed by TLC on aluminium-backed silica gel 60 F_{254} sheets from E-Merck, visualised by UV light.

Flash column chromatography was performed using Scharlau silica gel 60, 0.04 – 0.06 mm, 230 – 400 mesh. The length of silica was typically 20 cm and the diameter was varied according to reaction scale. The silica gel slurry was compacted with the specified solvent system of hexanes / EtOAc or CH_2Cl_2 / MeOH. The compound was then loaded onto the column an eluted with the specified solvent under positive pressure.

A.1.4 Characterisation

All compounds were characterised by nuclear magnetic resonance and mass spectrometry on in-house instruments. New compounds were sent for further characterisation by elemental analysis. One problem which was prevalent with most of the quino[7,8-*h*]quinolines was the fact they could not be purified by conventional silica gel column chromatography techniques unless extremely polar solvent MeOH gradients were used leading to dissolution of the silica. The quino[7,8-*h*]quinolines also did not recrystallise on a bulk scale. As such, elemental analysis results on these compounds were generally slightly outside publication standards, in these instances high resolution mass spectrometry and ^{13}C NMR spectras were recorded. X-ray crystal structures were recorded when suitable single crystals were available.

NMR spectra were collected on Bruker Avance 300, 400 and 500 MHz spectrometers; the particular instrument is specified for each compound. In $CDCl_3$, all chemical shifts are reported relative to TMS (^1H) and residual solvent (^{13}C). In all other deuterated solvents, the chemical shifts are reported relative to residual solvent (^1H, ^{13}C). Full NMR assignments were made using ^1H, ^{13}C, and when appropriate ^9Be, ^{11}B and ^{19}F spectra were recorded.

Electrospray mass spectra were recorded on a Mircomass ZMD spectrometer run in positive ion mode.

High resolution mass spectra were recorded on a micrOTOF-Q mass spectrometer, operating at a nominal voltage of 3500 V. This service was provided by The University of Auckland.

Elemental analyses were provided by the Campbell Microanalytical Laboratory, University of Otago.

UV-Vis spectra were recorded on a Shimadzu UV-3101PC spectrophotometer using UV Probe v1.1. Fluorescence measurements were made on a Perkin Elmer LS50B luminescence spectrometer using FL Winlab v4.00.02.

The X-ray data was collected at reduced temperature on a Rigaku Spider diffractometer equipped with a copper rotating anode X-ray source and a curved image plate detector. The crystals were mounted in an inert oil, transferred into the cold gas stream of the detector and irradiated with graphite monochromated Cu Kα (k = 1.54178 Å) X-rays. The data was collected by the Crystal Clear program (v.1.4.0) and processed with FS-PROCESS to apply the Lorentz and polarisation corrections to the diffraction spots (integrated 3 dimensionally). The structures were solved by direct methods SHELXS-97 and refined using the SHELXL-97 program. Absorption correction was carried out empirically. Hydrogens were calculated at their ideal positions unless otherwise stated.

A.1.5 Computational

Theoretical calculations were performed using the program GAUSSIAN03 for Linux running on the BESTGRID supercomputer operated at Massey University Albany. Becke's three-parameter hybrid exchange correlation functional containing the nonlocal gradient

correction of Lee, Yang, and Parr (B3LYP) in conjunction with the 6-311g++(2d,p) basis set in most instances unless noted otherwise.

A.2 Beryllium Coordination Chemistry Safety Considerations

A.2.1 Safe Handling

In order to conduct beryllium research safely, special precautions must be taken. The research should be conducted in an area separate from all other activities in order to prevent contamination, preferably a separate room. All handling of beryllium solids should be prepared in a negative phase; HEPA (high efficiency particulate air) filtered glove box. An example of such a setup is shown in Figure A.1.

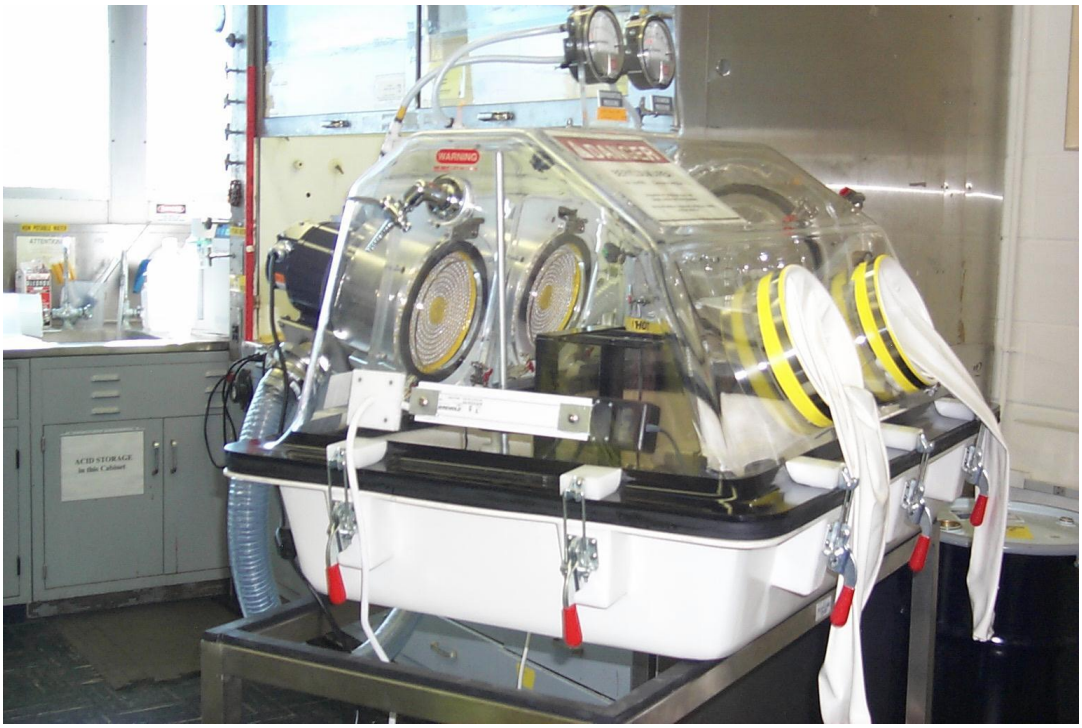

Reverse Phase, HEPA filtered glove box for the handling of Be solids

The gloves are sucked down due to the negative pressure. The negative pressure is necessary so that in the event of a glove rupture, or when simply taking items in and out of the box via the antechamber, no particulate beryllium is blown out. The reason for such strict measures is because the permissible exposure limit (The 8-hour time-weighted

average airborne concentration not to be exceeded) for beryllium is 2 µg/m^3. This is equivalent to grinding the tip off a pencil lead and scattering it in the area the size of a football field.

Once in a stock solution, Be may be handled out of the glove box in a normal fume hood that is separated for beryllium use. All liquid beryllium waste should be collected in a separate waste container and all disposables (gloves, pipette tips, scintillation vials etc) must be placed in a separate sealable bag for disposal, which is later double-bagged and collected separately. Teflon lined tubes must be used for NMR spectroscopy.

A.2.2 Testing for Contamination

The workspace should be regularly tested for contamination. A colorimetric test could be used that utilised the sulfonated hydroxybenzoquinoline to bind Be^{2+}, EDTA was used to bind interference elements. The elements validated for interference are Al, Fe, Pb, U, Cd, Cr, Hg, Ca, W, Ni, Co and Cu all at concentrations of up to 0.4 mM per 0.1µM Be.

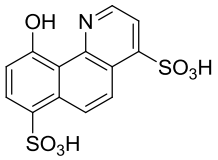

10-Hydroxybenzo[h]quinoline-4,7-disulfonic acid

The test is a convenient method for testing whether a surface contains beryllium contamination. Positively tested areas should be immediately be cleaned, with the waste being separated. A positive test would require review of handling procedures as there must be no chance for beryllium dust to occupy workspaces. When undertaking beryllium solution chemistry, this problem should not be encountered unless the worker drastically deviates from standard operating procedures.

A.3 Chapter 2 Experimental

A.3.1 Tetramethyl 2,2'-(naphthalene-1,8-diylbis(azanediyl))difumarate (205)

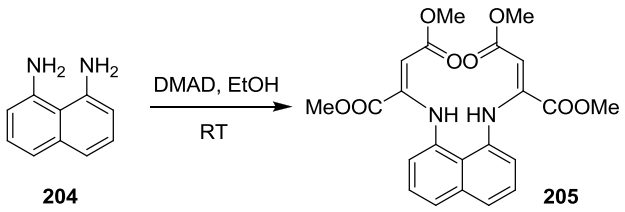

204 **205**

Tetramethyl 2,2'-(naphthalene-1,8-diylbis(azanediyl))difumarate (**205**) was synthesised according to the known literature procedure.[103] 1,8-Diaminonaphthalene (**204**) (10.0 g, 63.2 mmol) in EtOH (750 mL) was slowly added dropwise to dimethyl acetylenedicarboxylate (DMAD) (15.5 mL, 126.0 mmol) over 1 h, and the reaction was stirred for a further 1 h. The crude product precipitates as a yellow-brown material from the solution and was collected by filtration. Instead of recrystallisation, the crude **205** was partially purified by chromatography (1:1 EtOAc / hexanes), and washed and filtered with ether to give **205** as a yellow-orange crystalline powder (11.7 g, 41 %). R_f = 0.32 (2:1 hexanes / EtOAc). ^{1}H NMR (500 MHz, $CDCl_3$) δ 3.55 (s, 6H; COCH_3), 3.68 (s, 6H; COCH_3), 5.48 (s, 2H; C=C*H*), 6.93 (d, *J* = 7.4, 2H; 4,5-*H*), 7.34 (t, *J* = 7.8, 2H; 3,6-*H*), 7.65 (d, *J* = 8.2, 2H; 2,7-*H*), 10.11 (s, 2H, N*H*); ^{13}C NMR (125 MHz, $CDCl_3$) δ 51.0 (t), 52.6 (t), 93.8 (s), 121.6 (s), 123.3 (q), 125.8 (s), 126.4 (s), 136.1 (q), 137.0 (q), 147.9 (q), 164.9 (q), 169.5 (q). M.P. = 145 – 147 ^{o}C, Lit. M.P. = 146 ^{o}C;[103] 142 – 143 ^{o}C.[85]

A.3.2 Dimethyl 4,9-dioxo-1,4,9,12-tetrahydroquinolino[7,8-h]quinoline-2,11-dicarboxylate (206)

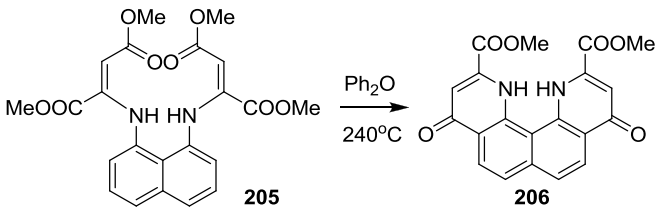

Dimethyl 4,9-dioxo-1,4,9,12-tetrahydroquinolino[7,8-*h*]quinoline-2,11-dicarboxylate (**206**) was synthesised according to the known literature procedure.[103] Tetramethyl 2,2'-(naphthalene-1,8-diylbis(azanediyl))difumarate (**205**) (2.5 g) was added to phenyl ether (60 mL) which was preheated to 240°C and stirred for 20 min. An insoluble pale yellow solid was formed which was filtered and washed with acetone (200 mL). Rinsing, sonication and filtration of the insoluble precipitate with acetone (3x 200 mL) removed the impurities locked into the clay-like product (1.21 g, 57 %). Analysis by NMR or MS experiments was not possible. $C_{20}H_{14}N_2O_6$ (378.33): calcd. C 63.49, H 3.73, N 7.40; found C 63.72, H 3.88, N 7.40. M.P. = 342 – 344°C, Lit. M.P. = ">300°C";[103] 276 - 278°C.[85]

A.3.3 Quinolino[7,8-h]quinoline-4-9-(1H,12H)-dione (208)

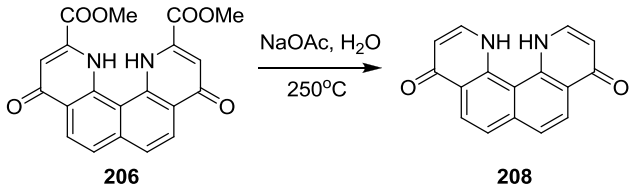

Dimethyl 4,9-dioxo-1,4,9,12-tetrahydroquinolino[7,8-*h*]quinoline-2,11-dicarboxylate (**206**) (0.800 g, 2.116 mmol) and sodium acetate (0.172 g, 2.116 mmol) were added to water (80 mL) in a stainless steel bomb with a Teflon inner container (100 mL capacity). The insoluble **206** was dispersed by vigorous agitation then left stationary and heated at 250 °C overnight (16 hr). An insoluble brown semi-crystalline solid was separated using centrifugation and decantation with water (3x 50 mL) resulting in the isolation of impure **208**. Purification of **208** was possible in the next step. $C_{16}H_{10}N_2O_2$ (262.26): calcd. C 73.27, H 3.84, N 10.68; found C 69.92, H 4.49, N 10.10. IR (KBr disc): 3433 br, 2556 br,

1786 br, 1617 s, 1584 w, 1550 w, 1500 m, 1472 m, 1432 m, 1411 m, 1375 s, 1302 m, 1284 m, 1193 m, 1167 w, 1103 m, 1072 w, 978 w, 865 w, 832 s, 805 w, 793 w, 742 w, 714 w, 652 w, 574 s, 509 s, 493 m, 476 w.

A.3.4 4,9-Dichloroquino[7,8-h]quinoline (L1)

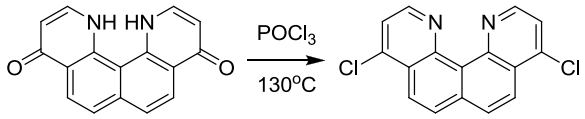

208 **L1**

4,9-Dichloroquinolino[7,8-*h*]quinoline (**L1**) was synthesised according to the known literature procedure.[85] Phosphorus oxychloride (4.02 g, 2.44 mL, 26.4 mmol) was added to quinolino[7,8-*h*]quinoline-4-9-(1*H*,12*H*)-dione (**208**) (0.520 g, 2.08 mmol) and the reaction was stirred at 130 °C for 8 minutes under Ar. The reaction mixture was diluted with CH_2Cl_2 (200 mL) and basified with 6M KOH (20 mL) followed by addition of water (200 mL), a small portion of decolourising carbon was added and the organic layer was filtered and dried over $MgSO_4$, and concentrated to give **L1** (0.427 g). The overall yield for the two steps (**206** – **L1**) is 68 %. ^{1}H NMR (500 MHz, $CDCl_3$) δ 7.71 (d, *J* = 4.5, 2H; 3,10-*H*), 8.03 (d, *J* = 8.9, 2H; 6,7-*H*), 8.48 (d, *J* = 8.9, 2H; 5,8-*H*), 9.28 (d, *J* = 4.5, 2H; 2,11-*H*); ^{13}C NMR (125 MHz, $CDCl_3$) δ 121.6 (s), 124.9 (s), 126.4 (q), 126.4 (q), 128.8 (s), 136.4 (q), 142.9 (q), 148.2 (q), 149.9 (s). MS for $C_{16}H_8N_2Cl_2$ (M^+) 299.25. The product was recrystallised by slow cooling of a saturated solution in $CHCl_3$ at 0 °C. $C_{16}H_8Cl_2N_2$ (299.15): calcd. C 64.24, H 2.70, N 9.36; found C 64.05, H 2.88, N 9.27. M.P. = 236 – 238 °C, Lit. M.P. = 234 – 235 °C.[85]

Crystal data for **L1**.2$CHCl_3$. $C_{18}H_{10}Cl_8N_2$, colourless needle, dimensions 1.25 x 0.25 x 0.20 mm, monoclinic, space group $P2_1/c$, a = 8.5924(17), b = 11.776(2), c = 21.225(4) Å, α = 90.00°, β = 92.47(3)°, γ = 90.00°, U = 2145.7(7) Å^3, μ = 1.058 mm^{-1}, Z = 4, D_c = 1.665 g cm^{-3}, F(000) = 1072, T = 173(2) K. 17488 Reflections were collected using a Bruker SMART four circle diffractometer in the range 2.94 < 2θ < 56.56°. A semi-empirical

absorption correction (SADABS-2004/1) was applied. The 5306 independent reflections were used to solve the structure by direct methods (SHELXS97) which resulted in the location of all non-hydrogen atoms. All non-hydrogen atoms were made anisotropic and the refinement (SHELXL97) of 253 parameters converged to R_1 = 0.0232 [for 4830 reflections having $I > 4\sigma(I)$], wR_2 = 0.0621 and goodness of fit 1.035 (for all 5306 F^2 data). Peak / hole 0.398 / -0.368 e Å^{-3}.

A.3.5 Quino[7,8-h]quinoline (L2)

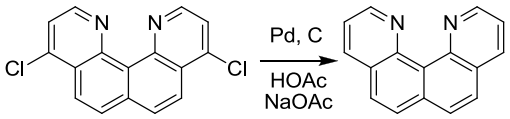

L1 **L2**

Quinolino[7,8-*h*]quinoline (**L2**) was synthesised according to the known literature procedure.[85] Water free sodium acetate (0.071 g, 0.862 mmol), 5 % Pd / C (0.037 g, 37 weight % of **L1**) and glacial acetic acid (10 mL) was added to 4,9-dichloroquino[7,8-*h*]quinoline (**L1**) (0.100 g, 0.334 mmol) and the reaction was shaken under H_2 at 60 psi for 2 hr. The acetic acid was removed *in vacuo* and product was basified with 6M KOH (20 mL) and extracted with CH_2Cl_2 (200 mL). A small portion of decolourising carbon was added and the organic layer was filtered and dried over $MgSO_4$ to give **L2** (0.055 g, 68 %). ^{1}H NMR (500 MHz, $CDCl_3$) δ 7.57 (dd, *J* = 4.3, 8.0, 2H; 3,10-*H*), 7.93 (‘s’, 4H; 5,8-*H* and 6,7-*H*), 8.28 (dd, *J* = 1.9, 8.0, 2H; 4,9-*H*), 9.43 (dd, *J* = 1.9, 4.3, 2H; 2,11-*H*); ^{13}C NMR (125 MHz, $CDCl_3$) δ 120.8 (s), 127.8 (s), 128.1 (q), 128.1 (q), 128.4 (s), 136.0 (q), 136.3 (s), 147.3 (q), 150.4 (s). MS for $C_{16}H_{10}N_2$ (MH^+) 231.31. M.P. = 191 – 192 ^{o}C, Lit. M.P. = 196 – 197 ^{o}C.[85]

A.3.6 [H(L1)]BF$_4$

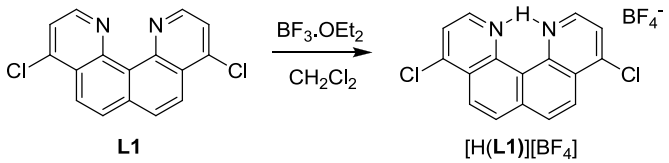

L1 [H(**L1**)][BF_4]

[H(**L1**)][BF_4] was a side-product of the reaction of **L1** with boron trifluoride diethyl etherate described in Chapter 4 and has been previously characterised as the perchlorate salt.[85] ^{1}H NMR (500 MHz, DMSO-d6) δ 8.42 (d, *J* = 5.5, 2H; 3,10-*H*), 8.53 (d, *J* = 9.1, 2H; 6,7-*H*), 8.62 (d, *J* = 9.1, 2H; 5,8-*H*), 9.34 (d, *J* = 5.5, 2H; 2,11-*H*) 19.29 (s, 1H; N*H*); ^{13}C NMR (125 MHz, DMSO-d6) δ 116.3 (q), 124.7 (s), 126.3 (q), 126.4 (q), 131.2 (s), 137.6 (q), 142.7 (q), 147.9 (s), 148.3 (s). MS for $C_{16}H_8N_2Cl_2.H^+$ (M^+) 299.60. The product was recrystallised by vapour diffusion of diethyl ether a MeCN solution of [H(**L1**)][BF_4]. $C_{16}H_8N_2Cl_2H^+ \bullet BF_4^-$ (386.02): calcd. C 49.66, H 2.34, N 7.24; found C 49.97, H 2.69, N 7.14. M.P. = 342 – 343 ^{o}C.

Crystal data for [H(**L1**)][BF_4]. $C_{16}H_9N_2Cl_2BF_4$, colourless rod, dimensions 0.5 x 0.1 x 0.05 mm, monoclinic, space group $P2_1/c$, a = 6.6569(13), b = 20.741(4), c = 11.169(2) Å, α = 90.00^o, β = 105.06(3)^o, γ = 90.00^o, U = 1489.1(5) Å^3, μ = 4.379 mm^{-1}, Z = 4, D_c = 1.726 g cm^{-3}, F(000) = 776, T = 173(2) K. 17488 Reflections were collected using a Rigaku MM007 rotating anode in the range 6.89 < 2θ < 144.74^o. A semi-empirical absorption correction (ABSCOR; Higashi, 1995) was applied. The 2846 independent reflections were used to solve the structure by direct methods (SHELXS97) which resulted in the location of all non-hydrogen atoms. All non-hydrogen atoms were made anisotropic and the refinement (SHELXL97) of 253 parameters converged to R_1 = 0.0429 [for 2303 reflections having $I > 4\sigma(I)$], wR_2 = 0.1075 and goodness of fit 1.041 (for all 2846 F^2 data). Peak / hole 0.305 / -0.339 e Å^{-3}.

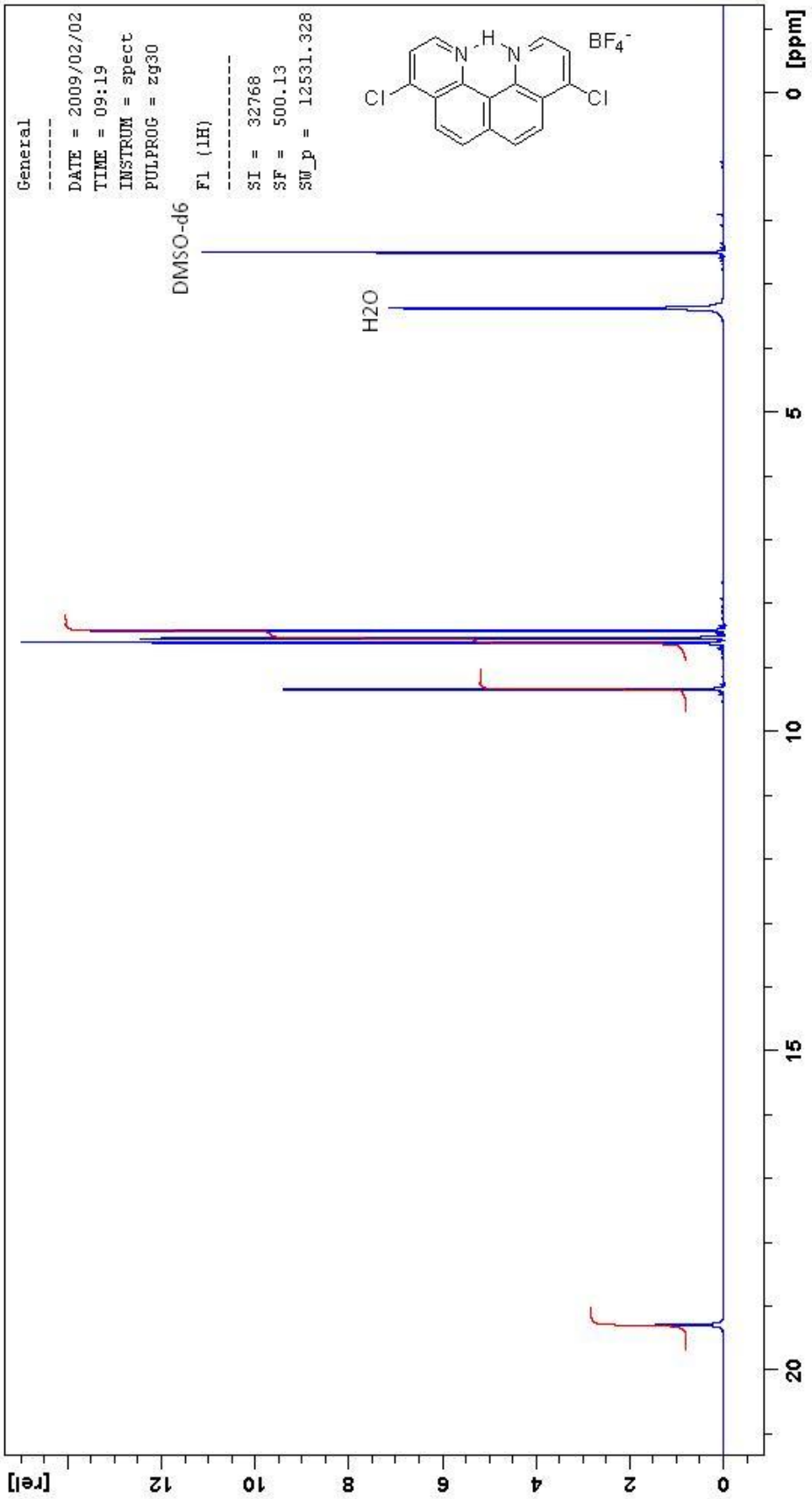
General
DATE = 2009/02/02
TIME = 09:19
INSTRUM = spect
PULPROG = zg30
F1 (1H)
SI = 32768
SF = 500.13
SW_p = 12531.328
DMSO-d6
H2O
Cl
Cl
N
H
N
BF4-
[rel]
[ppm]

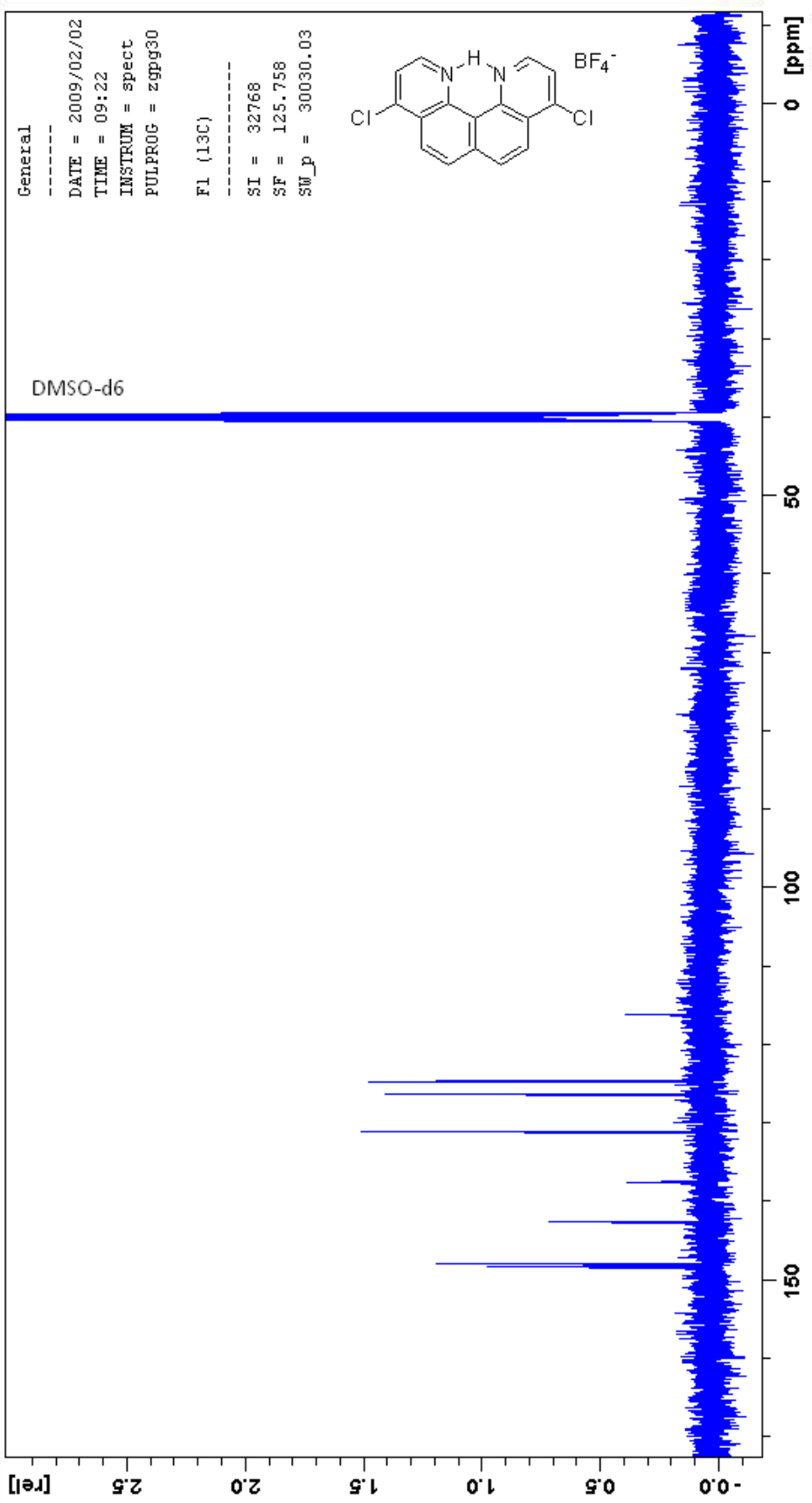
General
DATE = 2009/02/02
TIME = 09:22
INSTRUM = spect
PULPROG = zgpg30
F1 (13C)
SI = 32768
SF = 125.758
SW_p = 30030.03
DMSO-d6
Cl
Cl
BF4-
[rel]
[ppm]

A.3.7 [H(L2)]BF_4

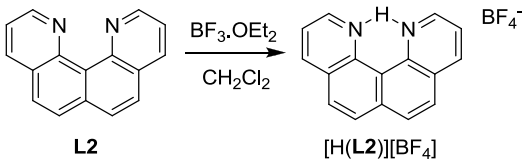

[H(**L2**)][BF_4] was a side-product of the reaction of **L2** with boron trifluoride diethyl etherate described in Chapter 4 and has been previously characterised as the perchlorate salt.[85] ^{1}H NMR (500 MHz, CD_3CN) δ 8.05 (dd, *J* = 5.0, 8.4, 2H; 4,6-*H*), 8.20 (d, *J* = 8.8, 2H; 6,7-*H*), 8.27 (d, *J* = 8.8, 2H; 5,8-*H*), 8.91 (dd, *J* = 1.6, 8.4, 2H; 3,10-*H*), 9.24 (m, 2H; 2,11-*H*), 19.61 (s, 1H; N*H*); ^{13}C NMR (125 MHz, CD_3CN) δ 117.0 (s), 124.3 (q), 129.3 (s), 130.5 (s), 130.8 (q), 138.2 (q), 143.1 (q), 143.7 (s), 147.7 (s). MS for $C_{16}H_{11}N_2$ (M^+) 231.31. M.P. = 235 – 237 ^{o}C.

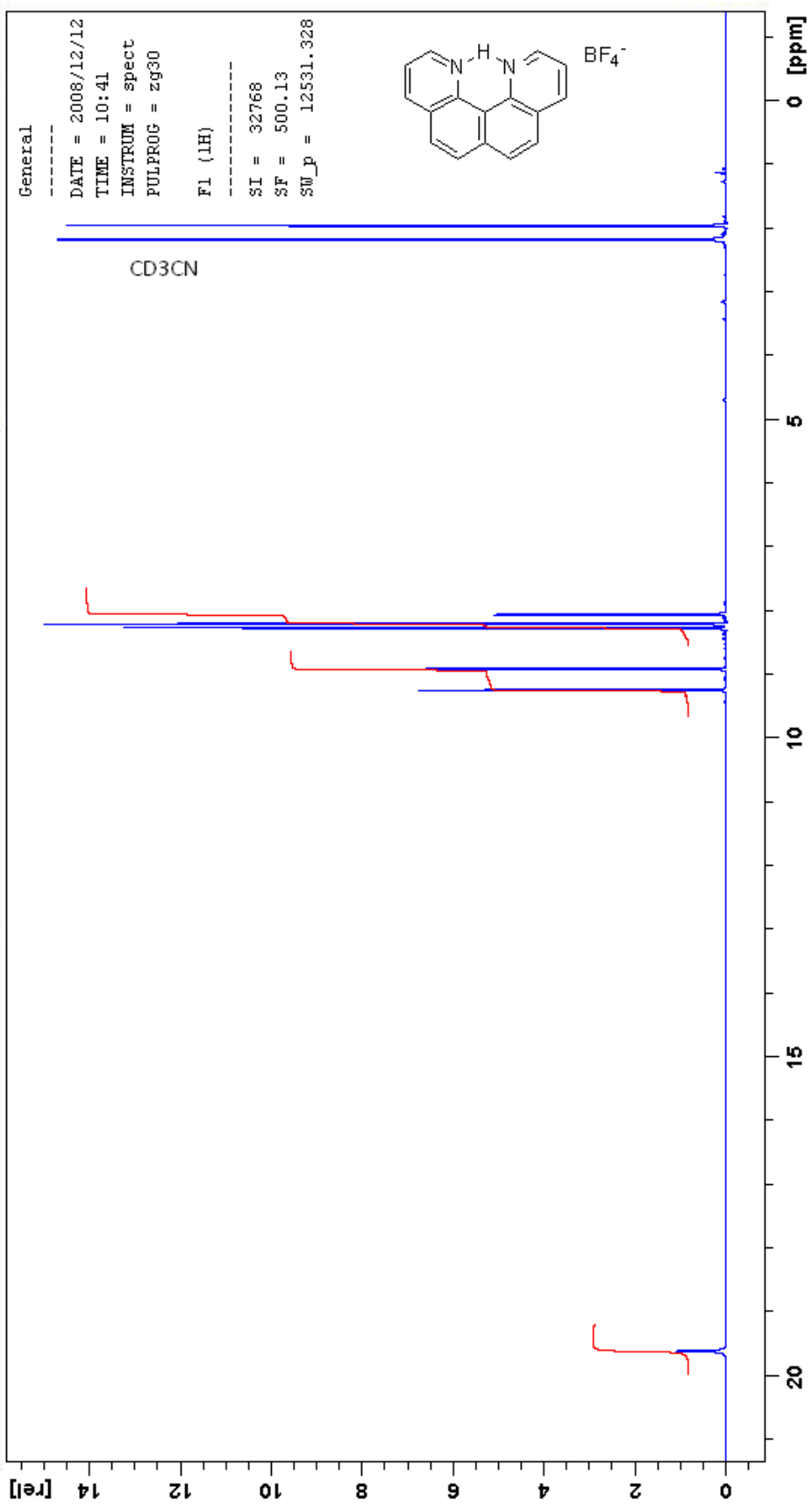
General
DATE = 2008/12/12
TIME = 10:41
INSTRUM = spect
PULPROG = zg30
F1 (1H)
SI = 32768
SF = 500.13
SW_p = 12531.328
CD3CN
BF4-
[rel]
[ppm]

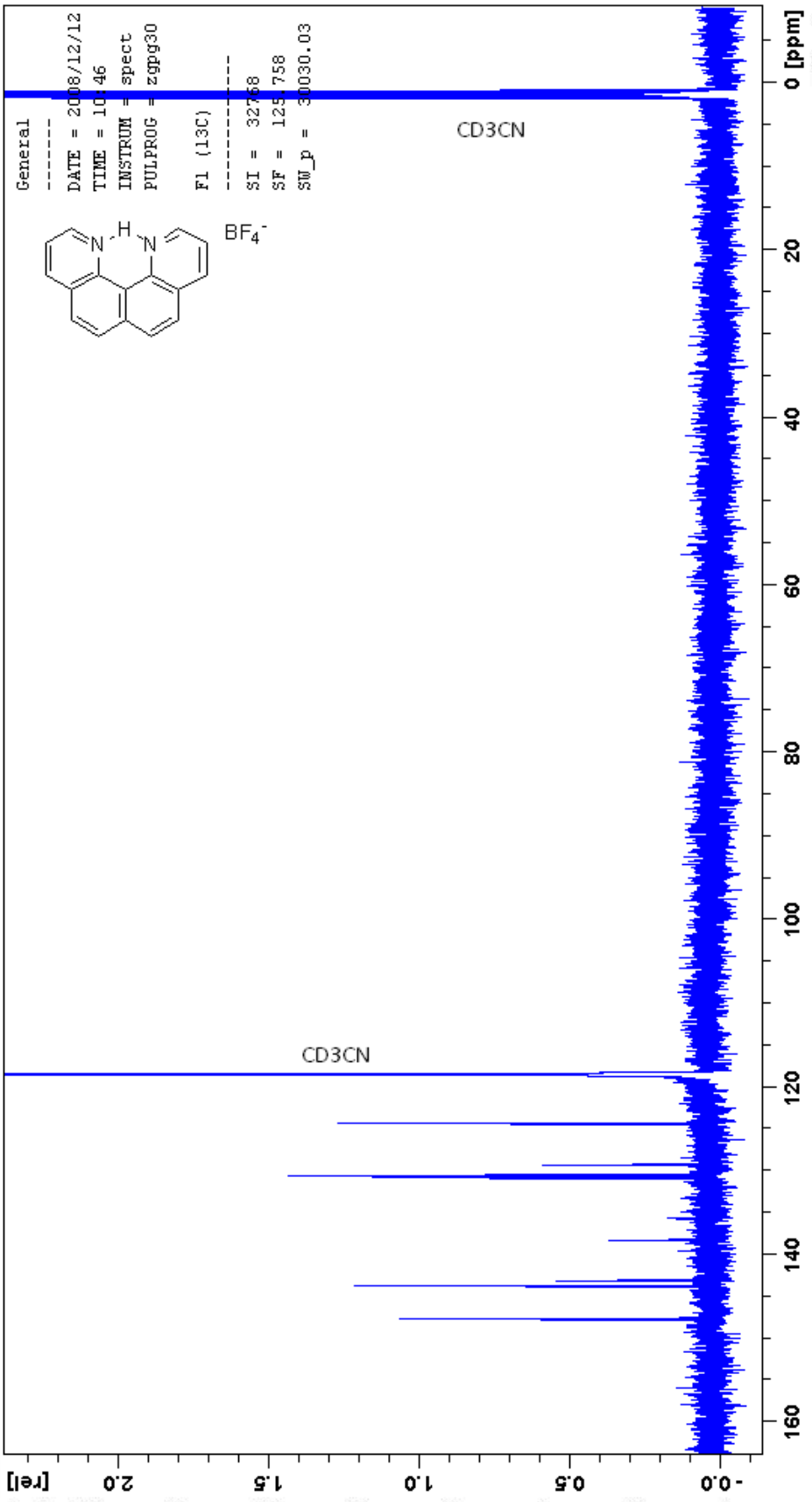
General
DATE = 2008/12/12
TIME = 10:46
INSTRUM = spect
PULPROG = zgpg30
F1 (13C)
SI = 32768
SF = 125.758
SW_p = 30030.03
BF4-
CD3CN
CD3CN
0 [ppm]
20
40
60
80
100
120
140
160
[rel]
2.0
1.5
1.0
0.5
0.0

A.3.8 3,3-bis(Methylthio)acrylaldehyde (217)

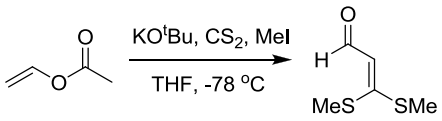

216 **217**

3,3-*bis*(Methylthio)acrylaldehyde (**217**) was synthesised according to the known literature procedure.[192] Vinyl acetate (**216**) (1.86 g, 2.00 mL, 21.6 mmol) in dry tetrahydrofuran (22 mL) was added slowly to a solution of potassium *tert*-butoxide (2.90 g, 25.9 mmol) in dry tetrahydrofuran (29 mL) under N_2 at -78 °C over 30 min. The reaction was stirred at this temperature for a further 1 hr. Then carbon disulfide (1.69 g, 1.30 mL, 21.6 mmol) was added dropwise over 15 min and the reaction was warmed to 0 °C and stirred at this temperature for a further 45 min. Methyl iodide (6.14 g, 2.70 mL, 43.2 mmol) was finally added and the reaction was stirred at 0 °C for 4 h. The reaction was poured onto ice-water (100 mL) and extracted with CH_2Cl_2 (3x 50 mL), dried over $MgSO_4$, filtered and concentrated. The product was purified by chromatography eluting with (1:6 EtOAc / hexanes) to give **217** as an orange oil (29 %). The product was used immediately in the next step and was not able to be stored long-term. R_f = 0.36 (2:1 hexanes / EtOAc). ^{1}H NMR (500 MHz, $CDCl_3$) δ 2.44 (s, 3H; SCH_3), 2.55 (s, 3H; SCH_3), 5.99 (d, J = 6.7, 1H; C=C*H*), 9.92 (d, J = 6.7, 1H; C*H*O); ^{13}C NMR (125 MHz, $CDCl_3$) δ 16.3 (t), 16.6 (t), 120.6 (s), 166.5 (q), 186.0 (q).

A.3.9 N-(2-(Methylthio)benzo[h]quinolin-10-yl)acetamide (214)

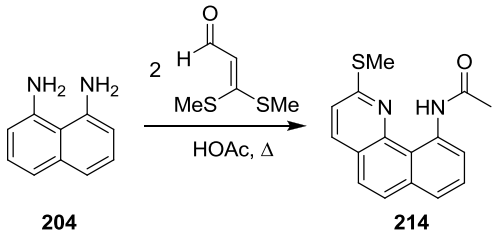

204 **214**

3,3-*bis*(Methylthio)acrylaldehyde (**217**) (0.300 g, 2.00 mmol) and 1,8-diaminonaphthalene (**204**) (0.174 g, 1.10 mmol) in glacial acetic acid (30 mL) was heated under reflux for 8 hr. The excess acetic acid was removed *in vacuo* and the residue quenched with a saturated $NaHCO_3$ solution. The residue was extracted with CH_2Cl_2 (200 mL) and the organic layer was washed with water (2 x 200 mL) and filtered and dried over $MgSO_4$. Purification by silica gel column chromatography eluting with 9:1 hexanes / EtOAc gave **214** as a pale brown solid which darkened upon storing (0.006 g, 2 %). R_f = 0.21 (2:1 hexanes / EtOAc). ^{1}H NMR (500 MHz, $CDCl_3$) δ 2.43 (s, 3H; C*H*$_3$), 2.69 (s, 3H; C*H*$_3$), 7.33 (d, *J* = 8.5, 1H), 7.51-7.68 (m, 4H), 8.05 (d, *J* = 8.5, 1H), 9.02 (d, *J* = 7.9, 1H), 14.3 (s, 1H; N*H*); ^{13}C NMR (125 MHz, $CDCl_3$) δ 14.7 (t), 25.9 (t), 116.6 (q), 117.0 (s), 118.0 (s), 122.8 (s), 124.3 (q), 124.8 (s), 128.1 (s), 129.0 (s), 135.4 (q), 136.9 (s), 139.2 (q), 147.3 (q), 158.0 (q), 169.4 (q).

Crystal data for **214**. $C_{16}H_{14}N_2OS$, colourless block, dimensions 0.55 x 0.34 x 0.33 mm, triclinic, space group *P*-1, *a* = 7.2715(2), *b* = 9.8011(2), *c* = 10.4908(2) Å, α = 106.4320(10)^o, β = 99.5190(10)^o, γ = 106.4390(10)^o, *U* = 662.88(3) Å^3, μ = 0.240 mm^{-1}, *Z* = 2, D_c = 1.415 g cm^{-3}, *F*(000) = 296, *T* = 173(2) K. 7336 Reflections were collected using a Bruker SMART four circle diffractometer in the range 2.31 < 2θ < 66.50^o. A semi-empirical absorption correction (SADABS-2004/1) was applied. The 2603 independent reflections were used to solve the structure by direct methods (SHELXS97) which resulted in the location of all non-hydrogen atoms. All non-hydrogen atoms were made anisotropic and the refinement (SHELXL97) of 181 parameters converged to R_1 = 0.0310 [for 2603 reflections having $I > 4\sigma(I)$], wR_2 = 0.0854 and goodness of fit 1.090 (for all 2603 F^2 data). Peak / hole 0.335 / -0.244 e Å^{-3}.

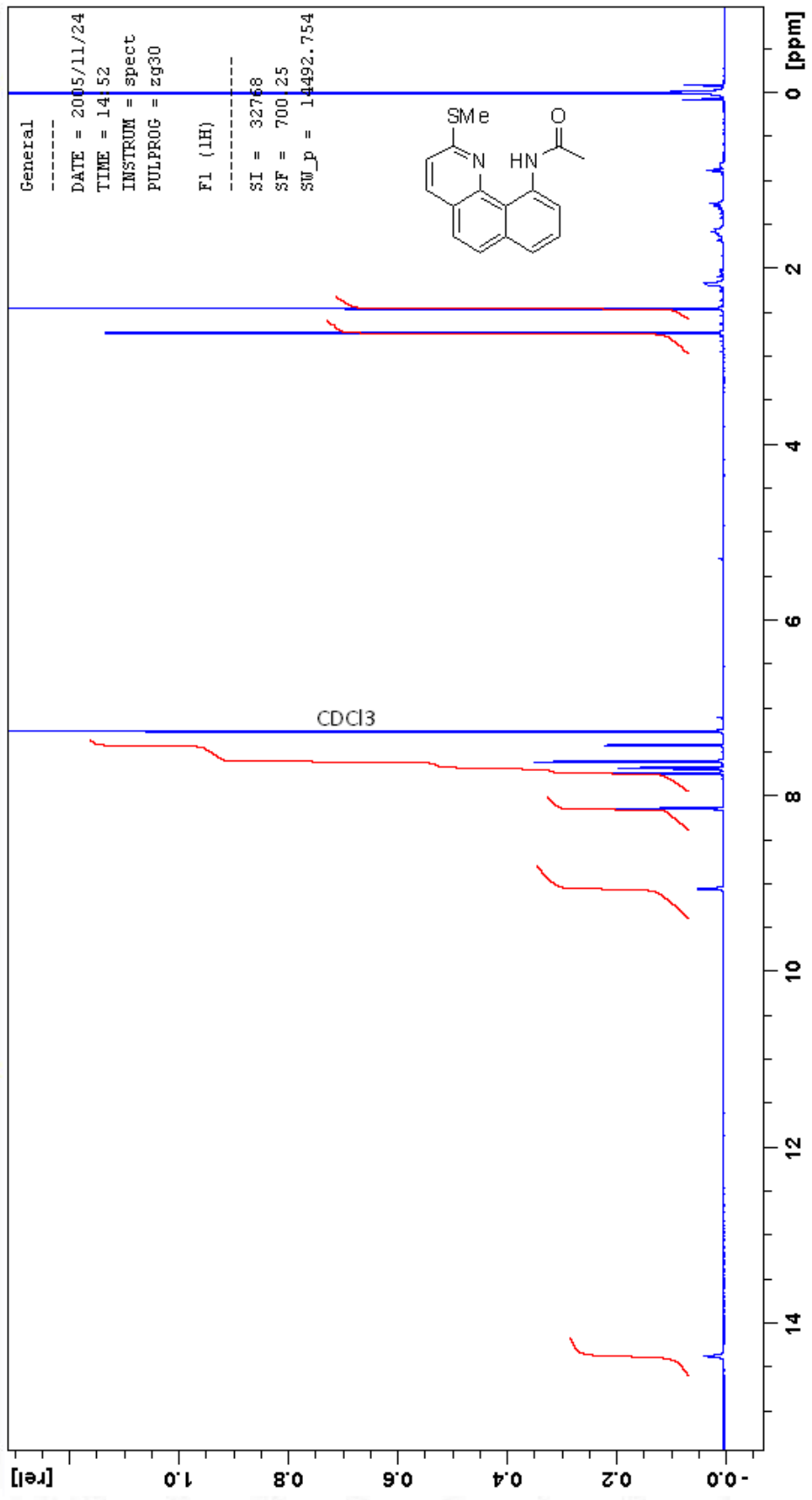
General
DATE = 2005/11/24
TIME = 14.52
INSTRUM = spect
PULPROG = zg30
F1 (1H)
SI = 32768
SF = 700.25
SW_p = 11492.754
SMe
N
HN
O
CDCl3
[rel]
[ppm]

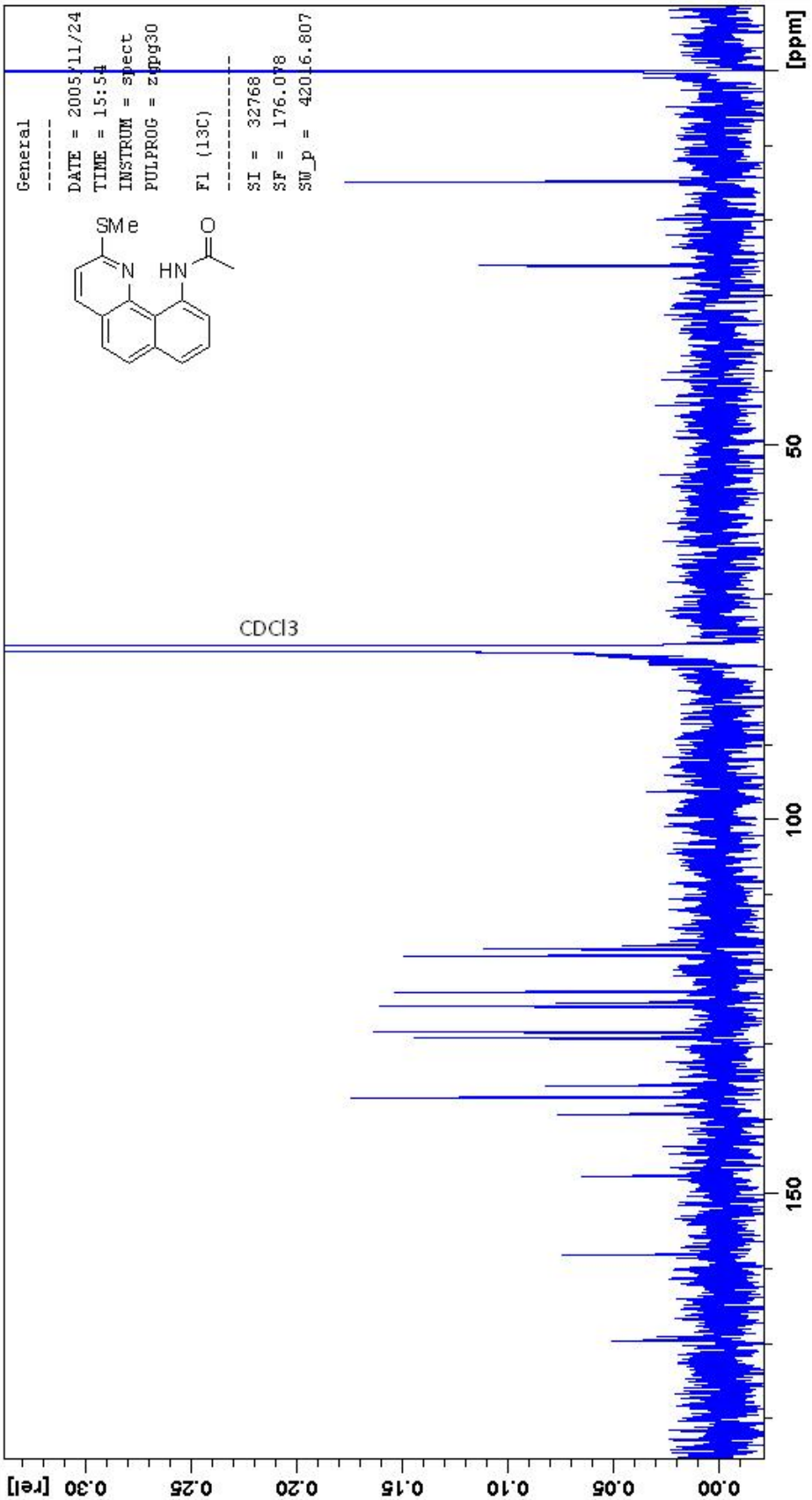
General
DATE = 2005/11/24
TIME = 15:54
INSTRUM = spect
PULPROG = zgpg30
F1 (13C)
SI = 32768
SF = 176.078
SW_p = 4201.6.807
SMe
N
HN
O
CDCl3
[ppm]
[rel]

A.4 Chapter 3 Experimental

A.4.1 9-(4-tert-Butylphenoxy)quinolino[7,8-h]quinolin-4(1H)-one (L4)

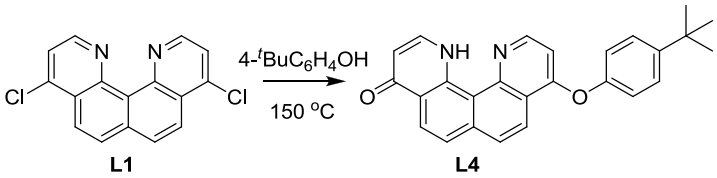

p-tert-Butylphenol (7.72 g, 51.2 mmol), potassium hydroxide (0.460 g, 9.35 mmol), and 4,9-dichloroquino[7,8-*h*]quinoline (**L1**) (0.200 g, 0.668 mmol) was stirred at 150 °C for 4 hr. The reaction was diluted with CH_2Cl_2 (200 mL) and washed with 2M HCl (10 mL) in water (200 mL) then basified with 6M KOH (10 mL). The organic layer was filtered and dried over $MgSO_4$. The product was purified by silica gel column chromatography using 95:5 CH_2Cl_2 / MeOH to give **L4** (0.258 g, 98 %). ^{1}H NMR (500 MHz, $CDCl_3$) δ 1.42 (s, 9H; C*H*$_3$), 6.84 (d, *J* = 6.2, 1H; 7-*H*), 6.87 (d, *J* = 5.4, 1H; 3-*H*), 7.21 (d, *J* = 8.6, 2H; Ar*H*), 7.56 (d, *J* = 8.6, 2H; Ar*H*), 7.78 (d, *J* = 8.7, 1H; 10-*H*), 7.93 (d, *J* = 6.2, 1H; 6-*H*), 8.09 (d, *J* = 6.2, 1H; 8-*H*), 8.50 (d, *J* = 6.2, 1H; 5-*H*), 8.62 (d, *J* = 8.7, 1H; 11-*H*), 8.80 (d, *J* = 5.4, 1H; 2-*H*); 16.30 (s, 1H; N*H*), ^{13}C NMR (125 MHz, $CDCl_3$) δ 31.5 (t), 34.6 (q), 105.4 (s), 111.1 (s), 115.0 (q), 116.7 (q), 119.5 (q), 120.6 (s), 122 (s), 124.1 (s), 125.6 (s), 126.1 (q), 127.4 (s), 127.7 (s), 137.0 (q), 138.4 (s), 140.4 (q), 148.5 (q), 148.7 (s), 149.3 (q), 151.4 (q), 162.8 (q). $C_{26}H_{22}N_2O_2$ (M^+) 395.55. $C_{26}H_{22}N_2O_2$ (394.47): calcd. C 79.16, H 5.62, N 7.10; found C 79.68, H 5.99, N 6.36. M.P. = 322 – 324 °C. The product was recrystallised by vapour diffusion of diethyl ether into a MeCN solution containing **L4** with an equimolar quantity of copper perchlorate. $C_{26}H_{22}N_2O_2$•$HClO_4$ (544.94): calcd. C 63.10, H 4.68, N 5.66; found C 63.00, H 4.60, N 5.70.

Crystal data for [H(**L4**)$_2$][ClO_4]. $C_{52}H_{45}N_4ClO_4$, colourless needle, dimensions 0.5 x 0.1 x 0.05 mm, monoclinic, space group $P2_1/c$, a = 16.964(3), b = 10.938(2), c = 24.162(5) Å, α = 90.00°, β = 101.65(3)°, γ = 90.00°, U = 4391.2(15) Å^3, μ = 1.282 mm^{-1}, Z = 4, D_c = 1.345 g cm^{-3}, F(000) = 1864, T = 100(2) K. 17488 Reflections were collected using a Rigaku

MM007 rotating anode in the range $6.65 < 2\theta < 144.18^{o}$. A semi-empirical absorption correction (ABSCOR; Higashi, 1995) was applied. The 10421 independent reflections were used to solve the structure by direct methods (SHELXS97) which resulted in the location of all non-hydrogen atoms. All non-hydrogen atoms were made anisotropic and the refinement (SHELXL97) of 587 parameters converged to R_1 = 0.0643 [for 8316 reflections having $I > 4\sigma(I)$], wR_2 = 0.1569 and goodness of fit 1.050 (for all 8316 F^2 data). Peak / hole 0.403 / -0.426 e $Å^{-3}$.

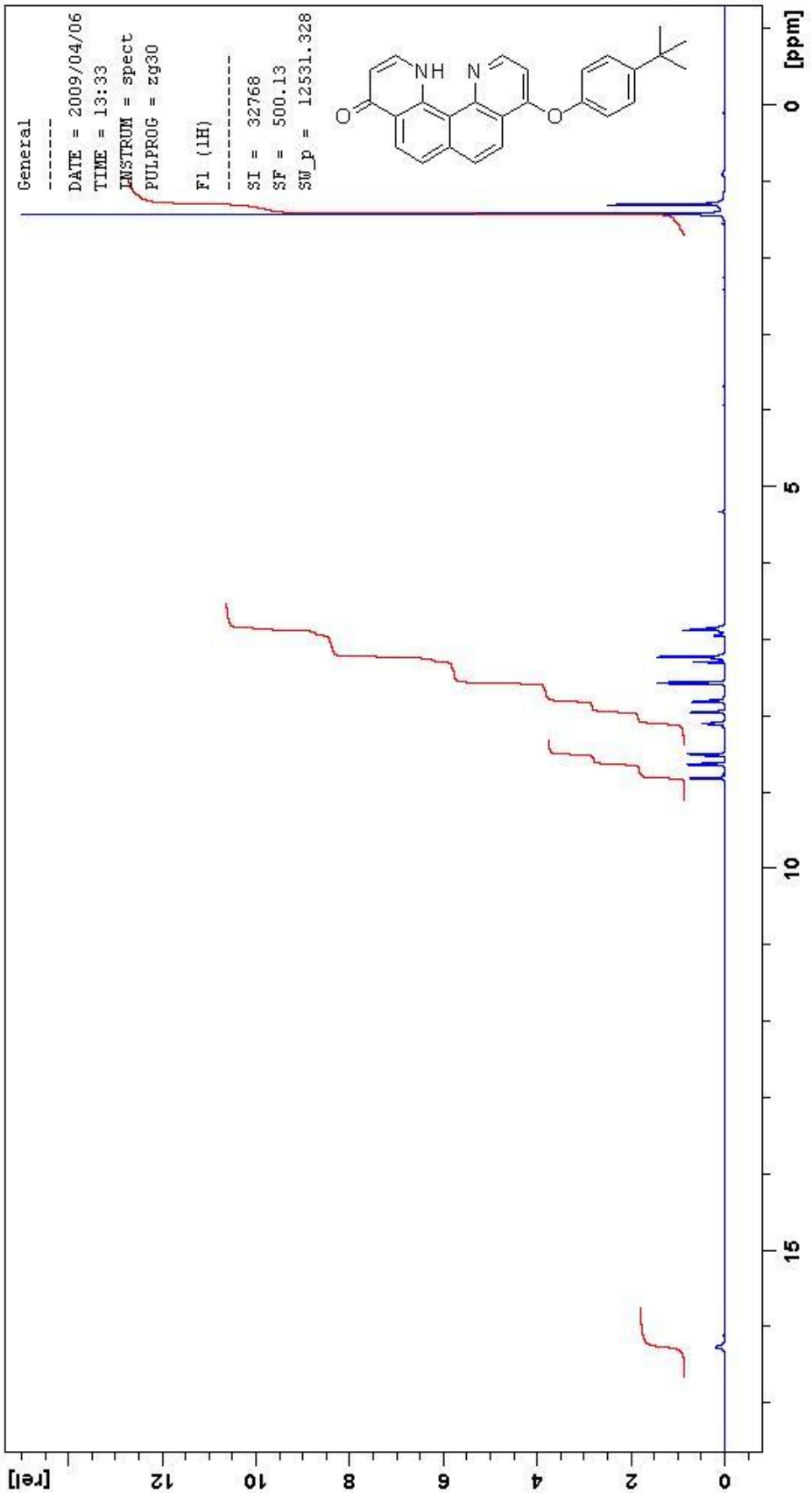
General
DATE = 2009/04/06
TIME = 13:33
INSTRUM = spect
PULPROG = zg30
F1 (1H)
SI = 32768
SF = 500.13
SW_p = 12531.328
NH
N
O
O
[rel]
[ppm]

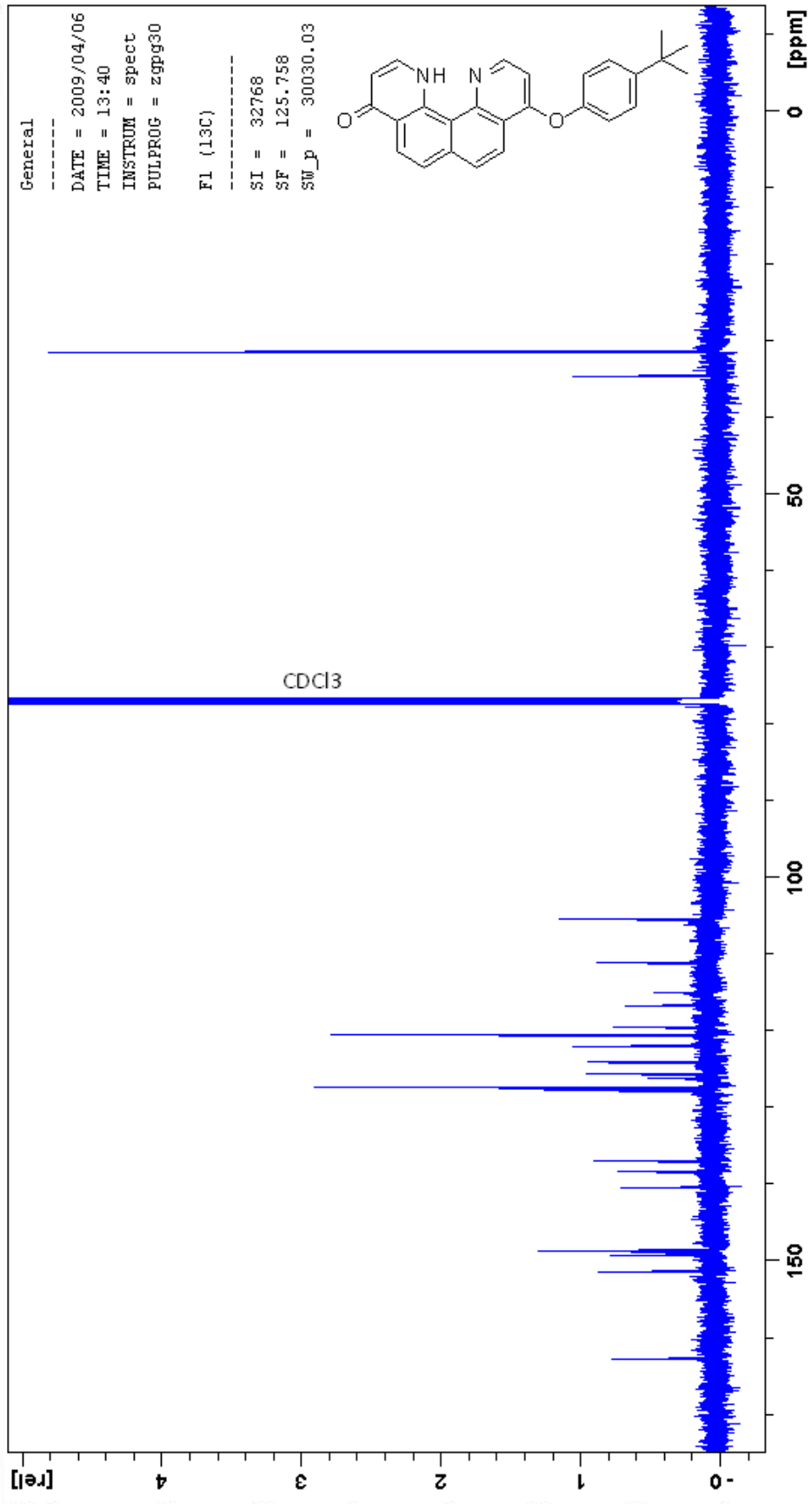
General
DATE = 2009/04/06
TIME = 13:40
INSTRUM = spect
PULPROG = zgpg30
F1 (13C)
SI = 32768
SF = 125.758
SW_p = 30030.03
NH
N
O
O
CDCl3
[rel]
[ppm]

A.4.2 4-(4-tert-Butylphenoxy)-9-chloroquinolino[7,8-h]quinoline (L5)

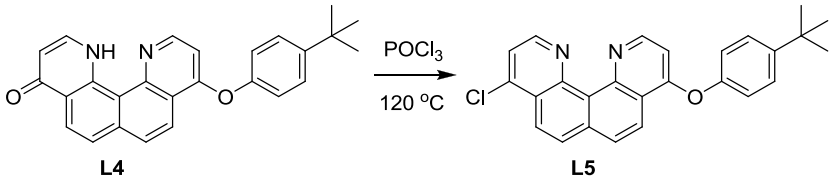

Phosphorus oxychloride (1.00 mL, 10.7 mmol) was added to 9-(4-*tert*-butylphenoxy)quinolino[7,8-*h*]quinolin-4(1*H*)-one (**L4**) (0.258 g, 0.655 mmol) and the reaction was stirred at 120 ^{o}C for 9 minutes under Ar. The reaction mixture was poured onto water (200 mL) and basified with 6M KOH (20 mL) and extracted with CH_2Cl_2 (200 mL). A small portion of decolourising carbon was added and the organic layer was filtered and dried over $MgSO_4$ to give **L5** (0.264 g, 98 %). ^{1}H NMR (500 MHz, $CDCl_3$) δ 1.42 (s, 9H; C*H*$_3$), 7.25 (d, *J* = 8.7, 2H; Ar*H*), 7.30 (d, *J* = 6.5, 1H; 10-*H*), 7.64 (d, *J* = 8.7, 2H; Ar*H*), 8.00 (d, *J* = 4.9, 1H; 3-*H*), 8.32 (d, *J* = 9.0, 1H; 7-*H*), 8.40 (d, *J* = 8.9, 1H; 6-*H*), 8.70 (d, *J* = 8.9, 1H; 5-*H*), 8.83 (d, *J* = 9.0, 1H; 8-*H*), 9.44 (d, *J* = 4.9, 1H; 2-*H*), 9.61 (d, *J* = 6.5, 1H; 11-*H*); ^{13}C NMR (125 MHz, $CDCl_3$) δ 31.1 (t), 34.6 (q), 105.7 (s), 116.6 (q), 120.0 (s), 120.1 (q), 122.6 (s), 123.6 (s), 126.0 (q), 126.7 (q), 127.1 (s), 127.9 (s), 128.8 (s), 129.8 (s), 137.6 (q), 140.0 (q), 145.0 (q), 146.5 (s), 146.6 (q), 149.8 (q), 150.0 (s), 151.1 (q). HRMS calculated for $C_{26}H_{21}N_2OCl$ (MH^+) 413.1415, found 413.1415 (ESI+). M.P. = 233 – 235 ^{o}C.

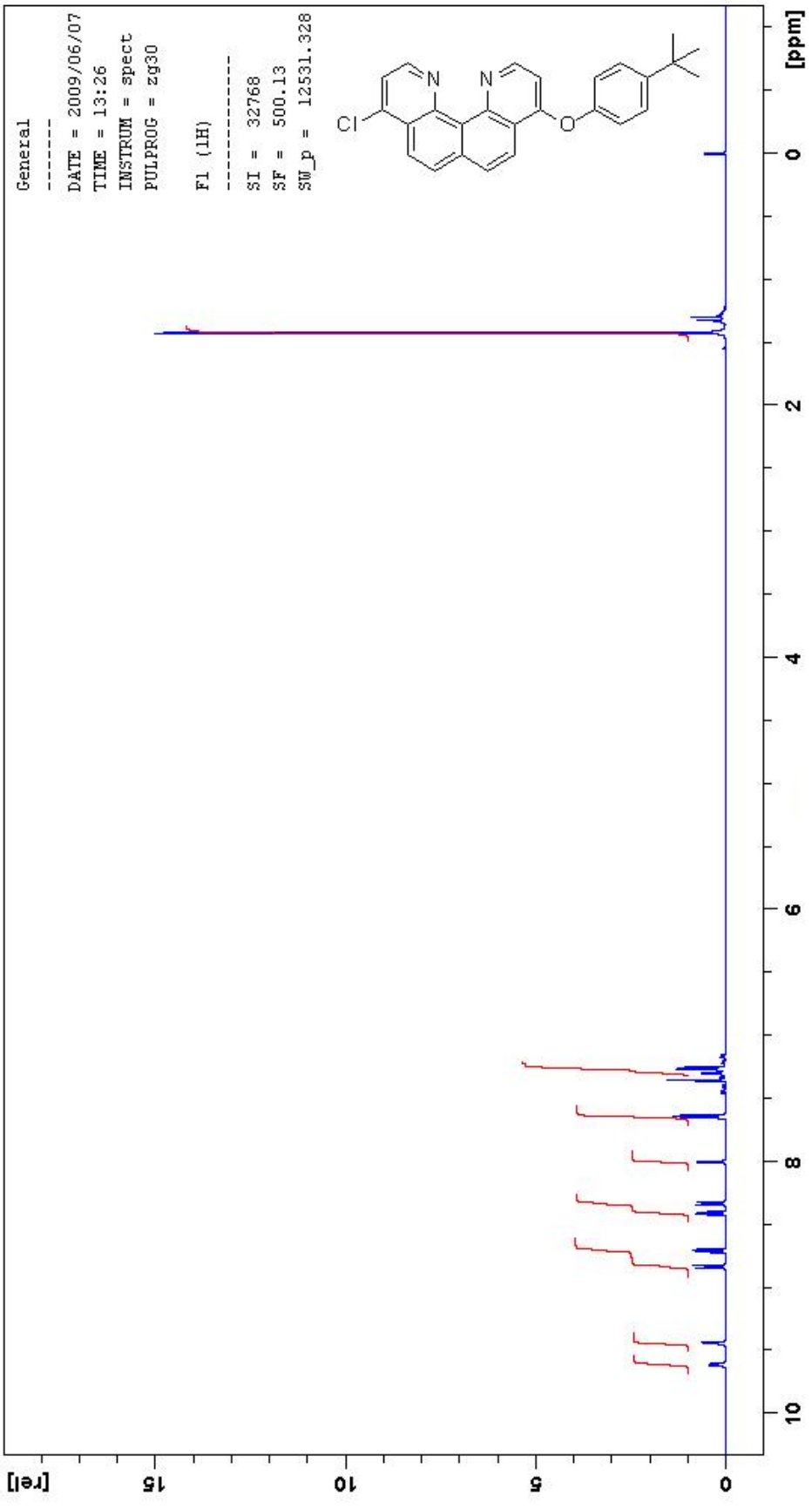
General
DATE = 2009/06/07
TIME = 13:26
INSTRUM = spect
PULPROG = zg30
F1 (1H)
SI = 32768
SF = 500.13
SW_p = 12531.328
Cl
N
N
O
[rel]
15
10
5
0
[ppm]
10
8
6
4
2
0

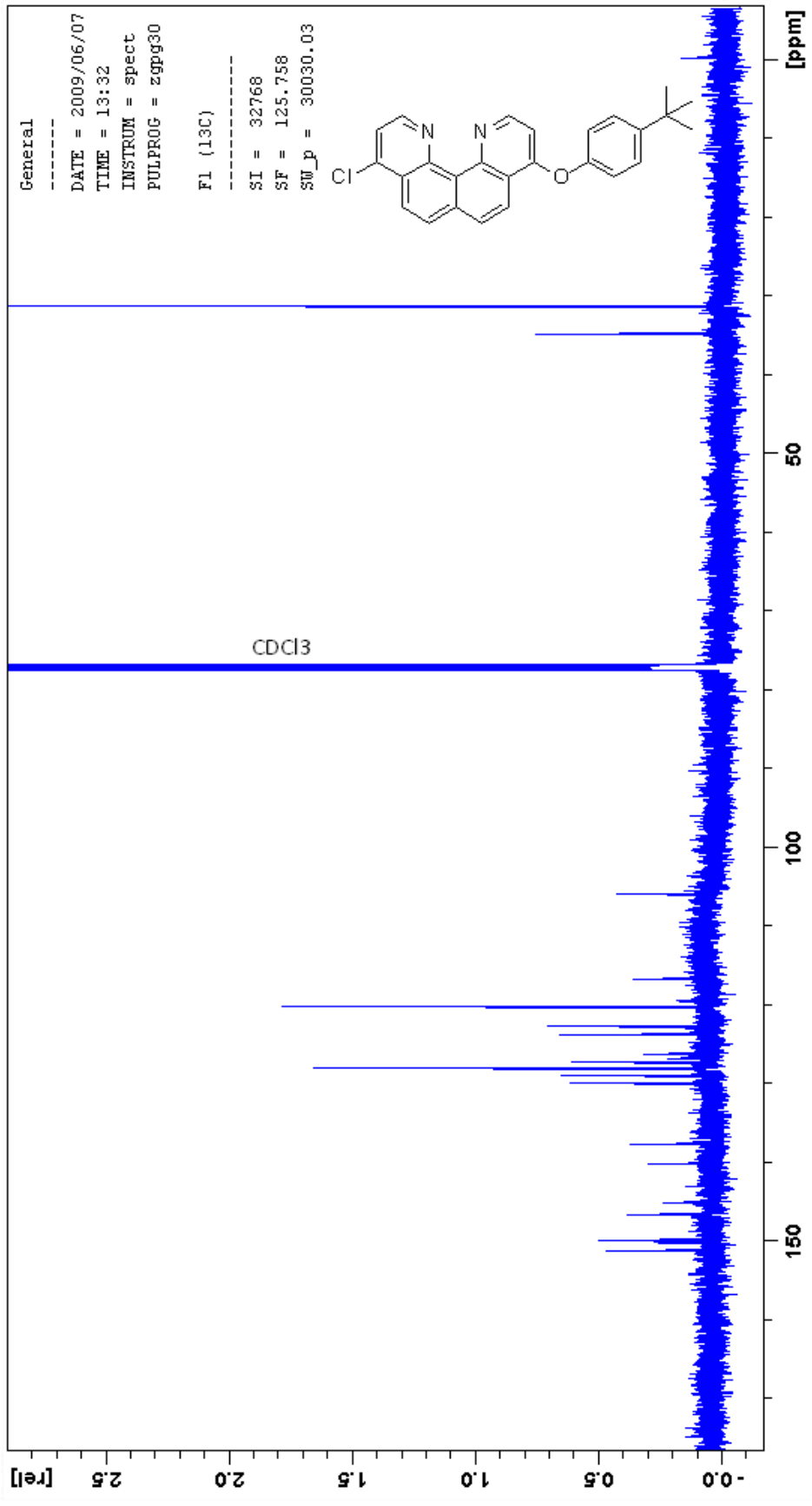
General
DATE = 2009/06/07
TIME = 13:32
INSTRUM = spect
PULPROG = zgpg30
F1 (13C)
SI = 32768
SF = 125.758
SW_p = 30030.03
Cl
N
N
O
CDCl3
[rel]
[ppm]
-0.0
0.5
1.0
1.5
2.0
2.5
50
100
150

A.4.3 (E)-N-(9-Chloroquinolino[7,8-h]quinolin-4(1H)-ylidene)-4-methylaniline (L6)

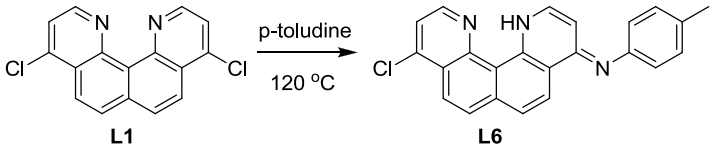

L1 **L6**

p-Toludine (0.143 g, 1.338 mmol) and 4,9-dichloroquino[7,8-*h*]quinoline (**L1**) (0.100 g, 0.334 mmol) was refluxed for 4 hr in toluene (20 mL). The precipitate of crude **L6** was filtered and dissolved in CH_2Cl_2 (200 mL) and MeOH (20 mL) and washed with water (200 mL) and 6M KOH (20 mL). The organic layer was filtered and dried over $MgSO_4$. **L6** was precipitated from hot DMSO by addition of EtOAc and filtered (0.099 g, 80 %). ^{1}H NMR (500 MHz, $CDCl_3$, MeOD) δ 2.37 (s, 3H; C*H*$_3$), 6.97 (d, *J* = 7.0, 1H; 3-*H*), 7.28 (m, 4H; Ar*H*), 7.84 (d, *J* = 5.0, 1H; 10-*H*), 8.09 (d, *J* = 9.0, 1H; 6-*H*), 8.12 (d, *J* = 9.0, 1H; 7-*H*), 8.40 (d, *J* = 9.0, 1H; 8-*H*), 8.57 (d, *J* = 7.0, 1H; 2-*H*), 8.68 (d, *J* = 9.0, 1H; 5-*H*), 9.03 (d, *J* = 5.0, 1H; 11-*H*), (in DMSO-d6) 14.62 (s, 1H; N*H*); ^{13}C NMR (125 MHz, $CDCl_3$, MeOD) δ 20.0 (t), 101.3 (s), 115.7 (q), 115.9 (q), 122.3 (s), 122.6 (s), 124.7 (s), 125.3 (s), 125.4 (s), 127.3 (q), 128.6 (s), 130.1 (s), 133.6 (q), 136.7 (q), 137.7 (q), 138.3 (q), 140.6 (s), 144.1 (q), 146.5 (q), 148.1 (s), 155.2 (q). The $C_{23}H_{16}N_3Cl$ (MH^+) 370.72. Elemental analysis was measured for the tetrafluoroborate salt. $C_{23}H_{17}ClN_3 \bullet BF_4 \bullet 0.75H_2O$ (471.17): calcd. C 58.63, H 3.96, N 8.92; found C 58.59, H 3.68, N 8.82.

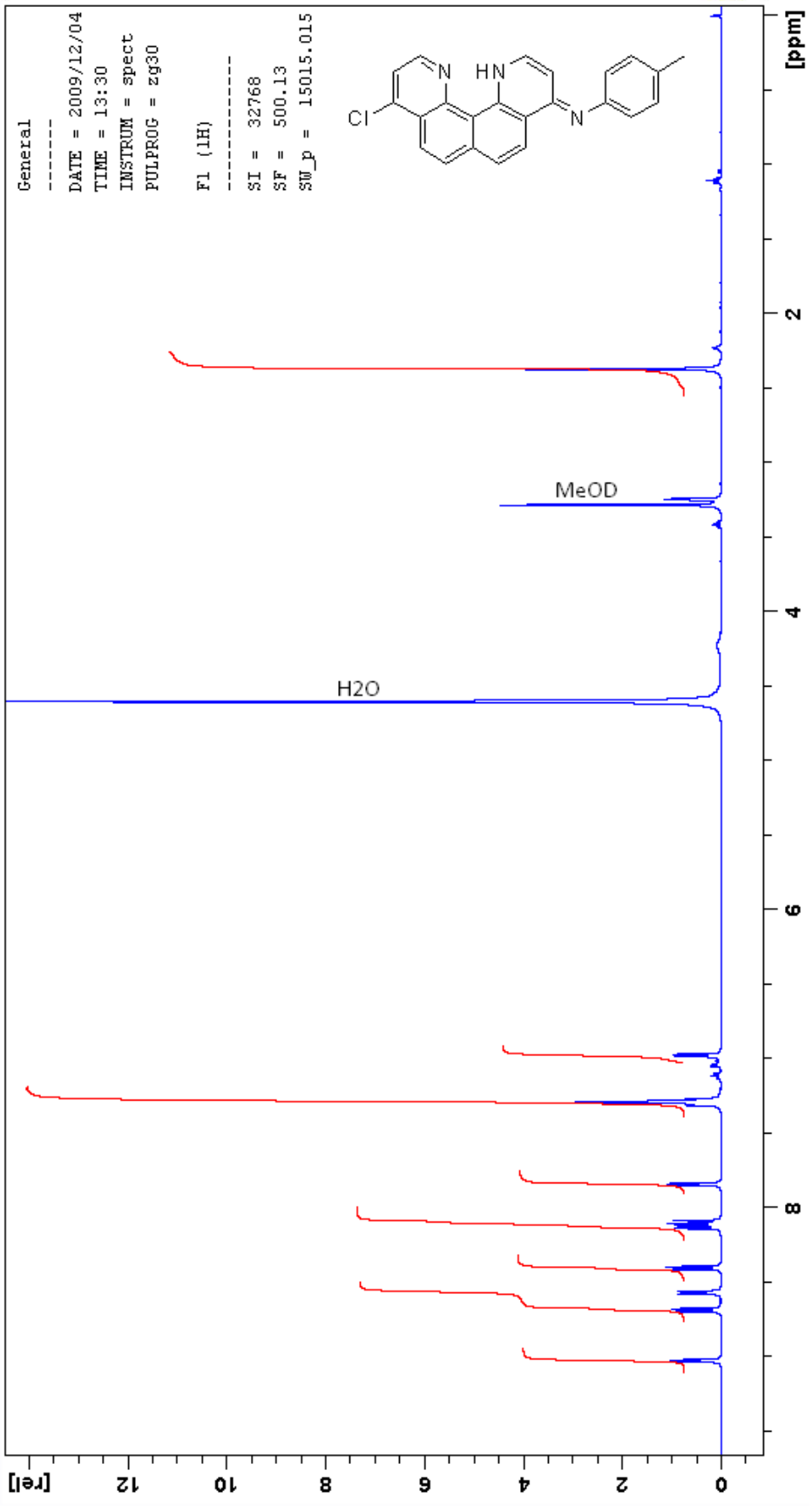
General
DATE = 2009/12/04
TIME = 13:30
INSTRUM = spect
PULPROG = zg30
F1 (1H)
SI = 32768
SF = 500.13
SW_p = 15015.015
Cl
N
HN
N
MeOD
H2O
[rel]
[ppm]
0
2
4
6
8
10
12

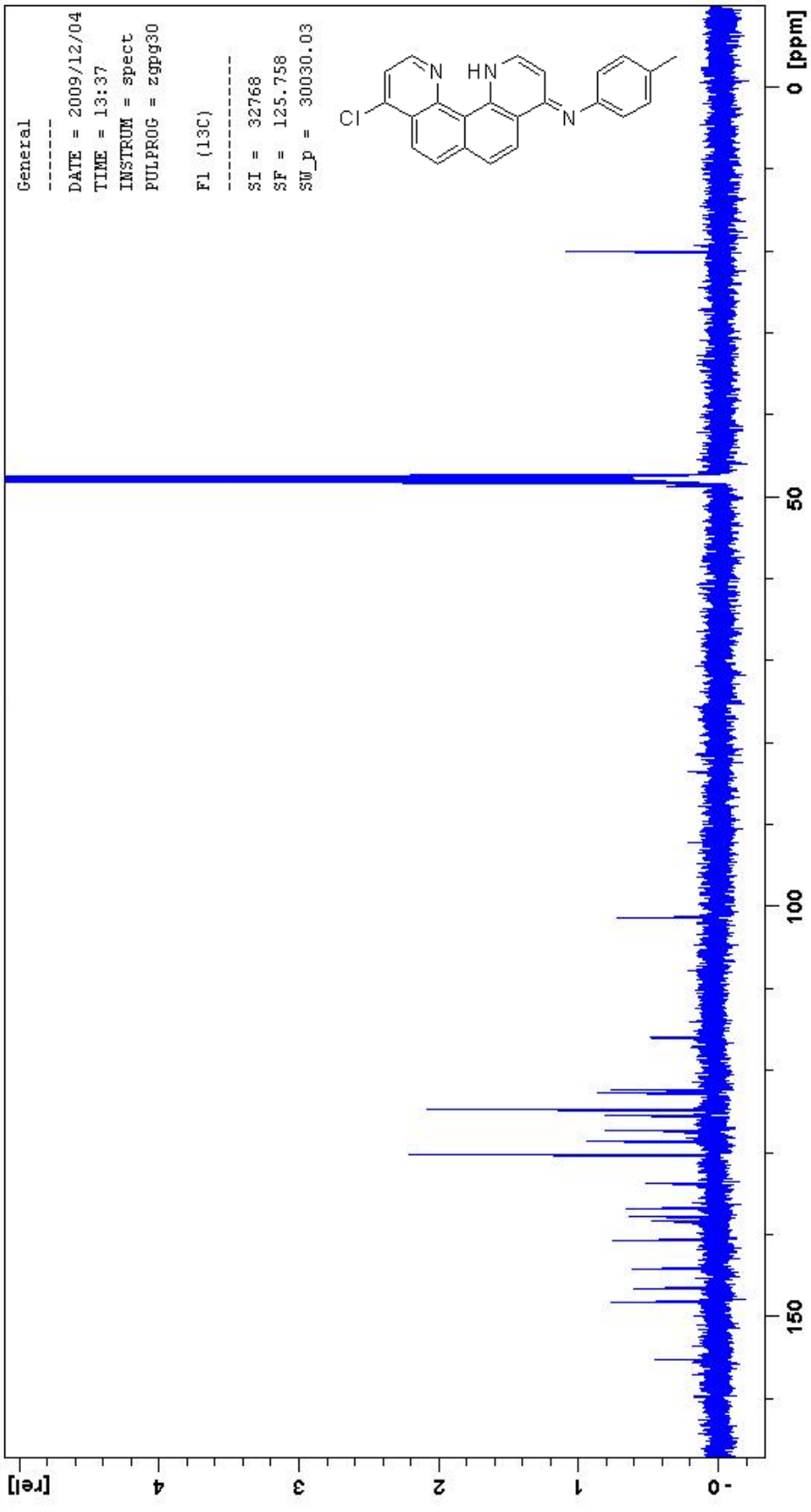
General
DATE = 2009/12/04
TIME = 13:37
INSTRUM = spect
PULPROG = zgpg30
F1 (13C)
SI = 32768
SF = 125.758
SW_p = 30030.03
Cl
N
HN
N
[rel]
0
1
2
3
4
150
100
50
0 [ppm]

A.4.4 (E)-N-p-tolyl-9-(p-tolylimino)-9,12-dihydroquinolino[7,8-h]quinolin-4-amine (L7)

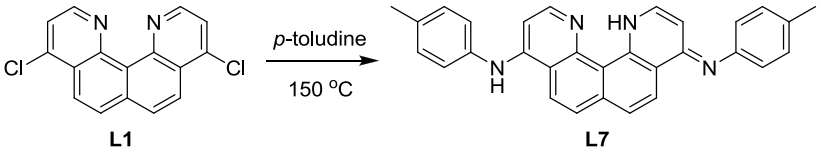

L1 **L7**

p-Toludine (2.75 g, 25.6 mmol) and 4,9-dichloroquino[7,8-*h*]quinoline (**L1**) (0.100 g, 0.334 mmol) was stirred at 150 ^{o}C for 4 hr. The reaction was diluted with CH_2Cl_2 (200 mL) and washed with water (200 mL) and 6M KOH (20 mL). The organic layer was filtered and dried over $MgSO_4$. The product was purified by silica gel column chromatography using 90:10 CH_2Cl_2 / MeOH then 50:50 CH_2Cl_2 / MeOH and finally 47:47:6 CH_2Cl_2 / MeOH / NEt_3 to give **L7** (0.136 g, 92 %). The product was recrystallised by cooling to 4 ^{o}C in CH_2Cl_2 / MeOH overnight. ^{1}H NMR (500 MHz, $CDCl_3$, DMSO-d6) δ 2.33 (s, 6H; C*H*$_3$), 6.66 (d, *J* = 6.4, 2H; 6,7-*H*), 7.12 (d, *J* = 7.9, 4H; Ar*H*), 7.23 (d, *J* = 7.9, 4H; Ar*H*), 7.95 (d, *J* = 8.8, 2H; 3,10-*H*), 8.25 (d, *J* = 6.4, 2H; 5,8-*H*), 8.61 (d, *J* = 8.8, 2H; 2,11-*H*), 16.41 (s, 1H; N*H*); ^{13}C NMR (125 MHz, $CDCl_3$, DMSO-d6) δ 20.6 (t), 101.8 (s), 116.2 (q), 118.3 (q), 123.1 (s), 123.2 (q), 124.7 (s), 130.0 (s), 133.0 (s), 135.8 (q), 141.4 (q), 142.6 (q), 143.4 (q), 152.2 (s). HRMS calculated for $C_{30}H_{24}N_4$ (MH^+) 441.2074, found 441.2068 (ESI+). M.P. = 302 – 304 ^{o}C.

Crystal data for **L7**.MeOH. $C_{31}H_{28}N_4O$, yellow chip, dimensions 0.4 x 0.15 x 0.15 mm, orthorhombic, space group $P2_12_12_1$, a = 7.8131(16), b = 14.208(3), c = 22.211(4) Å, α = 90.00^{o}, β = 90.00^{o}, γ = 90.00^{o}, U = 2465.6(9) Å^3, μ = 0.617 mm^{-1}, Z = 4, D_c = 1.273 g cm^{-3}, F(000) = 1000, T = 100(2) K. 9733 Reflections were collected using a Rigaku MM007 rotating anode in the range 6.54 < 2θ < 143.80^{o}. A semi-empirical absorption correction (ABSCOR; Higashi, 1995) was applied. The 4104 independent reflections were used to solve the structure by direct methods (SHELXS97) which resulted in the location of all non-hydrogen atoms. All non-hydrogen atoms were made anisotropic and the refinement (SHELXL97) of 329 parameters converged to R_1 = 0.0392 [for 3788 reflections having I > 4σ (I)], wR_2 = 0.1030 and goodness of fit 1.066 (for all 3788 F^2 data). Peak / hole 0.178 / -0.271 e Å^{-3}.

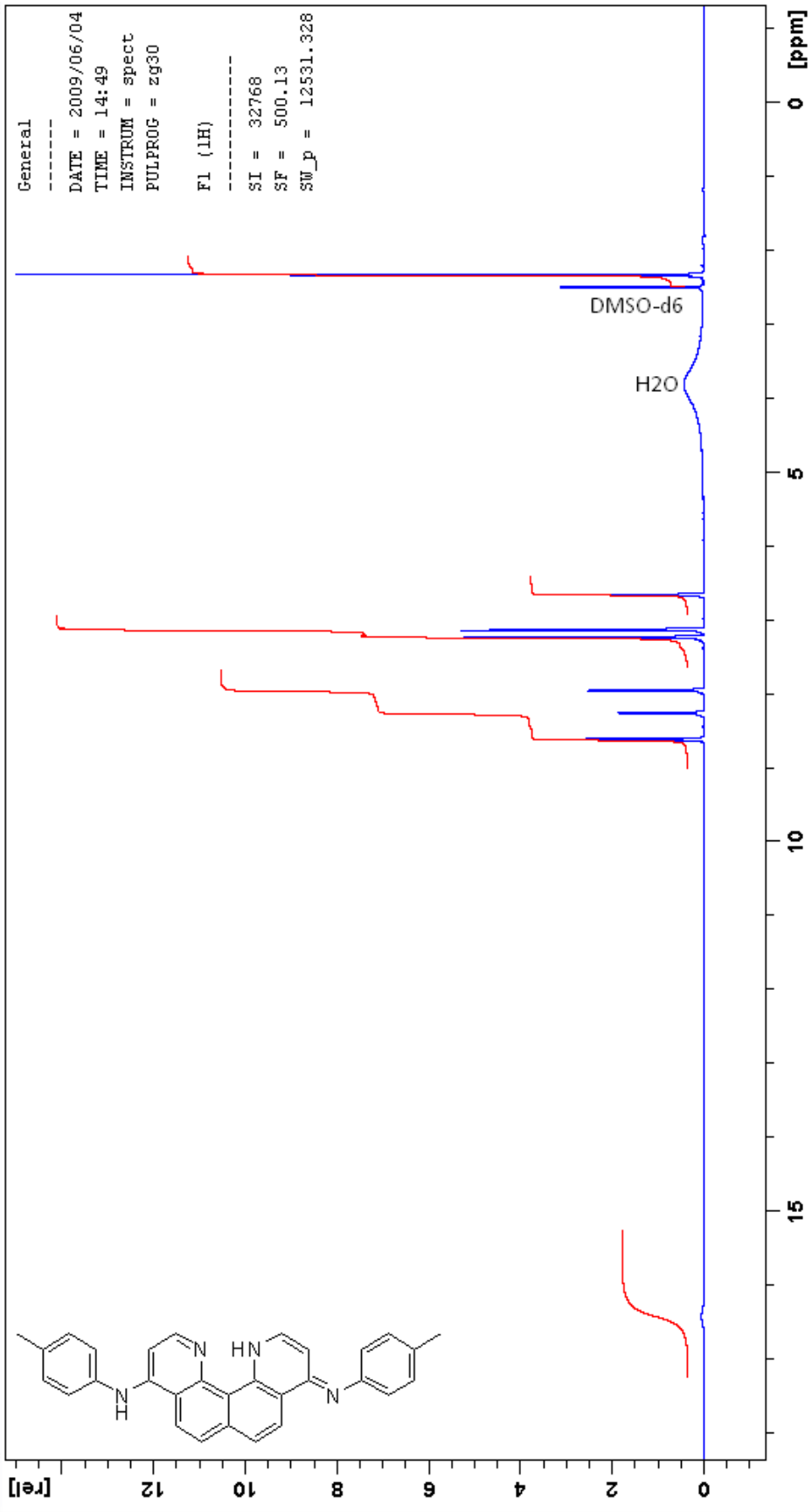
General
DATE = 2009/06/04
TIME = 14:49
INSTRUM = spect
PULPROG = zg30
F1 (1H)
SI = 32768
SF = 500.13
SW_p = 12531.328
DMSO-d6
H2O
[rel]
[ppm]
HN
N
N
H

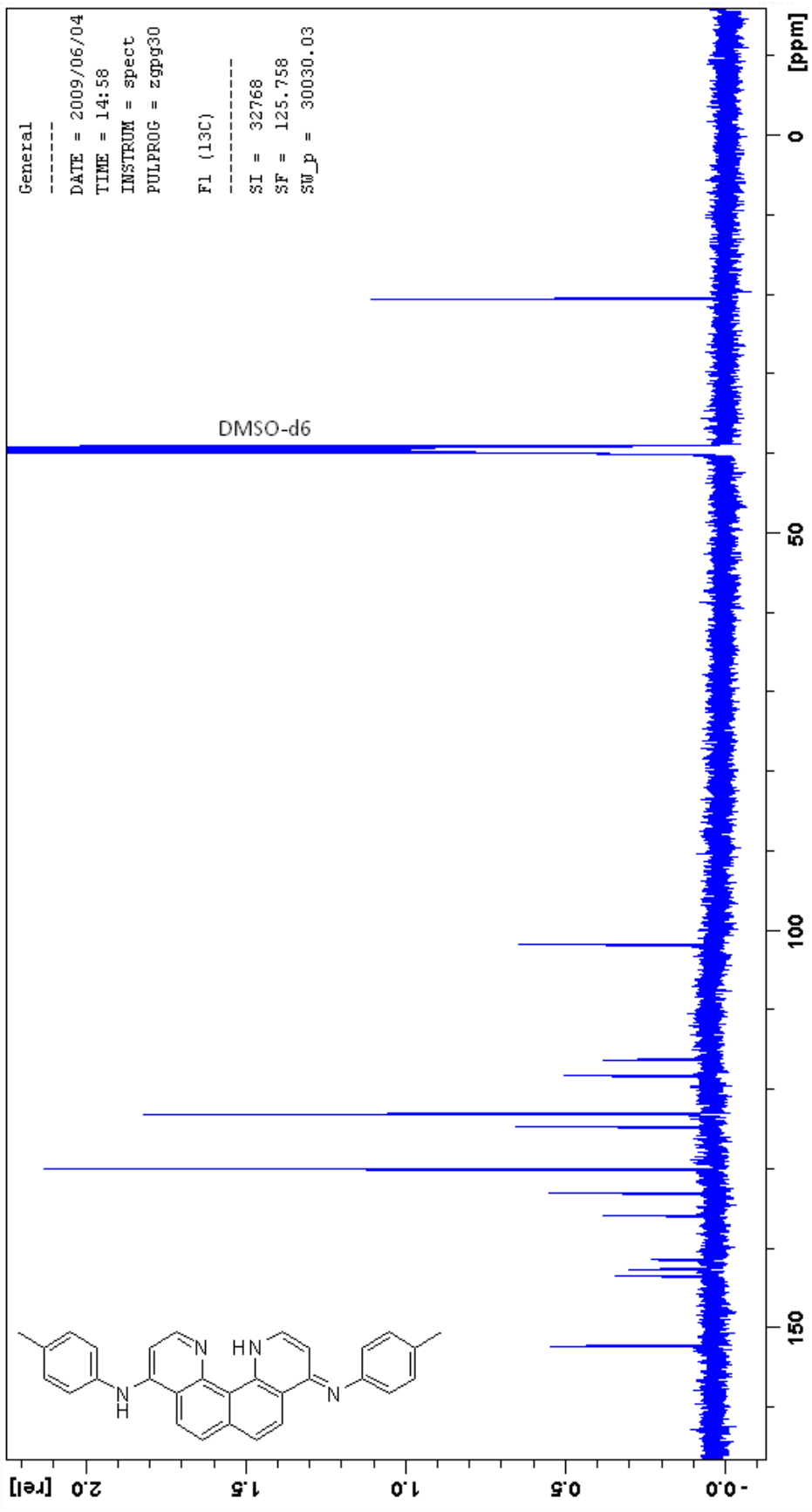
General
DATE = 2009/06/04
TIME = 14:58
INSTRUM = spect
PULPROG = zgpg30
F1 (13C)
SI = 32768
SF = 125.758
SW_p = 30030.03
DMSO-d6
[ppm]
[rel]
HN
N
N
H

A.4.5 [H(L7)]BF_4

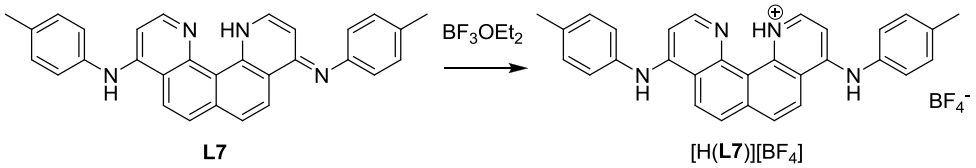

L7 [H(**L7**)][BF_4]

Boron trifluoride diethyl etherate (0.484 mL, 3.856 mmol) was added to (*E*)-N-p-tolyl-9-(p-tolylimino)-9,12-dihydroquinolino[7,8-h]quinolin-4-amine (**L7**) (0.100 g, 0.227 mmol) in dry CH_2Cl_2 (5 mL) under Ar and stirred at RT for 10 min. The reaction was diluted with diethyl ether and the solvent was separated from deposited [H(**L7**)][BF_4] and dried under vacuum. The product was then set up for crystallisation by vapour diffusion of diethyl ether into a MeOH solution containing [H(**L7**)][BF_4]. Yellow crystals suitable for X-ray crystallography were obtained after one day. ^{1}H NMR (500 MHz, DMSO-d6) δ 2.40 (s, 6H; C*H*$_3$), 7.06 (d, *J* = 6.3, 2H; 6,7-*H*), 7.38 (m, 8H; Ar*H*), 8.26 (d, *J* = 9.1, 2H; 3,10-*H*), 8.72 (d, *J* = 6.3, 2H; 5,8-*H*), 8.78 (d, *J* = 9.1, 2H; 2,11-*H*), 10.11 (s, 2H; N*H*), 18.79 (s, 1H; N*H*); ^{13}C NMR (125 MHz, DMSO-d6) δ 21.1 (t), 102.8 (s), 116.5 (q), 116.7 (q), 123.6 (s), 125.3 (s), 126.6 (s), 130.8 (s), 136.1 (q), 136.3 (q), 136.8 (q), 143.6 (q), 145.7 (s), 153.0 (q). HRMS calculated for $C_{30}H_{24}N_4$ (MH^+) 441.2074, found 441.2068 (ESI+).

Crystal data for [H(**L7**)][BF_4]. $C_{30}H_{25}N_4BF_4$, yellow rod, dimensions 0.8 x 0.3 x 0.05 mm, monoclinic, space group $P2_1/c$, a = 16.076(3), b = 17.296(4), c = 9.1906(18) Å, α = 90.00°, β = 97.00(3)°, γ = 90.00°, U = 2536.3(9) Å^3, μ = 0.858 mm^{-1}, Z = 4, D_c = 1.384 g cm^{-3}, F(000) = 1096, T = 123(2) K. 8257 Reflections were collected using a Rigaku MM007 rotating anode in the range 6.52 < 2θ < 143.40°. A semi-empirical absorption correction (ABSCOR; Higashi, 1995) was applied. The 4242 independent reflections were used to solve the structure by direct methods (SHELXS97) which resulted in the location of all non-hydrogen atoms. All non-hydrogen atoms were made anisotropic and the refinement (SHELXL97) of 355 parameters converged to R_1 = 0.0660 [for 2736 reflections having I > 4σ (I)], wR_2 = 0.1710 and goodness of fit 1.085 (for all 2736 F^2 data). Peak / hole 0.425 / -0.371 e Å^{-3}.

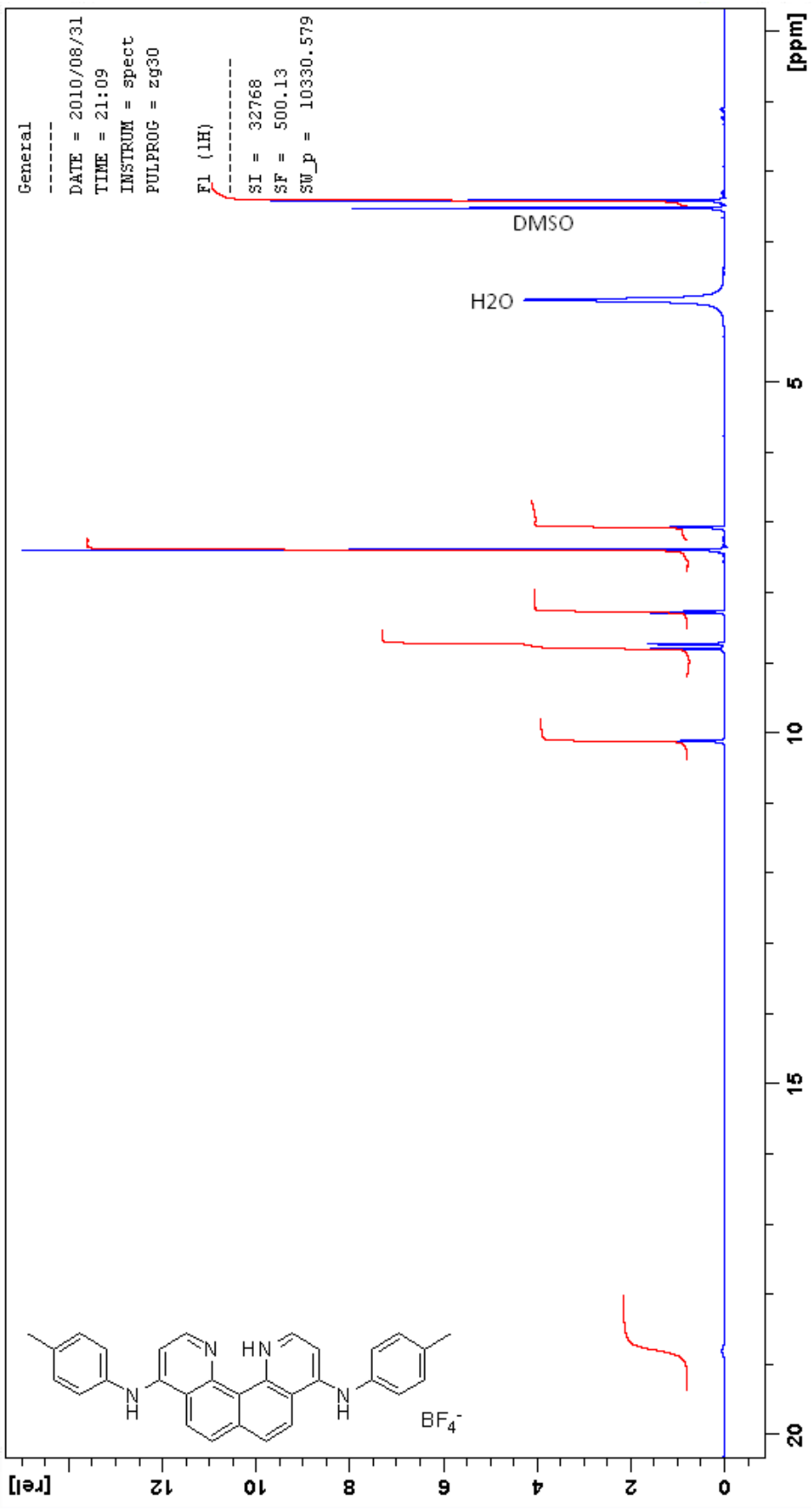
General
DATE = 2010/08/31
TIME = 21:09
INSTRUM = spect
PULPROG = zg30
F1 (1H)
SI = 32768
SF = 500.13
SW_p = 10330.579
DMSO
H2O
HN
N
H
N
H
BF4-
[ppm]
[rel]

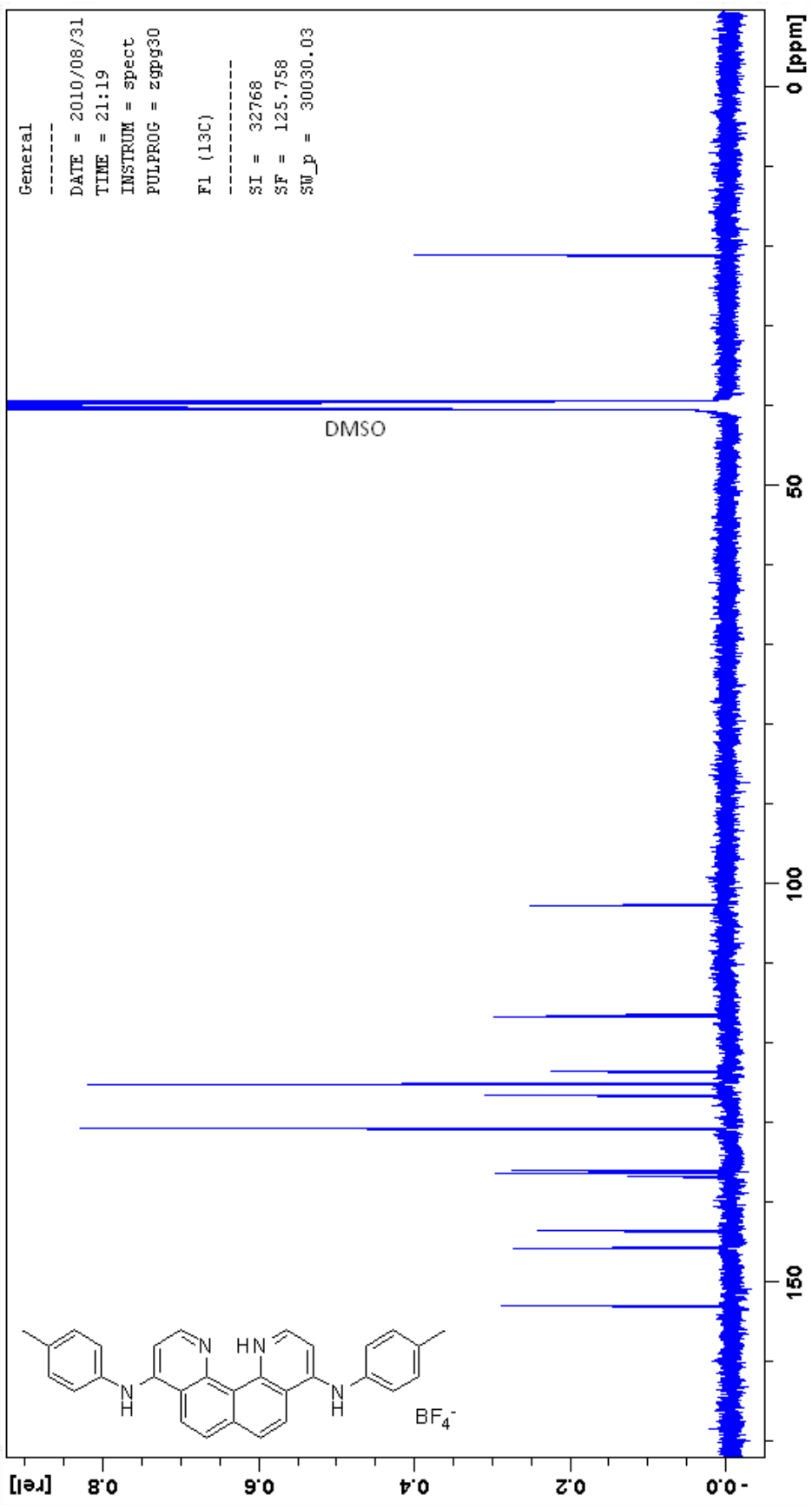
General
DATE = 2010/08/31
TIME = 21:19
INSTRUM = spect
PULPROG = zgpg30
F1 (13C)
SI = 32768
SF = 125.758
SW_p = 30030.03
DMSO
HN
N
H
N
H
BF4-
[rel]
0.8
0.6
0.4
0.2
0.0
150
100
50
0 [ppm]

A.4.6 (E)-Methyl 2-(9-(o-tolylamino)quinolino[7,8-h]quinolin-4(1H)-ylideneamino)benzoate (L8)

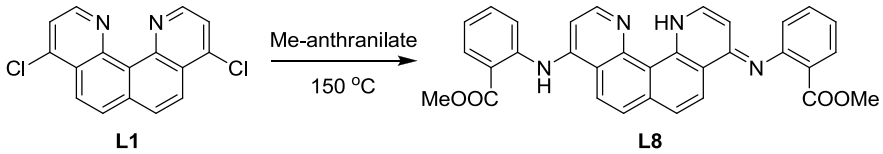

L1 **L8**

Methyl anthranilate (6.65 mL, 51.4 mmol) and 4,9-dichloroquino[7,8-*h*]quinoline (**L1**) (0.200 g, 0.668 mmol) was stirred at 120 °C for 2 hr. The reaction was diluted with CH_2Cl_2 (200 mL) and washed with water (200 mL) and 6M KOH (20 mL). The organic layer was filtered and dried over $MgSO_4$. The product was purified by silica gel column chromatography using 90:10 CH_2Cl_2 / MeOH then 50:50 CH_2Cl_2 / MeOH and finally 47:47:6 CH_2Cl_2 / MeOH / NEt_3 to give **L8** (0.093 g, 26 %). ^{1}H NMR (500 MHz, $CDCl_3$, MeOD) δ 3.97 (s, 6H; C*H*$_3$), 7.17 (m, 2H; Ar*H*), 7.57 (m, 4H; Ar*H*), 7.68 (d, *J* = 8.0, 2H; 3,10-*H*), 7.99 (d, *J* = 8.8, 2H; 6,7-*H*), 8.04 (d, *J* = 7.9, 2H; Ar*H*), 8.28 (d, *J* = 8.8, 2H; 5,8-*H*) 8.89 (m, 2H; 2,11-*H*), (in DMSO-d6) 15.69 (s, 1H; N*H*); ^{13}C NMR (125 MHz, $CDCl_3$, MeOD) δ 52.5 (t), 104.4 (s), 116.2 (q), 118.1 (q), 118.2 (q), 119.5 (s), 121.8 (s), 123.5 (s), 127.3 (s), 131.9 (s), 134.3 (s), 136.1 (q), 141.4 (q), 143.1 (q), 145.5 (s), 149.3 (q), 168.5 (q). HRMS calculated for $C_{32}H_{24}N_4O_8$ (MH^+) 529.1870, found 529.1866 (ESI+). M.P. = 230 – 232 °C.

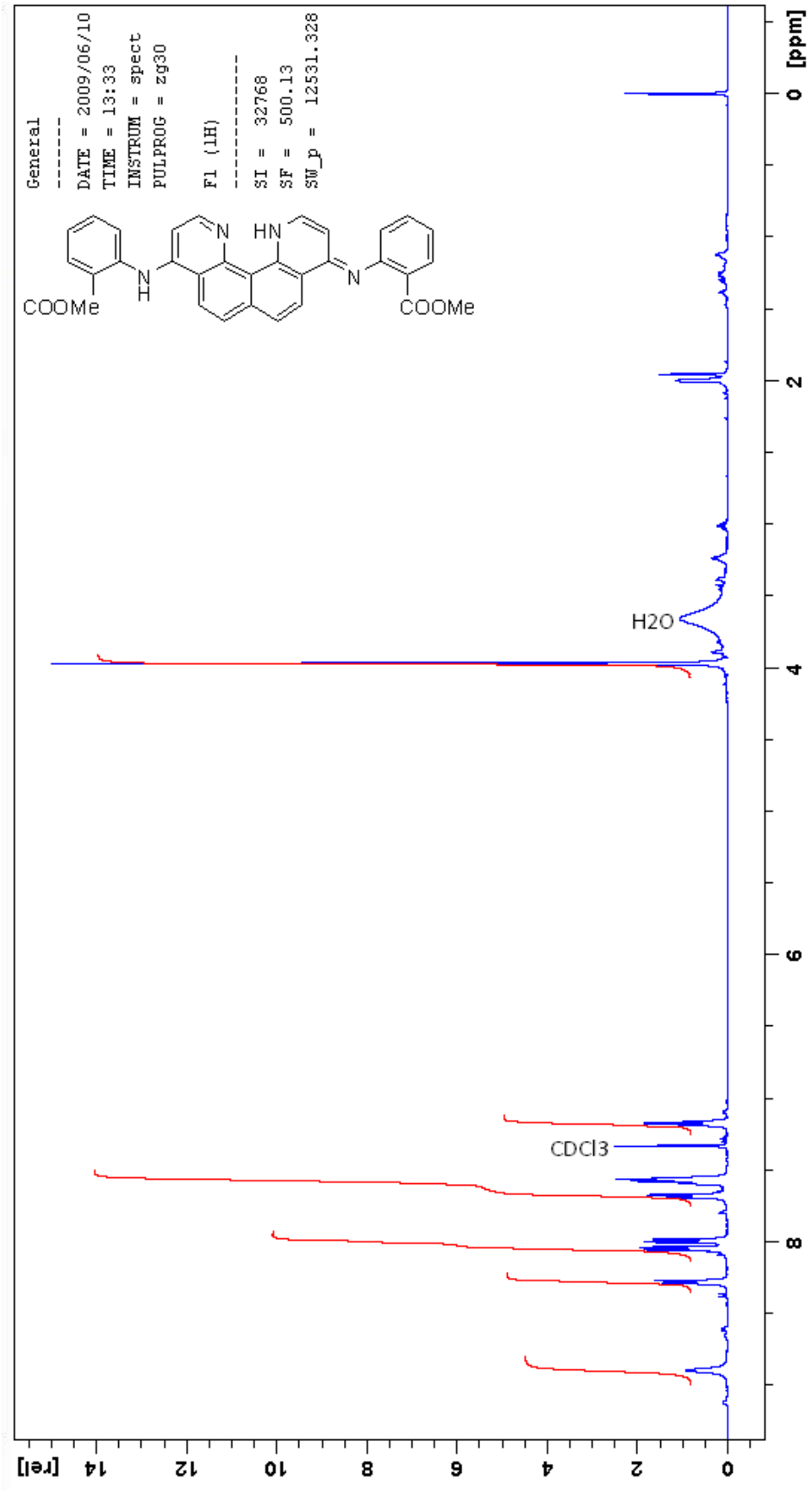
General
DATE = 2009/06/10
TIME = 13:33
INSTRUM = spect
PULPROG = zg30
F1 (1H)
SI = 32768
SF = 500.13
SW_p = 12531.328
COOMe
HN
N
N
COOMe
H2O
CDCl3
[rel]
[ppm]

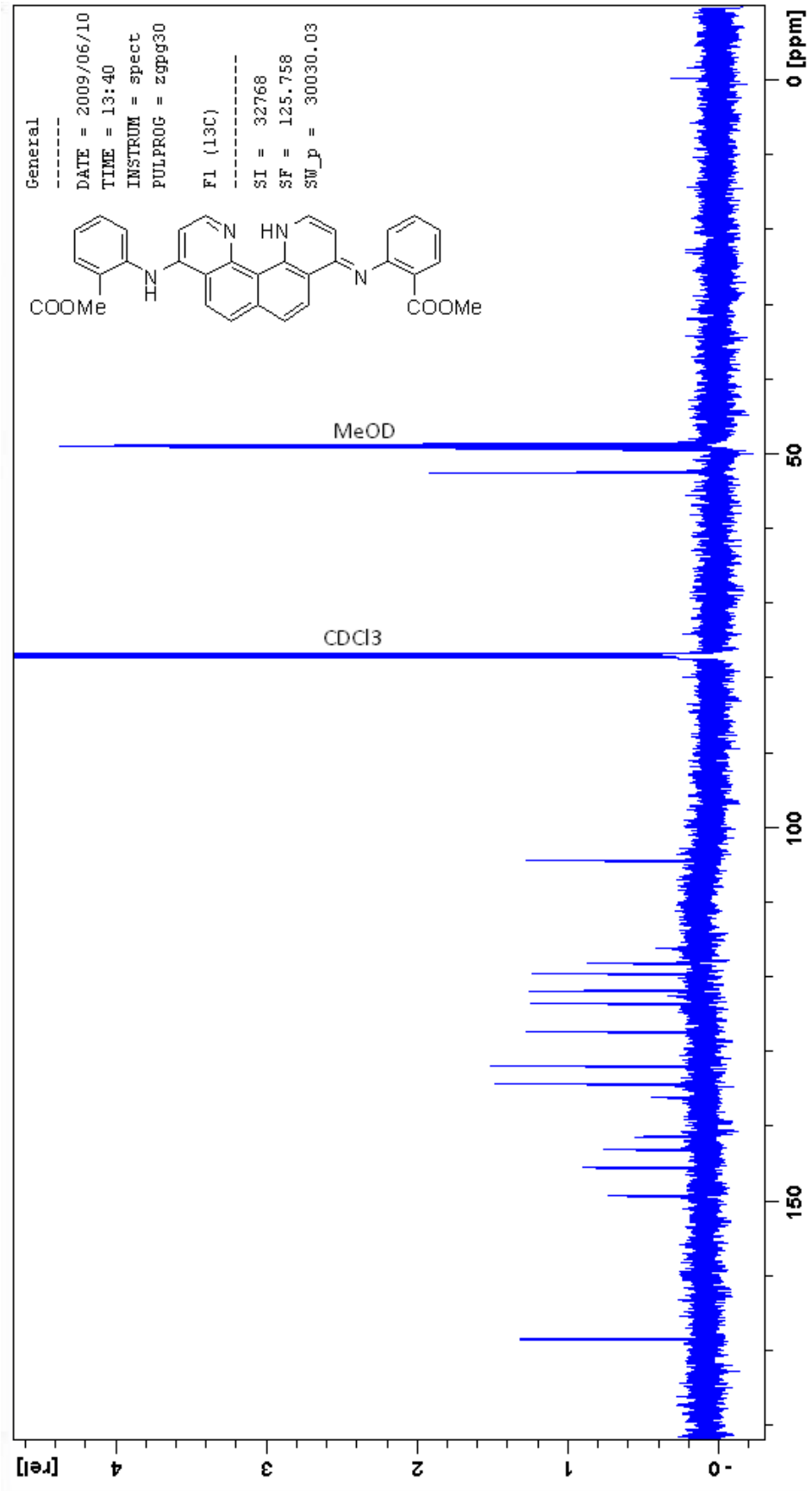
General
DATE = 2009/06/10
TIME = 13:40
INSTRUM = spect
PULPROG = zgpg30
F1 (13C)
SI = 32768
SF = 125.758
SW_p = 30030.03
COOMe
HN
N
COOMe
MeOD
CDCl3
0 [ppm]
50
100
150
[rel]
0
1
2
3
4

A.4.7 4,9-Dichloro-6,7-dinitroquinolino[7,8-h]quinoline (L9)

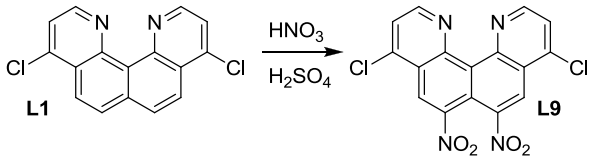

Fuming nitric acid (1 mL) and concentrated sulfuric acid (1 mL) were heated briefly to initiate NO_2 generation, 4,9-dichloroquino[7,8-*h*]quinoline (**L1**) (0.050 g) was added and the reaction was stirred for 2 min at 120 ^{o}C. The reaction was poured onto ice, 6M KOH (20 mL) diluted with CH_2Cl_2 (100 mL) and MeOH (10 mL). The organic layer was filtered and dried over $MgSO_4$ and the solvent was removed to give **L9** (0.023 g, 35 %). ^{1}H NMR (500 MHz, 70 ^{o}C, DMSO-d6) δ 6.52 (d, *J* = 7.4, 1H; 3-*H*), 8.34 (d, *J* = 5.0, 1H; 10-*H*), 8.37 (dd, *J* = 5.9, 7.4, 1H; 2-*H*), 9.09 (s, 1H; 8-*H*), 9.15 (s, 1H; 5-*H*), 9.31 (d, *J* = 5.0, 1H; 11-*H*), 15.59 (d, *J* = 5.2, 1H; N*H*); ^{13}C NMR (125 MHz, 70 ^{o}C, DMSO-d6) δ 111.1 (q), 113.4 (s), 120.1 (q), 121.3 (q), 123.7 (q), 123.8 (q), 124.9 (s), 125.1 (s), 126.3 (s), 140.5 (q), 141.8 (s), 142.8 (q), 145.3 (q), 145.6 (q), 148.3 (q), 152.8 (s). HRMS calculated for $C_{16}H_6N_4O_4Cl_2$ (MH^+) 388.9839, found 388.9832 (ESI+).

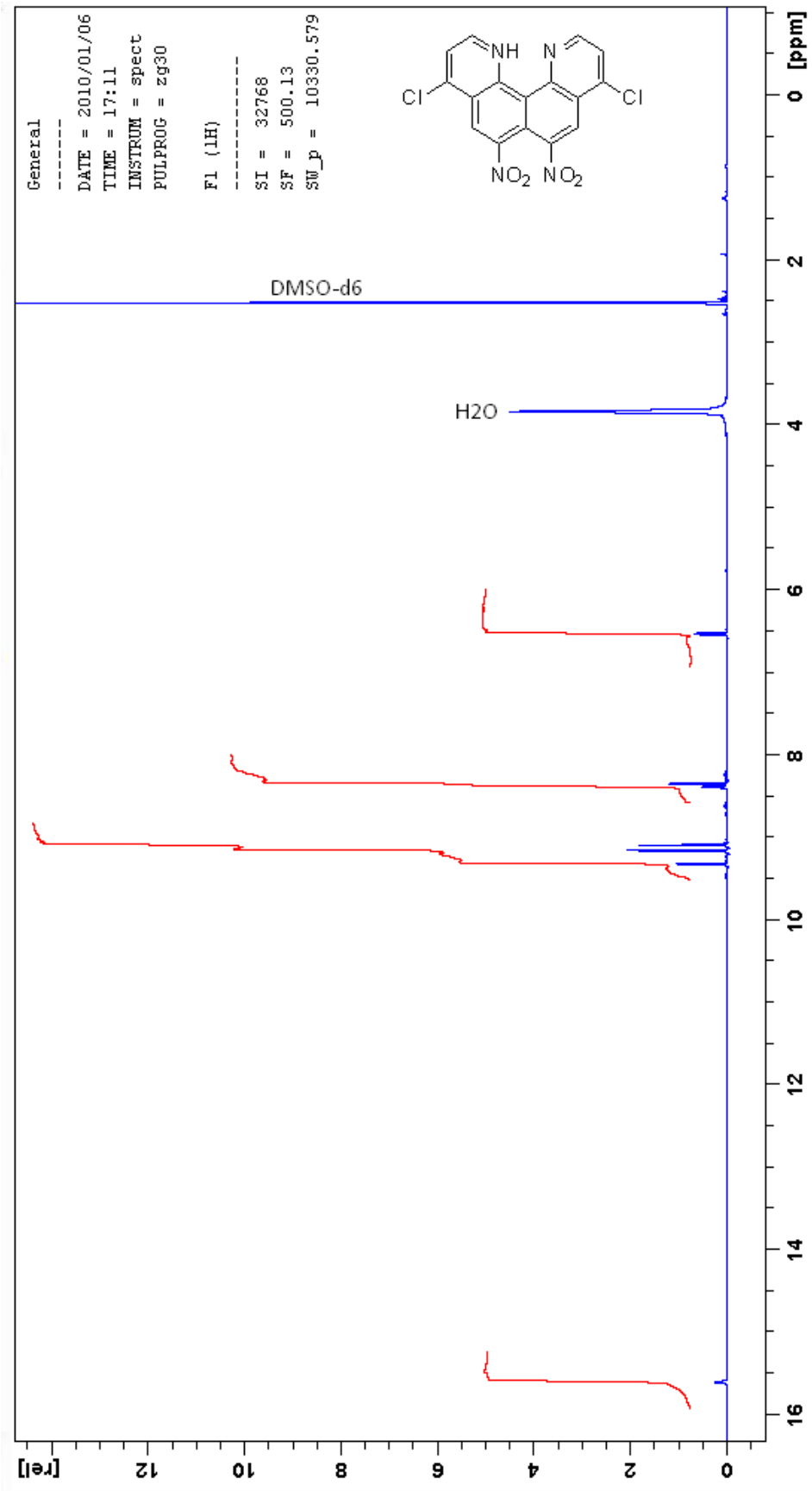
General
DATE = 2010/01/06
TIME = 17:11
INSTRUM = spect
PULPROG = zg30
F1 (1H)
SI = 32768
SF = 500.13
SW_p = 10330.579
NH
N
Cl
Cl
NO2
NO2
DMSO-d6
H2O
[rel]
[ppm]

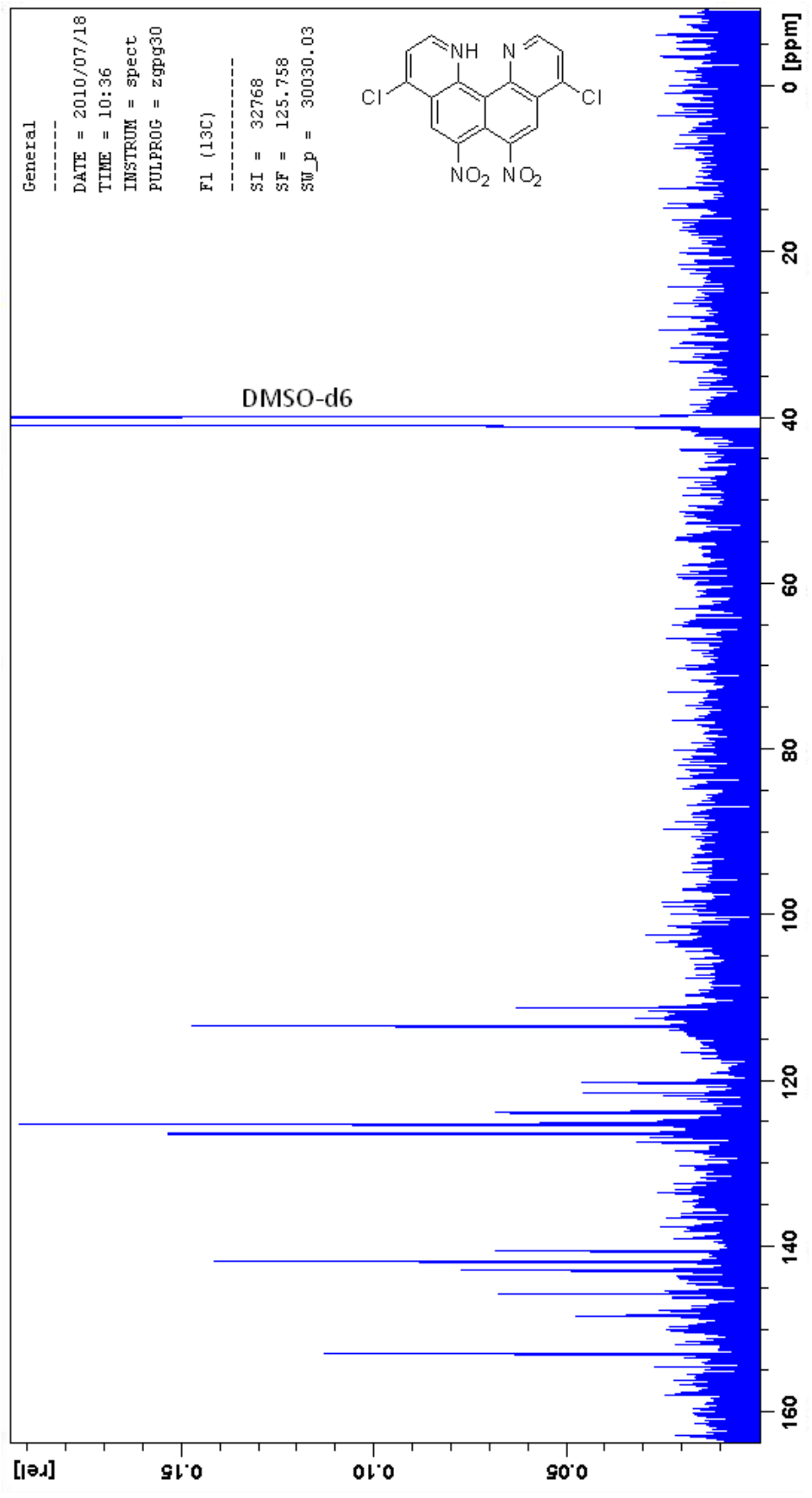
General
DATE = 2010/07/18
TIME = 10:36
INSTRUM = spect
PULPROG = zgpg30
F1 (13C)
SI = 32768
SF = 125.758
SW_p = 30030.03
NH
N
Cl
Cl
NO2
NO2
DMSO-d6
0 [ppm]
20
40
60
80
100
120
140
160
0.05
0.10
0.15
[rel]

A.4.8 9-Oxo-9,12-dihydroquinolino[7,8-h]quinoline-4-sulfonic acid (L10)

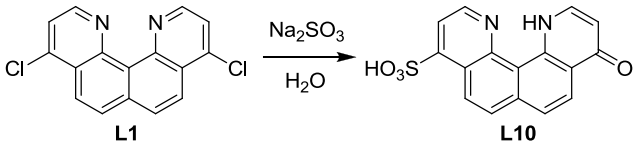

Sodium sulfite (0.084 g, 6.667 mmol) and 4,9-dichloroquino[7,8-*h*]quinoline (**L1**) (0.050 g, 0.167 mmol) in water (10 mL) was refluxed for 4 hr. The solvent was removed and the crude reaction mixture was dissolved in DMSO and filtered then precipitated with EtOAc (0.093 g, 26 %). ^{1}H NMR (500 MHz, DMSO-d6) δ 6.34 (d, *J* = 7.1, 1H; 7-*H*), 7.94 (d, *J* = 8.6, 1H; 6-*H*), 8.13 (d, *J* = 4.6, 1H; 10-*H*), 8.16 (d, *J* = 9.2, 1H; 3-*H*), 8.30 (t, *J* = 6.7, 1H; 8-*H*), 8.45 (d, *J* = 8.5, 1H; 5-*H*), 9.03 (d, *J* = 9.2, 1H; 2-*H*), 9.20 (d, *J* = 4.6, 1H; 11-*H*), 15.47 (d, *J* = 4.2, 1H; N*H*); ^{13}C NMR (125 MHz, DMSO-d6) δ 110.6 (s), 116.7 (q), 118.9 (s), 123.1 (q), 123.2 (s), 124.4 (q), 125.2 (s), 127.4 (s), 127.9 (s), 135.8 (q), 139.6 (q), 139.6 (q), 147.2 (q), 148.2 (s), 152.9 (s), 176.5 (q). HRMS calculated for $C_{16}H_{10}N_4O_2S$ (M-H) 325.0283, found 325.0289 (ESI-).

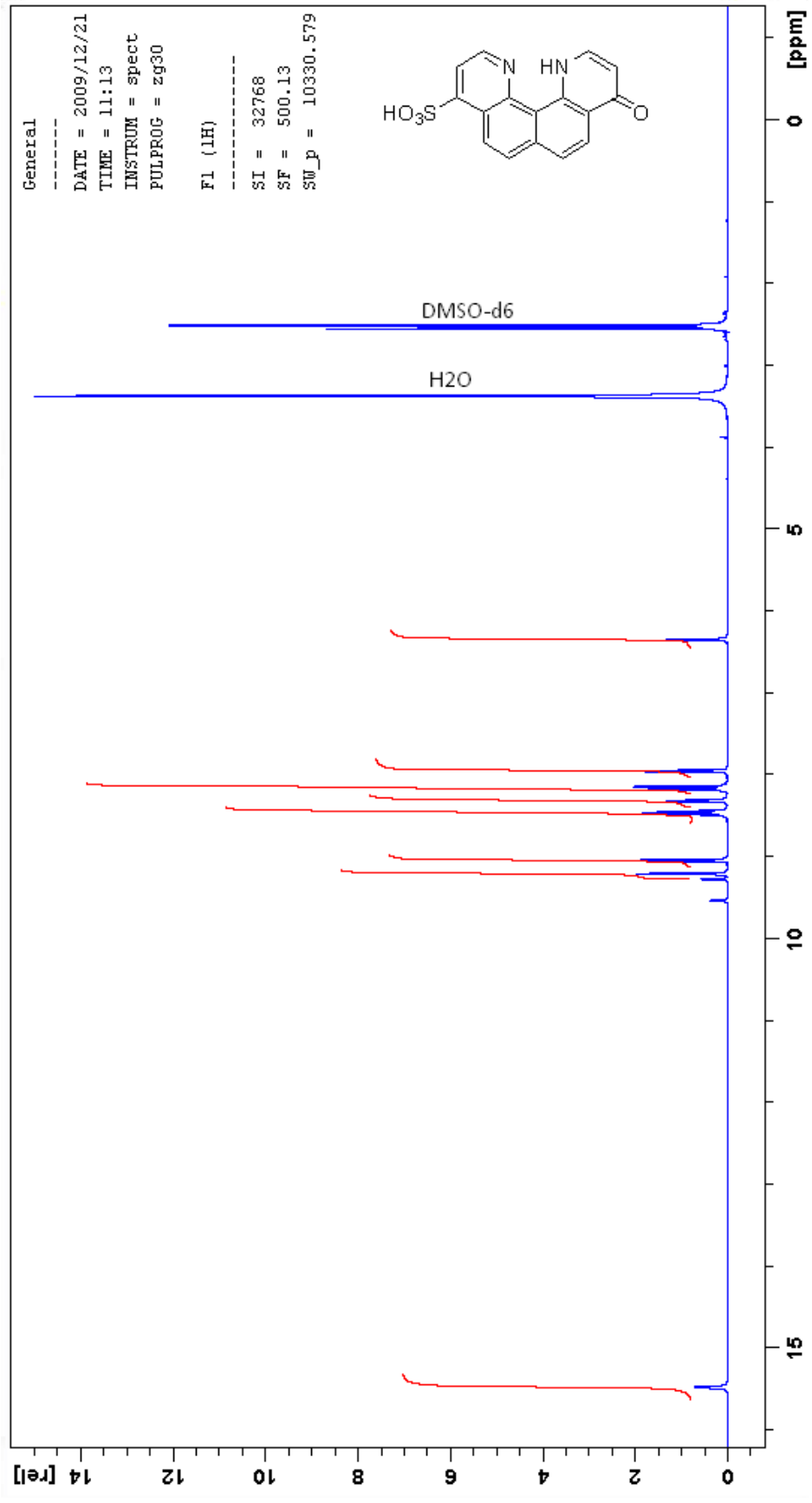
General
DATE = 2009/12/21
TIME = 11:13
INSTRUM = spect
PULPROG = zg30
F1 (1H)
SI = 32768
SF = 500.13
SW_p = 10330.579
HO3S
N
HN
O
DMSO-d6
H2O
[ppm]
[rel]

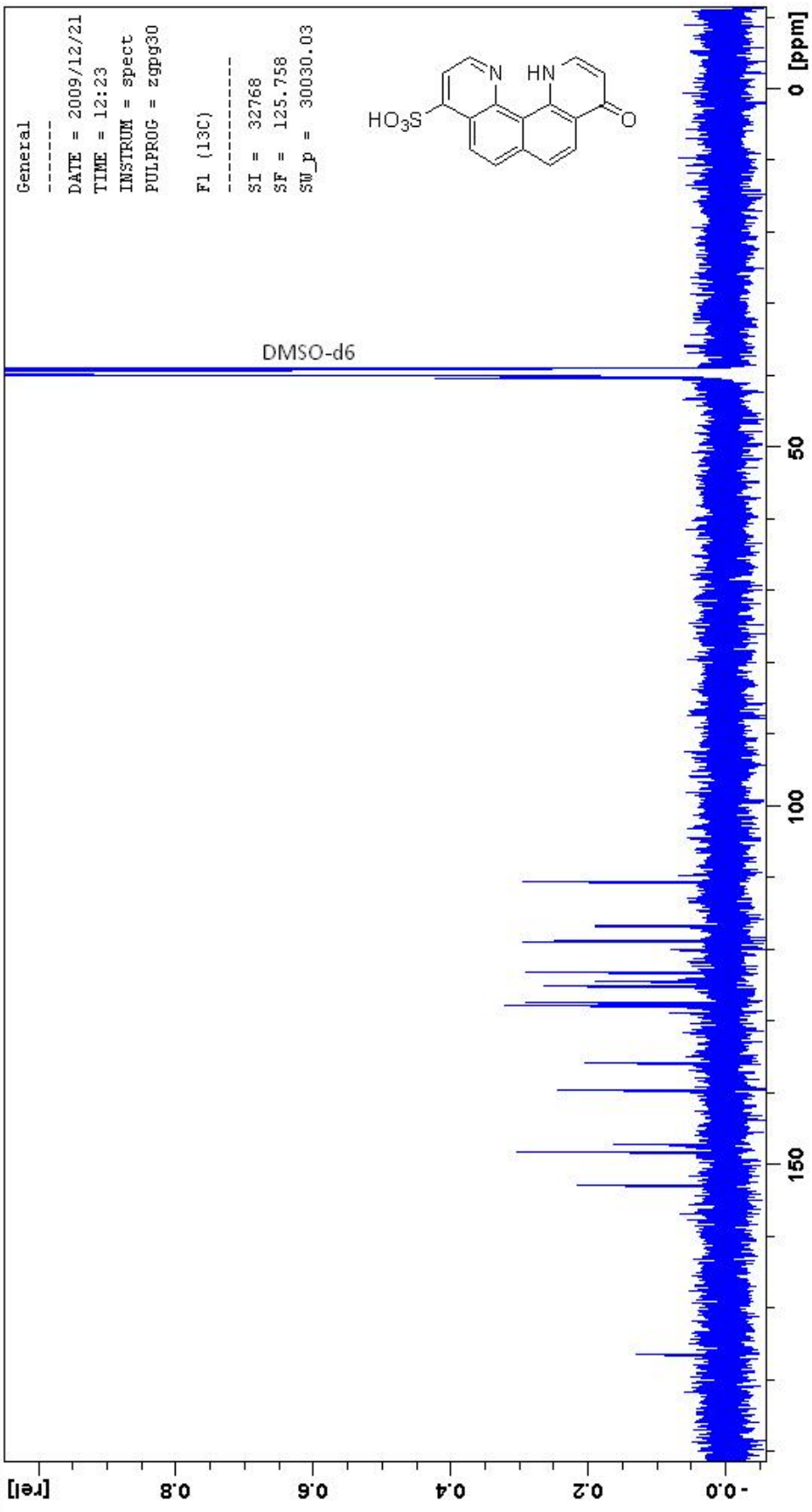
General
DATE = 2009/12/21
TIME = 12:23
INSTRUM = spect
PULPROG = zgpg30
F1 (13C)
SI = 32768
SF = 125.758
SW_p = 30030.03
DMSO-d6
HO3S
N
HN
O
[rel]
0.0
0.2
0.4
0.6
0.8
0 [ppm]
50
100
150

A.4.9 4,9-Dimethoxyquino[7,8-h]quinoline (L11)

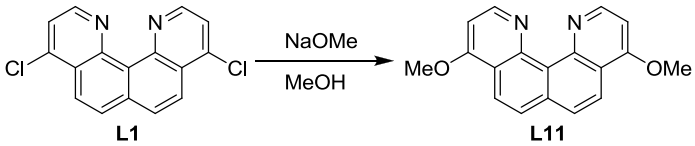

Sodium methoxide (0.072 g, 1.338 mmol) was added to 4,9-dichloroquino[7,8-*h*]quinoline (**L1**) (0.050 g, 0.167 mmol) in MeOH (10 mL) and refluxed for 2 hr under Ar. The reaction was diluted with CH_2Cl_2 (100 mL) and MeOH (10 mL) then washed with 2M KOH (10 mL) in water (100 mL). The organic layer was filtered and dried over $MgSO_4$ and the solvent was removed to give **L11** (0.048 g, 100 %). The product was recrystallised by heating to dissolution in hot DMSO then slowly cooling. ^{1}H NMR (500 MHz, MeOD) δ 3.35 (s, 6H; C*H*$_3$), 7.20 (d, *J* = 5.0, 2H; 3,10-*H*), 7.90 (d, *J* = 8.7, 2H; 6,7-*H*), 8.35 (d, *J* = 8.7, 2H; 5,8-*H*), 8.99 (d, *J* = 5.0, 2H; 2,11-*H*); ^{13}C NMR (125 MHz, MeOD) δ 50.0 (t), 102.9 (s), 121.7 (q), 123.1 (s), 125.7 (q), 128.2 (s), 137.9 (q), 148.4 (q), 151.6 (s), 164.4 (q). HRMS calculated for $C_{18}H_{14}N_2O_2$ (MH^+) 291.1128, found 291.1128 (ESI+).

Crystal data for **L11**. $C_{18}H_{14}N_2O_2$, colourless chip, dimensions 0.6 x 0.05 x 0.05 mm, monoclinic, space group P$2_1/c$, a = 6.9964(14), b = 12.597(3), c = 46.260(9) Å, α = 90.00°, β = 94.19(3)°, γ = 90.00°, U = 4066.3(14) Å^3, μ = 0.762 mm^{-1}, Z = 12, D_c = 1.423 g cm^{-3}, F(000) = 1824, T = 123(2) K. 7370 Reflections were collected using a Rigaku MM007 rotating anode in the range 6.70 < 2θ < 143.20°. A semi-empirical absorption correction (ABSCOR; Higashi, 1995) was applied. The 6224 independent reflections were used to solve the structure by direct methods (SHELXS97) which resulted in the location of all non-hydrogen atoms. All non-hydrogen atoms were made anisotropic and the refinement (SHELXL97) of 601 parameters converged to R_1 = 0.0940 [for 1963 reflections having I > 4σ (I)], wR_2 = 0.1984 and goodness of fit 0.828 (for all 1963 F^2 data). Peak / hole 0.299 / -0.487 e Å^{-3}.

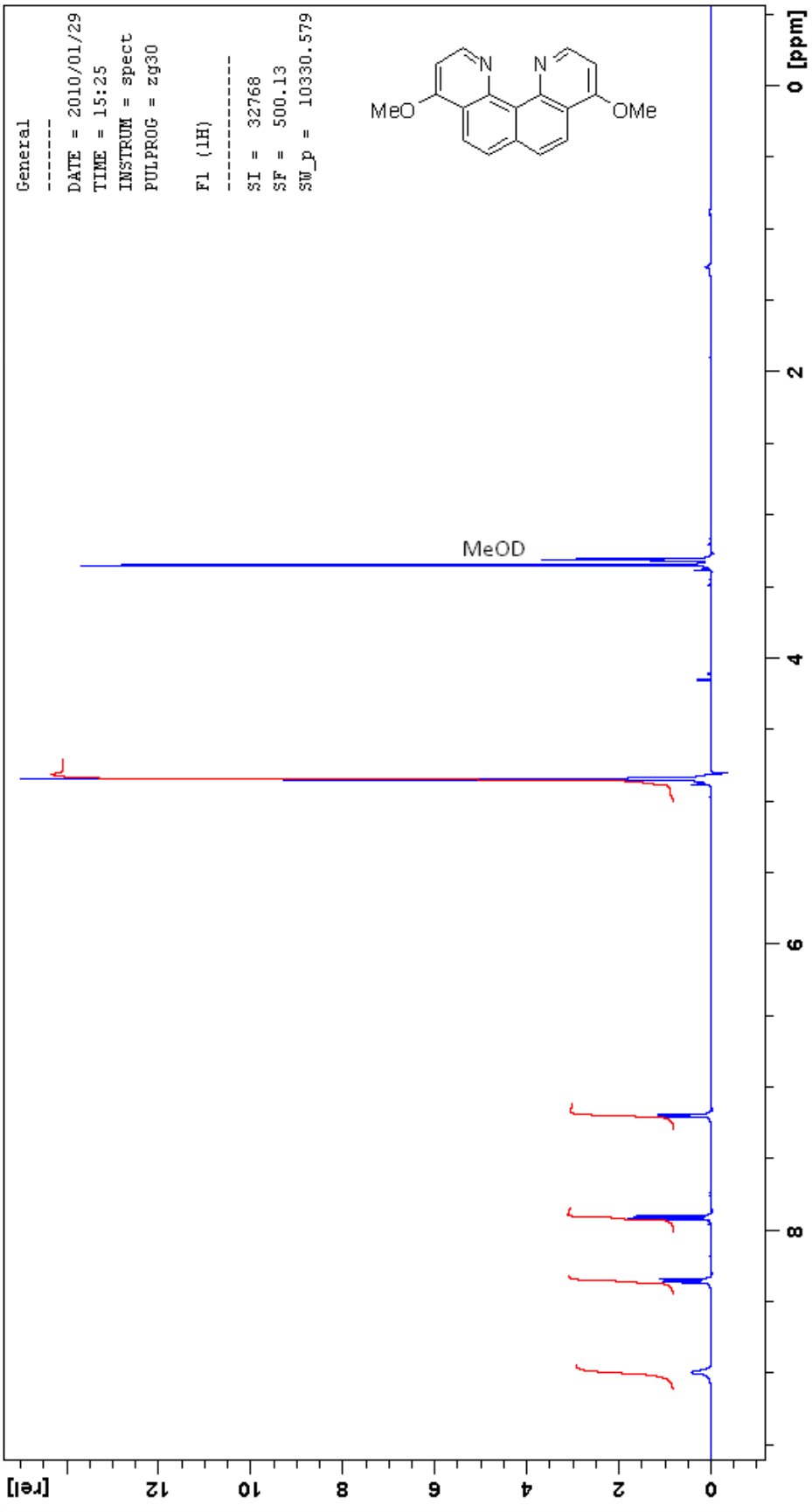
General
DATE = 2010/01/29
TIME = 15:25
INSTRUM = spect
PULPROG = zg30
F1 (1H)
SI = 32768
SF = 500.13
SW_p = 10330.579
MeO
OMe
N
N
MeOD
[rel]
0 [ppm]

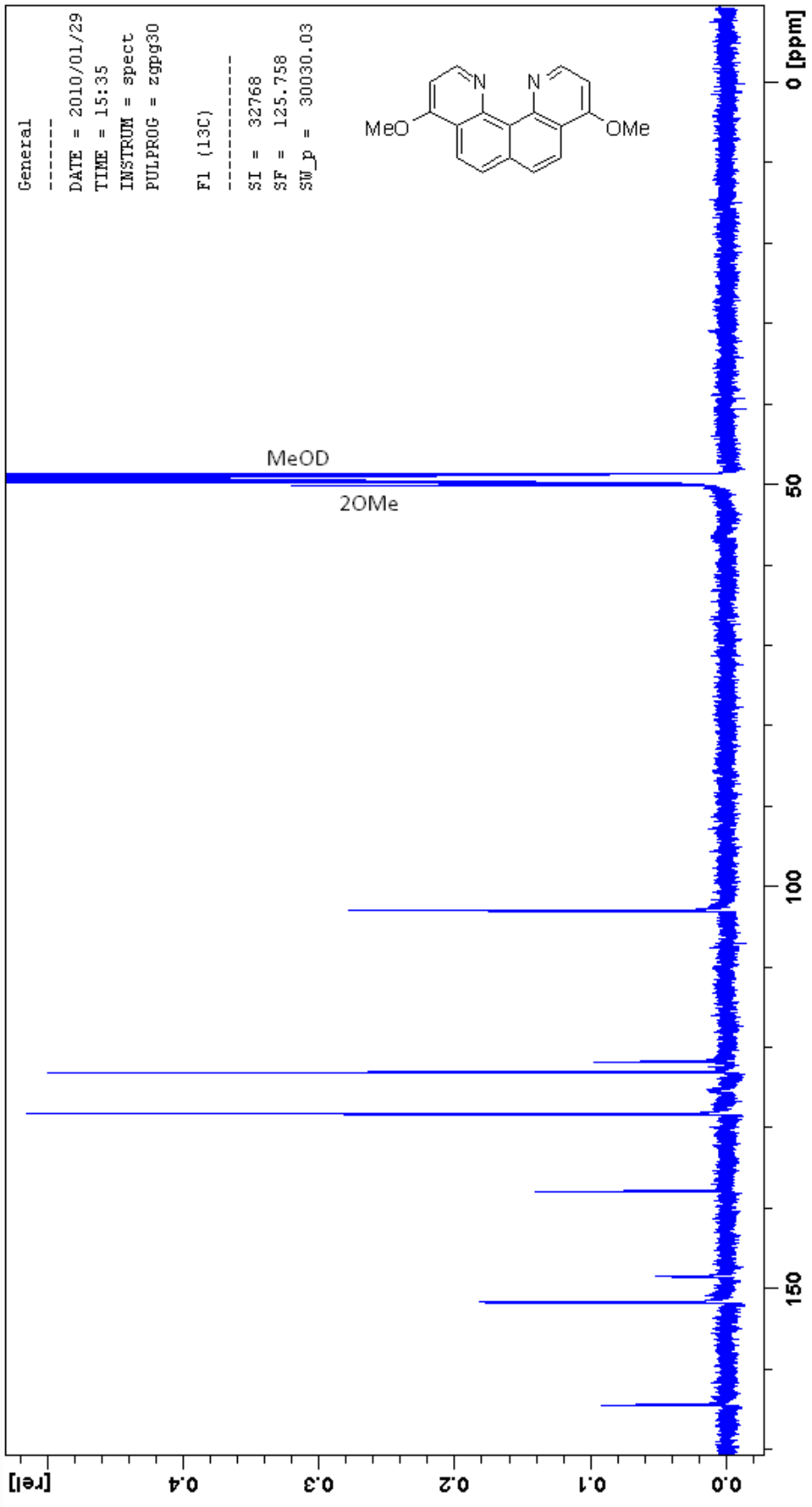
General
DATE = 2010/01/29
TIME = 15:35
INSTRUM = spect
PULPROG = zgpg30
F1 (13C)
SI = 32768
SF = 125.758
SW_p = 30030.03
MeO
N
N
OMe
MeOD
2OMe
0 [ppm]
50
100
150
[rel]
0.0
0.1
0.2
0.3
0.4

A.4.10 4,9-Dibromoquino[7,8-h]quinoline (L12)

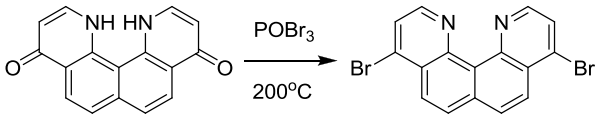

308 **L12**

L12 was synthesised by analogy to the known literature procedure for **L1**.[85] Phosphorus oxybromide (2.97 g, 10.4 mmol) was added to quinolino[7,8-*h*]quinoline-4-9-(1*H*,12*H*)-dione (**308**) (0.520 g, 2.08 mmol) and the reaction was stirred at 200 ^{o}C for 30 min under Ar. The reaction mixture was diluted with CH_2Cl_2 (200 mL) and MeOH (20 mL) and basified with 6M KOH (20 mL) in water (200 mL). A small portion of decolourising carbon was added and the organic layer was filtered and dried over $MgSO_4$ to give **L12** (0.533 g, 66 %). ^{1}H NMR (500 MHz, $CDCl_3$) δ 7.94 (d, *J* = 4.7, 2H; 3,10-*H*), 8.09 (d, *J* = 9.1, 2H; 6,7-*H*), 8.51 (d, *J* = 8.9, 2H; 5,8-*H*), 9.18 (brd, *J* = 4.5, 2H; 2,11-*H*); ^{13}C NMR (125 MHz, $CDCl_3$) δ 125.5 (s), 126.1 (q), 127.8 (s), 128.8 (q), 129.0 (s), 134.4 (q), 136.4 (q), 148.2 (q), 149.8 (s). HRMS calculated for $C_{16}H_8N_2Br_2$ (MH^+) 388.9107, found 388.9102 (ESI+).

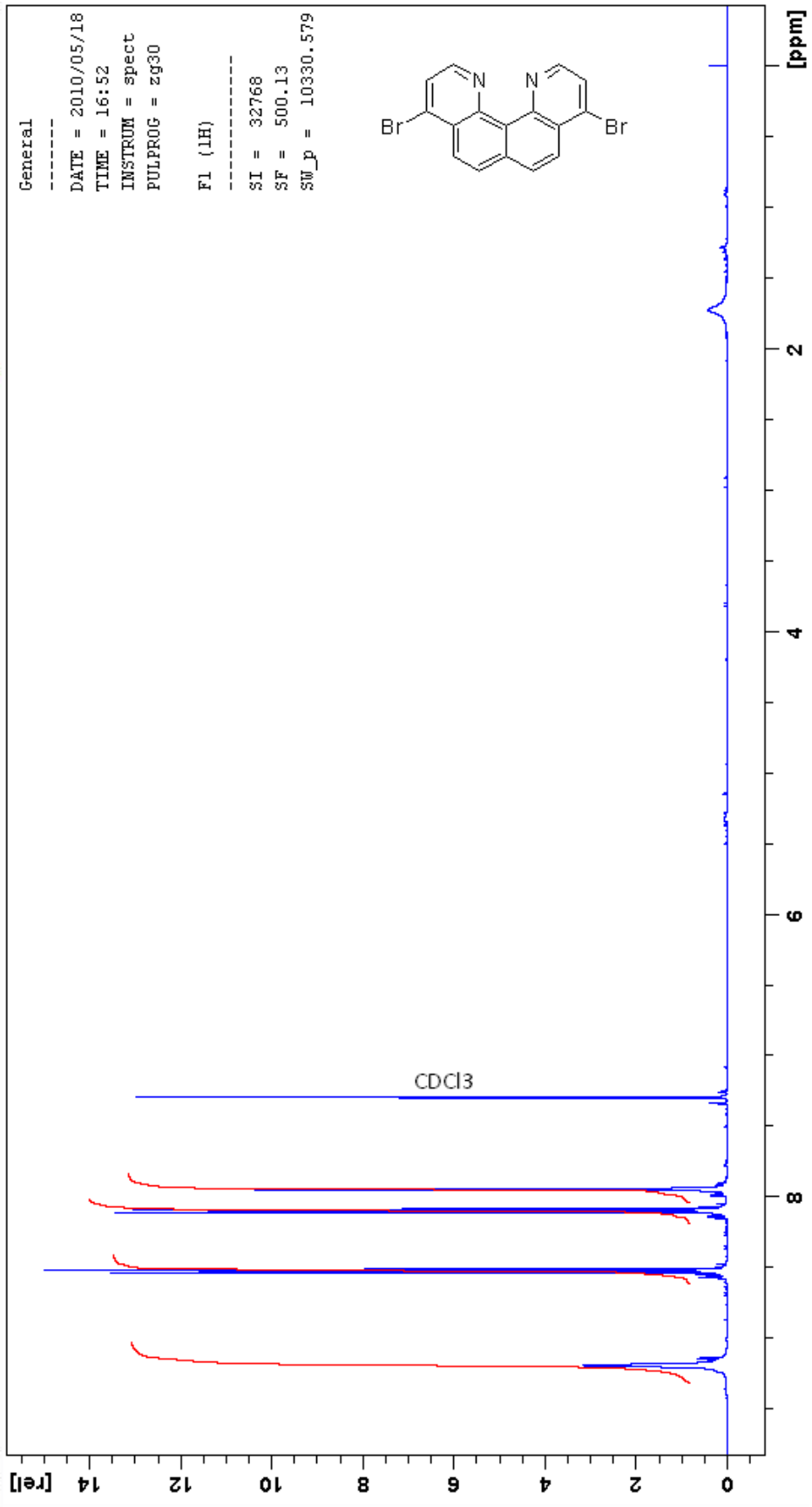
General
DATE = 2010/05/18
TIME = 16:52
INSTRUM = spect
PULPROG = zg30
F1 (1H)
SI = 32768
SF = 500.13
SW_p = 10330.579
Br
N
N
Br
CDCl3
[rel]
[ppm]
0
2
4
6
8
10
12
14

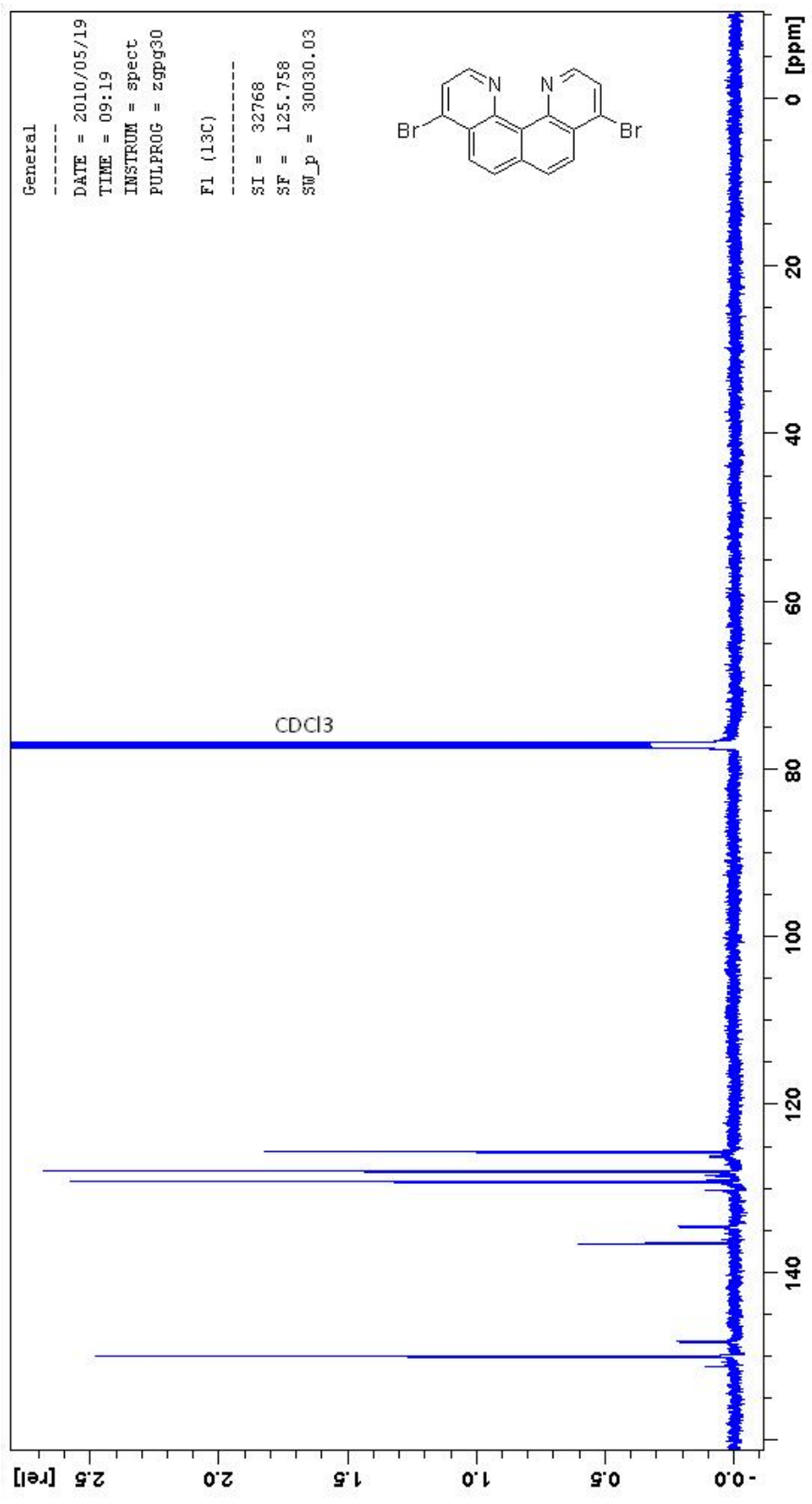
General
DATE = 2010/05/19
TIME = 09:19
INSTRUM = spect
PULPROG = zgpg30
F1 (13C)
SI = 32768
SF = 125.758
SW_p = 30030.03
Br
N
N
Br
CDCl3
[rel]
[ppm]

A.4.11 Dimethyl 4,9-Dichloroquinolino[7,8-h]quinoline-2,11-dicarboxylate (L13)

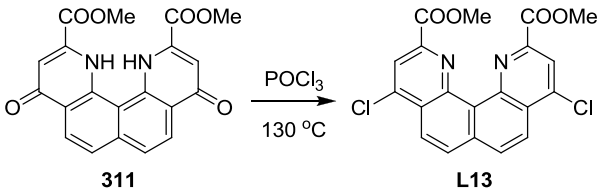

311 **L13**

Phosphorus oxychloride (1.25 mL, 13.5 mmol) was added to dimethyl 4,9-dioxo-1,4,9,12-tetrahydroquinolino[7,8-*h*]quinoline-2,11-dicarboxylate (**311**) (0.394 g, 1.06 mmol) and the reaction was stirred at 130 ^{o}C for 9 minutes. The reaction mixture was poured onto ice-water (200 mL) and basified with 6M KOH (20 mL) and extracted with CH_2Cl_2 (200 mL). The organic layer was filtered and dried over $MgSO_4$ to give **L13** (0.315 g, 72 %). ^{1}H NMR (500 MHz, $CDCl_3$) δ 4.19 (s, 6H; C*H*$_3$), 8.20 (d, *J* = 8.9, 2H; 6,7-*H*), 8.55 (s, 2H; 3,10-*H*), 8.60 (d, *J* = 8.8, 2H; 5,8-*H*); ^{13}C NMR (125 MHz, $CDCl_3$) δ 53.3 (t), 122.5 (s), 125.0 (s), 127.1 (q), 127.9 (q), 130.9 (s), 136.9 (q), 144.0 (q), 147.8 (q), 148.1 (q), 165.2 (q). MS for $C_{20}H_{12}N_2O_4Cl_2$ (M^+) 415.02. $C_{20}H_{12}N_2O_4Cl_2$•0.5H_2O (423.02): calcd. C 56.62, H 3.09, N 6.60; found C 56.73, H 3.08, N 6.60. M.P. = 171 – 172 ^{o}C.

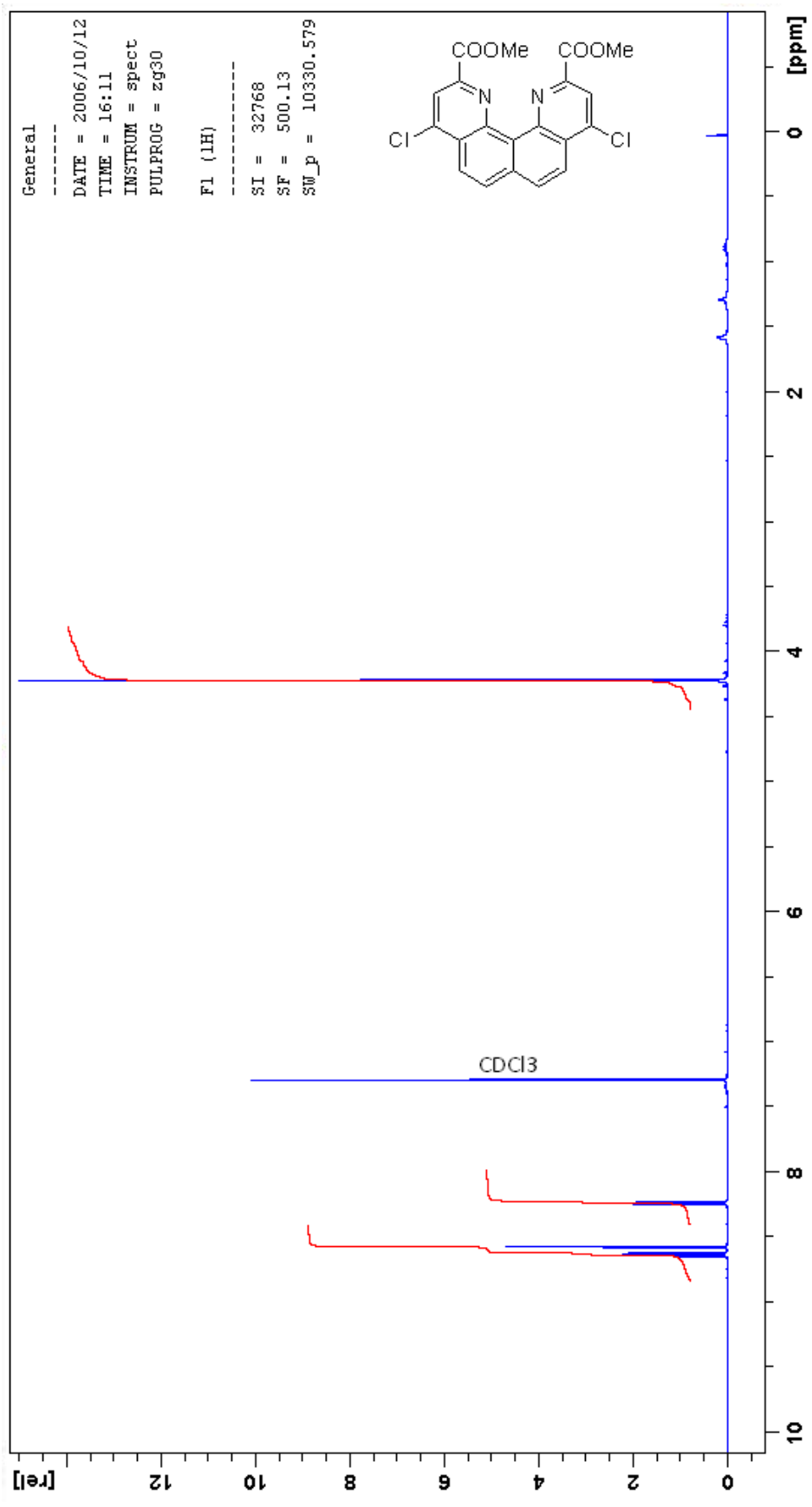
General
DATE = 2006/10/12
TIME = 16:11
INSTRUM = spect
PULPROG = zg30
F1 (1H)
SI = 32768
SF = 500.13
SW_p = 10330.579
COOMe
COOMe
N
N
Cl
Cl
CDCl3
[ppm]
[rel]

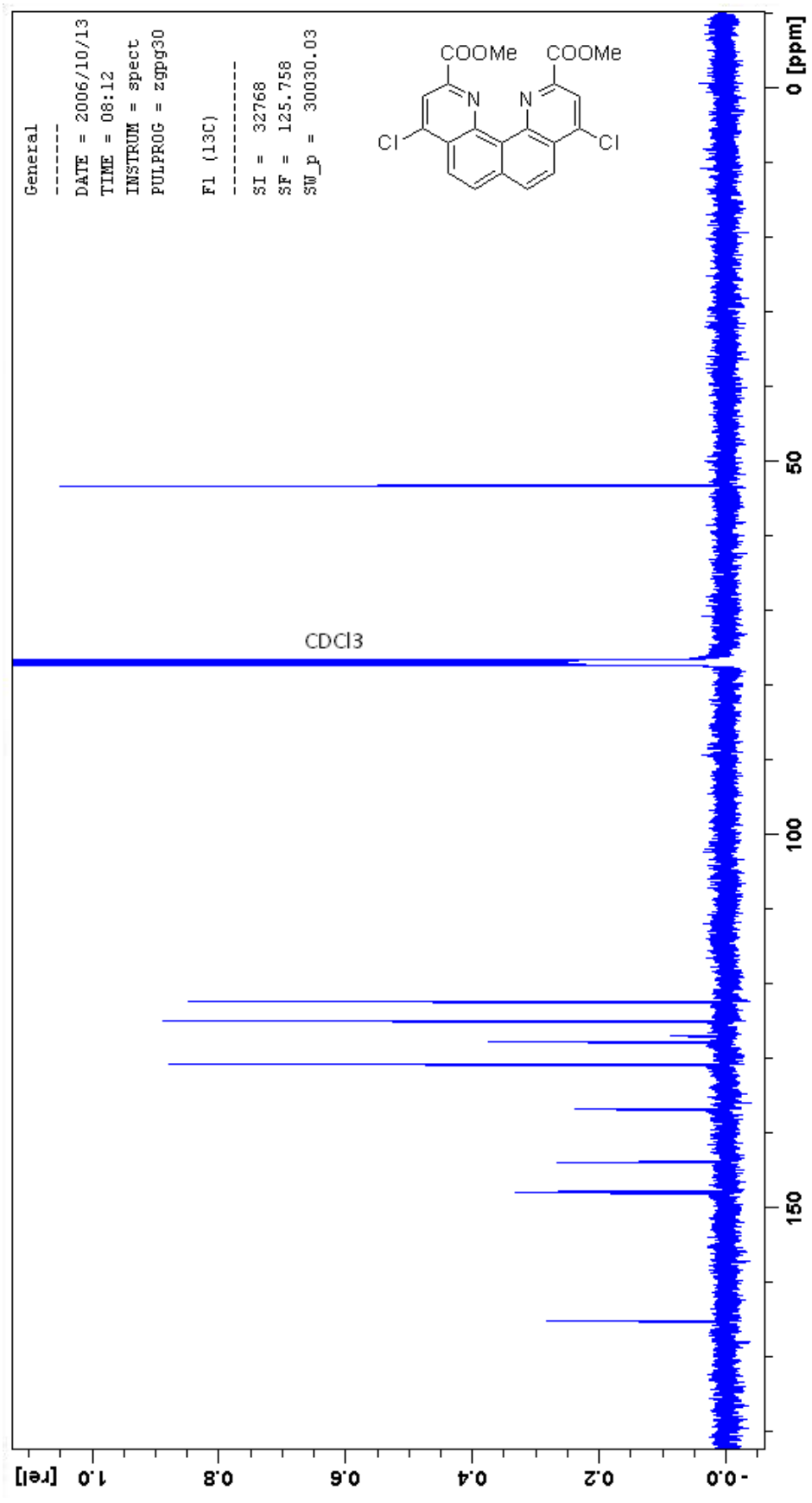
General
DATE = 2006/10/13
TIME = 08:12
INSTRUM = spect
PULPROG = zgpg30
F1 (13C)
SI = 32768
SF = 125.758
SW_p = 30030.03
COOMe
COOMe
N
N
Cl
Cl
CDCl3
0 [ppm]
50
100
150
-0.0
0.2
0.4
0.6
0.8
1.0
[rel]

A.4.12 [H(L13)]BF_4

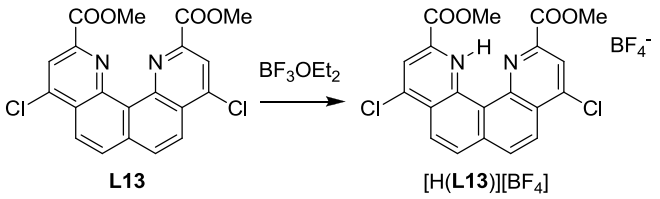

L13 [H(**L13**)][BF_4]

Boron trifluoride diethyl etherate (0.121 mL, 0.964 mmol) was added to 4,9-dichloroquino[7,8-*h*]quinoline-2,11-dicarboxylate (**L13**) (0.100 g, 0.241 mmol) in dry CH_2Cl_2 (5 mL) under Ar and stirred at RT for 8 hr. The reaction was diluted with CH_2Cl_2 and the solvent was separated from deposited [H(**L13**)][BF_4] and dried under vacuum. The product was then set up for crystallisation by vapour diffusion of diethyl ether into a MeCN solution containing [H(**L13**)][BF_4]. Brown crystals suitable for X-ray crystallography were obtained after one day. ^{1}H NMR (500 MHz, CD_3CN) δ 4.23 (s, 6H; C*H*$_3$), 8.43 (d, *J* = 9.1, 2H; 6,7-*H*), 8.64 (d, *J* = 9.1, 2H; 5,8-*H*), 8.68 (s, 2H; 3,10-*H*), 19.14 (s, 1H; N*H*); ^{13}C NMR (125 MHz, CD_3CN) δ 55.5 (t), 117.3 (q), 125.2 (s), 128.1 (s), 129.7 (q), 133.7 (s), 140.2 (q), 143.4 (q), 145.4 (q), 152.3 (q), 162.1 (q). MS for $C_{20}H_{13}N_2O_4Cl_2$ (M^+) 415.53. $C_{20}H_{13}N_2O_4Cl_2H^+ \bullet BF_4^-$ (503.04): calcd. C 47.75, H 2.60, N 5.57; found C 47.78, H 2.33, N 5.64. M.P. = 218 – 220 ^{o}C.

Crystal data for [H(**L13**)][BF_4]. $C_{20}H_{13}N_2O_2Cl_2BF_4$, yellow prism, dimensions 0.2 x 0.15 x 0.1 mm, triclinic, space group $P2_1/c$, a = 11.0327(2), b = 13.5997(2), c = 15.1206(3) Å, α = 113.4460(10)^o, β = 99.4340(10)^o, γ = 97.8210(10)^o, U = 2001.82(7) Å^3, μ = 3.573 mm^{-1}, Z = 4, D_c = 1.669 g cm^{-3}, F(000) = 1016, T = 100(2) K. 10378 Reflections were collected using a Rigaku MM007 rotating anode in the range 6.58 < 2θ < 144.00^o. A semi-empirical absorption correction (ABSCOR; Higashi, 1995) was applied. The 5797 independent reflections were used to solve the structure by direct methods (SHELXS97) which resulted in the location of all non-hydrogen atoms. All non-hydrogen atoms were made anisotropic and the refinement (SHELXL97) of 596 parameters converged to R_1 = 0.0406 [for 5280 reflections having $I > 4\sigma(I)$], wR_2 = 0.1095 and goodness of fit 1.080 (for all 5280 F^2 data). Peak / hole 0.336 / -0.391 e Å^{-3}.

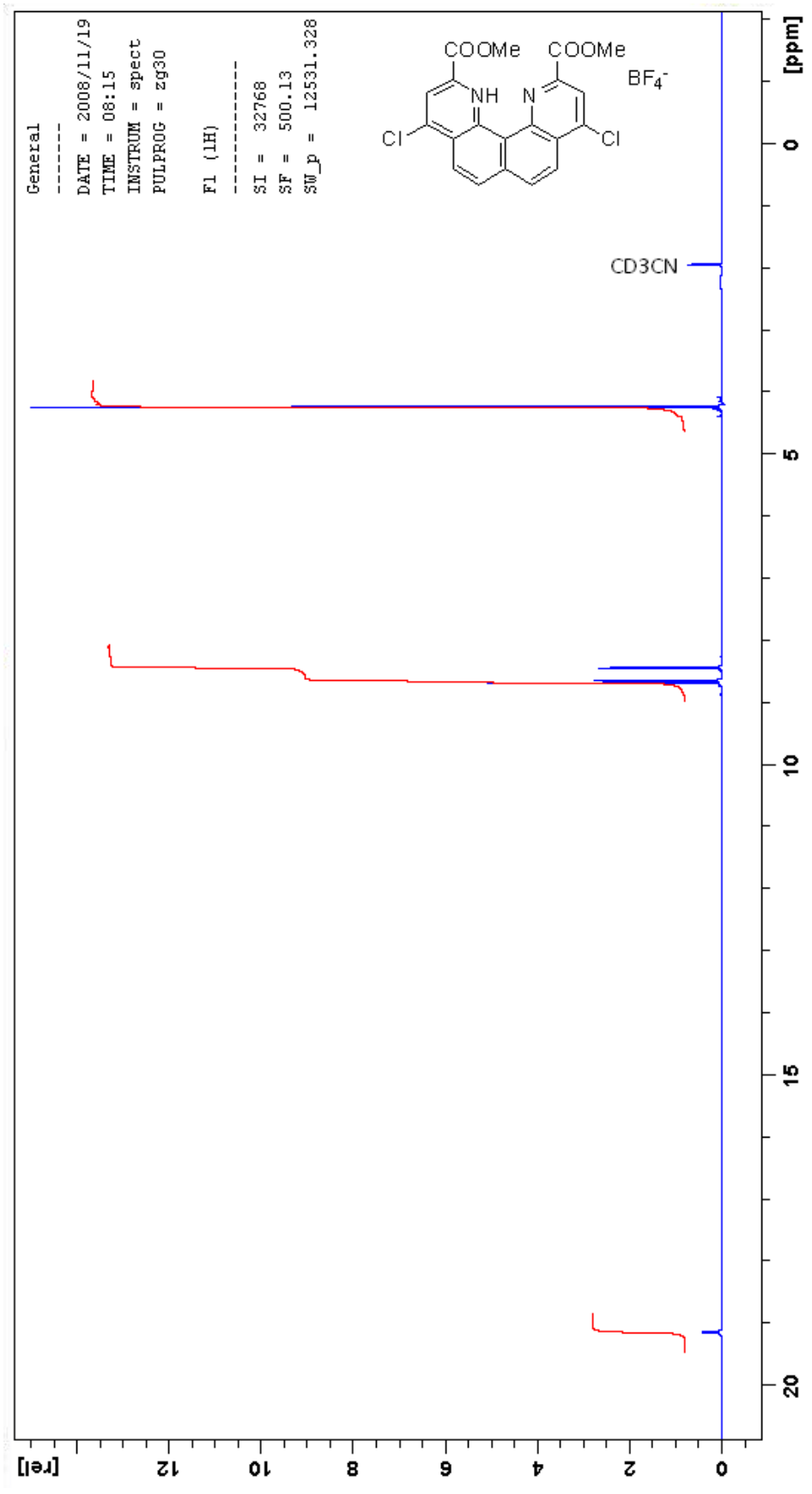
General
DATE = 2008/11/19
TIME = 08:15
INSTRUM = spect
PULPROG = zg30
F1 (1H)
SI = 32768
SF = 500.13
SW_p = 12531.328
COOMe
COOMe
NH
N
Cl
Cl
BF4-
CD3CN
[ppm]
[rel]

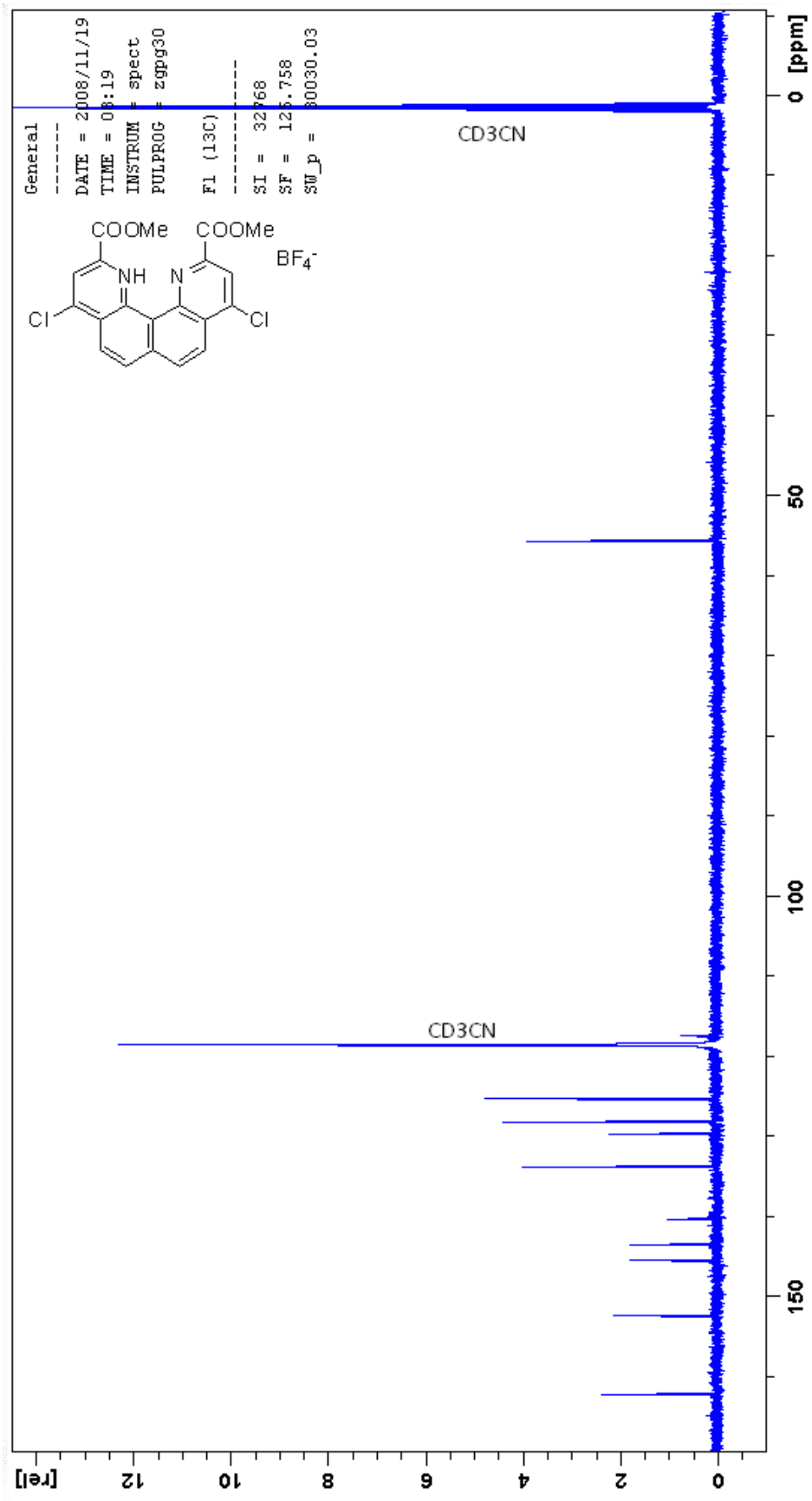
General
DATE = 2008/11/19
TIME = 08:19
INSTRUM = spect
PULPROG = zgpg30
F1 (13C)
SI = 32768
SF = 125.758
SW_p = 30030.03
COOMe
COOMe
NH
N
Cl
Cl
BF4-
CD3CN
CD3CN
[rel]
[ppm]

A.5 Chapter 4 Experimental

A.5.1 $[BF_2(L1)]BF_4$

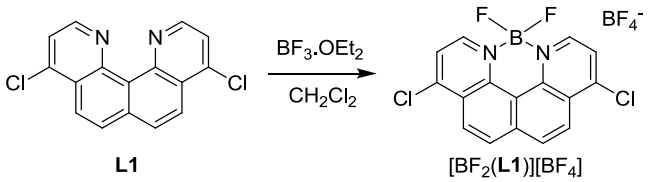

L1 $[BF_2(\mathbf{L1})][BF_4]$

Boron trifluoride diethyl etherate (0.168 mL, 1.336 mmol) was added to 4,9-dichloroquino[7,8-*h*]quinoline (**L1**) (0.100 g, 0.334 mmol) in dry CH_2Cl_2 (5 mL) under Ar and stirred at RT for 2 hr. The reaction was diluted with CH_2Cl_2 and the solvent was separated from deposited $[BF_2(\mathbf{L1})][BF_4]$ and dried under vacuum. The product was then set up for crystallisation by vapour diffusion of diethyl ether into a MeCN solution containing $[BF_2(\mathbf{L1})][BF_4]$. Pale brown crystals suitable for X-ray crystallography were obtained after one day, the crystals became darker over time, but, were stable when removed from solution and did not degrade. ^{1}H NMR (500 MHz, CD_3CN) δ 8.55 (d, *J* = 6.4, 2H; 3,10-*H*), 8.70 (d, *J* = 9.2, 2H; 6,7-*H*), 8.93 (d, *J* = 9.2, 2H; 5,8-*H*), 9.48 (m, 2H; 2,11-*H*); ^{13}C NMR (125 MHz, CD_3CN) δ 126.8 (s), 128.2 (s), 128.9 (q), 132.7 (s), 138.1 (q), 140.0 (q), 147.4 (s), 155.4 (q); ^{11}B NMR (160 MHz, CD_3CN) 1.79 (t, *J* = 27 Hz, 1B; *B*F_2), -1.17 (s, 1B; *B*F_4); ^{19}F NMR (376 MHz, CD_3CN) -134.8 (q, *J* = 27 Hz, 2F; B*F*$_2$), -151.71 (s, 4F; B*F*$_4$); MS for $C_{16}H_8N_2Cl_2.BF_2^+$ (M^+) 347.52. $C_{16}H_8N_2Cl_2BF_2^+ \bullet BF_4^-$ (434.02): calcd. C 44.20, H 1.85, N 6.44; found C 44.39, H 2.12, N 6.58. M.P. = 318 – 320 ^{o}C.

Crystal data for $[BF_2(\mathbf{L1})][BF_4]$. $C_{16}H_8N_2Cl_2B_2F_6$, yellow prism, dimensions 2.0 x 1.0 x 0.5 mm, monoclinic, space group $P2_1/n$, a = 9.1484(18), b = 17.528(4), c = 11.230(2) Å, α = 90.00^{o}, β = 111.42(3)^{o}, γ = 90.00^{o}, U = 1676.4(6) Å^3, μ = 4.138 mm^{-1}, Z = 4, D_c = 1.723 g cm^{-3}, F(000) = 864, T = 173(2) K. 4047 Reflections were collected using a Rigaku MM007 rotating anode in the range 6.59 < 2θ < 144.09^{o}. A semi-empirical absorption correction (ABSCOR; Higashi, 1995) was applied. The 2735 independent reflections were used to

solve the structure by direct methods (SHELXS97) which resulted in the location of all non-hydrogen atoms. All non-hydrogen atoms were made anisotropic and the refinement (SHELXL97) of 281 parameters converged to R_1 = 0.0617 [for 2405 reflections having $I > 4\sigma(I)$], wR_2 = 0.1738 and goodness of fit 1.146 (for all 2405 F^2 data). Peak / hole 0.549 / -0.567 e Å^{-3}.

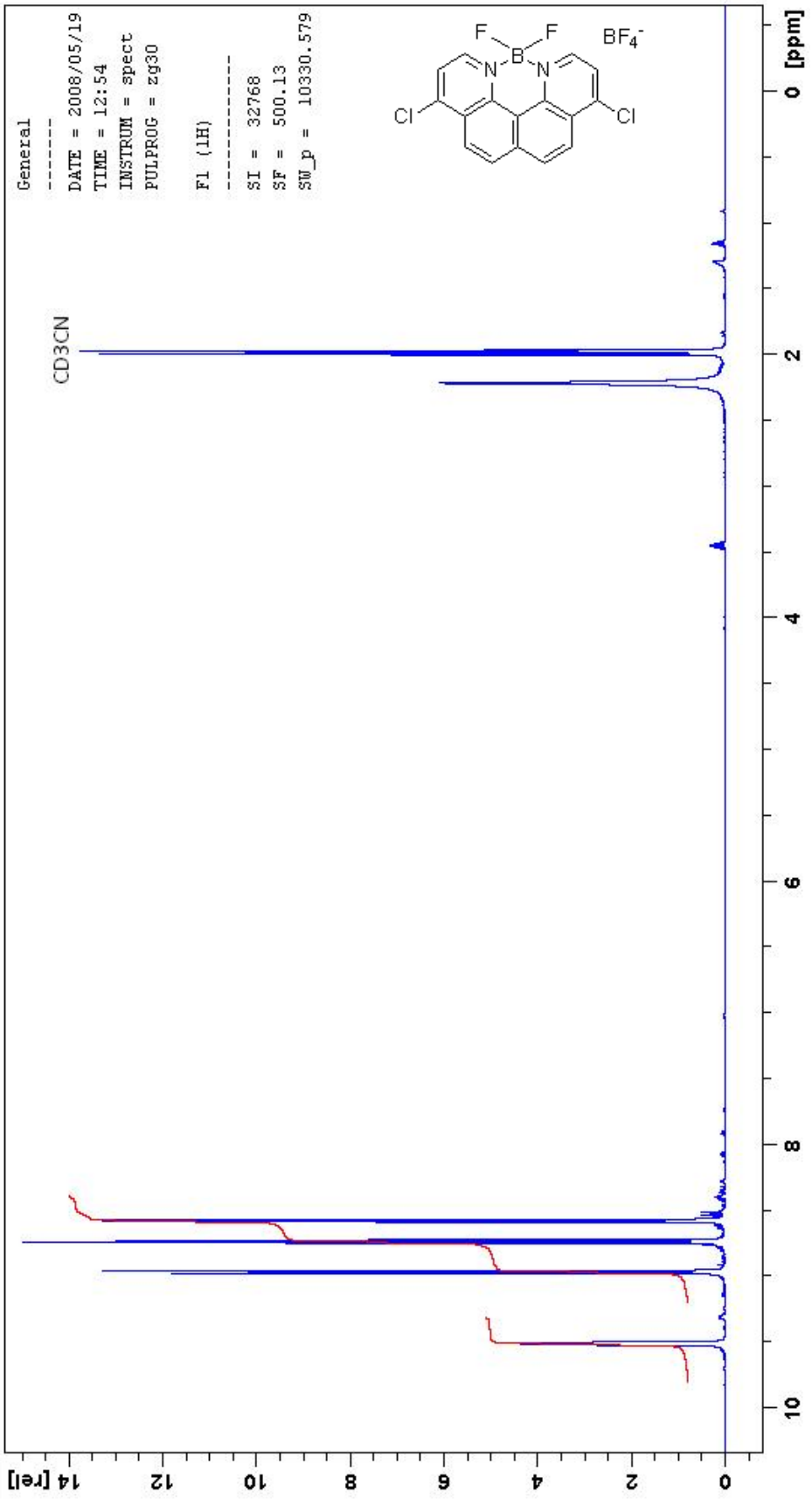
General
DATE = 2008/05/19
TIME = 12:54
INSTRUM = spect
PULPROG = zg30
F1 (1H)
SI = 32768
SF = 500.13
SW_p = 10330.579
CD3CN
F
F
B
N
N
Cl
Cl
BF4-
[rel]
[ppm]

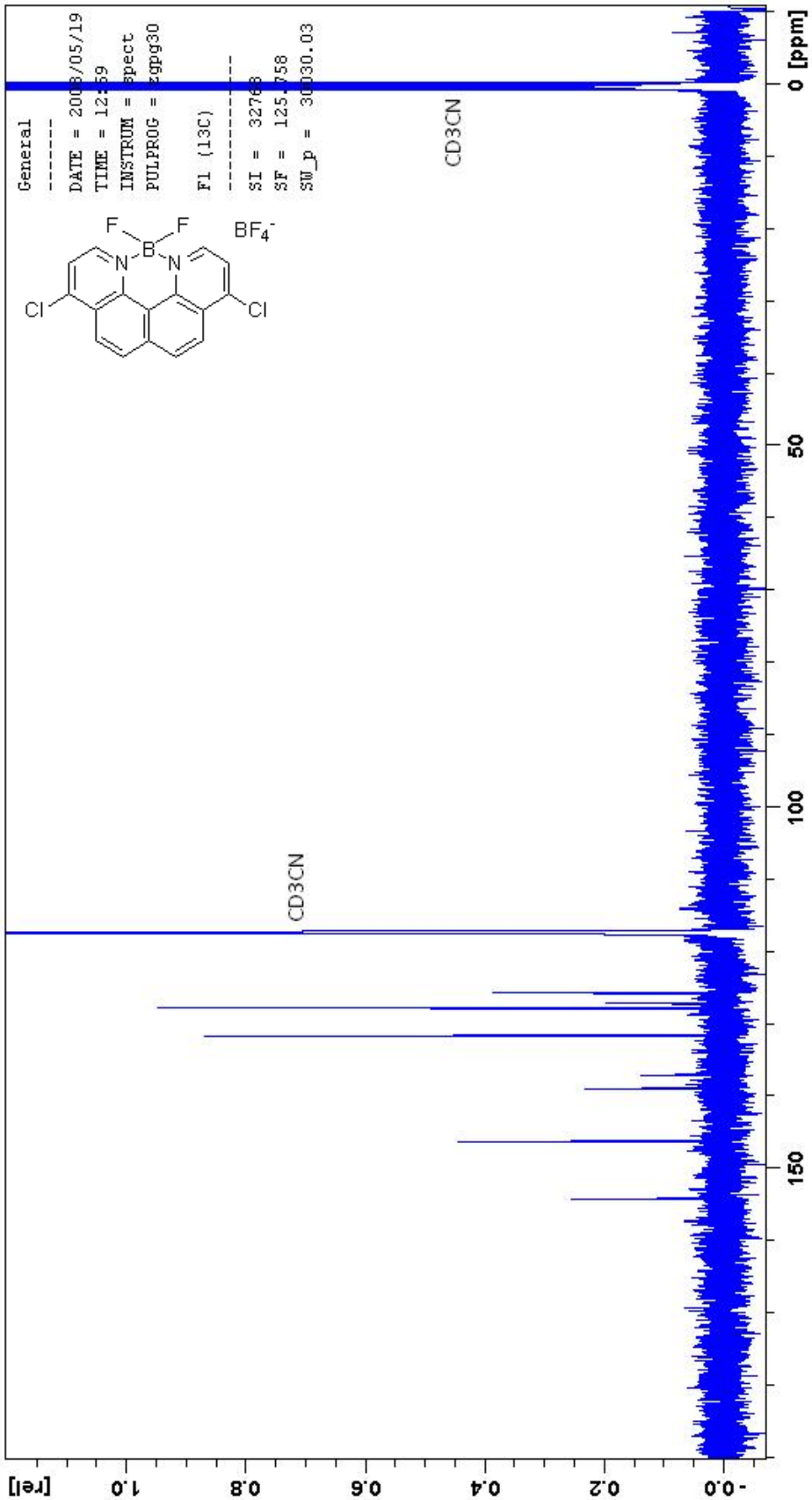
General
DATE = 2008/05/19
TIME = 12:59
INSTRUM = spect
PULPROG = zgpg30
F1 (13C)
SI = 32768
SF = 125.758
SW_p = 30030.03
CD3CN
CD3CN
F
F
B
N
N
Cl
Cl
BF4-
[rel]
1.0
0.8
0.6
0.4
0.2
0.0
0 [ppm]
50
100
150

A.5.2 [BF$_2$(L2)]BF$_4$

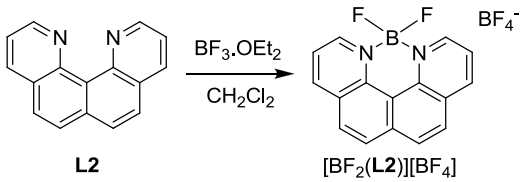

Boron trifluoride diethyl etherate (0.168 mL, 1.336 mmol) was added to 4,9-quino[7,8-*h*]quinoline (**L2**) (0.077 g, 0.334 mmol) in dry CH_2Cl_2 (5 mL) under Ar and stirred at RT for 2 hr. The reaction was diluted with CH_2Cl_2 and the solvent was separated from deposited [BF$_2$(**L2**)][BF$_4$] and dried under vacuum. The product was then set up for crystallisation by vapour diffusion of diethyl ether into a MeCN solution containing [BF$_2$(**L2**)][BF$_4$]. Colourless crystal needles formed after one day, however these did not diffract. A couple of the crystals formed as prisms and were suitable for X-ray crystallography. These crystals were shown to contain 10% of the chloride containing ligand, [BF$_2$(**L1**)][BF$_4$], which appeared to act as a template for the formation of X-ray suitable crystals of [BF$_2$(**L2**)][BF$_4$]. ^{1}H NMR (500 MHz, CD_3CN) δ 8.43 (dd, *J* = 5.7, 8.2, 2H; 3,10-*H*), 8.59 (d, *J* = 8.1, 2H; 6,7-*H*), 8.66 (d, *J* = 8.1, 2H; 5,8-*H*), 9.37 (dd, *J* = 1.3, 8.2, 2H; 4,9-*H*), 9.58 (m, 2H; 2,11-*H*); ^{13}C NMR (125 MHz, CD_3CN) δ 124.7 (s), 128.5 (q), 130.5 (s), 131.3 (s), 136.1 (q), 138.5 (q), 146.3 (s), 147.3 (s); ^{11}B NMR (160 MHz, CD_3CN) 1.97 (t, *J* = 27 Hz, 1B; *B*F$_2$), -1.17 (s, 1B; *B*F$_4$); ^{19}F NMR (376 MHz, CD_3CN) -134.1 (q, *J* = 27 Hz, 2F; B*F*$_2$), -151.71 (s, 4F; B*F*$_4$); MS for $C_{16}H_{10}N_2.BF_2^+$ (M^+) 279.27. $C_{16}H_{10}N_2BF_2^+ \bullet BF_4^- \bullet 0.75H_2O$ (384.10): calcd. C 50.65, H 3.06, N 7.38; found C 50.76, H 3.09, N 7.45.

Crystal data for [BF$_2$(**L2**)][BF$_4$].CH_3CN. $C_{18}H_{13}N_3B_2F_6$, green block, dimensions 0.4 x 0.3 x 0.1 mm, monoclinic, space group $P2_1/c$, a = 7.9589(16), b = 14.153(3), c = 15.609(3) Å, α = 90.00°, β = 95.54(3)°, γ = 90.00°, U = 1750.0(6) Å^3, μ = 3.573 mm^{-1}, Z = 4, D_c = 1.544 g cm^{-3}, F(000) = 824, T = 100(2) K. 10958 Reflections were collected using a Rigaku MM007 rotating anode in the range $6.52 < 2\theta < 143.98°$. A semi-empirical absorption correction (ABSCOR; Higashi, 1995) was applied. The 3289 independent reflections were used to solve the structure by direct methods (SHELXS97) which resulted in the location of

all non-hydrogen atoms. All non-hydrogen atoms were made anisotropic and the refinement (SHELXL97) of 264 parameters converged to R_1 = 0.0684 [for 2949 reflections having $I > 4\sigma(I)$], wR_2 = 0.1838 and goodness of fit 1.066 (for all 2949 F^2 data). Peak / hole 1.697 / -0.290 e Å^{-3}.

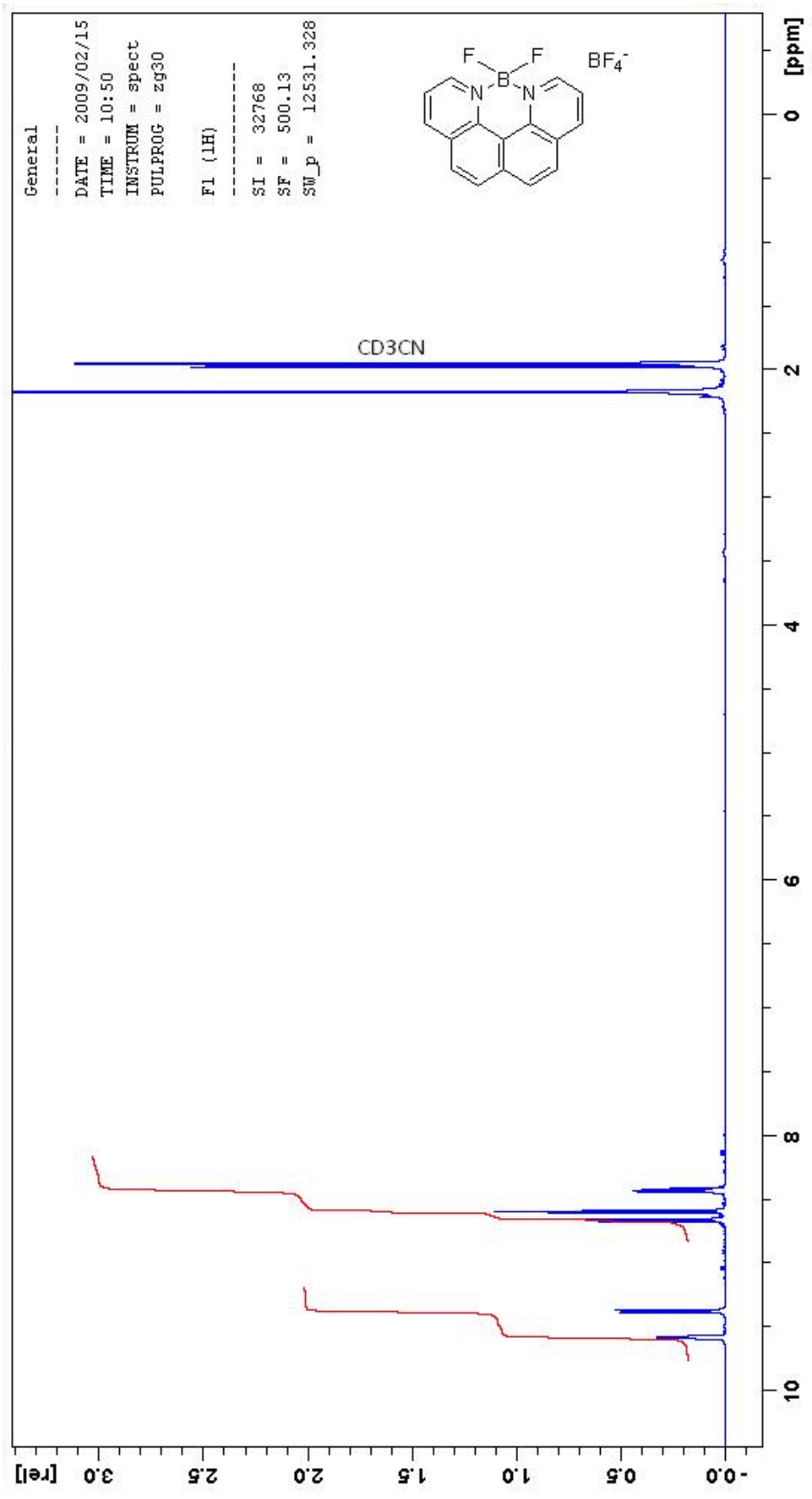
General
DATE = 2009/02/15
TIME = 10:50
INSTRUM = spect
PULPROG = zg30
F1 (1H)
SI = 32768
SF = 500.13
SW_p = 12531.328
CD3CN
BF4-
[rel]
[ppm]

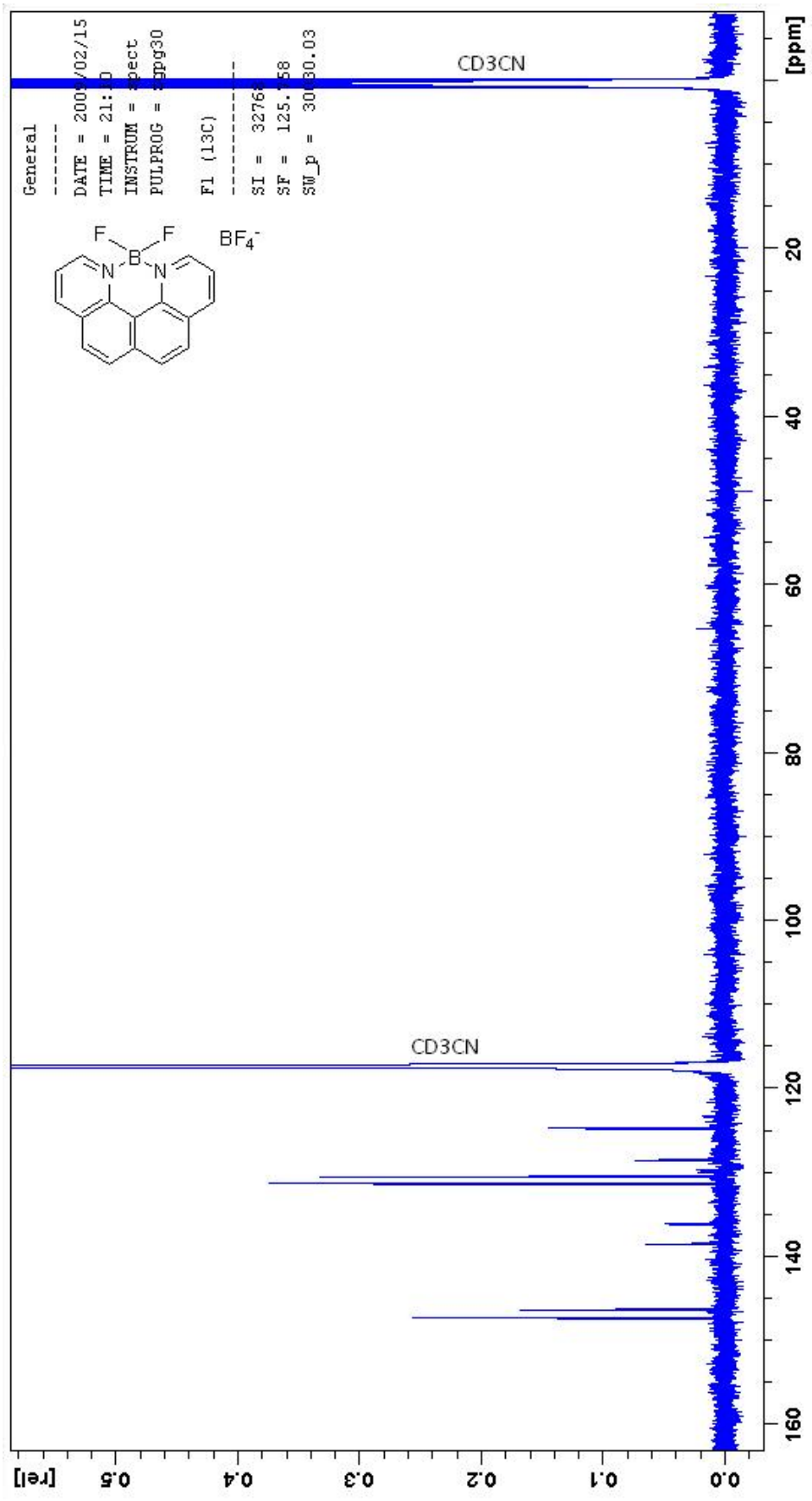
General
DATE = 2009/02/15
TIME = 21:10
INSTRUM = spect
PULPROG = zgpg30
F1 (13C)
SI = 32768
SF = 125.758
SW_p = 30030.03
F
F
B
N
N
BF4-
CD3CN
CD3CN
[ppm]
[rel]

A.5.3 Attempted beryllium complex with L1

4,9-Dichloroquino[7,8-*h*]quinoline (**L1**) (0.010 g, 33.4 µmol), beryllium sulfate 0.99 M in H_2O (24.0 µL, 33.4 µmol) and triethylamine (46.2 µL, 334 µmol) in DMF (1 mL) were stirred together for 16 h at 50 ^oC. The ^1H and ^{13}C NMR of the reaction mixture could not be measured due to use of non-deuterated solvents and incomplete complexation. ^9Be NMR (42.17 MHz, DMF) δ 2.25 (line width 220 Hz). The Mass Spectrum, Elemental Analysis and Melting Point were not measured as handling of beryllium solids would be involved.

A.5.4 Attempted beryllium complex with L5

4-Chloro-9-*p*-*tert*-butylphenylquino[7,8-*h*]quinoline (**L5**) (0.010 g, 24.2 µmol), beryllium sulfate 0.99 M in H_2O (26.0 µL, 24.2 µmol) and triethylamine (33.5 µL, 242 µmol) in DMF (1 mL) were stirred together for 16 h at 50 ^oC. The ^1H and ^{13}C NMR of the reaction mixture could not be measured due to use of non-deuterated solvents and incomplete complexation. ^9Be NMR (42.17 MHz, DMF) δ 1.69 (line width 210 Hz). The Mass Spectrum, Elemental Analysis and Melting Point were not measured as handling of beryllium solids would be involved.

A.5.5 $[Cu(L1)(CH_3CN)_3](ClO_4)_2$

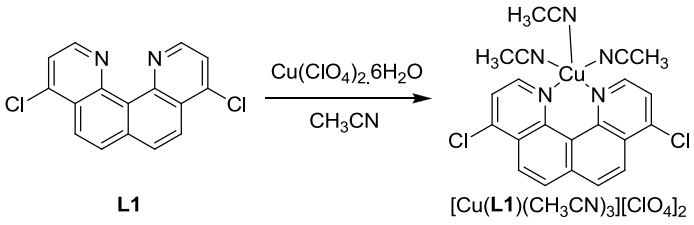

Copper perchlorate (0.068 g, 0.184 mmol) in dry MeCN (1 mL) was added to a suspension 4,9-dichloroquino[7,8-*h*]quinoline (**L1**) (0.050 g, 0.167 mmol) in dry MeCN (5 mL) under

Ar and stirred at RT for 30 min. The mother liquor was separated from deposited [Cu(**L1**)$(CH_3CN)_3$][ClO_4]$_2$ and dried under vacuum. The product was then set up for crystallisation by vapour diffusion of diethyl ether into a MeCN solution containing [Cu(**L1**)$(CH_3CN)_3$][ClO_4]$_2$. Green crystals suitable for X-ray crystallography were obtained after two days, and remained stable for one day whilst in solution. Elemental analysis did not match the crystal structure; however it was consistent with the most of the acetonitrile molecules being replaced by water molecules. $C_{16}H_8Cl_2CuN_2$•$2ClO_4$•$2.2H_2O$•$0.25CH_3CN$: calcd. C 32.41, H 2.17, N 5.15; found C 32.41, H 2.42, N 5.15.

Crystal data for [Cu(**L1**)$(CH_3CN)_3(ClO_4)$][ClO_4]. $C_{22}H_{17}N_5O_8CuCl_4$, green block, dimensions 0.2 x 0.1 x 0.05 mm, monoclinic, space group $P2_1/c$, a = 12.696(3), b = 13.902(3), c = 15.476(3) Å, α = 90.00°, β = 98.60(3)°, γ = 90.00°, U = 2700.8(10) Å^3, μ = 5.290 mm^{-1}, Z = 4, D_c = 1.684 g cm^{-3}, F(000) = 1380, T = 100(2) K. 904 Reflections were collected using a Rigaku MM007 rotating anode in the range 9.03 < 2θ < 143.44°. A semi-empirical absorption correction (ABSCOR; Higashi, 1995) was applied. The 3289 independent reflections were used to solve the structure by direct methods (SHELXS97) which resulted in the location of all non-hydrogen atoms. All non-hydrogen atoms were made anisotropic and the refinement (SHELXL97) of 364 parameters converged to R_1 = 0.0525 [for 2949 reflections having $I > 4\sigma(I)$], wR_2 = 0.1381 and goodness of fit 1.075 (for all 2949 F^2 data). Peak / hole 1.205 / -0.782 e Å^{-3}.

A.5.6 [Cu(L2)$(CH_3CN)_3$][ClO_4]$_2$

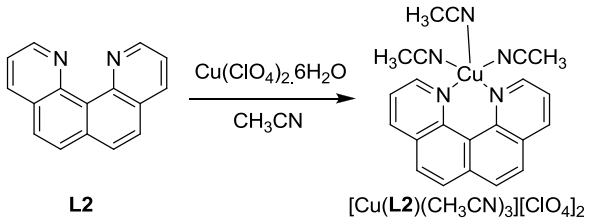

Copper perchlorate (0.080 g, 0.215 mmol) in dry MeCN (1 mL) was added to a suspension 4,9-dichloroquino[7,8-*h*]quinoline, **L2**, (0.045 g, 0.196 mmol) in dry MeCN (5 mL) under

Ar and stirred at RT for 30 min. The mother liquor was separated from deposited [Cu(**L2**)(CH_3CN)$_3$][ClO_4]$_2$ and dried under vacuum. The product was then set up for crystallisation by vapour diffusion of diethyl ether into a MeCN solution containing [Cu(**L2**)(CH_3CN)$_3$][ClO_4]$_2$. Green crystals suitable for X-ray crystallography were obtained after two days, and remained stable for one day whilst in solution. Elemental analysis did not match the crystal structure, however, was consistent with the three acetonitrile molecules being replaced by water molecules. $C_{16}H_{10}CuN_2$•2ClO_4•2.5H_2O: calcd. C 35.74, H 2.81, N 5.21; found C 35.81, H 2.68, N 5.21.

Crystal data for [Cu(**L2**)(CH_3CN)$_3$(ClO_4)][ClO_4]. $C_{22}H_{19}N_5O_8CuCl_2$, green block, dimensions 0.2 x 0.1 x 0.1 mm, triclinic, space group *P*-1, a = 8.6209(17), b = 10.128(2), c = 14.243(3) Å, α = 92.82(2)^o, β = 96.62(3)^o, γ = 90.68(4)^o, U = 1233.7(4) Å^3, μ = 3.767 mm^{-1}, Z = 2, D_c = 1.658 g cm^{-3}, F(000) = 626, T = 100(2) K. 10378 Reflections were collected using a Rigaku MM007 rotating anode in the range 6.72 < 2θ < 143.53^o. A semi-empirical absorption correction (ABSCOR; Higashi, 1995) was applied. The 3534 independent reflections were used to solve the structure by direct methods (SHELXS97) which resulted in the location of all non-hydrogen atoms. All non-hydrogen atoms were made anisotropic and the refinement (SHELXL97) of 347 parameters converged to R_1 = 0.0704 [for 2978 reflections having $I > 4\sigma(I)$], wR_2 = 0.1699 and goodness of fit 1.112 (for all 2978 F^2 data). Peak / hole 0.702 / -1.557 e Å^{-3}.

A.5.7 Fluorescence Experimental

Coumarin 153 (0.00743 g) was dissolved in acetonitrile and made up to the mark in a 100 mL volumetric flask. 0.100 mL of the stock solution was made up to 10 mL which gave an absorbance of 0.0501 at the λ_{max}, 421.5 nm. The excitation wavelength used in this study was 420 nm. The absorbance at the excitation wavelength (A_S) was 0.0499. On the fluorometer, both the emission and excitation slit widths were set to 2.5 nm to fit the spectras within the measurement scale. These parameters were arbitrary; however, they must be kept constant for each sample measurement. The integrated area under the fluorescence emission curve (F_S) was 44570. The literature value for the quantum yield in

acetonitrile was 0.56.[134] The refractive index of acetonitrile is 1.3441. The normalised absorption and emission spectras are shown below.

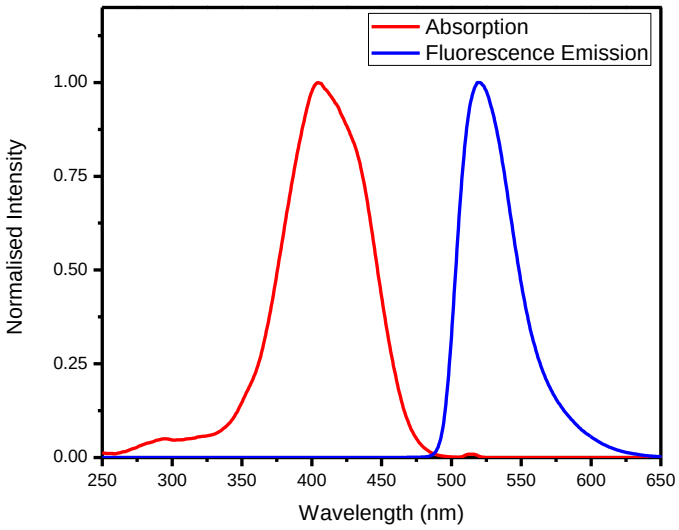

Normalised absorption and emission spectra of coumarin 153

Acridine orange (as hemi(zinc chloride) salt) (0.00735 g) was dissolved in basic ethanol (5 % triethylamine) and made up to the mark in a 100 mL volumetric flask. 0.150 mL of the stock solution was diluted to 10 mL which gave an absorbance of 0.0517 at the λ_{max}, 431.5 nm. The excitation wavelength used in this study was 420 nm. The absorbance at the excitation wavelength (A_S) was 0.0438. On the fluorometer, both the emission and excitation slit widths were set to 2.5 nm. The integrated area under the fluorescence emission curve (F_S) was 16053. The literature value for the quantum yield in basic ethanol was 0.20.[193] The refractive index of basic ethanol was measured as 1.3652. The normalised absorption and emission spectras are shown below.

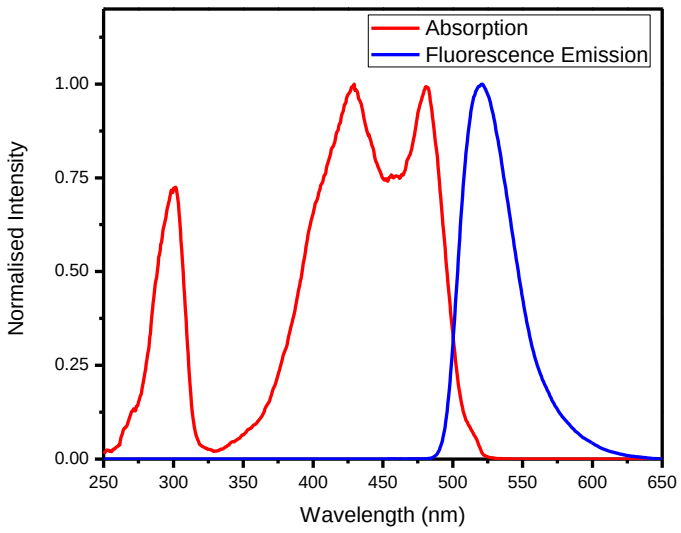

Normalised absorption and emission spectra of acridine orange

Crystals of $[BF_2(\mathbf{L1})][BF_4]$ (0.00567 g) were dissolved in acetonitrile and made up to the mark in a 100 mL volumetric flask. 0.500 mL of the stock solution was diluted to 10 mL which gave an absorbance of 0.0465 at the λ_{max}, 416.5 nm. The excitation wavelength used in this study was 420 nm. The absorbance at the excitation wavelength (A_S) was 0.0461. On the fluorometer, both the emission and excitation slit widths were set to 2.5 nm to fit the spectras within the measurement scale. The integrated area under the fluorescence emission curve (F_S) was 697.

$[BF_2(\mathbf{L2})][BF_4]$ was not fluorescent on the magnitude used for the other samples in the study.

A.5.8 Surface Enhanced Raman Spectroscopy Experimental

Silver colloids were prepared following Lee and Meisel's Method C.[194] Wavenumber calibration was performed using Raman bands from cyclohexane. $[BF_2(\mathbf{L1})][BF_4]$ was added to the solution in order to obtain a final concentration of about 5 mM. Excitation was provided by 514.5 nm radiation from a continuous wave mult-line Stellar-PRO 150

mW Argon laser and the samples were contained in capillary cells. The laser output was adjusted to give between 15 – 20 mW at the sample. The incident beam and the collection lens were arranged in a 135^{o} or 180^{o} back-scattering geometry to reduce Raman intensity reduction by self-absorption. An aperture-matched lens was used to focus scattered light a narrow band line-rejection (notch) filter (Kaiser Optical Systems) or long-pass edge filter (Irdian) and a quartz wedge (Spex) and onto the 100 um entrance slit of a spectrograph (Action Research SpectraPro 500i). The collected light was dispersed in the horizontal plane by a liquid nitrogen cooled back-illuminated Spec-10:100B CCD controlled by a ST-133 controller and WinSpec/32 (version 2.5.8.1) software (Roper Scientific, Princeton Instruments). The data was processed using Origin Pro 7.5.

A.6 Chapter 5 Experimental

A.6.1 2-(2-Pyridylmethyl)pyridine (504)

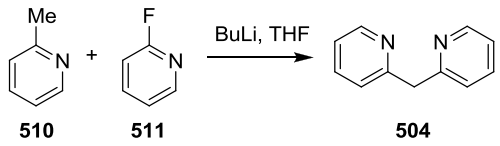

Dipyridin-2-ylmethane (**504**) was synthesised according to the known literature procedure.[147] 2-Picoline (**510**) (0.816 mL, 8.24 mmol) in dry THF (5 mL) was cooled to -78 ^{o}C under Ar. *N*-Butyllithium (0.515 mL, 8.24 mmol, as a 1.6 M solution in hexane) was added and the reaction stirred at -78 ^{o}C under Ar for 1 hr, slowly warming to -20 ^{o}C. 2-Fluoropyridine (**511**) (0.344 mL, 4.12 mmol) was added and the reaction was heated to reflux for 30 min. The reaction was diluted with CH_2Cl_2 (200 mL) and washed with water (200 mL). The organic layer was filtered and dried over $MgSO_4$. Concentration *in vacuo* gave **504** as a brown oil which was used without further purification (0.678 g, 97 %). ^{1}H NMR (500 MHz, $CDCl_3$) δ 4.36 (s, 2H; C*H*$_2$), 7.14 (dd, *J* = 4.8, 7.4, 2H; Ar*H*), 7.28 (d, *J* = 7.8, 2H; Ar*H*), 7.61 (td, *J* = 1.8, 7.8, 2H; Ar*H*), 8.55 (dd, *J* = 1.8, 4.8, 2H; Ar*H*); ^{13}C NMR (125 MHz, $CDCl_3$) δ 47.0 (d), 121.5 (s), 123.6 (s), 136.7 (s), 149.3 (s), 159.2 (q). MS for $C_{11}H_{10}N_2$ (MH^+) 171.23.

A.6.2 2-(2-Methoxyphenyl)pyridine (508)

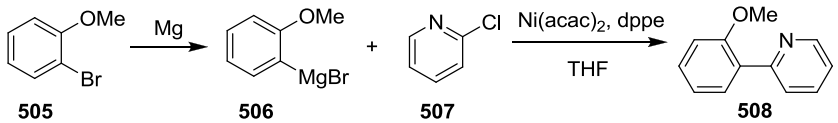

2-(2-Methoxyphenyl)pyridine (**508**) was synthesised according to the known literature procedure.[146] Magnesium (0.390 g, 16.2 mmol) was heated under vacuum for a short

period, a few crystals of iodine was added and 2-bromoanisole (**505**) (2.00 mL, 16.2 mmol) in dry THF (50 mL) was added. The mixture was stirred at RT under Ar for 2 hr. 2-Chloropyridine (**507**) (1.36 mL, 14.5 mmol), nickel acetylacetonate (0.190 g, 0.739 mmol) and 1,2-*bis*(diphenylphosphino)ethane (0.290 g, 0.739 mmol) in dry THF (20 mL) was added to the reaction mixture and then stirred at RT for 18 hr. The reaction was diluted with CH_2Cl_2 (200 mL) and washed with water (200 mL). The organic layer was filtered and dried over $MgSO_4$. The colourless liquid **508** was purified by silica gel column chromatography using 1:4 EtOAc / hexanes (1.87 g, 62 %). R_f = 0.14 (5:1 hexanes / EtOAc). ^{1}H NMR (500 MHz, $CDCl_3$) δ 3.81 (s, 3H; C*H*$_3$), 6.97 (d, *J* = 8.4, 1H; Ar*H*), 7.07 (td, *J* = 0.9, 7.6, 1H; Ar*H*), 7.17 (ddd, *J* = 0.9, 4.8, 7.6, 1H; Ar*H*), 7.35 (td, *J* = 1.8, 8.4, 1H; Ar*H*), 7.67 (td, *J* = 1.8, 8.0, 1H; Ar*H*), 7.77 (dd, *J* = 1.8, 7.6, 1H; Ar*H*), 7.80 (dt, *J* = 0.8, 8.0, 1H; Ar*H*), 8.69 (m, 1H; Ar*H*); ^{13}C NMR (125 MHz, $CDCl_3$) δ 55.4 (t), 111.2 (s), 120.9 (s), 121.5 (s), 125.0 (s), 128.9 (q), 129.8 (s), 131.0 (s), 135.6 (s), 149.1 (s), 155.9 (q), 156.8 (q). Not ionised in MS.

A.6.3 2-Chloro-6-(2-methoxyphenyl)pyridine (509)

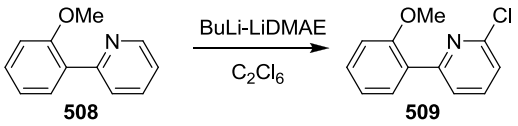

508 **509**

2-Chloro-6-(2-methoxyphenyl)pyridine (**509**) was synthesised according to the known literature procedure.[146] *N*-Butyllithium (0.266 mL, 4.26 mmol, as a 1.6 M solution in hexane) was added to 2-(dimethylamino)ethanol (0.212 g, 2.12 mmol) in dry toluene (20 mL) and the reaction stirred at -20 ^{o}C under Ar for 30 min. 2-(2-Methoxyphenyl)pyridine (**508**) (0.131 g, 0.704 mmol) was added and the reaction was stirred at -20 ^{o}C for 1 hr. The reaction was cooled to -78 ^{o}C and hexachloroethane (0.537 g, 2.26 mmol) in dry toluene (5 mL) was added and the reaction was allowed to warm to 0 ^{o}C over 1 hr. The reaction was diluted with diethyl ether (200 mL) and washed with water (200 mL). The organic layer was filtered and dried over $MgSO_4$. The yellow oil **509** was purified by silica gel column chromatography using 1:9 EtOAc / hexanes (0.101 g, 65 %). R_f = 0.30 (5:1 hexanes /

EtOAc). ^{1}H NMR (500 MHz, $CDCl_3$) δ 3.89 (s, 3H; C*H*$_3$), 7.01 (d, *J* = 8.3, 1H; Ar*H*), 7.10 (t, *J* = 7.6, 1H; Ar*H*), 7.25 (d, *J* = 8.0, 1H; Ar*H*), 7.40 (t, *J* = 7.4, 1H; Ar*H*), 7.67 (t, *J* = 7.6, 1H; Ar*H*), 7.84 (d, *J* = 8.0, 1H; Ar*H*), 7.89 (d, *J* = 7.6, 1H; Ar*H*); ^{13}C NMR (125 MHz, $CDCl_3$) δ 55.5 (t), 111.3 (s), 121.0 (s), 122.0 (s), 123.5 (s), 127.3 (q), 130.5 (s), 131.3 (s), 138.2 (s), 150.7 (q), 156.4 (q), 157.0 (q). MS for $C_{12}H_{10}NO^{35}Cl$ (MH^+) 220.19.

A.6.4 2-Bromo-6-(2-methoxyphenyl)pyridine (513)

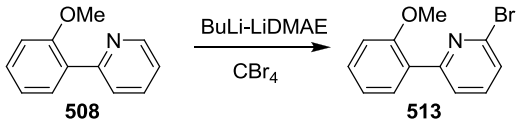

508 **513**

2-Bromo-6-(2-methoxyphenyl)pyridine (**513**) was synthesised by analogy to the known literature procedure.[146] *N*-Butyllithium (0.186 mL, 2.98 mmol, as a 1.6 M solution in hexane) was added to 2-(dimethylamino)ethanol (0.149 mL, 1.49 mmol) in dry toluene (10 mL) and the reaction stirred at -20 ^{o}C under Ar for 30 min. 2-(2-Methoxyphenyl)pyridine (**508**) (0.092 g, 0.497 mmol) was added and the reaction was stirred at -20 ^{o}C for 1 hr. The reaction was cooled to -78 ^{o}C and carbon tetrabromide (0.529 g, 1.59 mmol) in dry toluene (2.5 mL) was added and the reaction was allowed to warm to 0 ^{o}C over 1 hr. The reaction was diluted with diethyl ether (200 mL) and washed with water (200 mL). The organic layer was filtered and dried over $MgSO_4$. **513** was purified by silica gel column chromatography using 1:9 ethyl acetate / hexanes (0.080 g, 61 %). R_f = 0.34 (5:1 hexanes / EtOAc). ^{1}H NMR (500 MHz, $CDCl_3$) δ 3.89 (s, 3H; C*H*$_3$), 7.00 (d, *J* = 8.5, 1H; Ar*H*), 7.09 (t, *J* = 7.6, 1H; Ar*H*), 7.39 (m, 2H; Ar*H*), 7.56 (t, *J* = 7.8, 1H; Ar*H*), 7.88 (d, *J* = 7.8, 2H; Ar*H*); ^{13}C NMR (125 MHz, $CDCl_3$) δ 55.5 (t), 111.3 (s), 121.1 (s), 123.8 (s), 125.8 (s), 127.2 (q), 130.5 (s), 131.3 (s), 138.0 (s), 141.4 (q), 156.9 (q), 157.0 (q). HRMS calculated for $C_{12}H_{10}NO^{79}Br$ (MH^+) 264.0064, found 264.0057 (ESI+).

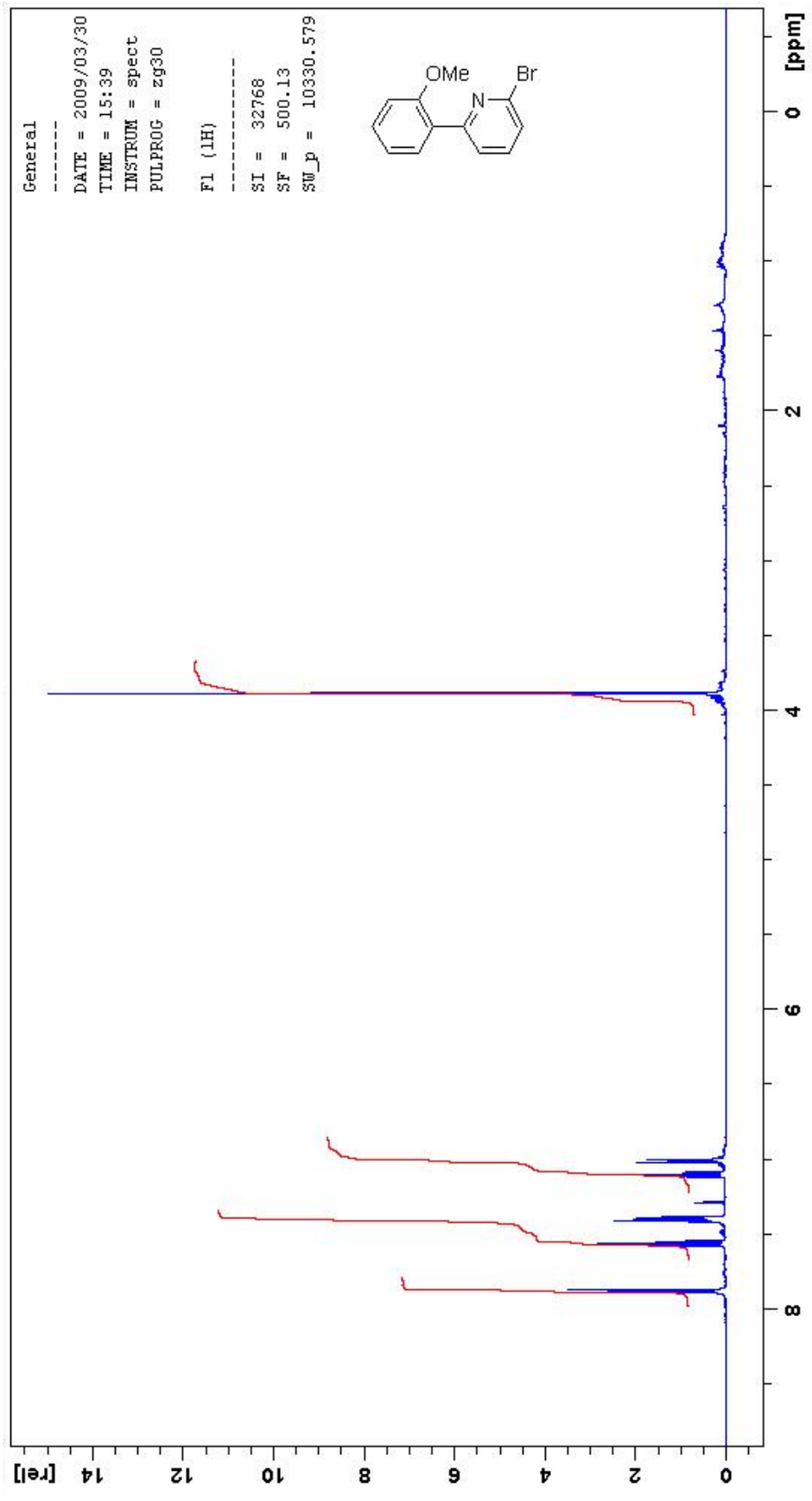
General
DATE = 2009/03/30
TIME = 15:39
INSTRUM = spect
PULPROG = zg30
F1 (1H)
SI = 32768
SF = 500.13
SW_p = 10330.579
OMe
Br
N
[rel]
[ppm]

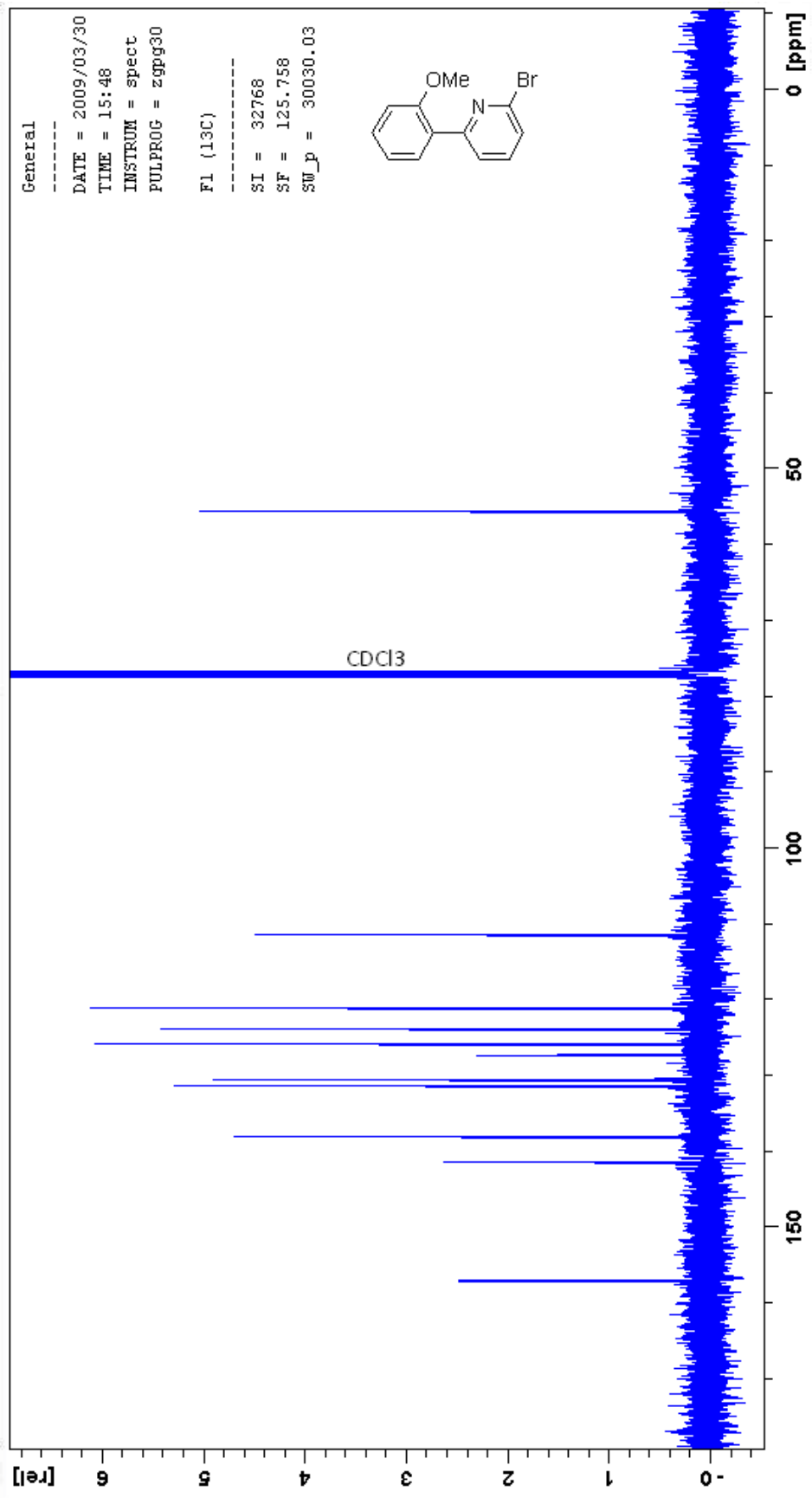
General
DATE = 2009/03/30
TIME = 15:48
INSTRUM = spect
PULPROG = zgpg30
F1 (13C)
SI = 32768
SF = 125.758
SW_p = 30030.03
OMe
Br
N
CDCl3
[rel]
[ppm]

A.6.5 2,2'-(Bromomethylene)dipyridine (514)

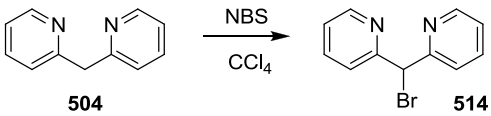

2,2'-(Bromomethylene)dipyridine (**514**) was synthesised according to the known literature procedure.[195] 2-(2-Pyridylmethyl)pyridine (**504**) (0.151 mL, 0.888 mmol) and *N*-bromosuccinimide (0.213 g, 0.903 mmol) in CCl_4 (2 mL) were refluxed for 30 min. The reaction was diluted with CH_2Cl_2 (200 mL) and washed with water (200 mL). The organic layer was filtered and dried over $MgSO_4$. The brown oil **514** was purified by silica gel column chromatography using 98:2 CH_2Cl_2 / MeOH (0.092 g, 42 %). R_f = 0.68 (9:1 CH_2Cl_2 / MeOH). ^{1}H NMR (500 MHz, $CDCl_3$) δ 4.36 (s, 1H; C*H*), 7.18 (ddd, *J* = 1.6, 4.8, 7.6, 2H; Ar*H*), 7.69 (td, *J* = 1.8, 7.6, 2H; Ar*H*), 7.72 (dt, *J* = 1.8, 7.6, 2H; Ar*H*), 8.57 (dd, *J* = 1.8, 4.8, 2H; Ar*H*); ^{13}C NMR (125 MHz, $CDCl_3$) δ 54.5 (s), 122.9 (s), 123.5 (s), 136.9 (s), 149.1 (s), 158.3 (q).

A.6.6 6-(2-Methoxyphenyl)-N,N-di(pyridin-2-yl)pyridin-2-amine (518)

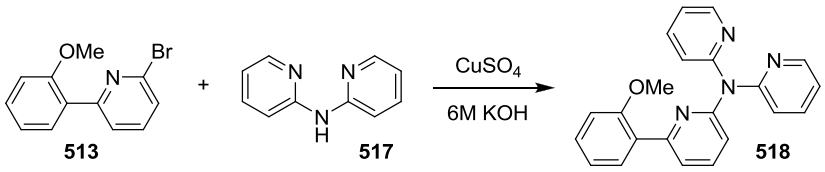

2-Bromo-6-(2-methoxyphenyl)pyridine (**513**) (0.313 g, 1.186 mmol), dipyridin-2-ylamine (**517**) (0.101 g, 0.591 mmol) and copper sulfate pentahydrate (0.030g, 0.120 mmol) in 6M KOH (1 mL) were heated under microwave irradiation for 15 min at 160 ^{o}C. The reaction was diluted with CH_2Cl_2 (200 mL) and washed with water (200 mL). The organic layer was filtered and dried over $MgSO_4$. The colourless oil **518** was purified by silica gel column chromatography using 99:1 CH_2Cl_2 / MeOH (0.197 g, 98 %). The oil could be collected as a colourless powder by adding a few drops of diethyl ether and removing the solvent on a high vacuum pump. R_f = 0.46 (9:1 CH_2Cl_2 / MeOH). ^{1}H NMR (500 MHz,

$CDCl_3$) δ 3.87 (s, 3H; C*H*$_3$), 6.96 (m, 3H; Ar*H*), 7.03 (dd, *J* = 4.8, 7.2, 2H; Ar*H*), 7.21 (d, *J* = 8.4, 2H; Ar*H*), 7.31 (dt, *J* = 1.5, 6.0, 1H; Ar*H*), 7.60 – 7.69 (m, 5H; Ar*H*), 8.31 (dd, *J* = 1.8, 4.8, 2H; Ar*H*); ^{13}C NMR (125 MHz, $CDCl_3$) δ 55.6 (t), 111.4 (s), 116.3 (s), 118.8 (s), 119.1 (s), 120.8 (s), 120.9 (s), 128.6 (q), 129.8 (s), 131.3 (s), 137.4 (s), 137.6 (q), 148.7 (s), 154.8 (q), 156.7 (q), 157.3 (q), 157.5 (s). HRMS calculated for $C_{22}H_{18}N_4O$ (MH^+) 355.1540, found 355.1547 (ESI+).

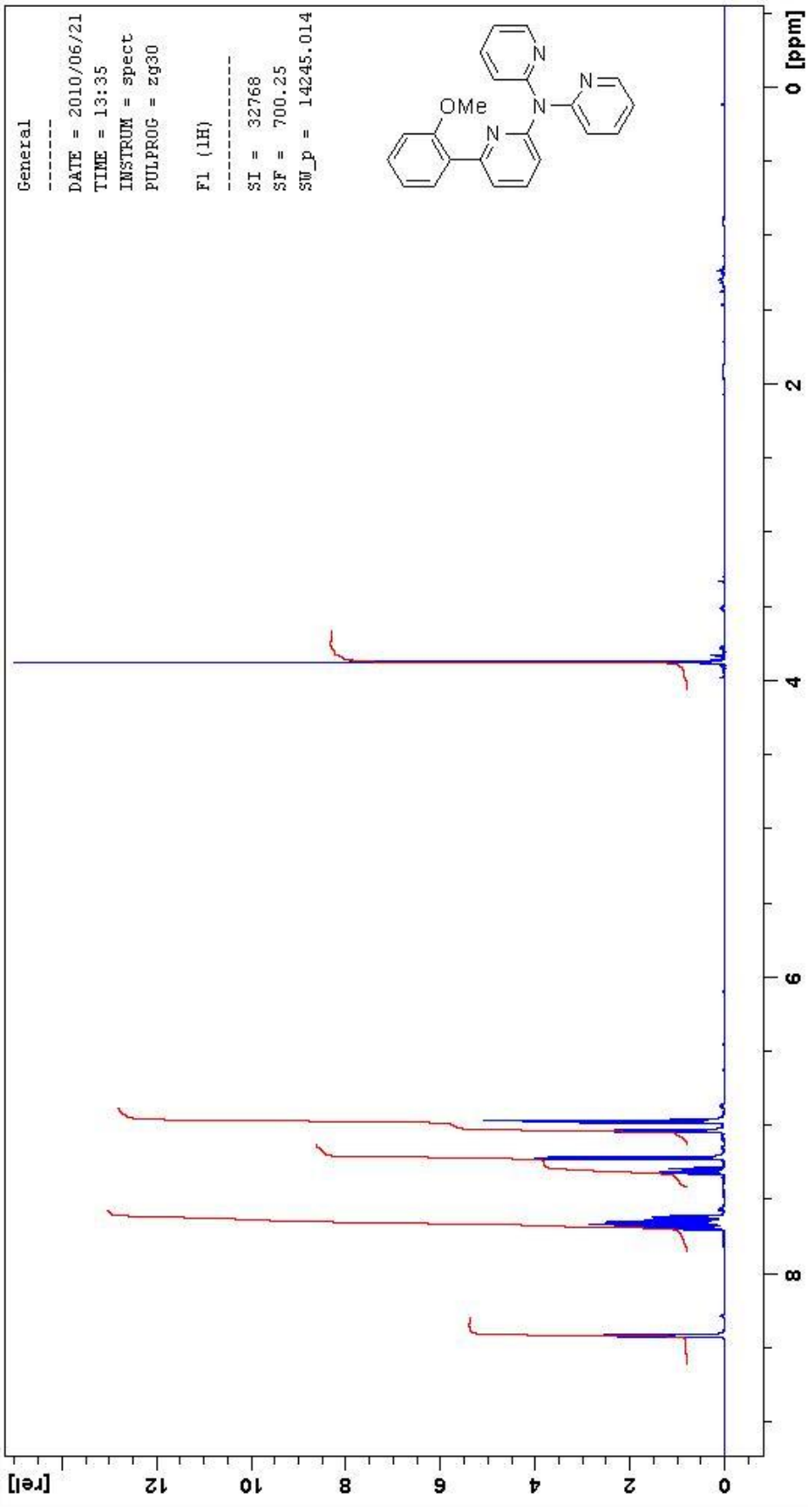
General
DATE = 2010/06/21
TIME = 13:35
INSTRUM = spect
PULPROG = zg30
F1 (1H)
SI = 32768
SF = 700.25
SW_p = 14245.014
OMe
N
N
N
N
[rel]
0
2
4
6
8
10
12
0 [ppm]
2
4
6
8

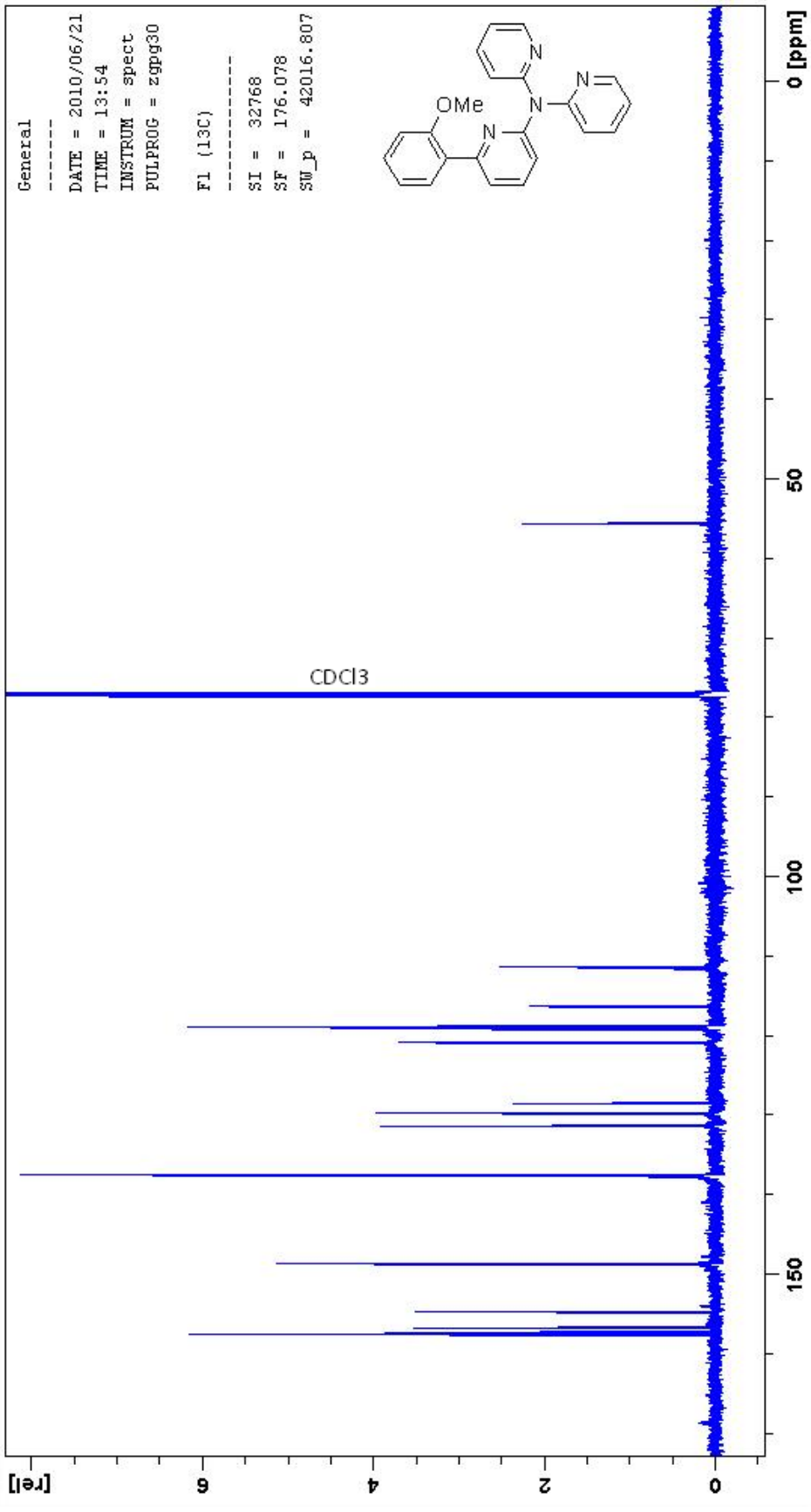
General
DATE = 2010/06/21
TIME = 13:54
INSTRUM = spect
PULPROG = zgpg30
F1 (13C)
SI = 32768
SF = 176.078
SW_p = 42016.807
OMe
N
N
N
N
CDCl3
[rel]
0
2
4
6
150
100
50
0 [ppm]

A.6.7 2-(6-(Dipyridin-2-ylamino)pyridin-2-yl)phenol (L14)

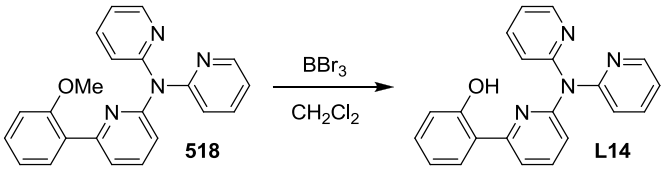

6-(2-Methoxyphenyl)-*N*,*N*-di(pyridin-2-yl)pyridin-2-amine (**518**) (0.050 g, 0.141 mmol) in CH_2Cl_2 (5 mL) was cooled to -78 ^oC and boron tribromide as a 1M solution in CH_2Cl_2 (0.706 mL, 0.706 mmol) was added and the reaction was left to stir at RT overnight. The reaction was diluted with CH_2Cl_2 (200 mL) and basified with 2M NaOH (20 mL) then washed with water (200 mL). The organic layer was filtered and dried over $MgSO_4$. The colourless oil **L14** was purified by silica gel column chromatography using 99:1 to 98:2 CH_2Cl_2 / MeOH (0.038 g, 79 %). The oil could be collected as a colourless powder by adding a few drops of diethyl ether and removing the solvent on a high vacuum pump. R_f = 0.62 (9:1 DCM / MeOH). ^{1}H NMR (500 MHz, $CDCl_3$) δ 6.87 (t, *J* = 8.2, 2H; Ar*H*), 7.08 (d, *J* = 4.8, 8.2, 1H; Ar*H*), 7.13 – 7.17 (m, 4H; Ar*H*), 7.23 (t, *J* = 6.7, 1H; Ar*H*), 7.58 (d, *J* = 7.9, 1H; Ar*H*), 7.71 – 7.79 (m, 4H; Ar*H*), 8.49 (dd, *J* = 0.9, 4.7, 2H; Ar*H*), 12.54 (s, 1H; O*H*); ^{13}C NMR (125 MHz, $CDCl_3$) δ 114.0 (s), 114.7 (s), 118.3 (s), 118.8 (s), 119.2 (s), 119.3 (q), 120.4 (s), 126.5 (s), 131.2 (s), 138.4 (q), 139.1 (s), 149.3 (s), 154.5 (q), 156.5 (q), 156.8 (s), 159.1 (q). HRMS calculated for $C_{21}H_{16}N_4O$ (MH^+) 341.1384, found 341.1387 (ESI+).

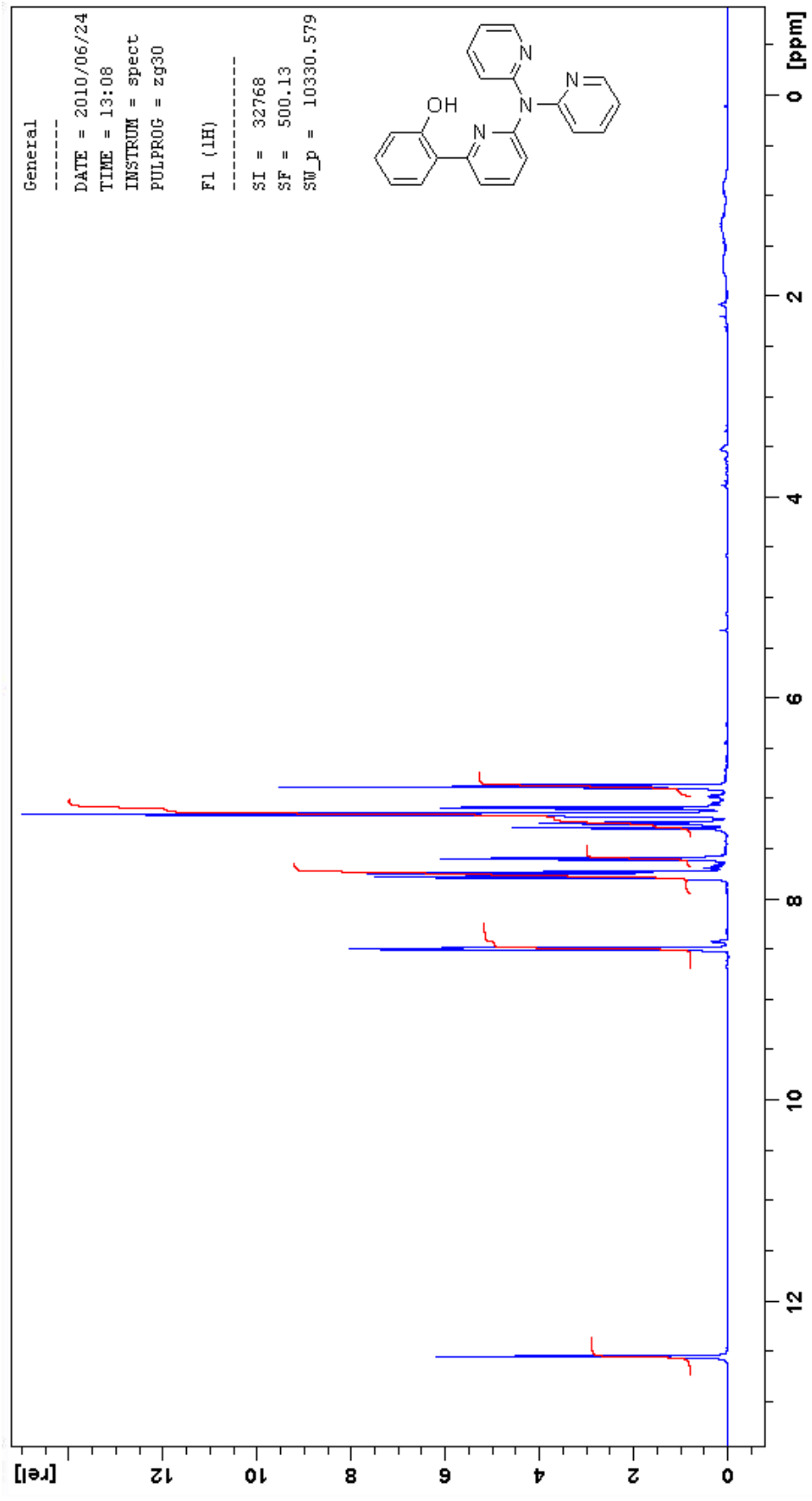
General
DATE = 2010/06/24
TIME = 13:08
INSTRUM = spect
PULPROG = zg30
F1 (1H)
SI = 32768
SF = 500.13
SW_p = 10330.579
OH
N
N
N
N
[rel]
[ppm]

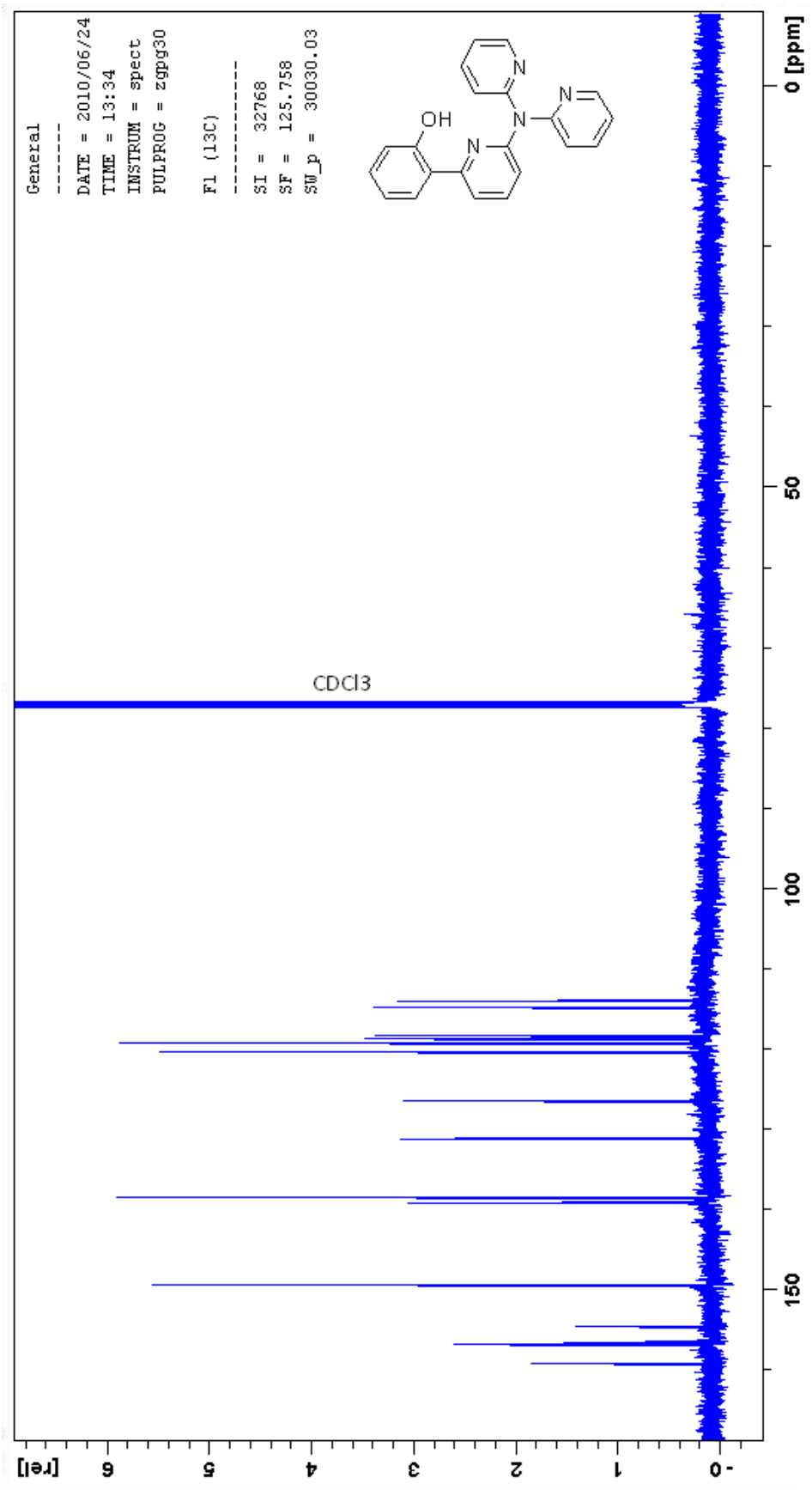
General
DATE = 2010/06/24
TIME = 13:34
INSTRUM = spect
PULPROG = zgpg30
F1 (13C)
SI = 32768
SF = 125.758
SW_p = 30030.03
OH
N
N
N
CDCl3
0 [ppm]
50
100
150
[rel]
0
1
2
3
4
5
6

A.6.8 N-(2-Bromophenyl)cinnamamide (533)

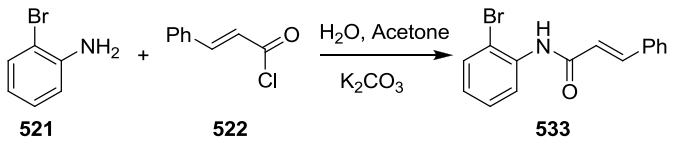

521 **522** **533**

N-(2-Bromophenyl)cinnamamide (**533**) was synthesised according to the known literature procedure.[156] To potassium carbonate (1.98 g, 14.5 mmol) dissolved in a mixture of water (20 mL) and acetone (16 mL) was added 2-bromoaniline (**521**) (1.66 g, 9.64 mmol) and cinnamoyl chloride (**522**) (1.60 g, 9.64 mmol). The mixture was sonicated (to ensure dissolution of reactants) then stirred for 2 hr at RT. Water (40 mL) was added to the reaction and the resulting precipitate was filtered and dried to give **533** as a white powder (2.66 g, 91 %) which was used directly without further purification. R_f = 0.70 (1:2 hexanes / EtOAc). ^{1}H NMR (500 MHz, $CDCl_3$) δ 6.58 (d, *J* = 15.5, 1H; C*H*), 6.98 (dt, *J* = 1.6, 7.6, 1H; Ar*H*), 7.31 (dt, *J* = 1.6, 7.6, 1H; Ar*H*), 7.36-7.39 (m, 3H; Ar*H*), 7.52-7.55 (m, 3H; Ar*H*), 7.75 (d, *J* = 15.5, 1H; C*H*), 7.83 (s, 1H; N*H*), 8.47 (d, *J* = 7.9, 1H; Ar*H*); ^{13}C NMR (125 MHz, $CDCl_3$) δ 113.5 (s), 120.6 (s), 122.1 (q), 125.2 (s), 128.0 (s), 128.4 (s), 128.8 (s), 130.1 (s), 132.2 (s), 134.4 (q), 135.8 (q), 141.8 (s), 142.9 (s), 142.2 (s), 163.8 (q). MS for $C_{15}H_{12}{}^{79}BrNO$ (MH^+) 304.37. M.P. = 148 – 149 ^{o}C.

A.6.9 8-Bromo-2(1H)-quinolinone (523)

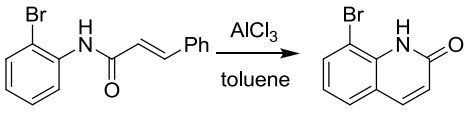

533 **523**

8-Bromoquinolin-2(1*H*)-one (**523**) was synthesised according to the known literature procedure.[156] To *N*-(2-bromophenyl)cinnamamide (**533**) (2.00 g, 6.62 mmol) dissolved in a dry toluene (60 mL) was added aluminium trichloride (5.28 g, 39.7 mmol) and the resultant solution was heated at 125 ^{o}C for 2 hr under Ar. The reaction was diluted with EtOAc (200 mL) then washed with water (200 mL). The organic layer was filtered and dried over

$MgSO_4$ then concentrated under reduced pressure. The white solid **523** was purified by silica gel column chromatography using 1:2 EtOAc / hexanes (0.814 g, 55 %). R_f = 0.34 (1:2 hexanes / EtOAc). ^{1}H NMR (500 MHz, $CDCl_3$) δ 6.68 (d, *J* = 9.6, 1H; Ar*H*), 7.11 (t, *J* = 7.9, 1H; Ar*H*), 7.53 (dd, *J* = 1.1, 7.8, 1H; Ar*H*), 7.72 (dd, *J* = 1.1, 7.8, 1H; Ar*H*), 7.73 (d, *J* = 9.6, 1H; Ar*H*), 9.11 (brs, 1H; N*H*); ^{13}C NMR (125 MHz, $CDCl_3$) δ 109.1 (s), 121.1 (q), 122.9 (q), 123.4 (s), 127.5 (s), 133.6 (s), 135.6 (q), 140.5 (s), 162.1 (q). MS for $C_9H_6NO^{79}Br$ (MH^+) 224.19. M.P. = 174 – 175 °C.

A.6.10 8-Bromo-2-chloroquinoline (524)

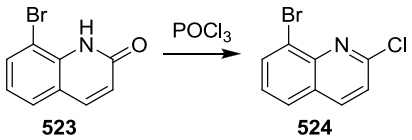

523 **524**

8-Bromo-2-chloroquinoline (**524**) was synthesised according to the known literature procedure.[156] 8-Bromo-2(1*H*)-quinolinone (**523**) (0.800 g, 3.57 mmol) and phosphorus oxychloride (1.60 mL, 17.3 mmol) were added and the reaction heated at 125 °C for 2 hr under Ar. The reaction was diluted with EtOAc (200 mL) and washed with water (200 mL). The organic layer was filtered and dried over $MgSO_4$ then concentrated under reduced pressure. The white solid **524** was purified by silica gel column chromatography using 1:2 EtOAc / hexanes (0.725 g, 84 %). R_f = 0.67 (1:2 hexanes / EtOAc). ^{1}H NMR (500 MHz, $CDCl_3$) δ 7.39 – 7.44 (m, 2H; Ar*H*), 7.78 (d, *J* = 8.1, 1H; Ar*H*), 8.05 (d, *J* = 7.4, 1H; Ar*H*), 8.10 (d, *J* = 8.5, 1H; Ar*H*); ^{13}C NMR (125 MHz, $CDCl_3$) δ 123.5 (s), 123.6 (q), 127.4 (s), 127.4 (s), 128.1 (q), 134.2 (s), 139.3 (s), 145.1 (q), 151.9 (q). Not ionised by MS. M.P. = 102 – 103 °C.

A.6.11 2-Chloroquinoline-8-carboxylic acid (519)

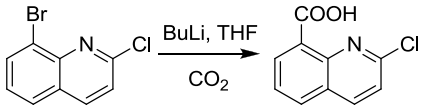

524 519

8-Bromo-2-chloroquinoline (**524**) (0.100 g, 0.413 mmol) in THF (10 mL) was cooled to -78 ^{o}C under Ar. *N*-butyllithium (0.258 mL, 0.413 mmol, as a 1.6 M solution in hexane) was added and the reaction stirred at -78 ^{o}C for 15 min. CO_2(g) was bubbled through the solution for 5 min. The reaction was warmed to RT, acidified with 2M HCl (5 mL), diluted with CH_2Cl_2 (200 mL) and washed with water (200 mL). The organic layer was filtered and dried over $MgSO_4$. The white solid **519** was purified by silica gel column chromatography using 1:1 hexanes / EtOAc (0.036 g, 42 %). R_f = 0.45 (1:2 hexanes / EtOAc). ^{1}H NMR (500 MHz, $CDCl_3$) δ 7.60 (d, *J* = 8.8, 1H; Ar*H*), 7.79 (t, *J* = 7.8, 1H; Ar*H*), 8.14 (dd, *J* = 1.5, 8.2, 1H; Ar*H*), 8.37 (d, *J* = 8.5, 1H; Ar*H*), 8.85 (dd, *J* = 1.5, 7.3, 1H; Ar*H*) 14.82 (s, 1H; O*H*); ^{13}C NMR (125 MHz, $CDCl_3$) δ 123.2 (s), 124.2 (q), 126.8 (q), 127.6 (s), 133.0 (s), 136.5 (s), 140.9 (s), 145.2 (q), 150.9 (q), 166.0 (q). MS for $C_{10}H_5ClNO_2$ (MH^+) 208.36. $C_{10}H_5{}^{35}ClNO_2$ (207.61): calcd. C 57.85, H 2.91, N 6.75; found C 58.26, H 3.15, N 6.59.

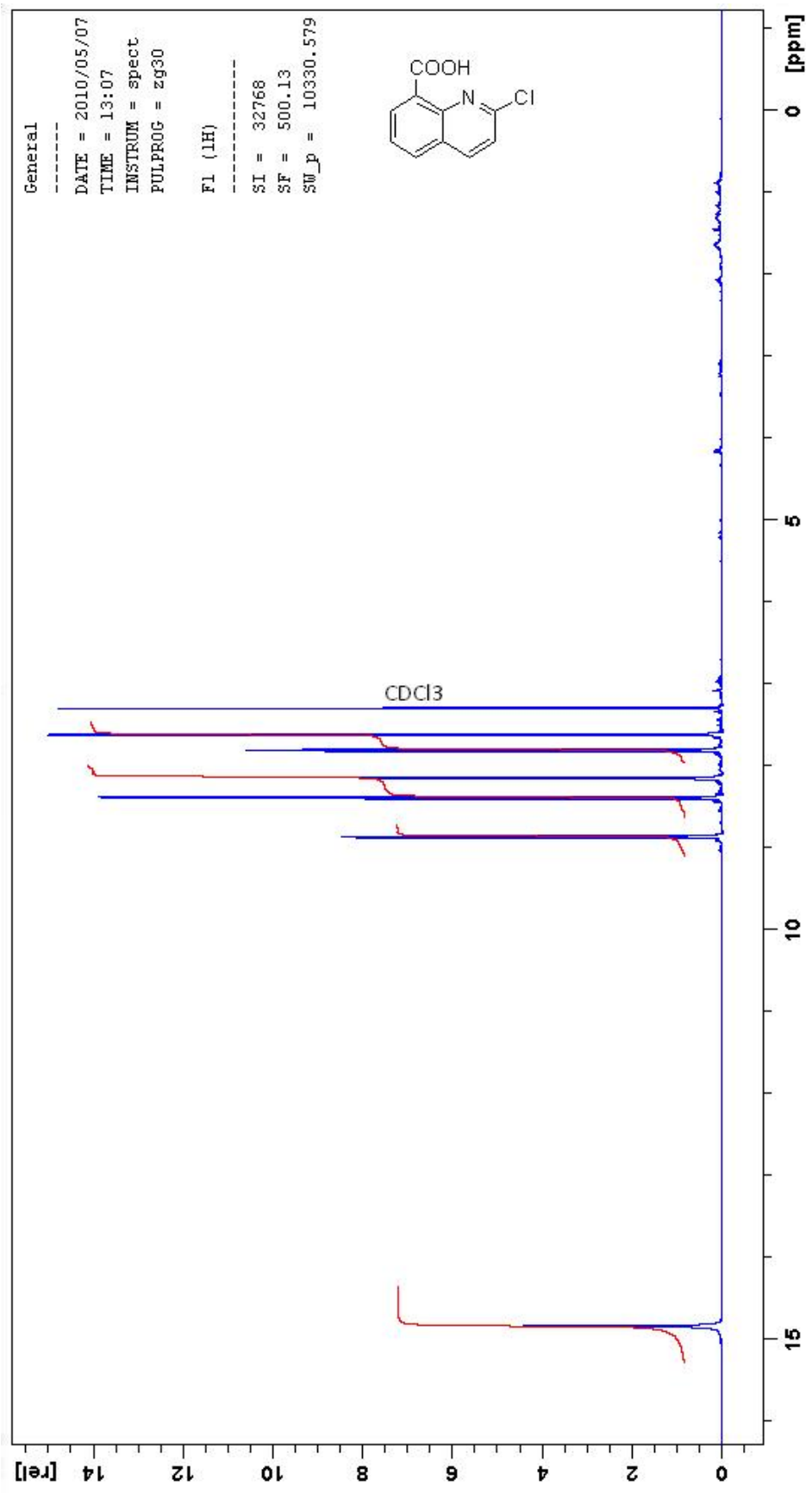
General
DATE = 2010/05/07
TIME = 13:07
INSTRUM = spect
PULPROG = zg30
F1 (1H)
SI = 32768
SF = 500.13
SW_p = 10330.579
COOH
N
Cl
CDCl3
[rel]
[ppm]

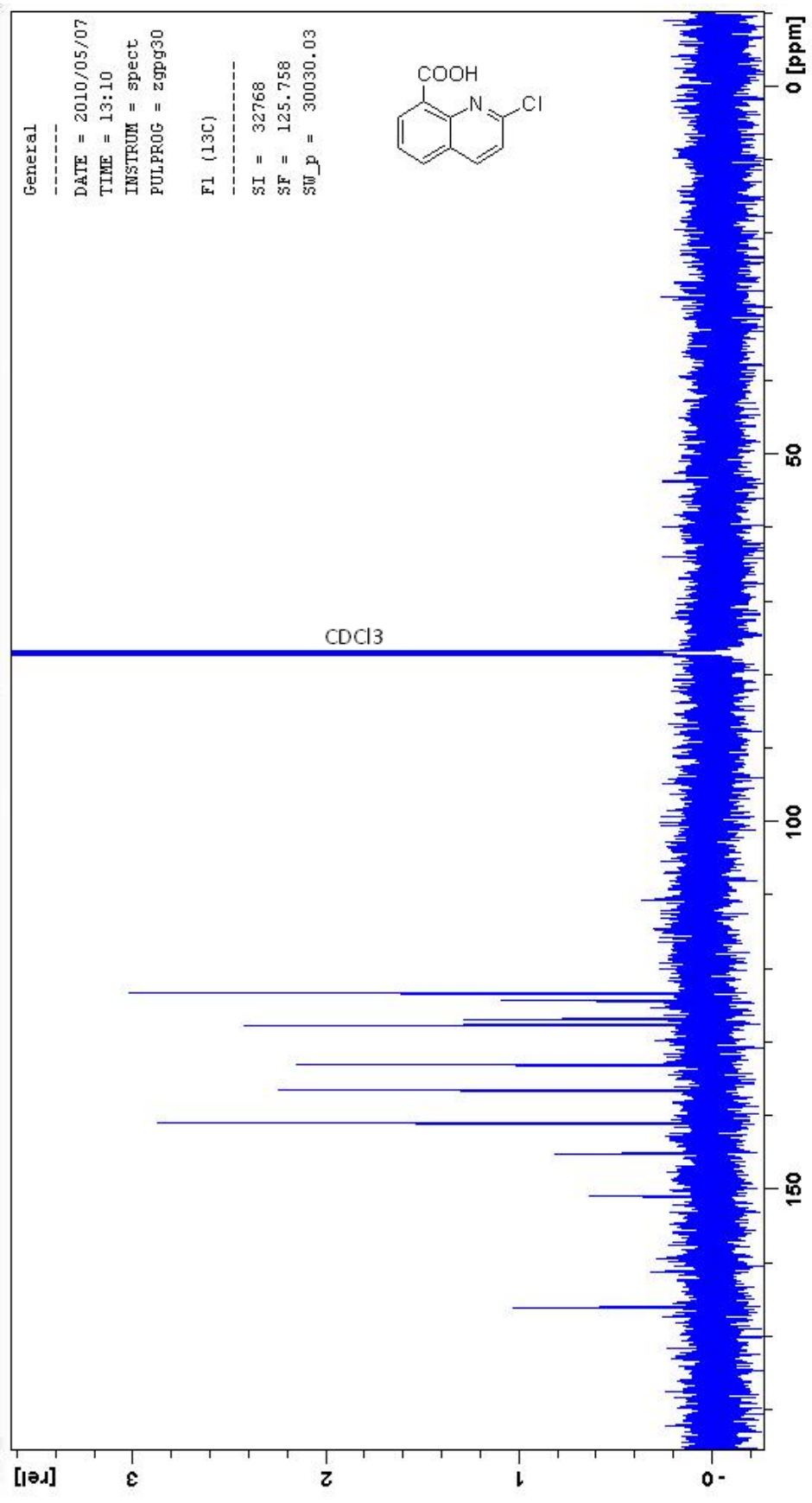
General
DATE = 2010/05/07
TIME = 13:10
INSTRUM = spect
PULPROG = zgpg30
F1 (13C)
SI = 32768
SF = 125.758
SW_p = 30030.03
COOH
N
Cl
CDCl3
[rel]
0 [ppm]
50
100
150

A.6.12 Methyl 2-chloroquinoline-8-carboxylate (535)

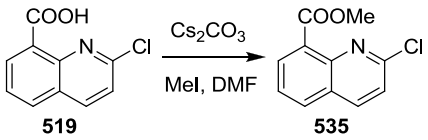

519 535

2-Chloroquinoline-8-carboxylic acid (**519**) (0.050 g, 0.240 mmol) and caesium carbonate (0.039 g, 0.120 mmol) in methanol (10 mL) were stirred at RT for 1 h. The solvent was removed and DMF (5 mL) and methyl iodide (0.018 mL, 0.288 mmol) were added and the reaction was stirred at RT overnight. The reaction was diluted with CH_2Cl_2 and washed with water. The organic layer was filtered and dried over $MgSO_4$ then concentrated under reduced pressure. The greasy white solid **535** was purified by silica gel column chromatography using 1:2 ethyl acetate / hexanes (0.049 g, 93 %). R_f = 0.66 (1:2 hexanes / EtOAc). ^{1}H NMR (500 MHz, $CDCl_3$) δ 4.07 (s, 3H; C*H*$_3$), 7.45 (d, *J* = 8.7, 1H; Ar*H*), 7.60 (dd, *J* = 7.2, 8.1, 1H; Ar*H*), 7.96 (dd, *J* = 1.3, 8.3, 1H; Ar*H*), 8.10 (dd, *J* = 1.5, 7.2, 1H; Ar*H*), 8.13 (d, *J* = 8.7, 1H; Ar*H*); ^{13}C NMR (125 MHz, $CDCl_3$) δ 52.7 (t), 123.2 (s), 126.1 (s), 127.0 (q), 130.8 (q), 131.1 (s), 131.6 (s), 138.9 (s), 145.0 (q), 151.9 (q), 167.4 (q). HRMS calculated for $C_{11}H_8{}^{35}ClNO_2$ (MH^+) 222.0316, found 222.0316 (ESI+).

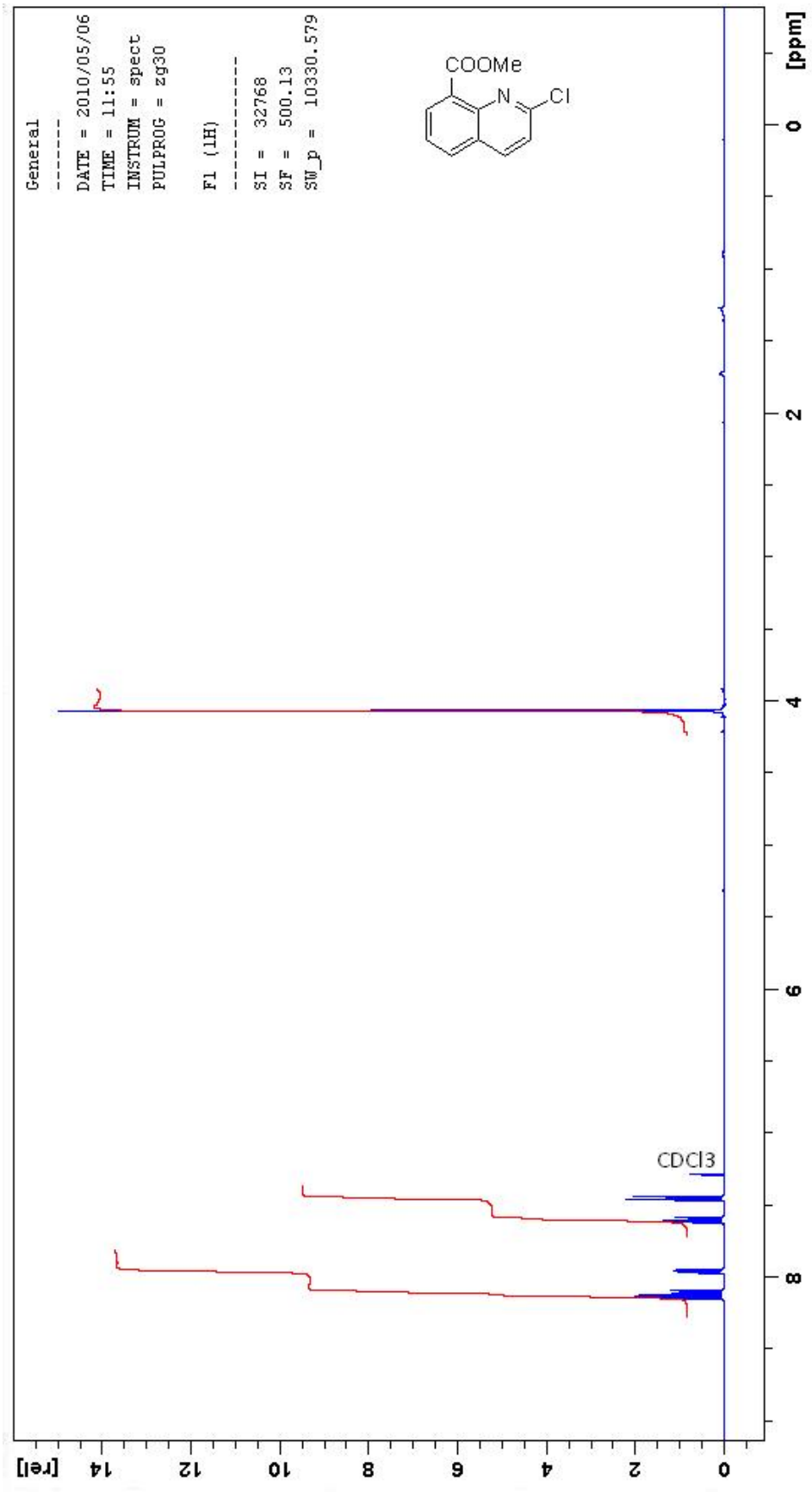
General
DATE = 2010/05/06
TIME = 11:55
INSTRUM = spect
PULPROG = zg30
F1 (1H)
SI = 32768
SF = 500.13
SW_p = 10330.579
COOMe
N
Cl
CDCl3
[rel]
[ppm]

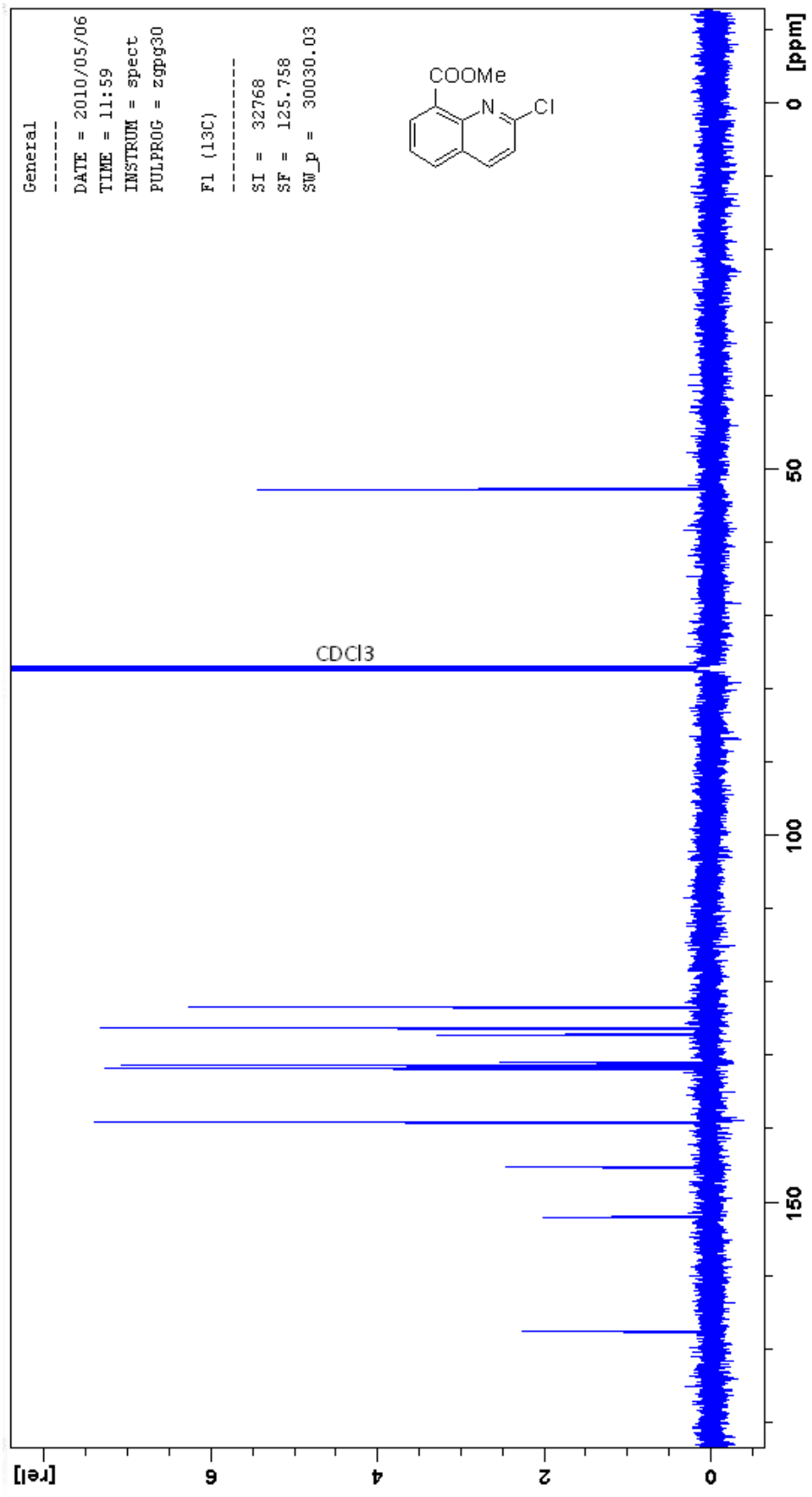
General
DATE = 2010/05/06
TIME = 11:59
INSTRUM = spect
PULPROG = zgpg30
F1 (13C)
SI = 32768
SF = 125.758
SW_p = 30030.03
COOMe
N
Cl
CDCl3
[rel]
[ppm]

A.6.13 Methyl 2-cinnamamidobenzoate (536)

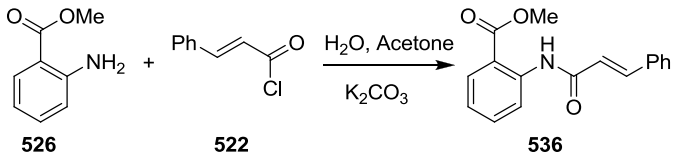

526 **522** **536**

Methyl 2-cinnamamidobenzoate (**536**) was synthesised by analogy to the preparation of **533**.[156] Potassium carbonate (0.248 g, 1.808 mmol), methyl 2-aminobenzoate (**526**) (0.156 mL, 1.204 mmol) and cinnamoyl chloride (**522**) (0.200 g, 1.204 mmol) were dissolved in acetone (10 mL) and the reaction was stirred overnight at RT. The reaction was diluted with EtOAc (200 mL) and washed with water (200 mL). The organic layer was filtered and dried over $MgSO_4$ then concentrated under reduced pressure. The white solid **536** was purified by silica gel column chromatography using 1:2 EtOAc / hexanes (0.320 g, 95 %). R_f = 0.58 (2:1 hexanes / EtOAc). ^{1}H NMR (500 MHz, $CDCl_3$) δ 3.95 (s, 3H, C*H*$_3$), 6.63 (d, *J* = 15.6, 1H, C*H*), 7.10 (dt, *J* = 1.1, 8.2, 1H; Ar*H*), 7.37-7.41 (m, 3H; Ar*H*), 7.56-7.59 (m, 3H; Ar*H*), 7.75 (d, *J* = 15.6, 1H, C*H*), 8.06 (dd, *J* = 1.6, 8.1, 1H; Ar*H*), 8.87 (dd, *J* = 1.0, 8.6, 1H; Ar*H*), 11.37 (s, 1H; N*H*); ^{13}C NMR (125 MHz, $CDCl_3$) δ 52.4 (t), 114.8 (q), 120.5 (s), 121.9 (s), 122.5 (s), 128.0 (s), 128.8 (s), 130.0 s), 130.8 (s), 134.6 (q), 134.7 (s), 141.8 (q), 142.2 (s), 142.2 (s), 164.5 (q), 168.9 (q). HRMS calculated for $C_{17}H_6NO_3$ (MH^+) 282.1130, found 282.1124 (ESI+).

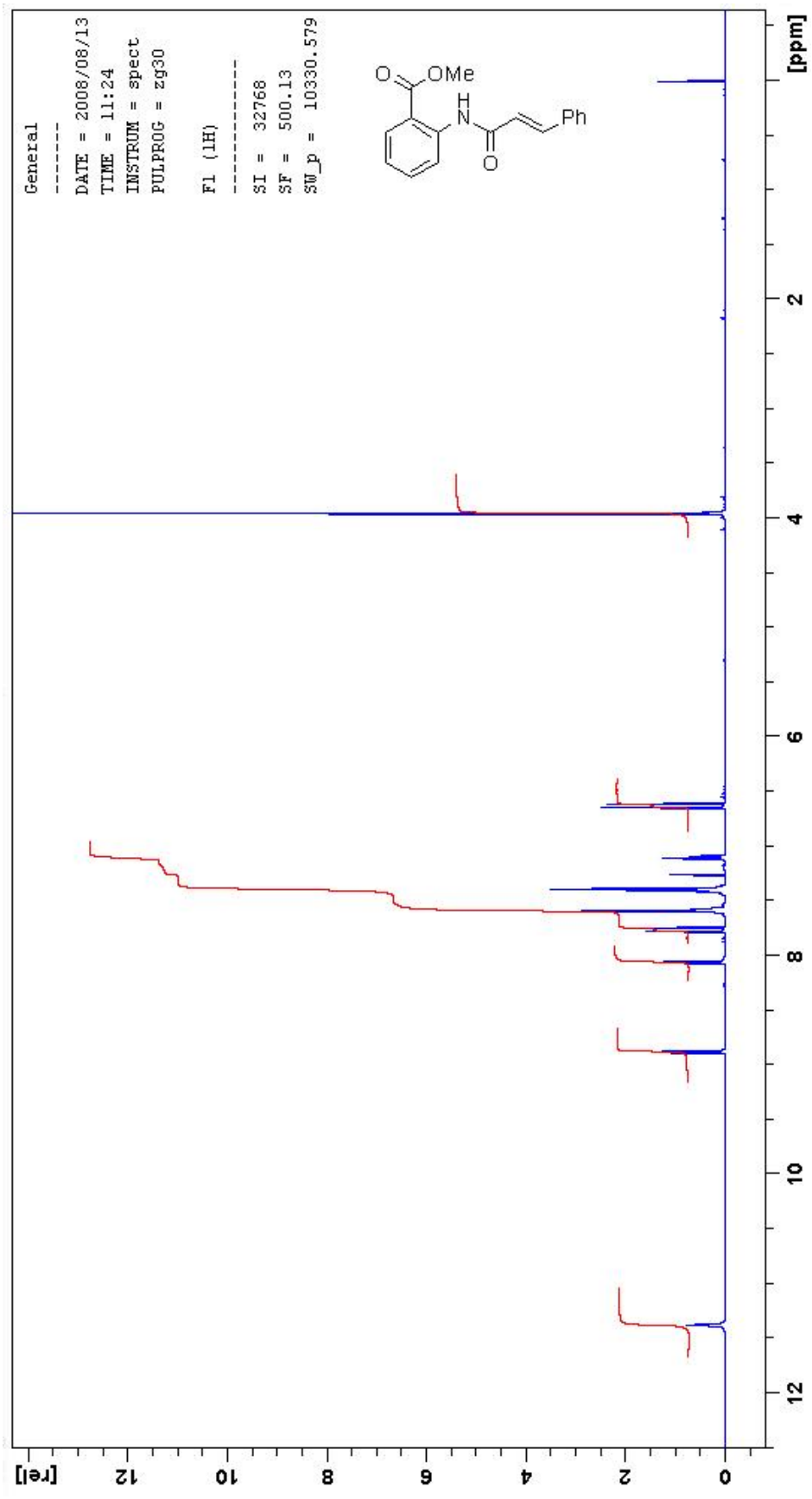
General
DATE = 2008/08/13
TIME = 11:24
INSTRUM = spect
PULPROG = zg30
F1 (1H)
SI = 32768
SF = 500.13
SW_p = 10330.579
OMe
Ph
[rel]
[ppm]

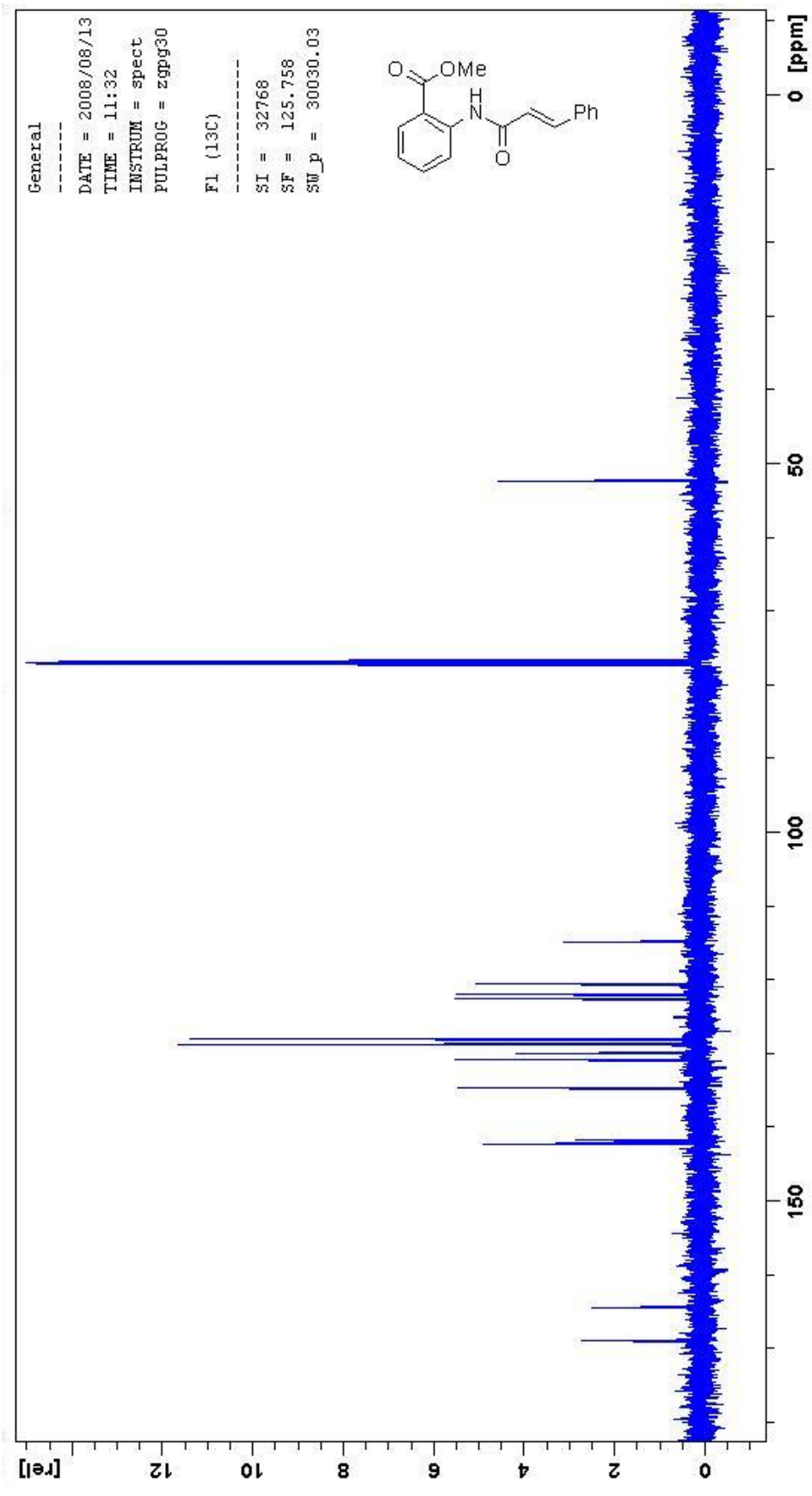
General
DATE = 2008/08/13
TIME = 11:32
INSTRUM = spect
PULPROG = zgpg30
F1 (13C)
SI = 32768
SF = 125.758
SW_p = 30030.03
O
OMe
H
N
O
Ph
[rel]
12
10
8
6
4
2
0
150
100
50
0 [ppm]

A.6.14 2-Chloroquinoline-8-carbonitrile (538)

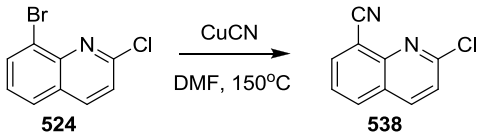

524 **538**

8-Bromo-2-chloroquinoline (**524**) (0.200 g, 0.828 mmol) and copper cyanide (1.92 g, 21.4 mmol) in dry DMF (5 mL) was heated at 120 ^{o}C for 18 h. The reaction was diluted with CH_2Cl_2 (200 mL) and washed with mixture of water (200 mL), 2,2',2",2'"-(ethane-1,2-diylbis(azanetriyl))tetraacetic acid (5 g), and a few drops of 6M KOH. The organic layer was filtered and dried over $MgSO_4$. The white solid **538** was purified by silica gel column chromatography using 1:4 EtOAc / hexanes (0.098 g, 63 %). R_f = 0.25 (1:2 EtOAc / hexanes). ^{1}H NMR (500 MHz, $CDCl_3$) δ 7.54 (d, *J* = 8.5, 1H; Ar*H*), 7.64 (t, *J* = 8.2, 1H; Ar*H*), 8.08 (d, *J* = 8.2, 1H; Ar*H*), 8.14 (d, *J* = 8.2, 1H; Ar*H*), 8.19 (d, *J* = 8.5, 1H; Ar*H*); ^{13}C NMR (125 MHz, $CDCl_3$) δ 112.4 (q), 116.4 (q), 124.5 (s), 126.3 (s), 126.7 (q), 132.5 (s), 136.4 (s), 138.9 (s), 147.1 (q), 153.5 (q). HRMS calculated for $C_{10}H_5{}^{35}ClN_2$ (MH^+) 189.0214, found 189.0209 (ESI+).

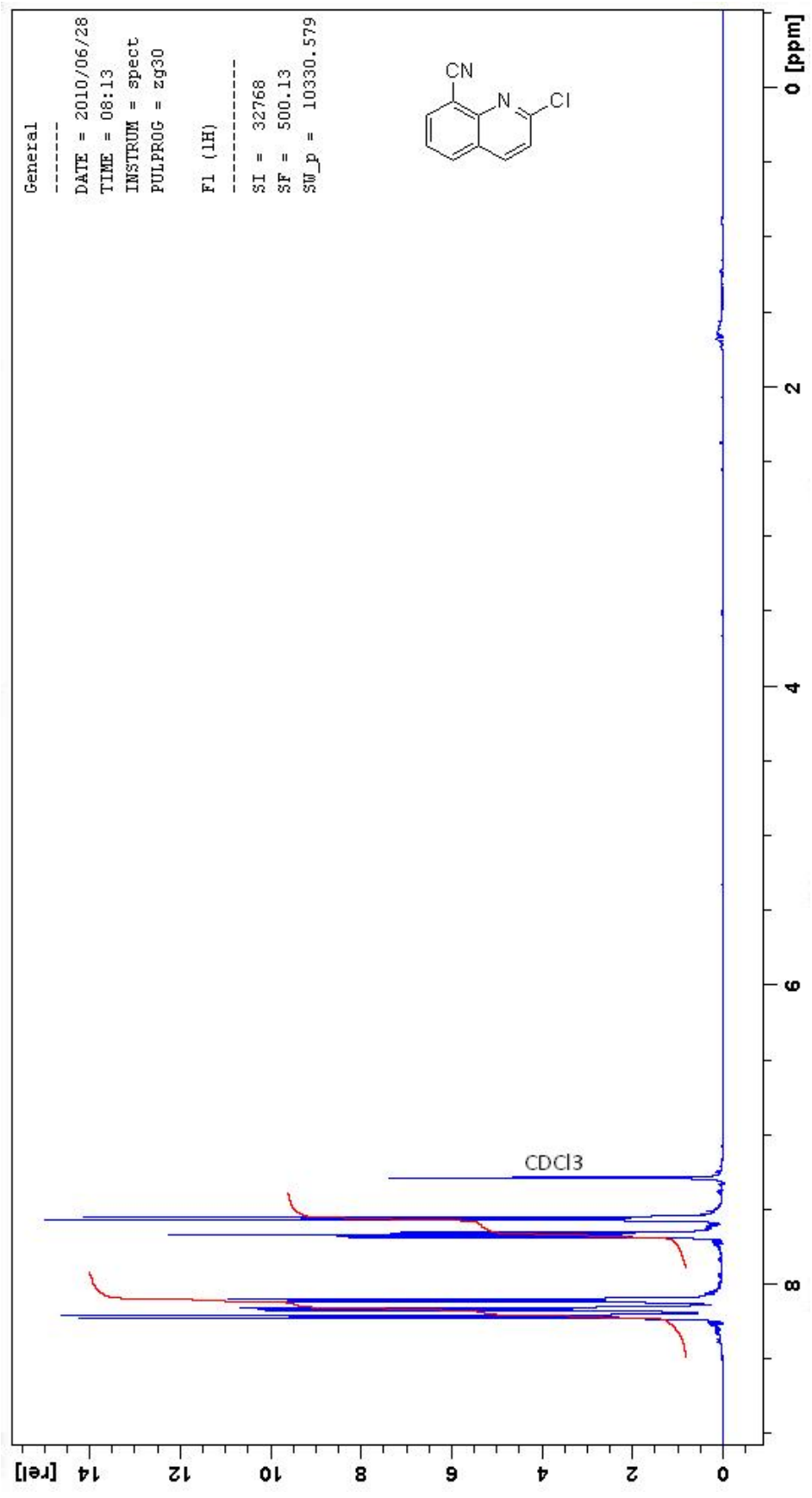
General
DATE = 2010/06/28
TIME = 08:13
INSTRUM = spect
PULPROG = zg30
F1 (1H)
SI = 32768
SF = 500.13
SW_p = 10330.579
CN
N
Cl
CDCl3
[rel]
0 [ppm]

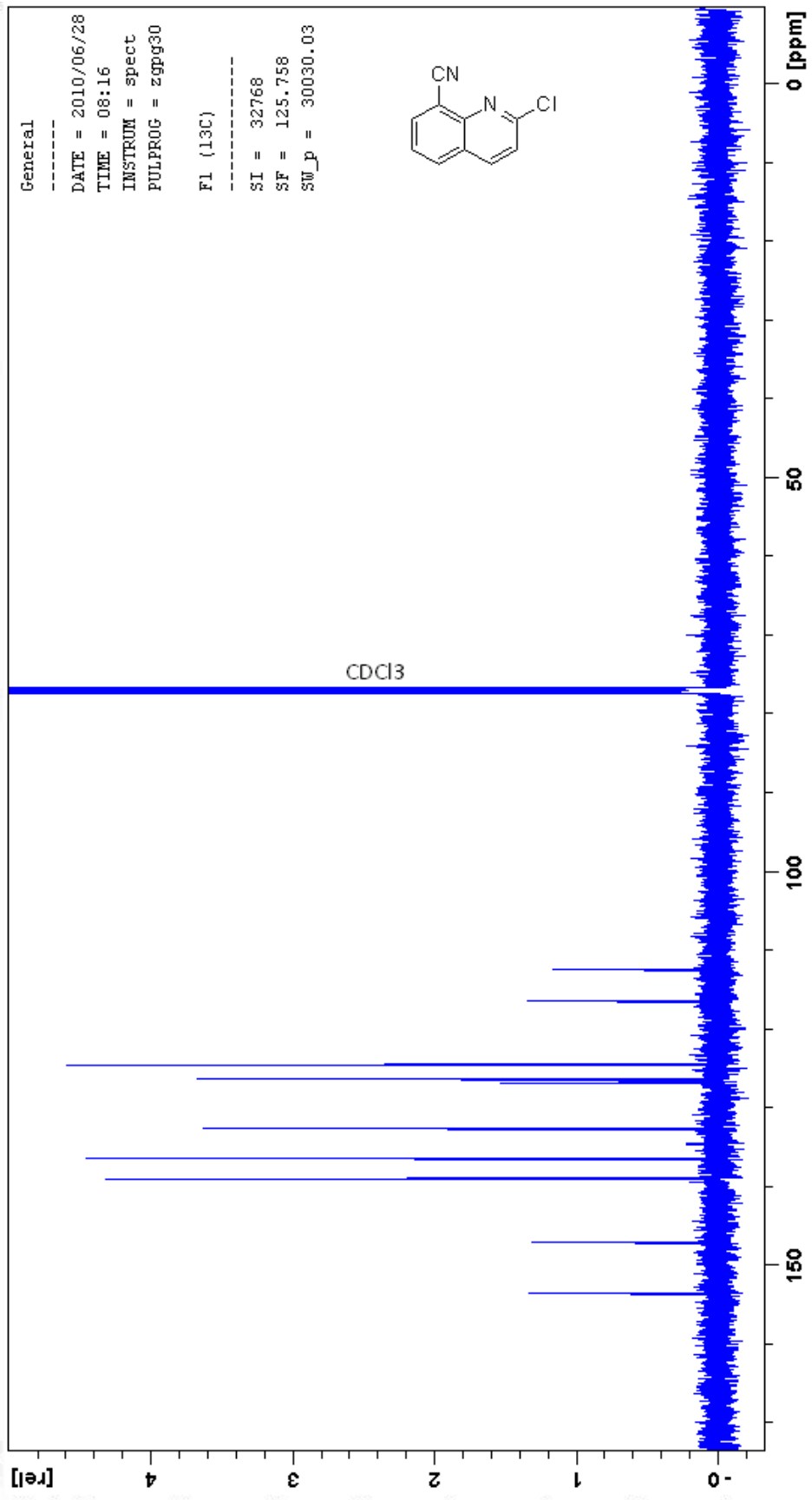
General
DATE = 2010/06/28
TIME = 08:16
INSTRUM = spect
PULPROG = zgpg30
F1 (13C)
SI = 32768
SF = 125.758
SW_p = 30030.03
CN
N
Cl
CDCl3
0 [ppm]
50
100
150
[rel]
0
1
2
3
4

A.6.15 8-Bromo-2-(dipyridin-2-ylmethyl)quinoline (537)

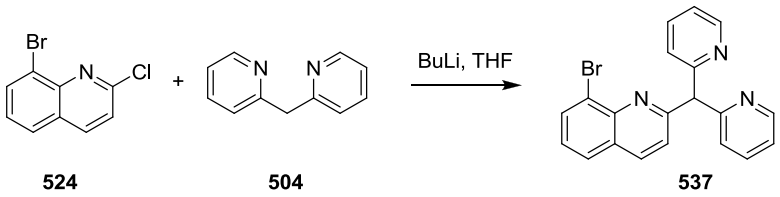

524 **504** **537**

2-(2-Pyridylmethyl)pyridine (**504**) (0.307 mL, 1.806 mmol) in dry THF (5 mL) was cooled to -78 ^{o}C under Ar. *N*-Butyllithium (1.13 mL, 1.806 mmol, as a 1.6 M solution in hexane) was added and the reaction stirred at -78 ^{o}C for 1 hr, then slowly warmed to -20 ^{o}C. 8-Bromo-2-chloroquinoline (**524**) (0.218 g, 0.903 mmol) was added and the reaction was heated to reflux for 30 min. The reaction was diluted with CH_2Cl_2 (200 mL) and washed with water (200 mL). The organic layer was filtered and dried over $MgSO_4$. The orange oil **537** was purified by silica gel column chromatography using 98:2 CH_2Cl_2 / MeOH (0.298 g, 88 %). R_f = 0.50 (9:1 CH_2Cl_2 / MeOH). ^{1}H NMR (500 MHz, $CDCl_3$) δ 6.25 (s, 1H; C*H*), 7.14 (m, 2H; Ar*H*), 7.30 (t, *J* = 7.8, 1H; Ar*H*), 7.59-7.71 (m, 6H; Ar*H*), 7.97 (dd, *J* = 1.2, 7.5, 1H; Ar*H*), 8.05 (d, *J* = 8.5, 1H; Ar*H*), 8.56 (m, 2H; Ar*H*); ^{13}C NMR (125 MHz, $CDCl_3$) δ 64.5 (s), 121.8 (s), 123.4 (s), 124.5 (s), 125.2 (q), 126.6 (s), 127.2 (s), 128.2 (q), 132.8 (s), 136.5 (s), 136.5 (s), 144.6 (q), 149.1 (s), 160.7 (q), 161.7 (q). HRMS calculated for $C_{20}H_{14}{}^{79}BrN_3$ (MH^+) 376.0444, found 376.0440 (ESI+).

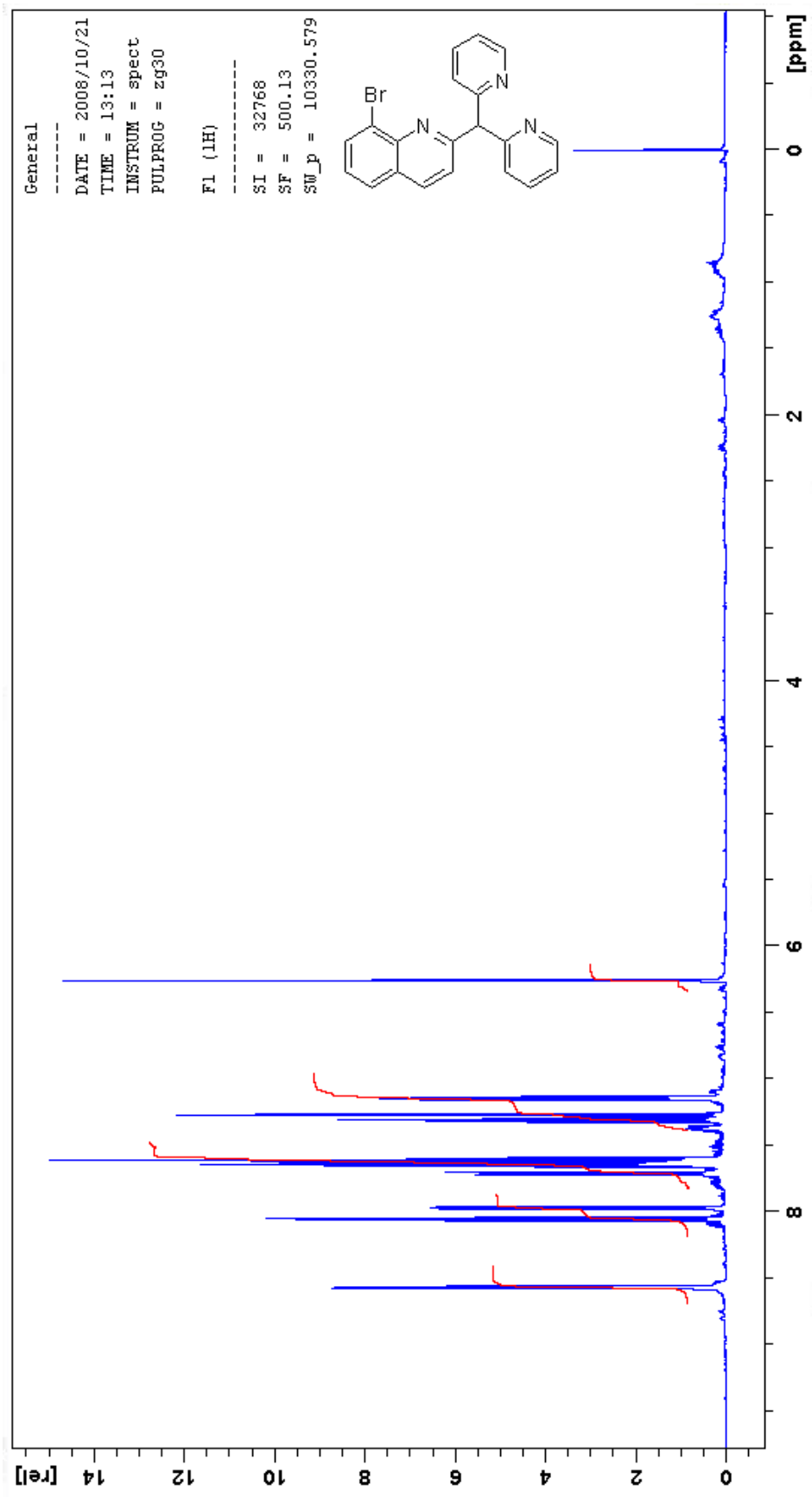
General
DATE = 2008/10/21
TIME = 13:13
INSTRUM = spect
PULPROG = zg30
F1 (1H)
SI = 32768
SF = 500.13
SW_p = 10330.579
Br
N
N
N
[rel]
[ppm]

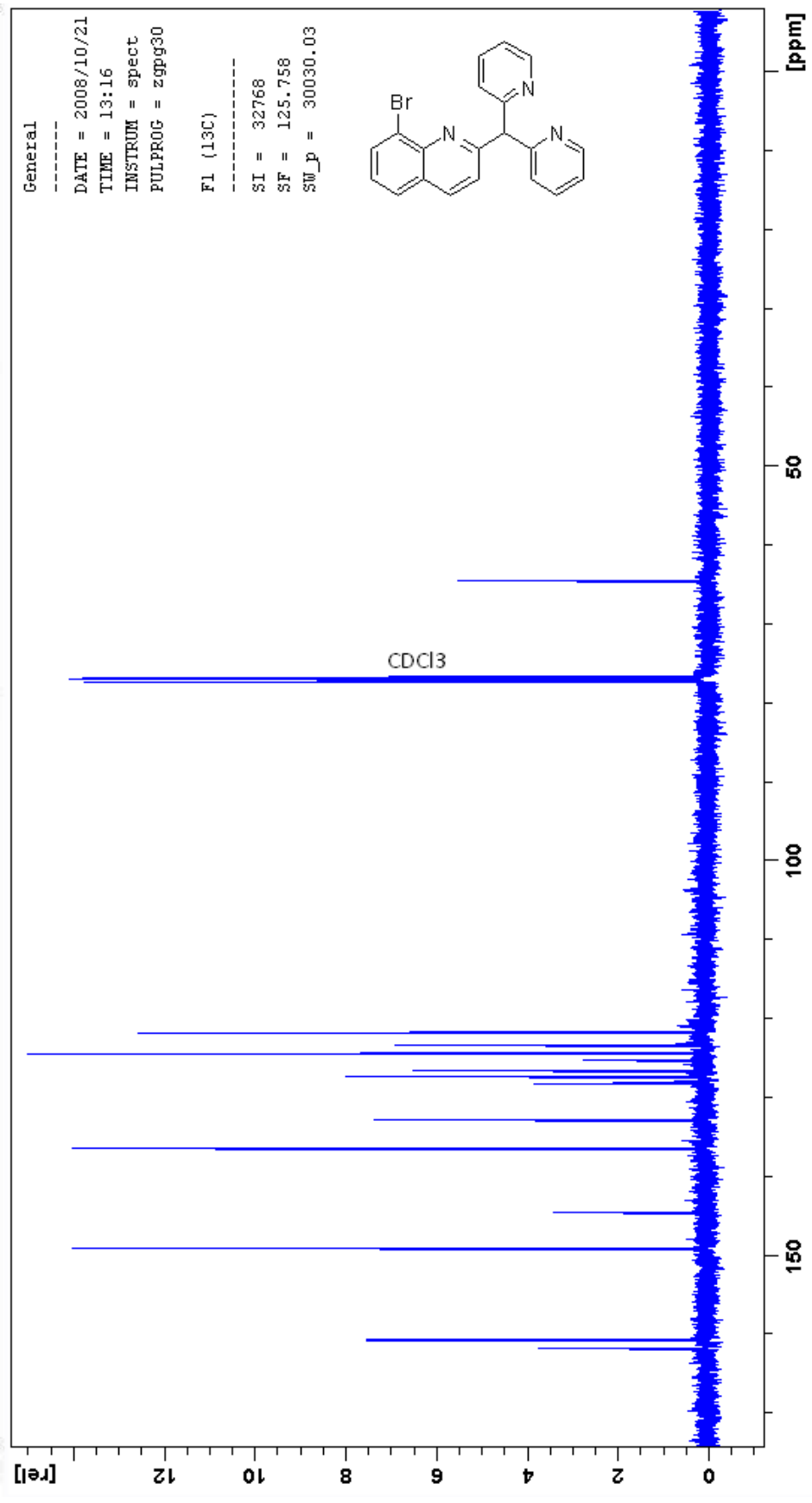
General
DATE = 2008/10/21
TIME = 13:16
INSTRUM = spect
PULPROG = zgpg30
F1 (13C)
SI = 32768
SF = 125.758
SW_p = 30030.03
Br
N
N
N
CDCl3
[rel]
[ppm]
0
2
4
6
8
10
12
50
100
150

A.6.16 2-(Dipyridin-2-ylmethyl)quinoline-8-carbonitrile (539)

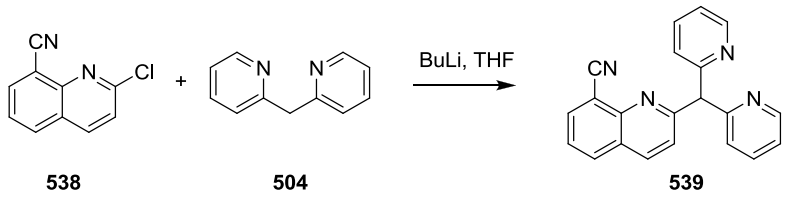

538 **504** **539**

2-(2-Pyridylmethyl)pyridine (**504**) (0.156 mL, 0.917 mmol) in dry THF (5 mL) was cooled to -78 ^{o}C under Ar. *N*-butyllithium (0.577 mL, 0.923 mmol, as a 1.6 M solution in hexane) was added and the reaction stirred at -78 ^{o}C for 1 hr, then slowly warmed to -20 ^{o}C. 2-Chloroquinoline-8-carbonitrile (**538**) (0.087 g, 0.462 mmol) was added and the reaction was heated to reflux for 30 min. The reaction was diluted with CH_2Cl_2 (200 mL) and washed with water (200 mL). The organic layer was filtered and dried over $MgSO_4$. The red oil **539** was purified by silica gel column chromatography using 98:2 CH_2Cl_2 / MeOH (0.103 g, 69 %). R_f = 0.57 (9:1 CH_2Cl_2 / MeOH). ^{1}H NMR (500 MHz, $CDCl_3$) δ 6.29 (s, 1H; C*H*), 7.16 (m, 2H; Ar*H*), 7.51 (m, 3H; Ar*H*), 7.66 (td, *J* = 1.8, 7.7, 2H; Ar*H*), 7.73 (d, *J* = 8.6, 1H; Ar*H*), 7.98 (dd, *J* = 1.2, 8.2, 1H; Ar*H*), 8.03 (dd, *J* = 1.2, 7.3, 1H; Ar*H*), 8.13 (d, *J* = 8.6, 1H; Ar*H*), 8.56 (m, 2H; Ar*H*); ^{13}C NMR (125 MHz, $CDCl_3$) δ 64.6 (s), 113.1 (q), 117.3 (q), 122.0 (s), 124.5 (s), 124.5 (s), 125.5 (s), 127.0 (q), 132.5 (s), 135.2 (s), 136.2 (s), 136.6 (s), 147.0 (q), 149.4 (s), 160.5 (q), 163.6 (q). MS for $C_{21}H_{14}N_4$ (MH^+) 323.76. HRMS calculated for $C_{21}H_{14}N_4$ (MH^+) 323.1291, found 323.1285 (ESI+).

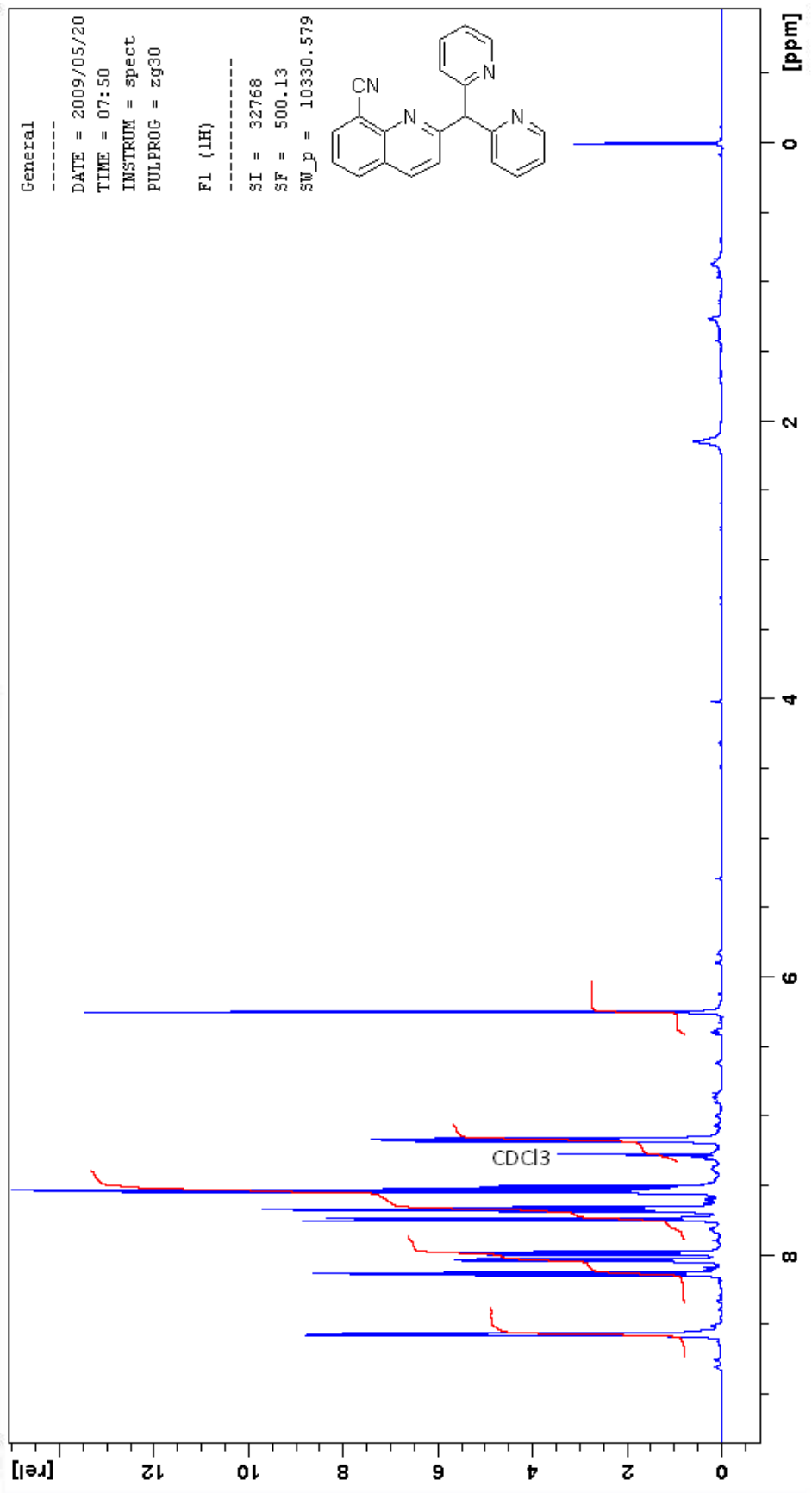
General
DATE = 2009/05/20
TIME = 07:50
INSTRUM = spect
PULPROG = zg30
F1 (1H)
SI = 32768
SF = 500.13
SW_p = 10330.579
CN
N
N
N
CDCl3
[rel]
[ppm]
0
2
4
6
8
10
12

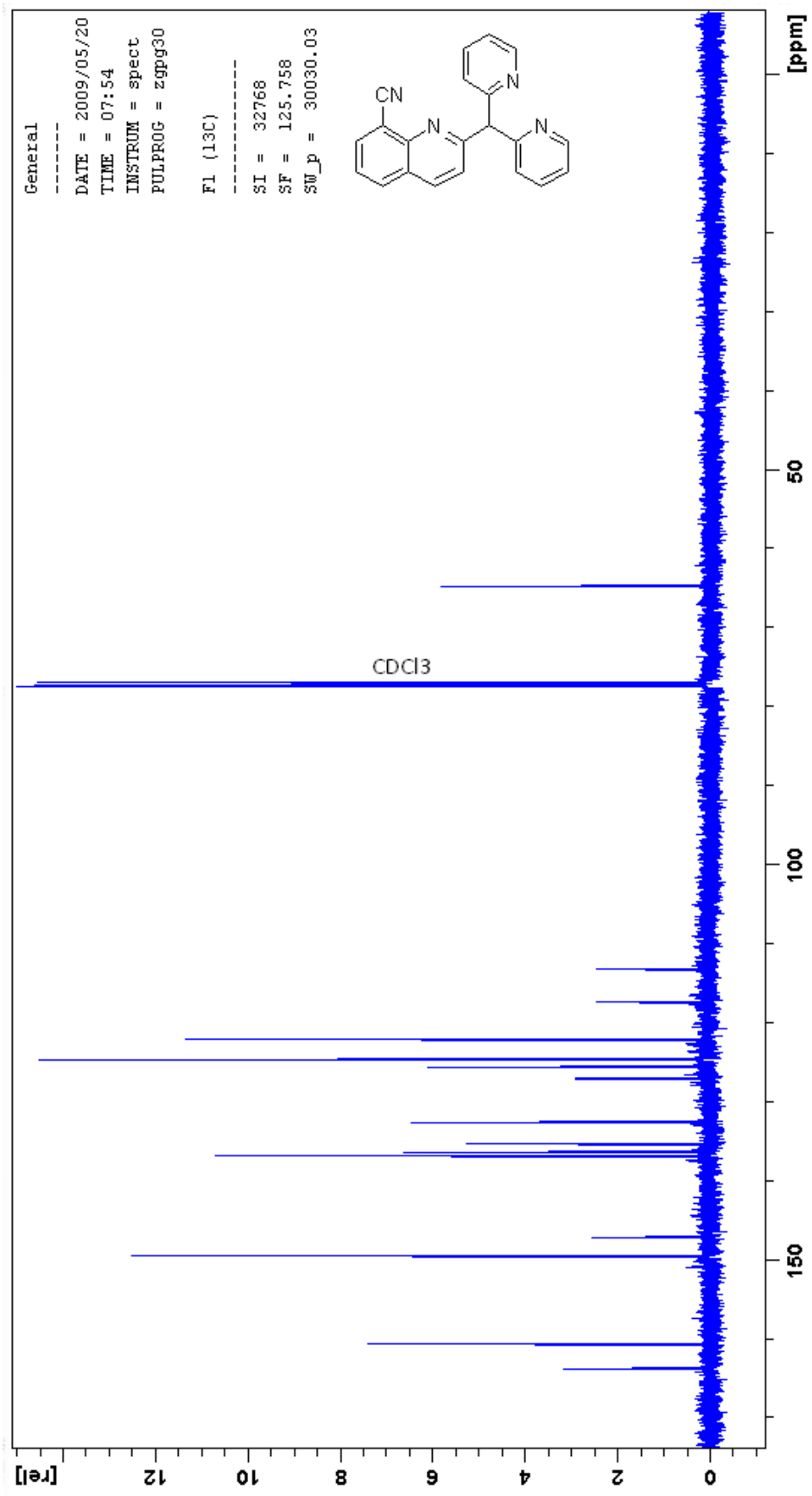
General
DATE = 2009/05/20
TIME = 07:54
INSTRUM = spect
PULPROG = zgpg30
F1 (13C)
SI = 32768
SF = 125.758
SW_p = 30030.03
CN
N
N
N
CDCl3
[ppm]
150
100
50
0
2
4
6
8
10
12
[rel]

A.6.17 2-((2-(Pyridin-2-yl)ethylamino)methyl)phenol (545)

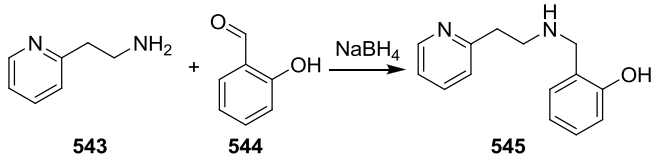

2-((Pyridin-2-ylethylamino)methyl)phenol (**545**) was a known compound and prepared according to the literature procedure.[196] Pyridin-2-ylethanamine (**543**) (0.490 mL, 4.10 mmol) and 2-hydroxybenzaldehyde (**544**) (0.500 g, 4.10 mmol) in MeOH (10 mL) were stirred for 30 min at RT. $NaBH_4$ (0.246 g, 6.48 mmol) and NaOH (0.033 g, 0.82 mmol) in H_2O (2 mL) were added to the reaction mixture and the resulting solution was stirred for 1 h. The reaction was diluted with CH_2Cl_2 (200 mL) and washed with water (200 mL). The organic layer was filtered and dried over $MgSO_4$ and the solvent removed. The colourless oil **545** was purified by silica gel column chromatography using 95:5 CH_2Cl_2 / MeOH (0.669 g, 72 %). ^{1}H NMR (500 MHz, $CDCl_3$) δ 2.96 (t, *J* = 6.7, 2H; C*H*$_2$), 3.12 (t, *J* = 6.7, 2H; C*H*$_2$), 4.01 (s, 2H; C*H*$_2$), 6.76 (td, *J* = 1.7, 7.8, 1H; Ar*H*), 6.81 (dd, *J* = 1.7, 5.0, 1H; Ar*H*), 6.98 (d, 1H; Ar*H*), 7.12-7.18 (m, 3H; Ar*H*), 7.61 (dt, *J* = 1.7, 7.8, 1H; Ar*H*), 8.52 (d, *J* = 5.0, 1H; Ar*H*). MS for $C_{14}H_{16}N_2O$ (MH^+) 229.13.

A.6.18 2-(((2-Hydroxybenzyl)(pyridin-2-ylethyl)amino)methyl)-4-nitrophenol (L15)

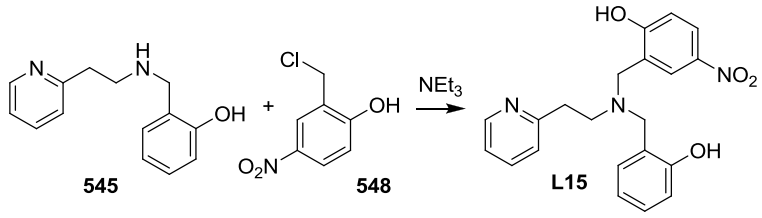

2-((Pyridin-2-ylethylamino)methyl)phenol (**545**) (0.669 g, 2.95 mmol), 2-(chloromethyl)-4-nitrophenol (**548**) (0.553 g, 2.95 mmol) and triethylamine (3.26 mL, 23.6 mmol) were refluxed together in $CHCl_3$ (20 mL) for 2 h. The reaction was diluted with CH_2Cl_2 (200 mL) and washed with water (200 mL). The organic layer was filtered and dried over

$MgSO_4$. The pale yellow oil **L15** was purified by silica gel column chromatography using 98:2 CH_2Cl_2 / MeOH. Residual MeOH caused **L15** to remain as an oil, this was removed by dissolving the residue in a minimum volume of CH_2Cl_2 and precipitating with hexane addition, decanting and drying under vacuum to give a pale yellow powder (0.590 g, 53 %). R_f = 0.29 (95:5 CH_2Cl_2 / MeOH). ^{1}H NMR (500 MHz, $CDCl_3$) δ 2.94 (t, *J* = 6.7, 2H; C*H*$_2$), 3.14 (t, *J* = 6.7, 2H; C*H*$_2$), 3.49 (brs, 2H; O*H*), 3.85 (s, 4H; C*H*$_2$), 6.69 – 6.82 (m, 3H; Ar*H*), 7.05 – 7.24 (m, 4H; Ar*H*), 7.64 (dt, *J* = 1.7, 7.8, 1H; Ar*H*), 7.94 (d, *J* = 2.2, 1H; Ar*H*), 8.00 (dd, *J* = 2.8, 8.9, 1H; Ar*H*), 8.54 (d, *J* = 5.0, 1H; Ar*H*); ^{13}C NMR (125 MHz, $CDCl_3$) δ 33.9 (d), 53.7 (d), 55.2 (d), 55.7 (d), 116.5 (s), 116.6 (s), 119.7 (s), 121.6 (q), 122.1 (s), 122.4 (s), 123.7 (s), 125.5 (s), 126.2 (q), 129.6 (s), 130.9 (s), 137.6 (s), 139.7 (q), 148.8 (s), 156.1 (q), 158.6 (q), 163.9 (q). MS for $C_{21}H_{21}N_3O_4$ (MH^+) 380.84. $C_{21}H_{21}N_3O_4$•0.25H_2O (383.91): calcd. C 65.70, H 5.64, N 10.95; found C 65.40, H 5.48, N 10.84. M.P. = 108 – 110 ^{o}C.

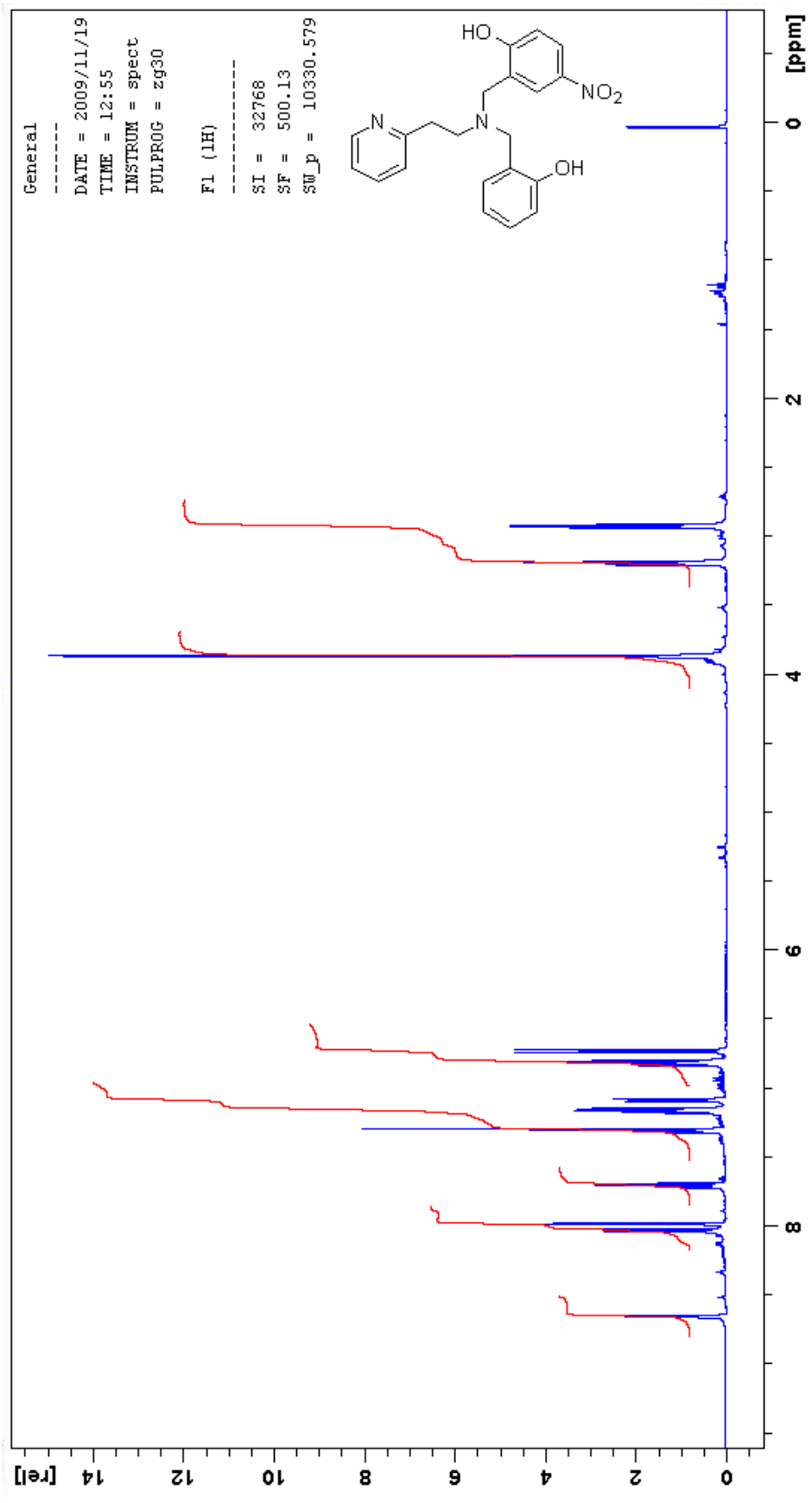
General
DATE = 2009/11/19
TIME = 12:55
INSTRUM = spect
PULPROG = zg30
F1 (1H)
SI = 32768
SF = 500.13
SW_p = 10330.579
HO
NO2
N
N
OH
[rel]
[ppm]

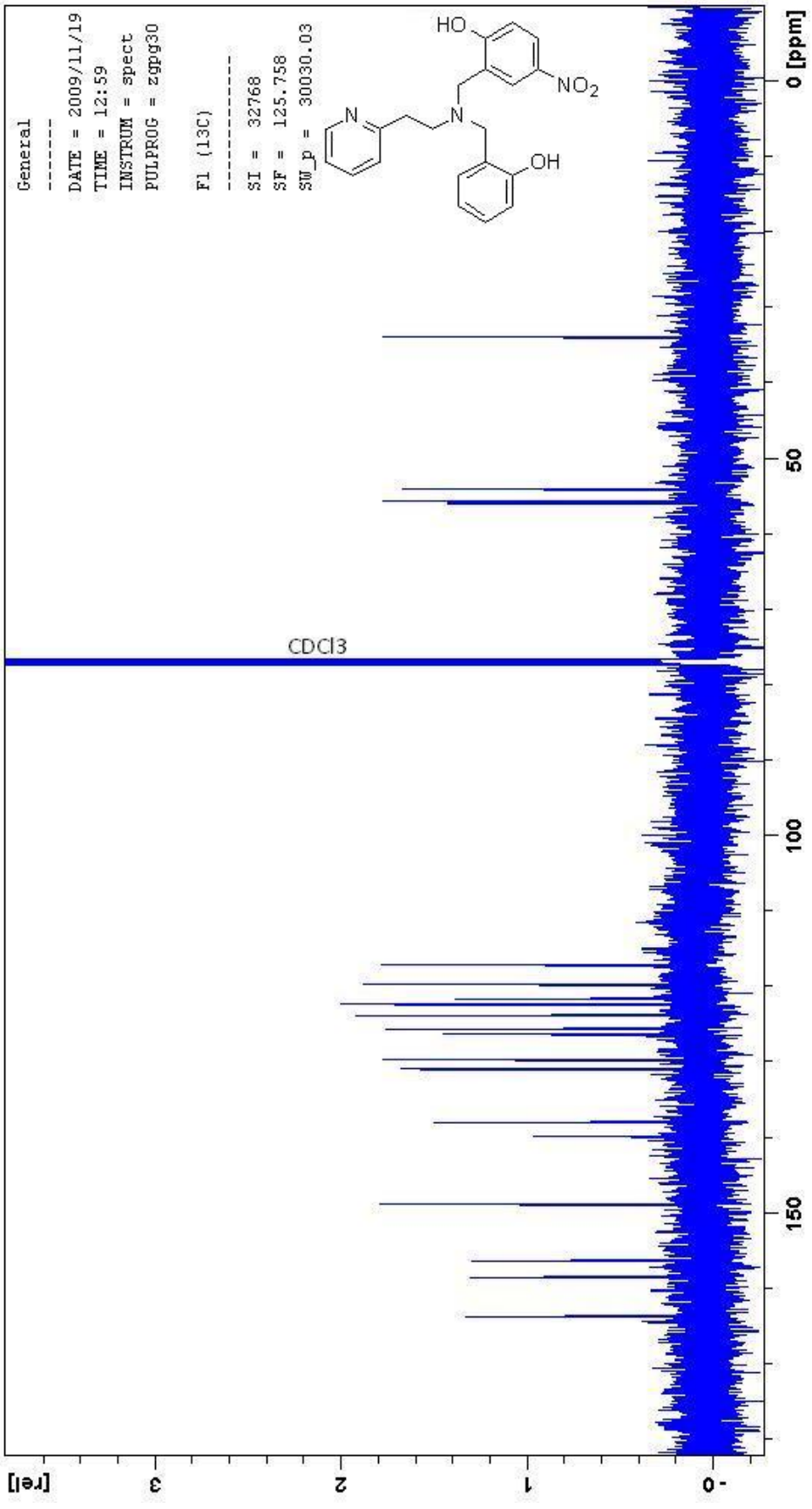
General
DATE = 2009/11/19
TIME = 12:59
INSTRUM = spect
PULPROG = zgpg30
F1 (13C)
SI = 32768
SF = 125.758
SW_p = 30030.03
HO
NO2
N
N
OH
CDCl3
[rel]
3
2
1
0
150
100
50
0 [ppm]

A.6.19 2-((2-(Pyridin-2-yl)methylamino)methyl)phenol (560)

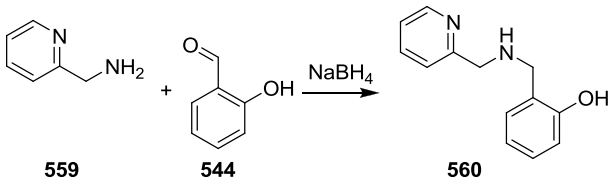

559 **544** **560**

2-((Pyridin-2-ylmethylamino)methyl)phenol (**560**) was a known compound and prepared according to the literature procedure.[197] Pyridin-2-ylmethanamine (**559**) (0.443 mL, 4.10 mmol) and 2-hydroxybenzaldehyde (**544**) (0.500 g, 4.10 mmol) in MeOH (10 mL) were stirred for 30 min at RT. $NaBH_4$ (0.246 g, 6.48 mmol) and NaOH (0.033 g, 0.82 mmol) in H_2O (2 mL) were added to the reaction mixture and the resulting solution was stirred for 1 h. The reaction was diluted with CH_2Cl_2 (200 mL) and washed with water (200 mL). The organic layer was filtered and dried over $MgSO_4$ and the solvent was removed. The colourless oil **560** was purified by silica gel column chromatography using 95:5 CH_2Cl_2 / MeOH (0.599 g, 68 %). ^{1}H NMR (500 MHz, $CDCl_3$) δ 3.87 (s, 2H; C*H*$_2$), 3.95 (s, 2H; C*H*$_2$), 6.73 - 6.75 (m, 2H; Ar*H*), 7.00 (dd, *J* = 1.6, 6.5, 1H; Ar*H*), 7.13 (dt, *J* = 6.5, 7.7, 1H; Ar*H*), 7.25 (dd, *J* = 1.6, 4.9, 1H; Ar*H*), 7.29 (t, *J* = 6.5, 1H; Ar*H*), 7.73 (dt, *J* = 1.6, 7.7, 1H; Ar*H*), 8.55 (d, *J* = 4.9, 1H; Ar*H*). MS for $C_{13}H_{14}N_2O$ (MH^+) 215.11.

A.6.20 2-(((2-Hydroxybenzyl)(pyridin-2-ylmethyl)amino)methyl)-4-nitrophenol (L16)

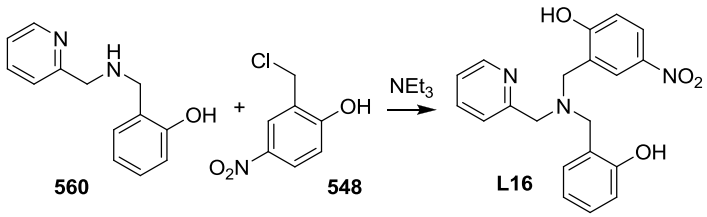

560 **548** **L16**

2-((Pyridin-2-ylmethylamino)methyl)phenol (**560**) (0.599 g, 2.80 mmol), 2-(chloromethyl)-4-nitrophenol (**548**) (0.525 g, 2.80 mmol) and triethylamine (3.10 mL, 22.4 mmol) were refluxed together in $CHCl_3$ (20 mL) for 2 h. The reaction was diluted with CH_2Cl_2 (200

mL) and washed with water (200 mL). The organic layer was filtered and dried over $MgSO_4$. The pale yellow oil **L16** was purified by silica gel column chromatography eluting with CH_2Cl_2. Residual polar solvents caused **L16** to remain as an oil, this was removed by dissolving the residue in a minimum volume of CH_2Cl_2 and precipitating with hexane addition, decanting and drying under vacuum to give a pale yellow powder (0.710 g, 69 %). R_f = 0.29 (95:5 CH_2Cl_2 / MeOH). ^{1}H NMR (500 MHz, $CDCl_3$) δ 3.89 (s, 2H; C*H*$_2$), 3.91 (s, 2H; C*H*$_2$), 3.99 (s, 2H; C*H*$_2$), 6.80 – 6.97 (m, 3H; Ar*H*), 7.07 – 7.22 (m, 3H; Ar*H*), 7.35 (t, *J* = 6.5, 1H; Ar*H*), 7.79 (dt, *J* = 1.6, 7.7, 1H; Ar*H*), 8.06 (d, *J* = 2.8, 1H; Ar*H*), 8.12 (dd, *J* = 2.8, 8.9, 1H; Ar*H*), 8.68 (d, *J* = 4.9, 1H; Ar*H*) 9.97 (brs, 2H; O*H*); ^{13}C NMR (125 MHz, $CDCl_3$) δ 56.0 (d), 56.3 (d), 56.8 (d), 117.0 (s), 117.6 (s), 119.5 (s), 120.8 (q), 122.0 (q), 123.0 (s), 123.4 (s), 126.0 (s), 126.6 (s), 129.8 (s), 130.3 (s), 138.2 (s), 140.0 (q), 148.0 (s), 155.5 (q), 157.0 (q), 163.9 (q). MS for $C_{20}H_{19}N_3O_4$ (MH^+) 366.72. $C_{20}H_{19}N_3O_4$ (379.41): calcd. C 65.74, H 5.24, N 11.50; found C 65.79, H 5.20, N 11.49. M.P. = 102 – 104 ^{o}C.

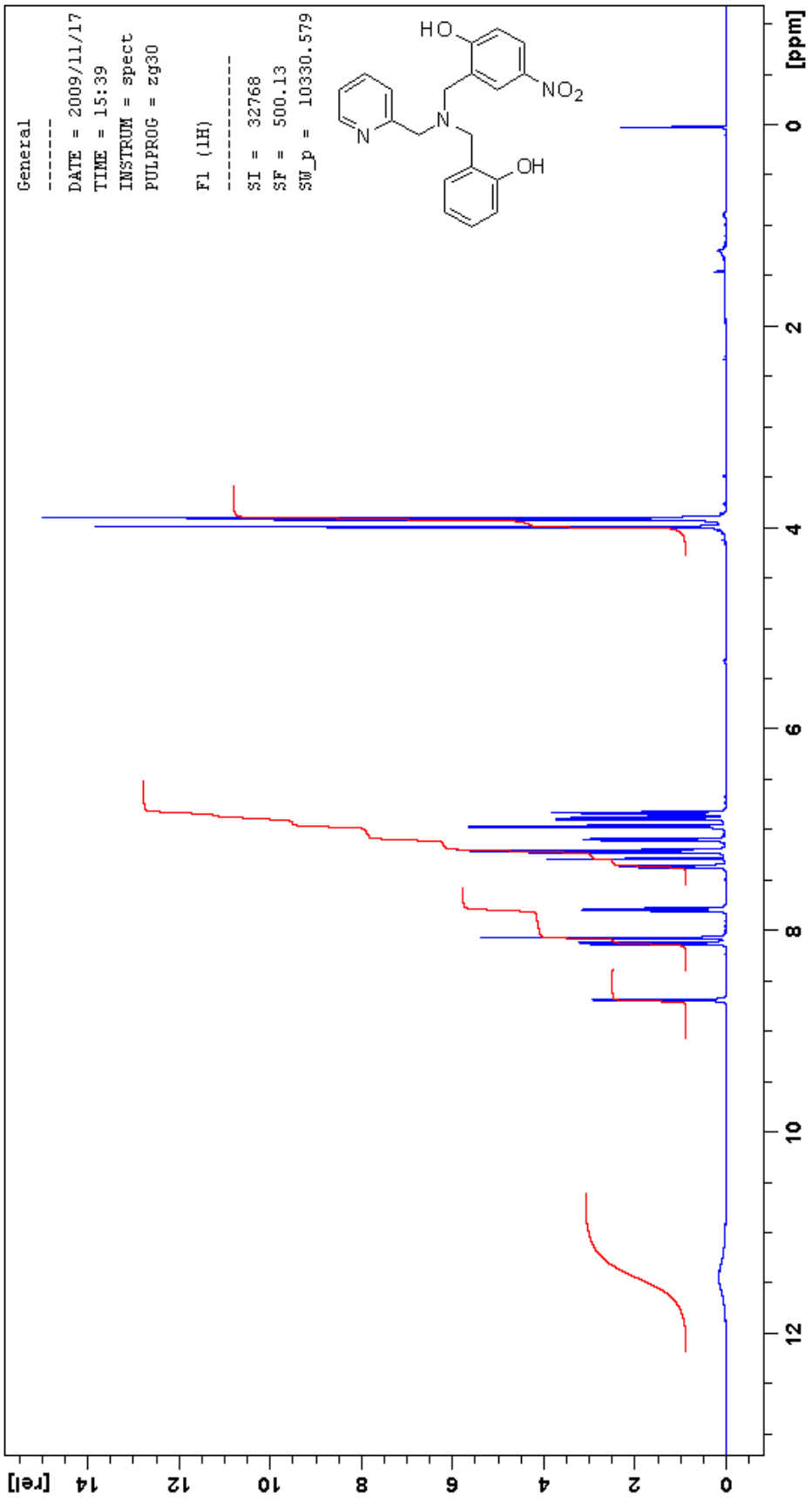
General
DATE = 2009/11/17
TIME = 15:39
INSTRUM = spect
PULPROG = zg30
F1 (1H)
SI = 32768
SF = 500.13
SW_p = 10330.579
HO
NO2
N
N
OH
[rel]
[ppm]

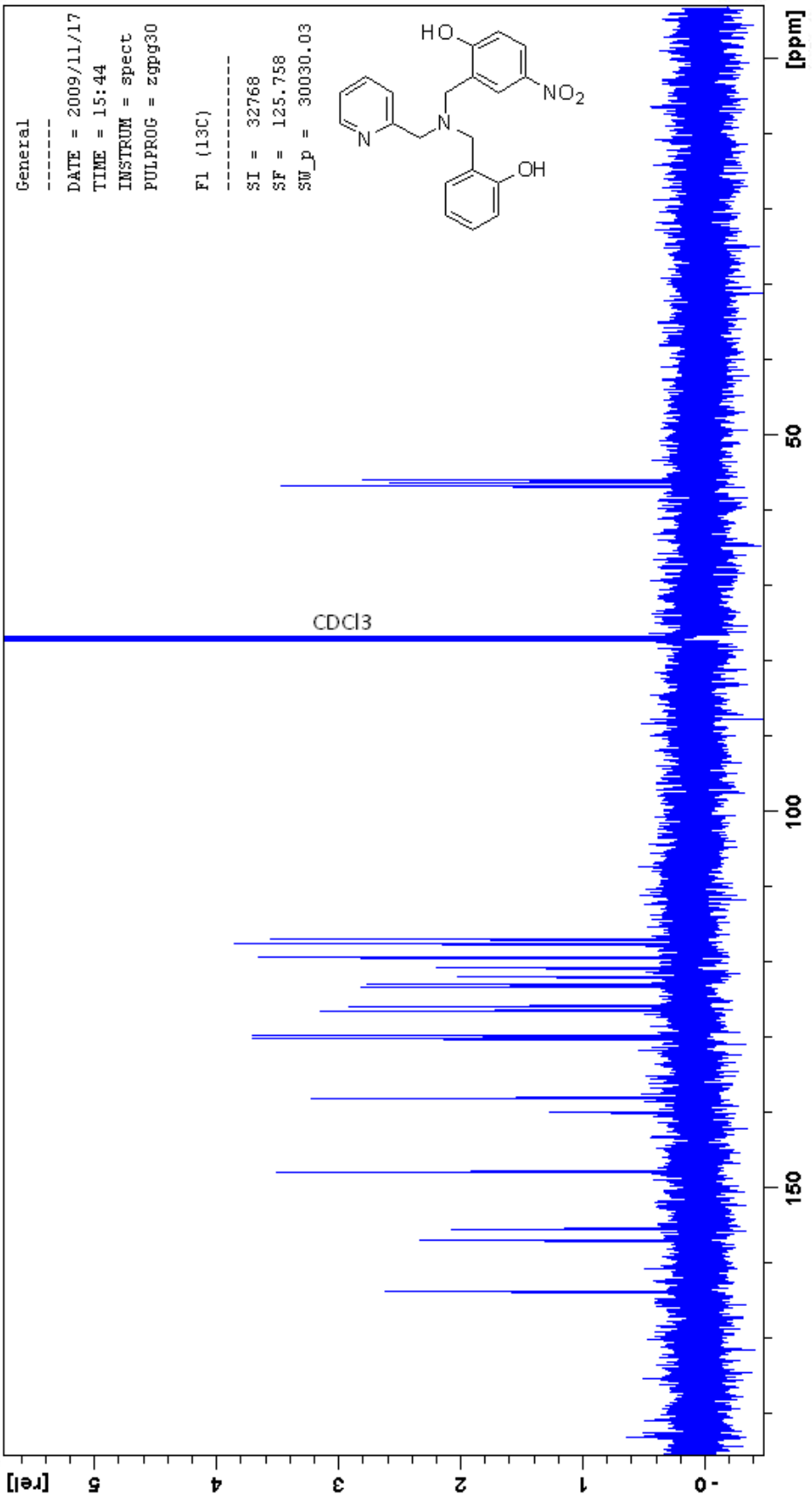
General
DATE = 2009/11/17
TIME = 15:44
INSTRUM = spect
PULPROG = zgpg30
F1 (13C)
SI = 32768
SF = 125.758
SW_p = 30030.03
HO
NO2
N
N
OH
CDCl3
[ppm]
[rel]

A.6.21 Methyl 3-(2-hydroxybenzylamino)propanoate (562)

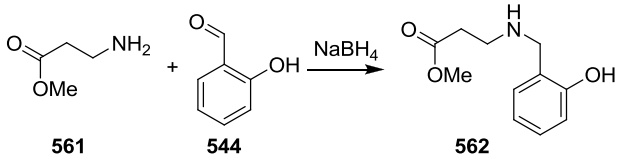

561 **544** **562**

Methyl 3-aminopropanoate hydrochloride (**561**) (0.572 mL, 4.10 mmol) and triethylamine (0.572 mL, 4.10 mmol) in MeOH (10 mL) were stirred together for 1 min to neutralise the hydrochloride salt of **561**. 2-Hydroxybenzaldehyde (**544**) (0.500 g, 4.10 mmol) was added and the resulting solution was stirred for 30 min at RT. Next $NaBH_4$ (0.246 g, 6.48 mmol) and NaOH (0.033 g, 0.82 mmol) in H_2O (2 mL) were added and the reaction mixture was stirred for 1 h. The reaction was diluted with CH_2Cl_2 (200 mL) and washed with water (200 mL). The organic layer was filtered and dried over $MgSO_4$ and the solvent was removed. The colourless oil **562** was purified by silica gel column chromatography using 95:5 CH_2Cl_2 / MeOH (0.722 g, 84 %). R_f = 0.29 (95:5 CH_2Cl_2 / MeOH). ^{1}H NMR (500 MHz, $CDCl_3$) δ 2.59 (t, *J* = 6.1, 2H; C*H*$_2$), 2.96 (t, *J* = 6.1, 2H; C*H*$_2$), 3.72 (s, 3H; C*H*$_3$), 4.02 (s, 2H; C*H*$_2$), 6.80 (td, *J* = 1.0, 7.3, 1H; Ar*H*), 6.85 (dd, *J* = 1.0, 8.1, 1H; Ar*H*), 7.01 (d, *J* = 6.7, 1H; Ar*H*), 7.18 (td, *J* = 1.0, 7.4, 1H; Ar*H*); ^{13}C NMR (125 MHz, $CDCl_3$) δ 33.6 (d), 43.6 (d), 51.8 (t), 52.4 (d), 116.3 (s), 119.0 (s), 122.2 (q), 128.4 (s), 128.8 (s), 158.1 (q), 172.8 (q). MS for $C_{11}H_{15}NO_3$ (MH^+) 210.61. $C_{11}H_{15}NO_3$•0.5H_2O (218.25): calcd. C 60.54, H 7.39, N 6.42; found C 60.96, H 7.10, N 6.69.

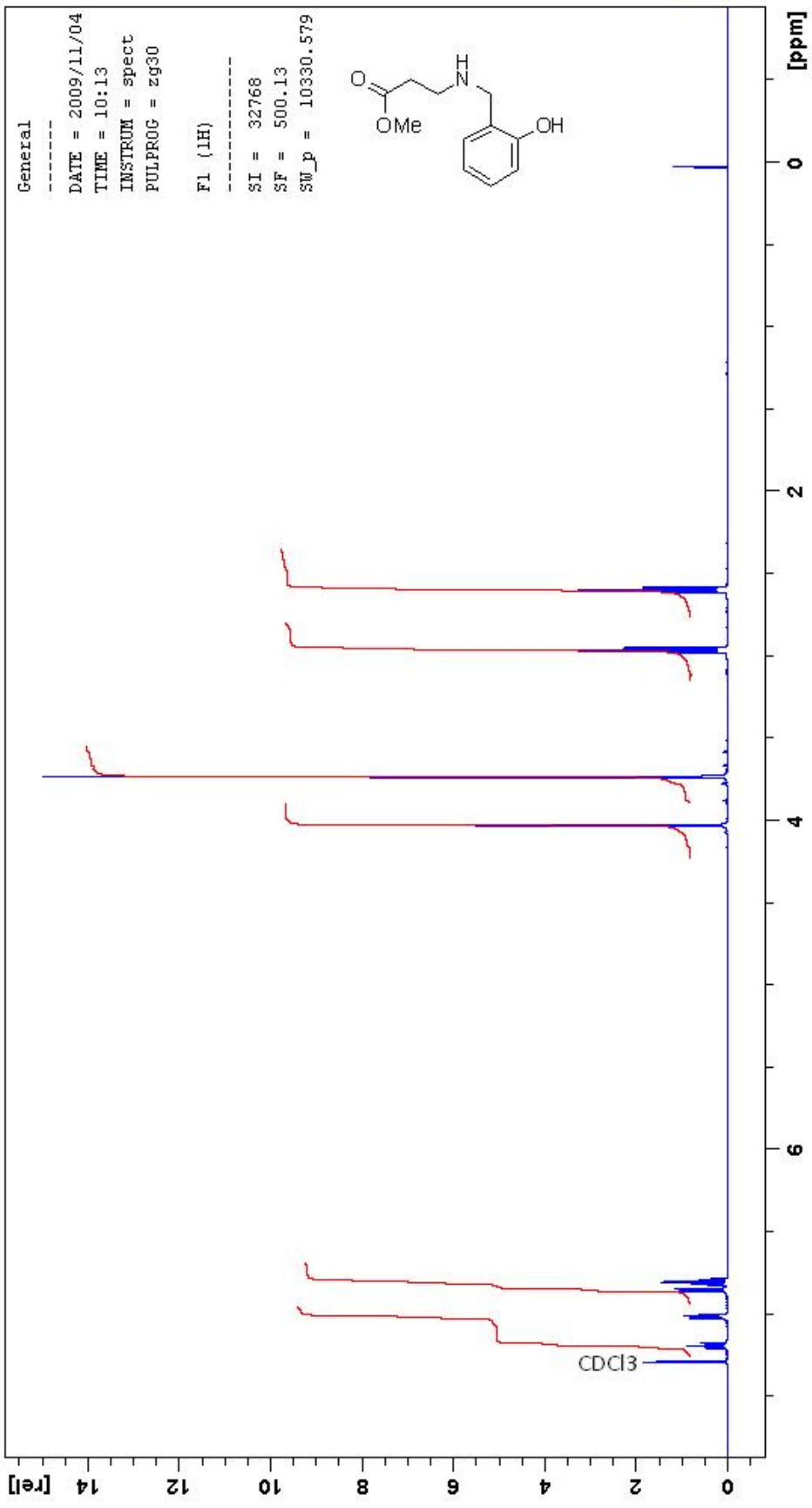
General
DATE = 2009/11/04
TIME = 10:13
INSTRUM = spect
PULPROG = zg30
F1 (1H)
SI = 32768
SF = 500.13
SW_p = 10330.579
O
OMe
NH
OH
CDCl3
[rel]
[ppm]

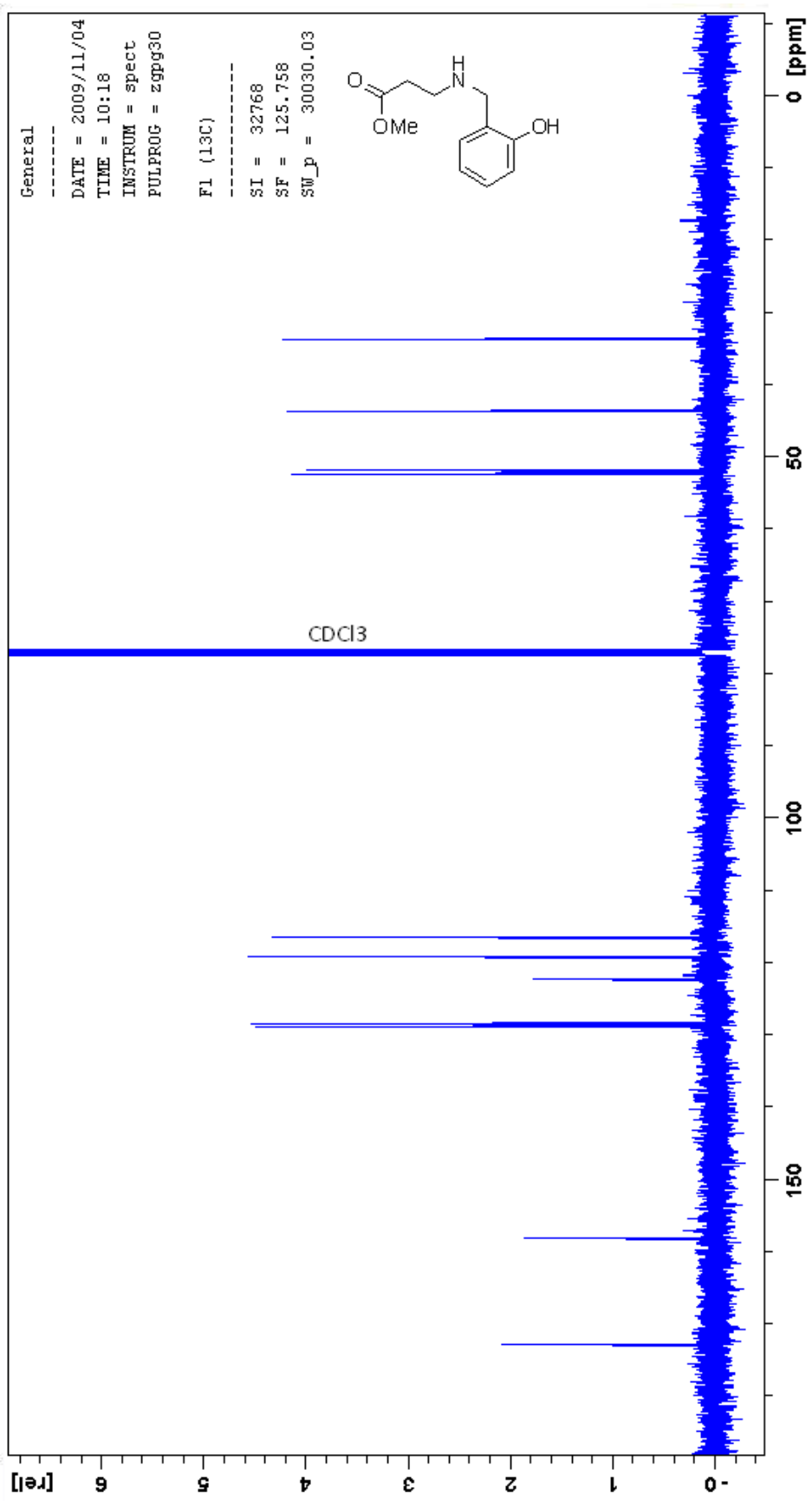
General
DATE = 2009/11/04
TIME = 10:18
INSTRUM = spect
PULPROG = zgpg30
F1 (13C)
SI = 32768
SF = 125.758
SW_p = 30030.03
O
OMe
H
N
OH
CDCl3
[rel]
[ppm]

A.6.22 Methyl 3-((2-hydroxy-5-nitrobenzyl)(2-hydroxybenzyl)amino)propanoate (549)

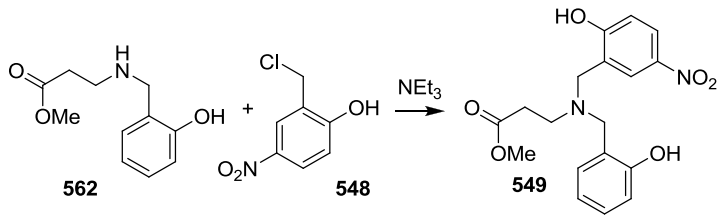

Methyl 3-(2-hydroxybenzylamino)propanoate (**562**) (0.722 g, 3.45 mmol), 2-(chloromethyl)-4-nitrophenol (**548**) (0.647 g, 3.45 mmol) and triethylamine (3.82 mL, 27.6 mmol) were refluxed together in $CHCl_3$ (20 mL) for 2 h. The reaction was diluted with CH_2Cl_2 (200 mL) and washed with water (200 mL). The organic layer was filtered and dried over $MgSO_4$. The yellow oil **549** was purified by silica gel column chromatography using 98:2 CH_2Cl_2 / MeOH. Residual MeOH caused **549** to remain as an oil, this was removed by dissolving the residue in a minimum volume of CH_2Cl_2 and precipitating with hexane addition, decanting and drying under vacuum to give a yellow powder (0.611 g, 46 %). R_f = 0.50 (95:5 CH_2Cl_2 / MeOH). ^{1}H NMR (500 MHz, $CDCl_3$) δ 2.73 (t, *J* = 7.4, 2H; C*H*$_2$), 3.02 (t, *J* = 7.4, 2H; C*H*$_2$), 3.69 (s, 3H; C*H*$_3$), 3.85 (s, 2H; C*H*$_2$), 3.89 (s, 2H; C*H*$_2$), 6.77 – 6.81 (m, 2H; Ar*H*), 6.88 (t, *J* = 7.4, 1H; Ar*H*), 7.13 – 7.20 (m, 2H; Ar*H*), 8.00 (d, *J* = 2.3, 1H; Ar*H*), 8.05 (dd, *J* = 2.7, 8.9, 1H; Ar*H*), 8.20 (brs, 2H; O*H*); ^{13}C NMR (125 MHz, $CDCl_3$) δ 31.2 (d), 49.2 (d), 52.1 (t), 55.0 (d), 56.2 (d), 116.0 (s), 116.5 (s), 120.5 (s), 121.0 (q), 121.7 (q), 125.9 (s), 130.0 (s), 131.1 (s), 139.7 (q), 155.4 (s), 157.0 (q), 164.4 (q), 172.3 (q). MS for $C_{18}H_{20}N_2O_6$ (MH^+) 361.73. $C_{18}H_{20}N_2O_6$ (360.36): calcd. C 59.99, H 5.59, N 7.77; found C 59.84, H 5.53, N 7.70.

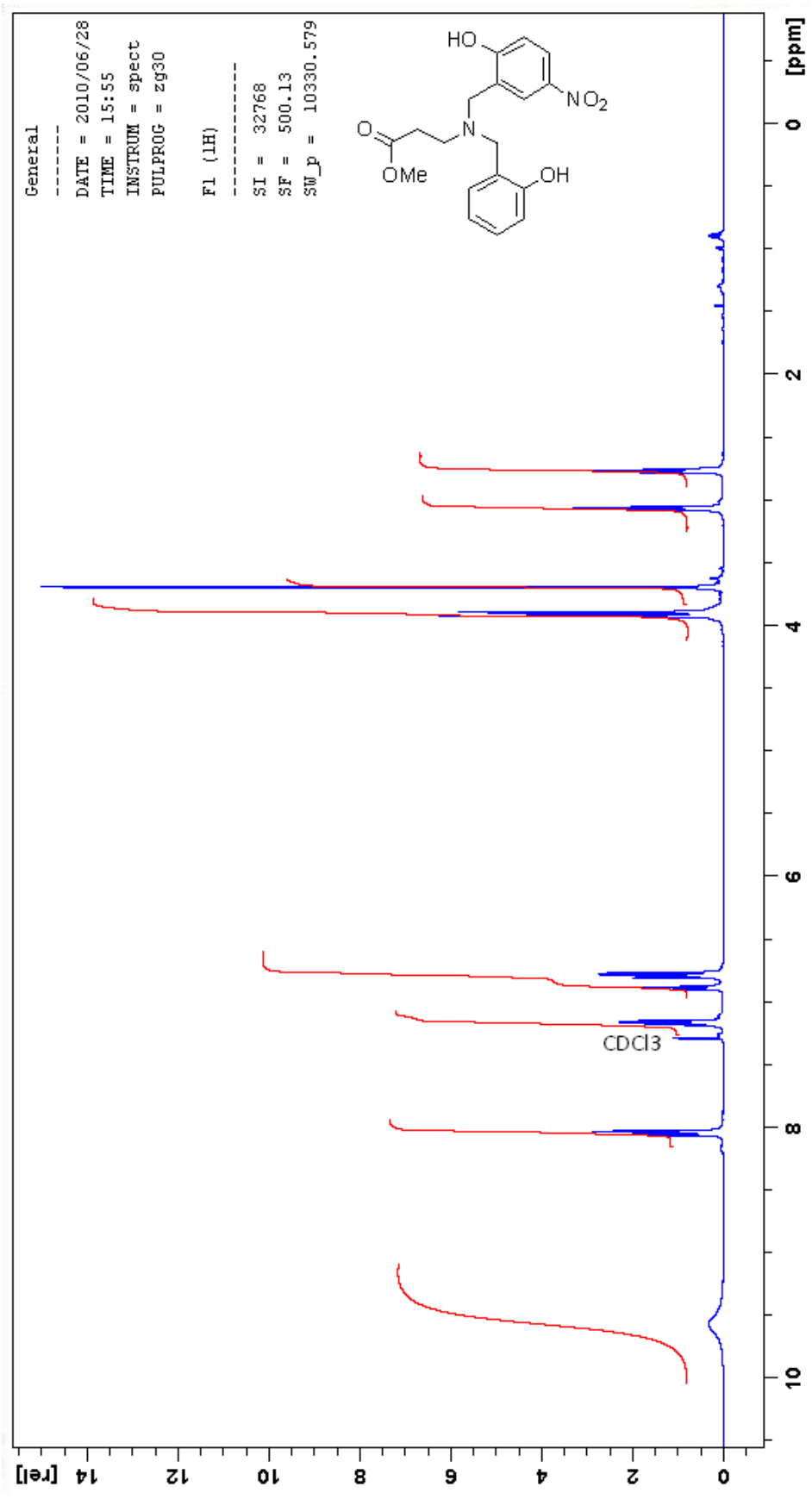
General
DATE = 2010/06/28
TIME = 15:55
INSTRUM = spect
PULPROG = zg30
F1 (1H)
SI = 32768
SF = 500.13
SW_p = 10330.579
HO
NO2
O
N
OMe
OH
CDCl3
[rel]
[ppm]

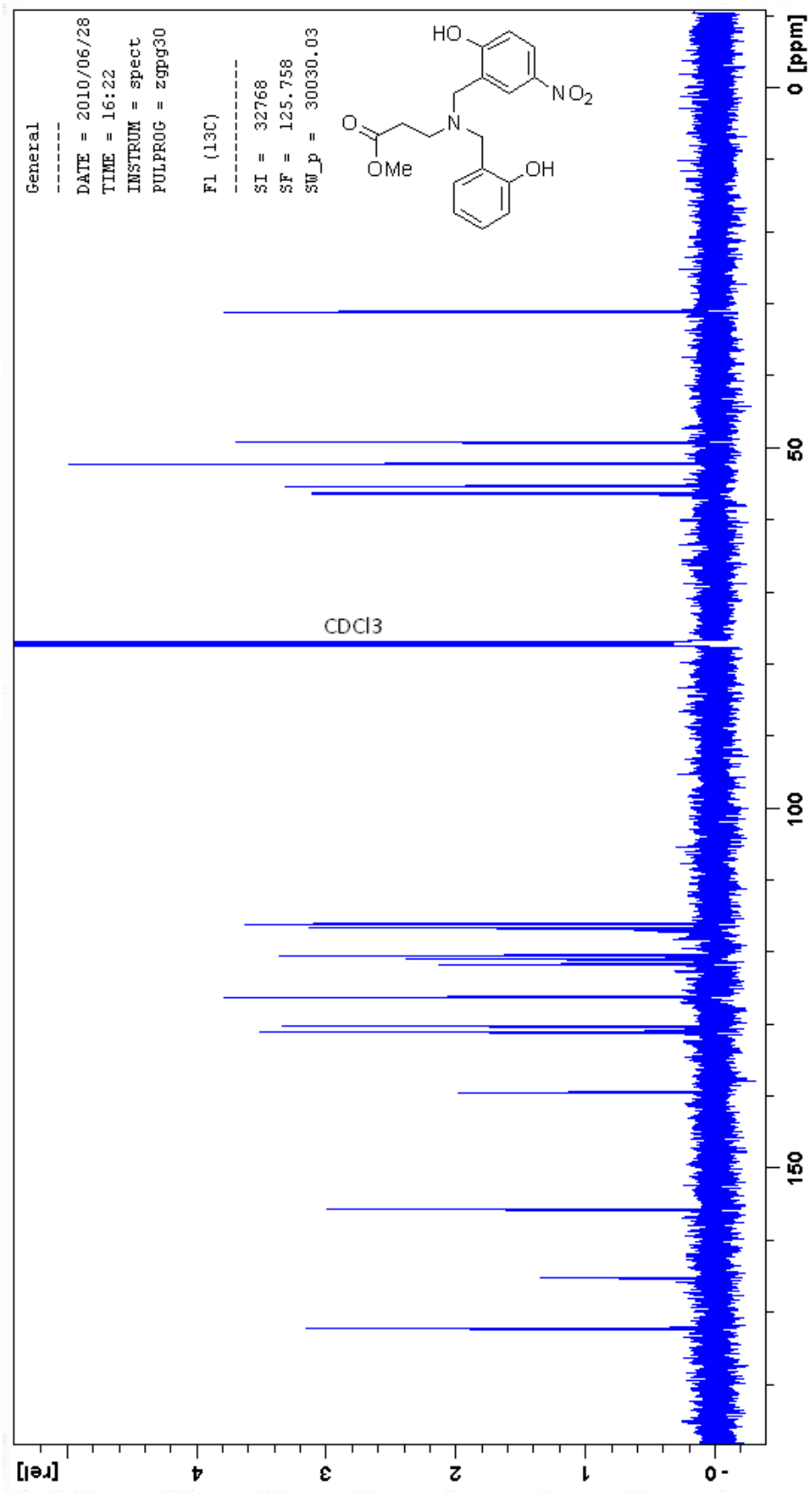
General
DATE = 2010/06/28
TIME = 16:22
INSTRUM = spect
PULPROG = zgpg30
F1 (13C)
SI = 32768
SF = 125.758
SW_p = 30030.03
HO
NO2
N
O
OMe
OH
CDCl3
0 [ppm]
50
100
150
[rel]
0
1
2
3
4

A.6.23 3-((2-Hydroxy-5-nitrobenzyl)(2-hydroxybenzyl)amino)propanoic acid (L17)

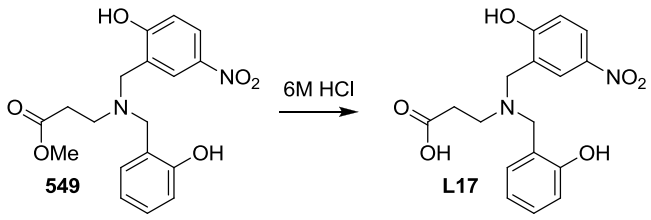

Methyl 3-((2-hydroxy-5-nitrobenzyl)(2-hydroxybenzyl)amino)propanoate (**549**) (0.100 g, 0.417 mmol) in 6M HCl (2 mL) was refluxed for 4 h at 110 ^{o}C. The reaction mixture was diluted with water (200 mL) and washed with CH_2Cl_2 (200 mL). The aqueous layer was separated and neutralised with 1M NaOH to pH 7 and **L17** was transferred into an organic layer of 9:1 CH_2Cl_2 / MeOH (200 mL). The organic layer was separated then filtered and dried over $MgSO_4$ and the solvent removed. The pale yellow solid **L17** was dissolved in CH_2Cl_2 and precipitated upon addition of hexane then filtered (0.047 g, 49 %). R_f = 0.36 (90:10 DCM / MeOH). ^{1}H NMR (500 MHz, DMSO-d6) δ 2.53 (t, *J* = 7.4 Hz, 2H; C*H*$_2$), 2.74 (t, *J* = 7.4 Hz, 2H, C*H*$_2$), 3.50 (brs, 1H; COO*H*), 3.70 (s, 2H; C*H*$_2$), 3.78 (s, 2H; C*H*$_2$), 6.77 (m, 2H; Ar*H*), 6.89 (t, *J* = 9.0, 1H; Ar*H*), 7.10 (td, *J* = 1.5, 7.4, 1H; Ar*H*), 7.17 (dd, *J* = 1.5, 7.4, 1H; Ar*H*), 8.03 (dd, *J* = 2.8, 9.0, 1H; Ar*H*), 8.14 (d, *J* = 2.8, 1H; Ar*H*); ^{13}C NMR (125 MHz, DMSO-d6) δ 31.0 (d), 48.6 (d), 53.2 (d), 53.6 (d), 115.7 (s), 116.2 (q), 119.3 (s), 123.1 (s), 124.7 (q), 125.3 (q), 126.3 (s), 129.0 (s), 130.7 (s), 139.5 (q), 156.8 (s), 164.2 (q), 173.6 (q). HRMS calculated for $C_{17}H_{18}N_4O_6$ (MH^+) 347.1238, found 347.1228 (ESI+).

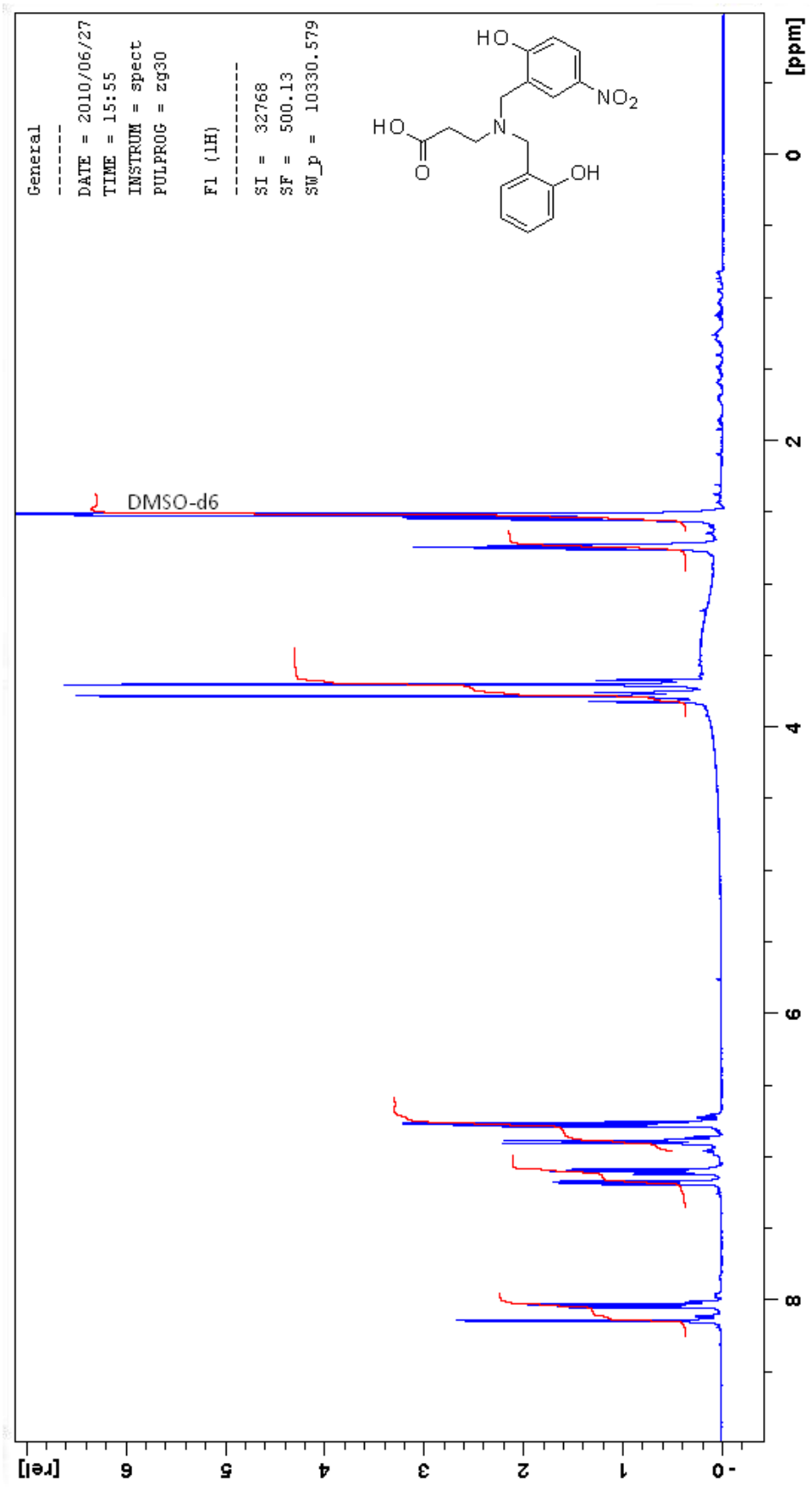
General
DATE = 2010/06/27
TIME = 15:55
INSTRUM = spect
PULPROG = zg30
F1 (1H)
SI = 32768
SF = 500.13
SW_p = 10330.579
HO
NO2
HO
O
N
OH
DMSO-d6
[ppm]
[rel]

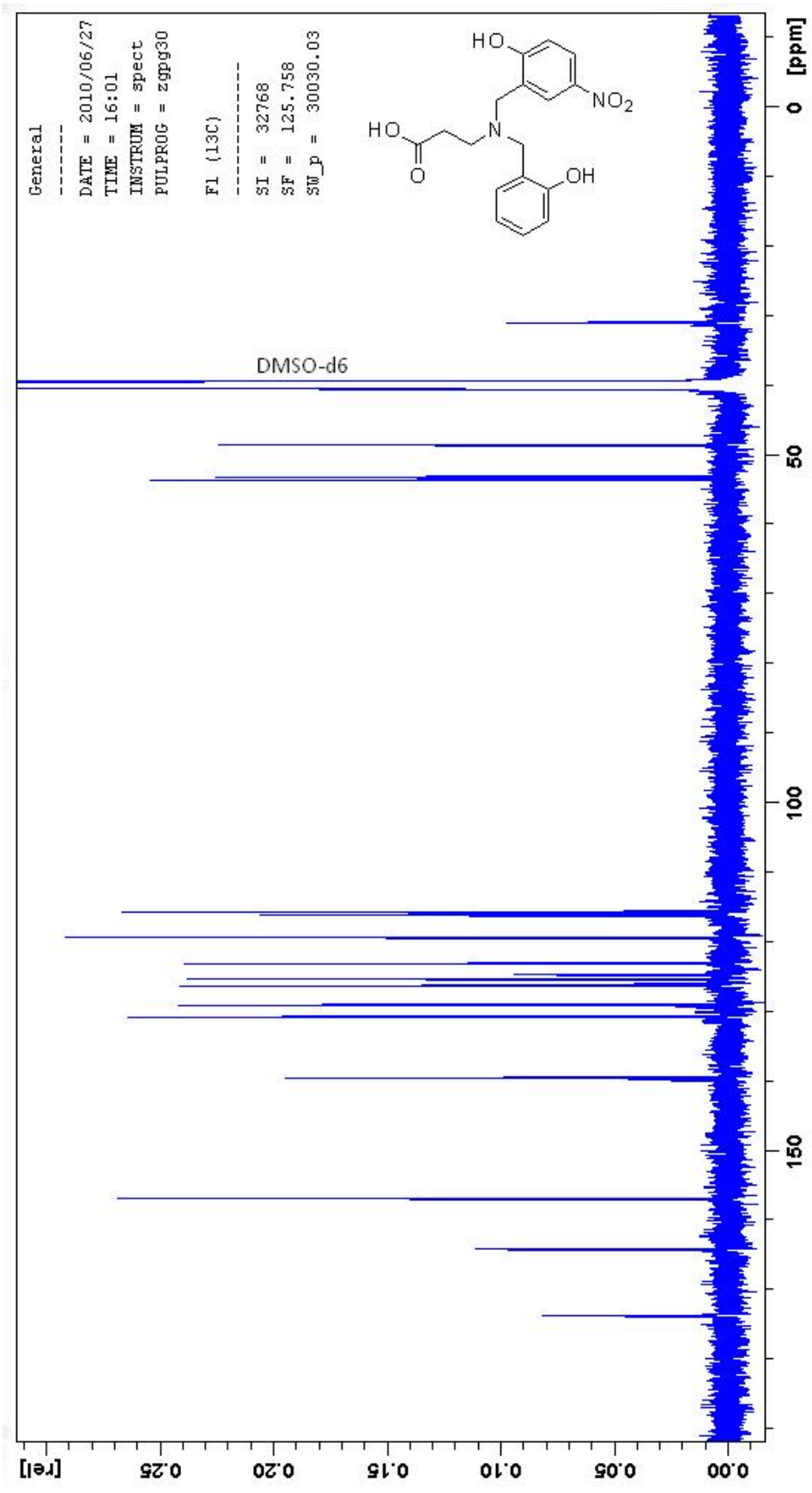
General
DATE = 2010/06/27
TIME = 16:01
INSTRUM = spect
PULPROG = zgpg30
F1 (13C)
SI = 32768
SF = 125.758
SW_p = 30030.03
HO
NO2
HO
O
N
OH
DMSO-d6
[ppm]
0
50
100
150
[rel]
0.00
0.05
0.10
0.15
0.20
0.25

A.6.24 2-(bis(2-Hydroxy-3,5-dimethylbenzyl)amino)acetic acid (L18)

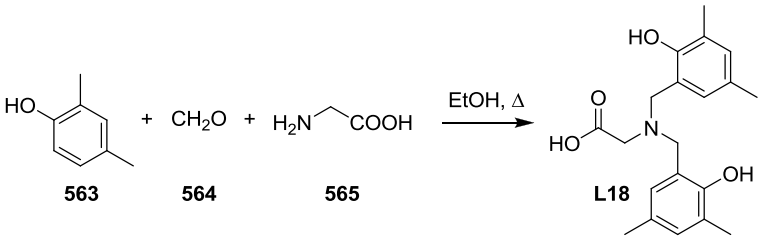

2-(*bis*(2-Hydroxy-3,5-dimethylbenzyl)amino)acetic acid (**L18**) was a known compound synthesised according to the literature procedure.[165] 2,4-Dimethylphenol (**563**) (1.00 g, 8.20 mmol), 2-aminoacetic acid (**565**) (0.614 g, 8.20 mmol) and formaldehyde (**564**) (0.327 g, 10.91 mmol) in EtOH (100 mL) were refluxed together overnight. The precipitate of **L18** was filtered and recrystallised from MeOH / pyridine (0.817 g, 29 %). ^{1}H NMR (500 MHz, DMSO-d6) δ 2.05 (s, 6H; C*H*$_3$), 2.12 (s, 6H; C*H*$_3$), 2.82 (s, 2H; C*H*$_2$), 3.52 (s, 4H; C*H*$_2$), 5.75 (brs, 1H; O*H*), 6.66 (s, 2H; Ar*H*), 6.77 (s, 2H; Ar*H*), 10.76 (brs, 1H; O*H*); ^{13}C NMR (125 MHz, DMSO-d6) δ 16.4 (t), 20.4 (t), 56.4 (d), 56.9 (d), 121.8 (x), 124.2 (x), 126.4 (x), 128.5 (x), 130.8 (x), 153.3 (x), 174.6 (q). MS for $C_{20}H_{25}NO_4$ (MH^+) 344.87.

A.6.25 2-(2-Hydroxybenzylamino)phenol (567)

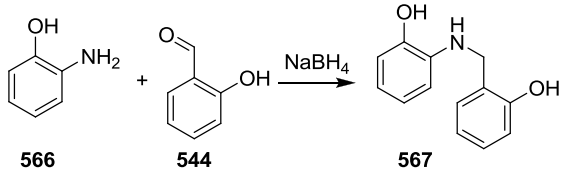

2-(2-Hydroxybenzylamino)phenol (**567**) was a known compound and prepared according to the literature procedure.[198] 2-Aminophenol (**566**) (0.449 mL, 4.10 mmol) and 2-hydroxybenzaldehyde (**544**) (0.500 g, 4.10 mmol) in MeOH (10 mL) were stirred for 6 hr at RT. $NaBH_4$ (0.246 g, 6.48 mmol) and NaOH (0.033 g, 0.82 mmol) in H_2O (2 mL) were added and the resulting mixture was stirred for 1 h. The reaction was diluted with CH_2Cl_2 (200 mL) and washed with water (200 mL). The organic layer was filtered and dried over

$MgSO_4$ and the solvent was removed. The brown powder **567** (0.766 g, 87 %) was used directly in the next step. ^{1}H NMR (500 MHz, $CDCl_3$) δ 4.44 (s, 2H; C*H*$_2$), 6.26 (brs, 1H; N*H*) 6.74 – 6.80 (m, 2H; Ar*H*), 6.86 – 6.94 (m, 4H; Ar*H*), 7.20 (m, 1H; Ar*H*), 7.25 (m, 1H; Ar*H*); ^{13}C NMR (125 MHz, $CDCl_3$) δ 48.9 (d), 114.8 (s), 115.5 (s), 116.7 (s), 120.3 (s), 120.9 (s), 121.6 (s), 123.3 (q), 128.7 (s), 129.1 (s), 135.8 (q), 145.0 (q), 156.6 (q). MS for $C_{13}H_{13}NO_2$ (MH^+) 216.19.

A.6.26 2-(((2-Hydroxybenzyl)(2-hydroxyphenyl)amino)methyl)-4-nitrophenol (L19)

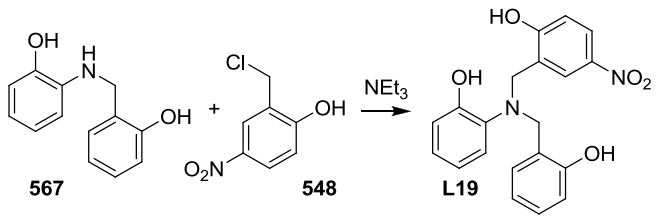

2-(2-Hydroxybenzylamino)phenol (**567**) (0.766 g, 3.37 mmol), 2-(chloromethyl)-4-nitrophenol (**548**) (0.632 g, 3.37 mmol) and triethylamine (3.80 mL, 27.5 mmol) were refluxed together in $CHCl_3$ (20 mL) for 2 h. The reaction was diluted with CH_2Cl_2 (200 mL) and washed with water (200 mL). The organic layer was filtered and dried over $MgSO_4$. The light brown oil **L19** was purified by silica gel column chromatography using 2:1 Hexanes / EtOAc. Residual EtOAc caused **L19** to remain as an oil, this was removed by dissolving the residue in a minimum volume of CH_2Cl_2 and precipitating with hexane addition, decanting and drying under vacuum to give a light brown powder (0.839 g, 68 %). R_f = 0.54 (95:5 CH_2Cl_2 / MeOH). ^{1}H NMR (500 MHz, $CDCl_3$) δ 4.22 (s, 2H; C*H*$_2$), 4.36 (s, 2H; C*H*$_2$), 6.77 (d, *J* = 9.0, 1H; Ar*H*), 6.87 – 6.95 (m, 4H; Ar*H*), 7.03 – 7.08 (m, 1H; Ar*H*), 7.11 (brs, 3H; O*H*) 7.20 – 7.26 (m, 3H; Ar*H*), 8.00 (dd, *J* = 2.8, 9.0, 1H; Ar*H*), 8.05 (d, *J* = 2.8, 1H; Ar*H*); ^{13}C NMR (125 MHz, $CDCl_3$) δ 54.0 (d), 57.9 (d), 116.1 (s), 116.5 (s), 116.9 (s), 120.9 (s), 121.2 (s), 121.6 (q), 121.6 (s), 122.4 (q), 125.7 (s), 126.2 (s), 127.1 (s), 130.3 (s), 131.6 (s), 133.8 (q), 140.5 (q), 151.0 (q), 154.5 (q), 163.4 (q). MS for $C_{20}H_{18}N_2O_5$ (MH^+) 367.72. $C_{20}H_{18}N_2O_5$ (366.37): calcd. C 65.57, H 4.95, N 7.65; found C 65.61, H 4.97, N 7.50. M.P. = 158 – 159 ^{o}C.

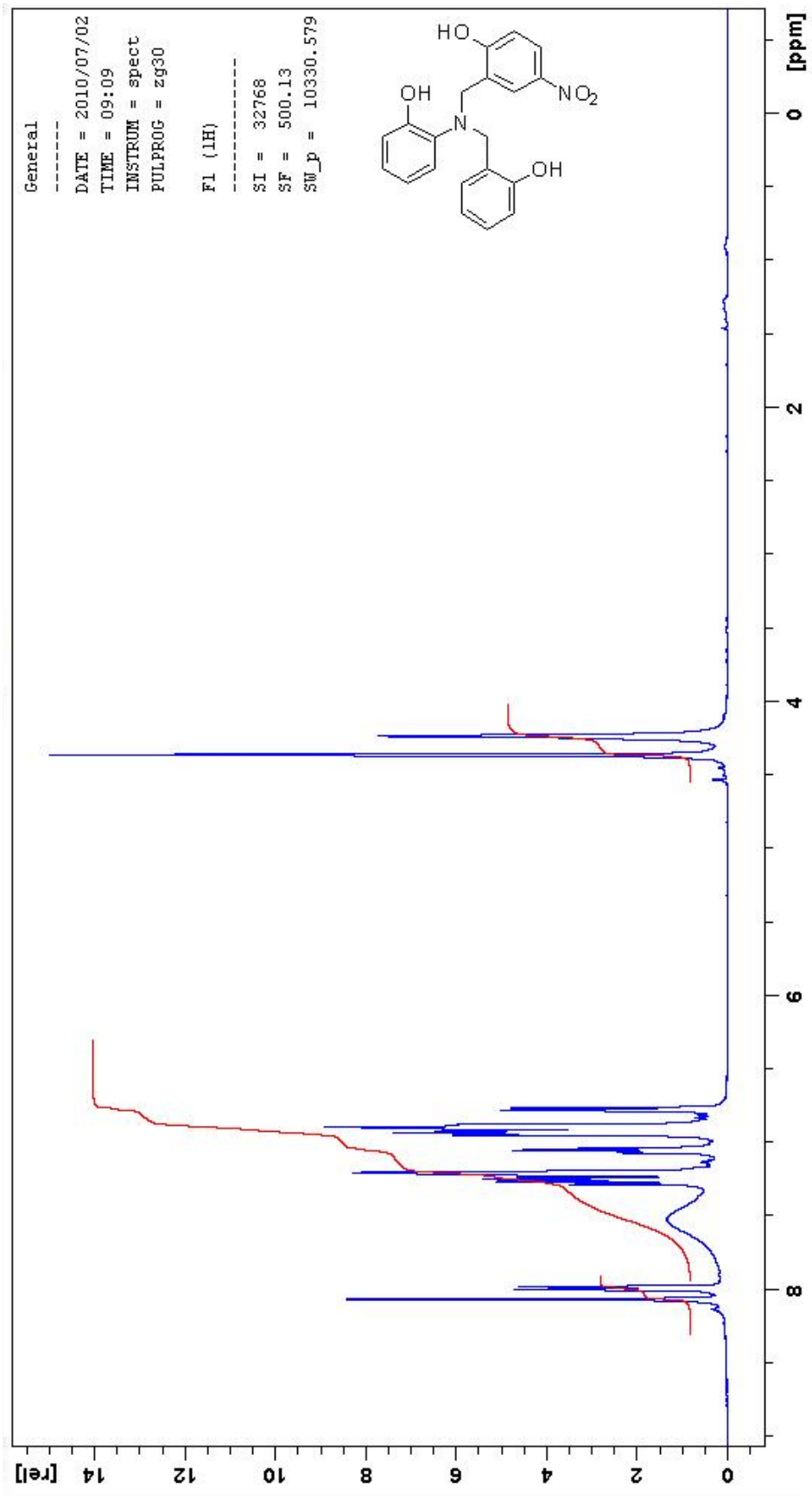
General
DATE = 2010/07/02
TIME = 09:09
INSTRUM = spect
PULPROG = zg30
F1 (1H)
SI = 32768
SF = 500.13
SW_p = 10330.579
HO
OH
N
NO2
OH
[rel]
[ppm]

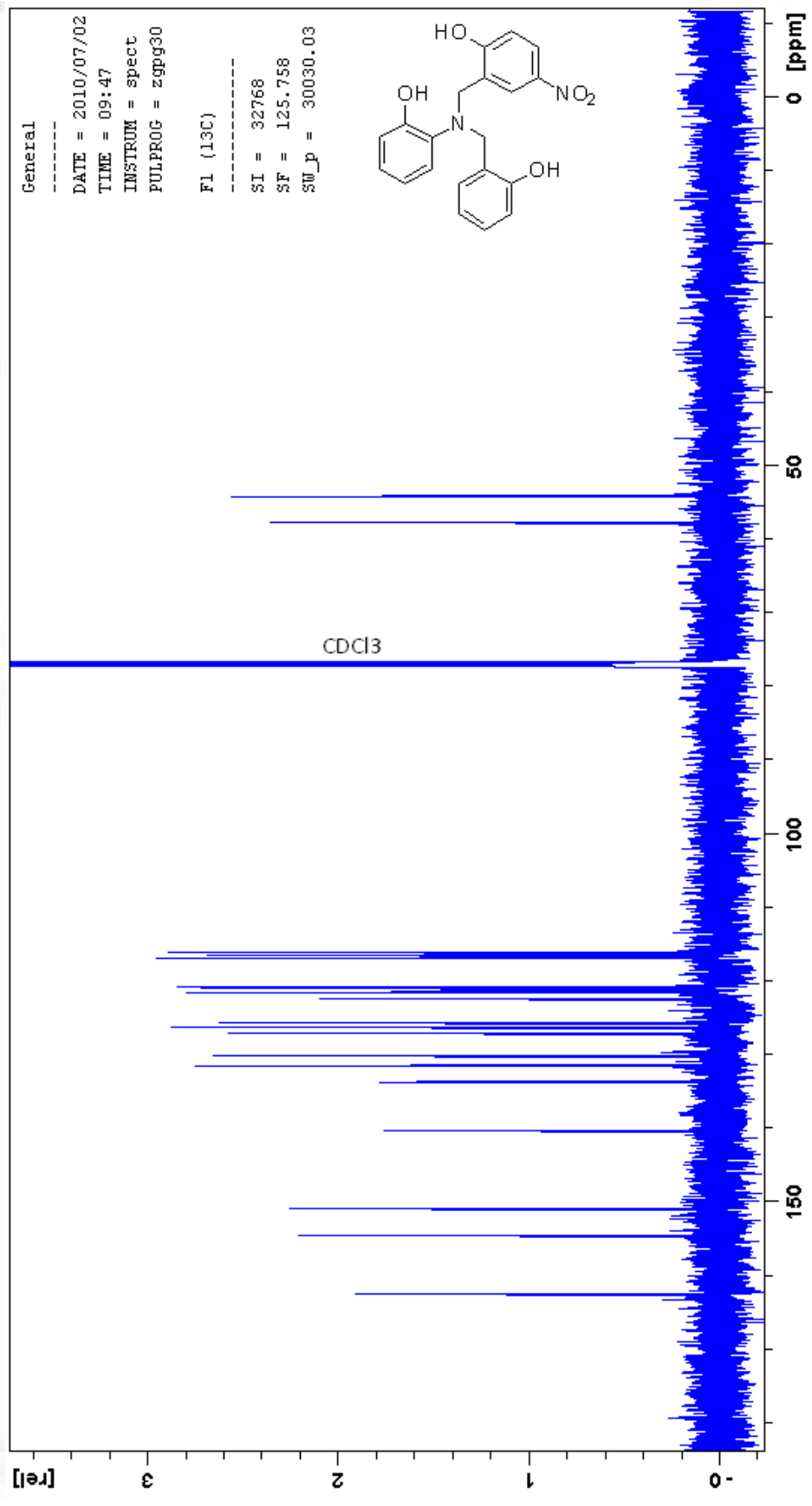
General
DATE = 2010/07/02
TIME = 09:47
INSTRUM = spect
PULPROG = zgpg30
F1 (13C)
SI = 32768
SF = 125.758
SW_p = 30030.03
HO
OH
N
NO2
OH
CDCl3
[rel]
[ppm]
0
50
100
150

A.6.27 2-((Quinolin-8-ylamino)methyl)phenol (569)

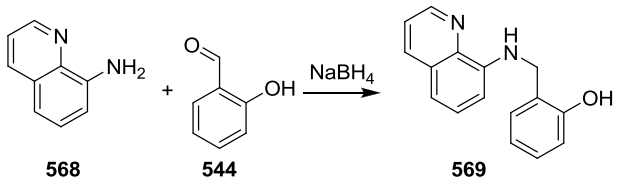

568 **544** **569**

2-((Quinolin-8-ylamino)methyl)phenol (**569**) was prepared according to the known literature procedure.[199] Quinolin-8-amine (**568**) (0.590 g, 4.10 mmol) and 2-hydroxybenzaldehyde (**544**) (0.500 g, 4.10 mmol) in MeOH (10 mL) were stirred for 1 week at RT. $NaBH_4$ (0.246 g, 6.48 mmol) and NaOH (0.033 g, 0.82 mmol) in H_2O (2 mL) were added and the resulting mixture was stirred for 1 h. The reaction was diluted with CH_2Cl_2 (200 mL) and washed with water (200 mL). The organic layer was filtered and dried over $MgSO_4$ and the solvent removed to give the yellow powder **569** (0.850 g, 83 %) was used directly in the next step. ^{1}H NMR (500 MHz, $CDCl_3$) δ 4.64 (d, *J* = 4.9, 2H; C*H*$_2$), 6.48 (brs, 1H; N*H*), 6.95 (m, 2H; Ar*H*), 6.99 (dd, *J* = 0.9, 7.6, 1H; Ar*H*), 7.24 – 7.28 (m, 3H; Ar*H*), 7.40 – 7.44 (m, 2H; Ar*H*), 8.13 (dd, *J* = 1.6, 8.3, 1H; Ar*H*), 8.24 (brs, 1H; O*H*), 8.78 (dd, *J* = 1.6, 4.2, 1H; Ar*H*); ^{13}C NMR (125 MHz, $CDCl_3$) δ 47.8 (d), 109.3 (s), 116.6 (s), 117.5 (s), 120.2 (s), 121.6 (s), 123.5 (q), 127.4 (s), 128.5 (q), 128.8 (s), 129.0 (s), 136.2 (s), 139.1 (q), 144.5 (q), 147.7 (s), 156.5 (q). MS for $C_{16}H_{14}N_2O$ (MH^+) 251.11.

A.6.28 2-(((2-Hydroxybenzyl)(quinolin-8-yl)amino)methyl)-4-nitrophenol (L20)

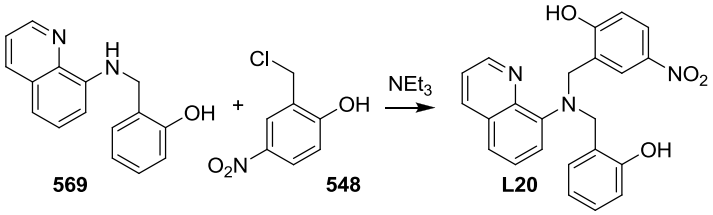

569 **548** **L20**

2-((Quinolin-8-ylamino)methyl)phenol (**569**) (0.850 g, 3.40 mmol), 2-(chloromethyl)-4-nitrophenol (**548**) (0.638 g, 3.40 mmol) and triethylamine (3.84 mL, 27.7 mmol) were

refluxed together in $CHCl_3$ (20 mL) for 2 h. The reaction was diluted with CH_2Cl_2 (200 mL) and washed with water (200 mL). The organic layer was filtered and dried over $MgSO_4$. The orange oil **L20** was purified by silica gel column chromatography using 2:1 Hexanes / EtOAc. Residual EtOAc caused **L20** to remain as an oil, this was removed by dissolving the residue in a minimum volume of CH_2Cl_2 and precipitating with hexane addition, decanting and drying under vacuum to give a light orange powder (0.695 g, 51 %). R_f = 0.82 (95:5 CH_2Cl_2 / MeOH). ^{1}H NMR (500 MHz, $CDCl_3$) δ 4.48 (s, 4H; C*H*$_2$), 6.80 – 6.85 (m, 2H; Ar*H*), 6.90 (d, *J* = 9.1, 1H; Ar*H*), 7.12 – 7.22 (m, 2H; Ar*H*), 7.47 (d, *J* = 5.0, 2H; Ar*H*), 7.59 (q, *J* = 4.1, 2H; Ar*H*), 8.05 (dd, *J* = 3.2, 8.6, 1H; Ar*H*), 8.17 (d, *J* = 2.7, 1H; Ar*H*), 8.31 (dd, *J* = 1.4, 8.6, 1H; Ar*H*), 9.01 (dd, *J* = 1.4, 4.6, 1H; Ar*H*), 10.46 (brs, 1H; O*H*), 12.59 (brs, 1H; O*H*); ^{13}C NMR (125 MHz, $CDCl_3$) δ 56.6 (d), 56.7 (d), 117.1 (s), 117.7 (s), 119.5 (s), 120.9 (q), 121.4 (s), 121.8 (s), 122.2 (q), 124.4 (s), 125.9 (s), 126.8 (s), 127.0 (s), 129.7 (s), 130.1 (q), 130.6 (s), 138.9 (s), 140.0 (q), 141.8 (q), 143.6 (q), 148.3 (s), 156.9 (q), 163.7 (q). MS for $C_{23}H_{19}N_3O_4$ (MH^+) 402.82. $C_{23}H_{19}N_3O_4$ (401.41): calcd. C 68.82, H 4.77, N 10.47; found C 69.03, H 4.69, N 10.50. M.P. = 184 – 185 ^{o}C.

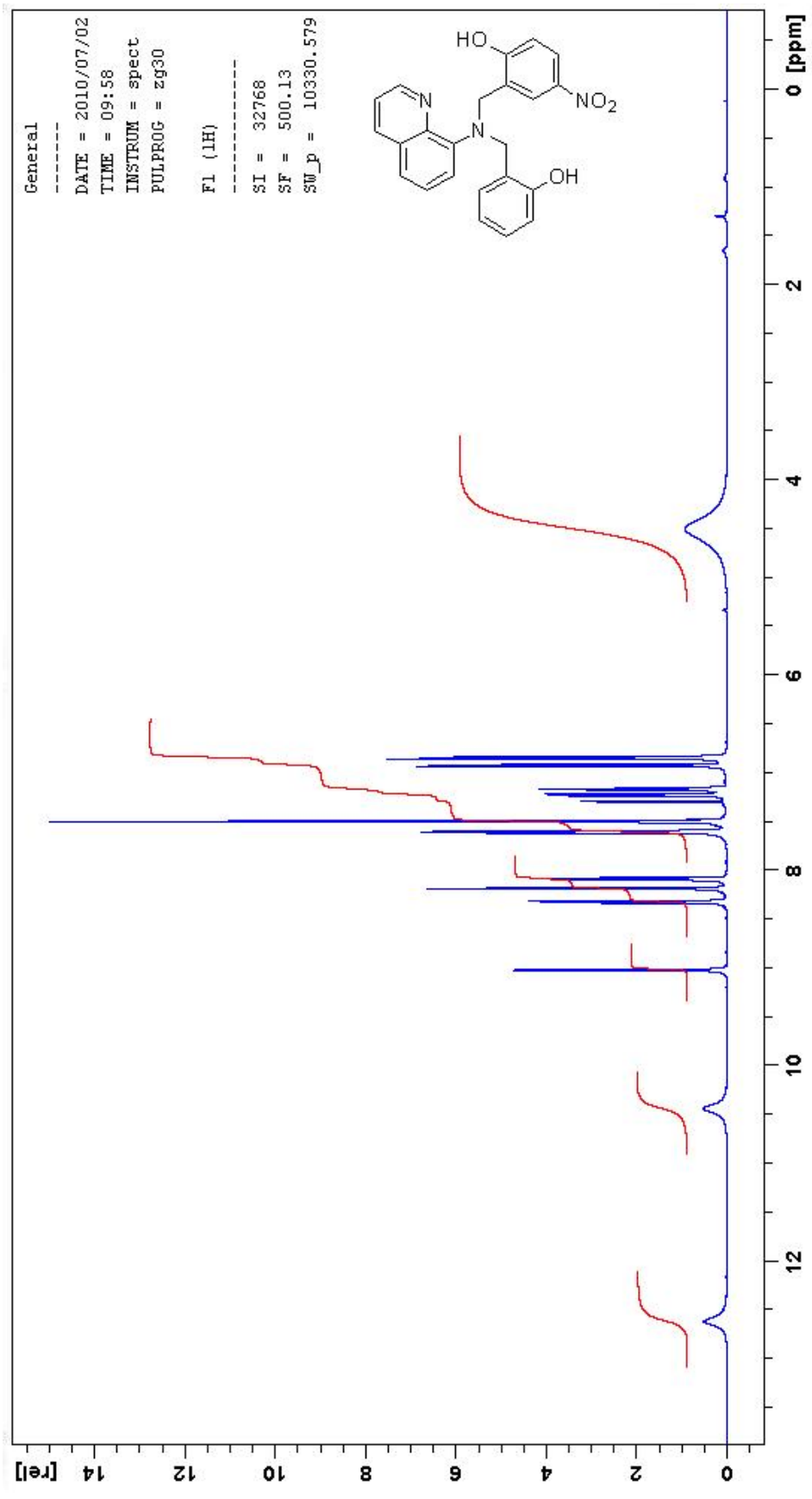
General
DATE = 2010/07/02
TIME = 09:58
INSTRUM = spect
PULPROG = zg30
F1 (1H)
SI = 32768
SF = 500.13
SW_p = 10330.579
HO
NO2
N
N
OH
[rel]
0 [ppm]

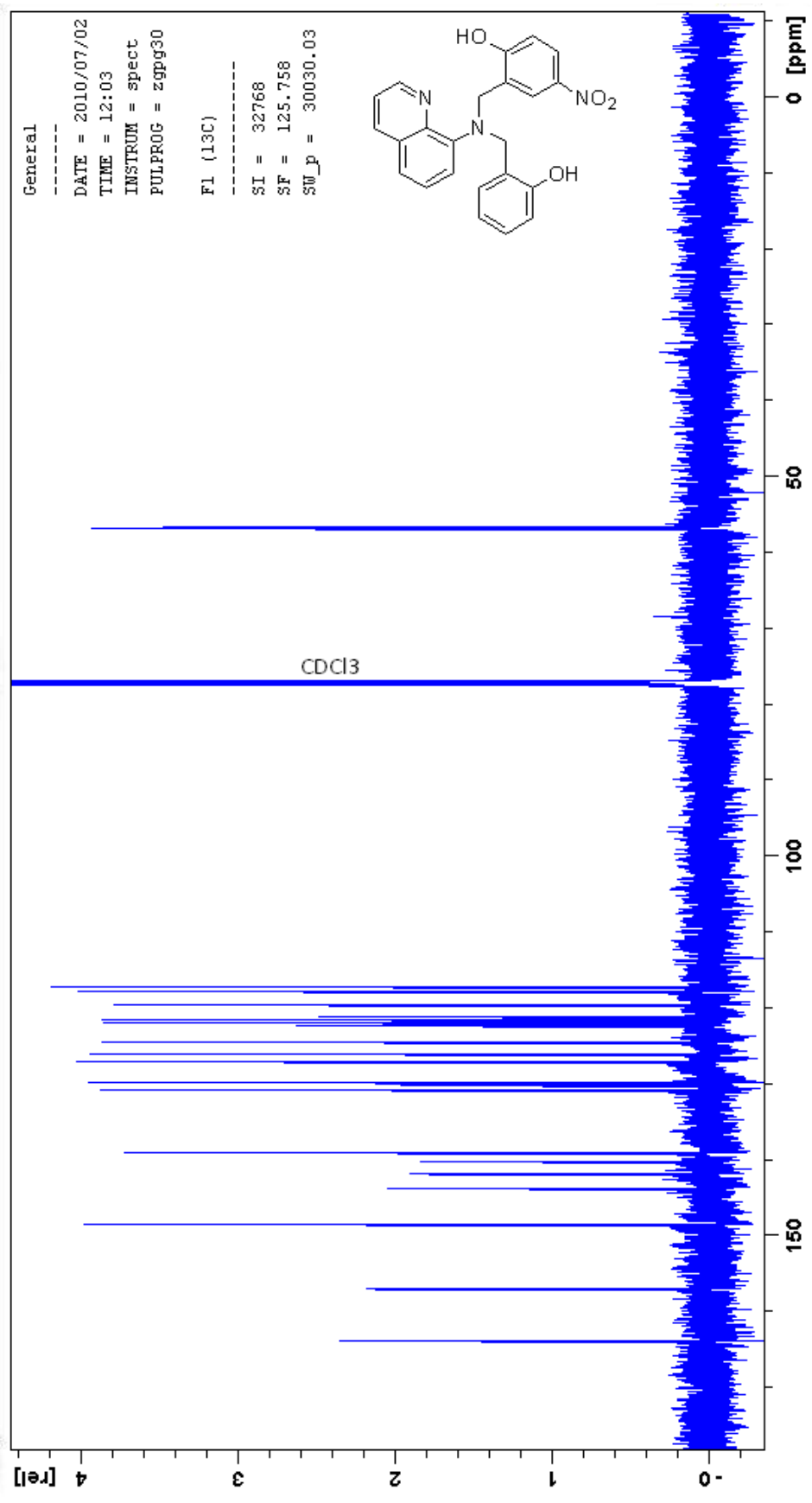
General
DATE = 2010/07/02
TIME = 12:03
INSTRUM = spect
PULPROG = zgpg30
F1 (13C)
SI = 32768
SF = 125.758
SW_p = 30030.03
HO
N
N
NO2
OH
CDCl3
[rel]
[ppm]

A.6.29 2-((2-Phenylquinolin-8-ylamino)methyl)phenol (571)

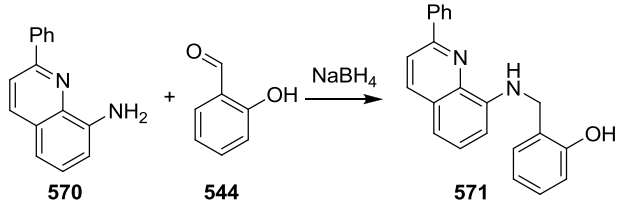

2-Phenylquinolin-8-amine (**570**) (0.902 g, 4.10 mmol) and 2-hydroxybenzaldehyde (**544**) (0.500 g, 4.10 mmol) in MeOH (10 mL) were stirred for 1 week at RT. $NaBH_4$ (0.246 g, 6.48 mmol) and NaOH (0.033 g, 0.82 mmol) in H_2O (2 mL) were added and the resultant solution was stirred for 1 h. The reaction was diluted with CH_2Cl_2 (200 mL) and washed with water (200 mL). The organic layer was filtered and dried over $MgSO_4$ the solvent removed. The light yellow powder **571** (1.189 g, 89 %) was used directly in the next step. R_f = 0.80 (95:5 CH_2Cl_2 / MeOH). ^{1}H NMR (500 MHz, $CDCl_3$) δ 4.66 (d, *J* = 3.8, 2H; C*H*$_2$), 6.67 (brs, 1H; N*H*), 6.90 – 6.98 (m, 3H; Ar*H*), 7.21 – 7.26 (m, 2H; Ar*H*), 7.34 (t, *J* = 7.8, 1H; Ar*H*), 7.42 – 7.52 (m, 3H; Ar*H*), 7.88 (d, *J* = 8.5, 1H; Ar*H*), 7.11 – 7.16 (m, 3H; Ar*H*), 8.31 (brs, 1H; O*H*); ^{13}C NMR (125 MHz, $CDCl_3$) δ 48.2 (d), 109.7 (s), 116.6 (s), 117.4 (s), 119.3 (s), 120.1 (s), 123.4 (q), 127.1 (s), 127.2 (q), 127.4 (s), 128.5 (s), 128.8 (s), 128.9 (s), 129.3 (s), 137.0 (s), 138.8 (q), 139.3 (q), 144.6 (q), 154.7 (q), 156.7 (q). HRMS calculated for $C_{29}H_{23}N_3O_4$ (MH^+) 478.1761, found 478.1756 (ESI+). M.P. = 136 – 137 ^{o}C.

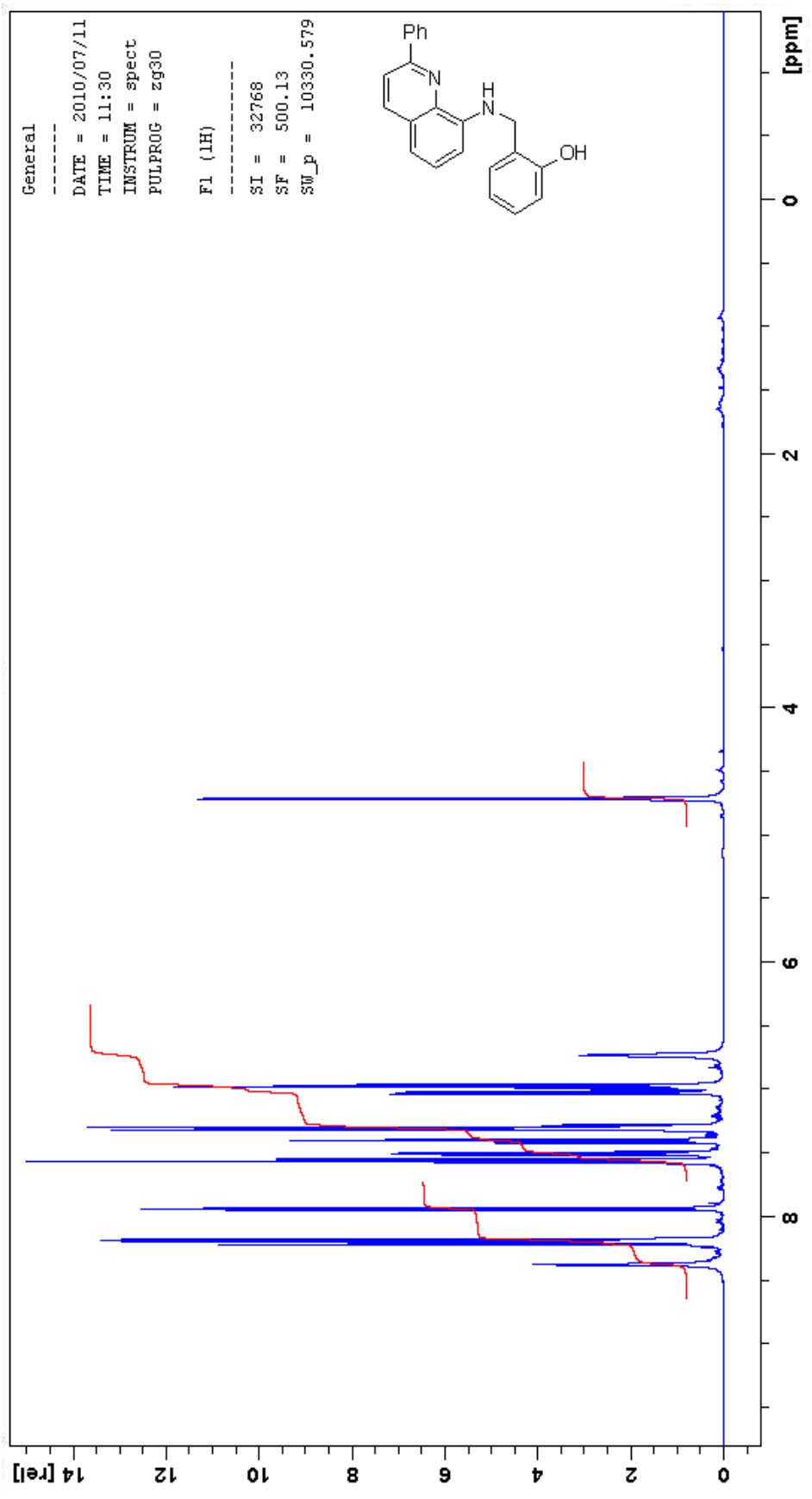
General
DATE = 2010/07/11
TIME = 11:30
INSTRUM = spect
PULPROG = zg30
F1 (1H)
SI = 32768
SF = 500.13
SW_p = 10330.579
Ph
N
H
N
OH
[rel]
[ppm]

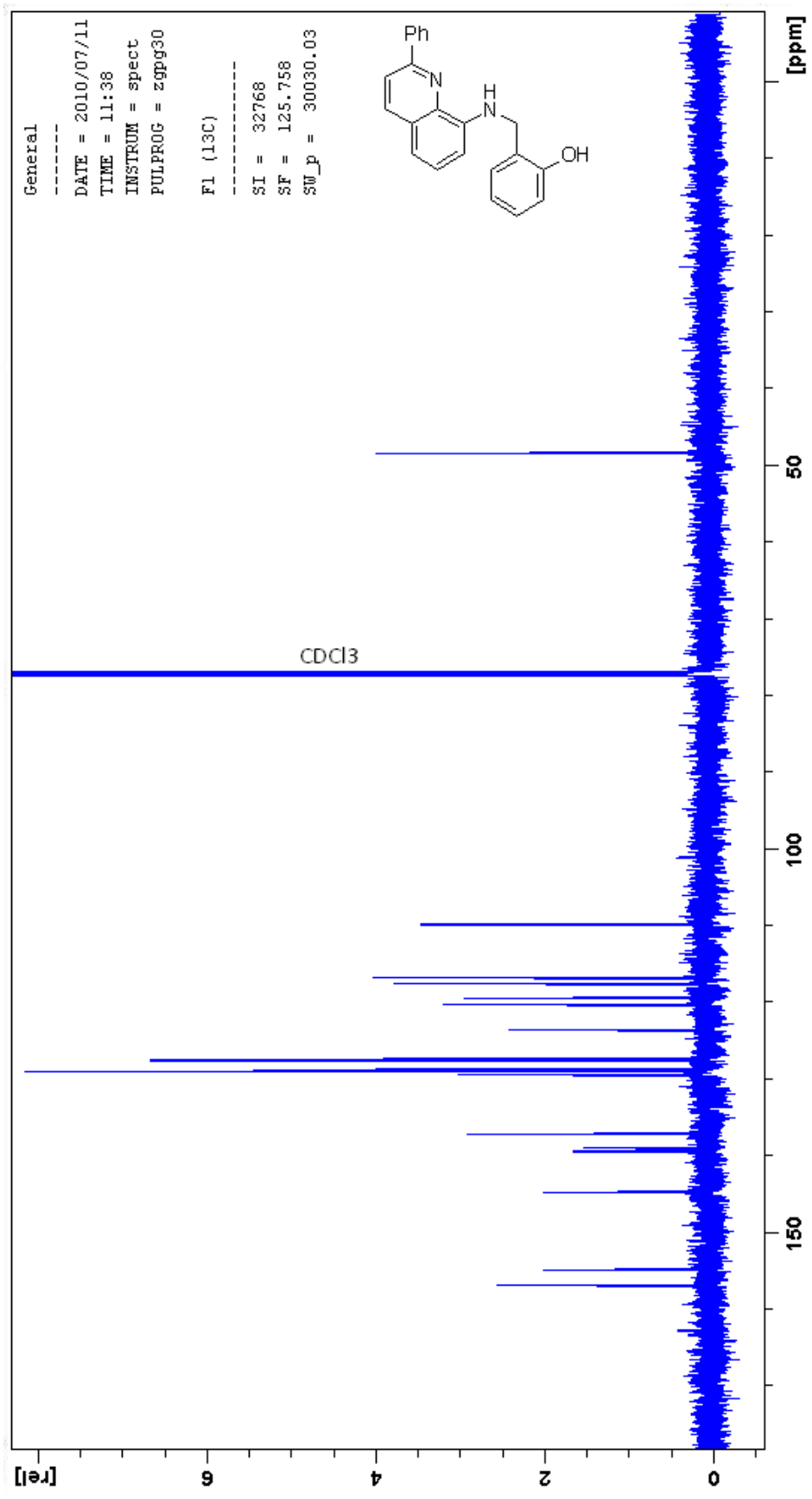
General
DATE = 2010/07/11
TIME = 11:38
INSTRUM = spect
PULPROG = zgpg30
F1 (13C)
SI = 32768
SF = 125.758
SW_p = 30030.03
Ph
N
H
N
OH
CDCl3
[rel]
[ppm]
0
2
4
6
50
100
150

A.6.30 2-(((2-Hydroxybenzyl)(2-phenylquinolin-8-yl)amino)methyl)-4-nitrophenol (L21)

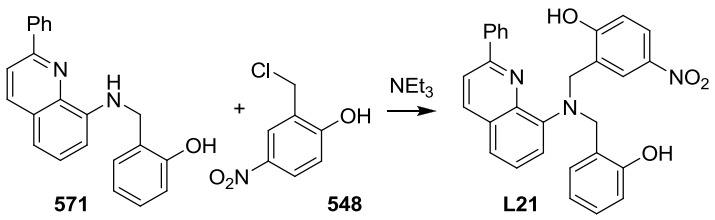

2-((2-Phenylquinolin-8-ylamino)methyl)phenol (**571**) (1.189 g, 3.64 mmol), 2-(chloromethyl)-4-nitrophenol (**548**) (0.683 g, 3.64 mmol) and triethylamine (4.12 mL, 29.7 mmol) were refluxed together in $CHCl_3$ (20 mL) for 2 h. The reaction was diluted with CH_2Cl_2 (200 mL) and washed with water (200 mL). The organic layer was filtered and dried over $MgSO_4$. The light yellow oil **L21** was purified by silica gel column chromatography using 2:1 Hexanes / EtOAc. Residual EtOAc caused **L21** to remain as an oil, this was removed by dissolving the residue in a minimum volume of CH_2Cl_2 and precipitating with hexane addition, decanting and drying under vacuum to give a light yellow powder (0.677 g, 39 %). R_f = 0.82 (95:5 CH_2Cl_2 / MeOH). ^{1}H NMR (500 MHz, $CDCl_3$) δ 4.48 (s, 2H; C*H*$_2$), 4.51 (s, 2H; C*H*$_2$), 6.77 – 6.85 (m, 3H; Ar*H*), 7.12 – 7.22 (m, 2H; Ar*H*), 7.46 – 7.64 (m, 6H; Ar*H*), 7.80 (d, *J* = 8.7, 1H; Ar*H*), 7.86 (m, 2H; Ar*H*), 8.03 (dd, *J* = 2.4, 9.0, 1H; Ar*H*), 8.17 (d, *J* = 2.4, 1H; Ar*H*), 8.32 (d, *J* = 8.7, 1H; Ar*H*), 10.59 (brs, 2H, O<u>H</u>); ^{13}C NMR (125 MHz, $CDCl_3$) δ 56.6 (d), 57.4 (d), 117.2 (s), 117.7 (s), 119.6 (s), 121.2 (s), 121.7 (s), 122.4 (s), 124.5 (s), 125.7 (s), 126.4 (s), 126.5 (s), 128.5 (s), 128.5 (s), 128.9 (q), 129.2 (s), 129.2 (s), 129.6 (s), 129.7 (s), 130.5 (s), 138.8 (q), 138.9 (q), 140.2 (q), 142.6 (q), 144.1 (q), 156.5 (q), 156.8 (q), 159.8 (q), 163.1 (q). MS for $C_{29}H_{23}N_3O_4$ (MH^+) 478.88. $C_{29}H_{23}N_3O_4$ (477.51): calcd. C 72.94, H 4.85, N 8.80; found C 71.76, H 4.55, N 8.67. M.P. = 175 – 176 ^{o}C.

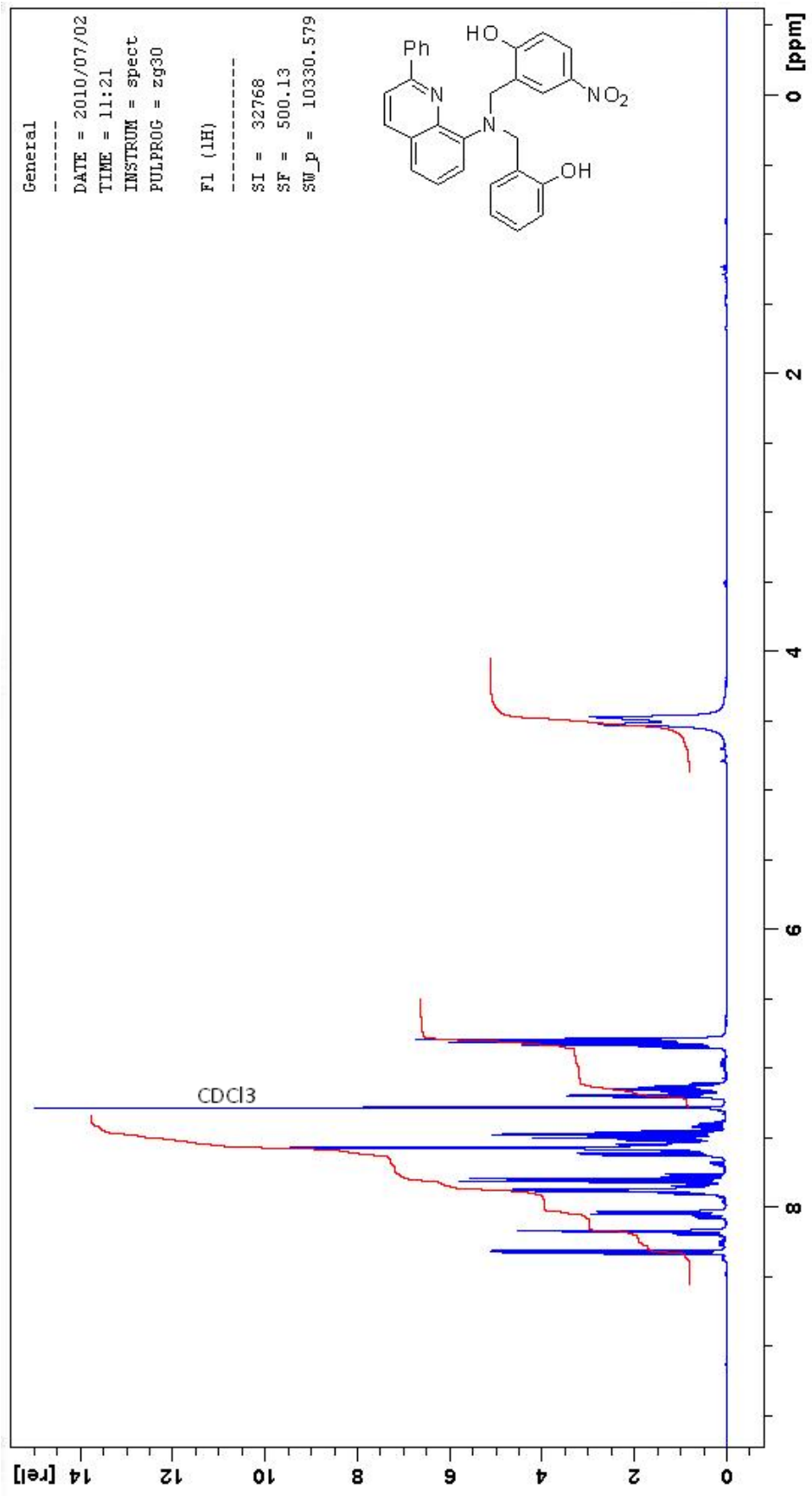
General
DATE = 2010/07/02
TIME = 11:21
INSTRUM = spect
PULPROG = zg30
F1 (1H)
SI = 32768
SF = 500.13
SW_p = 10330.579
Ph
N
HO
NO2
N
OH
CDCl3
[rel]
[ppm]

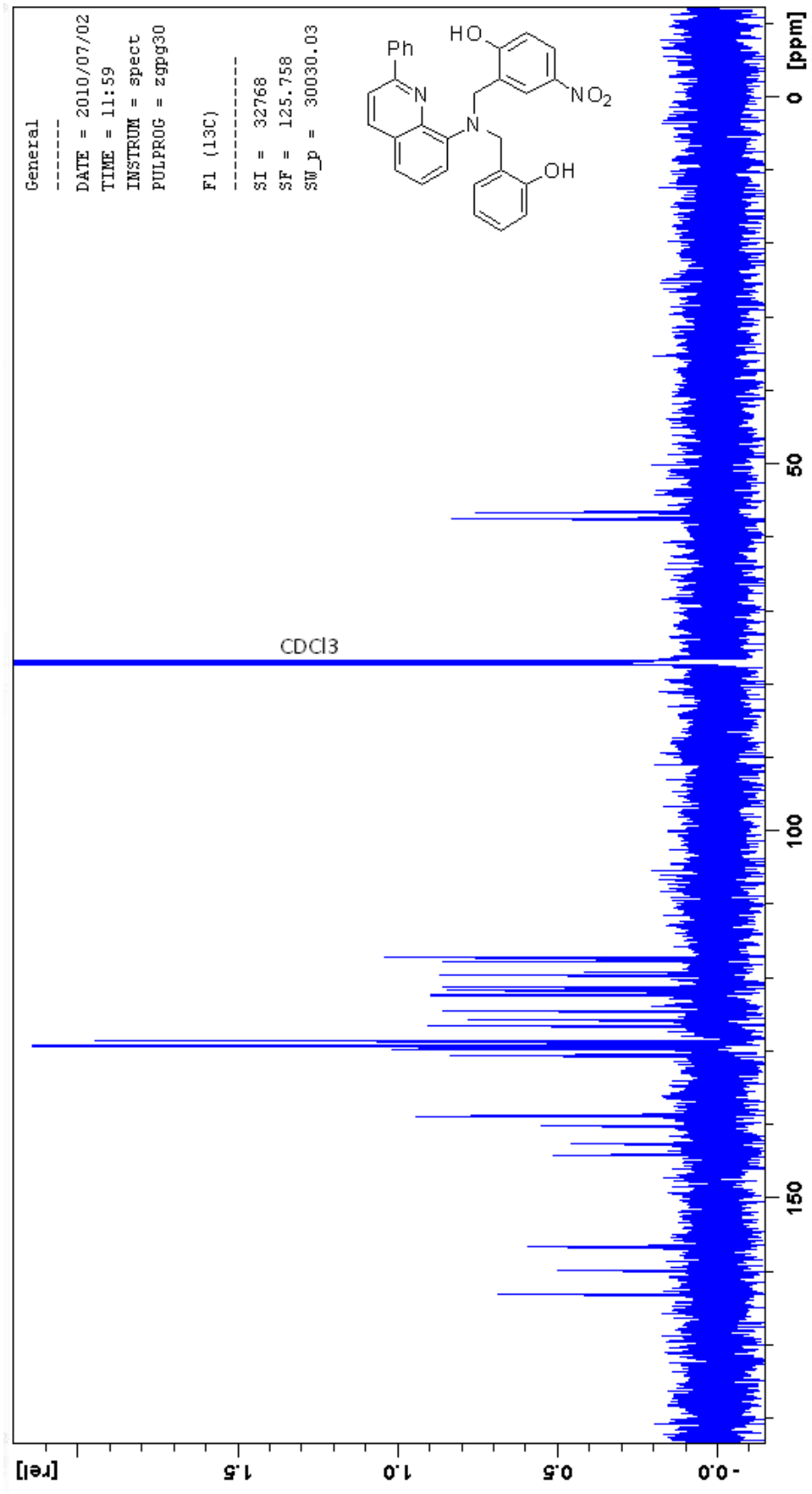
General
DATE = 2010/07/02
TIME = 11:59
INSTRUM = spect
PULPROG = zgpg30
F1 (13C)
SI = 32768
SF = 125.758
SW_p = 30030.03
Ph
N
N
HO
NO2
OH
CDCl3
[rel]
1.5
1.0
0.5
0.0
150
100
50
0 [ppm]

A.7 Chapter 6 Experimental

A.7.1 Be complex with L15

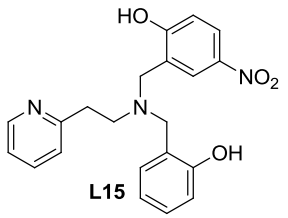

L15

2-(((2-Hydroxybenzyl)(pyridin-2-ylethyl)amino)methyl)-4-nitrophenol (**L15**) (0.010 g, 26.4 µmol), beryllium sulphate (26.5 µL, 26.4 µmol, 0.99 M in H_2O) and triethylamine (36.6 µL, 265 µmol) in DMF (1 mL) were stirred together for 16 h at 50 ^{o}C. The complex was characterised using DMSO-d6. ^{1}H NMR (400 MHz, DMSO-d6) δ CH_2 peaks not seen under solvent peaks and triethylamine, 6.51 (m, 2H; Ar*H*), 6.59 (d, *J* = 9.0, 1H; Ar*H*), 7.02 (m, 3H; Ar*H*), 7.53 (d, *J* = 7.9, 1H; Ar*H*), 7.64 (t, *J* = 6.7, 1H; Ar*H*), 7.96 (dd, *J* = 3.0, 9.0, 1H; Ar*H*), 8.04 (dd, *J* = 2.0, 6.7, 1H; Ar*H*), 8.72 (d, *J* = 5.2, 1H; Ar*H*); ^{13}C NMR (100 MHz, DMSO-d6) δ [29.2, 51.0, 55.5, 55.6] (CH_2), [115.8, 118.5, 118.8, 122.2, 123.2, 124.0, 126.0, 126.3, 126.8, 129.6, 130.0, 136.2, 141.2, 147.0, 157.5, 161.6, 170.0] (ArC).

NMR Analysis:

The ^{9}Be NMR of the mixture in DMF and showed a single peak 2.77 ppm (line width 62 Hz) for the complex. Analogous experiments in DMSO-d6 and MeOH gave a peak at 3.18 ppm (line width 123 Hz) and 2.94 ppm (line width 150 Hz) respectively. This ligand was not water soluble.

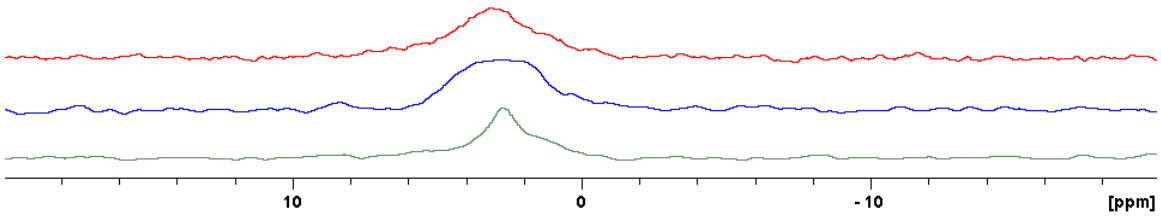

*^{9}Be NMR shift of **L15** coordinated to beryllium in DMF (**green**), MeOH (**blue**) and DMSO (**red**)*

UV-Vis and Fluorescence Spectroscopy:

A 20 µL aliquot of the reaction mixture was taken and diluted with DMF (10 mL) to give a concentration of 52.8 µmol L^{-1} and the UV-Vis spectra was measured against an identical sample containing only the free ligand, **L15**. The complex was not fluorescent.

A.7.2 Be complex with L16

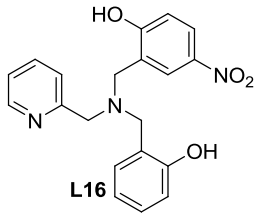

L16

2-(((2-Hydroxybenzyl)(pyridin-2-ylmethyl)amino)methyl)-4-nitrophenol (**L16**) (0.010 g, 27.4 µmol), beryllium sulphate (27.5 µL, 27.4 µmol, 0.99 M in H_2O) and triethylamine (37.9 µL, 274 µmol) in DMF (1 mL) were stirred together for 16 h at 50 ^{o}C. Full NMR characterisation using DMSO-d6 was not possible as complete conversion did not occur.

NMR Analysis:

The ^{9}Be NMR of the mixture in DMF showed weak coordination as the free beryllium signal at 0.99 ppm was present as well as a peak at 4.51 ppm (line width 67 Hz) for the complex. An analogous experiment in MeOH gave a peak at 4.18 ppm (line width 188 Hz) for the complex. This ligand was not water soluble.

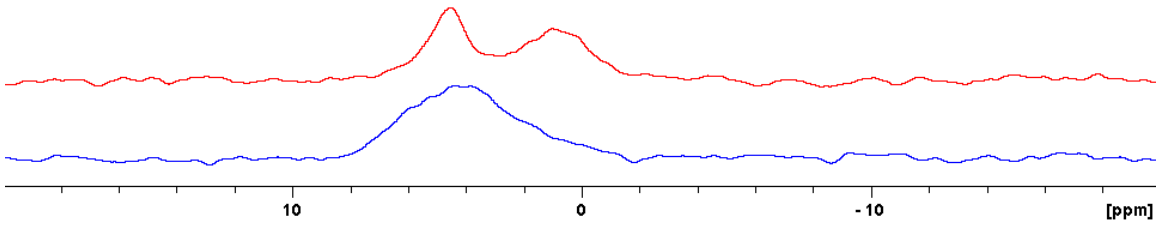

*^{9}Be NMR shift of [Be(**L16**)] in DMF (**red**) and MeOH (**blue**)*

UV-Vis and Fluorescence Spectroscopy:

A 20 µL aliquot of the reaction mixture was taken and diluted with DMF (10 mL) to give a concentration of 54.8 µmol L^{-1} which was measured against an identical sample containing only the free ligand, **L16**. The complex was not fluorescent.

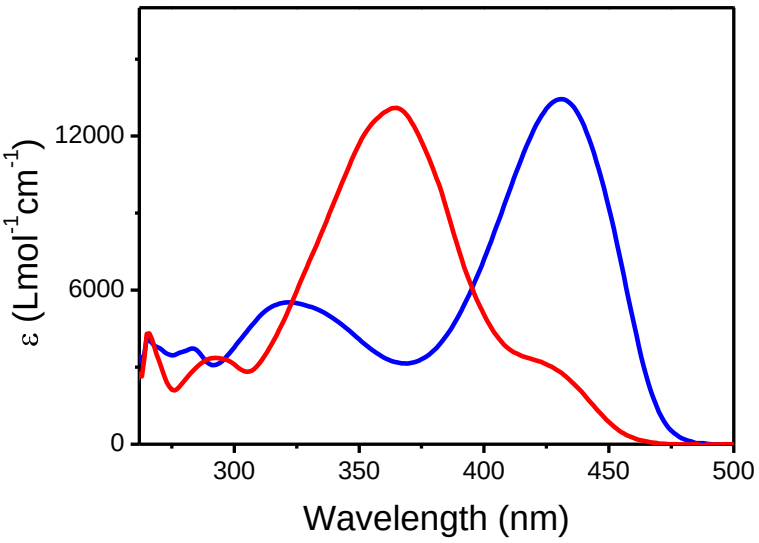

*Change in UV-Vis spectrum at 10^{-5} M of neutral **L16** (**blue**) and after $BeSO_4$ addition (**red**)*

A.7.3 Be complex with L17

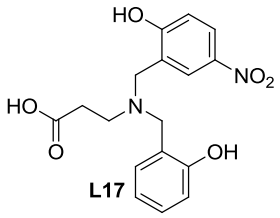

3-((2-Hydroxy-5-nitrobenzyl)(2-hydroxybenzyl)amino)propanoic acid (**L17**) (0.010 g, 28.9 µmol), beryllium sulphate (29.0 µL, 28.9 µmol, 0.99 M in H_2O) and triethylamine (40.0 µL, 289 µmol) in DMSO (1 mL) were stirred together for 16 h at 50 ^{o}C.

NMR Analysis:

The ^{9}Be NMR of the mixture in DMSO-d6 and showed a single peak at 2.11 ppm (line width 174 Hz) for the complex. Analogous experiments in D_2O and MeOH gave a peak at 2.60 ppm (line width 175 Hz) and 2.33 ppm (line width 151 Hz).

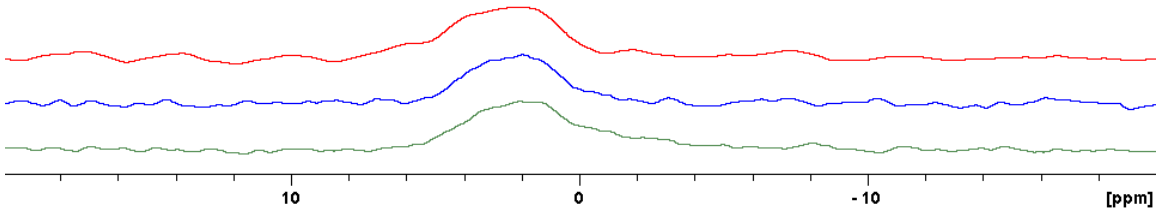

*^{9}Be NMR shift of **L17** coordinated to beryllium in DMSO-d6 (**green**), MeOH (**blue**) and D_2O (**red**)*

UV-Vis and Fluorescence Spectroscopy:

A 20 µL aliquot of the reaction mixture was taken and diluted with DMSO (10 mL) to give a concentration of 57.8 µmol L^{-1} which was measured against an identical sample containing only the free ligand, **L17**.

The carboxylic acid moiety enabled good water solubility and an analogous experiment to the one performed in DMSO was performed in H_2O. A 20 µL aliquot of the reaction mixture was taken and diluted with H_2O (10 mL) to give a concentration of 57.8 µmol L^{-1} which was measured against an identical sample containing only the free ligand, **L17**.

A.7.4 Be complex with L18

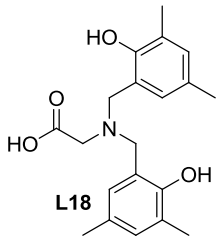

L18

2-(*bis*(2-Hydroxy-3,5-dimethylbenzyl)amino)acetic acid (**L18**) (0.010 g, 29.2 µmol), beryllium sulphate (29.5 µL, 29.2 µmol, 0.99 M in H_2O) and triethylamine (40.4 µL, 292 µmol) in DMF (1 mL) were stirred together for 16 h at 50 ^{o}C. The complex was

characterised using DMSO-d6. ^{1}H NMR (400 MHz, $DMSO_{d6}$) δ 2.00 (s, 6H; C*H*$_3$), 2.07 (s, 6H; C*H*$_3$), 2.97 (s, 2H; C*H*$_2$), C*H*$_2$ hidden under triethylamine peak, 6.54 (s, 2H; Ar*H*), 6.70 (s, 2H; Ar*H*); ^{13}C NMR (100 MHz, DMSO-d6) δ [17.2, 20.5] (C$\underline{H}_3$), [57.5, 57.8] ($\underline{C}H_2$), [121.7, 121.8, 126.1, 127.5, 131.1, 159.9, 174.4] (Ar$\underline{C}$).

NMR Analysis:

The ^{9}Be NMR of the mixture in DMF and showed a single major peak at 4.06 ppm (line width 66 Hz) for the complex. Analogous experiments in DMSO-d6 and D_2O gave peaks at 4.64 (line width 130 Hz) and 5.15 ppm (line width 104 Hz) respectively.

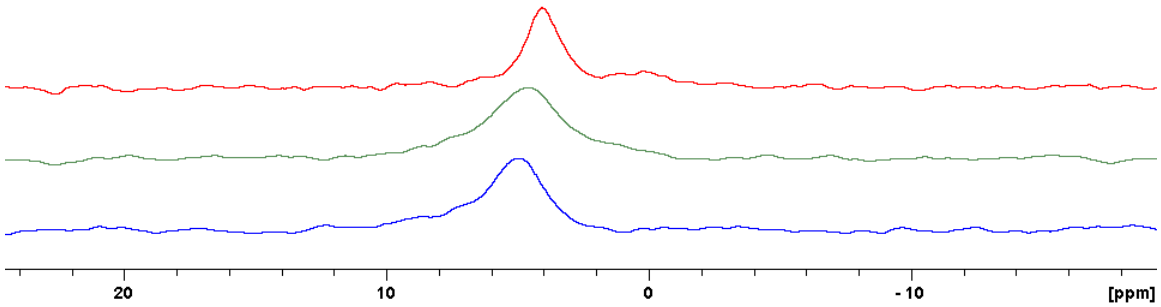

*^{9}Be NMR shift of **L18** coordinated to beryllium in DMF (**red**), DMSO-d6 (**green**) and D_2O (**blue**)*

UV-Vis and Fluorescence Spectroscopy:

A 20 µL aliquot of the reaction mixture was taken and diluted with DMF (10 mL) to give a concentration of 58.3 µmol L^{-1} which was measured against an identical sample containing only the free ligand, **L18**.

The carboxylic acid moiety enabled good water solubility and an analogous experiment to the one performed in DMF was performed in H_2O. A 20 µL aliquot of the reaction mixture was taken and diluted with H_2O (10 mL) to give a concentration of 58.3 µmol L^{-1} which was measured against an identical sample containing only the free ligand, **L18**.

A.7.5 Be complex with L19

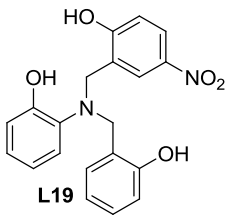

L19

2-(((2-hydroxybenzyl)(2-hydroxyphenyl)amino)methyl)-4-nitrophenol (**L19**) (0.010 g, 27.3 µmol), beryllium sulphate (27.5 µL, 27.3 µmol, 0.99 M in H_2O) and triethylamine (37.8 µL, 273 µmol) in DMF (1 mL) were stirred together for 16 h at 50 °C. The complex was characterised using DMSO-d6. ^{1}H NMR (400 MHz, $DMSO_{d6}$) δ C*H*$_2$ hidden under triethylamine peaks, 6.35 – 6.50 (m, 5H; Ar*H*), 6.79 (t, *J* = 7.2, 1H; Ar*H*), 6.90 – 6.97 (m, 2H; Ar*H*), 7.30 (d, *J* = 7.5, 1H; Ar*H*), 7.80 – 7.87 (m, 2H; Ar*H*), ^{13}C NMR (100 MHz, DMSO-d6) δ [55.1, 59.3] (CH_2), [114.1, 114.7, 116.0, 119.0, 119.1, 121.2, 123.3, 124.2, 126.0, 126.4, 128.5, 129.5, 129.6, 135.0, 137.8, 163.6, 163.8, 172.46] (ArC).

NMR Analysis:

The ^{9}Be NMR of the mixture in DMF and showed a single major peak at 4.40 ppm (line width 59 Hz) for the complex. An analogous experiment in DMSO-d6 and MeOH gave a peak at 5.10 ppm (line width 106 Hz) and 5.28 ppm (line width 159 Hz).

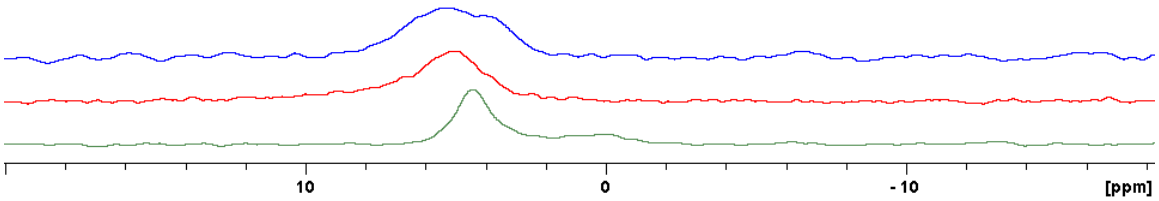

*Figure X: ^{9}Be NMR shift of **L19** coordinated to beryllium in DMF (**green**) and DMSO-d6 (**red**) and MeOH (**blue**)*

UV-Vis and Fluorescence Spectroscopy:

A 20 µL aliquot of the reaction mixture was taken and diluted with DMF (10 mL) to give a concentration of 54.6 µmol L^{-1} which was measured against an identical sample containing only the free ligand, **L19**.

A.7.6 Be complex with L20

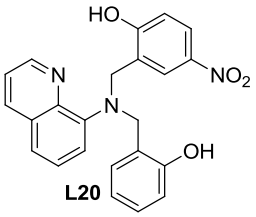

L20

2-(((2-hydroxybenzyl)(quinolin-8-yl)amino)methyl)-4-nitrophenol (**L20**) (0.010 g, 22.4 µmol), beryllium sulphate (25.0 µL, 22.4 µmol, 0.99 M in H_2O) and triethylamine (31.0 µL, 224 µmol) in DMF (1 mL) were stirred together for 16 h at 50 ^{o}C.

NMR Analysis:

The ^{9}Be NMR of the mixture in DMF and showed only weak coordination as the free beryllium signal at 0.30 ppm was present as well as a peak at 5.15 ppm (line width 89 Hz) for the complex.

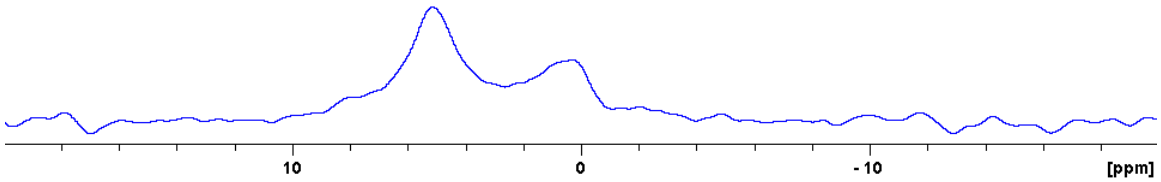

*^{9}Be NMR shift of **L20** coordinated to beryllium in DMF*

UV-Vis and Fluorescence Spectroscopy:

A 20 µL aliquot of the reaction mixture was taken and diluted with DMF (10 mL) to give a concentration of 49.8 µmol L^{-1} which was measured against an identical sample containing only the free ligand, **L20**.

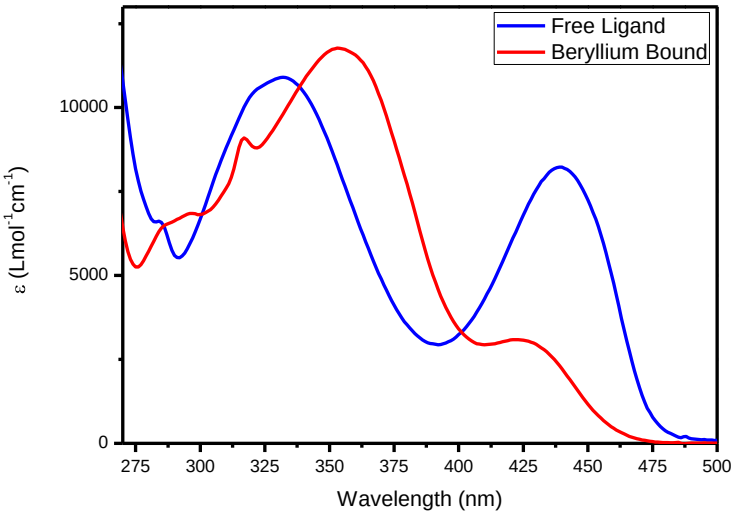

*Change in UV-Vis spectrum at 10^{-5} M of neutral **L20** (**blue**) and after $BeSO_4$ addition (**red**) in DMF*

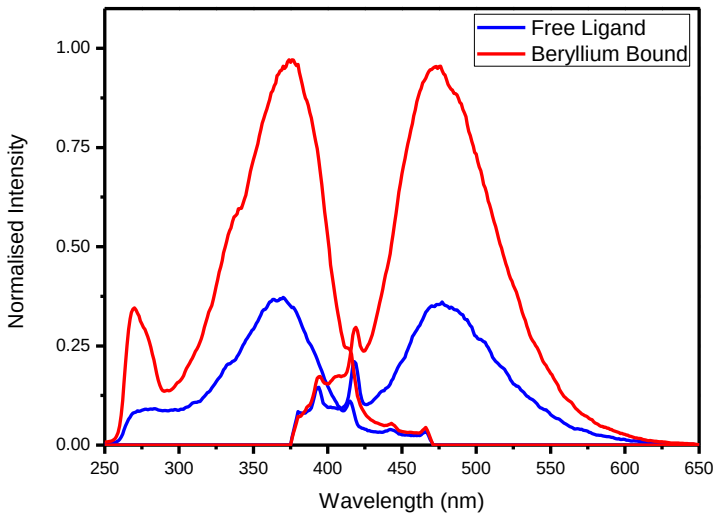

*Change in fluorescence at 10^{-5} M of neutral **L20** (**blue**) and after $BeSO_4$ addition (**red**) in DMF*

A.7.7 Be complex with L21

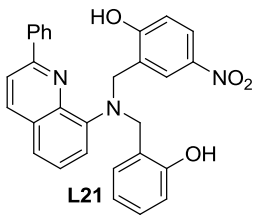

L21

2-(((2-Hydroxybenzyl)(2-phenylquinolin-8-yl)amino)methyl)-4-nitrophenol (**L21**) (0.010 g, 20.9 µmol), beryllium sulphate (21.0 µL, 20.9 µmol, 0.99 M in H_2O) and triethylamine (28.9 µL, 209 µmol) in DMF (1 mL) were stirred together for 16 h at 50 ^{o}C.

NMR Analysis:

No peaks were present in the ^{9}Be NMR of the mixture in DMF suggesting no coordination occurred.

UV-Vis and Fluorescence Spectroscopy:

A 20 µL aliquot of the reaction mixture was taken and diluted with DMF (10 mL) to give a concentration of 41.9 µmol L^{-1} which was measured against an identical sample containing only the free ligand, **L21**.

As there was no corresponding ^{9}Be NMR signal, the change in UV-Vis and fluorescence might be due to a central proton occupying the cavity.

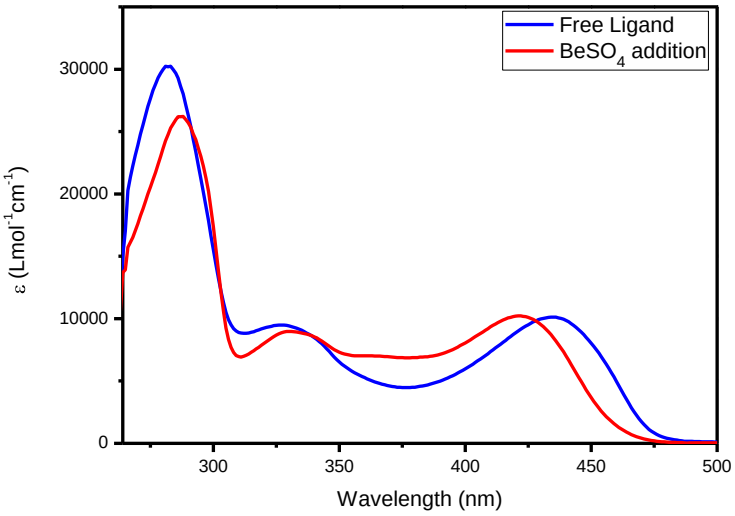

*Change in UV-Vis spectrum at 10^{-5} M of neutral **L21** (**blue**) and after $BeSO_4$ addition (**red**) in DMF*

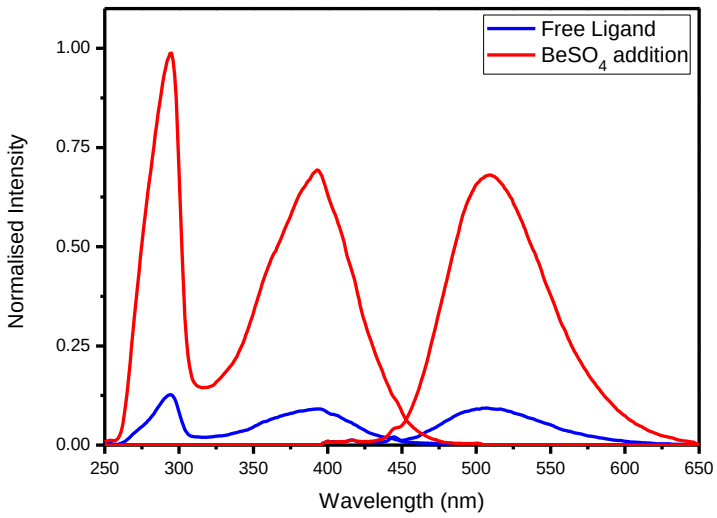

*Change in fluorescence at 10^{-5} M of neutral **L21** (**blue**) and after $BeSO_4$ addition (**red**) in DMF*

A.7.8 Cu complex with L16

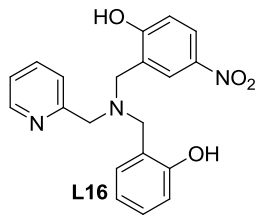

2-(((2-Hydroxybenzyl)(pyridin-2-ylmethyl)amino)methyl)-4-nitrophenol (**L16**) (0.048 g, 0.132 mmol) and copper acetate (0.026, 0.132 mmol) in MeOH (5 mL) were mixed together, MeCN (1 mL) was added and crystallisation was set up by vapour diffusion of diethyl ether. The green crystals obtained were completely insoluble and unsuitable for solution based analysis techniques.

Crystal data for [Cu(**L16**)]. $C_{20}H_{17}N_3O_4Cu$, green chip, dimensions 0.6 x 0.2 x 0.05 mm, triclinic, space group *P*-1, a = 8.9881(18), b = 9.3333(19), c = 12.050(2) Å, α = 91.39(3)°, β = 111.86(3)°, γ = 98.81(3)°, U = 923.5(4) Å^3, μ = 1.974 mm^{-1}, Z = 1, D_c = 1.564 g cm^{-3}, F(000) = 447, T = 100(2) K. 15723 Reflections were collected using a Rigaku MM007 rotating anode in the range 6.51 < 2θ < 143.94°. A semi-empirical absorption correction (ABSCOR; Higashi, 1995) was applied. The 2873 independent reflections were used to solve the structure by direct methods (SHELXS97) which resulted in the location of all non-hydrogen atoms. All non-hydrogen atoms were made anisotropic and the refinement (SHELXL97) of 269 parameters converged to R_1 = 0.0476 [for 2652 reflections having I > 4σ (I)], wR_2 = 0.1390 and goodness of fit 1.077 (for all 2652 F^2 data). Peak / hole 0.601 / -0.622 e Å^{-3}.

A.7.9 Zn complex with L16

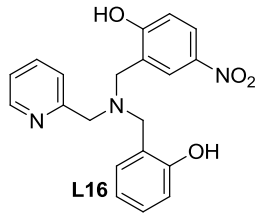

2-(((2-Hydroxybenzyl)(pyridin-2-ylmethyl)amino)methyl)-4-nitrophenol (**L16**) (0.020 g, 0.055 mmol) and zinc acetate (0.012, 0.055 mmol) in MeOH (2.5 mL) and CH_2Cl_2 (2.5 mL) and mixed and crystallisation was set up by vapour diffusion of diethyl ether. The yellow crystals obtained were completely insoluble and unsuitable for solution based analysis techniques.

Crystal data for [Zn(**L16**)]. $C_{20}H_{17}N_3O_4Zn$, yellow plate, dimensions 0.16 x 0.06 x 0.05 mm, monoclinic, space group $P2_1/n$, a = 16.915(3), b = 13.403(3), c = 19.396(4) Å, α = 90.00°, β = 105.61(3)°, γ = 90.00°, U = 4235.0(15) Å^3, μ = 1.858 mm^{-1}, Z = 4, D_c = 1.345 g cm^{-3}, $F(000)$ = 1760, T = 100(2) K. 44104 Reflections were collected using a Rigaku MM007 rotating anode in the range $6.61 < 2\theta < 133.10°$. A semi-empirical absorption correction (ABSCOR; Higashi, 1995) was applied. The 7399 independent reflections were used to solve the structure by direct methods (SHELXS97) which resulted in the location of all non-hydrogen atoms. All non-hydrogen atoms were made anisotropic and the refinement (SHELXL97) of 506 parameters converged to R_1 = 0.0907 [for 3956 reflections having $I > 4\sigma(I)$], wR_2 = 0.2370 and goodness of fit 1.047 (for all 3956 F^2 data). Peak / hole 1.103 / -0.738 e Å^{-3}.

Appendix B: Abandoned Proton Sponge Syntheses

B.1 Introduction

As the synthesis of **B01**[85] was not immediately successful a number of alternate routes were attempted early on in the investigation. The closest analogous heterocycles which had been synthesised in abundance were 1,10-phenanthroline, **B02**, and quinoline, **B03**, and promising new routes for these were attempted to be adapted for the synthesis of quino[7,8-*h*]quinoline.

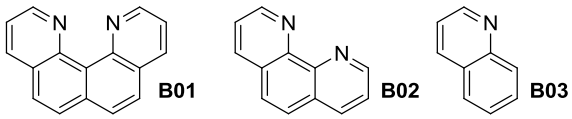

Figure B.1: Heterocycles with related synthetic methodologies

B.2 Muthusubramanian and Misra Synthesis[200]

B.2.1 Introduction

Muthusubramanian and Misra have reported on the synthesis of quinolines by cyanoethylation and in three steps they synthesised **B07**.

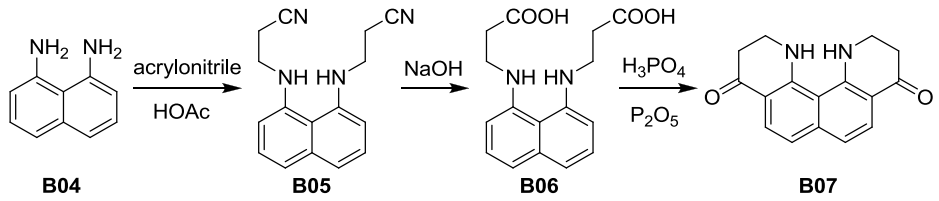

Scheme B.1: Synthesis of 4,9-dioxo-1,2,3,4,9,10,11,12-octahydroquinolino[7,8-h]quinoline, ***B07***

It was unknown whether any further reactions were attempted with **B07**, but dehydrogenation with Pd should give **B08** which could be converted to **B09** with phosphorus oxychloride. Chandrasekhar and co-workers[201] utilised a similar conversion with a substituted quinoline.

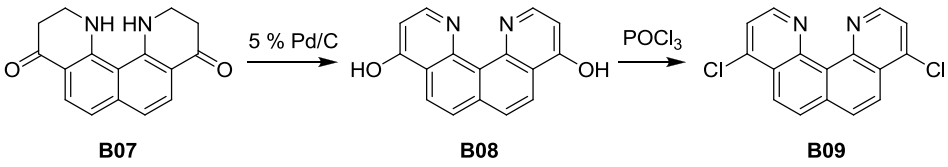

Scheme B.2: Proposed conversion of ***B07*** *to* ***B08*** *and* ***B09***

B.2.2 Results / Discussion

The first step of the reaction claimed to obtain a 48 % yield which was purified by crystallisation alone.

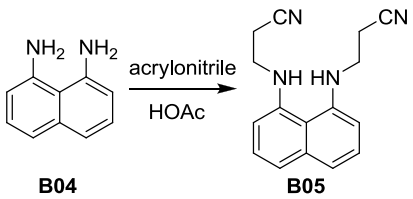

Scheme B.3: Synthesis of 3,3'-(naphthalene-1,8-diylbis(azanediyl))dipropanenitrile, ***B05***

Despite varying reaction time and temperature, the mono-substituted **B10** was predominantly formed in low yields with only trace formation of **B05**.

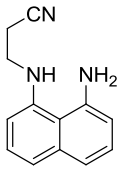

Figure B.2: 3-(8-Aminonaphthalen-1-ylamino)propanenitrile, ***B10***

Although this reaction scheme appeared promising, it was abandoned due to the unreliability of the first step. The literature was unable to be replicated in this case and it was unknown why the seemingly simple reaction did not work. In light of the research conducted during Chapter 3, **B08** would likely have limited utility due to the stable preferred tautomer, **B11**. This could be converted to **B09** with $POCl_3$; however, since Staab's original preparation already gave reasonable yields of **B09**, this route was not pursued further.

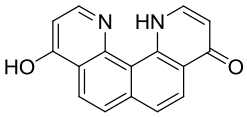

Figure B.3: ***B11****, the expected stable tautomer of* ***B08***

B.2.3 Experimental

B.2.3.1 3-(8-Aminonaphthalen-1-ylamino)propanenitrile (B10)

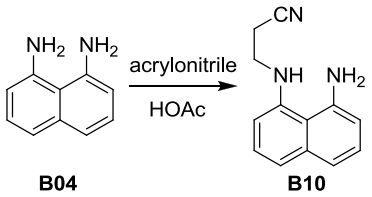

The reaction was performed as per the literature procedure. The products were purified by silica gel column chromatography eluting with 4:1 hexanes / EtOAc to give **B10** in 16 % yield and **B05** in 1 % yield. Characterisation data for **B05**: R_f = 0.17 (2:1 hexanes / EtOAc). ^{1}H NMR (500 MHz, $CDCl_3$) δ 2.69 (t, *J* = 6.5, 4H; C*H*$_2$), 3.50 (t, *J* = 6.5, 4H; C*H*$_2$), 6.37 (br s, 2H; N*H*), 6.70 (d, *J* = 7.1, 2H; Ar*H*), 7.29-7.36 (m, 4H; Ar*H*); ^{13}C NMR (125 MHz, $CDCl_3$) δ 17.9 (d), 42.0 (d), 110.5 (s), 117.9 (s), 118.9 (s), 121.5 (q), 126.3 (s), 137.0 (q), 143.3 (q). Characterisation data for **B10**: R_f = 0.20 (2:1 hexanes / EtOAc). ^{1}H NMR (500 MHz, $CDCl_3$) δ 2.69 (t, *J* = 6.5, 2H; C*H*$_2$), 3.50 (t, *J* = 6.5, 2H; C*H*$_2$), 4.41 (br s, 2H; N*H*$_2$), 6.25 (br s, 1H; N*H*), 6.46 (dd, *J* = 2.0, 6.7, 1H; Ar*H*), 6.66 (dd, *J* = 1.2, 7.2, 1H; Ar*H*), 7.17-7.27 (m, 4H; Ar*H*); ^{13}C NMR (125 MHz, $CDCl_3$) δ 17.7 (d), 40.8 (d), 106.5 (s), 113.8 (s), 117.3 (s), 118.5 (q), 119.6 (s), 120.8 (s), 126.2 (s), 137.0 (q), 143.3 (q), 144.5 (q).

B.3 Schmittel and Ammon Synthesis[112]

B.3.1 Introduction

Schmittel and Ammon, during their investigation into the synthesis of precursors to macrocyclic oligophenanthrolines, achieved the efficient synthesis of 3,8-dialkyl/diarylated 4,7-dihalo phenanthrolines. The generalised reaction scheme is shown below.

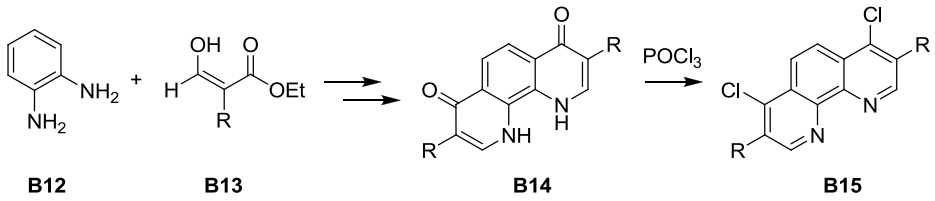

B12 **B13** **B14** **B15**

Scheme B.4: Synthesis of substituted phenanthrolines

In the synthesis by Staab,[85] the cyclisation step left esters at the 2,11 positions which could only be removed by a high-temperature, low-pressure thermal decarboxylation. This route would avoid the need for such a step and give alkylated substituents at the 3,10 positions.

B.3.2 Results / Discussion

The first step was the formation of the α-formylacetic ester. In the original literature the ester which gave the highest yield had *t*-butylphenyl R groups. A cheaper compromise which still gave reasonable yields had a phenyl group. **B16** could be purchased; however, it was much cheaper to alkylate phenylacetic acid by reacting the caesium salt with ethyl iodide. **B16** was then converted to **B18**.[202]

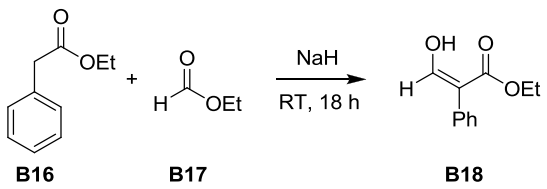

*Scheme B.5: Synthesis of (2)-ethyl-3-hydroxyl-2-phenylacetate, **B18***

The substitution of **B04** with **B18** gave none of the desired **B19**. The major by-product was the result of an internal reaction after mono-substitution. **B21** formed in near-quantitative yield.

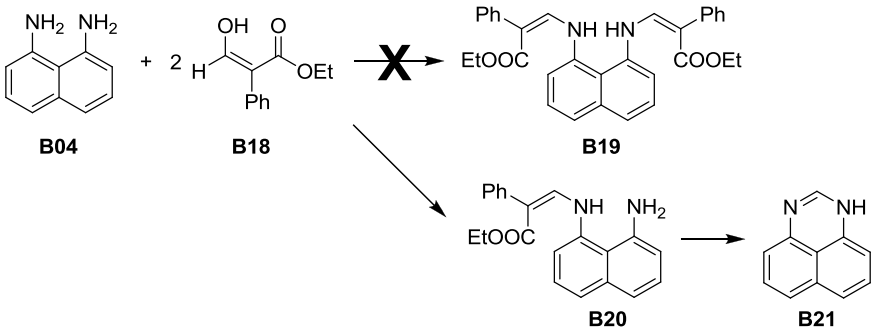

*Scheme B.6: Side reaction of **B04** and **B18** leading to the formation of **B21***

The inability to avoid the formation of **B21** meant the reaction scheme had to be abandoned.

B.3.3 Experimental

B.3.3.1 Ethyl-2-phenylacetate (B16)

Caesium carbonate (1.19 g, 3.68 mmol) was added to a suspension of phenylacetic acid (**B22**) (1.00 g, 7.35 mmol) in dry MeOH (14 mL). The homogeneous mixture was stirred at RT under N_2 for 2 h. The solvent was removed under reduced pressure and the colourless solid was dissolved in dry DMF (14 mL) and treated with ethyl iodide (0.700 mL, 1.37 g, 8.82 mmol). The resulting colourless suspension was stirred at RT overnight. The reaction mixture was diluted with EtOAc (200 mL), washed with water (3x 100 mL), dried over $MgSO_4$, filtered and concentrated to give the product **B16** as a yellow oil (92 %). R_f = 0.36 (5:1 hexanes / EtOAc). The product matched the literature characterisation data.[203] ^{1}H NMR (500 MHz, $CDCl_3$) δ 1.24 (t, *J* = 7.1, 3H; C*H*$_3$), 3.60 (s, 2H; C*H*$_2$), 4.15 (q, *J* = 7.1, 2H; C*H*$_2$), 7.23 – 7.33 (m, 5H; Ar*H*); ^{13}C NMR (125 MHz, $CDCl_3$) δ 14.1 (t), 41.3 (d), 60.7, (d), 126.9 (s), 128.4 (s), 129.1 (s), 134.1 (q), 171.5 (q).

B.3.3.2 Ethyl-3-hydroxy-2-phenylacetate (B18)

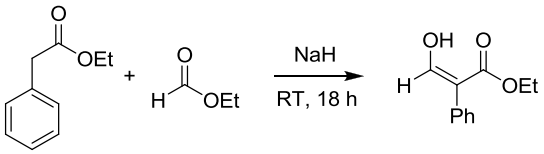

B16 **B17** **B18**

Sodium hydride as 60 % oil dispersion (0.228 g, 5.71 mmol) was added to a solution of ethyl-2-phenylacetate (**B16**) (0.468 g, 2.85 mmol) in dry DMF (6 mL) and was stirred for 30 min under N_2, allowing the H_2 to escape. Ethylformate (0.253 g, 3.42 mmol) was added and the reaction was left to stir overnight for 24 h. 5 % HCl (50 mL) was added and the aqueous layer was extracted with diethyl ether (2x 100 mL). The combined organic extracts were dried over $MgSO_4$, filtered and concentrated. The crude product was purified by silica gel column chromatography eluting with 6:1 hexanes / EtOAc to give **B18** in 25 % yield. R_f = 0.60 (2:1 hexanes / EtOAc). The product matched the literature characterisation data.[202] ^{1}H NMR (500 MHz, $CDCl_3$) δ 1.33 (t, *J* = 7.1, 3H; C*H*$_3$), 4.34 (q, *J* = 7.1, 2H; C*H*$_2$), 7.31 – 7.40 (m, 6H; Ar*H*), 12.19 (d, *J* = 13.1, 1H; O*H*); ^{13}C NMR (125 MHz, $CDCl_3$) δ 14.1 (t), 60.9,(d), 108.1 (q), 126.9 (s), 128.1 (s), 129.3 (s), 134.1 (q), 163.3 (s), 171.5 (q).

B.3.3.3 1H-Perimidine (B21)

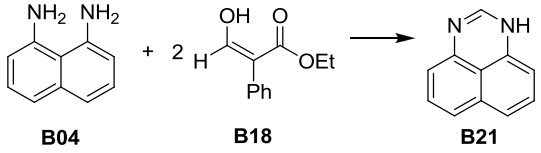

B04 **B18** **B21**

The reaction between **B04** and **B18** invariably lead to **B21**,[204] refluxing in CH_2Cl_2 for 2 h promoted quantitative formation of **B21**. ^{1}H NMR (500 MHz, MeOH) δ 6.77 (d, *J* = 7.4, 2H; 4,5-*H*), 7.33 (t, *J* = 7.8, 2H; 3,6-*H*), 7.41 (d, *J* = 8.4, 2H; 2,7-*H*), 8.24 (s, 1H; C*H*) ^{13}C NMR (125 MHz, MeOH) δ 94.3 (s), 102.6 (s), 108.2 (s), 123.1 (q), 128.3 (s), 131.7 (q), 150.0 (s). MS for $C_{11}H_8N_2$ (MH^+) 169.17.

B.4 Molock and Boykin Synthesis[205]

B.4.1 Introduction

Molock and Boykin reacted **B12** with **B23** to give **B25**.

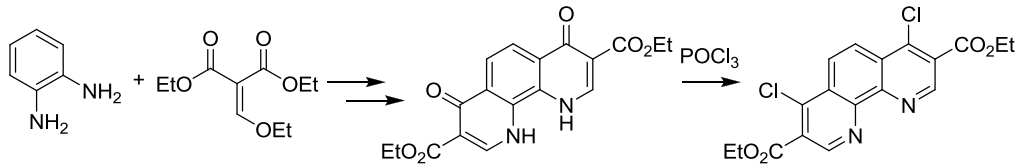

B12 **B23** **B24** **B25**

*Scheme B.7: Synthesis of diethyl 4,7-dichloro-1,10-phenanthroline-3,8-dicarboxylate, **B25***

This reaction was attempted with **B04** in place of **B12** to give the corresponding quino[7,8-*h*]quinoline.

B.4.2 Results / Discussion

The first step of this synthesis was the substitution of **B04** with **B26** to give **B27**.

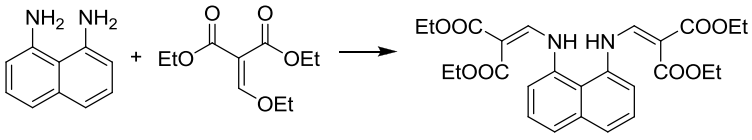

B04 **B26** **B27**

*Scheme B.8: Synthesis of tetraethyl 2,2'-(naphthalene-1,8-diylbis(azanediyl))bis(methan-1-yl-1-ylidene)dimalonate, **B27***

The reaction proceeded as indicated; however, only trace quantities of **B27** formed (1 %). The major by-product was **B21**, as seen in section B.3 above, over a wide range of reaction times and temperatures. Thermal cyclisation of the small amount of product isolated from the first step did not lead to a precipitate of **B28**.

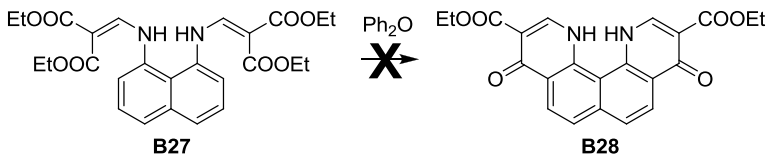

*Scheme B.9: Thermal cyclisation of **B27***

The very low yield of the first reaction step and the inability to obtain any product in the second step meant that this reaction scheme had to be abandoned.

B.4.3 Experimental

B.4.3.1 Tetraethyl 2,2'-(naphthalene-1,8-diylbis(azanediyl))bis(methan-1-yl-1-ylidene)dimalonate (B27)

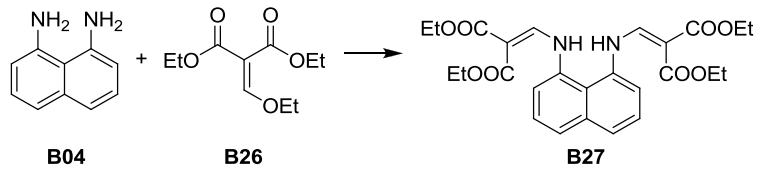

1,8-Diaminonaphthalene (**B04**) (0.200 g, 1.26 mmol) and diethyl ethoxymethylenemalonic ester (**B26**) (0.547 g, 0.506 mL, 2.53 mmol) were heated together at reflux (100°C) for 2 hours. The reaction was diluted with CH_2Cl_2, filtered, concentrated and then purified by column chromatography (1:2 EtOAc / hexanes). The fraction containing the product was crystallized in a small amount of hexane in the fridge overnight. This gave 5 mg (0.8 %) of **B27** as a colourless crystalline solid. R_f = 0.28 (2:1 hexanes / EtOAc). ^{1}H NMR (500 MHz, $CDCl_3$) δ 1.30-1.37 (m, 12H, C<u>H</u>$_3$), 4.17-4.28 (m, 8H, C<u>H</u>$_2$), 2.29 (d, *J* = 7.7 Hz, 2H, Ar<u>H</u>), 7.51 (t, *J* = 7.7 Hz, 2H, Ar<u>H</u>), 7.74 (d, *J* = 8.3 Hz, 2H, Ar<u>H</u>), 8.47 (d, *J* = 12.5 Hz, 2H, NHC<u>H</u>), 11.47 (d, *J* = 13.1 Hz, 2H, N<u>H</u>); ^{13}C NMR (125 MHz, $CDCl_3$) δ [14.2, 14.4] (<u>C</u>H$_3$), [59.9, 60.3] (<u>C</u>H$_2$), 95.5 (<u>C</u>=CH), [119.9, 120.0, 126.6, 126.9, 135.9, 136.1] (Ar<u>C</u>), 153.5 (C=<u>C</u>H), [165.6, 168.9] (<u>C</u>OCH$_2$CH$_3$).

B.5 Montalban et al. Synthesis[206]

B.5.1 Introduction

This was a similar reaction as in B.3 and B.4 above where a substitution of **B12** with an oxyethene derivative (in this case **B29**) and subsequent thermal cyclisation and dehydration lead to **B31**.

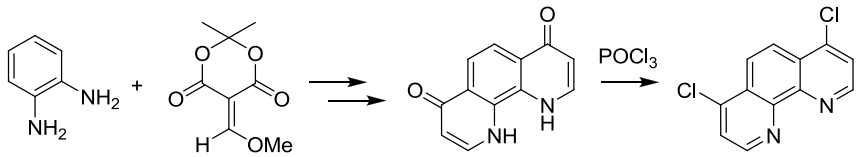

B12 **B29** **B30** **B31**

*Scheme B.10: Synthesis of 4,7-dichloro-1,10-phenanthroline, **B31***

This reaction was attempted with **B04** in place of **B12** to give the corresponding quino[7,8-*h*]quinoline.

B.5.2 Results / Discussion

Similarly to 7.3 and 7.4, the major by-product of the first step was **B21**, regardless of the reaction time or temperature.

B.6 Summary

The difficulty in synthesising quino[7,8-*h*]quinoline compared to other heterocycles (such as phenanthroline) can be rationalised by the unique separation of the nitrogens which promote the formation of the internal nitrogen-bridged species **B21**. The Staab synthesis is the only confirmed route to quino[7,8-*h*]quinoline as the ester substituents are crucial for hindering the formation of **B21**. The first step of the Staab synthesis gives **B32**, before the second amine is substituted. Likewise, the generalised **B33** would be formed in sections B.3, B.4 and B.5.

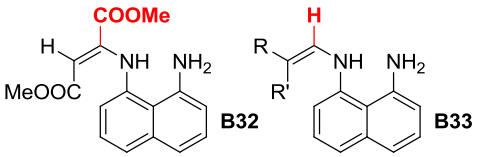

Figure B.4: Initial mono-substituted products

Unlike **B32**, the lack of steric hindrance in **B33** leads to a favourable side-reaction giving **B21**.

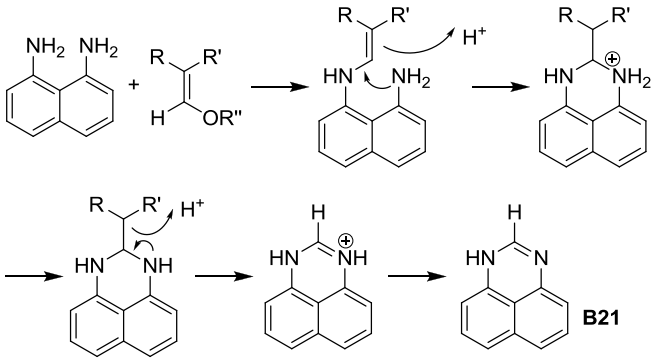

*Scheme B.11: Proposed side reaction leading to **B21***

In the Staab synthesis, one of the minor by-products was a bridged species with a methyl ester in place of the hydrogen on **B21**; however, the major product is the desired **B34**.

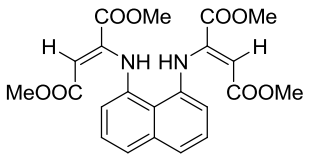

Figure B.5: Tetramethyl 2,2'-(naphthalene-1,8-diylbis(azanediyl))difumarate, ***B34***

The resistance of **B34** to **B21** is more likely due to steric reasons than electronic effects. The electron-withdrawing effect of the methyl esters would increase the electrophilicity of α carbon making it more susceptible to attack from the adjacent nitrogen. Instead it is likely that the methyl esters force the orientation of the α carbon away from the adjacent nitrogen so an internal reaction cannot occur. In contrast, with only a proton on the α carbon there is no steric hindrance to prevent formation of **B21**. To date, the only confirmed route to quino[7,8-*h*]quinoline is via the Staab synthesis.

References

1. US Agency for Toxic Substances and Disease Registry (ATSDR), Toxicological Profile for Beryllium, ATSDR, Atlanta, GA,. **2002**.
2. Taylor, T. P.; Ding, M.; Ehler, D. S.; Foreman, T. M.; Kaszuba, J. P.; Sauer, N. N., *J. Environ. Sci. Health* **2003**, *A38* (2), 439-469.
3. Eisenbud, M., *J. Appl. Occup. Environ. Hyg.* **1998**, *13* (1), 25-31.
4. Reeves, A. L., Toxicity of Detrimental Metal Ions. Beryllium. In *Handbook of Metal-Ligand Interactions. Biological Fluids: Bioinorganic Medicine*, Dekker: New York, NY, Vol. 2, pp 772-779.
5. Saltini, C.; Amicosante, M.; Franchi, A.; Lombardi, G.; Richeldi, L., *Eur. Resp. J.* **1998**, *12* (5), 1463-1475.
6. Toxicological Review of Beryllium. *U.S. Environmental Protection Agency* **1998**, *EPA/635/R-98/008*.
7. Bellamy, R. G.; Hill, N. A., Extraction and Metallurgy of Uranium, Thorium, and Beryllium. In *International Series of Monographs on Nuclear Energy*, Dunworth, J. V., Ed. The Macmillian Company: New York, 1963; Vol. 1.
8. Walsh, K. A., Beryllium. In *The Encyclopedia of Chemistry*, Hampel, C. A.; Hawley, G. G., Eds. Van Nostrand Reinhold Co.: New York, NY, 1973; Vol. 3.
9. Cunningham, L. D., *Minerals Yearbook - Beryllium*. US Geological Survey: Washington, DC, 2000.
10. Barthelmy, D., Mineralogy Database, Beryllium. *http://www.webmineral.com/chem/Chem-Be.html.* (Accessed May 2010).
11. United States Geological Survey (USGS), Mineral Commodity Summaries: Beryllium. USGS: Washington, D.C., 2001.
12. Parsonage, T., *Mater. Sci. Technol.* **2000**, *16* (7-8), 732-738.
13. Levoy, N. F.; Smith, B. J. In *Proc. 2nd Symp. Synth. Process Lightweight Metal Mater., Mineral., Metals Mater. Soc.: Warrendale, PA*, Beryllium Aluminum Alloy Development for Investment Casting., 1997.

14. Marder, J. M. In *P/M Aerospace Defense Technol. Proc., 2nd, Met. Powder Ind. Fed.: Princeton, NJ,*, An Overview of Beryllium Powder Metallurgy Technology., 1991.
15. Wong, C. Y.; Woollins, J. D., *Coord. Chem. Rev.* **1994**, *130*, 243-273.
16. Brush Wellman, Inc. *http://www.brushwellman.com* (Accessed May 2010).
17. National Jewish Medical and Research Center (NJMRC). Medfacts, Facts About Beryllium Disease. *http://www.nationaljewish.org/healthinfo/conditions/beryllium-disease/about-beryllium.aspx* (Accessed May 2010).
18. Kreiss, K.; Miller, F.; Newman, L. S.; Ojo-Amaize, E. A.; Rossman, M. D.; Saltini, C., *Clin. Immunol. Immunopathol.* **1994**, *71* (2), 123-129.
19. Newman, L.S. Hearing on Compensation for Beryllium-Related Illnesses, H.R.675, H.R. 3418, H.R. 3478, H.R. 3495, H.R. 4263, H.R. 4398. Testimony before Subcommittee on Immigration and Claims, Committee of the Judiciary, US House of Representatives. 2000.
20. Kreiss, K.; Mroz, M. M.; Zhen, B.; Martyny, J. W.; Newman, L. S., *Am. Rev. Respir. Dis.* **1993**, *148* (4), 985-991.
21. Kreiss, K.; Wasserman, S.; Mroz, M. M.; Newman, L. S., *J. Occup. Med.* **1993**, *35* (3), 267-274.
22. Richeldi, L.; Sorrentino, R.; Saltini, C., *Science* **1993**, *262* (5131), 242-244.
23. Wang, Z.; White, P. S.; Petrovic, M.; Tatum, O. L.; Newman, L. S.; Maier, L. A.; Marrone, B. L., *J. Immunol.* **1999**, *163* (3), 1647-1653.
24. Mederos, A.; Dominguez, S.; Chinea, E.; Brito, F.; Midollini, S.; Vacca, A., *Bol. Soc. Chil. Quim.* **1997**, *42* (2), 281-295.
25. Guy, R. H.; Hostynek, J. J.; Hinz, R. S.; Lorence, C. R., Beryllium. In *Metal and the Skin: Topical Effects and Systemic Absorption*, Marcel Dekker: New York, 1999; pp 91-97.
26. Griffitts, W. R.; Skilleter, D. N., Beryllium. In *Metals and Their Compounds in the Environment*, Merian, E., Ed. VCH: Weinheim: Fed. Rep. Ger., 1991; pp 775-787.
27. Scott, B. L.; McCleskey, T. M.; Chandhary, A.; Hong-Geller, E.; Gnanakaran, S., *Chem. Comm.* **2008**, (25), 2837-2847.

28. Diyabalanage, H. V. K.; Ganguly, K.; Ehler, D. S.; Collis, G. E.; Scott, B. L.; Chandhary, A.; Burrell, A. K.; McCleskey, T. M., *Angew. Chem., Int. Ed.* **2008**, *47* (38), 7332-7334.
29. Plieger, P. G.; John, K. D.; Burrell, A. K., *Polyhedron* **2007**, *26*, 472-478.
30. Alderighi, L. D., S.; Gans, P.; Midollini, S.; Sabatini, A.; Vacca, A., *J. Coord. Chem.* **2008**, *62* (1), 14-22.
31. Mederos, A.; Dominguez, S.; Chinea, E.; Brito, F.; Cecconi, F., *J. Coord. Chem.* **2001**, *53* (3), 191-222.
32. Schmidbaur, H., *Coord. Chem. Rev.* **2001**, *215* (1), 223-242.
33. Tulinsky, A.; Worthington, C. R.; Pignataro, E., *Acta Cryst.* **1959**, *12*, 623-626.
34. Keizer, T. S.; Sauer, N. N.; McCleskey, T. M., *J. Am. Chem. Soc.* **2004**, *126* (31), 9484-9485.
35. Keizer, T. S.; Sauer, N. N.; McCleskey, T. M., *J. Inorg. Biochem.* **2005**, *99* (5), 1174-1181.
36. Keizer, T. S.; Scott, B. L.; Sauer, N. N.; McCleskey, T. M., *Angew. Chem. Int. Ed.* **2005**, *44* (16), 2403-2406.
37. Alderighi, L.; Vacca, A.; Cecconi, F.; Midollini, S.; Chinea, E.; Dominguez, S.; Valle, A.; Dakternieks, D.; Duthie, A., *Inorg. Chim. Acta* **1999**, *285* (1), 39-48.
38. Schmidt, M.; Bauer, A.; Schier, A.; Schmidbaur, H., *Z. Naturforsch., B: Chem. Sci.* **1998**, *53* (7), 727-733.
39. Duc, G.; Faure, R.; Loiseleur, H., *Acta Cryst.* **1978**, *34*, 2115-2118.
40. Schmidt, M.; Bauer, A.; Schmidbaur, H., *Inorg. Chem.* **1997**, *36* (10), 2040-2043.
41. Alderighi, L.; Cecconi, F.; Ghilardi, C. A.; Mederos, A.; Midollini, S.; Orlandini, A.; Vacca, A., *Polyhedron* **1999**, *18* (25), 3305-3312.
42. Plieger, P. G.; Ehler, D. S.; Duran, B. L.; Taylor, T. P.; John, K. D.; Keizer, T. S.; McCleskey, T. M.; Burrell, A. K.; Kampf, J. W.; Haase, T.; Rasmussen, P. G.; Karr, J., *Inorg. Chem.* **2005**, *44* (16), 5761-5769.
43. Rivas, B. L.; Pooley, S. A.; Luna, M.; Geckeler, K. E., *J. Appl. Pol. Sci.* **2001**, *82* (2), 22-30.
44. Gohdes, J. W.; Duran, B. L.; Clark, N. C.; Robinson, T. W.; Smith, B. F.; Sauer, N. N., *Sep. Sci. Technol.* **2001**, *36* (12), 2647-2658.

45. Kontoghiorghes, G. J., *Toxicol. Lett.* **1995**, *80* (1-3), 1-18.
46. Cecconi, F.; Ghilardi, C. A.; Ienco, A.; Mariani, P.; Mealli, C.; Midollini, S.; Orlandini, A.; Vacca, A., *Inorg. Chem.* **2002**, *41* (15), 4006-4017.
47. Schmidbaur, H.; Kumberger, O.; Riede, J., *Inorg. Chem.* **1991**, *30* (21), 3101-3103.
48. Schmidbaur, H.; Kumberger, O., *Chem. Ber.* **1993**, *126* (1), 3-9.
49. Saarinen, H.; Raikas, T.; Lajunen, L., *Finn. Chem. Lett.* **1974**, (3), 109-111.
50. Kumberger, O.; Riede, J.; Schmidbaur, H., *Chem. Ber.* **1992**, *125* (12), 2701-2703.
51. Dubey, S. N.; Mehrotta, R. C., *J. Less-Common Met.* **1965**, *9* (2), 123-132.
52. Bartusek, M.; Zelinka, J., *Collect. Czech. Chem. Commun.* **1967**, *32* (3), 992-1005.
53. Klufers, P.; Mayer, P.; Schuhmacher, J., *Z. Anorg. Allg. Chem.* **1995**, *621*, 1373-1379.
54. Chinea, E.; Dominguez, S.; Mederos, A.; Brito, F.; Arrieta, J. M.; Sanchez, F.; Germain, G., *Inorg. Chem.* **1995**, *34* (6), 1579-1587.
55. Cecconi, F.; Chinea, E.; Ghilardi, C. A.; Midollini, S.; Orlandini, A., *Inorg. Chim. Acta.* **1997**, *260* (1), 77-82.
56. Li, Y.; Lui, Y.; Bu, W.; Lu, D.; Wu, Y.; Wang, Y., *Chem. Mater.* **2000**, *12* (9), 2672-2679.
57. Tong, Y.-P.; Zheng, S.-L.; Chen, X.-M., *Inorg. Chem.* **2005**, *44* (12), 4270-4275.
58. Hamada, Y.; Sano, T.; Fujita, M.; Fujii, T.; Nishio, Y.; Shibata, K., *Chem. Lett.* **1993**, (5), 905-906.
59. Guo, Z.; Dong, Z.; Zhu, R.; Jin, S.; Lui, B., *Spectrochem. Acta Part A* **2007**, *68*, 337-340.
60. Liao, S.-H.; Shui, J.-R.; Lui, S.-W.; Yeh, S.-J.; Chen, Y.-H.; Chen, C.-T.; Chow, T. J.; Wu, C.-I., *J. Am. Chem. Soc.* **2009**, *131* (2), 763-777.
61. Minogue, E. M.; Ehler, D. S.; Burrell, A. K.; McCleskey, T. M.; Taylor, T. P., *ASTM Spec. Tech. Pub.* **2006**, *1473*, 92-101.
62. van Niekerk, J. C.; Irving, H. M. N. H.; Nassimbeni, L. R., *S. Afr. J. Chem.* **1979**, *32* (3), 85-89.
63. Niemeyer, M.; Power, P. P., *Inorg. Chem.* **1997**, *36* (21), 4688-4696.
64. Fleischer, R.; Stalke, D., *Inorg. Chem.* **1997**, *36* (11), 2413-2419.

65. Thiele, K.-H.; Lorenz, V.; Thiele, G.; Zonnchen, P.; Scholz, J., *Angew. Chem. Int. Ed. Engl.* **1994**, *33* (13), 1372–1373.
66. Liu, S.-F.; Wu, Q.; Schmider, H. L.; Aziz, H.; Hu, N.-X.; Popovic, Z.; Wang, S., *J. Am. Chem. Soc.* **2000**, *122* (15), 3671-3678.
67. Chmely, S. C.; Hanusa, T. P., *Angew. Chem. Int. Ed.* **2010**, *49* (34), 5870-5874.
68. Okada, H. Electroluminescent Material. JP 2000-297278, Oct 24, 2000, Fuji Photo Film Co., Ltd., Japan.
69. Ke, Z.; Cundari, T. R., *Organometallics* **2010**, *29* (4), 821-834.
70. Furuya, T.; Kaiser, H. M.; Ritter, T., *Angew. Chem., Int. Ed.* **2008**, *47* (32), 5993-5996.
71. Dick, A. R.; Remy, M. S.; Kampf, J. W.; Sanford, M. S., *Organometallics* **2007**, *26* (6), 1365-1370.
72. Wustefeld, H.-U.; Kaska, W. C.; Schuth, F.; Stucky, G. D.; Bu, X.; Krebs, B., *Angew. Chem., Int. Ed.* **2001**, *40* (17), 3182-3184.
73. Schenkel, H.; Schenkel, M., *Helv. Chim. Acta* **1944**, *27*, 1456-1463.
74. Alder, R. W.; Bowman, P. S.; Steele, W. R. S.; Winterman, D. R., *Chem. Commun.* **1968**, (13), 723-724.
75. Alder, R. W.; Bryce, M. R.; Goode, N. C., *J. Chem. Soc., Perkin Trans. 2.* **1982**, (4), 477-483.
76. Ozeryanskii, V. A.; Pozharskii, A. F.; Koroleva, M. G.; Shevchuk, D. A.; Kazheva, O. N.; Chekhlov, A. N.; Shilov, G. V.; Dyachenko, O. A., *Tetrahedron* **2005**, *61* (17), 4221-4232.
77. Hibbert, F.; Simpson, G. R., *J. Chem. Soc., Perkin Trans. 2.* **1987**, (2), 243-246.
78. Hibbert, F.; Hunte, P. P., *J. Chem. Soc., Perkin Trans. 2.* **1983**, (12), 1895-1899.
79. Ozeryanskii, V. A.; Pozharskii, A. F.; Vistorobskii, N. V., *Russ. J. Org. Chem.* **1997**, *33* (2), 251-256.
80. Pozharskii, A. F.; Ozeryanskii, V. A., *Russ. Chem. Bull.* **1998**, *47* (1), 66-73.
81. Pozharskii, A. F.; Ryabtsova, O. V.; Ozeryanskii, V. A.; Degtyarev, A. V.; Kazheva, O. N.; Alexandrov, G. G.; Dyachenko, O. A., *J. Org. Chem.* **2003**, *68* (26), 10109-10122.

82. Ozeryanskii, V. A.; Pozharskii, A. F.; Bienko, A. J.; Sawka-Dobrowolska, W.; Sobczyk, L., *J. Phys, Chem. A.* **2005**, *109* (8), 1637-1642.
83. Staab, H. A.; Saupe, T.; Krieger, C., *Angew. Chem., Int. Ed. Engl.* **1983**, *22* (9), 731-732.
84. Saupe, T.; Krieger, C.; Staab, H. A., *Angew. Chem. Int. Ed. Engl.* **1986**, *25* (5), 451-453.
85. Zirnstein, M. A.; Staab, H. A., *Angew. Chem. Int. Ed. Engl.* **1987**, *26* (5), 460-461.
86. Krieger, C.; Newsom, I.; Zirnstein, M. A.; Staab, H. A., *Angew. Chem., Int. Ed. Engl.* **1989**, *28* (1), 84-86.
87. Raab, V.; Kipke, J.; Gshwind, R. M.; Sundermeyer, J., *Chem. Eur. J.* **2002**, *8* (7), 1682-1693.
88. Raab, V.; Harms, K.; Sundermeyer, J., *J. Org. Chem.* **2003**, *68*, 8790-8797.
89. Raab, V.; Gauchenova, E.; Merkoulov, A.; Harms, K.; Sundermeyer, J.; Kovacevic, B.; Maksic, Z. B., *J. Am. Chem. Soc.* **2005**, *127* (45), 15738-15743.
90. Yamasaki, T.; Ozaki, N.; Saika, Y.; Ohta, K.; Goboh, K.; Nakamura, F.; Hashimoto, M.; Okeya, S., *Chem. Lett.* **2004**, *33* (9), 928-929.
91. Wild, U.; Hubner, O.; Maronna, A.; Enders, M.; Kaifer, E.; Wadepohl, H.; Himmel, H.-J., *Eur. J. Inorg. Chem.* **2008**, (28), 4440-4447.
92. Polyakova, I. N.; Sergienko, V. S.; Poznyak, A. L., *Zh. Neorg. Khim.* **1996**, *41* (7), 1114-1118.
93. Fernandaz Martinez, M. T.; Sanchez Santos, F. J.; Gonzalez Garcia, S.; Niclos Gutierrez, J., *Ars Pharmaceutica* **1987**, *28* (4), 481-489.
94. Plieger, P. G.; John, K. D.; Burrell, A. K., *Polyhedron* **2007**, *26* (2), 472-478.
95. Hoshino, N.; Shiga, T.; Nihei, M.; Oshio, H., *Polyhedron* **2009**, *28* (9-10), 1754-1757.
96. Gonzalez-Arellano, C.; Corma, A.; Iglesias, M.; Sanchez, F., *Eur. J. Inorg. Chem.* **2008**, (7), 1107-1115.
97. Zhang, H. Y.; Ye, K. Q.; Zhang, J. Y.; Liu, Y.; Wang, W., *Inorg. Chem.* **2006**, *45* (4), 1745-1753.
98. Hartman, J. S.; Shoemaker, J. A. W., *Polyhedron* **2000**, *19* (2), 165-176.
99. Iwai, I.; Hara, S., *Yakugaku Zasshi* **1950**, *70*, 394-400.

100. Iwai, I.; Hara, S.; Sayegi, S., *J. Pharm. Soc. Jpn.* **1951**, *71*, 1152.
101. Dufour, M.; Buu-Hoi, N. P.; Pierre, J., *J. Chem. Soc. C.* **1967**, (15), 1415-1416.
102. Edel, A.; Marnot, P. A.; Sauvage, J. P., *Tetrahedron Lett.* **1985**, *26* (6), 727-728.
103. Honda, K.; Nakanishi, H.; Yabe, A., *Bull. Chem. Soc. Jpn.* **1983**, *56* (8), 2338-2340.
104. Strauss, C. R.; Trainor, R. W., *Aust. J. Chem.* **1998**, *51* (8), 703-705.
105. The Spectral Database for Organic Compounds, SDBS. National Institute of Advanced Industrial Science and Technology, AIST. *http://www.riodb01.ibase.aist.go.jp/sdbs/cgi-bin/cre_index.cgi?lang=eng* (Accessed July 2010).
106. Hunter, C. A.; Sanders, J. K. M., *J. Am. Chem. Soc.* **1990**, *112* (14), 5525-3324.
107. Janiak, C., *J. Chem. Soc. Dalton Trans.* **2000**, (21), 3885-3896.
108. Steiner, T., *Angew. Chem., Int. Ed. Engl.* **2002**, *41* (1), 48-76.
109. Jeffrey, G. A., *Cryst. Rev.* **2003**, *9* (2), 135-176.
110. Mallinson, P. R.; Wozniak, K.; Wilson, C. C.; McCormack, K. L.; Yufit, D. S., *J. Am. Chem. Soc.* **1999**, *121* (19), 4640-4646.
111. Panda, K.; Siddiqui, I.; Mahata, P. K.; Ila, H.; Junjappa, H., *Synlett* **2004**, (3), 449-452.
112. Schmittel, M.; Ammon, H., *Eur. J. Org. Chem.* **1998**, (5), 785-792.
113. Nasiri, H. R.; Bolte, M.; Schwalbe, H., *Heterocyclic Commun.* **2006**, *12* (5), 319-322.
114. Barth, T.; Krieger, C.; Neugebauer, F. A.; Staab, H. A., *Angew. Chem., Int. Ed. Engl.* **1991**, *30* (8), 1028-1030.
115. Ochiai, E.; Suzuki, I., *Pharmaceutical Bull.* **1954**, *2*, 247-249.
116. Rueping, M.; Ieawsuwan, W., *Synlett* **2007**, *2*, 247-250.
117. Miyaura, N.; Suzuki, A., *Chem. Commun.* **1979**, (19), 866-867.
118. Miyaura, N.; Yamada, K.; Suzuki, A., *Tetrahedron Lett.* **1979**, (36), 3437-3440.
119. Pozharskii, A. F.; Ozeryanskii, V. A., Proton Sponges. In *The Chemistry of Anilines Part 1*, Rappoport, Z., Ed. John Wiley & Sons , Ltd: Chichester, 2007; p 1180 pages.
120. Wozniak, K.; Krygowski, T. M.; Kariuki, B.; Jones, W.; Grech, E., *J. Mol. Struct.* **1990**, *240*, 111-118.

121. Kubiak, R.; Waskowska, A.; Sledz, M.; Jezierski, A., *Inorg. Chim. Acta* **2006**, *359* (5), 1344-1350.
122. Oi, R.; Sharpless, K. B., *Org. Syn., Coll* **1998**, *9*, 251.
123. Boechat, N.; da Costa, J.; Mendonca, J.; Paes, K.; Fernandes, E.; de Oliveira, P.; Vasconcelos, T.; de Souza, M., *Synth. Commun.* **2005**, *35* (24), 3187-3190.
124. O'Regan, B.; Gratzel, M., *Nature* **1991**, *353* (6346), 737-740.
125. Umezawa, K.; Nakamura, Y.; Makino, H.; Citterio, D.; Suzuki, K., *J. Am. Chem. Soc.* **2008**, *130* (5), 1550-1551.
126. Mascal, M.; Armstrong, A.; Bartberger, M. D., *J. Am. Chem. Soc.* **2002**, *124* (22), 6274-6276.
127. Quinonero, D.; Garau, C.; Rotger, C.; Frontera, A.; Ballester, P.; Costa, A.; Deya, P. M., *Angew. Chem., Int. Ed. Engl.* **2002**, *41* (18), 3389-3392.
128. Alkorta, I.; Rozas, I.; Elguero, J., *J. Am. Chem. Soc.* **2002**, *124* (29), 8593-8598.
129. Loudet, A.; Burgess, K., *Chem. Rev.* **2007**, *107* (11), 4891-4932.
130. Fery-Forgues, S.; Lavabre, D., *J. Chem. Ed.* **1999**, *76* (9), 1260-1264.
131. Li, L.; Han, J.; Nguyen, B.; Burgess, K., *J. Org. Chem.* **2008**, *73* (5), 1963-1970.
132. Andersson, M. P.; Uvdal, P., *J. Phys, Chem. A.* **2005**, *109* (12), 2937-2941.
133. Tantirungrotechai, T.; Phanasant, K.; Roddecha, S.; Surawatanawong, P.; Sutthikhum, V.; Limtrakul, J., *J. Mol. Struct: (THEOCHEM)* **2006**, *760* (1-3), 189-192.
134. Jones, G.; Jackson, W. R.; Kanoktanaporn, S.; Bergmark, W. R., *Photochem. Photobiol.* **1985**, *42* (5), 477-483.
135. Soep, B.; Kellman, A.; Martin, M.; Lindqvist, L., *Chem. Phys. Lett.* **1972**, *13* (3), 241-244.
136. Coates, G. E.; Green, S. I. E., *J. Chem. Soc.* **1962**, 3340-3348.
137. Alderighi, L.; Gans, P.; Midollini, S.; Vacca, A., *Adv. Inorg. Chem.* **2000**, *50*, 109-172.
138. Plieger, P. G.; John, K. D.; Keizer, T. S.; McCleskey, T. M.; Burrell, A. K., *J. Am. Chem. Soc.* **2004**, *126* (44), 14651-14658.
139. Hofmeister, F., *Arch. Exp. Pathol. Pharmacol.* **1888**, *24*, 247-260.
140. Irving, H. M. N. H.; Williams, R. J. P., *J. Chem. Soc.* **1953**, 3192-3210.

141. Kirk, S. Cyclo- and Polyphosphazenes Containing 2-oxypyridine Moieties Coordinated to Selected Transition Metals. Massey University, Palmerston North, 2008.
142. Lever, A. B. P., *Inorganic Electronic Spectroscopy*. 2nd ed.; Elsevier: New York, 1984.
143. Yokoi, H.; Addison, A. W., *Inorg. Chem.* **1977**, *16* (6), 1341-1349.
144. Ainscough, E. W.; Brodie, A. M.; Jameson, G. B.; Otter, C. A., *Polyhedron* **2007**, *26* (2), 460-471.
145. Wang, X.; Spear, K. L.; Fulp, A. B.; Seconi, D.; Suzuki, T.; Ishii, T.; Moritomo, A.; Kubota, H.; Kazami, J.-I. Preparation of polycyclic pyridines as potassium ion channel modulators. WO 2005100349, Oct 27 2005, USA.
146. Parmentier, M.; Gros, P.; Fort, Y., *Tetrahedron* **2005**, *61* (13), 3261-3269.
147. Dyker, G.; Muth, O., *Eur. J. Org. Chem.* **2004**, (21), 4319-4322.
148. Sumby, C. J., *Aust. J. Chem.* **2008**, *61* (11), 894-904.
149. Hagel, M.; Lui, J.; Muth, O.; Rivera, H. J. E.; Schwake, E.; Sripanom, L.; Henkel, G.; Dyker, G., *Eur. J. Org. Chem.* **2007**, (21), 3573-3582.
150. Ye, M.-C.; Zhou, J.; Tang, Y., *J. Org. Chem.* **2006**, *71* (9), 3576-3582.
151. Saha, S.; Majumdar, R.; Roy, M.; Dighe, R. R.; Chakravarty, A. R., *Inorg. Chem.* **2009**, *48* (6), 2652-2663.
152. Matsumoto, K.; Ikeda, J.; Kurata, H.; Kawase, T.; Oda, M., *Chem. Lett.* **2006**, *35* (1), 74-75.
153. Toganoh, M.; Harada, N.; Furuta, H., *J. Organomet. Chem.* **2008**, *693* (19), 3141-3150.
154. Aubouy, L.; Huby, N.; Hirsch, L.; Van der Lee, A.; Gerbier, P., *New. J. Chem.* **2009**, *33* (6), 1290-1300.
155. Rudine, A. B.; Walter, M. G.; Wamser, C. C., *J. Org. Chem.* **2010**, *75* (12), 4292-4295.
156. Cottet, F.; Marmull, M.; Lefebvre, O.; Schlosser, M., *Eur. J. Org. Chem.* **2003**, (8), 1559-1568.
157. Polozov, A. M.; Hategan, G.; Cao, H.; Kiselyov, A. S.; Zeller, W.; Singh, J., *Tetrahedron Lett.* **2010**, *51* (4), 575-578.

158. Arnold, P. J.; Davies, S. C.; Dilworth, J. R.; Durrant, M. C.; Griffiths, D. V.; Huges, D. L.; Richards, R. L.; Sharpe, P. C., *J. Chem. Soc., Dalton Trans.* **2001**, (5), 736-746.

159. Hamada, M.; Inami, I.; Nagai, Y.; Higashi, T.; Shoji, M.; Ogawa, S.; Umezawa, K.; Sugai, T., *Tetrahedron Asymm.* **2009**, *20* (18), 2105-2111.

160. Lu, Z.; Zhan, F.; Xue, L.; Zhu, J., *Jingxi Shiyou Huagong* **2006**, *23* (6), 37-40.

161. Tandon, S. S.; Chander, S.; Thompson, L. K.; Bridson, J. N.; McKee, V., *Inorg. Chim. Acta* **1994**, *219* (1-2), 55-65.

162. Mukherjee, A.; Lloret, F.; Mukherjee, R., *Inorg. Chem.* **2008**, *47* (11), 4471-4480.

163. Philibert, A.; Thomas, F.; Philouze, C.; Hamman, S.; Saint-Aman, E.; Pierre, J.-L., *Chem. - Eur. J.* **2003**, *9* (16), 3803-3812.

164. Whitelaw, E. L.; Jones, M. D.; Mahon, M. F.; Kociok-Kohn, G., *Dalton Trans.* **2009**, (41), 9020-9025.

165. Short, J. H.; Ours, C. W., *J. Heterocyclic Chem.* **1975**, *12* (5), 869-876.

166. Nielson, A. J.; Waters, J. M., *Polyhedron* **2010**, *29* (7), 1715-1726.

167. Singh, R.; Banerjee, A.; Gordon, Y.; Rajak, K. K., *Transition Met. Chem.* **2009**, *34* (6), 689-694.

168. Schnieders, D.; Hammerschmidt, A.; Merkel, M.; Schweppe, F.; Krebs, B., *Z. Anorg. Allg. Chem.* **2008**, *634* (15), 2933-2939.

169. Boyd, C. L.; Toupance, T.; Tyrrell, B. R.; Ward, B. D.; Wilson, C. R.; Cowley, A. R.; Mountford, P., *Organometallics* **2003**, *24* (2), 309-330.

170. Wong, Y.-L.; Tong, L. H.; Dilworth, J. R.; Ng, D. K. P.; Lee, H. K., *Dalton Trans.* **2010**, *39* (19), 4602-4611.

171. Phomphrai, K.; Chumsaeng, P.; Sangtrirutnugul, P.; Preeyanuch, K.; Palangpon, P. M., *Dalton Trans.* **2010**, *39* (7), 1865-1871.

172. Dean, R. K.; Granville, S. L.; Dawe, L. N.; Decken, A.; Hattenhauser, K. M.; Kozak, C. M., *Dalton Trans.* **2010**, *2* (39), 548-559.

173. van Gorkum, R.; Berding, J.; Mills, A. M.; Kooijman, H.; Tooke, D. M.; Spek, A. L.; Mutikainen, I.; Turpeinen, U.; Reedijk, J.; Bouwman, E., *Eur. J. Inorg. Chem.* **2008**, (9), 1487-1496.

174. Hasan, K.; Fowler, C.; Kwong, P.; Crane, A. K.; Collins, J. L.; Kozak, C. M., *Dalton Trans.* **2008**, (22), 2991-2998.
175. Nagataki, T.; Itoh, S., *Chem. Lett.* **2007**, *36* (6), 748-749.
176. Lui, X.; Shang, X.; Tang, T.; Hu, N.; Pei, F.; Cui, D.; Dongmei, C.; Xuesi, J. X., *Organometallics* **2007**, *26* (10), 2747-2757.
177. Chmura, A. J.; Davidson, M. G.; Jones, M. D.; Lunn, M. D.; Mahon, M. F.; Johnson, A. F.; Khunkamchoo, P.; Roberts, S. L.; Wong, S. S. F., *Macromolecules* **2006**, *39* (21), 7250-7257.
178. Mondal, A.; Sarkar, S.; Chopra, D.; Row, T. N.; Guru, R.; Kajal, K., *Dalton Trans.* **2004**, (20), 3244-3250.
179. Thomas, F.; Gellon, G.; Gautier-Luneau, I.; Saint-Aman, E.; Pierre, J. L., *Angew. Chem. Int. Ed. Engl.* **2002**, *41* (16), 3047-3050.
180. John, A.; Shaikh, M. M.; Ghosh, P., *Dalton Trans.* **2008**, (21), 2815-2824.
181. Abrahams, A.; Cowley, A. R.; Gerber, T. I. A.; Imrie, C.; Mayer, P., *J. Coord. Chem.* **2003**, *56* (15), 1299-1306.
182. Tshuva, E. Y.; Goldbery, I.; Kol, M.; Goldschmidt, Z., *Organometallics* **2001**, *20* (14), 3017-3028.
183. Taki, M.; Kumei, H.; Nagatomo, S.; Kitagawa, T.; Itoh, S.; Fukuzumi, S., *Inorg. Chem. Acta.* **2000**, *300-302*, 622-632.
184. Hinshaw, C. J.; Peng, G.; Singh, R.; Spence, J. T.; Enemark, J. H.; Bruck, M.; Kristofzski, J.; Merbs, S. L.; Ortega, R. B.; Wexler, P. A., *Inorg. Chem.* **1989**, *28* (25), 4483-4491.
185. Ceccato, A. S.; Neves, A.; De Brito, M. A.; Drechsel, S. M.; Mangrich, A. S.; Werner, R.; Haase, W.; Bortoluzzi, A. J., *Dalton* **2000**, (10), 1573-1577.
186. Shongwe, M. S.; Kaschula, C. H.; Adsetts, M. S.; Ainscough, E. W.; Brodie, A. M.; Morris, M. J., *Inorg. Chem.* **2005**, *44* (9), 3070-3079.
187. Roy, M.; Saha, S.; Patra, A. K.; Nethaji, M.; Chakravarty, A. R., *Inorg. Chem.* **2007**, *46* (11), 4368-4370.
188. Tong, L. H.; Wong, Y.-L.; Pascu, S. I.; Dilworth, J. R., *Dalton Trans* **2008**, (35), 4784-4791.

189. Shimazaki, Y.; Huth, S.; Odani, A.; Yamauchi, O., *Angew. Chem. Int. Ed.* **2000**, *39* (9), 1666-1669.

190. Shimazaki, Y.; Huth, S.; Hirota, S.; Yamauchi, O., *Inorg. Chem. Acta.* **2002**, *331*, 168-177.

191. Whittaker, M. M.; Duncan, W. R.; Whittaker, J. W., *Inorg. Chem.* **1996**, *35* (2), 382-386.

192. Mahata, P. K.; Barun, O.; Ila, H.; Junjappa, H., *Synlett* **2000**, (9), 1345-1347.

193. Soep, B.; Kellman, A.; Martin, M.; Lindqvist, L., *Chem. Phys. Lett.* **1972**, *13*, 241-244.

194. Lee, P. C.; Meisel, D., *J. Phys. Chem.* **1982**, *86* (17), 3391-3395.

195. Vedernikov, A. N.; Fettinger, J. C.; Mohr, F., *J. Am. Chem. Soc.* **2004**, *126* (36), 11160-11161.

196. Yajima, T.; Shimazaki, Y.; Ishigami, N.; Odani, A.; Yamauchi, O., *Inorg. Chim. Acta* **2002**, *337*, 193-202.

197. Biswas, S.; Mitra, K.; Chattopadhyay, S. K.; Adhikary, B.; Lucas, C. R., *Transition Met. Chem.* **2005**, *30* (4), 393-398.

198. Abreu, A.; Jesus, A. S.; Beltran, H. I.; Santillan, R.; Farfan, N., *J. Organomet. Chem.* **2006**, *691* (3), 337-348.

199. Usatyuk, V. G.; Yalchin, B.; Aydin, A.; Medzhidov, A. A., *Azerbaidzhanskii Khim. Zh.* **2004**, (2), 129-136.

200. Muthusubramanian, L.; Misra, G. S., *Ind. J. Chem.* **1987**, *26B* (12), 1192-1193.

201. Chandrasekhar, B.; Prasad, A. S. R.; Eswaraiah, S.; Venkateswaralu, A., *Org. Process Res. & Development* **2002**, *6* (3), 242-245.

202. Beccalli, E. M., *J. Org. Chem.* **1984**, *49* (22), 4287-4290.

203. Kazuyoshi, T.; Kanoko, T.; Keiko, Y.; Haruo, O., *J. Org. Chem.* **1985**, *50* (2), 273-275.

204. Herbert, J. M.; Woodgate, P. D.; Denny, W. A., *J. Med. Chem.* **1987**, *30* (11), 2081-2086.

205. Molock, F. F.; Boykin, D. W., *J. Heterocyclic Chem.* **1983**, *20* (3), 681-686.

206. Graf, G. I.; Hastreiter, D.; da Silva, L. A.; Rebelo, R. A.; Montalban, A. G.; McKillop, A., *Tetrahedron* **2002**, *58* (44), 9095-9100.